CROSS-REGIONAL AND LOCAL AIR POLLUTION HISTORIES FROM SEDIMENTS OF SMALL URBAN PONDS IN THE LOWER MERSEY REGION, UK.

ANN LOUISE POWER

A thesis submitted to the Department of Natural, Geographical and Applied Science, Edge Hill University, in partial fulfilment of the requirements for the degree of Doctor of Philosophy.

Degree awarded by Edge Hill University.

JANUARY 2011

ABSTRACT

Retrospective urban air quality assessments are imperative in understanding human health effects of long-term (lifetime) exposures to pollution; however, historical pollution data are limited. Therefore, air pollution records captured in the sediments of small urban ponds, sedimentary archives sensitive to localised urban activity, have been explored within the lower Mersey region (LMR), a heavily industrialised area with poor health amongst the population.

Proxy pollution profiles derived from isotope chronologies and magnetic, trace metal, flyash and geochemical properties of sediments from four small urban ponds have yielded high-resolution air pollution histories (<300 years). These site specific air pollution signals reveal air quality impacts of localised urban development and demonstrate the integrity of sediment records from urban ponds. A cross-regional air pollution history, reconstructed using these local contamination signals, details spatial variations in pollution deposition across the LMR, spanning pre-industrial times to present day. Low ~pre-1830 pollution levels reflect a time of pre-intensified industry in the LMR with ~post-1830 increases signifying the Industrial Revolution and establishment of the early chemical industry. Distinct pollution enhancement from ~1900 to 1950 is attributed to population increases, industrial diversification and war-time demands on industry, pre-Clean Air Acts (1959). A complex cross-regional post-1950 signal reveals intra-urban variations reflecting urban expansions within the region, with pollution reductions observed post-1970, due to increasingly stringent air quality legislations, however, pollution does not consistently decline throughout the LMR, potentially, due to air quality impacts from increased road and air travel.

This high-resolution cross-regional *urban* air pollution signal provides an alternative to reliance upon *background* air pollution signals recorded by remote UK lakes. Furthermore, these ponds are set amongst populations most as risk to exposure of urban PM, and demonstrate important spatial variations in pollution characteristics, as well as revealing how air pollution has changed over time. These air pollution histories may, therefore, be used to better understand possible health linkages in the LMR.

ACKNOWLEDGEMENTS

I would like to express my gratitude to Halton Primary Care Trust (NHS), in particular Dr Julia Miller, for funding this work and thank Alex Stewart and the Health Protection Agency for championing this research. Also, thanks to Edge Hill University for funding via the Research Development Fund, and the support received from Alistair McCulloch, Julia Hedley, Julie Proud and the Research Office. Thanks are also extended to the University of Liverpool and the University of Wolverhampton for the use of laboratory equipment and technical assistance.

There are also many individuals I would like to thank for their continued help and generous support I have received whilst completing this work. Sincere thanks to the Director of Studies, Professor Annie Worsley, for all of her guidance, support, inspiration, and faith in her research student! Thank you for everything! Thanks, also, to the meticulous Dr Colin Booth (University of Wolverhampton), who first introduced me to the wonderful world of environmental magnetism and has been a valued supervisor. A special thank you to Dr Vanessa Holden, your support (academic, editorial, emotional and chocolate-related) has been truly appreciated!

A heartfelt thank you to all the staff at Edge Hill University's Geography Department for your encouragement! I would like to also express my sincere gratitude to Kathryn Coffey and Rob Hart (and all technicians past and present) for the fabulous technical support I have received, as well as cups of tea and a lending ear! I truly appreciate everyone's willingness to get covered in mud for the good of this work!

Also, I would like to recognise Professor Peter Appleby (University of Liverpool) for undertaking radiometric dating and his valued expertise. Thanks also to Paul Oldfield (Halton Borough Council) and Tim Kirwin (Woodland trust) for 'insider information' regarding various ponds and assistance in obtaining permission to carryout fieldwork.

I would not have been able to complete this thesis without the help of my family- Nan, Patty, Jacqui, Jackie and Melvyn. Thanks for all the encouragement and financial assistance when called on! I am sincerely indebted to my partner Paul Fryer, who bravely made the move 'up north' with me and has been providing financial support, allowing me to carry out this work, ever since, as well as assisting with fieldwork, listening to me rant on about the wonders of mud and helping me through the tough bits! Thank you so much!

CONTENTS

LIST OF FIGURES:

LIST OF PLATES:

LIST OF TABLES:

THESIS OVERVIEW:

The use of small urban ponds as air pollution archives is explored using sediment records obtained in the lower Mersey region (LMR), an area including and surrounding the borough of Halton, northwest England. The thesis is presented in three main sections:

(A) Introduction, aims and background: The aims and objectives, the utilisation of urban ponds as sedimentary archives and the reconstruction and importance of air pollution histories are introduced (Chapter 1). The need to investigate air pollution histories in the LMR is justified; highlighting the extensive industrial history and present day ill health within Halton (Chapter 2). A comprehensive account of the applied methodology details desktop analyses, fieldwork, laboratory techniques and data analyses (Chapter 3).

(B) Results: Site descriptions of the investigated ponds are presented (Chapter 4). Textural properties (particle size distributions, organic content) and established isotope chronologies of sediment stratigraphies are included (Chapter 5). Local proxy pollution signals from each pond are revealed via down-core variations in magnetic properties, trace metals, spheroidal carbonaceous particles (SCPs) and particulates <10 μm in master cores from each site as concentration profiles, with corresponding isotope chronologies (Chapter 6). The conversion of concentration data to flux profiles, using sediment accumulation rates, demonstrates the 'real-time' supply of magnetic grains, trace metals and SCPs to each pond (Chapter 7). The local proxy pollution records are then combined, to produce a cross-regional signal which is presented and described (Chapter 8).

(C) Discussion and conclusions: The integrity of small urban ponds as archives of air pollution is initially explored to test that the sediment records obtained are 'intact' and that an atmospheric, opposed to catchment-derived, depositional history is captured, devoid of post-depositional changes (Chapter 9). Local pollution histories revealed by each pond are then discussed in turn, relating to documented surrounding urban development (Chapter 10). The importance of these detailed, high-resolution *local*, rather than *regional* pollution signals is highlighted via comparison of the urban pond histories with the background depositional history of pollution for the UK determined from remote UK lakes (Chapter 10). The cross-regional pollution signal, further enhanced by pollution records from other sedimentary evidence, most notably Speke Hall Lake, adds a spatial dimension to temporal pollution trends, revealing intra-urban variations in the deposition of pollution throughout the LMR conurbation (Chapter 11). The main findings of this research, potential implications and suggestions of future work conclude the thesis (Chapter 12).

SECTION A: INTRODUCTION, AIMS, BACKGROUND AND METHODOLOGIES

This section of the thesis introduces the research project and the aim and objectives of this work. A background into the utilisation of lakes as sedimentary archives of environmental change and pollution histories is detailed, along with the potential for urban, manmade ponds as suitable archives of local temporal pollution signals (Chapter 1).

The justification for reconstructing long-term urban air pollution histories from urban lake sediments is presented (Chapter 1). Also, a background into the need for investigating a regional historical air pollution signal in and surrounding Halton, termed in this work as the 'Lower Mersey Region' (LMR), is detailed (Chapter 2). Methodologies applied in this work to reconstruct detailed dated proxy pollution records from urban lake sediment stratigraphies, are also explained and justified (Chapter 3).

1 CHAPTER ONE: INTRODUCTION, AIMS AND BACKGROUND

1.1. Chapter overview

This chapter introduces the aims and objectives of the thesis and presents a background to inferring proxy air pollution histories from sediment records retrieved from urban ponds. The benefits of utilising urban ponds, rather than more commonly investigated remote, rural lakes, are detailed; most notably, their potential to yield site specific, local air pollution histories that can be used to explore temporal cross-regional urban pollution signals. The importance of investigating air pollution deposition records, beyond contemporary monitored emissions data (i.e. pre-1990s), to determine the air quality impacts of industrialisation and urbanisation, which subsequently contributes to the toxicology of urban air, is also presented.

1.2. Introduction to project

Small (<1 ha), man-made lakes of >100-year longevity, set within established urban landscapes are important and unique sedimentary archives of industrial and urban activities, acting as sinks for atmospherically-derived pollution particulates [Charlesworth and Lees, 2001; Meriläinen *et al.*, 2003; Tylmann, 2005]. These particulates form part of the accretionary lake sediment matrix, from which proxy environmental histories can be reconstructed (Figure 1.1). However, small urban ponds are rarely utilised in this way [Charlesworth and Lees, 2001; Worsley *et al.*, 2006]. It is possible to test the integrity of urban ponds to yield air pollution histories by adopting a range of environmental proxy analyses, routinely applied to large, natural, rural lakes [Charlesworth and Lees, 1997, 2001; Dauval'ter, 2004; Tylmann, 2005].

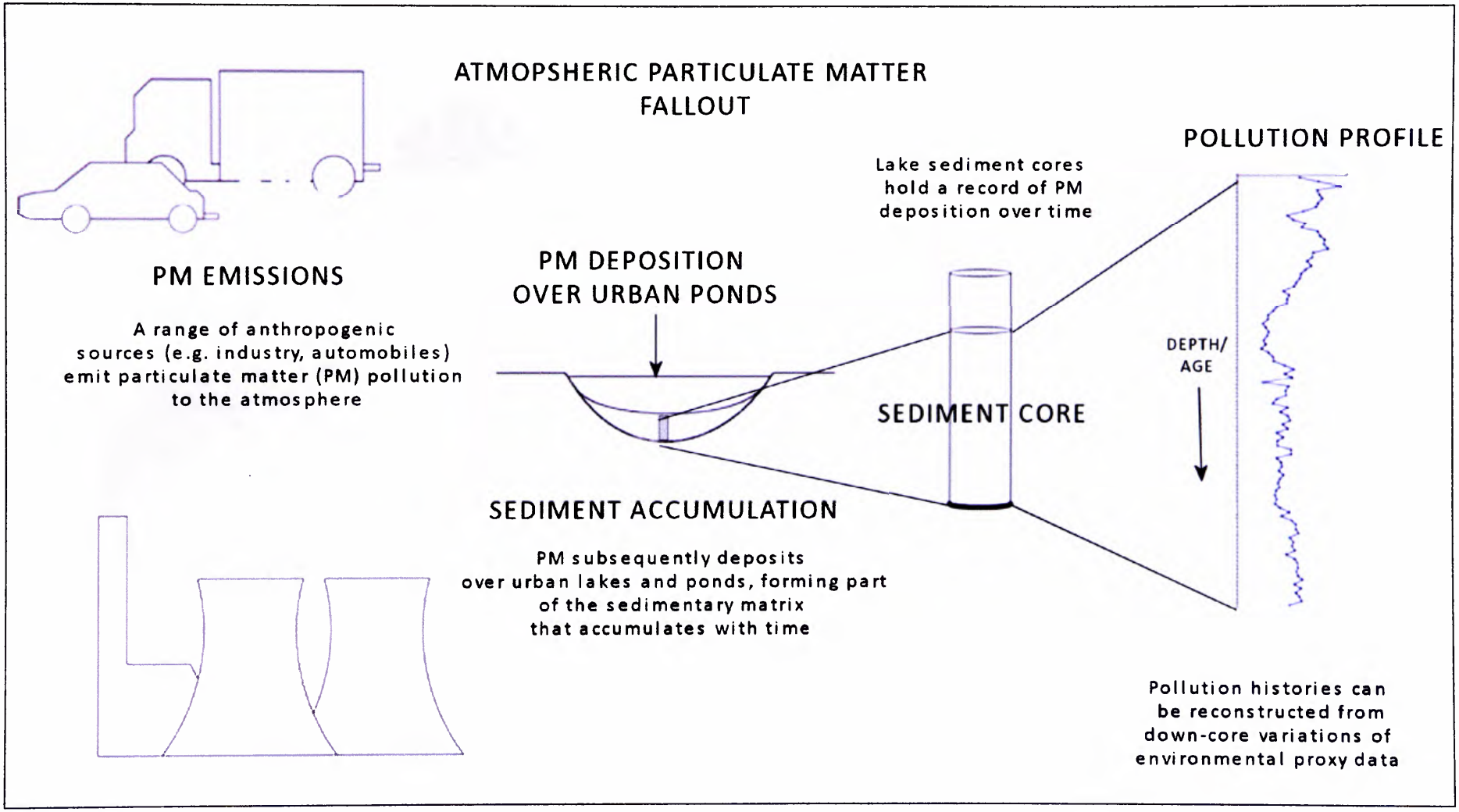

Figure 1.1: Formation of air pollution stratigraphies in urban lakes and ponds.

Due to insufficient historical (i.e. pre 1960s) pollution data, it is important to investigate air pollution histories recorded in natural sedimentary archives, such as urban lakes and ponds, as they can retain the *only* known available data to reconstruct past air pollution trends, which can span from pre-intensified industrial times to present day [Worsley *et al.*, 2006]. A detailed chronology of air pollution for a heavily industrialised urban centre such as Halton and its surrounding area termed in this work as the lower Mersey region (LMR), northwest England, is especially important, as indiscriminate releases of pollutants to air have been experienced there since the 1800s [Halton Borough Council (HBC), 1991]. By investigating several urban ponds and lakes within the LMR, a historical cross-regional pollution signal can be proposed that allows a retrospective assessment of temporal pollution deposition across the conurbation. Records of historical air quality in the LMR, spanning from the intensification of industry during the early 19th century to present day, may potentially benefit the exploration of novel linkages between the environment and public health.

1.3. Aims and objectives

The aim of the research project is to investigate sediment records from urban ponds to yield local air pollution signals, from which a cross-regional history of pollution deposition in the LMR can be reconstructed.

The objectives are:

(i) To test the integrity of urban ponds as sinks of atmospheric particulates by:

  (a) identifying, and subsequent extraction at, suitable urban pond sites that may yield intact, undisturbed sediment cores;

  (b) determining sediment chronologies using isotope dating;

  (c) characterising urban sediment stratigraphies using a range of environmental proxy analyses including mineral magnetism, x-ray fluorescence, fly ash particle analysis, particle size analysis and geochemistry techniques; and

  (d) teasing out the air pollution record from the natural/catchment signal.

(ii) To produce detailed local air pollution histories from urban ponds via:

  (a) concentration profiles of proxy pollution characteristics such as mineral magnetic properties, trace metals, particle size distributions and spheroidal carbonaceous particulates (SCPs), highlighting how variations in these proxy pollution characteristics change over time using corresponding isotope chronologies; and

(b) reconstructing flux profiles to determine the deposition of magnetic grains, trace metals and SCPs to the ponds over time.

(iii) To investigate the cross-regional pollution signal for the LMR by:

(a) combining proxy pollution concentration and flux profiles collected from urban ponds within and surrounding Halton to characterise spatial variations in pollution deposition since the intensification of industry in the area from ~1800.

(iv) To retrospectively assess the effects of urbanisation and industrialisation on the air pollution signal in the LMR by:

(a) interpreting local proxy pollution histories using documented industrial activity and urban development in the region.

1.4. Reconstructing air pollution histories from urban lake sediments

1.4.1. Lakes as archives of environmental change

Lakes are important terrestrial archives of palaeoenvironmental and palaeoclimatic information [Bell and Walker, 1992; Last and Smol, 2001; Mingram *et al.*, 2004]. Their still, low energy conditions allow natural sediment accumulation to occur within the lake basin* [Boggs, 1995]. With time, younger sediments become deposited on top of older sediments which, if undisturbed, can produce a sedimentary sequence (stratigraphy) with a depth-time profile [Oldfield and Appleby, 1984; Smol, 2002]. This lacustrine sediment is composed of material originating from within the lake (autochthonous), such as algae and plant remains, and allochthnonous inputs derived from groundwater, the surrounding catchment† and the atmosphere (Figure 1.2) [Goudie *et al.*, 1990; Lowe and Walker, 1997; Smol, 2002]. These inputs are determined by environmental pressures, therefore lakes act as sedimentary archives, recording local (catchment) and regional environmental 'signals' [Fernandéz *et al.*, 2002; Rose *et al.*, 2002; Smol, 2002; Tylmann, 2005].

* Lake basin: term used to define the bowl-like shape of the lake itself, not to be confused with the catchment basin.

† Lake catchment: the drainage basin of the lake, area surrounding the lake from which water drains into the lake basin.

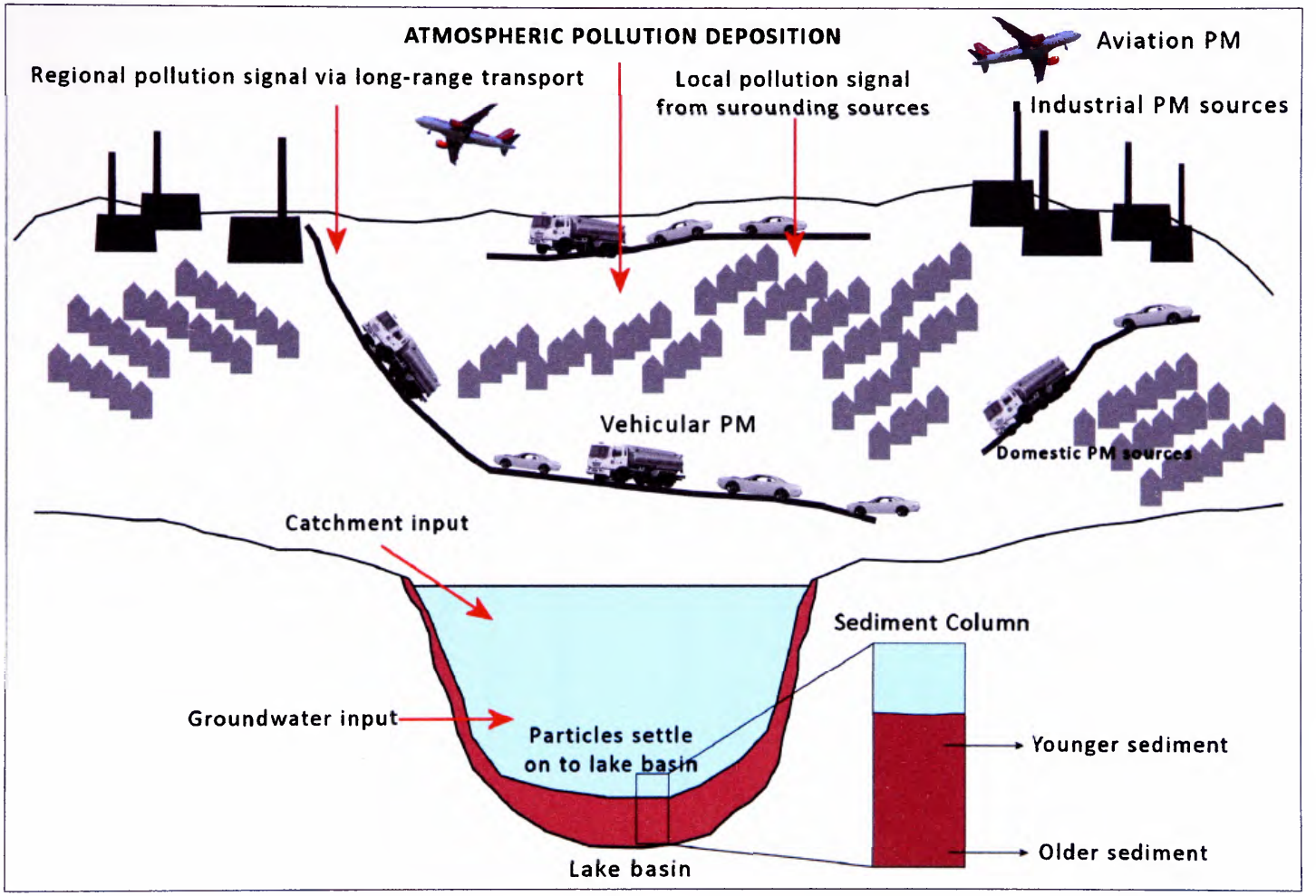

Figure 1.2: Sediment accumulation processes in urban lakes and ponds.

By retrieving lake sediment cores (columns of sediment), a history of environmental change can be 'captured' and analysed using environmental proxy analyses, to reveal a wealth of chemical, biological and physical information, to reconstruct past environmental conditions [Smol, 2002; Birks *et al.*, 2004]. Palaeolimnology, the study of past environments inferred from lake sediments [Oldfield *et al.*, 1983; Last and Smol, 2001], has revealed palaeoclimatic and environmental changes spanning back thousands of years, [Robinson, 1986; Stockhausen and Zolitschka, 1999; Dean and Schwalb, 2000; Anker *et al.*, 2001; Ariztegui *et al.*, 2001; Rolph *et al.*, 2004], to more recent time scales (<300 years) [Roberts, 1989; Oldfield, 1990; Birks *et al.*, 2004; Yeloff *et al.*, 2005].

Sediment records have been used to identify trends in climate [Lotter *et al.*, 1992; Bjöck *et al.*, 2000; Colman *et al.*, 2000; Kaplan *et al.*, 2002; Watanabe *et al.*, 2004; Demroy *et al.*, 2005], lake water levels [Farr *et al.*, 1990; Caballero and Guerrero, 1998; Digerfeldt *et al.*, 2000], seismic/tectonic and volcanic activity [Haberle and Lumley, 1998; Hallett *et al.*, 2001; Leroy *et al.*, 2002], erosion events [Eriksson and Sandgren, 1999; Huang and O'Connell, 2000; Doner, 2003; Ng and King, 2004], human activities [Edwards and Whittington, 2001; Mingram *et al.*, 2004; Punning *et al.*, 2007], land use changes [Huang 2002; Kim, 2005], and human impacts on water sheds [Berge *et al.*, 1990; Faegri, 1990; Cohen *et al.*, 2005].

1.4.2. Air pollution histories stored in lake sediments

Lakes also act as sinks for atmospheric pollution particulates [Heit *et al.*, 1981; Griffin and Goldberg, 1983; Renberg, 1986; Oldfield, 1990; Veselý *et al.*, 1993; Rose and Harlock, 1998; Rose *et al.*, 1998(a), 2004; Couillard *et al.*, 2004; Solovieva *et al.*, 2005]. Particulate matter (PM) is comprised of solid particles or liquid droplets (aerosols) small enough to remain suspended in the atmosphere (<100 μm) [Phalen, 2002; Harrison, 2004]. The main origins of PM are:

(i) natural sources, including volcanic dust, sea salt, forest fires and pollen [Colls, 1997];

(ii) anthropogenic sources (e.g. industry, traffic and domestic combustion) which, in turn, can be classified as mobile (e.g. road vehicles, aeroplanes and trains) or stationary (e.g. power generation plants, factories, industrial stacks, mines and homes) [Artiola, 1996; Alloway and Ayeres, 1997;

Harrison and Grieken, 1999; Morwaska and Zhang, 2002; Phalen, 2002]; and

(iii) secondary formation of PM, occurring in the atmosphere via chemical and physical conversions of gaseous precursors (e.g. nitrogen oxides, sulphur oxides, ammonia and volatile organic compounds), to form solid sulphates, nitrates and organic aerosols [Goodwin *et al.*, 1999; Phalen, 2002; Wilson *et al.*, 2005].

PM is classified by size fractions that reflect the physical behaviour of particulates in the atmosphere (e.g. transport, suspension and deposition) and inhalation potential and, therefore, toxicity* (Table 1.1).

Table.1.1: Size classifications and physical behaviour of particulate matter (PM) [Alloway and Ayres, 1997; Morwaska and Zhang, 2002: Harrison, 2004; Wilson *et al.*, 2005].

PM size classification	Aerodynamic diameter (μm)	Transport and deposition	Health linkage
Total suspended particulates (TSP)	<100	Settle quickly from the atmosphere and, therefore, deposit close to source: <10 km.	Filtered by the nasal tract.
PM_{10} (coarse)	<10	Remain suspended in the atmosphere and can deposit hundreds to thousands of km from source.	Penetrate the lower respiratory system.
$PM_{2.5}$ (fine) PM_1 (fine) $PM_{0.1}$ (ultrafine)	<2.5 <1.0 <0.1	Less effectively removed from the atmosphere and subject to long range transport.	Deposit deep in the lung (gas–exchange portions).

PM composition is complex, varying according to source, airborne duration and atmospheric conditions [Claes *et al.*, 1998; Morwaska and Zhang, 2002; Celis *et al.*, 2004; Schmeling, 2004; Götchi *et al.*, 2005], and includes minerals, metals, magnetic spherules, organics, sulphates and nitrates (Table 1.2) [Matthias, 1996; Allen *et al.*, 2001; Phalen, 2002; Kukier *et al.*, 2003]. Generally, coarse urban PM (>2.5 μm) is dominated by soil particles as well as non-combusted industrial and road dusts (e.g. metallurgical dusts and vehicular abrasion particulates); whereas fine PM (<2.5 μm) are products of combustion (e.g. high-temperature combustion processes, power generation and vehicular combustion emissions) and gas-to-particle conversions (secondary PM) detailed in Table 1.2 [McElroy *et al.*, 1982; Morwaska *et al.*, 1998; Morwaska and Zhang, 2002; Phalen, 2002; Schmeling, 2004].

* Discussed further in section 1.5.2: Air pollution and epidemiology.

Table 1.2: Typical sources and composition of PM_{10} divided into particle diameter ranges [Phalen, 2002].

PM classification	Composition	Examples of source
PM_{10} Coarse (2.5 µm – 10 µm)	Minerals	Soil, road dust, industrial dust.
	Trace metals	Soil and combustion of oil and coal.
	Organic carbon	Tyre rubber and asphalt road wear.
	Bioaerosols	Animals, plant, fungi, bacteria.
	Aqueous droplets	Fogs, water sprays.
	Associated gases	Ammonia, sulphur dioxide (SO_2), hydrogen sulphide (H_2S), carbon dioxide (CO_2).
$PM_{2.5}$ Fine (<2.5 µm)	Minerals	Soil, road dust, industrial dust.
	Trace metals	Oil and coal combustion, machinery wear, industrial processes (e.g. smelting, welding).
	Carbonaceous	Wildfires, liquid fuel, solid fuel and waste combustion, cooking, engine exhaust, tyre wear.
	Sulphates and nitrates	Volcanoes, oceans, oxidation of SO_2 and nitrogen oxides (NO_x), fires, engine exhaust.
	Ammonium compounds	Reactions of ammonia produced by animals, sewage, fertilisers and engine exhaust.
	Bioaerosols	Viruses and bacteria.
	Associated gases	Formaldehyde, SO_2, NO_x, ozone (O_3), carbon monoxide (CO).
$PM_{0.1}$ Ultrafine (<0.1 µm)	Trace metals	Incombustible constituents of fuel.
	Organics	Condensation of volatile emissions from complex plants, microbes, fuel combustion.
	Carbon	Fuel combustion.
	Miscellaneous	Gas-to-particle conversion reactions.

Particulate size, emission source, meteorological and topographical conditions also influence the transport, deposition and ambient concentrations of PM [Wu *et al.*, 2006]. Airborne particulates are removed from the atmosphere via wet and dry deposition [Alloway and Ayres, 1997]. Due to greater settling velocities PM >10 µm are effectively removed from the atmosphere under gravity and, therefore, deposit close to source (~<10 km) [Yang *et al.*, 1999; Alloway and Ayres, 1997; Morwaska and Zhang, 2002; Phalen, 2002; United Nations: Economic and Social Council, 2005]. Finer PMs (<10 µm) remain suspended in the atmosphere for longer periods (days to months) and, therefore, can be transported great distances from source (potentially hundreds to thousands of km) [ApSimon *et al.*, 2001; Phalen, 2002; Harrison, 2004; United Nations: Economic and Social Council, 2005]. Particles <1 µm are even less effectively removed from the atmosphere and have longer residency times and are, therefore, subject to long-range (transboundary) transport [ApSimon *et al.*, 2001].

Atmospheric particulates have become an important and abundant contribution to lake sediments since the 20th century [Yang *et al.*, 1997; Dearing, 1998; Petrovský and Ellwood, 1999; Rose, 2001]. Therefore, recent (<100 years) lacustrine sediments allow

monitoring of environmental contaminants, heavily influenced by the intensification of industry and urbanisation [Last and Smol, 2001; Smol, 2002; Tylmann, 2005]. PM enters lakes via direct atmospheric fallout or from surface runoff within the catchment (Figure 1.3). Particulates settle through the lake's water column and deposit onto the lake basin where, with time, lacustrine sediment accumulation 'traps' these particulates, preserving a record of atmospheric pollution deposition [Oldfield *et al.*, 1983; Last and Smol, 2001; Smol, 2002].

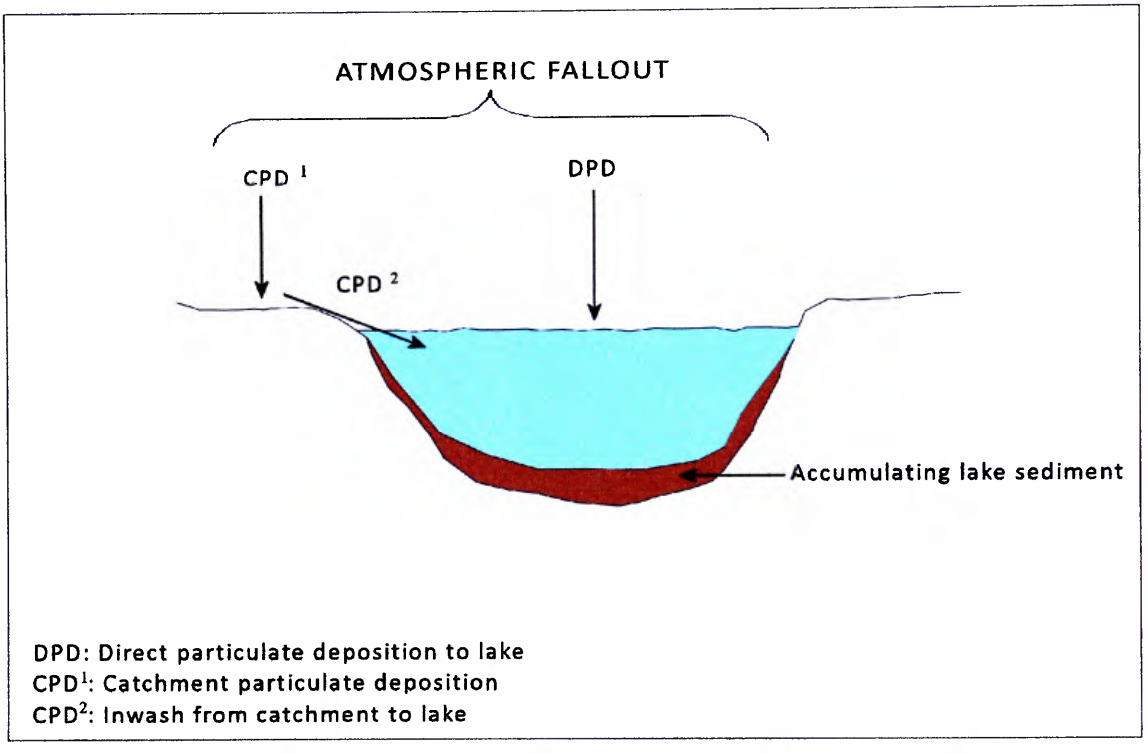

Figure 1.3: Deposition of atmospheric particulates in lake sediments [adapted from Worsley & Power, 2007].

A multiple proxy approach, using a range of environmental analyses to characterise lake sediments, allows a detailed, datable reconstruction of the pollution record held within the lake stratigraphy [Heit *et al.*, 1981; Veselý *et al.*, 1993; Lowe and Walker, 1997; Couillard *et al.*, 2004; Rose *et al.*, 2004(a); Solovieva *et al.*, 2005]. An important advantage is that these 'pollution profiles' provide unique temporal air pollution data, where long-term conventional monitoring is inconsistent, crude or unavailable (Section 1.5.1.).

1.4.3. Environmental proxies in lake sediments

Environmental proxies enter lakes via the atmosphere, catchment, groundwater and within the lake itself (Figure 1.4).

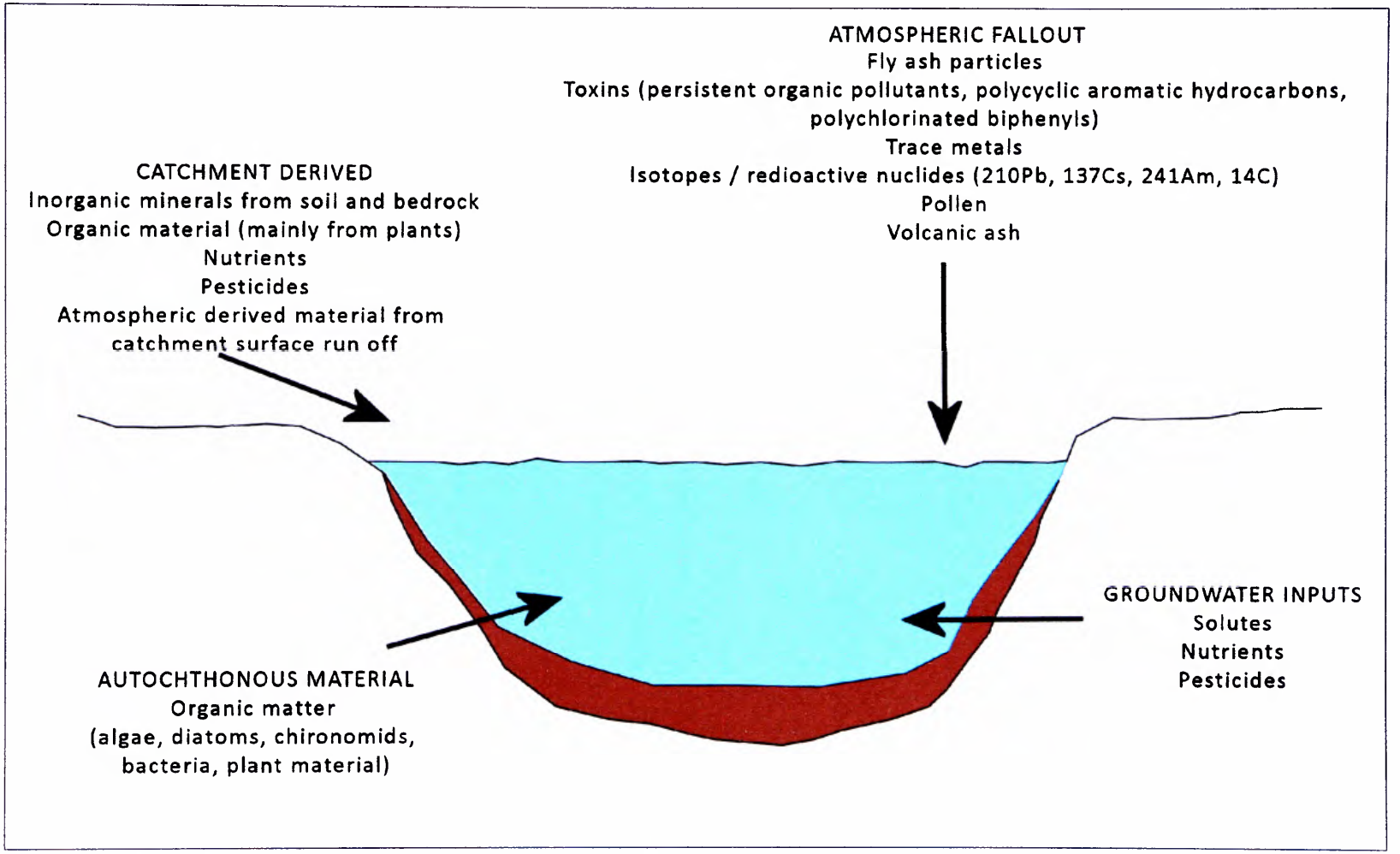

Figure 1.4: Inputs and pathways of environmental proxies in lake and pond sediments.

Due to lacustrine sedimentation, an environmental record of a lake catchment history accumulates, on which an atmospheric pollution signal is superimposed [Heit *et al.*, 1981; Norton, 1986; David *et al.*, 1998; Meriläinen *et al.*, 2003]. Therefore, lake sediment stratigraphies can be used to:

(i) infer a history of the watershed, for example land-use, erosion events and fluctuating water levels [David *et al.*, 1998; Boyle *et al.*, 1999; Ng and King, 2004];

(ii) discriminate between catchment, atmospheric and autochthonous derived material [Oldfield *et al.*, 1983; Norton *et al.*, 1992; Rose *et al.*, 1998(b), 1998(c); Birks *et al.*, 2004; Dinescu *et al.*, 2004];

(iii) identify and characterise temporal air pollution deposition 'signals' [Renberg, 1986; Birks *et al.*, 2004]; and

(iv) infer a corresponding chronology [Norton, 1986; Vesleý *et al.*, 1993; von Gunten *et al.*, 1997; Rose *et al.*, 1998(c)].

The integrity of lake sediment records can be compromised by physical disturbance; for example, due to human management (desilting and dredging) and bioturbidation (the mixing of sediments by benthic (bottom dwelling) organisms); and by chemical diagenesis within the sediment column, disrupting the stratigraphy sequence [Norton, 1986; Couillard *et al.*, 2004]. By adopting a multi-proxy approach to reconstruct environmental histories, disturbed sediments can be identified. This allows confidence in the sediment sequence and, therefore, a reliable air pollution history to be inferred [Norton, 1986; Boyle *et al.*, 1999; Smol, 2002; Solovieva *et al.*, 2005].

Available expertise and facilities have influenced the environmental proxies adopted in this work:

- Magnetic minerals (Section 1.4.3.1.)
- Trace metals (Section 1.4.3.2.)
- Fly ash particles (Section 1.4.3.3.)
- Organic matter (Section 1.4.3.4.)
- Isotopes (Section 1.4.3.5.)
- Particle size data (Section 1.4.3.6.)

These analyses have been adopted to test the integrity of urban ponds and lakes as archives of air pollution [Van Metre and Callender, 1997; Charlesworth and Lees, 1999(a); Meriläinen *et al.*, 2003; Dauval'ter, 2004; Tylmann, 2005].

1.4.3.1. Magnetic minerals

Lakes receive a range of mineral magnetic grains (Figure 1.5) originating from:

(i) the catchment: detrital material originating from the erosion of bedrock, subsoil and topsoil within the drainage basin of the lake [Oldfield *et al.*, 1983; Demroy *et al.*, 2005]. This minerogenic material deposits within the lake after transport from streams or over land [Smol, 2002; Evans and Heller, 2003].

(ii) the atmosphere: direct atmospheric fall out of particulates from natural sources such as volcanic activity [Haberle and Lumley, 1998; Hallett *et al.*, 2001], cosmic sources [Thompson *et al.*, 1980; Taylor *et al.*, 1996] and dust from storms [Bloemendal *et al.*, 1988; Dinarès-Turell *et al.*, 2003], as well as anthropogenic pollutants from the burning of fossil fuels [Oldfield *et al.*, 1983; Hunt *et al.*, 1984; Oldfield 1990; Oldfield and Richardson, 1990(a); Georgeaud *et al.*, 1997].

(iii) authigenic/*in situ* magnetic formation: subsequent to deposition of magnetic minerals, post depositional diagenetic processes can alter the magnetic assemblage, for example by bacterial magnetosomes [Vali *et al.*, 1987; Snowball, 1994; Bazylinski, 1996; Oldfield, 1999], reductive diagenesis and authigenic iron sulphides [King and Channell, 1991; Dearing 1999(a); Evans and Heller, 2003].

The application of environmental magnetic techniques can discriminate between these sources to investigate the environmental processes within the atmosphere, lithosphere and hydrosphere that transport, deposit or transform magnetic minerals within lake sediments [Oldfield *et al.*, 1985; Yu and Oldfield, 1989, 1993; Caitcheon, 1993; Crowther and Barker, 1995; Verosub and Roberts, 1995; Dearing *et al.*, 1996; Oldfield, 2007].

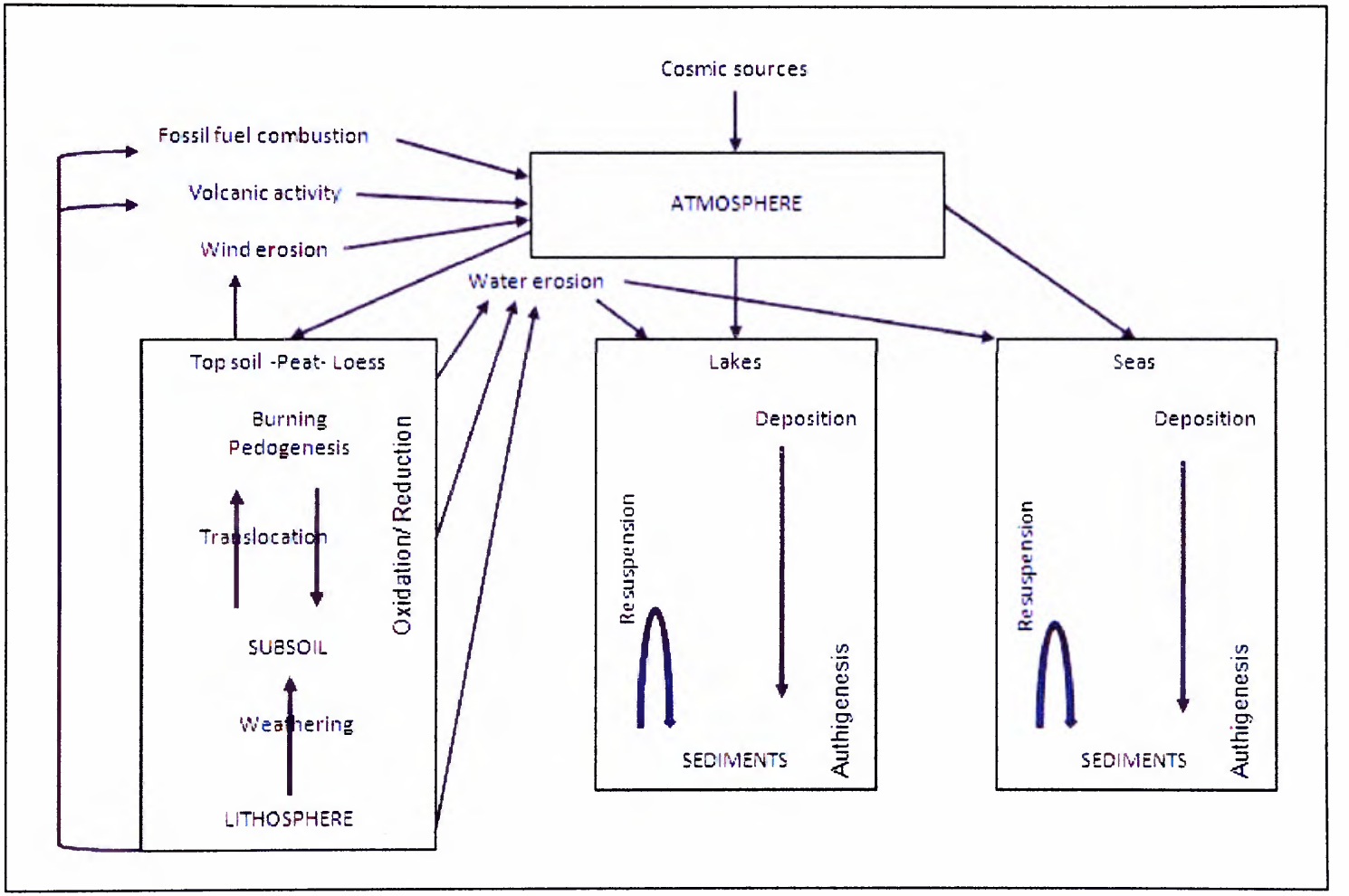

Figure 1.5: Sources of magnetic minerals in the environment [Smith, 1999].

Due to sub-atomic structure, *all* substances display magnetic properties, not only *perceived* 'magnetic' substances, such as metallic iron [Thompson and Oldfield, 1986; Smith, 1999; Xie *et al.*, 1999(a)]. Types of magnetic behaviour are influenced by the spinning of electrons (negatively charged particles) on their axis, and interactions within and between electrons of constituent atoms (such as pairing and spacing) [Smith, 1999]. The magnetic properties of environmental materials can be characterised by applying a range of magnetic 'tests'. By inducing a range of magnetic fields within a sample and measuring the resulting magnetisation whilst in the field, the amount of magnetisation retained (remanence) when removed from an applied field, and the alignment of magnetic moments within a sample to the direction of the applied field; information regarding the magnetic composition, granulometery and concentration of environmental samples can be inferred [Verosub and Roberts, 1995; Maher and Thompson, 1999; Sandgren and Snowball, 2001; Evans and Heller, 2003; Peters and Dekkers, 2003]. An understanding of these magnetic attributes provides the basic approach to characterising sediments.

1.4.3.1.1. Magnetic behaviour

There are three general classifications of magnetic behaviour, defined in Table 1.3:

(i) 'diamagnetism', in substances displaying weak or negative magnetisation (e.g. plastic);

(ii) 'paramagnetism', positive weak magnetism, although relatively greater than diamagnetism (e.g. iron-containing minerals); and

(iii) 'ferromagnetism', strongly magnetic, and unlike diamagnetism and paramagnetism, ferromagnetic substances have a spontaneous (naturally occurring) magnetic moment (e.g. pure iron) [Dekkers, 1997; Smith, 1999; Sandgren and Snowball, 2001; Evans and Heller, 2003].

Variations in this spontaneous net magnetic moment occur within ferromagnets, which can be further divided into ferromagnetic, antiferromagnetic, canted-antiferromagnetic and ferrimagnetic behaviour, relating to the structure of the crystal lattice within magnetic grains [Dekkers, 1997; Smith, 1999; Evans and Heller, 2003] (Table 1.3).

Table 1.3: Magnetic behaviour and magnetisation. [Thompson and Oldfield, 1986; Dekkers, 1997; Maher and Thompson, 1999; Smith, 1999; Evans and Heller, 2003].

Magnetic behaviour	Atomic structure	Magnetic susceptibility (concentration) behaviour	Example of minerals
Diamagnetic	Displayed only when a magnetic field is applied to a substance that has no unpaired electrons. Electron orbits align in the opposite direction to the applied magnetic field producing a magnetic moment. This behaviour is fundamental to all substances but becomes masked when other behaviours are present.	Weak and negative	Water, plastic, organic matter, quartz, feldspars, calcium carbonate
Paramagnetic	Substance has some atoms with unpaired electrons, which creates a magnetic moment, however the interaction between these atoms is small as the electrons are widely spaced. Therefore a weak magnetic moment is produced with the application of a magnetic field. This paramagnetic effect is stronger than diamagnetic substances and relatively weaker than ferromagnetic behaviour.	Weak positive	Fe-containing minerals and salts e.g. biotite, olivine, ferrous sulphite, pyrite
Ferromagnetic	Substances with unpaired electrons in atoms that are regularly and closely spaced, resulting in strong interaction between atoms and a spontaneous magnetic moment. This interaction between atoms is important as the arrangement of atoms within the crystal lattice produces four different types of ferromagnetic behaviour:		
	• **Ferromagnetic:** Parallel coupling of all unpaired electrons occurs resulting in strong magnetisation.	Strong positive	Pure iron, nickel, chromium, cobalt
	• **Antiferromagnetic:** Anti-parallel (alternate layers of magnetisation direction) crystal lattices with equal number of unpaired electrons creating no overall ferromagnetic moment.	Moderate positive	Some iron oxides e.g. haematite, goethite
	• **Canted antiferromagnetic:** Similar arrangement to antiferromagnetic behaviour, but not perfectly anti-parallel, therefore producing a small net spontaneous magnetisation.		
	• **Ferrimagnetic:** Alternating crystal lattices, but with an unequal magnetic moment producing a net spontaneous magnetic moment.	Strong positive susceptibility but weaker than ferromagnetism	Some iron oxides and sulphides e.g. Magnetite, maghaemite, greigite, pyrrhotite

Ferromagnetic minerals can also be further classified by their 'magnetic domain' structure, which is influenced by the size and shape of magnetic grains [Smith, 1999; Evans and Heller 2003]. Magnetic domains are chambers of magnetism, within magnetic grains that occur due to competition between magnetic forces within a ferromagnet, which result in domain walls positioned to achieve a minimal total magnetic energy state [Smith, 1999]. Generally, a division between small (<0.7 μm), single domain (SD) grains and large (>10 μm), multi-domain (MD) grains occur, which behave differently on the application of an external magnetic field in relation to their domain structure (Table 1.4) [Banerjee *et al.*, 1981; Dekkers, 1997; Maher and Thompson, 1999; Smith, 1999]. Due to known magnetic properties of environmental materials, the characterisation of sediments using magnetic parameters provides a discriminatory and diagnostic tool [Oldfield, 1991; Bloemendal *et al.*, 1992; Lees, 1999; Sandgren and Snowball, 2001] (Table 1.5).

Table 1.4: Size classification of ferromagnetic (magnetite) grains [Dunlop, 1973; Smith, 1999; Walden, 1999(a); Evans and Heller, 2003; Thompson and Oldfield, 1986].

Magnetic domain structure	Behaviour from applied magnetic fields	Grain size* (typical of a ferromagnetic)
Super-paramagnetic (SP)	Very small grains have very short relaxation times (i.e. the time it takes for an induced magnetic field to revert back to its original direction is very short). When removed from a magnetic field, SP grains lose their magnetisation as the natural thermal energy within SP grains is sufficient to re-orientate the direction of the induced magnetic field. Therefore these ultrafine grains do not hold a measurable remanence, but do display large magnetisations during in-field measurements.	<0.05 μm
Stable single domain (SSD)	Magnetic moments within a SD grain are all aligned in the same 'easy' direction with the absence of an applied magnetic field. When a field is applied opposite to this easy direction, electron magnetic spin moments simultaneously reverse to align with the direction of the applied field. On removal of this field the SD grains retain this new direction of magnetisation, which in turn produces a remanence. True SD grains demonstrating this behaviour are referred to as stable single domain grains.	0.07-0.7 μm
Viscous single domain (VSD)	Slightly larger than SP grains, VSD grains demonstrate an increased stability of remanence.	0.05-0.07 μm
Pseudo single domains (PSD)	Transitional phase occurring between the SD / MD boundary. PSD grains only consist of a few domains and exhibit both SD and MD behaviour.	0.7-10 μm
Multi-domain (MD)	Magnetic remanence of MD grains is less stable and lower than that of SD grains. When an external field is applied, the domain walls move to favour the growth of domains which have a magnetic moment in the direction of the applied field. If the applied field crosses the direction of the domain magnetisation, domains may rotate and domain walls will cross energy barriers to reach minimal energy positions. On the removal of the applied field the domains are unable to re-cross these energy barriers, resulting in a remanence induced in the sample. If energy barriers are not crossed and new low energy positions not reached then the domain will revert back to their original patterns and no remanence occurs.	>10 μm

* Exact size boundaries are dependent upon mineral type and grain shape. Therefore, published boundaries vary between authors, however data from Smith [1999] are presented.

Table 1.5: Explanation of mineral magnetic parameters [Robinson, 1986; King and Channel, 1991; Verosub and Roberts, 1995; Dearing *et al.*, 1996; Dekkers, 1997; Dearing, 1999(a), 1999(b); Oldfield, 1999; Snowball, 1999; Walden, 1999; Maher and Thompson, 1999].

Magnetic parameter and unit	Measurement	Interpretation of parameter
Low frequency mass specific susceptibility (χ_{LF}) $10^{-6}\ m^3\ kg^{-1}$	Magnetization of sample induced by a weak applied field of 0.46 kHz, normalised by sample mass.	Indicates magnetic concentration within the sample. χ_{LF} values are proportional to the amount of ferrimagnetic minerals within the sample. Lower values may also indicate the presence of paramagnetic minerals. However the signal may be dominated by antiferromagnetic content if the sample has little or no ferrimagnetic component.
High frequency mass specific susceptibility (χ_{HF}) $10^{-6}\ m^3\ kg^{-1}$	Magnetization of sample induced by a higher applied field of 4.6 kHz (compared to χ_{LF}).	Unlike χ_{LF}, high frequency susceptibility does not recognise the SP size range, instead groups these ultrafine grains within the SSD range, and therefore comparatively lower values of χ_{HF} indicate that SP grains are present. Generally χ_{LF} and χ_{HF} produce very similar results with only slight differences in values if SP grains are present.
Susceptibility frequency dependence (χ_{FD}%) and (χ_{FD}) $10^{-9}\ m^3\ kg^{-1}$	χ_{FD}% is the calculated ratio of the percentage difference between (χ_{HF}) and (χ_{LF}). χ_{FD} is the raw difference between (χ_{HF}) and (χ_{LF}).	The presence of SP grains can be identified by calculating the percentage difference between χ_{LF} and χ_{HF}. High χ_{FD}% reveals a SP component and low χ_{FD} % indicates a lack of SP grains within a sample. χ_{FD} can also identify the presence of ferrimagnetic grains (0.018–0.02 μm) [Dearing *et al.*, 1996], indicative of soil in wash from the lake catchment.
Anhysteretic Remanence Magnetism (ARM) $10^{-6}\ Am^2\ kg^{-1}$ or χ_{ARM} $10^{-6}\ m^3\ kg^{-1}$	Relatively small magnetic field applied (but higher than χ) with a peak alternating field of 100 mT induced in the sample with a DC biasing field of 0.04 mT (which is equivalent to the earth's magnetic field). The magnetic field is slowly built up from zero, peaks at 100 mT and then falls back to zero. The amount of magnetism retained by the sample is measured outside of the magnetic field in the magnetometer. Mass specific values are calculated. Calculated ratio of ARM x 31.84 (equivalent to the 0.04 mT biasing field adjustment).	This type of magnetic exposure at a low field magnetises the fine magnetic grains within a sample, therefore ARM is sensitive to concentrations of fine grained magnetic particles, particularly those of the SSD grain size (0.03-0.5 μm) [Dekkers, 1997]. A more accurate parameter than ARM as corrected by the biasing field. This ratio is "highly selective of true stable single domain ferromagnetic grains in the 0.02 to 0.4 μm range" [Walden *et al.*, 1999]. Values drop dramatically with the presence of ferrimagnetic grains above and below this size range.

Table 1.5 (continued from previous page).

Magnetic parameter and unit	Measurement	Interpretation of parameter
Saturated Isothermal Remanence Magnetism (SIRM) *10^{-3} Am^2 kg^{-1}*	High magnetic field applied (800 mT) aligning all the magnetic grains within the sample in a forward direction. All of the remanence carrying minerals are saturated with a magnetic field. The amount of magnetism the sample remembers is measured once the sample is removed from the field and placed in the magnetometer. Data are normalised for sample mass.	SIRM is the highest amount of remanence in a sample induced by a large magnetic field. SIRM measurements reflect the concentration of all remanence-carrying minerals in a sample (minerals that can retain magnetisation once removed from the magnetic field). 800 mT has been used for SIRM measurements in this study, however, although this field will saturate most minerals, some antiferromagnetic minerals may not be saturated (not all of the antiferromagnetic content of the sample may be magnetised e.g. goethite). Also, SIRM is sensitive to magnetic grain size and reflects the magnetic mineral assemblage of a sample. Therefore samples with high levels of SIRM may not necessarily have the highest concentration of magnetic minerals, so an understanding of the magnetic grain size and behaviour is also important when interpreting SIRM values. Low levels of fine grained (SSD) ferrimagnetic grains in a sample can mask large quantities of coarse ferrimagnetic grains and antiferromagnetic components.
Backfield Isothermal Remanence Magnetism Ratios *(no units)*	Samples already saturated (from SIRM) are exposed to reverse magnetic fields of 20, 40, 100, 300 and 500 mT, realigning the magnetic grains in the reverse direction to SIRM. Magnetic remanence is measured once sample is removed from the applied magnetic field.	The application of gradually building up reverse magnetic fields in a saturated sample has a demagnetising effect on the sample. The backfield ratios are expressed as a percentage difference between IRM and SIRM. Therefore, 0 % represents SIRM (sample totally saturated) and 100 % represents total reversal of magnetic field. The backfield ratios are expressed as IRM/SIRM and, therefore, fall between 1 (saturated SIRM value) and -1 (sample totally reversed). The gradual 'knocking out' of the magnetisation in the forward direction from the SIRM provides results relating to the magnetic behaviour of the sediment. Samples that easily revert to the reverse field direction are known as displaying 'soft' behaviour, characteristic of MD ferrimagnetic minerals. Samples that resist realignment (usually past 100 mT) are described as 'hard', therefore indicative of antiferromagnetic minerals and or fine grained (SSD) ferrimagnetic grains. Therefore IRM_{-20} mT and IRM_{-40} mT are used as parameters for ferrimagnetic content and IRM_{-300} mT and IRM_{-500} mT are used to indicate antiferromagnetic content. In this work IRM_{-20} and IRM_{-300} have been selected, termed '$SOFT_{-20mT}$' and '$HARD_{-300mT}$'.

Table 1.5 (continued from previous page).

Magnetic parameter and unit	Measurement	Interpretation of parameter
$SOFT_{-20mT}$ $10^{-3}\ Am^2\ kg^{-1}$	Calculation of IRM-$_{20}$ mT to the SIRM signal corrected for sample volume and mass*. ((IRM$_{-20}$ – SIRM)*12.9)/mass	It is unlikely that at a low field magnetisation of -20 mT 'hard'/antiferromagnetic grains will become magnetised. Therefore, IRM_{20} values can be used as an indicator of 'soft'/MD ferrimagnetic grains.
$HARD_{-300mT}$ $10^{-3}\ Am^2\ kg^{-1}$	Calculation of IRM_{300} to the SIRM signal corrected for sample volume and mass. ((IRM$_{-300}$ + SIRM)*12.9)/mass	At a higher magnetic field of -300 mT, MD ferrimagnetic grains will have already reversed and, therefore, any further changes in demagnetisation will be from 'hard'/antiferromagnetic and or fine (SSD) ferrimagnetic grains to this IRM value and can be used as an indicator of hard/ antiferromagnetic content.
S-RATIO *(no units)*	Interparametric ratio of IRM_{100}/SIRM.	At -100 mT all soft magnetic minerals are magnetised and is therefore used to indicate contributions of soft and hard minerals in a sample. S-RATIO values ~-1 are indicative of 'soft' magnetic behaviour (i.e. ferrimagnetic MD grains), whereas higher values, ~-0.3to -0.6, highlight a 'hard' antiferromagnetic component. Intermediate values ranging from ~-0.4 to ~0.6 indicate a dominant SD ferrimagnetic signal.
SIRM/ARM *(no units)*	Interparametric ratio.	This ratio is indicative of magnetic grain size variations in samples dominated by ferrimagnetic minerals as SIRM indicates total concentration of remanence carrying minerals, whereas ARM is sensitive to SSD ferrimagnetic grains. A low ratio reflects the presence of SSD grains and high ratios indicate MD grains.
χ_{ARM}/SIRM $10^{-3}\ Am^{-1}$	Interparametric ratio.	This parameter also discriminates variations in magnetic grain size, with high ratios highlighting SSD ferrimagnetic grains, and low values indicate the presence of coarser (MD) grains.
SIRM/χ_{LF} $10^{3}\ Am^{-1}$	Interparametric ratio.	As SIRM values reflect the concentration of all remanence carrying minerals, and χ_{LF} indicates the contribution of ferrimagnetic grains, this ratio determines the contribution of non-remanence carrying minerals. Low ratios indicate paramagnetic minerals, whereas canted-antiferromagnetic minerals are highlighted by high ratios. For samples with similar mineralogy, SIRM/χ_{LF} can also be use to assess grain size variations, with high values indicating SSD grains, and low values highlighting SP/ MD grains.

*12.9 value corresponds to the assumed volume measured by the magnetometer (12.87 10^{-6} cm^3).

1.4.3.1.2. Mineral magnetism as a proxy for environmental change

Since its development in the 1960s, mineral magnetic techniques have been widely applied to a range of lake, peat and marine sediments, as well as soils and dusts in palaeoclimatic [Robinson, 1986; Colman *et al.*, 2000; Demroy *et al.*, 2005] and palaeoenvironmental studies [Yu and Oldfield, 1993; Hu *et al.*, 1999; Stockhausen and Zolitschka, 1999]; in sedimentology [Caitcheon, 1998; Booth *et al.*, 2005; Holden, 2009], land-use and human activity research [Thompson *et al.*, 1975; Eriksson and Sandgren, 1999; Oldfield *et al.*, 2003]; and environmental contamination studies [Scoullos and Oldfield, 1979; Oldfield, 1981; Tolonen and Oldfield, 1986; Clifton *et al.*, 1999; Hoffmann *et al.*, 1999; Pozza *et al.*, 2004]. Mineral magnetism has been widely applied in palaeolimnology to establish chronologies [Oldfield, 1991; Verosub and Roberts, 1995], correlate sediments stratigraphies within and between lake sites [Bloemendal *et al.*, 1995; Thompson *et al.*, 1975; Rolph *et al.*, 1996], and infer environmental lake histories from down-core variations in magnetic properties [Thompson *et al.*, 1975; Oldfield *et al.*, 1983, 2003].

Magnetic particles produced from anthropogenic processes have increased in abundance within the environment since the industrial revolution (~post-19th century), primarily from the combustion of fossil fuels [Dekkers, 1997; Dearing, 1999; Petrovský and Ellwood, 1999]. Iron occurs as an impurity in fossil fuels which, when unburned, have low magnetisations [Flanders, 1994]; however, on combustion (industrial, domestic, vehicular) carbon and organic material are lost by oxidation and highly magnetic iron oxide (magnetite and haematite) spherules are produced [Petrovsky and Ellwood, 1999; Muxworthy *et al.*, 2002; Kukier *et al.*, 2003]. Combustion temperature and fuel type determines the magnetic grain size, mineralogy and concentration of these particulates [Flanders, 1994; Matzka and Maher, 1999; Robertson *et al.*, 2003]. The magnetic signature of anthropogenic combustion particulates within lake stratigraphies can be separated out from natural inputs, to produce a pollution 'signal' [Locke and Bertine, 1986; Oldfield, 1991; Dearing, 1999; Rose *et al.*, 2004(a)]. Concentration magnetic parameters susceptibility (χ) and saturation isothermal remanence magnetism (SIRM) are widely used as proxies of particulate pollution concentration [Oldfield and Richardson, 1990(a); Verosub and Roberts, 1995; Petrovský *et al.*, 2000; Moreno *et al.*, 2003]. A range of magnetic parameter ratios can also help to separate a pollution signal from natural inputs, such as soil/catchment derived grains [Dearing *et al.*, 1996] and bacterial magnetite [Oldfield, 1994, 2007].

The mineral magnetic analysis of urban sediments is increasingly acknowledged as a viable inexpensive, reliable and complimentary diagnostic tool to characterise particulate pollution [Shu *et al.*, 2000; Muxworthy *et al.*, 2003], distinguish pollutant sources [Oldfield *et al.*, 1985; Hunt *et al.*, 1984; Hunt, 1986], and identify spatial [Ďurža, 1999; Strzyszcz *et al.*, 1996; Kapička *et al.*, 1999; Hoffman *et al.*, 1999] and temporal [Tolonen and Oldfield, 1986; Berry and Plater, 1998; Lee and Cundy, 2001; Worsley *et al.*, 2005] PM trends; when applied to soils [Strzyszcz and Magiera, 1996; Heller, 1998; Hoffmann *et al.*, 1999; Kapička *et al.*, 2001; Hanesch and Scholger, 2002; Klose *et al.*, 2003; Berqúo *et al.*, 2004]; biomonitors (leaves, mosses, tree barks) [Schädlich *et al.*, 1995; Matzka and Maher, 1999; Hanesch *et al.*, 2003; Moreno *et al.*, 2003; Urbat *et al.*, 2004; Gautam *et al.*, 2005], atmospheric filter samples [Flanders, 1994; Muxworthy *et al.*, 2001, 2003; Shu *et al.*, 2001; Spassov *et al.*, 2004] and street dusts [Beckwith *et al.*, 1986; Morris *et al.*, 1995; Xie *et al.*, 1999(b), 2000, 2001; Robertson *et al.*, 2003; Gautam *et al.*, 2004; Shilton *et al.*, 2005].

Mineral magnetic parameters are also reported as suitable proxies for trace metals [Strzyszcz *et al.*, 1996; Georgeaud *et al.*, 1997; Scholger, 1997, 1998; Chan *et al.*, 1998 Petrovský *et al.*, 2001], grain size [Oldfield and Yu, 1994; Muxworthy, 2001; Booth *et al.*, 2005] and organic content [Xie *et al.*, 2000; Shilton *et al.*, 2005]; as well as a surrogate for PM pollution [Matzka and Maher, 1999; Hanesch *et al.*, 2003; Moreno *et al.*, 2003; Muxworthy *et al.*, 2003] and mutagenicity of urban PM [Morris *et al.*, 1995] (Table 1.6).

Table 1.6: Key publications within the literature of environmental proxy analyses of contemporary urban sediments.

Author	Environmental setting	Main findings
Xie *et al.*, 2000; 2001	Liverpool, UK: roadside street dusts	Xie *et al.*, [2000] report good correlation between organic matter (OM) content with χ_{LF}, χ_{HF} and χARM. Correlations between OM and χ_{FD} suggest that soil is an important contribution of organic material in street dusts. Magnetic signal dominated by MD ferrimagnetic grains. Xie *et al.*, [2001] observed statistical relationships between χ_{LF}, χARM, SIRM, and 'soft' magnetic behaviour with Ti, Fe, Pb and Zn; suggesting roadside dust is composed of a mixture of both natural and urban sources.
Robertson *et al.*, 2003	Manchester, UK: street dusts	Magnetic and trace metal analysis of Manchester road dusts revealed a dominance of vehicular derived particulates characterised by high metal concentrations, primarily lead, zinc and iron and a ferrimagnetic multi domain magnetic component.
Gautam *et al.*, 2004	Kathmandu, Nepal: roadside dusts and soils	Used magnetic susceptibility to quantify intra-urban environmental pollution. Magnetic mapping allowed identification of pollution 'hotspots' attributed to vehicular and/or industrial emissions and decreasing magnetic concentrations observed with distance from road. Microscopy identified anthropogenic magnetic spherules as a dominant contribution to the magnetic signal.
Hay *et al.*, 1997	England and Wales: top soils	Produced a national database of spatial pollution contamination in soil. Strong positive relationships occur between heavy metal concentrations and magnetic parameters in anthropogenic produced particles. The majority of polluted top soils existed in zones of high sulphur dioxide concentrations. Coarse particles of fly-ash material dominated the polluted material within the top soils, reflecting high concentrations of lead and copper. Copper, lead and zinc demonstrated the strongest correlations with SSD and MD grains. A weak correlation was identified between metals and SP grains in polluted top soils.
Heller, 1998	Poland: forest soils	Identified χ as a rapid and sensitive tool to monitor soil contamination. Metallurgical dusts reported as having only local importance to soil enrichment, due to large particle sizes (90 % >100 μm). Fly ash magnetic particles (4-20 μm) were observed to play a more important role in enrichment due to transportation greater distances.
Hoffmann *et al.*, 1999	Germany: Roadside soils	Magnetic susceptibility was used as a proxy measurement for the contamination of roadside soils by vehicular emissions. Magnetic susceptibility values were mapped to trace contaminated areas along highways, providing a cheap, efficient, and sensitive alternative method. Vehicular emissions were magnetically characterized as being dominated by magnetite with grain size decreasing with distance from road.
Petrovský *et al.*, 2001	Prague: alluvial soils	Highlights the suitability of magnetic susceptibility as a proxy to discriminate between polluted and unpolluted areas. Relationships between magnetic concentration and heavy metals were statistically investigated, significant relationships identified in bottom layers of soil opposed to surface layers.

Table 1.6 (continued from previous page).

Author	Environmental setting	Main findings
Kapička *et al.*, 1999	Czech Republic: industrial soils	Monitored the spatial distribution of fly-ash in soils around a brown-coal-burning power plant in a heavily industrialised area of the Czech republic. Comparisons of heavy metal concentrations with susceptibility measurements, suggest that magnetic mapping can be successfully used as a proxy indicator of industrial contamination.
Matzka and Maher, 1999	Norwich, UK: tree leaves	Highlights the potential for tree leave magnetisations to be used as a proxy for monitoring vehicle pollution loadings. High magnetic concentrations were observed at proximal sides of the trees to the road, at locations adjacent to major roads. Maximum magnetisation values occurred at an uphill dual carriageway site. The magnetic signal was dominated by ferrimagnetic grains, chiefly falling within the respirable $PM_{2.5}$ (0.3-3 μm) size fraction and attributed to combustion/exhaust derived PM (opposed to abrasion grains).
Hansech *et al.*, 2003	Leoben, Austria: tree leaves	The magnetic properties of tree leaves were used to characterise contemporary urban dusts. The magnetic signal was dominated by a soft ferrimagnetic phase, which reflected long-term pollution deposition in soils, highlighting the suitability of the method to monitor ongoing emissions.
Moreno *et al.*, 2003	Rome, Italy: tree leaves	Identified high magnetic concentrations (χ) along roadsides, with a decrease in magnetic grain size and concentration with distance from road. The urban dust was dominated by magnetite-type minerals, indicating adsorption of vehicle-derived pollutants on leaf surfaces.
Gautam *et al.*, 2005	Kathmandu, Nepal: tree leaves	Highlights the application of magnetic properties of leaves as an effective method of identifying spatial pollution hotspots within cities. Accumulated PM on leaves is characterized as being magnetite with a predominant grain size range of 2-20 μm attributed to tail pipe emissions. Suggests χ is an effective proxy indictor of metal pollution due to significant relationships observed between χ and heavy metal concentrations.
Hunt *et al.*, 1984	West Midlands and Liverpool, UK: leaf, fly ash and atmospheric samples	Characterised the magnetic signal of vehicular and industrial (fly ash) particulates and used IRM/SIRM ratios to distinguish between the sample sets. Fly ash samples were found to be dominated by 2 μm magnetite and haematite particulates. A higher component of haematite was observed in the industrial dust when compared to the roadside samples, which are dominated by magnetite grains. Highlights the diamagnetic effect of organic material, weakening the magnetic susceptibility signal; however ARM and IRMs were not influenced by OM, but by grain size variations and haematite components.
Flanders, 1994	Various locations and sediments	Measured magnetisation of surface 'moist tissue wipes' and direct atmospheric samples using tape and analysed using mineral magnetism, SEM and chemical analyses. Spheroidal magnetite 2-10 μm, from coal combustion and iron/steel manufacturing, dominated the airborne samples.The magnetic component of fly ash from coal combustion was identified as being primarily magnetite spheroidal particles with an orange peel-like surface. Also identified greater PM deposition in the direction of prevailing wind.

Table 1.6 (continued from previous page).

Author	Environmental setting	Main findings
Morris *et al.*, 1995	Hamilton, Ontario, Canada: Atmospheric filter samples	Correlations were observed between magnetic susceptibility of urban airborne particulates and mutagenicity potencies of the organic extracts and presence of polycyclic aromatic hydrocarbons (PAH).
Muxworthy *et al.*, 2001; 2002	Munich, Germany: atmospheric filter samples, street dusts	Mineral magnetic analyses were applied to filter methods, street dust collections and biomonitoring techniques to characterise urban particulate pollution in Munich. 57Fe Mössbauer spectra, high temperature thermomagnetic and low temperature thermomagnetic curves and hysteresis curves were produced. Maghemite, reported as originating from vehicular emissions (opposed to magnetite in previous studies) and metallic iron particles, derived from street trams, comprise the primary magnetic components of the urban dust, with mean magnetic particle size ranging from 0.1 to 0.7 μm [Muxworthy *et al.*, 2002]. A comparison of magnetic parameters of urban atmospheric pollution filter samples and meteorological data was made in Munich Germany. Magnetite was the primary magnetic mineral with a dominant grain size of 0.2 to 5 μm. The use of magnetic susceptibility for measuring bulk atmospheric particulates is termed as possibly misleading. Examined the effects of grain assemblages on frequency dependent susceptibility [Muxworthy *et al.*, 2001].
Spassov *et al.*, 2004	Switzerland: atmospheric filter samples	Present a new method for the magnetic quantification of urban atmospheric particulates opposed to chemical analysis. Filter samples collected in Switzerland of differing exposure levels to atmospheric particulate pollution were analysed using demagnetisation curves of ARM. Vehicular particulate matter was identified as the dominating source of PM emissions.

The interpretation of magnetic proxies as indicators of palaeoenvironments is not always straightforward, due to the 'blurring' of magnetic properties, when studying mixed mineral assemblages, such as lake sediments [Dekkers, 1997]. Land-use changes, which can accelerate soil erosion, may result in increased catchment-derived eroded material, contributing to the sedimentary matrix. This can potentially dilute or, if contaminated, strengthen the pollution signal [Dearing *et al.*, 1998; Smol, 2002]; however, magnetic parameters can also be used to identify this eroded lake catchment signal [Oldfield, 1991; Dearing *et al.*, 1998]. The formation of magnetic minerals from bacterial magnetosomes (magnetic grains produced by living magnetotactic bacteria, to navigate via the earth's magnetic field) [Vali *et al.*, 1987; Snowball, 1994; Bazylinski, 1996; Gibbs-Eggar *et al.*, 1999] and post-deposition transformation of magnetic grains [King and Channell, 1991; Williams, 1991; Ariztegui and Dobson, 1996; Dearing *et al.*, 1998] can also complicate the magnetic record. However, a range of magnetic parameters can be used to distinguish between natural and anthropogenic inputs [Yu and Oldfield, 1989; Crowther and Barker, 1995; Oldfield, 1994; Xie *et al.*, 1999; Petrovský *et al.*, 2000; Oldfield, 2007]. In order to reconstruct a robust history of pollution, it is necessary to augment magnetic data with other environmental proxies.

1.4.3.2. Trace metals

Trace metals, also known as heavy metals, are a group of elements, which include zinc, cadmium, lead, copper, nickel and chromium and are commonly associated with pollution and toxicity to humans in excessive concentrations [Alloway and Ayres, 1997; Goyer, 1997]. Trace elements are ubiquitous in most natural materials, and sources include wind blown dust, volcanic activity, sea-spray and soil erosion [Cleas *et al.*, 1998]. However, levels of trace elements within the environment have intensified from industrial and agricultural processes [Artiola 1996; Gao *et al.*, 1996; Turner *et al.*, 1999] (Table 1.7). Atmospheric heavy metal loadings have increased since the Industrial Revolution, due to high-temperature combustion processes, fossil fuel consumption (Figure 1.6 and Table 1.8), metallurgical dusts, manufacturing processes [Meij, 1995; Alloway and Ayers, 1997] and vehicle use [Hopke *et al.*, 1980; de Miguel *et al.*, 1997; Williams, 2000; Robertson and Taylor, 2007].

Trace metals are released to air as aerosols or coatings on combustion particulates [Turner *et al.*, 1993; Godbeer and Swaine, 1995; Morwaska and Zhang, 2002] (Figure 1.6). They are an important component of urban PM due to high trace metal loadings and, therefore,

elevated burdens of toxicity, observed in fine and ultrafine particulates [Al-Rajhi *et al.*, 1996; Allen *et al.*, 2001]. Sulphur, a non-metal, major element, is also associated with anthropogenic particulate emissions, especially the release of sulphur dioxide from fossil fuel combustion [Alloway and Ayers, 1997]. S has, therefore, been grouped with the typically anthropogenic trace metals for convenience in presenting and interpreting the anthropogenic-derived elemental composition of sediments in this work.

Table 1.7: Sources of anthropogenic trace metals: Br, Cl, Cr, Cu, Ni, Pb and Zn, and S [Cox, 1995; Alloway and Ayers, 1997; Van Loon and Duffy, 2005].

Trace metal	Anthropogenic sources
Br (Bromine)	Commonly used as an indicator of air quality. Br is mostly used in industry as a source of brine, however it is also converted into organic bromine compounds and used as ethylene dibromide, a fuel additive as a scavenger for lead, in pesticides and fire retardants and extinguishers. Industrially produced organobromine compounds are an important source of Br in the atmosphere.
Cl (chlorine)	Chlorine gas is produced by the electrolysis of sodium chlorine solutions (e.g. in mercury cells). Hydrochloric acid is a widely used industrial chemical, a by-product of organic chlorine compound production. Chlorine is primarily used to manufacture chlorinated organic compounds such as vinyl chloride used to produce plastics (e.g. PVC).
Cr (chromium)	Used in metallurgy as a constituent of stainless steel and in chrome plating, also chromate compounds are used as pigments. Fossil fuel combustion, metallurgical industries, agricultural materials.
Cu (copper)	Principally mining and extraction of metals. Also fossil fuel combustion, metallurgical industries, agricultural materials.
Ni (nickel)	Primarily used in alloys. Mining and extraction of metals (Used in the Mond process as tetracarbonyl (Ni(Co)4)). Fossil fuel combustion, (including diesel exhausts) battery manufacturing, metallurgical industries, agricultural materials.
Pb (lead)	Used in lead-acid storage batteries, pigments, and as tetraethyl lead as a petrol additive. Released into the atmosphere by smelting, refuse incineration and combustion of petrol. The use of lead dates back to pre-industrial times (pre-1750) in metals (e.g. tools, coins, etc.) and in glass, ceramics and dyeing. Fossil fuel combustion (primarily leaded and unleaded petrol from vehicle exhausts), metallurgical industries, agricultural materials, manufacture of batteries, paints, plastics and printing.
S (sulphur)	Used to make sulphuric acid an important industrial chemical. The most significant anthropogenic source is sulphur dioxide from the combustion of fossil fuels, in particular coal-fired power stations. Pre-industrial uses in pharmaceuticals.
Zn (zinc)	Used in anti-corrosion coatings (galvanised iron), batteries and alloys. Fossil fuel combustion, manufacture of pigments, paints and plastics, metallurgical industries, agricultural materials.

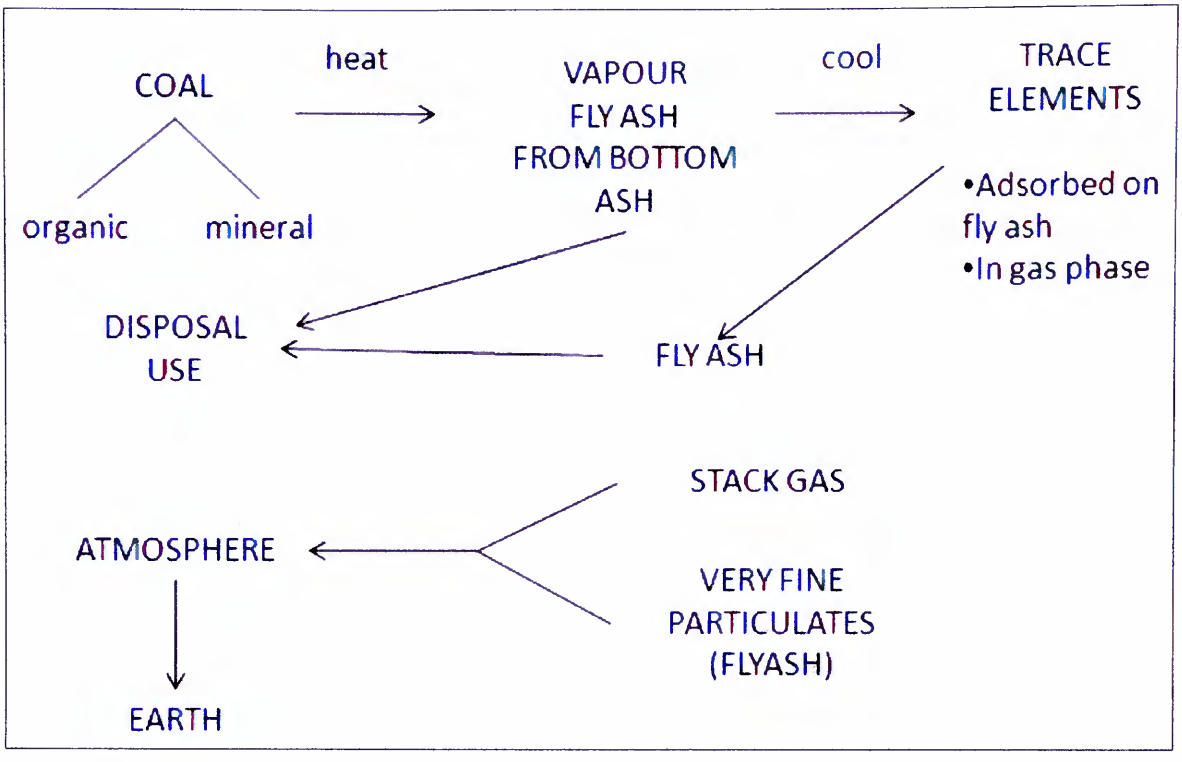

Figure 1.6: Formation of trace metals in fly ash [Swaine, 1995].

Table 1.8: Content of trace elements in UK coal derived fly ash [Swaine, 1995].

Trace element (and chemical symbol)	Content (ppm)	Trace element (and chemical symbol)	Content (ppm)
Antimony (Sb)	<10	Mercury (Hg)	<10
Arsenic (As)	40-600	Manganese (Mn)	200-1300
Boron (B)	100-300	Molybdenum (Mo)	8-190
Barium (Ba)	20-100	Nickle (Ni)	100-400
Beryllium (Be)	<10-40	Phosphorous (P)	570-1140
Cadmium (Cd)	0.1-8	Selenium (Se)	2-23
Chlorine (Cl)	200-300	Thallium (Tl)	<3
Chromium (Cr)	100-500	Vanadium (V)	50-800
Copper (Cu)	100-1000	Zinc (Zn)	90-700
Lead (Pb)	17-800		

Trace metals enter lake systems, most notably, via atmospheric deposition, groundwater and surface water runoff that scavenges metals from the surrounding catchment [Galloway *et al.*, 1982; Smol, 2002]. Once metals enter the water column they settle (if insoluble) or adhere to fine particulates (if soluble) and become deposited on the lake basin forming part of the sediment profile. Therefore, trace metals associated with anthropogenic emissions such as Pb, Zn, Cu, Cd, Cr and Ni, and S (Table 1.4) [Artiola, 1996; Pacyna and Pacyna, 2001; Pacyna *et al.*, 2007] can be used as a proxy for air pollution [Couillard *et al*, 2004; Veselý *et al.*, 1993; Nowierski *et al.*, 2006; Chalmers *et al.*, 2007] and, due to observed relationships with magnetic proxies, can be used to support the magnetic record [Beckwith *et al.*, 1986; Georgeaud *et al.*, 1997; Hay *et al.*, 1997; Scholger, 1997, 1998; Kapička *et al.*, 1999; Gautam *et al.*, 2005].

For some elements, post-deposition mobility can occur [Damman, 1978; Norton, 1986; Smol, 2002]; for example, the migration of zinc and aluminium with increased lake acidity; however, generally less mobility occurs in lakes than other sedimentary environments, such as ombriotrophic peat bogs, which are typically acidic [Galloway *et al.*, 1982; Smol, 2002]. Elevated levels of anthropogenic trace metals can be distinguished from natural, background lake inputs by measuring trace element concentrations and calculating accumulation rates and fluxes [Boyle *et al.*, 1999; Boyle, 2001; Dinescu *et al.*, 2004; Yang and Rose, 2005]. This makes heavy metals suitable tracers of environmental pollutants [Manta *et al.*, 2002], which have been used to reconstruct temporal contamination profiles in peat bogs [Richardson, 1986; Tolonen and Oldfield, 1986; Sanders *et al.*, 1995; Gilbertson *et al.*, 1997], estuarine sediments [Allen and Rae, 1986; Croudace and Cundy, 1995; Lee and Cundy, 2001; Ip *et al.*, 2004; Shi *et al.*, 2007] marine sediments [Santschi *et al.*, 1984; Bricker, 1993; Chan *et al.*, 2001], lakes [Norton, 1986; Norton *et al.*, 1992; von Gunten *et al.*, 1997; Yang and Rose, 2005] and urban ponds [Charlesworth and Lees, 2001; Graney and Eriksen, 2004; Worsley *et al.*, 2006].

1.4.3.3. Fly ash

Fly ash, the collective term for spheroidal carbonaceous particles (SCPs) and inorganic ash spheres (IAS), is produced during the high-temperature combustion of fossil fuels, primarily from energy generation and industrial activity [Locke and Bertine, 1986; Rose, 2001]. IAS, non-combustible material and SCPs are produced by incomplete combustion of fuel [Rose *et al.*, 1995; Rose, 1996], and emitted into the atmosphere [Puffer *et al.*, 1980; Swaine, 1995]. They subsequently deposit in lakes (via direct atmospheric fallout or

catchment soil inwash) and become incorporated within the sedimentary matrix [Renberg and Wik, 1984; Locke and Bertine, 1986; Rose *et al.*, 1999(a), 2002]. The morphological characteristics of fly ash particles (Table 1.9) [Fisher *et al.*, 1978; Griffin and Goldberg, 1979, 1981; Rose, 2001] allow SCPs and IASs to be identified and counted in lake sediments [Rose, 1990, 1994(a)] to reconstruct spatial [Alliksaar and Punning, 1998; Bowman and Harlock, 1998; Fott *et al.*, 1998; Rose and Harlock, 1998] and historical impacts of fuel combustion [Goldberg *et al.*, 1981; Rose, 1994(b); Rose *et al.*, 1998(c); Boyle *et al.*, 1999].

Table 1.9: Main differences between IAS and SCP particles [Rose, 2001].

Fly ash component	General description
Inorganic Ash Sphere (IAS)  © Neil Rose, Univeristy College London www.ecrc.ucl.ac.uk	Spherical, hollow ash sphere with smooth surfaces and a variety of internal structures containing encapsulated smaller spheres. Unable to distinguish between combustion sources.
Spheroidal Carbonaceous Particle (SCP) 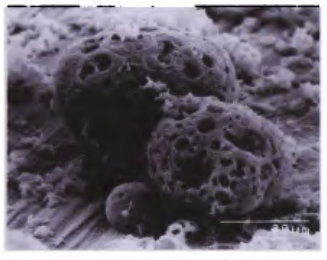 © Neil Rose, Univeristy College London www.ecrc.ucl.ac.uk	Non-spherical (but display sphericity in their morphology), porous, convoluted, rough or smooth surface textures. Coal and oil derived SCPs can be distinguished from composition, surface properties and particle size.

Coal is the dominant industrial fuel type in the UK, and Rose [1996], therefore reports that the majority of fly ash released to air is coal derived IAS. However, SCPs are more commonly used in palaeolimnology as, unlike IAS, which has natural sources (e.g. volcanic emissions), SCPs are solely derived from the combustion of fossil fuels, making them unambiguous indicators of anthropogenic pollution [Rose *et al.*, 1994(c); 1996; 1999(a)]. The varying surface properties of SCPs also allow discrimination between combustion source [Fisher *et al.*, 1978; Griffin and Goldberg, 1981; Rose *et al.*, 1994(c); Kutchko and Kim, 2006].

Collaboration of various studies within the UK, Europe and America, most notably by Rose [2001], has identified regional SCP records from lake sediments, complemented by radiometric dating [Renberg and Wik, 1984, 1985; Charles *et al.*, 1990; Tolonen *et al.*,

1990; Toro *et al.*, 1993; Punning *et al.*, 1997; Alliksaar *et al.*, 1998]. Attributed to the industrial revolution, the UK record starts at ~1830-1910, with a general rapid increase in SCP concentrations during the mid-20th century, showing agreement with national energy demands and power generation [Rose *et al.*, 1995, 1999(b); Rose, 2001]. Fly ash analysis has also been applied to infer lake sediment chronologies supporting other dating methods [Renberg and Wik, 1984, 1985; Rose *et al.*, 1999(b), 1999(c)], as well as the identification of pollution inputs (i.e. distinguishing coal/oil combustion particulates) [Rose, 1996; Rose *et al.*, 1999(a), 1999(b); Solovieva *et al.*, 2005].

SCP profiles have demonstrated correlations with other contaminants, such as persistent organic pollutants (polychlorinatedbiphenyls (PCBs) and polycyclic aromatic hydrocarbons (PAHs)) [Hueglin *et al.*, 1997; Fernandés *et al.*, 2002], making them a proxy of overall pollution deposition. Fly ash particles are also highly magnetic, containing magnetite and haematite fractions [Dekkers and Pietersen, 1992; Kukier *et al.*, 2003] and are also composed of a range of trace metals (Table 1.5) [Mamane *et al.*, 1986; Sager, 1993; Swaine, 1995; Cachier, 1998]. Therefore, as well as unambiguous indicators of PM deposition, fly ash spheres can verify magnetic [Locke and Bertine, 1986; Dekkers and Pietersen, 1992; Dearing *et al.*, 1998] and trace metal proxies [Goldberg *et al.*, 1981; Oldfield, 1990; Rose *et al.*, 1998].

1.4.3.4. Organic matter

Organic matter is an important component of lake sediments, routinely investigated in palaeolimnology [Avnimelech *et al.*, 1984; Boggs, 1995; Meyers and Teranes, 2001]. Derived from organisms that have lived in the lake or the surrounding catchment (mostly originating from plant material), organic matter can be used to infer the history of the lake catchment [Smol, 2002]. Organic matter in lakes can be derived from both natural and anthropogenic origins. The natural organic fraction is primarily derived from plant and microbial residues. The biomass of decaying plants and microorganisms adds to soil, which can be washed into the lake from the surrounding catchment. Also plant material and leaf litter can become deposited on the lake surface which, subsequently decay, providing a further source of organic matter in the water column. *In situ* production of organic matter can also occur within lakes, which support the growth of aquatic plants. Anthropogenic sources of organic matter include sewage that can sometimes be discharged into lakes, agricultural chemicals and a wide range of organic compounds which are by-products of the organic chemical industry [Van Loon and Duffy, 2005].

Biological indicators, including microfossils such as pollen, spores and algae, plant macrofossils and charcoal are widely used to infer palaeoenvironmental conditions [Roberts, 1989; Farr *et al.*, 1990; Jenkins *et al.*, 1990; Peglar, 1998]. For example, due to differences in species' tolerance to pH, diatoms (a group of algae) are commonly used as a proxy indicator of lake acidity [Round, 1990; Clarke *et al.*, 2005]. However, this work is concerned with using the overall organic content (%) to characterise the sediment and infer limnological conditions, such as lake productivity, land use and erosion events [David *et al.*, 1998; Meyers and Teranes, 2001; Smol, 2002; Birks *et al.*, 2004; Boyle *et al.*, 2004; Ng and King, 2004; Punning *et al.*, 2007].

1.4.3.5. Isotopes

Isotopes in lake sediments have been used to track sources of pollutants (for example, using metal isotope ratios) [Nageotte and Day, 1998; Brännvall *et al.*, 1999; Renberg *et al.*, 2001; Solovieva *et al.*, 2005]; however, in this work, inventories of natural and artificial radioactive isotopes have been used to determine a sediment chronology. Naturally occurring ^{210}Pb (lead) isotopes are commonly used in palaeolimnology to date recent sediments over a 100-200 year time scale [Batterbee *et al.*, 1985; Norton *et al.*, 1992; Appleby, 1993; Rose, 1995; von Guten *et al.*, 1997]. A member of the ^{238}U (uranium) decay series, ^{210}Pb can be formed from the radioactive decay of ^{226}Ra (radium), which forms the inert gas ^{226}Rn (radon) which, in turn, forms ^{210}Pb [Appleby and Oldfield, 1983].^{226}Ra enters lake systems in eroded material from within the catchment. The *in situ* decay of this radium is referred to as the 'supported' ^{210}Pb (Figure 1.7, 2b). However, it is the 'unsupported' ^{210}Pb component from atmospheric and catchment deposition that is used for dating since, once incorporated into the lake sediment layers, it decays exponentially with time in accordance with the 'radioactive decay law' [Oldfield and Appleby, 1984]. By subtracting the 'supported' from 'total' ^{210}Pb activity and applying models to determine sediment accumulation rates, a detailed chronology can be reconstructed [Appleby and Oldfield, 1979, 1982; Goudie *et al.*, 1990].

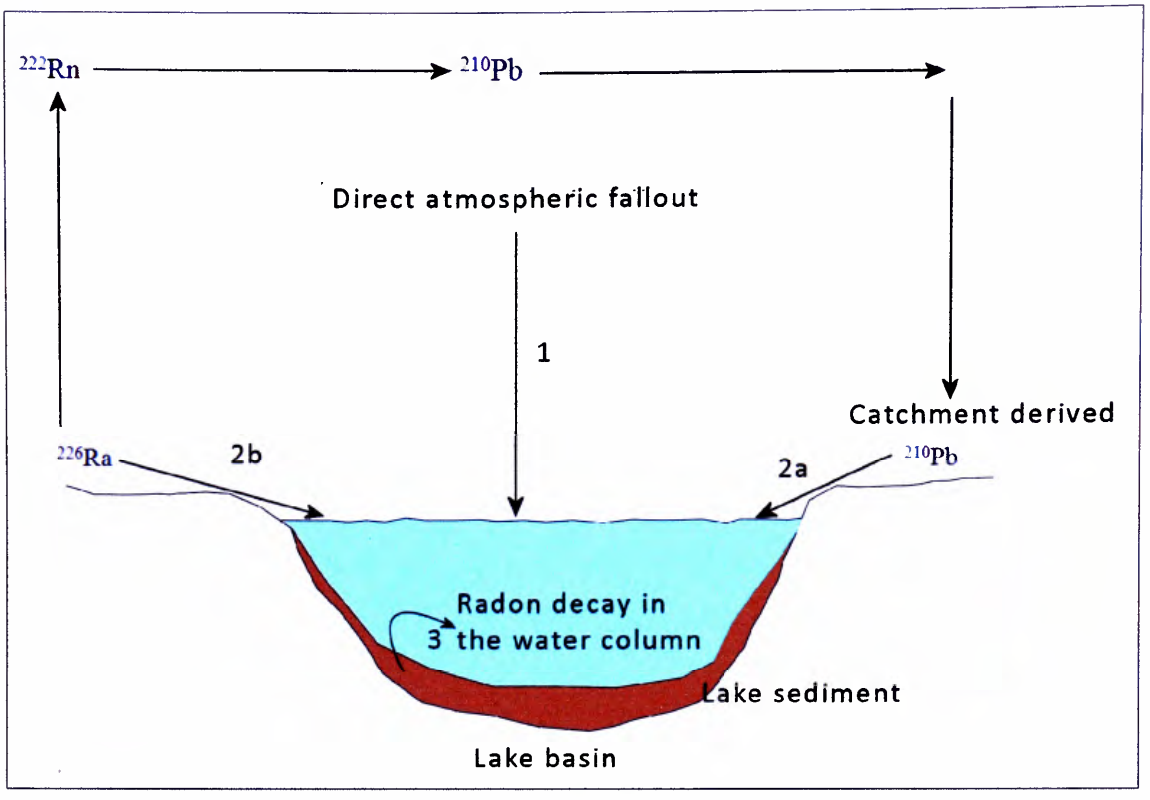

Figure 1.7: Pathways of ^{210}Pb in lake sediments [Oldfield and Appleby, 1984].

Sources of unsupported ^{210}Pb in lake sediments demonstrated in Figure 1.7 include:

- Direct atmospheric fallout (1)

  The principle source of unsupported ^{210}Pb is atmospherically derived. Diffusion of ^{226}Ra from decay in soils into the atmosphere, along with decay of radon (^{222}Rn) in the atmosphere, produces ^{210}Pb. By either wet deposition or dry fallout, ^{210}Pb enters the lake and adsorbs to sediment particles which then become deposited on the bed of the lake [Appleby and Oldfield, 1982; Oldfield and Appleby, 1985; Smol, 2002].

- Catchment derived (2)

  There is also an indirect atmospheric input where ^{210}Pb becomes incorporated into the catchment and quickly reaches the lake, or is detained on fine surface particles within the catchment, where long residence times can occur before eventually reaching the lake as erosive input (2a). Also ^{226}Ra enters the lake via eroded catchment material (2b) [Appleby and Oldfield, 1982; Oldfield and Appleby, 1984].

- Radon Decay within the water column (3)

  Radon enters the lake water by diffusion from underlying sediments. ^{210}Pb is formed from the decay of ^{226}Ra in the water column [Oldfield and Appleby, 1984].

^{137}Cs (caesium) isotopes, artificially produced from nuclear weapons testing, which enter lake systems primarily via atmospheric fallout, can also be traced in lake sediments [Olsson, 1986; Goudie *et al.*, 1990]. ^{137}Cs was introduced into the environment in 1945 and, therefore, can be used to corroborate recent ^{210}Pb dates, in particular the ^{137}Cs peak from maximum output in 1963 [Appleby, 1993]. ^{210}Pb and ^{137}Cs isotope records are widely adopted in palaeolimnology [Jordan *et al.*, 2002; Hu *et al.*, 2003; Tylmann, 2005] to provide accurate chronologies to accompany inferred pollution trends from environmental proxies [Appleby and Oldfield, 1978; Heit *et al.*, 1981; Appleby and Oldfield, 1983; Veselý *et al.*, 1993; Dearing *et al.*, 1998; Rose *et al.*, 1998(c); Solovieva *et al.*, 2005] and to allow calculation of rates of sediment supply to the lake and, therefore, trace metal accumulation rates [Appleby and Oldfield, 1982; Boyle, 2001].

1.4.3.6. Particle size distributions

Particle size is a fundamental diagnostic property of the inorganic component of the lake sediment matrix, as particle size is characteristic of sediment source [Lowe and Walker, 1997; Last 2001; Smol, 2002]. Fluctuations in clay sized (<0.002 mm in diameter) components of lake sediments have been used to identify erosion inputs, indicative of human impact within the catchment [Van Metre and Callender, 1997; Charlesworth and Lees, 2001; Frignani *et al.*, 2004; Tylmann, 2005]. Also, it is important to understand down-core variations in particle size distributions, due to the particle size effect on magnetic properties [Banerjee *et al.*, 1981; Oldfield and Yu, 1994; Han and Jiang, 1999; Muxworthy, 2001; Peters and Dekkers, 2003; Booth *et al.*, 2005]. Particle size is also an important attribute of PM (section 1.4.2) due to affinities with trace metals, sulphur and PAH observed in the finer fraction of fly ash [Mamme *et* al., 1986; Rose, 2001] and may, therefore, be adopted to aid identification and characterisation of PM signals (e.g. PM_{10} and $PM_{2.5}$). Important particle size boundaries and their descriptive terms (e.g. coarse and fine) investigated in this work are defined in Table 1.10 and Figure 1.8, to clarify distinctions between textural particle sizes, pollution and respiratory particle size boundaries, and magnetic grain domains.

Table 1.10: Definitions of particulate size boundaries, respiratory particulate size fractions and magnetic grain size boundaries used in this work.

Pollution classification and particle size		**Magnetic description and grain size**		**Textural description and particle size**	
Coarse	TSP Total suspended particulates <100 µm PM_{10} <10 µm	**Coarse**	Multi domain (MD) >10 µm Pseudo single domain (PSD) 0.7 – 10 µm	**Sand**	>63 µm
				Silt	1.95-63 µm
Fine	$PM_{2.5}$ <2.5 µm	**Fine**	Single stable domain (SSD) 0.7-0.07 µm Superparamagetic (SP) <0.05 µm	**Clay**	<1.95 µm
Ultrafine	$PM_{0.1}$ <0.1 µm				

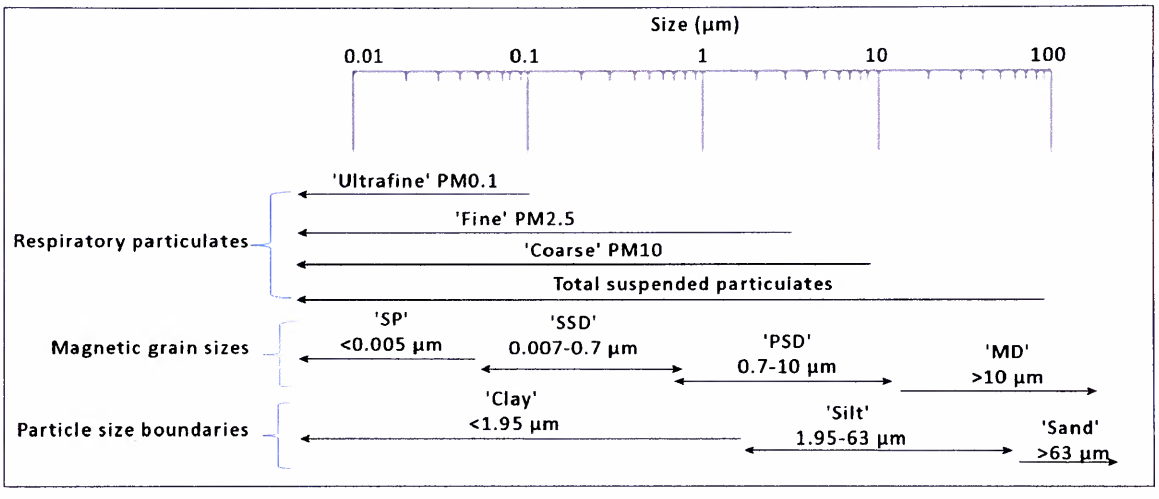

Figure 1.8: Definitions of particulate size boundaries, respiratory particulate size fractions and magnetic grain size boundaries used in this work.

The presentation of down-core variations in environmental proxies expressed as concentrations, flux (accounting for sedimentation rate), or by combining different proxies as ratios can reconstruct a detailed history of lake inputs [Heit *et al.*, 1981; Croudace and Cundy, 1995; Rose *et al.*, 1995; Van Metre and Callender, 1997; Couillard *et al.*, 2004; Rose *et al.*, 2004(b); Yang and Rose, 2005] from which a temporal atmospheric pollution signal can be derived [Oldfield *et al.*, 1983; Maher, 1986; Yu and Oldfield, 1989; Oldfield and Richardson, 1990(a); Dearing *et al.*, 1998; Petrovský *et* al., 2000].

1.4.4. Air pollution histories retrieved from natural sediment archives

As well as lakes [Renberg, 1986; Norton *et al.*, 1992; Birks *et al.*, 2004], wetland [Conner and Thomas, 2003; Kim, 2005], saltmarsh [French, 1996; Fox *et al.*, 1999; Lecoanet *et al.*,

2001], estuarine [Camacho-Ibar and McElroy, 1996; Berry and Plater, 1998; French, 1998; Plater and Appleby, 2004; Cantwell *et al.*, 2007] and peat bog [Oldfield *et al.*, 1981; Tolonen and Oldfield, 1986; Sanders *et* al., 1995; Gilbertson *et al.*, 1997] sediments have been used to reconstruct pollution histories.

Temporal background/regional contamination trends have been inferred from data derived from peat bogs and lakes in rural, upland locations [Pirrone *et al.*, 1998; Brännvall *et al.*, 1999; Dearing and Jones, 2003; Yang and Rose, 2005; Yang *et al.*, 2010], whereas local pollution signals have been identified from coastal, estuary and lake sites adjacent to industry [Vesleý *et al.*, 1993; Tikkanen *et al.*, 1997; Boyle *et al.*, 2004; Frignani *et al.*, 2004; Ullrich *et al.*, 2007]. Sedimentary pollution histories reflect trends in industrial activities (expansion/closures of industrial sites) [Norton, 1986; Bricker, 1993; Rose and Harlock, 1998; Hu *et al.*, 2003; Couillard *et al.*, 2004], transport activity derived pollutants (i.e. road vehicles and aviation) [von Gunten *et al.*, 1997; Boonyatumanond *et al.*, 2007], impacts of air quality regulations and pollution controls [Sanders *et al.*, 1995], and the introduction of new pollutants (e.g. persistent organic pollutants) into the environment [Bonnett *et al.*, 1988; Croudace and Cundy, 1995; Sanders *et al.*, 1995; Fox *et al.*, 1999] (Table 1.11).

Table 1.11: Examples of contamination records established from sedimentary archives.

Author	Environmental setting	Employed environmental proxies	Main findings
Allen and Rae, 1986	Severn Estuary, UK: Estuarine sediments	Trace metals, radioisotope dating	Increases in Zn, Cu and Pb in post industrial sediments, identified coal and local industry as important sources of trace metals.
Berry and Plater, 1998; Plater *et al.*, 1998; Plater and Appleby, 2004	Tees Estuary north-east UK: Estuarine sediments	Magnetic properties, radioisotope dating, trace metals	Onset of metal pollution occurs during the late 19th century, with a peak in metals during the 1950s and decline in metal pollution from 1980, trends related to local mining events and industry.
Brännvall *et al.*, 1999	Sweden: Lake sediments	Pb isotopes	Produced a 3000 year atmospheric Pb profile in annually laminated sediments. Identified a 2000 year old pollution signal from Roman and Greek activities, followed by subsequent increases from Medieval metal production in Europe. More recent peaks are attributed to the industrial revolution.
Connor and Thomas, 2003	Sydney, Australia: Wetland sediments	Magnetic properties, trace metals, pollen	Reconstructed heavy metal pollution history dated using pollen histories. Demonstrated elevated levels of trace metals relating to documented pollution and industrial events.
Couillard *et al.*, 2004	Québec, Canada: Lake sediments	Trace metals, radioisotope dating	Variations in Pb, Cu, Zn and Cd metal profiles reflected the start of industrialisation in 1926, and subsequent histories in local mining operations.
Fox *et al.*, 1999, 2001	Mersey Estuary, UK: Estuarine and salt marsh sediments	Persistent organic pollutants, radionuclides, trace metals	Radionuclide signals used to date cores, and reflect the introduction of POPs in the environment during the mid 20th century. Metal profiles show increases in Zn, Hg, As, Cr, Cu, Pb since the 1900s, which generally decline after mid century peaks. Decline in POPs observed reflecting regulatory controls since the 1970s. Contamination attributed to the production of organic chemicals and pesticides, and other industrial activities.
Gilbertson *et al.*, 1997	Sheffield, UK: Bog sediments	mineral magnetic, charcoal, pollen and trace metals	Profiles reflect local impact of known steel works on the environment during the 19th and 20th century.
Goldberg *et al.*, 1981; Griffin and Goldberg, 1983;	Lake Michigan, USA: Lake sediments	Fly ash, trace metals, radioisotope dating	Observed fly ash particles derived from the burning of biomass in pre-1900 sediments, followed by an increase in combustion derived particulates and trace metals post-1900 attributed to increased use of coal and oil.
Lee and Cundy, 2001	Humber Estuary, UK: Estuarine, saltmarsh and mud flat sediments	Trace metals, radioisotope dating, magnetic properties	Trace metals increase in the salt marsh cores relating to ~ 1900 and demonstrate peaks in Cu, Pb and Zn during the mid-20th century.

Table 1.11 (continued from previous page).

Author	Environmental setting	Employed environmental proxies	Main findings
Norton *et al.*, 1992	30 sites throughout USA: Lake sediments	Major elements, trace metals, radioisotope dating	Accumulation rates of Pb, due to coal burning, sulphide ore smelting and gasoline additives were seen to increase at ~ 1850-1900, from pre-industrial values. Increased use in oil in 1920-1940 is reflected by increases in Vanadium. Variation in metal profiles between sites due to localised industry and pollution, sediment disturbance.
Nowierski *et al.*, 2006	Québec, Canada: Lake sediments	Trace metals	Identified elevated levels of Pb, Cd and Cu in recent sediments compared to lower (pre-industrial sediments) and tested the bioavailability of trace elements, which revealed that pre industrial sediments were less/non toxic compared to recent sediments.
Oldfield, 1981	Finland: Ombriotrophic peat bog	Magnetic properties and moss increments	Profile of atmospheric particle deposition showing increase in magnetic particulates, due to the industrial revolution (~1860), and peak values during the mid 20th century. Magnetite spherules significantly contribute to the magnetic record in recent sediments.
Pirrone *et al.*, 1998	Great lakes, USA: Lake sediments	Radioisotope dating, trace elements	Reconstructed mercury trends, which were compared to emission estimates. Atmospheric deposition was the main contributor of accumulated levels of Hg in the lake sediments. With silver and gold mining the major source in pre industrial sediments.
Renberg, 1986	Sweden: Lake sediments	Trace metals	Presents pollution histories from several Swedish Lakes, which reveal increases in trace metal concentrations during the 19th century attributed to atmospheric deposition from industrialisation which increases further in the 20th century, reflecting the known development and increased combustion of fossil fuels in the area. The local influence of industrial emissions between the different lake sites and prevailing wind direction are highlighted. Also suggests that trace metal analysis should not be solely used as indicators of pollution.
Rose *et al.*, 1998(c)	Siberia: Lake sediments	Fly ash, radioisotope dating	Spatial variation in SCP concentrations between core sites showed deposition higher near to sources in industry, also temporal trends reflect the development of industry in the area since the 1940s.
Rose *et al.*, 2004(b)	China: Lake sediments	Fly ash, magnetic properties, trace metals, radioisotope dating	Contamination trends observed since 1940 show a steady increase in SCPs, Cd, Cu, Pb and Zn.
Solovieva *et al.*, 2005	Russia: Lake sediments	SCPs, diatoms, radioisotope dating	Demonstrates a pollution signal from SCPs that starts ~1950 and peaks ~1980.

Table 1.11 continued from previous page.

Author	Environmental setting	Employed environmental proxies	Main findings
Tolonen and Oldfield, 1986	Canada: Ombriotrophic peat bog	Magnetic properties, trace metals, moss increment and bulk-density based chronologies	Magnetic profiles appear to indicate primary deposition of magnetic particles from industrial and urban fossil fuel combustion processes reflecting documented histories of industry and urbanisation. Metal profiles appear to be less consistent.
Veselý *et al.*, 1993	Czech Republic: Lake sediments	Trace metals, pollen, diatoms, radioisotope dating	Profiles reveal a 350 year history of Cu and Pb pollution. High Pb and Cu concentrations in older sediments, attributed to local glassworks and iron production occurred from 1676 to 1905. Pb increases in from mid 20th century to present day reflected by increased gasoline consumption. 150 years of Zn pollution is reflected by the cores and recent pollution is observed with an increase in vanadium since ~1980 due to increased oil consumption.
Worsley *et al.*, 2006	South Merseyside, UK: urban lake sediments	Trace metals, SCPs, magnetic properties, radioisotope dating	Retrieved a continuous history of air pollution from sediments of Speke Hall Lake. Proxy pollution profiles reflect pre-industrial times, the Industrial Revolution and 20th century urban development.

1.4.5. Urban lakes as historical sinks of air pollution

The majority of paleolimnological studies have focused on natural, upland, rural lakes to infer historical impacts of industrialisation and urbanisation (Figure 1.9, Table 1.12). These lakes are generally remote from pollution sources, receiving atmospheric particulates via long-range transport [Rose, 1995; Yang *et al.*, 1999].

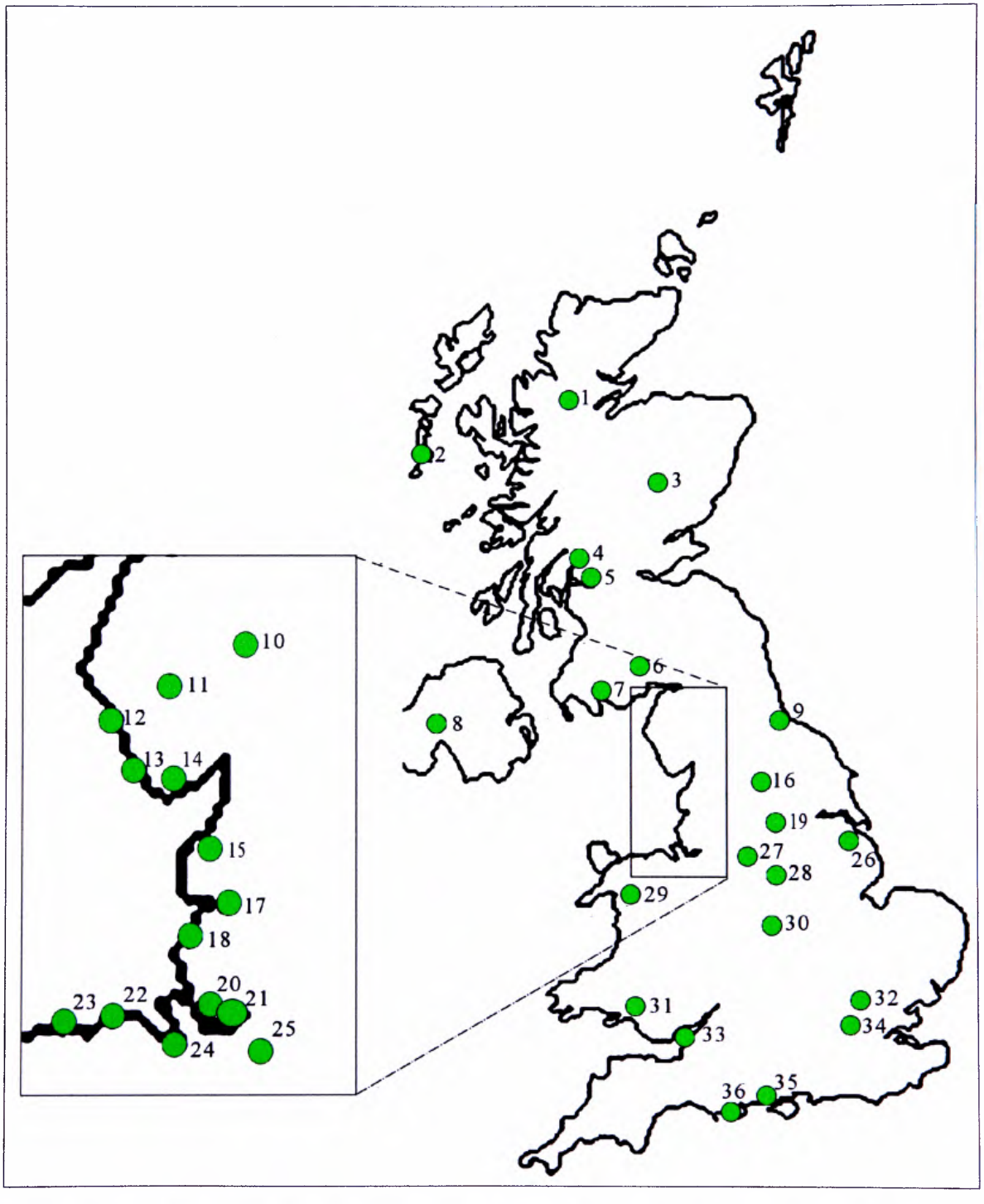

Figure 1.9: Location of some peat, lake and estuarine sediment stratigraphies investigated in the UK (see Table 1.12).

Table 1.12: Peat, lake and estuarine sediments investigated in the UK (corresponding to Figure 1.9).

Site	Location	Author	Sediments
1	Loch Coire nan Arr, Scotland	Rose *et al.*, 1999(b)	Rural lake
2	Loch Teanga, Outer Hebridies	Rose, 1996(b)	Rural lake
3	Lochnagar, Aberdeenshire, Scotland	Yang *et al.*, 2001(b); Yang and Rose, 2005	Rural lake
4	Loch Tinker, Scotland	Rose, 1996	Rural lake
5	Loch Chon, Scotland	Yang and Rose, 2005	Rural lake
6	Ellergower Moss, Scotland	Tolonen and Oldfield, 1986	Rural peat bog
7	Loch Grannoch, Scotland	Yang and Rose, 2005	Rural lake
8	Friary Lough, Co. Tyrone, Northern Ireland	Jordan *et al.*, 2002	Rural lake
9	Tees Estuary	Plater *et al.*, 1998	Estuarine
10	Ponsonby Tarn,. Cumbria	Oldfield *et al.*, 1999	Rural lake
11	Burnmoor Tarn, Cumbria	Yang and Rose, 2005	Rural lake
12	Sellafield, Cumbria	Bonnett *et al.*, 1988; Clifton *et al.*, 1999	Coastal/estuarine
13	Duddon Estuary, Cumbria	Bonnett *et al.*, 1988; Clifton *et al.*, 1999	Estuarine
14	Leven Estuary, Cumbria	Bonnett *et al.*, 1988; Clifton *et al.*, 1999	Estuarine
15	Wyre River , Lancashire	Thomson *et al.*, 2002	Estuarine
16	March Haigh Reservoir, South Pennine	Yeloff *et al.*, 2005	Rural man-made reservoir
17	Ribble Estuary	Bonnett *et al.*, 1988; Clifton *et al.*, 1999	Estuarine
18	Southport	Bonnett *et al.*, 1988	Coastal/estuarine
19	Tinsley Park Bog, Sheffield	Gilbertson *et al.*, 1997	Urban peat bog
20	Mersey Estuary	Fox *et al.*, 2001; 1999; Bonnett *et al.*, 1988; Clifton *et al.*, 1999	Coastal/estuarine
21	Speke Hall, South Merseyside	Worsley *et al.*, 2006	Urban lake
22	Colwyn Bay, North Wales	Clifton *et al.*, 1999	Coastal/estuarine
23	Conwy Bay, North Wales	Clifton *et al.*, 1999	Coastal /estuarine
24	Dee Estuary	Bonnett *et al.*, 1988	Estuarine
25	Flaxmere Bog, Cheshire	Sanders *et al.*, 1995	Rural peat bog
26	Humber Estuary	Lee and Cundy, 2001	Estuarine
27	Ringlow Bog, South Pennines	Tolonen and Oldfield, 1986	Rural peat bog
28	Leicestershire (Groby Pool)	David *et al.*, 1998	Semi rural lake
29	Llyn Llagi, Wales	Yang and Rose, 2005	Rural lake
30	Swanswell Pool and Wyken Pool, Coventry	Charlesworth and Foster, 1999; Charlesworth and Lees, 2001	Urban lakes
31	Swansea Valley, Wales	Blake, 2007	Urban lake
32	Hampstead Heath, London	Rose, 1996	Rural lake
33	Severn Estuary,	French, 1996; Allen and Rae, 1986	Estuarine
34	Banbury Reservoir	Yang and Rose, 2005	Urban reservoir
35	Southampton Water, South England	Croudace and Cundy, 1995	Estuarine
36	Beaulieu Marsh, South England	Thomson *et al.*, 2002	Estuarine

Although rural sites are affected by human activity, there is an observed gradient of decreasing atmospheric deposition with distance from source [Puffer *et al.*, 1980]. Although useful background *regional* pollution signals can be gathered from large, natural, rural lakes (Table 1.11), small, urban ponds (Plate 1.1) can be used to investigate *local* urban pollution signals [Van Metre and Callender, 1997; Meriläinen *et al.*, 2003; Tylmann, 2004; Worsley *et al.*, 2006] and potentially cross-regional signals over a large urban area.

Plate 1.1: An example of an urban pond: Halton Moss (SJ 356961, 384369) facing northeast to surrounding industry and nearby Fiddlers Ferry power station 07/12/2005.

Sediment records from urban lakes and ponds are site specific and therefore unique to their environment. Unlike pristine, natural rural lakes, urban ponds are heavily impacted by human activity, receiving a complexity of atmospheric urban particulates from various industrial and transport sources [Van Metre and Callender, 1997; Charlesworth and Foster, 1999; Callender and Rice, 2000]. Also different PM characteristics are experienced in an urban environment compared to rural areas [Charlesworth and Lees, 1999(b); Weber *et al.*, 2000; Wilson *et al.*, 2005; Chalmers *et al.*, 2007], with elevated levels of trace metal deposition observed in urban catchments [Chalmers *et al.*, 2007].

Favourable attributes of urban ponds as sinks of air pollution include:

(i) Urban ponds are generally closed systems. The absence of output and/or input channels such as drains, allows a more consistent preservation of the paleo-lake record [Sack, 2001] and, therefore, air pollution signal [Charlesworth and Lees, 2001].

(ii) Urban ponds have small surface areas, making them sensitive to changes within their catchment (i.e. contamination) and produce high-resolution sedimentary stratigraphies, detailing environmental transformations [Tylmann, 2005].

(iii) Urban ponds have small catchments and, therefore, high lake-to-catchment ratios. Their catchments are typically defined by the rim of the lake basin and, therefore, the primary sedimentary contribution to the pond derives from the atmosphere (via direct atmospheric fallout). Vegetation from trees and shrubs that immediately surround the pond may also contribute. The potential 'extended' catchment area for some urban ponds, defined by land height and urban/constructed areas, may also influence the flow of sediment to the pond from catchment run off. However, this input is potentially negligible due to the typically small area of this extended catchment in urban environments and highly vegetated margins typical of urban ponds.

(iv) Urban ponds are heavily impacted by anthropogenic activities, due to their setting amongst sources of pollution. This makes them representative of the complexity of PM experienced within an urban environment [Graney and Eriksen, 2004; Chalmers *et al.*, 2007].

(v) Urban pond sediments are site specific [Van Metre and Callender, 1997; Charlesworth and Lees, 1999(a)], receiving inputs from adjacent industry and, therefore, can potentially be used to identify spatial variations within a large-scale conurbation.

(vi) Urban ponds allow the reconstruction of local urban pollution histories instead of relying on remote/background signals picked up by rural lakes [Charlesworth and Lees, 1999(a); Tylmann, 2005].

Urban lake sediment stratigraphies have been used to infer human impacts on lake ecosystems, water quality and eutrophication [Tikkanen *et al.*, 1997; Meriläinen *et al.*, 2003]. Surface sediments from urban lakes or lakes adjacent to industrial sources have also been used to characterise pollutant inputs and their origin [Blake *et al.*, 2007; Ullrich *et al.*, 2007]. However, minimal research has utilised small urban ponds as *temporal* sinks of air pollution (Table 1.13). Although contamination of urban lakes has been explored, very few high-resolution, dated, detailed air pollution histories have been reconstructed [Dauval'ter, 2004; Tylmann, 2005; Worsley *et al.*, 2006] and there is limited work on cross-regional pollution signals within a conurbation [Charlesworth and Lees, 1999(a), 2001; Chalmers *et al.*, 2007].

By employing environmental proxy techniques, comprehensively applied to rural lakes, to ponds with verified longevity in an urban landscape, it may be possible to reconstruct datable, high-resolution detailed trends in air pollution deposition, spanning pre-industrial times to present day (i.e. the last 200-300 years). Distinct elemental, magnetic and grain size signatures of PM may also allow discrimination between pollution sources (e.g. vehicular / industrial) [Hunt *et al.*, 1984; Hunt, 1986; Schmeling, 2004; Wilson *et al.*, 2005].

The potential for urban ponds to reconstruct temporal patterns of air pollutants has only recently been recognised [Dauval'ter, 2004; Tylmann, 2005; Worsley *et al.*, 2006]. Preliminary investigations into atmospheric deposition in urban catchments in Coventry, UK, by Charlesworth and Lees [1997(a), 2001] and Charlesworth and Foster [1999] have highlighted some potential issues regarding the integrity of urban lake stratigraphies. The aforementioned authors applied mineral magnetic proxies, trace metal analysis and radiometric dating to two small urban lakes and contemporary urban sediments. Elevated trace metal concentrations were observed in recent sediments (1954-1991), when compared to older core sections (1850-1954); however, detailed continuous, down-core trends of proxy pollution characteristics are not presented. Their main findings highlight:

(i) the potential of PM to undergo biogeochemical processes within the urban environment prior to deposition within the lake, complicating the use of magnetic proxies as effective pollution tracers;

(ii) problematic unmixing of the sediment record due to multiple sources of pollutants entering an urban lake; and

(iii) inconsistent associations between magnetic proxies and trace metals, potentially due to physical and chemical transformations of urban PM during transport; altering initial characteristics of PM during atmospheric deposition, to the final characteristics of PM which eventually deposits in urban lakes.

A further important factor when investigating urban lakes is the potential of catchment disturbance in the urban environment, which can disrupt the sediment sequence [Charlesworth and Lees, 2001]. Unlike rural locations, where the infill of lakes is relatively consistent, urban lake sedimentation is more sporadic [Knight, 1979; Lazaro, 1979; Charlesworth and Lees, 2001]. With urban expansion there is an increase in impermeable surfaces (concrete/tarmac), combined with increased erosion due to exposed surfaces, which results in increased surface run off so that urban lakes receive sediment in 'pulses' with continued development and construction [Wolman, 1967; Douglas, 1985; Lazaro, 1979; Charlesworth and Lees, 2001], and which may raise levels of pollutants entering urban lakes [Graney and Eriksen, 2004]. This is especially important for lakes with large catchments or altered catchment boundaries due to urban development.

Elevated contributions of trace metals, via run off of urban impervious surfaces, were utilised by Graney and Eriksen [2004] who investigated long-term levels of pollutants in sediments from a storm water pond in New York, USA. A history of pollution trends from ~1940 was archived within the sediments, reflecting local development and industry. A post-1920s air pollution history has also been reconstructed from lakes adjacent to an industrialised area in Vorkuta, Russia [Dauval'ter, 2004]; whereby, lake contamination trends reflected local industrial emissions. A more extensive history has been reconstructed by Tylmann [2005] using a relatively small (7.5 ha) and shallow (<3 m) lake in a heavily industrialised region of Gdańsk, Poland, which demonstrated a clear record of local anthropogenic change, detailing the urbanisation and industrial development of the region throughout the 19th and 20th century.

Table 1.13: Exploration of contamination records from urban lake and pond sediments.

Author	Environmental setting	Lake characteristics	Employed environmental proxies	Main findings
Rose, 1996	Lake sediments: Hampstead Heath, London, UK	Lake area: 0.309 ha	SCPs	SCP record demonstrates good agreement with the known combustion history of coal and oil in the UK during the 20th century.
Van Metre and Callender, 1997	Lake sediments: Texas, USA	Lake area: 440 ha Maximum water depth: 6 m	Trace metals, pollen, grain size, radiometric dating, POPs	Used sediment cores from a man-made reservoir to explore a history of pollution since its construction in 1912. Pollution impacts are observed from the 1950s due to urban development in the area at this time, which include increased trace metals, POPs and changing sedimentation rates and grain size. Increased Pb levels from 1952 are attributed to gasoline use, with a decrease observed ~1978 ascribed to reductions of Pb in petrol. Also PCB and DDT levels appear from the 1950s and peak during the mid- late 1960s.
Charlesworth and Lees, 1999(a); 2001	Lake, stream, wetland, street sediments: Coventry conurbation, UK	Site 1: Swanswell Pool Lake area: 0.73 ha Maximum water depth: 1.3 m Site 2: Wyken Pool Lake area: 2.25 ha Maximum water depth: 0.8 m	Magnetic proxies, trace metals, radiometric dating	Properties of sediments from polluted urban lakes in Coventry, UK, were compared to street dusts. A lack of relation between levels of heavy metals and mineral magnetic measurements revealed the importance of chemical changes during transport within the urban environment and deposition and various sources of sediment. Complex processes occurring in an urban environment causes sediment delivery to be unsynchronised with time, unlike natural environments. Noted difficulty in tracing sediments through this disruptive urban environment. When the sediment chronology was divided into two periods 1: 1850-1954 and 2: 1954-1991 an increase in trace metals in the later period was observed. However, continuous down-core trends are not presented.
Meriläinen *et al.*, 2003	Urban lake sediments: Finland	Lake area: 340 ha Maximum water depth: 2.7 m	Diatoms, chironomids, trace elements, SCP, radiometric dating	Although the lake received municipal waste water from local industry a SCP record starts during the 1930s, and peaks at ~ mid 1980s attributed to coal fired power plant operations. ^{210}Pb chronology proved unreliable due to the disturbance of the chronology from large amounts of eroded material due to intensive land use of lake shores. Temporal trends in POPs and trace metals are attributed to discharge of waste waters to the lake from a local sewage works opposed to atmospheric deposition.

Table 1.13 (continued from previous page).

Author	Environmental setting	Lake characteristics	Employed environmental proxies	Main findings
Dauval'ter, 2004	Lake sediments: industrial coal mining region in Vorkuta, Russia	Lake area: 44 ha Maximum water depth: 8.7 m	Fly ash, trace metals, diatoms, radiometric dating	Reconstructs a detailed history of 20th century pollution. Suggests that long-range transboundary pollution transfer from other areas contributes to high concentrations of heavy metals. Cadmium concentrations are thought to be related to coal combustion with Cd temporal trends reflecting the local history of coal production. Highest concentrations of identified SCPs occur in sediments at ~ 1970s and 1980s, a time of maximum coal production in the area. More recent sediments show a decline in SCP counts. Metal and diatom analyses reveal the alkalising effects of industrial emissions in the region. A time lag was observed between local pollution source and heavy metal concentrations within the sediments, attributed to migration of metals and effects of the buffer capacity of soil and vegetation cover.
Graney and Eriksen, 2004	Pond sediments: New York, USA	Urban pond site: Lake area: 0.55 ha Maximum water depth: 1.2 m	Trace metals, radiometric dating	Metal concentrations in urban and rural pond sediments were used to construct archives of anthropogenic activities in Binghamton, New York. Elevated levels of pollutants in an urban storm water pond were observed when compared to rural ponds. Metal concentrations reflect emissions of local industry and consumption of leaded gasoline and coal. A 50-year chronology of trace metal trends highlight a Pb peak at 1980, then Pb decline due to the introduction of unleaded petrol.
Tylmann, 2005	Lake sediments: Poland	Lake area: 7.5 ha Maximum water depth: 3 m	Trace metals, organic matter, particle size, radiometric dating	Cu, Zn, Cd and Pb profiles reflect lake contamination during the 19th century from a health spa, and subsequent 20th century increases attributed to industrial plants. Elevated levels of metals were observed in post industrial sediments.
Worsley *et al.*, 2006	Lake sediments: Merseyside, UK	Lake area: 0.309 ha Maximum water depth: 3 m	Magnetic properties, trace metals, radiometric dating, SCP	Reconstructed ~350-year sediment pollution records using cores taken from a small, man-made urban pond. Magnetic and trace metal data reveal trends in pollution from the construction of the pond in the 17th century to present day. High pollution levels are observed from ~1800-1850, attributed to the maximum industrial output during the Industrial Revolution, following relatively low pre-industrial levels. Mid-20th century peaks are observed with subsequent reductions in pollution levels, potentially due to Clean Air Acts. Post-1980 increases in pollution data are attributed to road and air travel.
Chalmers *et al.*, 2007	Stream and lake sediments: throughout New England, USA	Lake surface area and depth not specified	POPs, trace metals, radionuclides	Identified pollutants in lake sediments from elevated levels of pollutants from natural background concentrations. Noticed higher burdens of pollutants in urban lakes opposed to rural locations. Identified Attributes fluvial pollution inputs, as well as atmospheric fall out, as an important contribution of pollutants in urban lake sediments. Cd, Cr, Cu, Hg, Ni, Pb and Zn correlated with urbanisation. Higher levels of pollutants observed in urban, opposed to rural sediments.

Worsley *et al.*, [2006] demonstrate that a continuous air pollution record, which encompasses the Industrial Revolution to present day, can be reconstructed from environmental analysis of urban lakes. Three-hundred and fifty-year sediment proxy pollution records were obtained, using mineral magnetic, trace metal, SCP and ^{210}Pb analyses, from a small (~0.309 ha), anthropogenic lake at Speke Hall, set in urban south Merseyside, which detail a local pollution history. Distinct phases of anthropogenic activity were identified in the Speke Hall Lake sediment record:

(i) Relatively low-level pollution concentrations highlighting localised activity from the construction of the pond in c.1520 to ~1800.

(ii) Intensive industrialised activity noted by high pollution peaks from ~1800-1850, reflecting the maximum activity of the Industrial revolution in the south Merseyside region.

(iii) Late 19th and early 20th century decreases potentially due to the changing nature of chemical productivity in the region.

(iv) Early to mid-20th century pollution increases, possibly due to the industrial demands of two World Wars.

(v) Mid to late 20th century reduction in pollution proxy data, suggestive of the Clean Air Acts introduced post-1950.

(vi) Recent increase from ~1980, possibly due to increase in road and air travel.

(vii) Mid-1990s reduction in pollution levels and subsequent rise at the start of the 21st century.

This clear, high-resolution air pollution record highlights the potential for small urban lakes as archives of local air pollution depositional histories, revealing pollution trends related to localised industrial and urban activity.

The sediment records from Speke Hall Lake (SHL) provide an initial insight into an air pollution history for the lower Mersey region (LMR). A preliminary comparison of the sulphur record retrieved from an urban pond in north Cheshire, Daresbury Delph Pond (SJ 353630, 383290), with the sulphur profile obtained from SHL, reveal several similar features (Figure 1.10).

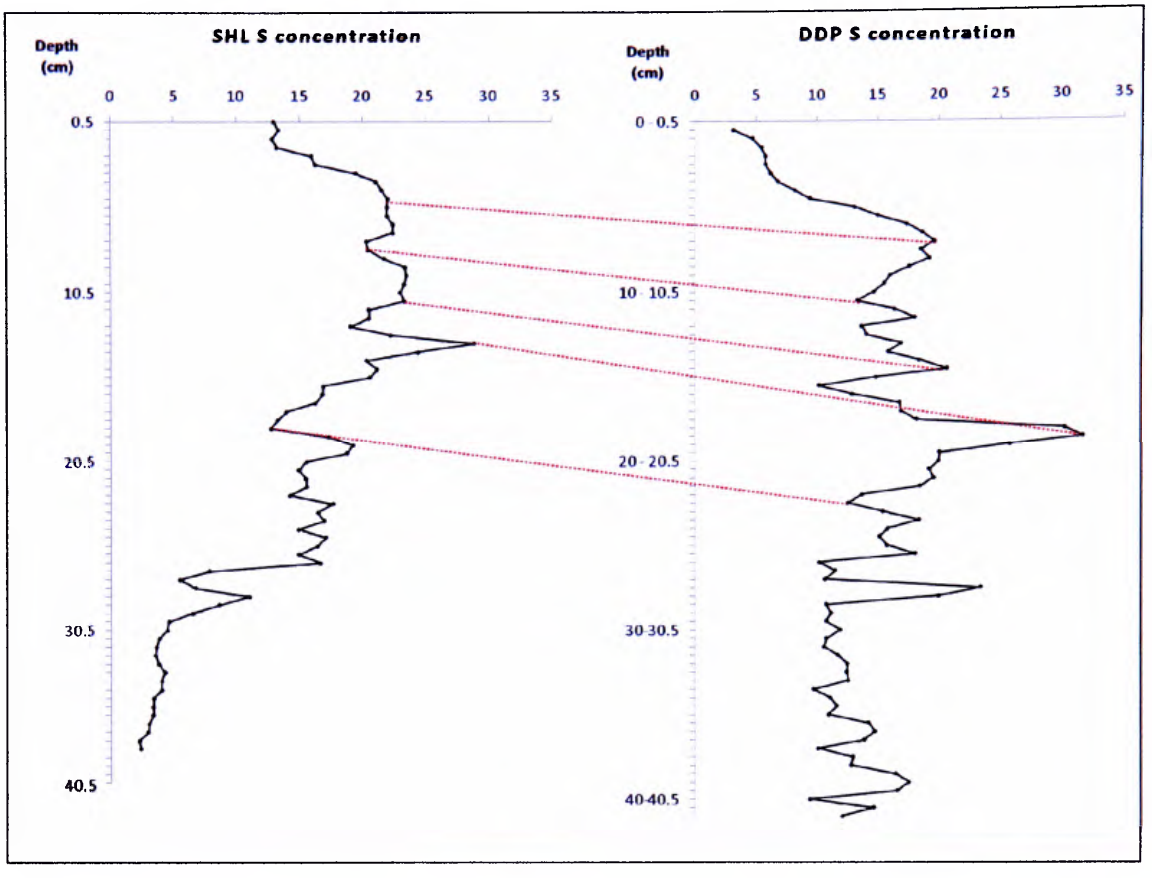

Figure 1.10: Sulphur concentration (mg/g) profiles obtained from Speke Hall Lake (SHL) and Daresbury Delph Pond (DDP), urban lakes within the lower Mersey region. Similar features are highlighted.

This suggests that there are possible corresponding features between urban ponds within the LMR and supports the reliability and reproducibility of sediment records retrieved from small (<1 ha) lakes and ponds set within complex urban environments; justifying further investigation into urban sediment stratigraphies.

1.5. The need for urban sedimentary air pollution histories

Despite potential limitations, it is important to further investigate urban ponds as archives of air pollutants as they:

(i) hold the only available pre-1960 (and sufficient pre-1990s) urban air pollution data [Rose, 1996; Meriläinen *et al.*, 2003; Dauval'ter, 2004; Rose *et al.*, 2004(a)];

(ii) can be used to monitor the impacts of industrialisation and urbanisation on urban air quality [Van Metre and Callender, 1997; Meriläinen *et al.*, 2003; Dauval'ter, 2004] since the intensification of industry during the 19th century [Tylmann, 2005; Worsley *et al.*, 2006]; which in turn

(iii) may, potentially, be used to retrospectively assess the toxicology of urban PM.

1.5.1. Air pollution monitoring

Since the mid-20th century, black smoke and sulphur dioxide concentrations have been measured in the UK using filter reflectance and acid titration techniques (respectively) [Goodwin *et al.*, 1999]. Crude methods and inconsistent measurements of only two pollutants is insufficient to fully understand historical trends in air pollution. However, this monitoring represents the only available long-term (i.e. post-1960s) air pollution measurements, prior to current, technologically advanced, real-time monitoring.

Listed as one of the eight major pollutants monitored as part of the 1997 National Air Quality Strategy, ambient PM (TSP, PM_{10} and $PM_{2.5}$) concentrations for UK cities have been automatically recorded since the 1990s, using gravimetric particulate mass measurements via expensive and spatially limited (usually one station per city) monitoring 'boxes' [DEFRA, 2007]. Although these monitoring systems record useful, detailed, temporal concentration data (allowing hourly and daily mean values to be expressed), and reveal diurnal and seasonal variations in urban atmospheric quality, they do not provide any long-term (i.e. pre-1990s) historical data, or spatial information *within* urban areas.

The Environment Agency has published a 'Pollution Inventory' of industrial emissions data (www.environment-agency.gov.uk/pi), detailing releases of pollutants to air, water and land from industrial activities. Emissions data are gathered for each company by either measurements at point sources, calculations using standard used estimations and non-standardized estimations from best assumptions, which are then calculated as annual discharge [Environmental Agency, 2007]. These data are useful in understanding the types of substances released from industry, however due to estimates there is some doubt over the accuracy of the quantities of these released substances, and data only extends back to 1998.

1.5.2. Urban air quality

Concerns of urban air quality are not recent. The urban growth of major UK conurbations (e.g. London, Liverpool, Manchester, Birmingham and Bristol) during the industrial revolution in the late 18th century, saw economic growth from the development of manufacturing industries and, as a consequence, rapid population increases [Stobart, 1996; Barker and Harris, 1959]. Subsequent 19th century industrial intensification shaped the urban landscape [Warren 1980; Douglas *et al.*, 2002]. Growing industrial towns were characterised by poor terrace housing occupied by labourers and factory workers, living on the doorstep of industry, and a variety of industrial chimney stacks [Allen, 1906; Halton Borough Council, 1991]. Nineteenth century urban environments were renowned for their black smogs and gases 'offensive to sight and smell' that would often destroy vegetation [Allen, 1906]. Technological advancements and continued industrial expansion throughout the 20th century, in particular the shift from inorganic to organic chemical production and petrochemicals, led to the introduction of new pollutants in the environment (e.g. persistent organic pollutants) [Alloway and Ayres, 1997], and potential variations in emissions due to changing industrial processes [Wilson *et al.*, 2005].

In order to improve UK urban air quality, a series of legislations have been introduced and amended since 1845 (Table 1.14). Since the Clean Air Acts of 1956, 1968 and 1993, smoke emissions have been reduced due to emission controls from industrial chimney stacks and shifts in domestic fuel from coal to electricity and gas [Goodwin *et al.*, 1999; DEFRA 2007]. Recent concerns focus on the degradation of urban air quality due to fine ($PM_{2.5}$) and ultrafine particulate ($PM_{0.1}$) emissions, from industrial high-temperature combustion processes and increased vehicular use [Vermette *et al.*, 1991; Penttinen *et al.*, 2000; Boffetta, 2004; Harrison, 2004; Wilson *et al.*, 2005].

Table 1.14: UK air quality legislations [adapted from http://www.air-quality.org.uk].

Year	Legislation	Details
1845	Railway Clauses Consolidation Act	Requires railway engines to consume their own smoke.
1846	The Improvement Clauses Act	Contained a section dealing with factory smoke.
1866	The Sanitary Act	Empowered sanitary authorities to take action in cases of smoke nuisances.
1875	The Public Health Act	Contained a section on smoke abatement from which legislation to the present day has been based.
1906	The Alkali, etc. Works Regulation Act	Extended and consolidated previous Acts and embodied the prevention of discharge of noxious or offensive gases from scheduled works by the use of best practicable means.
1926	Public Health (Smoke Abatement) Act	By which the Acts of 1875 and 1891 were amended and extended.
1956	Clean Air Act	Introduced smoke control areas, controlled chimney height and prohibited emissions of dark smoke from chimneys, with some exceptions.
1968	Clean Air Act	Extended the smoke control provisions of the 1956 Act and further prohibitions in dark smoke emissions.
1970	EC Directive 70/220/EEC	Relating to measures to be taken against air pollution by gases from positive ignition engines of motor vehicles. Limited emissions of carbon monoxide and hydrocarbons from petrol engines. Came in to force in 1971.
1972	EC Directive 72/306/EEC	Measures to be taken against emissions from diesel engines for use in motor vehicles. Limited black smoke emissions from heavy duty vehicles.
1974	Control of Pollution Act	Allowed for the regulation of the composition of motor fuels. In addition the Act limited the amount of sulphur in fuel oil.
1975	EC Directive 75/441/EEC	Set up a procedure for exchanging air quality information between Member states. Repeated in 1982.
1975	EC Directive 75/716/EEC	Concerned with the sulphur content of certain liquid fuel. Defined two types of gas oil (diesel and heating oil). Introduced in two stages, sulphur limits for these fuels. (1) the motor fuel (sulphur content of gas oil) and (2) the oil fuel (sulphur content of gas).
1978	EC Directive 78/611/EEC	Concerning the lead content of petrol. Limited the maximum permissible lead content of petrol to 0.4 gl^{-1}.
1979	International Convention on Long Range Transboundary Pollution	Introduced to control the transboundary effects of acid rain and to limit emission of acidifying pollutants.
1980	EC Directive 80/779/EEC	Air quality limit values and limit values for sulphur dioxide and suspended particles.
1981	The Motor Fuel (lead content of petrol) Regulation	Limited the maximum amount of lead in petrol to 0.4 gl^{-1}.
1982	EC Directive 82/884/EEC	Limit value for lead in the air.
1984	EC Directive 84/360/EEC	Established a common framework directive on combating pollution from industrial plants throughout the Community.
1985	EC Directive 85/210/EEC	Allowed for the introduction of unleaded petrol.
1987	EC Directive 87/77/EEC	Specified the measures to be taken against the emission of gaseous pollutants from diesel engines for use in vehicles. Controlled emissions of gaseous pollutants from heavy duty vehicles.
1988	EC Directive 88/609/EEC	Limited emissions of sulphur dioxide and nitrogen oxides particulates from power stations and other large combustion plants.
1989	The Air Quality Standards Regulations	Brought into UK law as the limit values for sulphur dioxide and suspended particulates, lead in air and nitrogen dioxide set by the EC.

Table 1.14 (continued from previous page).

Year	Legislation	Details
1989	EC Directive 89/427/EEC	Limit values of air quality for sulphur dioxide and suspended particulates. Harmonised measurement methods.
1989	EC Directive 89/429/EEC	Directive on air pollution from existing municipal waste incinerators. Set limits on new waste incinerators.
1989	EC Directive 89/369/EEC	Directive on air pollution from new municipal waste incinerators. Set emission limits on new waste incinerators.
1990	Environmental Protection Act	Brings many smaller emission sources under air pollution control by local authorities for the first time and established a system of integrated pollution control for the most potentially polluting industrial processes.
1991	The Road Vehicles Regulations	Set standards for service emissions of carbon monoxide and hydrocarbons to be included in the MOT test for petrol cars and light good vehicles.
1992	EC Directive 92/72/EEC	Air pollution by ozone. Establishes a harmonised procedure for monitoring, exchange of information and warnings to be issued to the public about ozone pollution.
1995	The Environment Act	This provides a new statutory framework for local air quality management. The Act requires publication of a National Strategy which will set air quality standards and targets for the pollutants of most concern.
1996	EC Directive 96/62/EEC	This provides a new statutory framework for controlling levels of sulphur dioxide, nitrogen dioxide, particulate matter, lead, ozone, benzene, carbon monoxide, and other hydrocarbons.
1997	The National Air Quality Strategy	The final version of the National Air Quality Strategy was published in response to The Environment Act on March 12th 1997 with commitments to achieve new air quality objectives throughout the UK by 2005, and is periodically reviewed.
2000	The Air Quality Strategy for England, Scotland, Wales and Northern Ireland	The second National Air Quality Strategy was published with new air quality objectives for local authorities.

1.5.3. Health effects of PM

Associations between ill health and air pollution have been recognised since industry intensified in the 19th century [Dingle, 1982]. Accusations of industrial emissions causing ill health amongst local residents and industrial workers during the 19th century, are widely documented [Allen, 1906; Dingle, 1982; Jenner, 1995; Szneter and Mooney, 1998]; although, no link between air pollution and health was proved at this time. However, it was the numerous deaths that arose from the 1952 London smog events that raised awareness of the potential for air pollution to harm health [Stone, 2002; Raloff, 2003]. In recent years (post-1990s), with the introduction of sophisticated pollution monitoring and modelling, and advancements in epidemiology, more precise relationships between air pollution and disease have been identified and are widely reported [Dockery *et* al., 1993; Spurny, 1996;

Diaz *et al.*, 1999; Peters *et al.*, 2000; Englert, 2004; Evans and Smith, 2005; von Klot *et al.*, 2005; Mukhopadhyay and Forssell, 2005; Rainham *et al.*, 2005].

Although air quality is perceived to have improved since the mid-20th century (observed by reductions in black smoke and sulphur dioxide) with the introduction of emission controls and regulations [Goodwin *et al.*, 1999], recent epidemiological studies demonstrate that even low levels of pollution (below ambient guidelines) can effect health [Spurny, 1996; Maynard, 2004]. This has been shown to be especially important for particulate pollution [Ballester *et al.*, 1999; Brunekreef and Holgate, 2002; Maynard, 2004], whereby no threshold exists below which PM does not affect health [Vinzents *et al.*, 2005].

The relevance of PM emissions on health has been widely investigated [Brunekreef and Holgate, 2002; Le Tertre *et al.*, 2002; Harrison, 2004]. Particulates with an aerodynamic diameter of <10 μm (PM_{10}) are especially important since, due to their small size, they are not filtered by the nasal tract and are, therefore, able to penetrate deep into the human lung and are thought to cause cardiorespiratory mortality and morbidity [Katsouyanni *et al.*, 1996; Anderson *et al.*, 1998; Donaldson *et al.*, 1998; Adamson *et al.*, 2000; LeTetre *et al.*, 2002; Englert, 2004; Hosseinpoor *et al.*, 2005; Janssen *et al.*, 2005; Jerrett *et al.*, 2005; Peled *et al.*, 2005]. Further size divisions of fine $PM_{2.5}$, and ultrafine $PM_{0.1}$ are increasingly raising concerns because of their higher burdens of toxicity (heavy metals and polycyclic aromatic hydrocarbons), potential to penetrate deep in the alveoli, and ability to become absorbed into the body (via gas-exchange portion of the lung), potentially targeting specific organs [Vedal, 1997; Oberdörster, 2000; Morawska and Zhang, 2002; Raloff, 2003; Englert, 2004; Harrison, 2004; Wilson *et al.*, 2005].

As well as size, Wilson *et al.*, [2005] report that PM composition is also an important factor due to the potential for some particulates to act as carriers of absorbed chemicals or gases, which may act as triggers for various health effects. The toxicological role of metallic components of particles has also been identified as important [Meade *et al.*, 1988; Zhang *et al.*, 1998; Maynard, 2004]. Also, sources of PM_{10} may determine pathogencicity, with combustion source particulates reported as being more toxic than soil-derived particulates [Vedal, 1997].

An important factor in understanding relationships between disease and PM in epidemiology is exposure assessment [Smith, 1993]. Socio-economical, occupational and demographical factors are of significant importance in assessing exposure to pollutants

[Revich *et al.*, 2001; O'Neil *et al.*, 2003; Vineis *et al.*, 2004; Bell *et al.*, 2005; Jerret *et al.*, 2005] and although life style, smoking and diet are potential causes of disease, pollution emissions from transport and industrial activities are important considerations [McCally, 2002; Vargas, 2003], especially as many studies demonstrate trends in mortality and morbidity associated with short-term changes in air pollution amongst populations within the urban environment, and within close proximity to industry [Dockery and Pope, 1994; Brunkreef *et al.*, 1995; Kozlov, 2004; Yang *et al.*, 2004] (Table 1.15).

The short-term health effects of PM are also influenced by long-term pollutant exposures due to the accumulation of residuals in the body [Englert, 2004; Wilson *et al.*, 2005]. Long-term pollution exposure is especially important for populations within close proximity to extensive industrial activity [Kozlov, 2004; Pless-Mulloli *et al.*, 1998]. For diseases with long latency times, such as cancer, it is imperative to understand the historical account of pollution exposure, as well as that of the present day, due to the life-time accumulation of toxicity in humans that can trigger disease [Schwartz, 1993; Pope *et al.*, 2002; Ahrens and Stewart, 2003; Englert, 2004].

Contemporary health data (e.g. hospital admissions) can be compared with short-term temporal pollution trends obtained from centralised monitoring stations; however, long-term (decades and centuries) associations cannot be made as this requires investigating pollution levels that extend far back in time beyond the current technologies of monitoring ambient air quality (i.e. pre 1990s). Retrospective exposure assessments are, therefore, difficult as they rely upon proxies for pollution exposure such as land-use [Sainsbury *et al.*, 1996] and proximity of residence to industry [Hodgson *et al.*, 2004], or inconsistent historical pollution records and emissions estimates [Lall *et al.*, 2004; Mukhopadhyay and Forssell, 2005]. Sedimentary archives, such as urban ponds can, however, be used as an alternative to extend existing monitored air pollution data back to pre-industrial times [Dauval'ter, 2004; Tylmann, 2005] and reconstruct a detailed history of the complexity of pollutants experienced in an urban environment, influenced by various types and rates of industrial emissions, transport activities, air quality legislations and specific pollution episodes.

Table 1.15: Key texts in the epidemiological literature.

Author and date	Study area	Main findings
Bhopal *et al.*, 1998	Teeside , UK	Potential for air pollution to explain higher incidences of lung cancer in women living in close proximity to industry.
Brunekreef and Holgate, 2002	Europe	Reviewed various research conducted in Europe. Effects on health were experienced at low levels of exposure, concluding that a low or no threshold exists below which particulate pollution would have an effect on health.
Colvile *et al.*, 2001	Slovakia	Valley topography influenced the spatial distribution of exposure to atmospheric emissions of arsenic from a power plant.
Dubnov *et al.*, 2007	Israel	Identified a negative effect long-term exposure to air pollutants on lung function in children living in the vicinity of a coal-fired power station.
Hodgson *et al.*, 2004; 2006	Halton, UK	Excess kidney disease mortality in a heavily industrialised area with mercury emissions and land contamination.
Jerrett *et al.*, 2005	Hamilton, Canada	Long-term ambient PM exposure associated with premature cardiovascular and cancer mortality in an industrialised city. Although data 'corrected' for socioeconomic and demographic factors, this did not eliminate the pollution effect on mortality.
Kamat *et al.*, 1987	Bombay, India	Observed greater standard mortality ratio (SMR) in cardio-respiratory and malignant diseases related to sulphur dioxide and PM pollution.
Keegan *et al.*, 2002	Slovakia	Identified higher exposure of arsenic with close proximity to a power station.
Le Tetre *et al.*, 2002	European cities	Attributes increase risk of heart disease from particulate pollution to vehicle emissions.
Lin *et al.*, 2001	Taipei, Taiwan	Identified decrease in renal function from low-level long term exposure to lead.
Lopez *et al.*, 2005	Mexico	Despite complying with national standards PM emissions from a coal-fired power plant were reported to be impacting health.
Mohorvic, 2004	Croatia	A retrospective study, identified adverse pregnancy outcomes from coal fired power plant emissions.
Parodi *et al.*, 2005	Italy	Lung cancers clusters identified in females living close to a coke oven plant.
Peled *et al.*, 2005	Israel	Ultrafine particulate pollution significantly associated with decreased lung function in asthmatic children.
Peng, 2002	Shijiazhuang, China	Sulphate, derived form coal combustion, was identified as having significant health effects and exposure levels. A spatial model was developed to identify emission sources and dose-response functions were used to assess impact on human health. It is suggested that the use of cleaner coal is the most cost effective method of reducing human exposure.
Pless-Mulloli *et al.*, 1998	Teesside, UK	Highlights the use of proximity to industry as a surrogate for assessing pollution exposure and the use of female health data opposed to male data, which may be dominated by occupational exposure to pollutants rather than environmental.

Table 1.15 (continued from previous page).

Author and date	Study area	Main findings
Pope *et al.*, 1995	United States	Noted health effects of particulate air pollution in US cities including respiratory symptoms, decreased lung function and cardiovascular disease. Reported a 10 μgm^{-3} in PM_{10} was associated with a 1-10 % increase in respiratory symptoms (e.g. cough and asthma attacks) and an increase of 10 μgm^{-3} $PM_{2.5}$ was associated with a 7 % increase of total mortality.
Pope, 1989	Utah Valley (USA)	Composition of PM less toxic during a Steel mill strike compared to when mill operative.
Revich *et al.*, 2001	Russia	Identified high dioxin concentrations in populations close to industry. Chemical workers were the most exposed to dioxins, and high levels of dioxins were observed in the blood of residents living adjacent to a chemical plant.
Romieu *et al.*, 1996	Mexico	Identified decreases in pulmonary function related to PM_{10} exposure.
Sainsbury *et al.*, 1996	Cheshire, UK	Identified higher mortality rates in populations in wards of high industrial land use, after controlling for deprivation. Identified stronger relationship between deprivation and health than pollution and health.
Schwartz, 1996	Six USA cities	Short term increases in $PM_{2.5}$ associated with mortality.
Smith, 1993	Global	Smith highlights the effects of combustion of solid fuels on the environment through history, with local environment contamination due to biomass combustion in prehistoric times to the present day global problem of pollutant transport of urban air pollution. Smith suggests that ambient air pollution concentrations are not an accurate indication of human exposure to pollutants, to assess the effects of air pollution on health the dose of pollutant inhaled is more important that ambient air pollution concentrations. Therefore highlighting a need for air pollution to be measured in places 'used' by people to assess exposure. Recommends that total exposure assessments should concentrate on public exposure to pollution opposed to ambient concentrations.
Stone, 2002	London, UK	After the London smog events of 1952 unexplained deaths occurred in the area, reported by the government as the result of influenza. By researching historic pollution and health records, the increased mortality may be explained by prolonged health effects of lingering air pollution.
Wang *et al.*, 2006	China	Identified power station emissions as having a lower 'intake fraction' (potential of exposure to population) than industries such as cement, chemical or metallurgical plants.

1.6. Chapter summary

Urban ponds, uncommonly used in palaeolimnology, are important archives of local temporal pollution signals, specific to their urban environmental setting. Data derived from environmental proxies stored within urban lake sediment stratigraphies can reveal down-core trends in trace metals, fly ash, magnetic grains, organic matter and isotopes, enabling the reconstruction of detailed, datable, high-resolution histories of their catchments, on which an air pollution history is superimposed. Urban lakes hold the *only* known available data to determine historical trends in urban air pollution, due to the absence of sufficient long-term (i.e. pre 1990s) monitored pollution data. Therefore, the reconstruction of cross-regional urban air pollution histories is fundamental to investigate the long-term impacts of industrialisation and urbanisation on air quality, which in turn, may be impacting community health.

2. CHAPTER TWO: THE NEED FOR URBAN AIR POLLUTION HISTORIES IN THE LOWER MERSEY REGION

2.1. Chapter overview

The location and geo-characteristics of the borough of Halton, located within the lower Mersey region (LMR) are introduced. Details of the dominance of the chemical industry in the area are presented, with a history of industrial development and subsequent contamination. Ill health amongst the Halton population and potential epidemiological links with the borough's renowned industrial legacy are reviewed, highlighting the importance of investigating air pollution histories in the LMR.

2.2. Introduction

The lower Mersey region (LMR) is termed in this work to describe south Merseyside/north Cheshire region which includes and surrounds the borough of Halton (Figure 2.1). Located in the northwest of England (Figure 2.1 A), the River Mersey broadly divides the LMR into the northwest LMR and southeast LMR (Figure 2.1 B). The river also separates the two towns of Halton, with Runcorn to the south and Widnes to the north of the Mersey (Figure 2.1 C). Renowned as 'chemical towns', an extensive amount of chemical and associated industries have developed in Halton since the early 19th century. As a consequence, there has been a vast amount of water, air and land contamination, from a variety of sources, over the past 200 years [Halton Borough Council (HBC), 1991]. The extent of this 'industrial legacy' was realised in 1974 with a re-organising of local government (Widnes joined Runcorn to form the borough of Halton) and several remediation projects were subsequently introduced. Recent concerns have arisen over the potential of the industrial legacy to affect the health of the current population, especially as Halton experiences some of the highest mortality and morbidity rates throughout the UK [Halton Primary Care Trust (HPCT), 2004]. However, due to a lack of contemporary and historical pollution data, such associations cannot be fully investigated [Burgess *et al.*, 2003] and urban air quality impacts remain unknown.

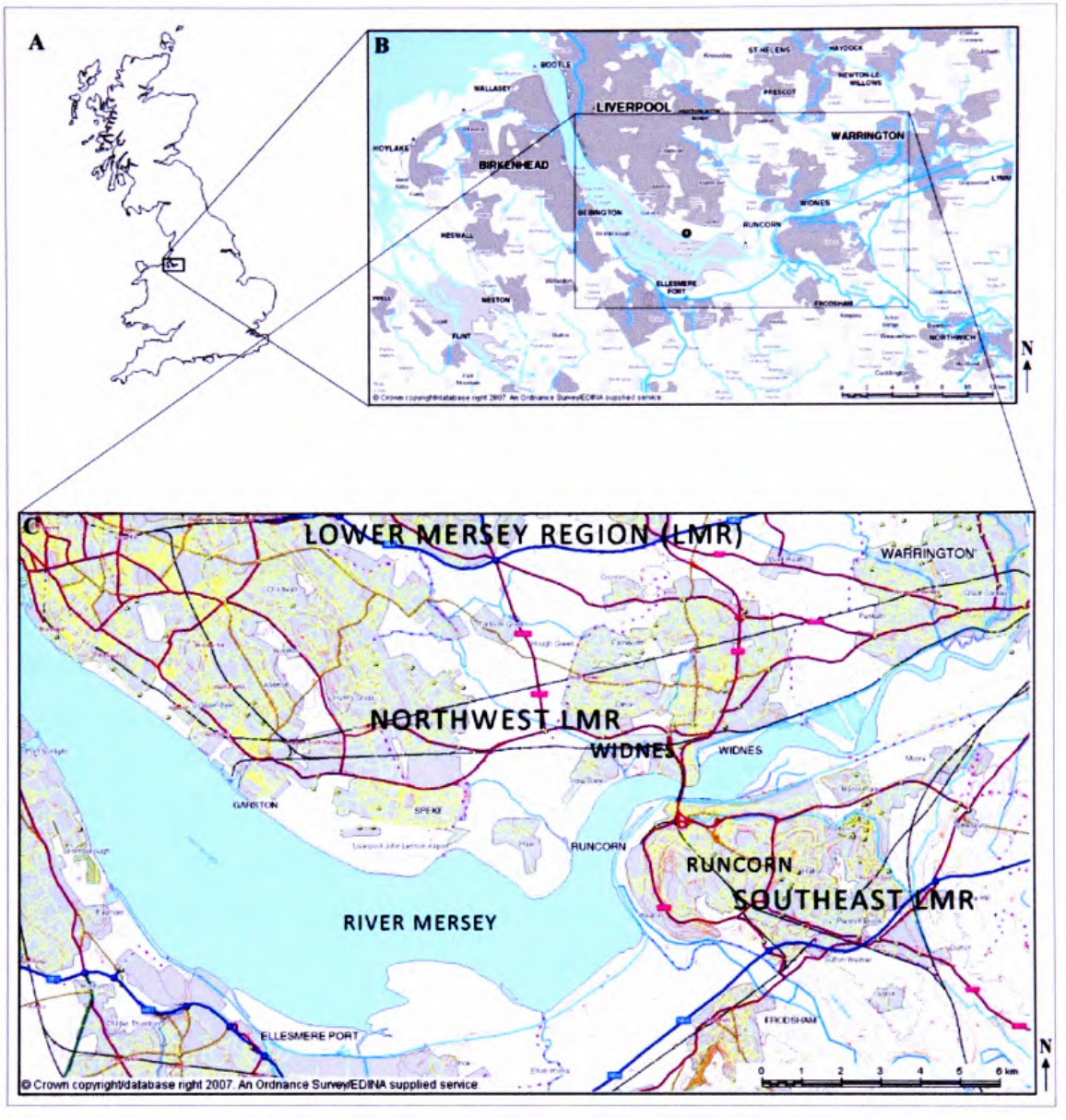

Figure 2.1: Location of the lower Mersey region (LMR). (A): location in northwest England, (B): north Cheshire/south Merseyside and (C) the 'lower Mersey region' termed in this work. Reproduced from the 2007 Ordnance Survey Strategi 1:185196 (B) and 1:92597 (C) maps with the permission of Ordnance Survey on behalf of The Controller of Her Majesty's Stationery Office © Crown Copyright Edge Hill University, Ormskirk, Lancashire licence number: ED100020392.

2.3. Geo-characteristics of Halton

Located on the northern margin of the Cheshire basin, Halton lies within a broad river valley landscape (the Mersey Valley) and is characterised by estuarine, low relief topography generally lying below 20 m AOD (Above Ordnance Datum) in the west (Hale), and below 40m AOD in Widnes, north of the River Mersey, which gently inclines to 55m AOD. South of the River Mersey, in Runcorn, the topography rises more steeply to 78 m AOD at Weston and Daresbury, and 75 m AOD at Halton Hill in Runcorn (Figure 2.2).

The bedrock geology of Halton is mainly composed of Triassic sandstone of the Sherwood Sandstone group (Figure 2.3). The sandstone is overlain with silt and mudstones from the Mercia Mudstone group in the south and east of Runcorn. Extensive faulting has occurred throughout the area with a direction of north and northwest, which has exposed underlying carboniferous coal measures. Superficial drift deposits cover a wide area of the bedrock in Halton, mainly tidal flat deposits to the north of the River Mersey in Widnes, characteristic of tidal zones, and till further in land and throughout Runcorn (Figure 2.3) [HBC, 1991; Greenwood, 1999]. There are occasional sandstone outcrops in Halton, for example at Runcorn Hill (SJ 350650, 381628) and Halton Hill (SJ 353776, 382066). There is considerable 'made ground' in Halton, where ditches, pits, quarries and marshlands have been filled-in with artificial deposits, mainly a result of the industrial legacy of the borough [HBC, 1991].

Runcorn and Widnes are major urban centres, with vast industrial activities generally located along the coastal margins of the River Mersey. The Mersey Estuary is a highly industrialised catchment with predominating chemical and petrochemical industries existing in the northwest at Liverpool (SJ 336262, 39136), to the southwest at Ellesmere Port (SJ 340416, 377723) and Stanlow (SJ 342899, 375996), and coal-fired power generation to the northeast at Warrington (SJ 354367, 386335). Industrial, residential and urban developments dominate land-use in Halton, with some agricultural land away from the town centres in Daresbury (SJ 358247, 382867) to the east and Hale (SJ 347100, 382353) in the northwest.

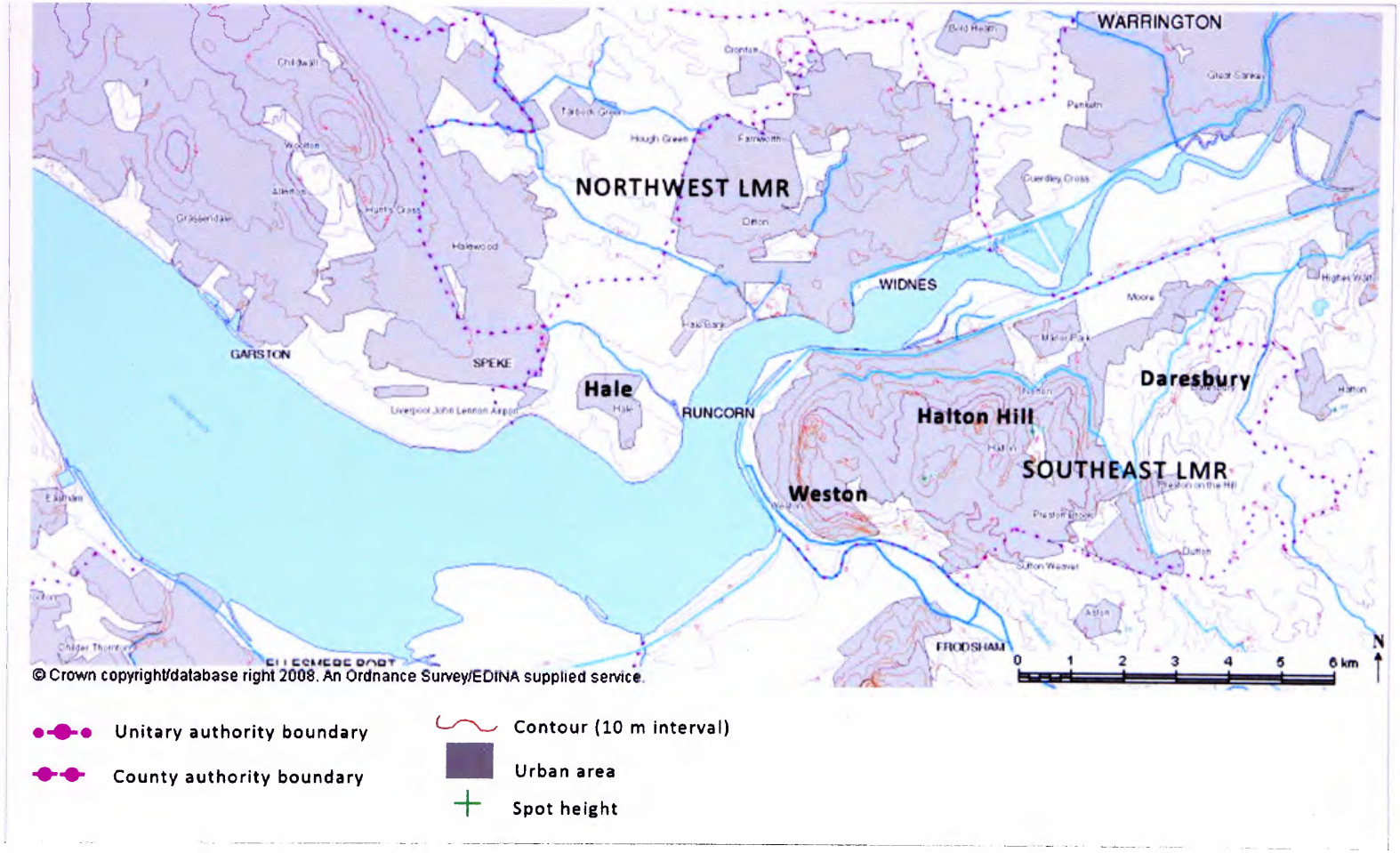

Figure 2.2: Relief and unitary authority boundaries within the lower Mersey region (LMR) 1:92597. Reproduced from the 2008 Ordnance Survey Strategi 1:92597 map with the permission of Ordnance Survey on behalf of The Controller of Her Majesty's Stationery Office © Crown Copyright Edge Hill University, Ormskirk, Lancashire licence number: ED100020392.

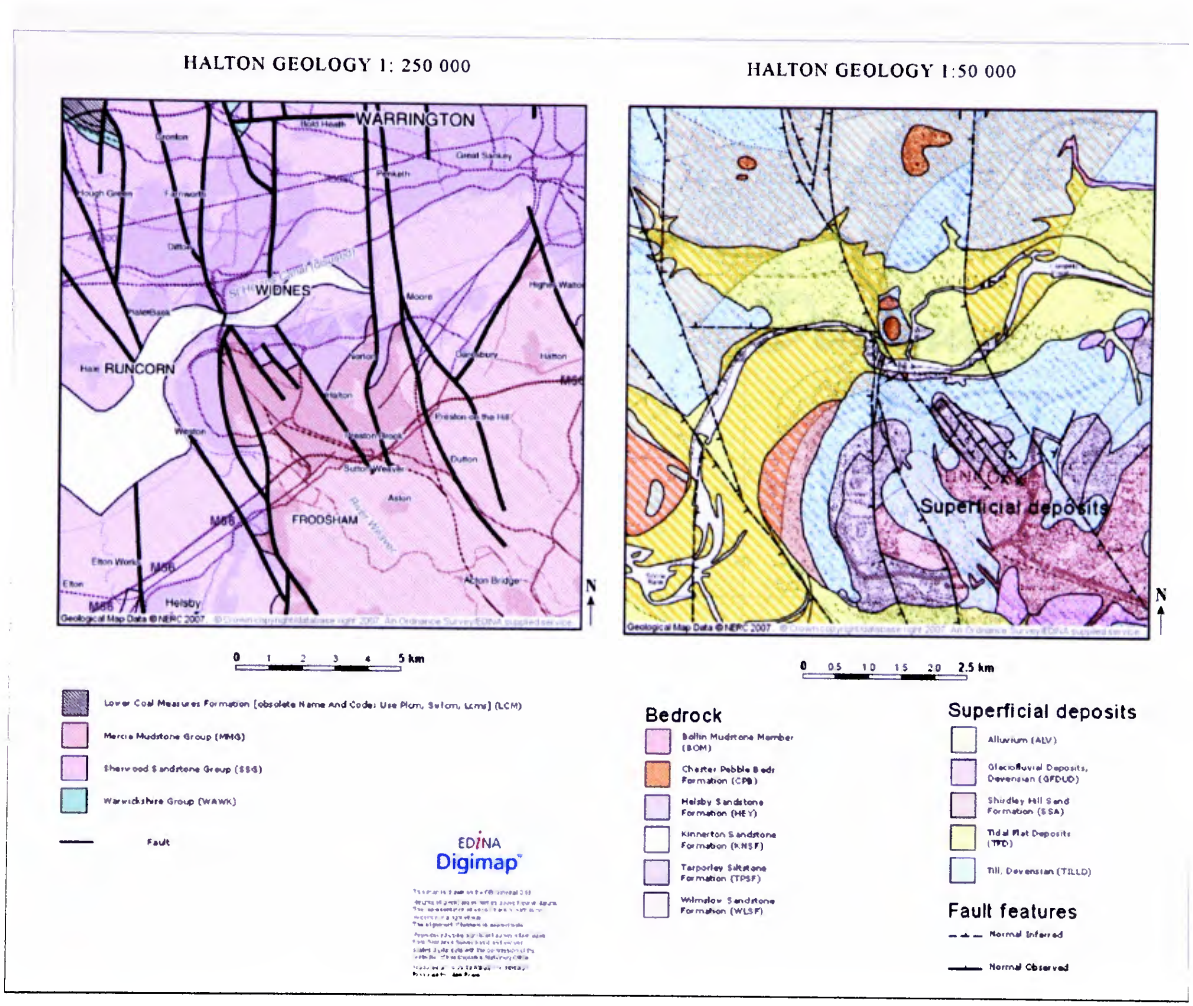

Figure: 2.3: Geology maps of Halton and the lower Mersey region. Reproduced from the 2007 Ordnance Survey British Geological Survey 1:250 000 and 1:50 000 maps with the permission of Ordnance Survey on behalf of The Controller of Her Majesty's Stationery Office © Crown Copyright Edge Hill University, Ormskirk, Lancashire licence number: ED100020392.

2.4. Industrial Legacy of Halton

2.4.1. Present day industry and monitored pollution data

Halton is renowned as a heartland of the chemical industry in Britain.

"Not a day passes without every household in the UK using a product manufactured from raw materials made in Widnes or Runcorn" [HBC, 1991].

Currently over 20 main industrial sites exist throughout Halton (Figure 2.4). Power generation occurs at Fiddlers Ferry in Warrington (SJ 354367, 386335) (Plate 2.1) and the Rocksavage site south of Weston (SJ 351847, 380054), and radioactive, metal, water and waste industries exist throughout the borough; however, it is the chemical industry that dominates industrial activity. A diverse range of chemical manufacturing occurs with ~68 companies operating in Runcorn and Widnes producing polymers, plastics, polishes, perfumes, soaps, detergents, metal alloys, pharmaceuticals and agrochemicals (e.g. pesticides) [HBC, 2005(a); Environment Agency, 2005]. Also Ineos, a major petrochemical and chlor alkali producer (globally the third largest chemical company) is based at Runcorn, manufacturing chlorine and fluorine-based products (used in refrigeration and pharmaceuticals) in the village of Weston [HBC, 2005(b)].

Plate 2.1: Fiddlers Ferry power station in Warrington (SJ 354352, 386358) facing southwest 07/12/2005.

This variety of industrial processes (Figure 2.4) has released a cocktail of emissions to the atmosphere, including inorganic pollutants such as heavy metals, nitrogen and sulphur oxides, and organic (carbon containing) substances including hydrocarbons and organohalides (pesticides, PCBs and dioxins) [Environment Agency, 2005]. Table 2.1 demonstrates the range of substances currently released to air in Halton [Environment Agency, 2005], each with differing potentials to pollute and toxicological effects [Meade *et al.*, 1988; Madden and Fowler, 2000; US EPA, 2003].

Table 2.1: Organic and inorganic substances released to air in Halton [Environment Agency, 2005 (Pollution Inventory data) http://www.environment-agency.gov.uk].

Inorganic substance	Organic substance
Ammonia	1,1,2,2, Tetrachloroethane
Antimony (Stibnium)	1,3, Butadiene
Arsenic	Acetaldehyde
Beryllium	Acetonitrite
Boron	Benzo (A) Pyrene
Cadmium	Bromodifluoromethane (HBFC)
Carbon dioxide	Carbon tetrachloroethane
Carbon monoxide	Carbon tetrachloride
Chlorides	Chloroform (Trichloromethane)
Chromium	Chlorofluorocarbons (CFCs),
Copper	Dichloride
Hydrogen chloride	Dimethylformarmide
Hydrogen fluoride	Dioxins and Furans
Inorganic chlorine compounds	Ethanol
Inorganic fluoride compounds	Ethene (Ethylene)
Lead	Ethylene dichloride
Manganese	Formaldehyde
Mercury	Hexachlorobenzene
Nickel	Hydrofluorocarbons (HCFCs)
Nitrogen oxides	Hydrogen cyanide
Selenium	Maleic anhydride
Sulphur oxides	Methane
Vanadium	Methhylamine
Zinc	Methyl bromide
	Methylene
	Methylene chloride
	Methyl chloroform
	Para-bichlorobenzene
	Phosgene
	Polychlorinatedbiphenyls (PCBs)
	Polycyclic aromatic hydrocarbons (PAHs)
	Tetrachloride
	Tetrachloroethylene
	Toluene
	Trichloroethylene
	Vinyl chloride
	VOCs (Volatile organic compound)s
	Xylene

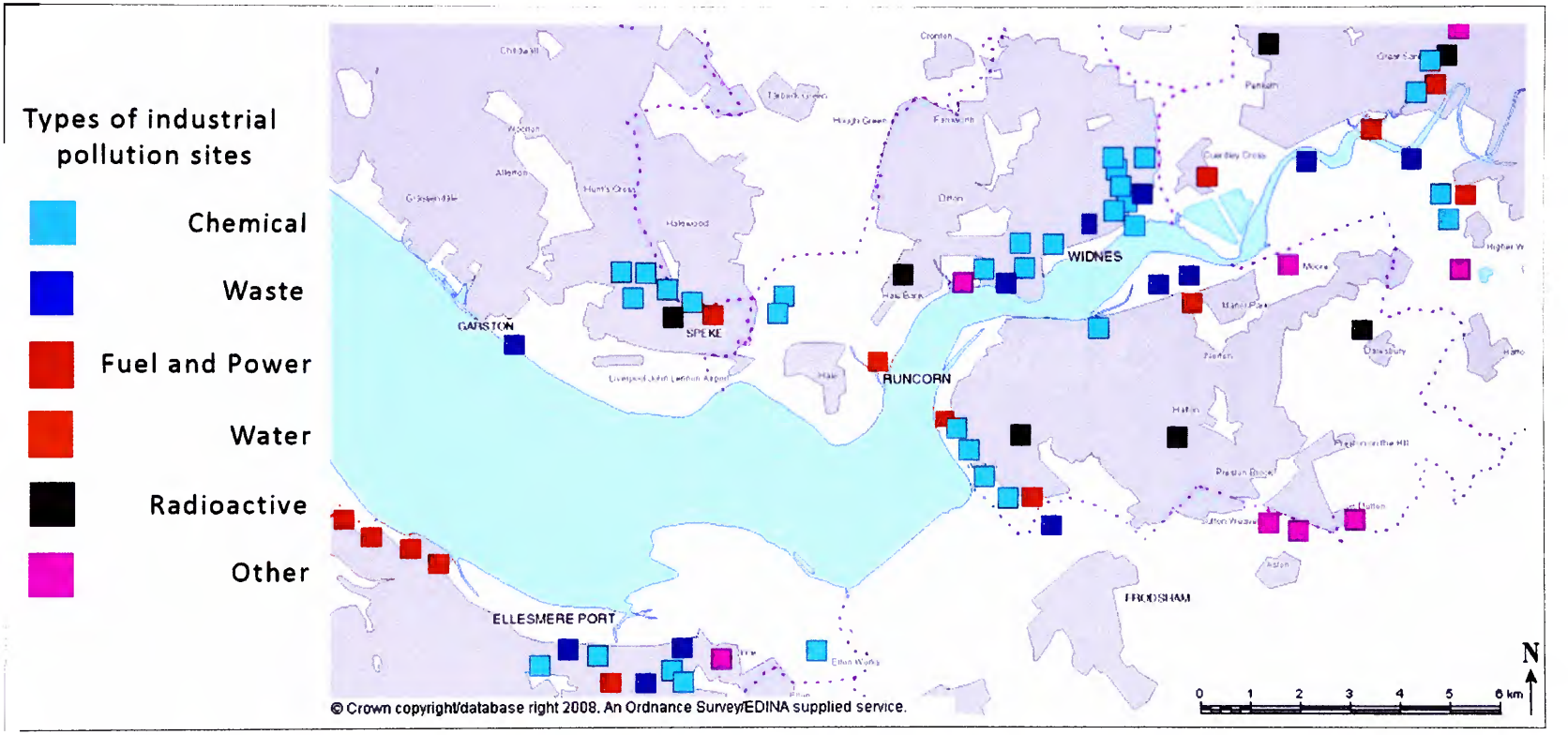

Figure 2.4: Map of industrial pollution sites in the lower Mersey region (1:925915). Reproduced from the 2008 Ordnance Survey Strategi 1:925915 map with the permission of Ordnance Survey on behalf of The Controller of Her Majesty's Stationery Office © Crown Copyright Edge Hill University, Ormskirk, Lancashire licence number: ED100020392. Information obtained from the Environment Agency, 2005 (Pollution Inventory data) http://www.environment-agency.gov.uk.

There are no National Air Quality Strategy (NAQS) pollution 'stations' monitoring ambient air pollutant concentrations in Runcorn or Widnes. The nearest monitoring station is located at Speke (SJ 343828, 383616, ~7 km west from Widnes and 8 km northwest from Runcorn) that has monitored ambient PM_{10} from 21/05/2003 to 13/03/2007. The only long-term pollution data that exists for Halton are levels of sulphur dioxide (measured by acid titration); and black smoke (measured by reflectance from a filter) from 1962 to present day (Figures 2.5 and 2.6). Reductions in these two pollutants have been observed, especially from the mid-1970s, due to the introduction of pollution controls and the subsequent and continual stringent regulations and monitoring of industrial emissions. These two pollution trends suggest that air quality has improved since the 1960s; however, this provides only a snap shot of the pollution experienced, considering the industrial history of Halton extends to the early 1800s [Warren, 1980; HBC, 1991].

Due to a lack of historical data, the use of urban ponds to reconstruct temporal air pollution trends is fundamental in investigating the history of emissions experienced in Halton and the LMR. Historical information regarding the onset of industry in the area, industrial development, and the location and processes of operating companies, needs to be researched to understand the release of pollutants over ~200 years. As chemicals have dominated industry in Halton, it is important to understand the timescale of chemical manufacturing in the borough as technological advances and economic changes have shaped industrial activity and, therefore, pollution emissions [Jones, 1969; HBC, 1991, 2005; Vardy, 2005].

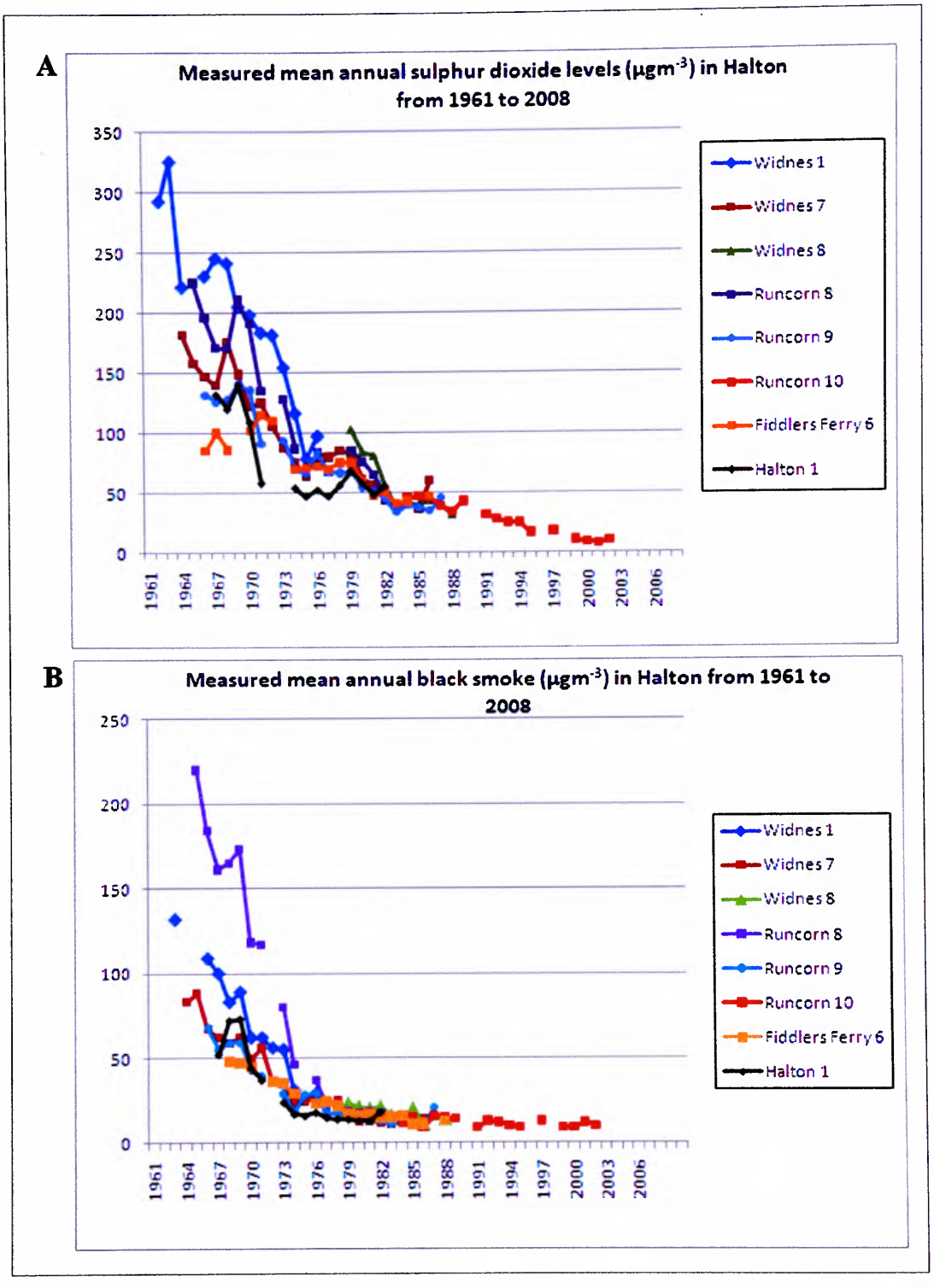

Figure 2.5: Available historical mean annual black smoke (A) and sulphur dioxide (B) concentration data for Halton, produced from the UK National Air Quality Archives.

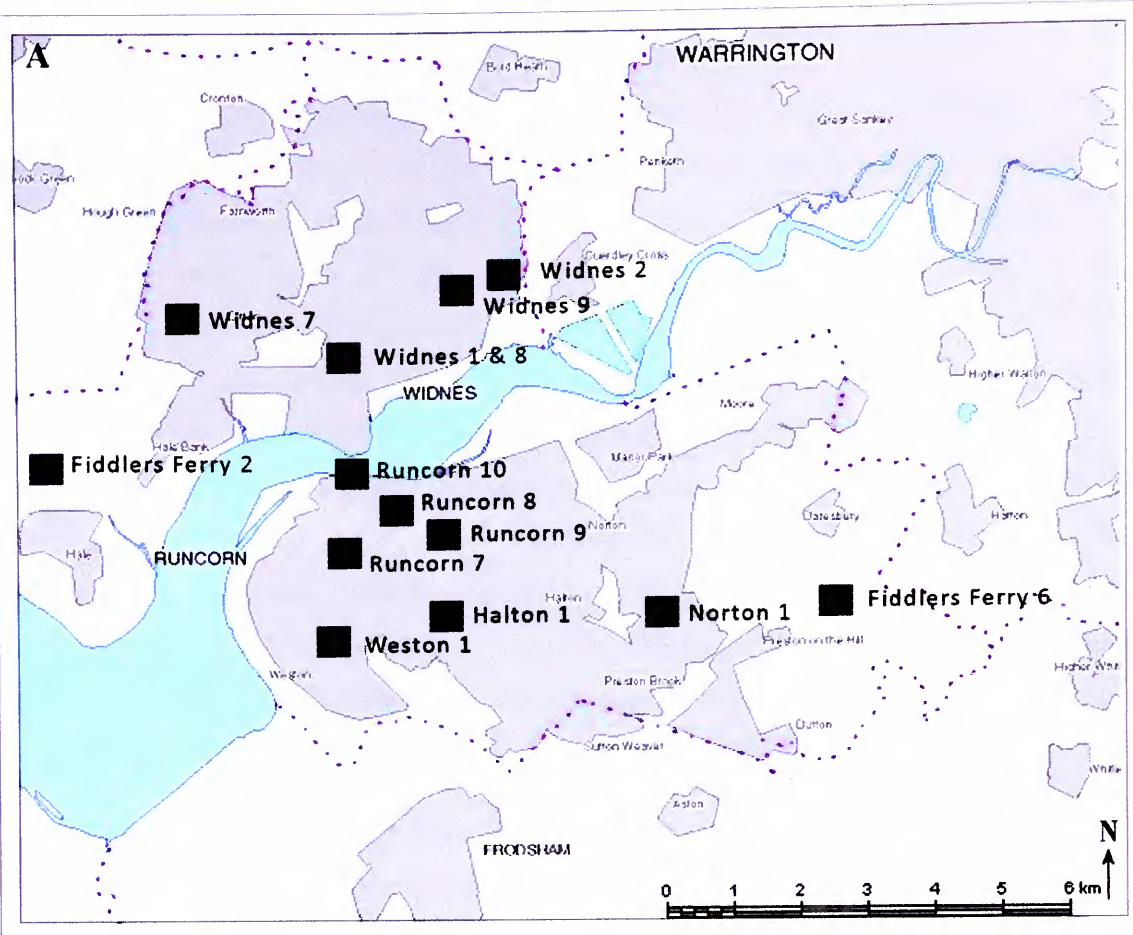

B

Site	Start Date	End Date
Fiddlers Ferry 2	06/04/1965	31/03/1986
Fiddlers Ferry 6	06/04/1967	31/03/1986
Halton 1	04/04/1967	29/03/1982
Norton 1	05/04/1966	31/03/1986
Widnes 1	03/04/1962	03/04/1978
Widnes 2	03/04/1962	02/04/1979
Widnes7	03/04/1962	31/03/1986
Widnes 8	04/04/1978	28/03/1988
Widnes 9	04/04/1978	30/03/1987
Runcorn 7	02/04/1963	04/04/1966
Runcorn 8	02/04/1964	02/04/1984
Runcorn 9	06/04/1965	30/03/1987
Runcorn 10	29/03/1983	31/03/2001
Weston 1	26/03/1968	29/03/1982

Figure 2.6: Location of monitored historical air pollution data (A) and table of sites with available data (B). Monitoring information obtained from the UK National Air Quality Archives. (A): adapted and reproduced from the 2008 Ordnance Survey Strategi 1:925915 map with the permission of Ordnance Survey on behalf of The Controller of Her Majesty's Stationery Office © Crown Copyright Edge Hill University, Ormskirk, Lancashire licence number: ED100020392.

2.4.2. Pre-chemical Halton

Both Runcorn and Widnes are perceived to have been quiet idyllic agricultural villages during the 1700s as transport routes bypassed the towns [Poole, 1906]. Pre-industrial Widnes was described as a charming picturesque village: "*The rustic beauties of the once fair Widnes charmed the eye and produced a pleasant sense of gratification to the one who looked upon them... The rolling flood which for ages upon ages has swept past Widnes Point was then a pure stream, alive with fresh-water fish... Truly Widnes was a charming spot, the superior of which did not exist at any other point either up or down the whole length of the river*" [Poole, 1906]. A serene and pleasant rural Runcorn had the reputation of a health resort: "*Runcorn has always been celebrated for its situation being surrounded by a beautifully romantic and picturesque scenery. It has also the advantages of a salubrious air and mild temperature...*" [Fowler, 1834]; providing air so clean that people came to the town to recuperate from illness and bathe in the Mersey during summer months [Vardy, 2005].

Industry intensified in Runcorn with the completion of the Bridgewater Canal in 1770 [Vardy, 2005], resulting in an increase in barge and ship repairing industries and the export of limestone [Jones, 1969]. However, by the 19th century, quarrying declined and during the early 1800s soap and chemical manufacturing joined quarrying and ship building as the main industries in Runcorn. It was not until the mid-19th century that the chemical industry established in Widnes; prior to this, principle trades included watch making, tool making, file cutting, wire drawing, farming and beer selling, as recorded in the 1841 Census [Warren, 1980].

2.4.3. A history of contamination

The early 'Leblanc' chemical industry involved the production of sodium carbonate, caustic soda, chlorine, ammonia and copper smelting by 'inorganic' chemical industrial methods, for use in textiles, soap and glass manufacturing [Warren, 1980]. Throughout the 19th century Leblanc alkali production dominated the chemical industry. Despite developments in production, methods remained largely unchanged, and involved heating salt with sulphuric acid in lead chambers to produce saltcake, which in turn was heated with coal and limestone to produce black ash, from which alkali was recovered [Dingle, 1982]. Smoke, from the burning of coal and hydrochloric acid gas were emitted via tall

chimneys, and a sulphur rich residue mud known as 'galligu,' were by-products of this process [HBC, 1991].

The first soapworks (Johnson's) in Halton was established in 1803 along the Bridgewater canal (SJ 351411, 382835), followed by Hazlehurst in 1818 [Warren, 1980] (Plate 2.2). The 1828 trade directory lists these works as 'soap boilers and turpentine distillers' [Pigot and Co., 1828]. During the 1830s, soap production rapidly increased at the sites and Johnsons became the second largest works out of Liverpool [Barker and Harris, 1959]. In 1834 the first soapworks in Weston was established, marking the transformation of the village by the chemical industry, with expansion and development of new works. During the mid-19th century Wiggs alkali works was established at Astmoor saltmarsh (SJ 352676, 383435) and other existing industries at this time included tanneries, shipyards, slate works, iron foundries, steam mills, brewery, skin yards, windmill, pin manufacturer, chain works, ropery, gas works, brickyard, pottery and malt kiln, as well as soap boilers and chemical manufacturers [Pigot and Co., 1834; Jones, 1969]. This development was reflected by a six-fold increase in the population of Runcorn between 1800 and 1850 [Vardy, 2005]. In the 1860s the Runcorn Soap and Alkali Company formed, who prospered in the boom in alkali trade in 1861-1875, and constructed a copper works at Weston [Rintoul, 1984; Vardy, 2005].

Plate 2.2: Artwork by Hedley Fitton in: 'History of Runcorn' [Nickson, 1887] depicting Hazlehurst's factory (left) and Johnson's (right) on the Bridgewater Canal.

The opening of the Runcorn Gap and St Helens Railway (1831), and development of the Widnes docks [Poole, 1906] made Widnes an attractive location for prospective chemical manufacturers and soon became an epicentre of the chemical industry [Barker and Harris, 1959; HBC, 1991], which dominated in the northwest of England (Figure 2.7). The first alkali works (Gossage) in Widnes was built along the Sankey canal (SJ 351279, 384290) in 1847 [Warren, 1980] and a boom in chemical trade in 1855 soon made Widnes 'a chemical town' with five chemical works, one oil manufacturer, three sail makers, four file makers, nine wheelwrights, joiner and iron works and 33 furnaces [Warren, 1980].

Approximately 22 Leblanc works were constructed in Widnes between 1847 and 1884 [Warren, 1980]. The establishment of soap works moved from the initial location of the canal to Widnes Marsh (SJ 350281, 384167) (with works constructed here from 1866-1873), and Ditton Road (SJ 350152, 384886) (1870 to 1874) [Warren, 1980], marking a period of outstanding development at Widnes [Warren, 1980; HBC, 1991] (Figure 2.8, Plate 2.3).

The development of the chemical industry in Halton brought immediate consequences of landscape change and pollution [HBC, 1991] (Plate 2.4, Figure 2.9). This was especially noticed in Widnes, when after only a few years of development it was noted that: *"the works that were belching forth volumes of most deleterious gases and clouds of black smoke from chimneys of inadequate height, with trees that stood leafless in June, and hedgerows that were shrivelled in May. The air reeked with gases offensive to the sight and smell, and large heaps of stinking refuse began to accumulate"* [Allen, 1906].

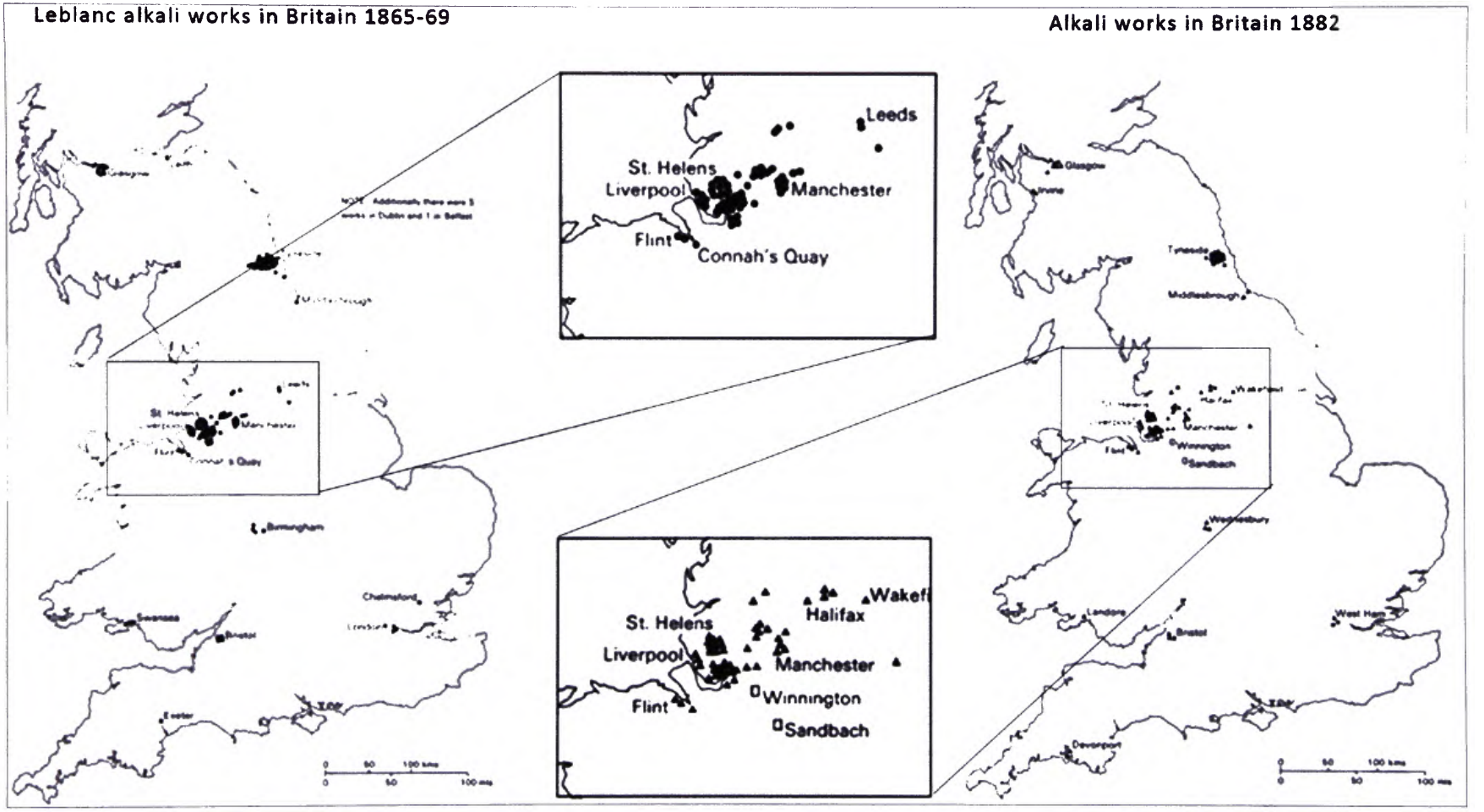

Figure 2.7: Location of alkali works in Britain during the 19th century [Warren, 1980].

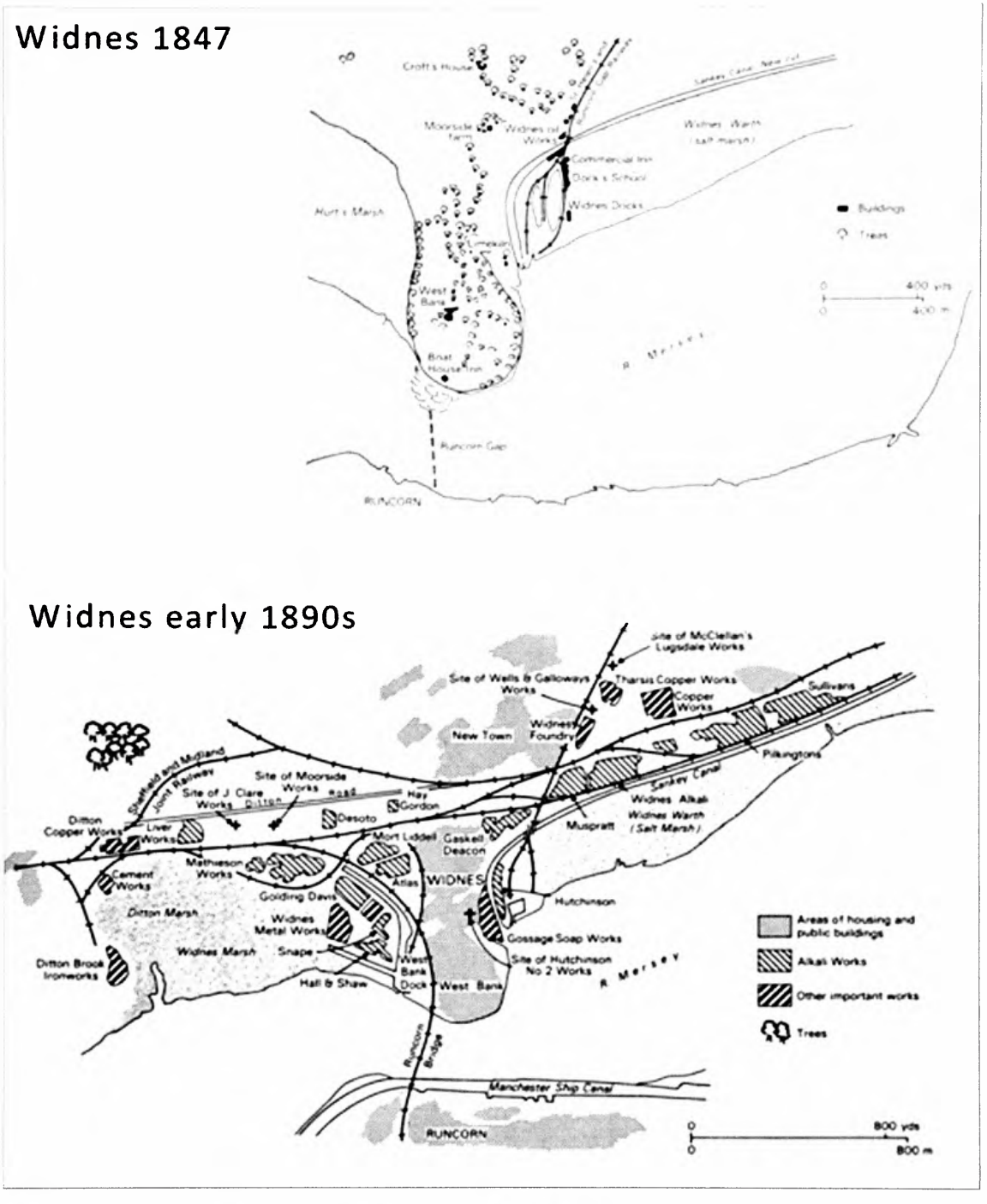

Figure 2.8: Location of industries in Widnes in 1847 and 1890 [Warren, 1980].

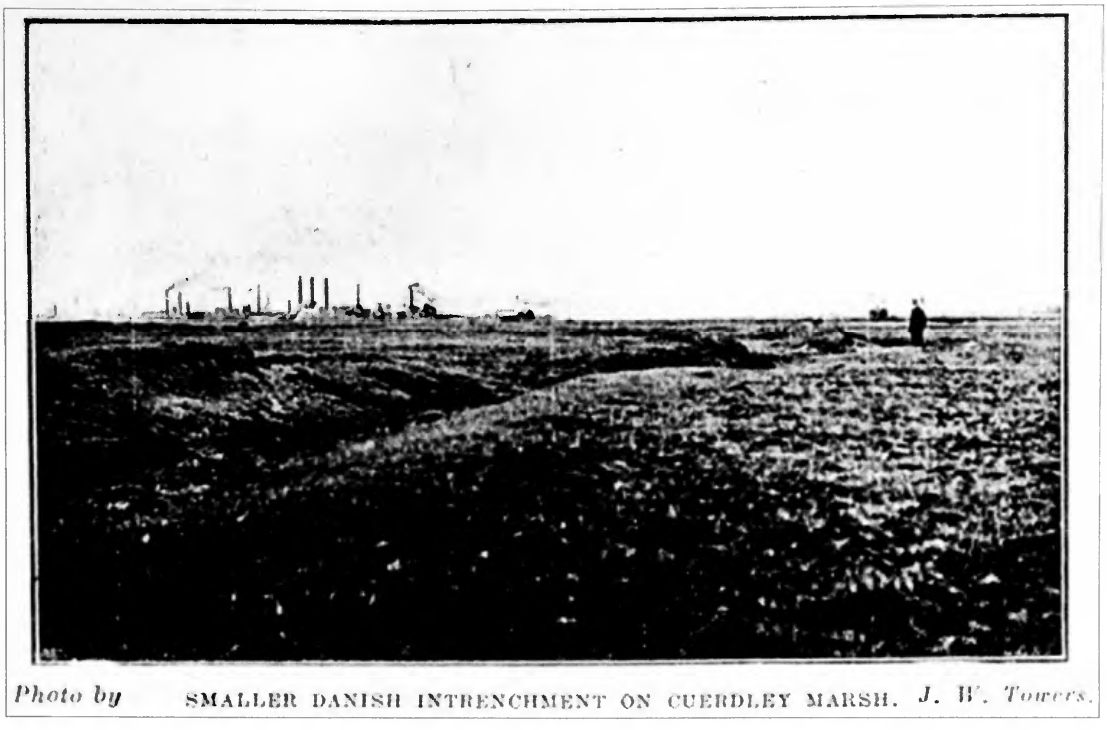

Plate 2.3: Chemical industries at Widnes as seen from Cuerdley Marsh [Poole, 1906].

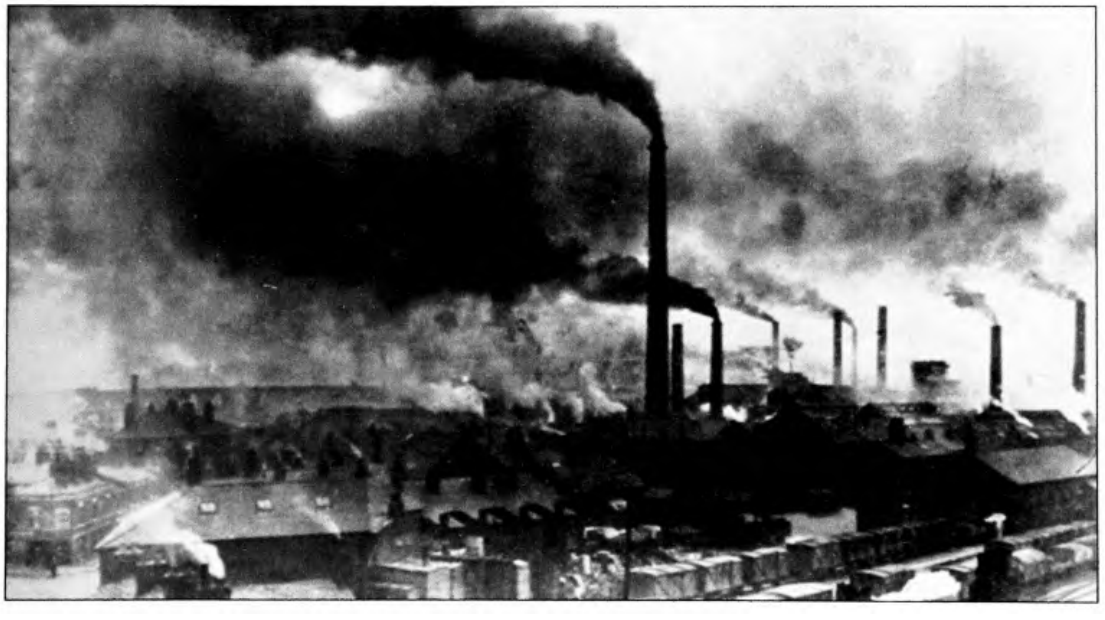

Plate 2.4: Industrial emissions from chimney stacks in Widnes [Hardie, 1950].

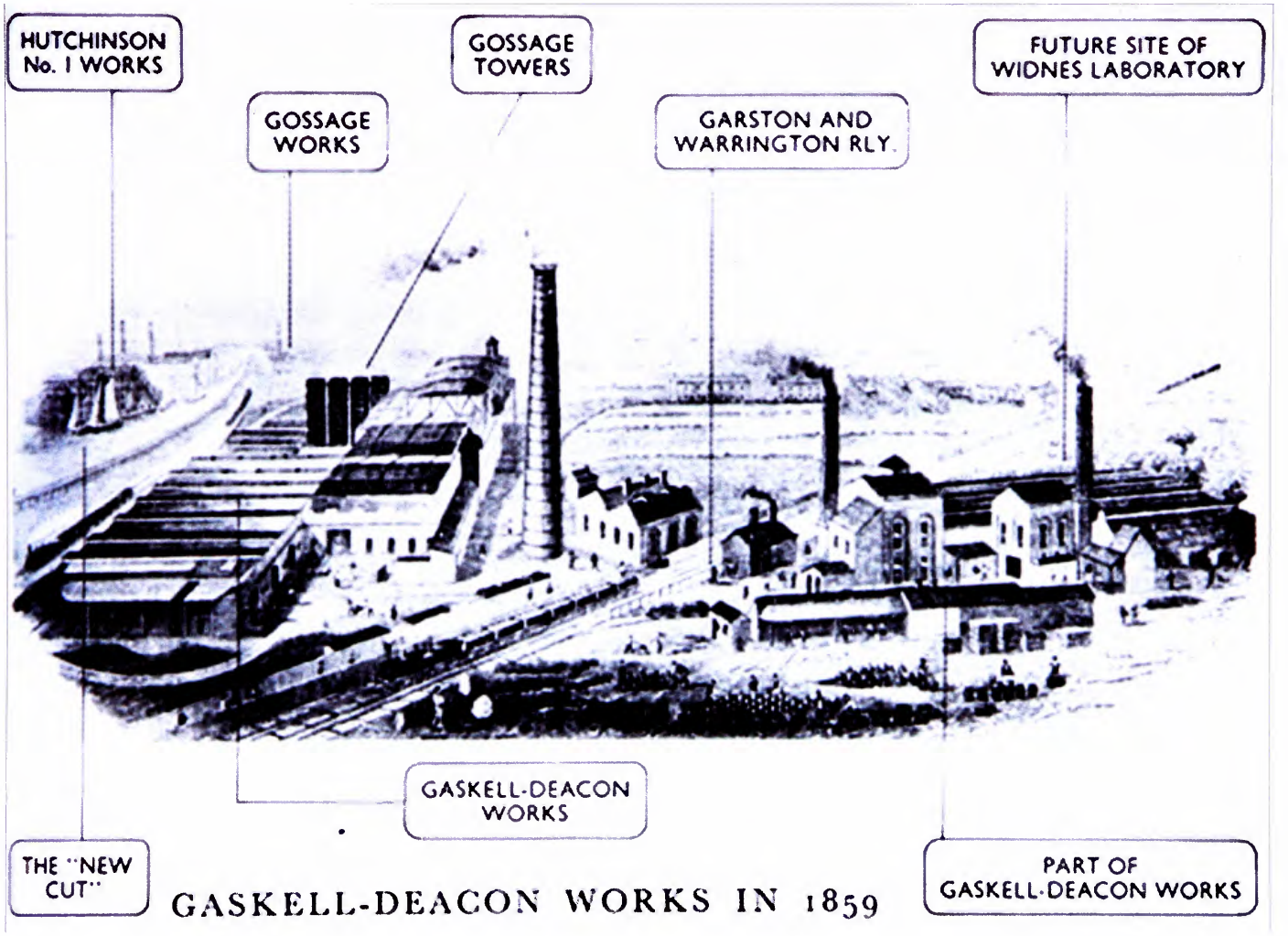

Figure 2.9: Chemical works landscape in Widnes, 1859 [Hardie, 1950].

Described in 1855 as a resort for sunbathing visitors [Warren, 1980] the detrimental consequences for the landscape were also noted in Runcorn: "*All the land within a quarter of a mile from works at Weston and towards Halton from the Runcorn works was useless as a result of the gases and had been acquired by the manufacturers*" by Smith, (Alkali Inspector) in 1867 [Warren, 1980]. Also, Runcorn was described as being *"exposed to the irritating vapour cast off so freely by the large industrial chemical works in its vicinity"* [Annon, 1880]. Smoke was a persistent problem associated with the chemical industry and in 1887, it is estimated that 960 000 tons of coal were used in Widnes [Warren, 1980]; consequently, in 1888 Widnes was described as *"the dirtiest, ugliest and most depressing town in England"* [Diggle, 1961].

In 1872 there were 35 industrial plants in Widnes, 24 of these were chemical works, also three copper works were established to support and diversify chemical manufacturing [Warren, 1980]. By 1884 Leblanc works in Halton started to close due to a recession in the chemical trade, which continued into the 20th century, as electrolytic alkali production superseded the Leblanc process [Warren, 1980]. This less labour intensive method involved the electrolysis of a brine solution to produce caustic soda and bleaching powder [Warren, 1980]. In 1914 the Castner Kellner works at Weston started production using mercury cell technology, and war time demand for chlorine (WW1 1914-18) that continued into the 1920s, sustained production at this site [Rintoul, 1984].

Twentieth century technological advances in the chemical industry, particularly the synthesis of organic chemical compounds and petrochemicals, led to corporate mergers in Halton, most notably the formation of Imperial Chemicals Industry (ICI) in 1926 [Carter, 1964; HBC, 2005]. The ICI merger bridged the gap between old and new chemical methods and led to a diversification of different types of manufacturing processes and the expansion of organic chemicals, such as fertilisers, plastics, polymers, pesticides and pharmaceuticals [Campbell, 1971; HBC, 1991, 2005]. Tanneries began to close from the 1950s due to the introduction of plastics, which led to ICI replacing tanneries as major employers in Halton [Jones, 1969]. Chemical production expanded throughout the 20th century. However, ICI dominated the industry with several sites existing throughout Halton producing fertilisers, dyestuffs, industrial chemicals, printing materials, paints, polymers, plastics and pharmaceuticals, chlorine and chlorinated solvents, fluorinated refrigerants, aerosol propellants, insecticides and pesticides [Carter, 1964; Jones, 1969].

A 1956 survey of industrial process in Widnes identified 52 major factories manufacturing heavy chemicals, metals, soap, gelatin, glue, bone meal, animal food and fertilizers. Also, cement, asbestos, insulating materials, furniture and light engineering products were produced in premises throughout Halton. Sixty-two chimneys attached to boiler plants and 37 chimneys from other processes were identified, as well as numerous vents and openings that emitted smoke and fumes from industrial processes [HBC, 2001]. The demise of tanneries continued throughout the 1950s and 1960s in Runcorn [Runcorn and District Historic Society, n.d.].

Rapid growth and industrial expansion were experienced in Halton in the 1960s and 1970s when Runcorn was designated as a 'New Town' [Ling, 1967; HBC, 2003] (Figure 2.10). Despite this, many industrial closures occurred throughout Halton from 1976 and 1986 with a rapid decline in the chemical industry [HBC, 1991]. In the 1990s, ICI factories were taken over by petrochemical company INEOS, who have since expanded production and technologies, to shape the present day industry in the borough [HBC, 2003, 2005(a)].

Although chemical manufacturing has dominated industry in Halton (Figure 2.10), other industrial processes have occurred in the area, such as the manufacturing of leather, asbestos, alloys, gasworks, coke works and power generation (Table 2.2), resulting in a mixture of chemicals and pollutants released to air, water and land. A legacy of environmental contamination remains from the extensive amount of industry Halton has experienced since the 19th century. In particular, the early chemical industry and the wasteful Leblanc process widely used in the area from 1800s-1920 has caused extensive land contamination and released unknown quantities of pollutants into the air from coal combustion and the use of metal vats and equipment for chemical processes [HBC, 1991].

The contamination of land and waterways is a persistent problem, especially from the tipping of galligu throughout Halton and Widnes Marsh prior to controls. The full extent of contamination is unknown, with vast areas in Halton classified as 'potentially contaminated land' [HBC, 1991, 2003]. This is also true for the extent of air pollution experienced in the borough, the history of which is difficult to quantify due to inconsistent pollution data and, unlike the disposal of solid waste from industry, the composition of past atmospheric emissions are more difficult to 'rediscover'.

Figure 2.10: Runcorn New Town Development [Ling, 1967].

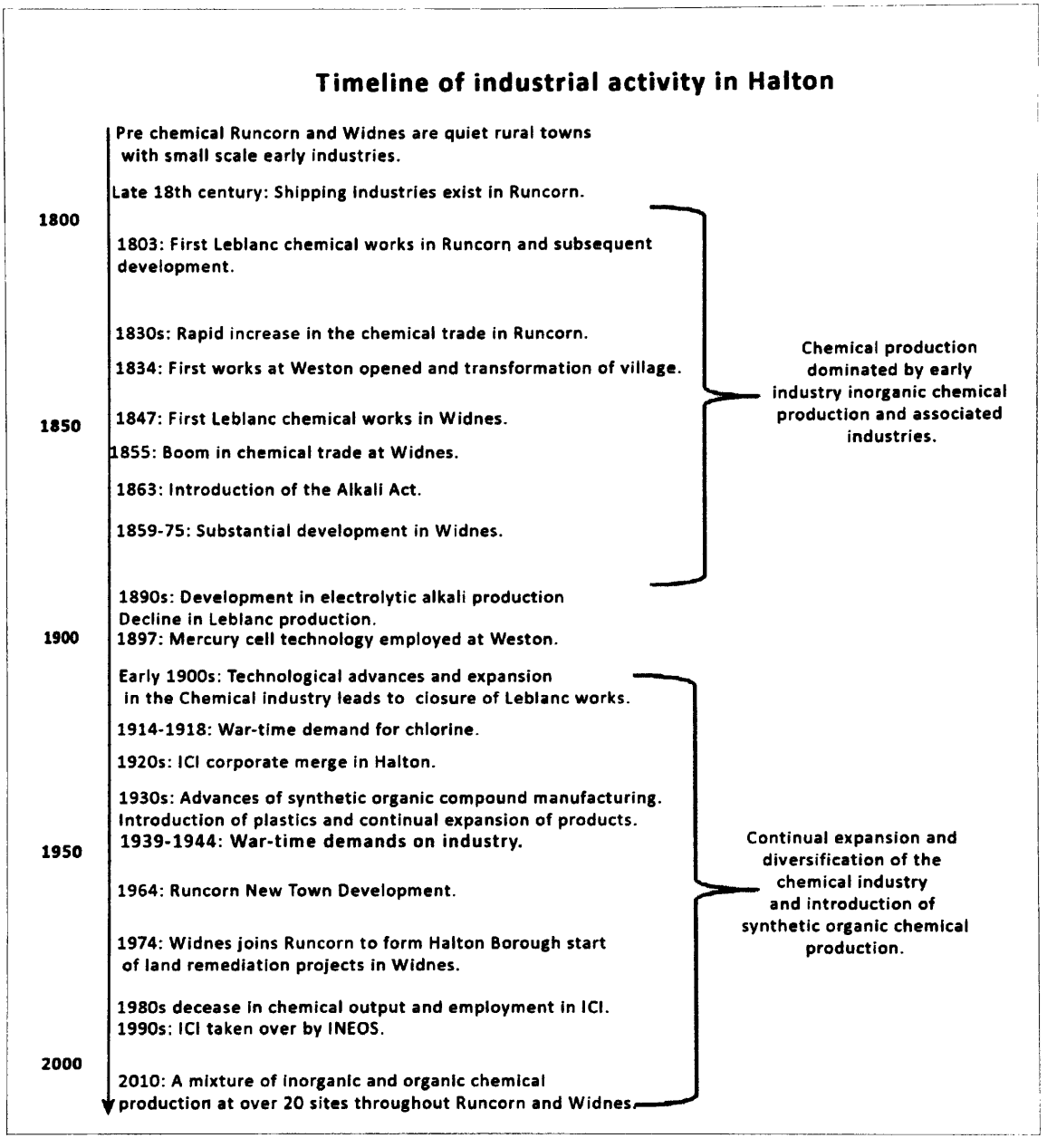

Figure 2.11: Timeline of industry in Halton.

Table 2.2: Estimated number of historical sites in Halton over time for each land use [HBC, 1991].

Land use	Estimated number of sites
Asbestos manufacture and use	2
Organic and inorganic chemical production (not included elsewhere)	62
Gasworks, coke works, coal carbonisation etc.	3
Radioactive materials, processing and disposal	1
Waste disposal sites, including hazardous wastes, landfills, filled pits and quarries, incinerators, sanitary depot, drum and tank cleaning, solvent recovery	40
Oil refining petrochemical production and storage	0
Pesticide manufacturing	1
Fine chemicals, dyestuffs and pigments manufacturing	1
Paint, varnished and ink manufacturing	1
Animal slaughtering and by-products (including soap, candle and bone works, detergent manufacture)	11
Tanning and leather works	10
Metal smelting and refining	5
Explosives manufacturing	0
Iron and steel works	2
Scrap yards	20
Engineering	3
Rubber products and processing	0
Tar bitumen, linoleum, vinyl and asphalt works	0
Concrete, ceramics, cements and plaster works	10
Mining and extractive industries	1
Electricity generation	1
Film an photography processing	0
Manufacture of disinfectants	0
Paper and printing works	0
Glass manufacturer	0
Fertiliser manufacturer	2
Timber treatment works	4
Sewage treatment works	2
Garages (including sale of automobile fuel)	50
Transport depots	10
Railway land (yard and tracks)	10
Electrical and electrics manufacture	3
Textiles manufacturing and dying	0
Laundries and dry-cleaning	0
Plastic products manufacture, building materials, fibreglass	5
Dockyards and wharves	3
Food processing	2
Airports	0

2.5. Health in Halton

Perceived health concerns amongst the Halton population has resulted from the extensive industrial legacy, contamination incidents, industrial emissions and industrial odours experienced within the borough; combined with the known health effects of pollutants and increased exposure via residency at close proximity to industry [Burgess *et al.*, 2003]. Repeated ranking with some of the highest mortality and morbidity rates in the UK [HPCT, 2004; Association of Public Health Observations (APHO), 2007] has prompted the local health authority, Halton Primary Care Trust (HPCT), to investigate the causes of ill health among the population.

2.5.1. Health inequalities

Halton is an unhealthy borough, ranked as having the worst rate of early deaths from cancer in the whole of England and Wales, followed by Liverpool and Manchester, respectively (Table 2.3) [APHO, 2007]. This is a 41% difference from the national average [APHO, 2007] and has risen by 10% in Halton from 2006 to 2007 [APHO, 2007]. Halton has the third lowest female life expectancy at birth in England and Wales [APHO, 2007], and the sixth lowest for males (74.3 years, with the lowest male life expectancy of 74.2 years occurring in Manchester). Standard mortality ratios (SMR) of several diseases and illnesses in Halton also reveal elevated levels of ill health when compared to the northwest region and the national average (Table 2.4).

There are several health indicators with prominent SMRs in Halton including all cancers, all circulatory diseases and coronary heart disease, with coronary heart disease accounting for 40% of all deaths in Halton [HCPT, 2004]. Although SMRs for bronchitis, emphysema and asthma are below the national and regional averages, incidences of lung disease are higher (Table 2.3). Mortality from liver disease in Halton is 50% higher than national average with mortality rates higher than 70% compared to the national average in females [HCPT, 2004]. Over 20% of Halton residents have a limiting long-term illness, again higher than the national average [HPCT, 2004]. These health indicators depict a low standard of health in Halton and have justified further investigation as to why, compared to the rest of England, Halton stands out as having poor health.

Table 2.3: 2004-2006 data for two health indicators that demonstrates 'unhealthy' boroughs within the UK [http://www.apho.org.uk APHO, 2007].

Borough	Life expectancy at birth for females (years)	Borough	Early deaths from cancer (SMR)
Liverpool	78.7	Halton	167.8
Hartlepool	78.6	Liverpool	166.0
Halton	78.4	Manchester	165.8
Manchester	78.3	Corby	157.0
Blackpool	78.3	Knowsley	155.7

Table 2.4: Health indicators for Halton, England and the Northwest. Source: adapted from Burgess *et al.*, [2003]. (North West Public Health Observatory local area statistics and Department of Health compendium of clinical health and health indicators, 2001). Highlighted data illustrates poorer health compared to England and Northwest region.

Health Factor	England	Northwest	Halton
Mortality from all causes, all ages (SMR) 1998 to 2000	100.00	111.52	120.02
Mortality from all cancers, all ages (SMR) 1998 to 2000	100.00	109.42	127.90
Mortality from coronary heart disease, all ages (SMR) 1998 to 2000	99.00	115.65	133.26
Mortality from all circulatory diseases, all ages (SMR) 1998 to 2000	100.00	112.75	123.43
Mortality from Bronchitis and Emphysema, all ages (SMR) 1998 to 2000	99.00	94.78	95.14
Mortality from Asthma, all ages (SMR) 1998 to 2000	100.00	100.04	91.60
Incidence of lung cancer, indirectly Standardised Registration Ratios (SSR) all ages 1996 to 1998	100.00	124.17	159.60
Mortality from stroke, all ages (SMR) 1998 to 2000	100.00	113.69	113.35
Mortality from suicide, all ages (SMR) 1998 to 2000	99.00	114.19	127.84
Life expectancy at birth, number of years 1997 to 1999 males	75.20	73.69	72.70
Life expectancy at birth, number of years 1997 to 1999 females	80.10	78.73	76.79

Spatial variations of health inequalities are also demonstrated throughout Halton at ward level. Mortality rates for all causes and all ages are highest in the wards of Appleton and Broadheath (Widnes), Norton South, Halton Lea and Heath (Runcorn) (Figure 2.12). However, these mortality rates show a more detailed indicator of ill health when standardised for premature mortality among the population under 75 years of age. These mortality rates, when divided into deaths from all circulatory diseases (Figure 2.14) and all cancers (Figure 2.13) demonstrate that Riverside, Broad Health, Appleton, Grange, Windmill Hill and Norton South experience high mortality from both causes. These potential 'clusters' of ill health are also reflected by high rates of residents with a limiting long-term illness and, self-reported, 'not good health' [HPCT, 2004]. The healthier wards within Halton appear to be Hale, Birchfield, Norton North and Daresbury, which display lower mortality rates.

Reasons for these health inequalities have been initially explored in Halton, and a recent report by Burgess *et al.*, [2003] compared the health in Halton to 'comparative boroughs' and stated that the overall picture of health 'was not markedly different from rates experienced in similar areas elsewhere' [Burgess *et al.*, 2003]. However, this study compared the ill health of Halton alongside other relatively 'unhealthy' boroughs of St Helens, Knowsley, Hartlepool and Middlesbrough [APHO, 2007]. The report also highlights high levels of airborne pollution loads experienced in Halton; however, due to insufficient spatial and temporal pollution data, no link with health could be identified and emphasis was instead placed on socio-economic factors (such as deprivation and lifestyle). Environmental factors, not fully explored in previous studies, may be playing a greater part in the ill health of the population and should not be underestimated in a heavily industrialised area such as Halton.

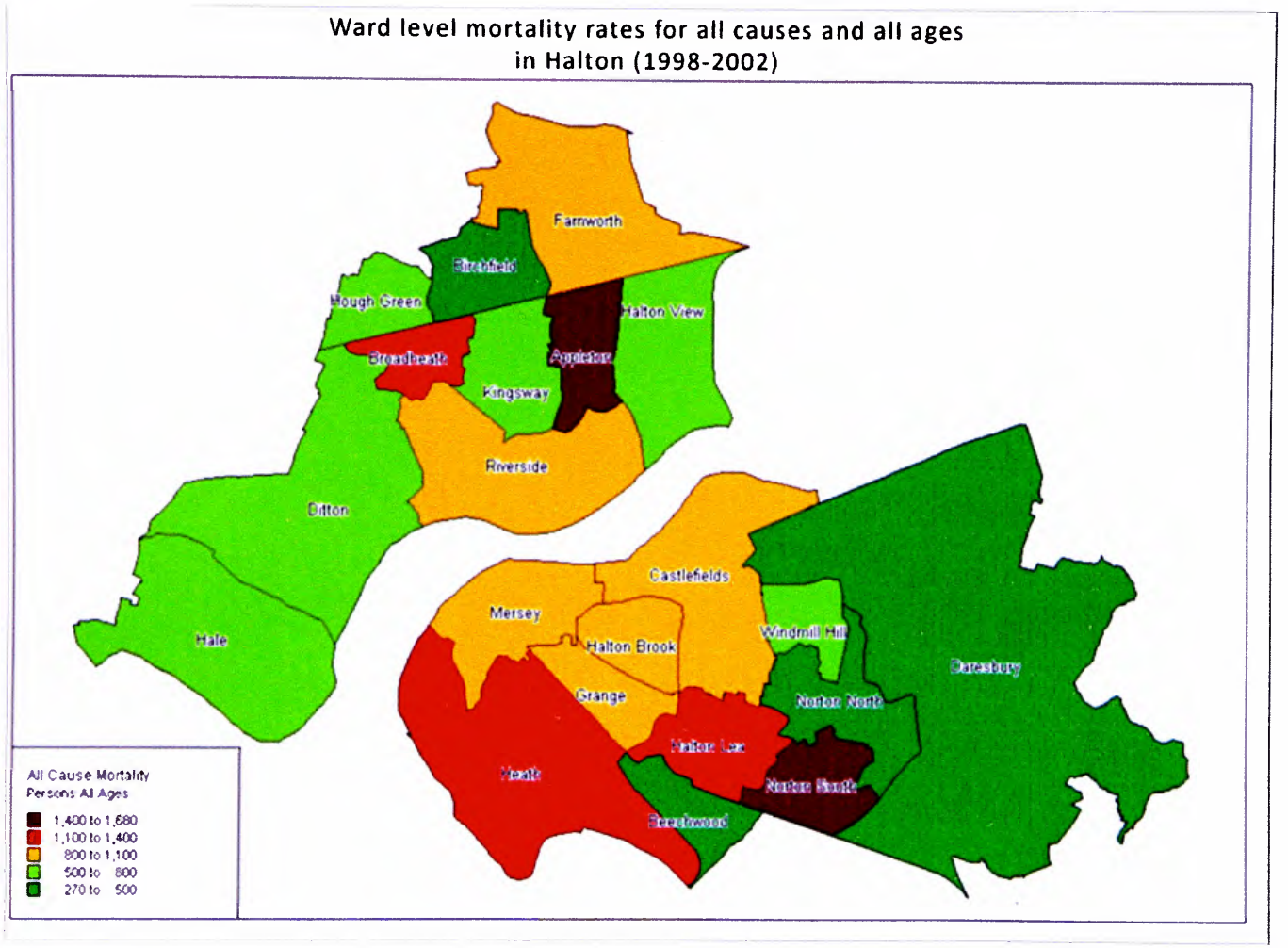

Figure 2.12: Ward level mortality rates in Halton for all causes and ages (1998-2002) [HCPT, 2004].

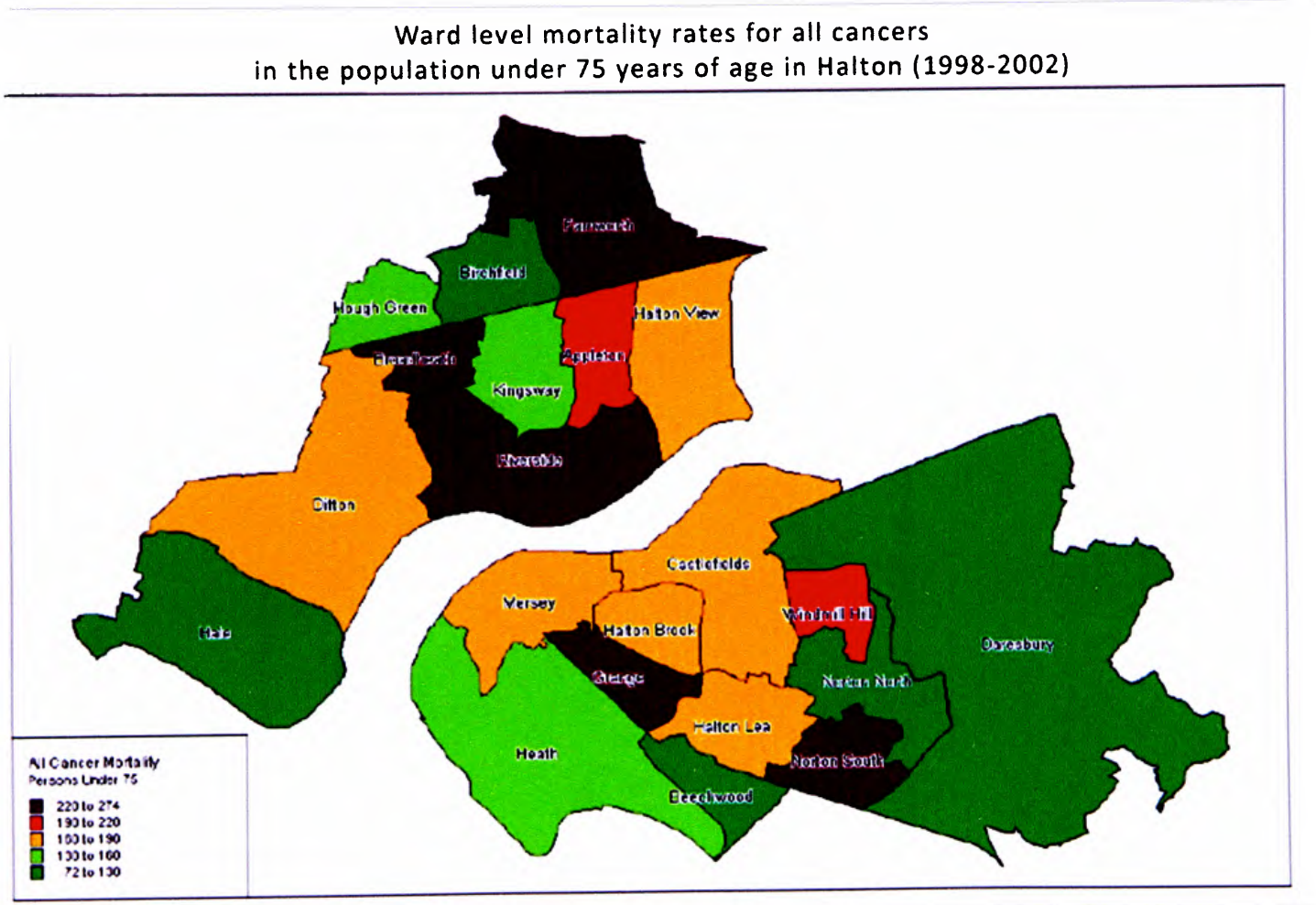

Figure 2.13: Ward level premature mortality rates in Halton for all cancers (1998-2002) [HCPT, 2004].

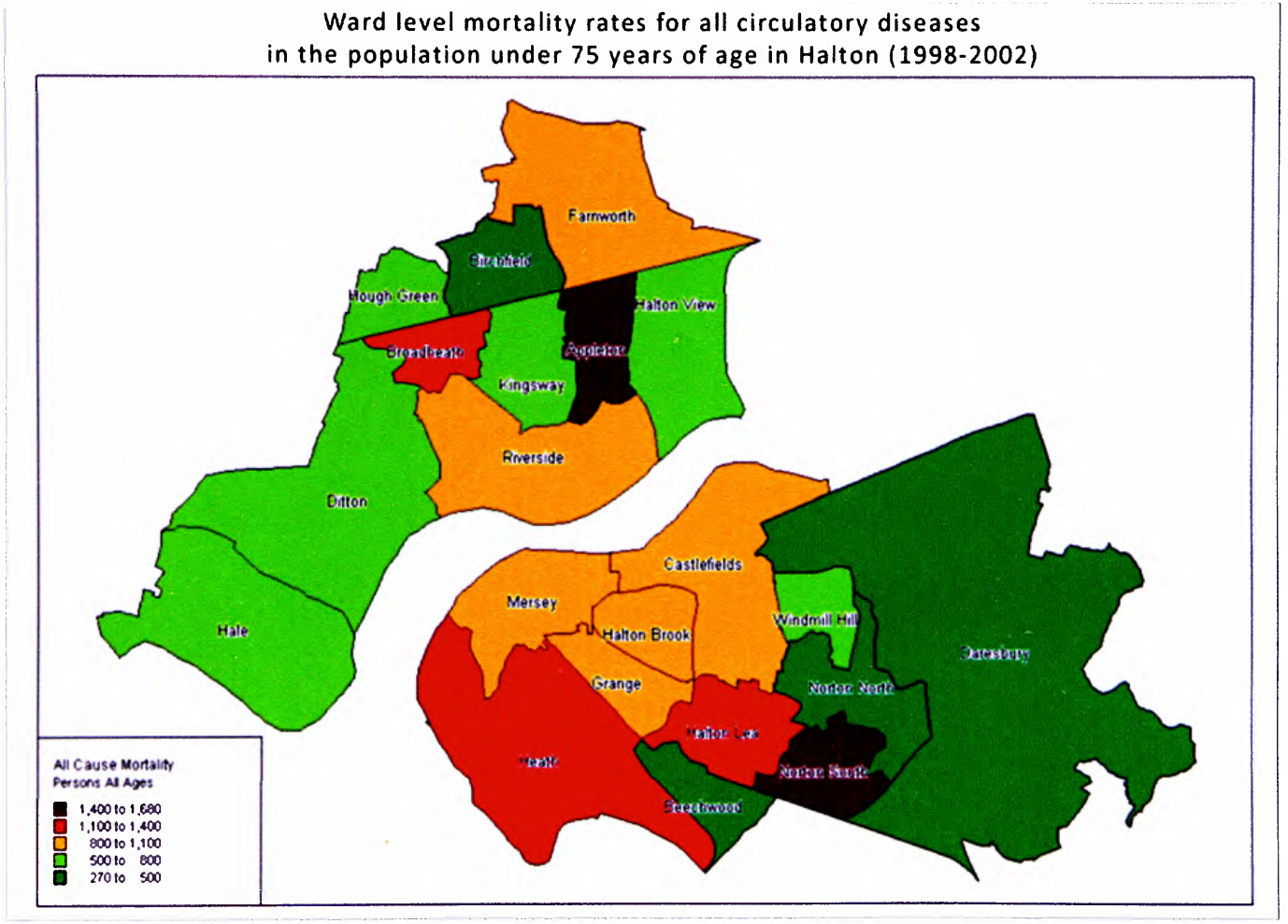

Figure 2.14: **Ward level premature mortality rates in Halton for all circulatory diseases (1998-2002) [HCPT, 2004].**

2.5.2. A cause for concern: the contamination of Halton

In the 1990s, ICI conducted a voluntary investigation called the 'Pathways Project' to assess any human risk from local industry in Halton [Hodgson, 2005] which, in 1999, revealed a contamination incident at Weston (Plate 2.5). Two redundant quarries previously used to dispose industrial waste (lime, demolition waste, chlorinated solvents, chemical catalysts and boiler ash) from 1917 to 1972 were investigated. The analysis of boreholes identified the presence of a toxic, chemical gas hexachlorobutadiene (HCBD), a renal toxicant produced as a by-product from the manufacture of chlorinated hydrocarbons. Further investigation revealed 140 homes in Weston with elevated HCBD levels, and residents were relocated to Daresbury [Vidal, 2000; Staples *et al.*, 2003].

Plate 2.5: View of Ineos Chlor Ltd, Ineos Fluor Ltd and SE Generation Ltd industrial sites at Weston Point (SJ 349763, 381014) from nearby residential village of Weston Point. Facing west 07/06/2007.

Health checks identified renal abnormalities, which reduced after relocation; however, the defects were not specific to HCBD exposure [Staples *et al.*, 2003; Hodgson, 2005]. A wider investigation into the health of the Halton population was requested by the Department of Health. Small area health studies unit (SAHSU) data of kidney disease were mapped throughout the borough. Results revealed a higher than expected risk not only in Weston, but also throughout Halton, suggesting that other toxic pollutants, released to air across the borough may be causing a larger contamination incident than originally thought,

[Hodgson *et al.*, 2004; Alex Stewart *Pers. Comm.*]. This was further investigated by Hodgson *et al.*, [2004, 2006] who observed a pronounced relationship between mortality from renal disease and historical exposure estimates (from 1981 to 2001) in areas at close proximity to nephrotoxic emitting industries, such as chlor alkali plants, solvent emitting industries and power stations.

These initial studies, investigating potential links between environmental pollution and community health in Halton, highlight the importance of investigating the *historical*, as well as contemporary, releases of air pollutants, to better understand the toxic effects of industrial emissions [Burgess *et al.*, 2003; Hodgson *et al.*, 2004; Staples *et al.*, 2003; Hodgson, 2005]. Therefore, the cross-regional air pollution signal preserved in urban pond sediments throughout Halton and the LMR, requires investigation to reconstruct a detailed history of air pollution experienced since the intensification of industry in Halton during the 19th century.

2.6. Chapter summary

Halton is an extensively industrialised borough that has experienced indiscriminate releases of pollutants to air since the intensification of industry in the early 19th century. Due to limited available historical pollution data, it is important to investigate the sedimentary air pollution signal of Halton and the LMR, especially as the borough experiences high mortality and morbidity amongst its population. There is high potential for the industrial legacy of the past to be impacting present day community health, an important epidemiological link that requires a retrospective assessment of population exposure to air pollution.

3. CHAPTER THREE: METHODOLOGY

3.1. Chapter overview

This chapter details the desktop, field and laboratory techniques and data analyses applied to reconstruct proxy pollution histories from the sediments of urban ponds.

3.2. Introduction

Although the potential for urban pond sediments to be used as archives of pollution contamination has only recently been recognised (Section 1.4.5.), the environmental analyses adopted in this work are widely used in palaeolimnology [Norton *et al.*, 1992; Veselý *et al.*, 1993; Solovieva *et al.*, 2005; Cantwell *et al.*, 2007]. The range of methodologies employed to retrieve a long-term (~300-year) record of pollution from urban ponds can be divided into four main stages of analyses (Table 3.1):

(i) identifying suitable sites (Section 3.3.);

(ii) retrieving urban lake sediments (Section 3.4.);

(iii) analysing the composition of the lake basin (Section 3.5.); and

(iv) distinguishing the atmospheric pollution signals (Section 3.6.).

Table 3.1: Stages of the methodology applied to reconstruct pollution histories from urban lakes.

Stage of method	Techniques employed	Main aims	Section
(I) Identification of suitable sites.	Desktop survey and site visit (site selection process) studies of historical maps (supported by Pb^{210} dating in phase III).	To identify potential sites of suitable longevity (~150 – 200 years) within the urban landscape.	3.3.
(II) Retrieval of sediment cores and basin morphology.	Fieldwork: core sample collection.	Sediment core retrieval.	3.4.
	Basic sediment description.	Identification of artificial clay lining.	3.5.2.
(III) Characterisation of basin fill composition.	Mineral magnetism characterisation.	Identify down-core trends in magnetic properties, determine contributions of catchment, atmospheric and authigenic sources of magnetic grains.	3.5.4.
	Particle size analysis.	Assess down-core variations in particle size distributions.	3.5.5.
	Elemental analysis.	Determine the composition of the lake sediment.	3.5.6.
	^{210}Pb analysis.	Determine a chronology for the lake stratigraphy.	3.5.7.
	Organic matter content.	Assess contribution of OM to lake stratigraphy.	3.5.8.
	Spheroidal carbonaceous particulate analysis.	Determine a record of anthropogenic atmospheric particulate deposition.	3.5.9.
(IV) Data analysis and identifying the pollution signal.	Presentation of down-core variations in environmental proxies.	Investigate down-core trends in trace metal concentrations.	3.6.1.
	Establishing and extrapolating the ^{210}Pb chronology.	Extrapolate dates for the entire lake stratigraphy, calculate sediment accumulation rates to assess the supply of sediment to the lake over time.	3.6.2.
	Correlation coefficients and statistical analyses.	Identify statistically significant relationships between the environmental proxies.	3.6.4.
	Trace metal enrichment factors.	Assess the anthropogenic contribution of total trace metal concentrations to the lake.	3.6.5. and 3.6.6.
	Flux data.	Assess the supply of magnetic grains and trace metals to the lake over time.	3.6.7.

3.3. Identification of suitable urban ponds

The use of urban pond sediments in palaeolimnological studies is limited [Charlesworth and Lees, 2001; Meriläinen *et al.*, 2003; Dauval'ter, 2004; Tylmann, 2005], therefore, the retrieval of intact, undisturbed and reliable sediment cores from within the urban environment is of the utmost importance and requires extensive investigation [Norton, 1986]. A systematic site selection process was adopted (Figure 3.1), which involved investigating over 100 pond sites within the LMR (Appendix A, Table A1). A specific set of criteria for urban ponds were applied in order to identify sites that had the potential to yield appropriate sediment stratigraphies and environmental histories: (i) suitable location; (ii) sufficient age and (iii) limited sediment disturbance.

(i) Suitable location:

Proven longevity within the urban landscape is imperative in reconstructing an historical urban air pollution record. Therefore a range of Ordnance Survey (OS) maps of various scales and editions (Table 3.2) were used to identify potential sites that have been part of the urban environment since the mid 1800s as ponds within Halton will have potentially received atmospheric fall out from a range of various local industrial sources that have existed throughout and surrounding the borough. However, sites outside of this modern urban sprawl, have also been investigated to explore the cross-regional (LMR) pollution signal. It is important to explore this large scale regional urban signal since the transport of air pollution is not restricted to administrative boundaries and, therefore, pollution sources in surrounding urban areas, such as Warrington and Liverpool, may also contribute to the air pollution experienced in Halton. Site location is, therefore, crucial to reconstruct an historical cross-regional pollution signal for the LMR.

Table 3.2: Collections of maps used to determine age and permanence of potential pond sites.

	Map collection and scale	Map age
Contemporary	Ordnance Survey Explorer 275 1:25000	2000
	Online Ordnance Survey collection (Available via digimap.edina.ac.uk/carto) Variety of scales from 1:1250 to 1:250 000	2004-2008
Post 1846 Historic Landmark Collection (available via digimap.edina.ac.uk/historic)	Country Series 1: 10560 (1846 – 1969)	1st Edition: 1849-1899 1st Revision: 1888-1914 2nd Revision: 1900-1949 3rd Revision: 1922-1969
	National Grid 1: 10560 (1948 – 1976)	1st Imperial edition: 1948-1977 1st Revision: 1949-1981 2nd Revision: 1959-1982 3rd Revision: 1967-1976
Tithe maps 1840s	Parish of Runcorn 1: 24000	1844

(ii) Sufficient age:

The permanence of each pond site was determined from historical maps. Ponds that have existed for ~200 years are imperative in order to reconstruct an environmental history of pollution contamination that spans back to before industry intensified in the Halton area (circa. 1800). First edition OS maps (circa. 1849-1899) provided a baseline date of ~150 years, then Tithe maps (dating back to the early 19th century) further helped to validate the longevity of sites. Eliminating ponds of insufficient age helped to condense an extensive database of potential sites. To further determine the age of sites, historical records from local libraries and record offices provided additional supporting evidence.

(iii) Limited sediment disturbance:

Ponds with minimal sediment interference are favoured to yield accurate undisturbed stratigraphies. However, many urban ponds and lakes undergo management in which sediment at the bottom of the pond is dredged to maintain a healthy ecosystem, and to prevent the pond from naturally drying up. By identifying historical changes in the shape and size of ponds, and their surroundings, the anthropogenic influence on each site was assessed using a series of OS map editions and revisions. To further assess possible

management and sediment disturbance, favourable attributes such as muddy lake margins, absence of duckweed (*Lemnaceae)* on the water's surface and absence of structures such as fishing posts and fallen trees were observed and noted during site visits. The management histories of the sites were further investigated via consultations with land owners/managers. However, some sites lacked any documented management records and the only way to determine the suitability of the site was to attempt core extraction and to employ magnetic analyses to ensure that the sediment column was undisturbed [Thompson *et al.*, 1980].

For potential sites that met the necessary criteria, landowners/managers were approached to obtain permission to extract sediment cores and subsequent method statements and risk assessment documents were produced; however, permission was not granted in all cases, which restricted the number of potential sites investigated. The sampling protocol is summarised in Figure 3.1 which details the steps applied to identify suitable urban ponds.

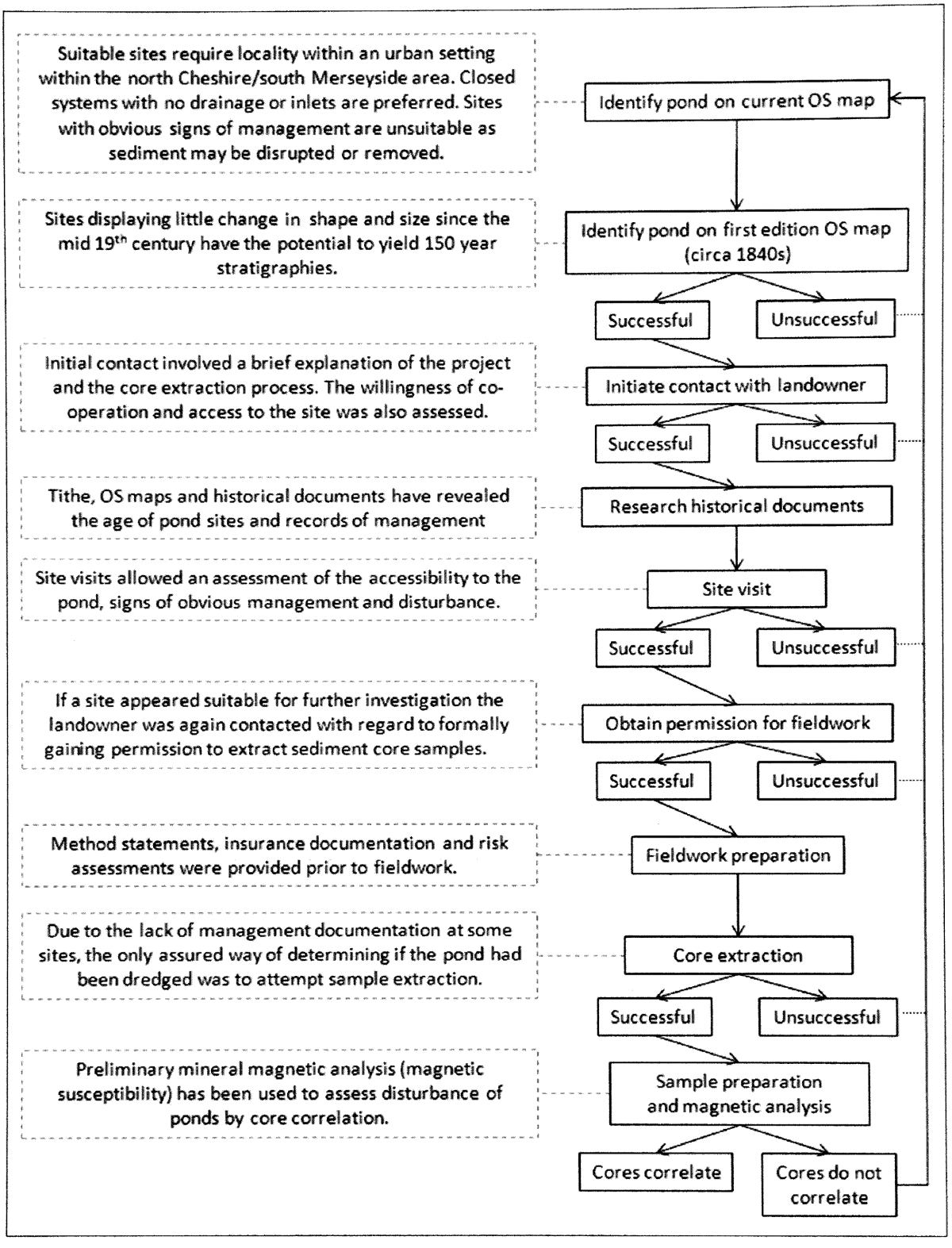

Figure 3.1: Protocol of the site selection process.

3.4. Retrieval of urban lake sediments: collection of sediment cores

A Gilson hand-held gravity corer, designed for collection of sediment from soft-bottomed shallow lakes (http://www.duncanandassociates.co.uk/equip.htm#corer) typical of urban ponds, was used to retrieve short (<1 m) sediment cores samples [Pirrone *et al.*, 1998; Frignani *et al.*, 2004; Rose *et al.*, 2004(a); Kienel *et al.*, 2005; Blake *et al.*, 2007]. The Gilson mechanism was fitted with a plastic sample tube with an inside diameter of 0.06 m and either 0.5 m or 1 m length. A series of interlocking aluminium rods were then attached to the corer and, with the aid of a small boat secured in position by ropes tied to nearby trees, the corer was lowered into the centre of the pond (Plate 3.1). The centre of the lake is commonly the deepest part, with the greatest accumulation of sediment at the basin [Boggs, 1995].

Maintaining the corer in a vertical position at all times, the Gilson was gently lowered through the water column and pushed through the soft bottom sediment. A valve within the Gilson allowed water to pass through freely as the corer was lowered through the water column. The valve was then closed as the corer was lifted back to the water surface, creating a vacuum-like condition within the tube and reducing hydrostatic pressure. This prevented the sediment sample from sliding out of the bottom of the plastic core tube [Wright, 1991; Smol, 2002] (Figure 3.2). To retain the sediment sample, a rubber bung was inserted into the bottom of the plastic tube before the corer was raised out of the water. The plastic sample tube was then detached from the Gilson, and a second bung inserted into the top of the tube to secure the sediment core sample for transportation.

The top of the resulting core sample demonstrates the water-sediment interface and, therefore, the most recent layers of sediment, with age progressing with core depth. Where possible, multiple replicate cores were taken from each site. However, due to the small size of some of the ponds, this was limited due to disturbance of the lake sediment when collecting previous cores. Care was taken to keep the sample in an upright vertical position so as not to disturb the sediment sequence. Cores were then labelled and secured for transportation (Plate 3.2). Samples were returned to Edge Hill University and stored in a refrigerated room (<5 °C) to restrict biological activity from occurring within the sediment and, therefore, sediment disruption.

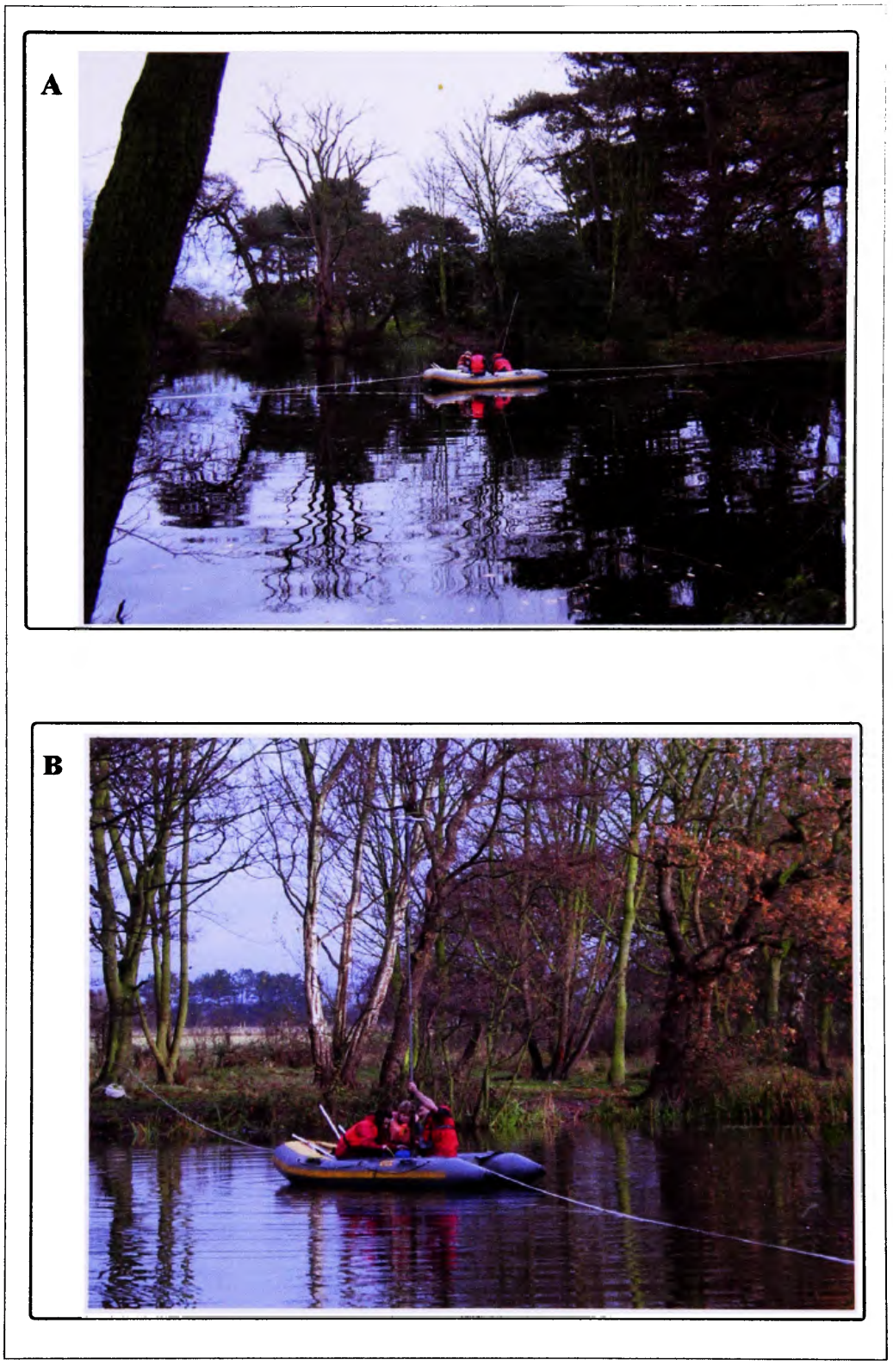

Plate 3.1: Core collection at: Speke Hall: SJ 341960, 382789, 03/12/2004. Showing central positioning of boat in lake with corer lowered into the water (A) and retrieval of sediment core (B). Source: Ann Worsley.

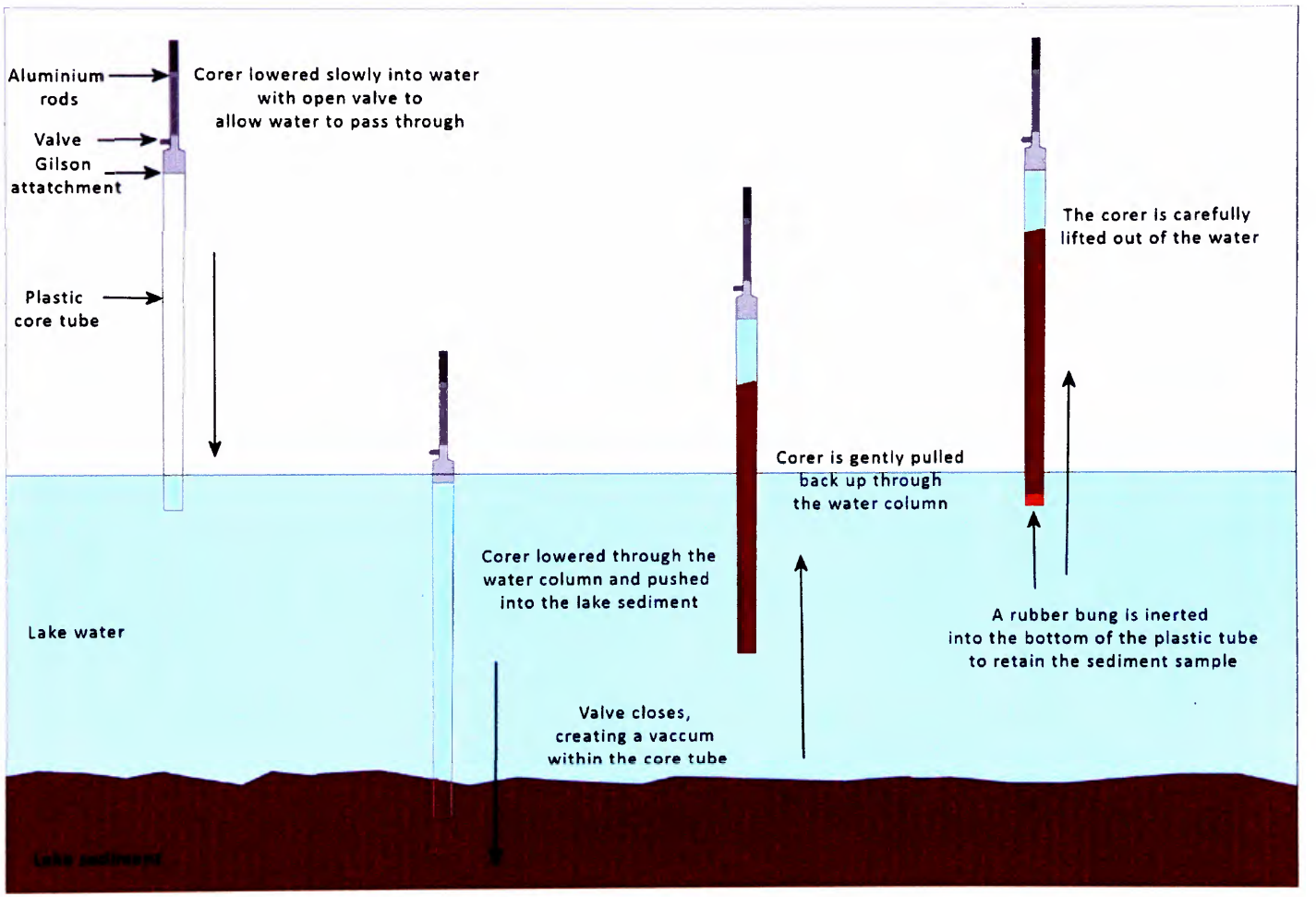

Figure 3.2: Collection of sediment cores using the Gilson gravity corer.

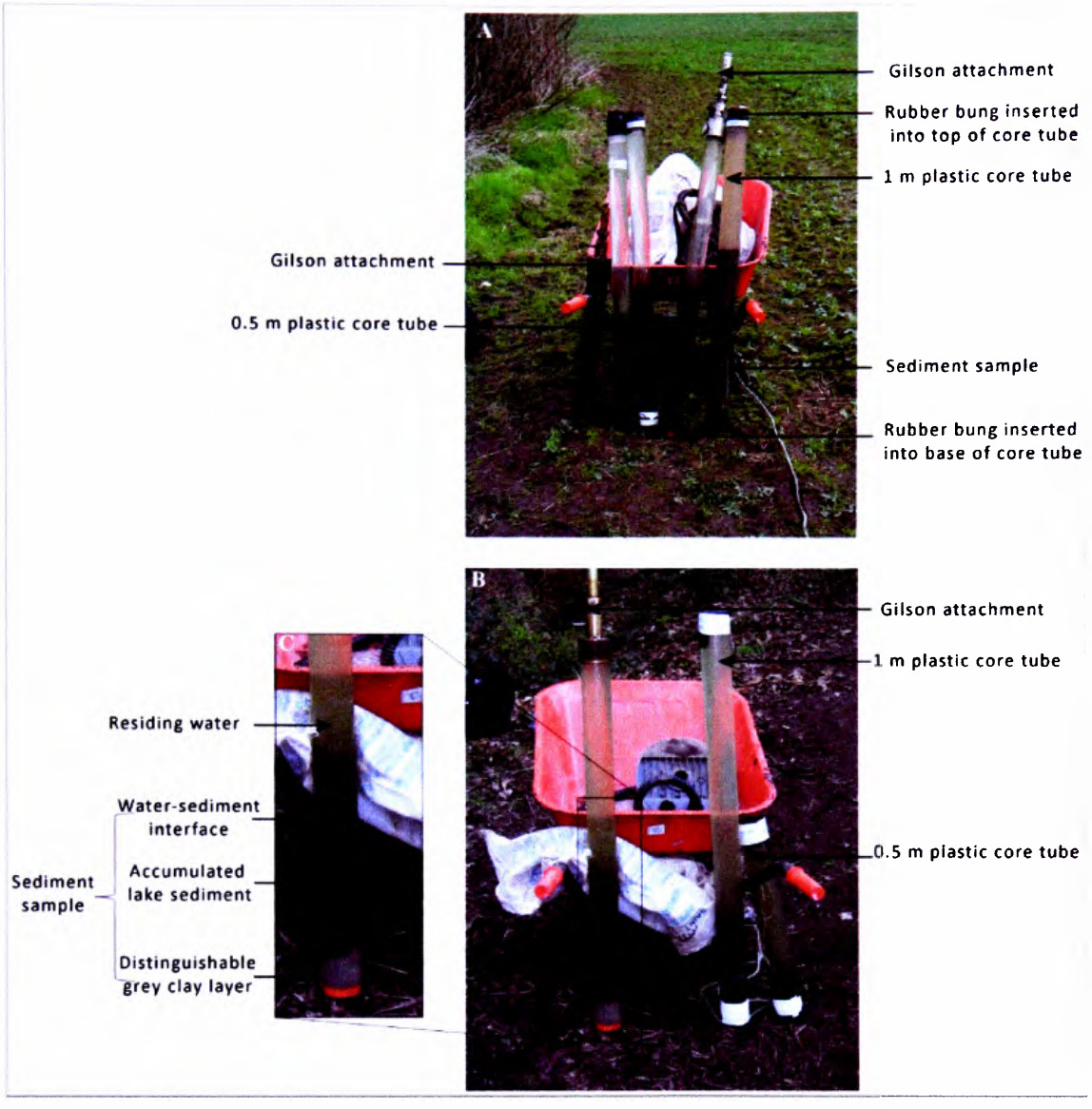

Plate 3.2: Collected sediment cores from Daresbury Delph pond (A); Windmill Hill pond (B); and retrieved sediment stratigraphy (C).

3.5. Analysis of sediment composition: laboratory work

A range of environmental analyses have been applied to the lake sediment cores, to obtain detailed proxy pollution histories. Typically the retrieved cores were <50 cm in length, resulting in small sediment sample masses; therefore, sequential laboratory analyses were applied with care (see Figure 3.3), especially as some of the methods used are destructive. During sample preparation and analysis, potential sample contamination was prevented and, furthermore, all samples were stored, prepared and analysed, as consistently as possible, to ensure an accurate comparability of results.

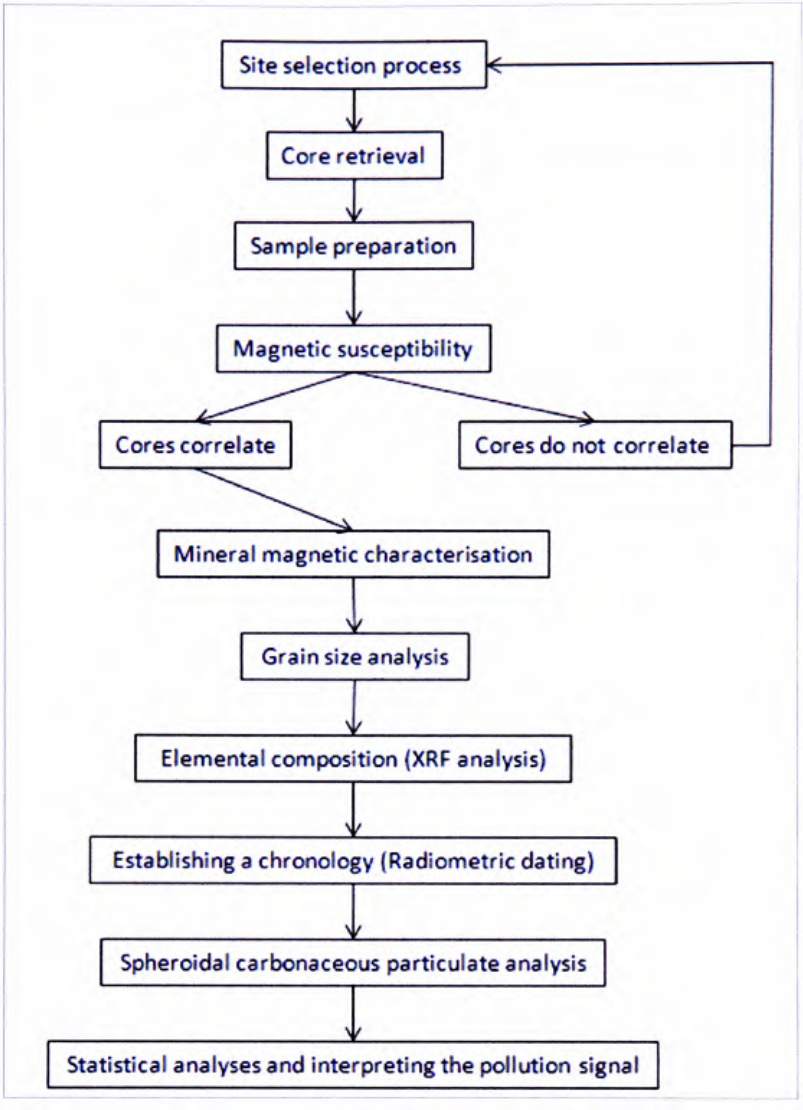

Figure 3.3: Methodological protocol for reconstruction of temporal pollution profiles from lake sediments.

3.5.1. Core extrusion

In order to extrude the core samples, the majority of residing water trapped above the sediment, within the top of the core tube, was siphoned away using a hand vacuum pump attached to a rubber tube. A trigger initiated the draining of the water from the core, and was removed to allow the water to drain out of the plastic tube. Approximately 3 cm of water above the top sediment layer was not drained, to prevent disturbance of the water-sediment interface. The sediment cores were then extruded into 5 mm samples in order to obtain a high-resolution stratigraphic sequence [Norton, 1992; Rose *et al.*, 1995; Boyle *et al.*, 1998; Dearing *et al.*, 1998; Pirrone *et al.*, 1998].

To do this, a rubber bung, attached to a wooden rod, was carefully inserted into the bottom of the plastic core sample tube, replacing the original bung inserted in the field. The device

was then pushed slowly upwards until the sediment reached the top of the tube. A plastic collar (with a diameter of the plastic core tube and a height of 5 mm) was then placed on the top of the plastic core tube, and used to accurately 'slice' the core sample into 5 mm intervals. The sediment was pushed up through the tube, and sectioned in this way, until the entire core had been extruded [Wright, 1980]. Sediment slices were then placed into plastic Petri dishes and, labelled with site location and sample depth. At all times plastic (opposed to metal) tools were used to prevent altering subsequent mineral magnetic measurements [Sandgren and Snowball, 2001].

3.5.2. Sample description

A basic sample description [Boyle, 2001] using the Troels-Smith (1955) method [West, 1977] was carried out for all core samples, to identify the layers of sand and clay, commonly used to line anthropogenic ponds, which are typically distinguishable in colour from the natural lacustrine sedimentation. Detailed descriptions were not necessary, due to the homogenous nature of the detritus sediment and lack of structures (e.g. laminations or varves) [Oldfield and Richardson, 1990(b)].

3.5.3. Sample preparation for magnetic analysis

To avoid contamination and alternation of subsequent magnetic measurements, care was taken to prevent: (i) contact between the sediment and metal; (ii) exposure to temperatures >40 °C and electromagnetic fields; and (iii) the physical destruction of magnetic grains during sample preparation [Walden *et al.*, 1999(b); Sandgren and Snowball, 2001]. The first stage of sample preparation involved drying the sediment samples to reduce transformation of magnetic minerals in the moist state [Oldfield *et al.*, 1992], decrease the diluting (diamagnetic) effect of water on the magnetic signal of the magnetically weak samples [Sandgren and Snowball, 2001] and for mass specific measurement [Walden, 1999(b)]. A plastic spoon was used to primarily break up the sediment within the Petri dish, before oven drying (at 35 °C) overnight. This helped to reduce the amount of potential mechanical damage when samples were disaggregated after drying.

A ceramic pestle and mortar were used to gently disaggregate the sediment, and then washed and dried after each sample to avoid cross contamination. Large organic matter (i.e. pieces of wood) and stones were removed from the sample, where necessary, using plastic tweezers, to make the sample as homogenous as possible and more representative of

the lake sediment. The samples were then packed into pre-weighed and labelled 10 cc plastic pots; the sediment was compacted whilst filling the pot using a wooden 'pot packer' (Appendix B, Plate B1). Once the pots were filled they were re-weighed (using a Precisa 125A analytical balance for all measurements to ensure accuracy) to obtain sample mass.

For accurate mineral magnetic measurements it is essential that, during analyses, sediment is unable to move within the pot [Walden, 1999(b)]. Therefore, using the wooden 'pot packing' device, cling-film ('non magnetic') was compressed over the top of the sediment, filling the remainder of the pot prior to the lid being securely fastened, whilst not contributing to the magnetic content of the sample. Each plastic lid had a small pointed tab which was used to align samples during magnetic analyses.

3.5.4. Mineral magnetic measurements

Mineral magnetic techniques are considered a routine form of analysis for the characterisation of soils, dusts and sediments [Thompson and Oldfield, 1986; Dekkers, 1997; Maher and Thompson, 1999; Walden *et al.*, 1999(a)]. Based on the principle that all substances are magnetic [Smith, 1999], a suite of mineral magnetic analyses have been carried out to characterise the magnetic concentration, behaviour and grain size of samples (Section 1.4.3.1.1.).

Mineral magnetic analyses boast many advantages as an inexpensive, rapid, reliable and non destructive compositional tool, with a quick and simple sample preparation [Oldfield, 1991; Dekkers, 1997; Walden *et al.*, 1999(a)]. The technique also allows analysis of bulk material; therefore, data is representative of the whole sample and complements sub-sampled techniques used in this research (such as spheroidal carbonaceous particulate (SCP) and particle size analyses). Mineral magnetism is also sensitive to low concentration levels and detects grains in the ultrafine size range [Dekkers, 1997].

Samples were exposed to a range of induced magnetic fields. The measured magnetisation of the sample whilst in the field and the amount of magnetisation 'remembered' (remanence) by the sample when removed from the field, were used to reveal the magnetic characteristics of the sample. As varying magnetic field strengths were induced, the order of these measurements is important so that they do not influence each other (Figure 3.4).

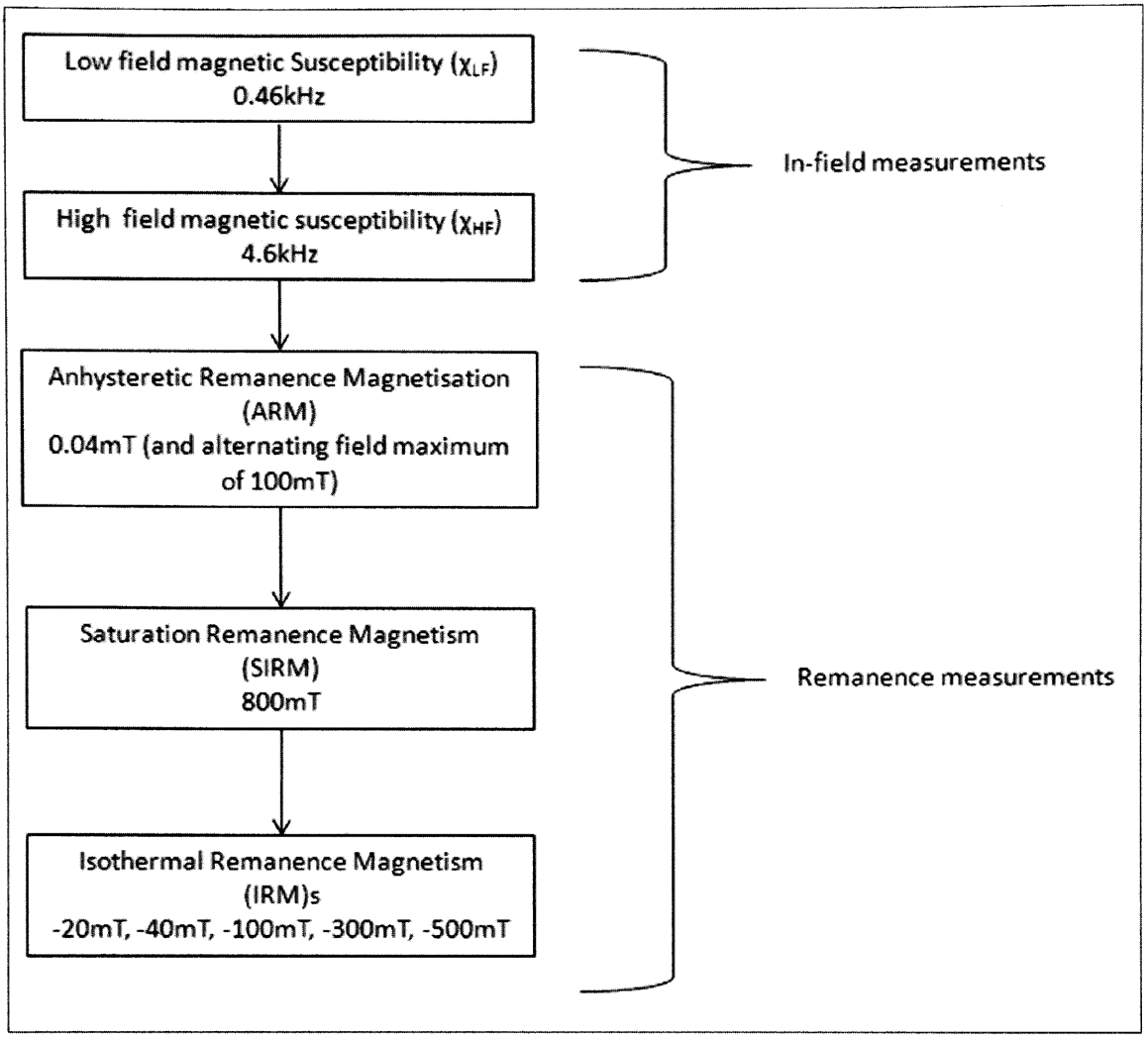

Figure 3.4: Sequence of mineral magnetic analyses [Walden *et al.*, 1999(a)].

3.5.4.1. Magnetic susceptibility

Magnetic susceptibility (χ) was measured at two frequencies: low (0.46 kHz) and high (4.6 kHz) using a Bartington (Oxford, England) MS2B dual frequency susceptibility sensor connected to a MS2 magnetic susceptibility meter. The MS2 sensor is very sensitive to electromagnetic fields, temperature changes, vibrations, movement and magnetic materials [Dearing, 1999(b)]. Therefore, a 'quiet' environment without any background 'noise' in which to carry out susceptibility measurements was essential. To reduce this background noise the sensor was stabilised to a worktop, all PCs, mobile phones and electrical equipment (especially other magnetic field generating devices in the laboratory) other than the meter were turned off, the working temperature was kept constant and the equipment was shaded from sunlight, and metal objects were distanced from the sensor. Due to the inevitable background drift in susceptibly measurements [Dearing, 1999(b)], the machine

was turned on 15 minutes prior to recording, to promote the equipment to stabilise (minimise drift).

Low field (χ_{LF}) susceptibility was measured before high field (χ_{HF}) in all samples. The method for both was the same (except for the variation in field strengths); whereby, an automated six measurement cycle in continuous mode at the 0.1 scale was used [Dearing, 1999(b)]. This method was selected (over the manual method using fewer measurements), to give greater precision as samples were generally magnetically weak and low in mass, with a high potential for background noise and drift to influence readings.

When the sample was placed in the MS2 Bartington sensor it was exposed to an electromagnetic field (generated by a coil); therefore, by subtracting the background readings (B1 and B2) from the 'in field' measurements (R1 and R2), χ can be calculated using equation 1.

$$\chi = ((R1 + R2)/2) - ((B1 + B2)/2)) \qquad \text{(Eq 1)}$$

Mass specific values were then obtained by dividing χ by sample weight.

As a precaution, measurements that displayed high variations (>0.4) in the two background and or in-field readings were repeated. Also in order to compare the dual frequencies measured, the magnetic pots were aligned using the small tab on the pot lid, for both high and low field measurements [Dearing *et al.*, 1999(b)]. Also, as some samples reduced dramatically in weight after drying, most notably the top layers of the cores, repeat measurements were taken to ensure reliability of data.

3.5.4.2. Anhysteretic remanence magnetisation

Anhysteretic remanence magnetisation (ARM) was induced in samples using a Molspin (Newcastle-upon-Tyne, England) A.F. demagnetiser, whereby a DC biasing field of 0.04 mT (comparable to the earth's magnetic field intensity) was generated in the presence of an alternating magnetic field, which reached a maximum of 100 mT [Verosub and Roberts, 1995; Walden, 1999(a)]. This anhysteretic field was produced within the main coil chamber, where a rapidly alternating field was created, which, if was equal, would have a demagnetising effect on the sample; however, with the presence of a biasing field, a small magnetic field is generated. This magnetises the single domain (SD) grain size range of the sample as finer super-paramagnetic (SP) grains are too small to hold a remanence and

coarser multi-domain (MD) gains require higher magnetic fields to become magnetised [Walden, 1999(a); Peters and Dekkers, 2003].

Once induced, this remanence was measured in a Molspin 1A magnetometer. Sample pots were aligned within the magnetometer sample-holder in the same direction as the induced remanence. Samples were lowered into a coil and spun (for ~ six seconds). Electrical currents produced by the coil are proportional to the remanence a sample holds [Walden, 1999(a)] and, therefore, subsequent 'north' and 'east' readings reflect this. For confidence in the accuracy of the magnetometer data the machine was calibrated after every 10 sample measurements by material of a known magnetism. Care was taken, when inserting and removing samples, not to adjust the delicate settings of the machine. Also the ARM and magnetometer were allowed 15 minutes to warm-up in order to reach a constant operating temperature prior to taking measurements [Walden, 1999(a)].

3.5.4.3. Saturation isothermal remanence magnetism and back-field IRMs

Saturation isothermal remanence magnetisations (SIRM) and backfield isothermal remanence magnetisations (IRM) were induced in samples using a Molspin Pulse Magnetiser, in which an electrical current builds-up to produce a short magnetic charge of a programmed intensity [Walden, 1999(a)]. On receiving this magnetic 'pulse', samples were immediately transferred to the magnetometer to measure the remanence induced. Samples were exposed to a SIRM of 800 mT in the forward field and then subjected to a series of reverse fields of progressively increasing intensities: -20 mT, -40 mT, -100 mT, -300 mT and -500 mT, respectively. By inducing IRM in this way the behaviour of magnetic grains within the sample can be assessed. The SIRM initially magnetises all magnetic grains in the forward field direction, then the series of reverse fields realigns the magnetisation of the sample in the opposite direction to the SIRM [Thompson and Oldfield, 1986]. This essentially 'knocks out' the SIRM forward field with increasing magnetic intensities until the magnetisation of the sample is reversed. The point at which this happens is determined by either 'soft' or 'hard' magnetic behaviour. Samples that easily align to the reverse field display soft (ferrimagnetic) behaviour; and samples that resist 'flipping' to the reverse direction are known as hard (antiferromagnetic) [Smith, 1999].'

3.5.5. Particle size analysis

Down-core particle size distributions have been analysed to characterise the composition of lacustrine sediment (Table 3.3) [McCave and Syvitski, 1991; Last and Smol, 2001], to determine detrital sedimentation, and erosion signals [Smol, 2002], identify potential particle size effects and relationships with magnetic behaviour and also heavy metal content [Fisher *et al.*, 1978; Flanders, 1994; Morris *et al.*, 1995; Al-Rajhi *et al.*, 1996] and to determine possible temporal trends in particulate size, a key attribute of the toxicity of particulate pollution [Keywood *et al.*, 1999; Ghio and Cohen, 2005].

Table 3.3: Particle size scale [adapted from McCave and Syvtski, 1991; Last, 2001].

Descriptive terms		Particle diameter (mm)
Boulder		256
Cobble		64
Pebble		2
Sand	Very coarse	1
	coarse	0.5
	Medium	0.25
	Fine	0.125
	Very fine	0.0625
Silt	Very coarse	0.03125
	Coarse	0.01563
	Medium	0.00781
	Fine	0.00391
	Very fine	0.00195
Clay		

Particle size analysis was conducted at the University of Wolverhampton using laser diffraction instrumentation. Based on the principle that there is an increase in the angle that light is diffracted from particles with decreasing particulate size, laser diffraction analysis allows a rapid, reliable and reproducible measurement of particles ranging in size from 0.1

μm to 2000 μm [Malvern Instruments, n.d.; Agrawal *et al.*, 1991; McCave and Syvitski, 1991]. The application of the Mie light scattering theory properly analyses submicron material, boasting advantages over other techniques such as sieving and settling of suspensions, which are limited in measuring fine and ultrafine particles [McCave and Syvitski, 1991]. Also, despite this being a destructive process, only a very small subsample is required for analysis.

Using a Malvern Mastersizer Long-bed X with a MSX1 Small Volume Presentation Unit (SVPU) connected to a PC with Malvern v1.2 software capabilities, each sample was measured for two separate size ranges (0.1-80 μm and 4-2000 μm) with the use of two lens sizes, 45 mm and 1000 mm, respectively. A small amount of sediment, sub-sampled from the original sample, was disaggregated using a rubber pestle and a dropwise addition of a calgon solution (40 mg sodium hexametaphosphate $(NaPO_3)_6$ per one litre of distilled water) from a pipette. Visible organic matter was then manually removed, using tweezers, to prevent organic material disrupting the size measurement of the sediment grains [Booth, 2002].

The sample procedure (Figure 3.5) involved filling the MSX1 Small Volume Presentation Unit with water and configuring the Malvern hardware. A background reading of the water was then recorded and stored. The sediment sample was then added to the instrument (SVDU) until an appropriate obscurity level (10%) was reached (to ensure enough sediment in dilution for an accurate reading). Applied ultrasonics constantly pumped and stirred a flow of suspended sediment received by the laser. Light from the laser was shone onto the suspended particulates, which caused a scattering effect due to the diffraction of light at an angle inversely proportional to particle size [Agrawal *et al.*, 1991]. As the diluted sediment sample passes the laser beam, the light becomes diffracted creating diffraction patterns. A series of photo-detectors placed at different angles within the instrument are able to divide the patterns into particle size values using the Mie light scattering theory [Malvern Instruments, n.d.; Bohren and Huffman, 1998; Lehner *et al.*, 1998]. The diffraction patterns received by the photo-detectors are averaged for a fixed time period and deconvolved into particle size values [McCave and Syvitski, 1991; Booth, 2002]. The Malvern software then blended the two sample runs (0.1-80 μm and 4-2000 μm) to produce particle size distribution graphs and a table of descriptive statistics for each sample.

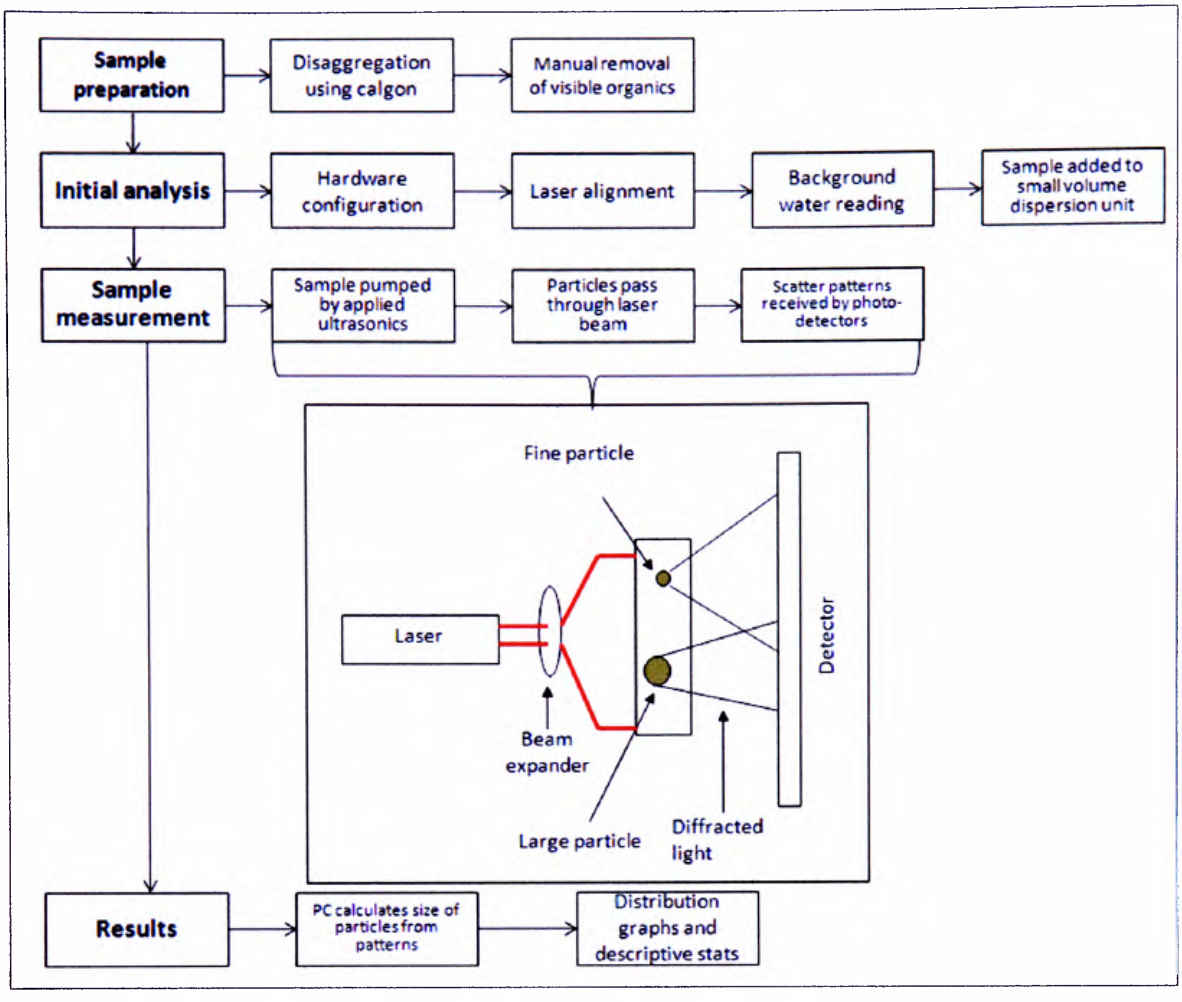

Figure 3.5: Schematic laser diffraction size analyser [adapted from Last and Smol, 2001].

3.5.6. Elemental composition (X-ray fluorescence)

Characterising the elemental composition of lake sediments can reveal natural (catchment derived) and anthropogenic (fossil fuel combustion) inputs [Heit *et al.*, 1981; Norton *et al.*, 1992; Plater *et al.*, 1998; Dauval'ter, 2004]. Elevated levels beyond natural background concentrations and accumulation rates can also be calculated, to assess the impact of pollution [Allen and Rae, 1986; Dearing and Jones, 2003; Graney and Eriksen, 2004]. Furthermore, the elemental composition of particulate pollution is an important factor in understanding the impact of particulate pollution on health [Harrison, 2004; Johnson *et al.*, 2005; Xie *et al.*, 2005].

Energy dispersive radioisotope-source X-Ray Fluorescence (XRF-ED) has been used to characterise the elemental composition of the lake sediment cores. XRF analysis is based on the photoelectric fluorescence of secondary x-rays generated within a sample by irradiation. The secondary x-rays produced are characteristic of source elements within the

sample, and the emission rates are a function of concentration [Boyle, 2000]; therefore, elemental composition can be determined directly by allowing for instrument geometry, detector efficiency, fluorescence yield of elements and absorption of radiation by the sample [Boyle, 2001]. XRF analysis has been widely applied to sediments, to interpret elemental characteristics of pollution and temporal contamination trends [Versteeg *et al.*, 1995; French, 1996; Lee and Cundy, 2001; Roberston *et al.*, 2003; Yang and Rose, 2005].

XRF-ED is a highly precise, reliable and rapid (~70 samples per day) method for determining total elemental sediment analysis on bulk samples [Al-Merey *et al.*, 2005]. Compared to alternative techniques (for example, energy dispersive x-ray spectrometry), XRF-ED has poorer detection limits; however, for many elements, observed levels are above this detection limit [Boyle, 2001]. Also, XRF is non-destructive and there is minimal handling of samples, advantageous when analysing samples of small sample mass, reducing potential errors and contamination [Boyle, 2001].

XRF analysis was carried out at the University of Liverpool using a Metorex (Finland) XMET920 system comprising two analysis probes connected to X-Met PC system boards (XPCS) and XMET software [Boyle, 2000]. Two metallic sample holders containing a cadmium (heavy metal) probe and an iron (light element) probe were attached to a PC. Prior to sample measurements, the machine was calibrated using a range of reference materials, which contain certified levels of element concentrations [Boyle, 2001].

Sample preparation involved transferring sediment into polythene sample pots, with a lining of propylene film on which the sediment sat. Pots were filled with ~1-2 g of sediment to provide a sample depth of >1 mm, and sediment was compressed lightly using a plunger. Boyle [2000] recommends using >0.5 g of sediment to reach this sample thickness, above which the fluorescence signal is independent of sample mass for all measured elements. Samples were then placed in the metallic holders for analysis and each sample was measured separately in both the heavy element and light element probes, using 200 second count times. Concentration data for elements displayed in Table 3.4 were stored electronically. Using DECONV software (Department of Geography, University of Liverpool), the heavy and light element analyses were combined and normalised for organic content, using loss on ignition (LOI) values (mg/g) and tabulated in an Excel (Microsoft Office 2007) spreadsheet.

Table 3.4: Elements measured by XRF.

Chemical Symbol	Element	Chemical Symbol	Element
Al	Aluminium	Nb	Niobium
Br	Bromine	K	Potassium
Ca	Calcium	Rb	Rubidium
Cl	Chlorine	S	Sulphur
Cr	Chromium	Si	Silicon
Cu	Copper	Sr	Strontium
Fe	Iron	Ti	Titanium
Pb	Lead	Y	Yttrium
Mn	Manganese	Zn	Zinc
Ni	Nickel		

For samples that consisted of minimal sediment (<0.5 g), 'masks' (thin disc of metal with a small hole in the centre) were inserted into the sample holders to reduce the surface area measured, by concentrating sediment into the centre of the holder to produce an accurate XRF reading [John Boyle, *Pers. Comm.*]. An aluminium (light element) mask was used in the heavy element probe, and a copper (heavy metal) mask was used in the light element probe so as not to contribute to the measured composition. Results were then corrected by taking a series of extra 'masked' measurements of samples of an adequate sample amount. A comparison was then made between the masked and non-masked results of these extra samples, to provide a correction concentration equation (2) [John Boyle *Pers. Comm.]:*

(1/m)* 'masked' concentration result (Eq 2)

Where m is the slope of the trend line (with interception at zero) of a scatter plot of 'no-mask' (x axis) verses 'masked' (y axis). This correction was advised by John Boyle of Liverpool University [*Pers. Comm.*]. He recommended that these corrected results would provide accurate results for the elements (Si, Ti, Ca, K, Fe, Mn, S, Pb Zn, Zr, Rb Zn Sr); however, no other element results would be useable for 'masked' samples. Data obtained from reference materials measured prior to and following measurement of each sample batch revealed that no other correction was needed to account for instrument variability [John Boyle, *Pers. Comm.*].

3.5.7. Establishing the chronology

A reliable chronology is essential in reconstructing detailed temporal changes in pollution from natural archives, and allows dating of specific pollution episodes [Croudace and Cundy, 1995; Rose *et al.*, 1998(b); Graney and Eriksen, 2004; Plater and Appleby, 2004],

calculation of sedimentation rates, magnetic and heavy metal flux (Heit *et al.*,1981; Oldfield and Appleby, 1984; Battarbee *et al.*,1985; Norton, 1986] and comparison of proxy pollution trends from various sites with industrial histories [Veselý *et al.*, 1993; Couillard *et al.*, 2004; Tylmann, 2005].

Isotope dating is widely accepted as a standard tool in palaeolimnology for reliable sediment chronologies [Norton, 1986; Appleby, 1993; Veselỳ *et al.*, 1993; Couillard *et al.*, 2004; Tylmann, 2005]. Based on the disappearance of isotopes due to radioactive decay [Olsson, 1986], the ^{210}Pb radioactive decay series is acknowledged as the most accurate method for dating a 100 – 200 year timescale [Oldfield and Appleby, 1984] and was, therefore, crucial in order to establish an accurate, high-resolution chronology of industrial pollution since the 19th century. Limitations include the possible migration of ^{210}Pb isotopes within the lake sediment column, or redistribution of sediment [Oldfield and Appleby, 1984]. Interpolation of dates for sample between measured data points provides a high-resolution sediment chronology; however, for sediment below the depth at which supported and unsupported ^{210}Pb reaches equilibrium, dates have to be extrapolated. Due to the high expense of the analyses, not all cores could be analysed.

Radiometric dating was conducted by Professor Peter Appleby at the Liverpool University Environmental Radioactive Laboratory. Using direct gamma assay, an Ortec HPGe GWL series well-type coaxial low background intrinsic germanium detectors counted the presence of ^{210}Pb, ^{226}Ra, ^{137}Cs and ^{241}Am isotopes within the lake cores [Appleby *et al.*, 1986]. Unsupported ^{210}Pb (atmospherically derived) content was established by subtracting the supported ^{210}Pb (gathered from the ^{226}Ra content of the sample) from the total ^{210}Pb activity. The age of the unsupported ^{210}Pb within the sediment layer was then calculated using the radioactive decay law [Appleby and Oldfield, 1983]. Radiometric dates for each core were calculated from the CRS (constant rate of supply) [Appleby and Oldfield, 1979] model to account for temporal variations of accumulation rates and supply of unsupported ^{210}Pb to the lake [Appleby and Oldfield, 1978; Oldfield and Appleby, 1984; Oldfield and Appleby, 1985; Olsson, 1986]. The processes of ^{210}Pb entering and depositing in lake sediments and the application of models is described in more detail by Appleby and Oldfield [1978], Appleby and Oldfield [1983], Olsson [1986], Appleby [1993].

^{137}Cs data were used to complement the ^{210}Pb chronologies. As a consequence of nuclear weapons testing, ^{137}Cs is artificially formed and has been detectable in the environment since 1945, with a pronounced increase in 1954, reduction in 1960 and maximum in 1963

[Appleby, 2001]. The accuracy of the calculated ^{210}Pb position for the year 1963 was assessed using the ^{137}Cs peak representative of this year that experienced a maximum release of ^{137}Cs from nuclear weapons testing [Olsson, 1986] (Figure 3.6).

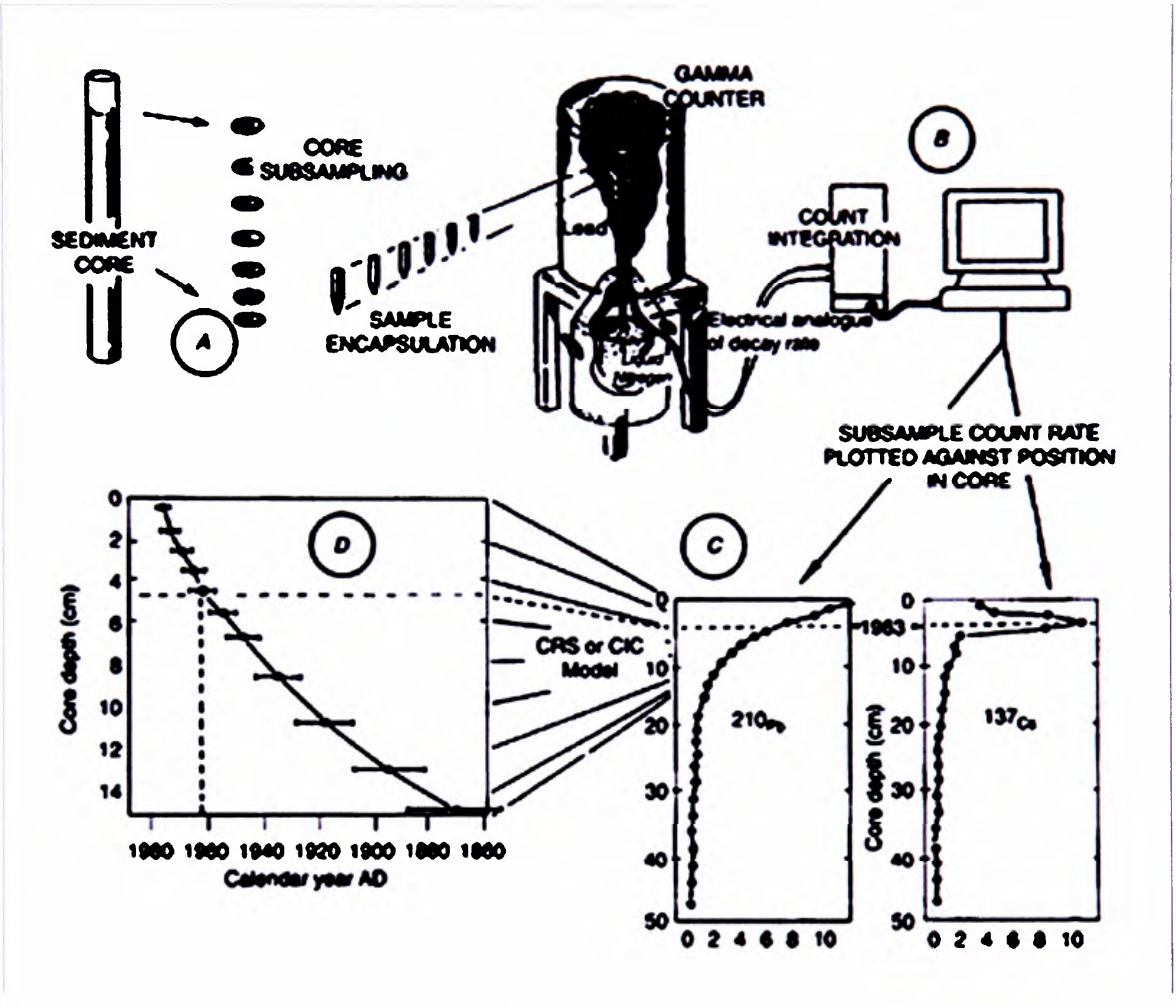

Figure 3.6: Four main steps in determining ^{210}Pb dates in lake sediments [Smol, 2000]. (A) 5 mm interval core samples were sent for analysis. (B) Using a low-background gamma counter radioisotopes (^{210}Pb, ^{226}Ra, ^{137}Cs and ^{241}Am) are counted. (C) Activities of total and supported ^{210}Pb and ^{137}Cs versus depth of core. The peak in ^{137}Cs activity is assumed to represent 1963, the year of maximum fall out from nuclear weapons testing. (D) Depth of 1963 from the ^{137}Cs stratigraphy was used as a reference level to correct CRS model ^{210}Pb dates. Raw ^{210}Pb dates, corrected ^{210}Pb dates and sedimentation rates typically displayed.

3.5.8. Determining organic matter

Loss on ignition (LOI) is the simplest method to determine organic content of sediment samples [Charlesworth and Lees, 1999(b); Xie *et al.*, 1999(b); Heiri *et al.*, 2001; Robertson *et al.*, 2003]. Igniting samples at high temperatures oxidises organic carbon to carbon dioxide and ash; therefore, organic matter is calculated by measuring this weight loss [Heiri *et al.*, 2001]. However, there is some debate as to the temperature at which LOI is performed, with ignition temperatures ranging from 375 °C [Beaudoin, 2003], 450 °C

[Oldfield *et al.*, 1999], 550 °C [Solovieva *et al.*, 2005] to 580 °C [Vesleý *et al.*, 1993]. With differing ignition temperatures there is variation in the loss of volatile salts, structural water (held within the lattices of clay particles), sulphides and inorganic carbonates [Heiri *et al.*, 2001] demonstrated in Table 3.5. Therefore, LOI at 450 °C, as applied to lake sediments by Oldfield *et al.*, [1999], Williams [1991], and Jordan *et al.*, [2002], has been used as an estimate of organic matter content in this work. This temperature was selected as at 450 °C decomposition of organic matter, including fatty acids, peptides, carbohydrates such as cellulose and less thermally stable humified organic substances are decomposed [Boyle, 2001]. At higher temperatures an overlap in decomposition of carbonates in soils occurs that can results in misleading OM values, which is negligible at <450 °C [Leong and Tanner, 1999; Beaudoin, 2003]. Also samples exposed to lower temperatures for shorter times may also result in incomplete combustion of organic material [Beaudoin, 2003].

Table 3.5: Loss of organic matter phase at various temperatures. Adapted from Boyle [2001].

Decomposition of organic matter phase	LOI temperature °C
Dehydration of plant matter	40-135
Decomposition of organic matter (e.g., fatty acids, peptides and carbohydrates)	250-350
Decomposition of less thermally stable humified organic substances	370-420
Decomposition of more thermally stable organic substances	530-540
Inorganic carbon / carbonate breakdown	650-750

Despite reported inter-laboratory variations and potential intra-laboratory discrepancies in the LOI method [Leong and Tanner, 1999; Heiri *et al.*, 2001], it remains a reliable, rapid and inexpensive means of determining organic content [Dean, 1974; Boyle, 2001]. LOI values compliment magnetic measurements, by allowing normalisation of data for the diluting effects of organic content on the magnetic signal. LOI data is also required for determining XRF values in order to understand the sample composition and to calculate effects of mass attenuation (absorption process of fluoresced x-rays) by the sample during XRF measurement.

Ceramic crucibles were labelled, weighed and filled with a 0.5-1 g sub sample of sediment and reweighed (W1). To assure consistency in the result, the same analytical balance (Precisa 125A) was used for all measurements (to three decimal places). Samples were then oven dried (105 °C) overnight to remove the moisture content of the samples. Following this, samples were allowed to cool in a dessicator at room temperature, to

prevent the absorption of moisture from air, and then re-weighed (W2). Samples were then placed in a muffle furnace and ignited at 450 °C for five hours, enough time for the furnace to heat up to the desired temperature (one hour) and then four hours exposure time to burn off the organic carbon content. Samples were then cooled in the dessicator and re-weighed (W3).

Organic matter content of the sample was then calculated by Equation 3.

$$LOI\ \% = 100 * (W2-W3) / W2 \qquad \text{(Eq 3)}$$

3.5.9. Spheroidal carbonaceous particulate analysis

Spheroidal carbonaceous particles (SCPs) are unambiguous indicators of atmospheric pollution and have been widely used to investigate temporal particulate matter deposition [Goldberg *et al.*, 1981; Griffin and Goldberg, 1981; Renberg and Wik, 1984; Renberg, 1986; Rose *et al.*, 1994(a); Rose *et al.*, 1998(b); Rose, 2001; Rose *et al.*, 2002]. As the start of the SCP record in the UK begins at ~1850/1860 [Rose *et al.*, 1995], SCPs can be used to allocate dates to lake cores [Rose, 2001]. SCP profiles can also be used to validate proxy indicators of atmospheric pollution established from magnetic and XRF interpretation. However, due to time constraints, SCP analysis was only conducted on one core from Daresbury Delph pond.

Sample preparation (Table 3.6) involved a destructive procedure consisting of centrifuging, and the digestion of samples in polypropylene tubes in a water bath to remove the unwanted fraction of the sample by sequential chemical attack. The chemical procedure was undertaken in a fume cupboard using nitric acid (HNO_3), hydrofluoric acid (HF) and hydrochloric acid (HCl) to remove organic, siliceous and carbonate fractions, respectively, from the sample [Rose, 1990, 1994(a)]. Using this technique, >99.3% of the original sediment mass was reduced [Rose, 1994(a)]. However, SCPs are immune to this digestion due to their elemental carbon composition, and the residue was then viewed under a microscope to identify and count the intact SCPs, to provide concentrations expressed in particles per gram dry weight.

Table 3.6: Sequential chemical attack for SCP preparation.

Step	Sequential chemical attack
1	A 0.10-.15 g of sub sample was transferred into 12 cm^3 polypropylene centrifuge tube.
2	1.5 cm^3 of concentrated nitric acid was added to sample and left overnight in a fume cupboard.
3	A further 1.5 cm^3 of nitric acid was added and the tube was placed in a water bath for three hours at a temperature of 80-90 °C.
4	Tubes were then removed from the water bath and allowed to cool.
5	A dropper pipette was used to transfer the supernatant into a labelled collection vessel for disposal.
6	3 cm^3 of 40% hydrofluoric acid was added to the tube which was then placed into the water bath for 23 hours at a temperature of 80-90 °C.
7	Tubes were removed from the water bath and allowed to cool.
8	A dropper pipette was used to transfer the supernatant into an appropriately labelled collection vessel for disposal.
9	3 cm^3 of 6M hydrochloric acid was then added to each tube and returned to the water bath for a further two hours.
10	The residue was washed and centrifuged twice.
11	The residue was transferred into a pre-weighed and labelled glass vial.

3.6. Data analysis

The data obtained from the aforementioned analyses are presented as concentration-depth profiles along with ^{210}Pb dates and extrapolated timescales to assess variations in sediment characteristics over time. Data analysis included statistical analysis to identify relationships between the lake sediment properties and separating out 'natural' from 'pollution' derived inputs throughout the core. Data are also converted to flux profiles to assess the temporal supply of magnetic minerals and trace metals to the lake.

3.6.1. Concentration-depth profiles

In accordance with the majority of palaeolimnological studies data have primarily been presented in graphical form, with depth of sediment core (relative to time) forming the y axis and unit of environmental proxy forming the x axis. For each lake site concentration-depth profiles have been constructed to highlight down-core variations in mineral magnetic parameters (concentration per dry weight) and quotients, grain size assemblages (relative abundance % per dry weight), trace metal composition (concentration per dry weight), organic matter (%), sedimentation rates (sediment accumulation per time interval) and, where applicable, spheroidal carbonaceous particulate counts (particles per dry weight).

Isotope chronologies dates have been superimposed on the profiles, to visually assess temporal changes in the sediment record.

3.6.2. Extrapolating the isotope chronology

^{210}Pb chronologies can only be derived for the recent section of the sediment cores, due to concentrations of ^{210}Pb and ^{226}Ra reaching radioactive equilibrium depths [Appleby and Oldfield, 1982; Kunzendorf *et al.*, 1998; Ruiz-Fernandez *et al.*, 2005]. Below this ^{210}Pb dating horizon the chronology requires extrapolation. As the exact age of the pond sites were unknown (only the existence of the lakes determined using historical maps), to extrapolate the chronology back to the start of the sediment record, scatter plots of depth (y) versus age (x) were constructed using excel (Windows 2008). A polynomial trend line was then fitted and the corresponding equation, from which the age of any depth in the core could be calculated, was applied to the remainder of the core [Vesléy *et al.*, 1993; Appleby unpublished document]. The extrapolated dates and dry bulk density data were then used to calculate sediment accumulation rates, outside of the CRS (constant rate of supply) model.

3.6.3. Separating out the pollution-detrital-diagenesis magnetic signal

3.6.3.1. Inorganic content correction

Magnetic profiles were normalised using inorganic matter (content per dry gram) to assess the potential diluting effects of organic content on the magnetic properties of the pond sediments [Dearing *et al.*, 1996]. Original magnetic concentration depth profiles are plotted alongside normalised parameters (Appendices F).

3.6.3.2. Magnetic bi-plots

For samples that are dominated by fine (<0.7 μm) magnetic grains, as identified by criteria set out by Oldfield [1994]; bi-logarithmic plots of χ_{ARM}/χ_{FD} versus χ_{ARM}/χ_{LF} were constructed and compared to those published by Oldfield, [2007]. The primary source of the fine-grained magnetite are identified by samples plotting within proposed 'bacterial' and 'soil/catchment' envelopes [Oldfield, 1994; Oldfield *et al.*, 1999; Oldfield, 2007] highlighting a SSD bacterial magnetite signal, or a finer SP soil-derived signature.

Also by plotting (SIRM-IRM$_{20}$)/SIRM against SIRM/ARM [after Oldfield, 1990] for temporal or depth phases, ferrimagnetic magnetic grain size variations throughout the sediment cores can be identified. Oldfield reports that a trend towards increases in both of

these parameters indicates a general increase in ferrimagnetic grain size. Therefore samples that plot in the bottom left of the graph are relatively fine compared to sample which plot in the top right [Oldfield, 1990].

3.6.4. Statistical relationships

In order to assess significant relationships between the various environmental proxies, statistical analyses were conducted using Minitab (version 13). Due to non-normal data distributions (identified via histograms and Anderson-Darling normality tests), variables were ranked prior to Pearsons correlation coefficients analysis to determine R values. Statistically significant relationships were identified at 99.5%, 99.9% and 99.99% confidence levels.

3.6.5. Trace metal enrichment factors

The supply of trace metals to lakes originate naturally from the catchment, as well as anthropogenic sources. Therefore, 'enrichment factors' (EF) have been adopted to distinguish the anthropogenic fraction of total trace metal concentrations, directly related to human activity [Renberg, 1986; Norton *et al.*, 1992; Tylmann, 2005]. The normalisation of trace metal concentration data by natural inputs allows assessment of the enhanced pollution signal:

Anthropogenic input= total input / natural input (or total input - natural input) (Eq 4)

Therefore, it is important to establish the natural trace element supply to the lake if stratigraphies are to be used as records of pollution [Boyle, 2001; Yang and Rose, 2005]. Al and Ti have been selected to assess the naturally derived component of trace metals in this work. Due to the high natural abundance of Al, a major constituent of soil and sediments and a structural element of clays, it is commonly used as a passive tracer for normalisation of trace metal data [Van Metre and Callender, 1997; Milko *et al.*, 2003; Tylmann, 2005]. Ti is also a suitable passive tracer as is relatively insoluble, not used biologically and does not undergo mobilisation via water acidification [Clark, 1989; Norton *et al.*, 1992; Rose *et al.*, 2004]. Pb, Zn, Cu, S, Br and Ni have been used as pollution tracers in this work as are typically associated with anthropogenic activity [Clark, 1989; Norton *et al.*, 1992; Van Metre and Callender, 1997; Charlesworth and Foster, 1999; Couillard *et al.*, 2004; Dauval'ter, 2004; Graney and Eriksen, 2004; Rose *et al.*, 2004; Blake *et al.*, 2007]. The use of EFs allow anthropogenic increases in trace metal

concentrations to be separated out from the natural background input, revealing enhanced pollution *trends*, rather than actual *concentrations*.

A simple normalisation of trace metal concentrations by elements associated with natural inputs, such as Al and Ti, has been applied to allow for variations in the natural supply [Kemp and Thomas, 1976; Bertine and Mendeck, 1997; Van Metre and Callender, 1997; Milko *et al.*, 2003]:

$$EF = TM_{anthro\ (x)} / TM_{natural\ (x)}. \quad \text{(Eq 5)}$$

whereby TM = trace metal concentration and suffix: $_{anthro}$ = trace metal associated with anthropogenic activity; $_{natural}$ = trace metal associated with natural inputs; $_{(x)}$ = any depth interval.

Trace metal baseline data, the natural constant supply, were incorporated into the EF calculation according to Tylmann, [2005], whereby, ratios of trace metal concentrations to Al and Ti in sediment intervals are normalised by ratios of trace elements to Al and Ti in unpolluted sediments. A reference level of pre-1800 sediment was assumed to represent background (pre-industrial intensification) concentrations of trace metals, having minimal influence from anthropogenic activity, from which mean trace metal: natural supply ratios were calculated using Al and Ti as passive tracers [Norton *et al.*, 1992; Van Metre and Callender, 1997; Rose *et al.*, 2004; Tylmann *et al.*, 2005; Yang and Rose, 2005].

$$EF = (TM_{anthro} / TM_{natural})_{(x)} / (TM_{anthro} / TM_{natural})_{(b)}. \quad \text{(Eq 6)}$$

Where suffix $_{(b)}$ = background pre-1800 mean.

Both of these EF models are included to assess the anthropogenic fraction, opposed to absolute values, to determine down-core trends in trace metal enhancement.

3.6.6. Cultural enrichment factors

Also a 'cultural enrichment factor' (CEF) demonstrated by Heit *et al.*, [1981] was applied to identify elevated levels of trace metals associated with pollution in relation to baseline values. Defined as the ratio of trace metal concentration in recent sediments (associated with contamination by anthropogenic activity) to the constant baseline concentration of the trace metal [Heit *et al.*, 1981], CEF was calculated using:

$$CEF = TM_{(x)} / TM_{(b)}. \quad \text{(Eq 7)}$$

The interpretation of the CEF values are: CEF ~1 suggests no significant anthropogenic input; CEF 1-2 highlights evidence of some anthropogenic input; and CEF >2 is indicative of increasingly greater anthropogenic contributions [Heit *et al.*, 1981]. CEFs have been tabulated for Pb, Zn, Cu and S levels in the lake cores, to assess the anthropogenic contribution of trace metals to the sediment column.

3.6.7. Trace metal inventories

In order to compare the amount of Pb, S, Zn and Cu supply to each lake for certain time periods, trace metal inventories were calculated according to Yang and Rose [2005] for a given depth of sediment interval representative of a certain time period (e.g. post 1950):

Total Inventory = sum of (dry sediment $mass_{(i)}$ * $TM_{TOTAL(i)}$) (Eq 8)

Whereby: TM_{TOTAL} = total trace metal concentration and suffix $_{(i)}$ = per interval.

To evaluate anthropogenic inventories the 'excess' trace metal concentrations were calculated from:

$$TM_{EXCESS} = TM_{TOTAL} - TM_{(b)} \quad \text{(Eq 9)}$$

Where TM_{EXCESS} = excess trace metal concentration,

and then applied to:

Pollution Inventory = sum of (dry sediment $mass_{(i)}$ * $TM_{EXCESS(i)}$). (Eq 10)

Pollution inventories for Pb, Zn, Cu and S are tabulated to assess the supply of total and anthropogenic trace metals.

3.6.8. Flux profiles

As well as concentration profiles, magnetic and trace metal flux data are also presented. Original concentration data have been converted into flux using the ^{210}Pb-derived sediment accumulation rates to demonstrate the supply of magnetic minerals and trace metals over time. Despite unknown bias added due to interpolation and extrapolation of ^{210}Pb dates and accumulation rates, flux profiles are more representative of temporal variations and therefore have been included in this work [Norton *et al.*, 1992; Vesléy *et al.*, 1993; Croudace and Cundy, 1995; Charlesworth and Foster, 1999; Boyle, 2001; Rose *et al.*, 2004; Tylmann, 2005].

3.6.8.1. Magnetic flux

To assess temporal trends in the supply of magnetic minerals to the ponds, magnetic flux data were calculated for SIRM, SOFT-$_{20mT}$ and HARD-$_{300mT}$ [after Richardson Pers. Comm., Oldfield, 1990; Tolonen and Oldfield, 1986]:

Magnetic flux (10^3A y^{-1}) = (Dry sediment accumulation rate g cm^{-2} y^{-1}*100) * magnetic parameter 10^{-6} Am^2 kg^{-1} /1000 (Eq 11)

3.6.8.2. Trace metal flux

Total trace metal flux profiles have been produced for all lake sites using normalisation by inorganic sediment accumulation rates and total (gross) sediment accumulation rates. Where pre-1800 data are available, the anthropogenic trace metal contribution to the total flux has been determined. Total trace metal flux data, corrected for inorganic content, was calculated using a series of calculations published by Vesléy *et al.*, [1993]:

Accumulation rate of inorganic material (g cm^2 y^{-1}) = dry sediment accumulation rate (g cm^2 y^{-1}) * inorganic content (/g) (Eq 12)

and

TMF_{TOTAL} (µg cm^2 y^{-1}) = accumulation rate of inorganic material (g cm^2 y^{-1})* trace metal concentration (µg/g) (Eq 13)

Whereby TMF=Trace metal flux and suffix $_{TOTAL}$= total flux.

Vesléy *et al.*, [1993] state that the anthropogenic proportion of the total trace metal flux can be obtained by:

$TMF_{ANTHRO} = TMF_{TOTAL} - TMF_{NATURAL}$. (Eq 14)

Whereby, natural flux is estimated as the mean accumulation rate of trace metals in pre-industrial sediments. Anthropogenic trace metal flux data are presented alongside total flux for Pb, Zn, Cu and S (where applicable).

Also Norton *et al.*, [1992] apply a flux model to determine the anthropogenic fraction of trace metal flux, using TiO_2 (rutile) as a soil mineral tracer*, which acts as a background tracer, so that by subtracting the background from the total concentration, the proportion of atmospheric input can be found [Norton *et al.*, 1992]:

TMF_{TOTAL} = Trace metal concentration per interval * dry sediment accumulation rate per interval (Eq 15)

Therefore Norton *et al.*, [1992] state:

$$TMF_{ANTHRO(x)} = TMF_{TOTAL(x)} - (TiO_2\,FLUX_{(x)} / TiO_2\,FLUX_{(b)}) * TMF_{(b)}. \quad \text{(Eq 16)}$$

Where suffix: (x) = any depth and (b) = pre-1800 mean and TiO_2 FLUX = flux of TiO_2.

$$Pb\ FLUX_{anthro(x)} = Pb\ FLUX_{total(x)} - (Ti\ FLUX_{(x)} / Ti\ FLUX_{(b)}) * Pb\ FLUX_{(b)}. \quad \text{(Eq 17)}$$

The model assumes that there is a constant supply of Ti and Pb entering the lake system from within the catchment, however this calculation will be in error if the catchment supply of Pb and Ti is not in constant proportion, potentially due to atmospheric deposition of TiO_2 or changing sedimentation trend [Norton *et al.*, 1992].

3.6.8.3. SCP flux

Temporal supply of SCPs are calculated as:

number of SCPs per dry mass (no. g^{-1}) * dry sediment accumulation rate (g cm^{-2} y^{-1}) = SCP flux (no. cm^{-2} y^{-1}) (Eq 18)

after Rose [2001] and Rose and Monteith [2004].

3.6.9. Inter-site comparison

Due to variations in sample size, accumulation rates and timescales, relationships between lake sites cannot be statistically proven. Therefore down-core lake sediment characteristics for each site are presented alongside each other and using the ^{210}Pb chronologies time phases are overlain to allow a visual comparison of temporal trends. Magnetic and trace metal concentrations and fluxes are presented in this way. Also box and whisker plots have

* Norton *et al.*, [1992] used Atomic Absorption Spectroscopy to analyse the elemental composition of lake sediments and reports major elements (Al, Ti, etc.) as the oxide "regardless of their actual state in the sediment". Therefore, Ti concentration data are used, not TiO_2, validating the use of Ti in this work.

been produced using Minitab (version 13) to assess variations between sites [Blake *et al.*, 2007].

3.7. Chapter summary

Criteria are set out for the process of identifying potential suitable lake sites for investigation. The procedure for the of retrieving lake sediment cores is presented, which have been characterised using a range of environmental analyses. Sample preparation, analysis procedure and type of data obtained for each stage of the employed laboratory methodology protocol are explained, which include:

(i) mineral magnetic analysis,
(ii) trace metal analysis,
(iii) particle size analysis,
(iv) ^{210}Pb radiometric dating,
(v) loss on ignition and
(vi) spheroidal carbonaceous particulate analysis.

To demonstrate the temporal variations of the environmental proxy data and therefore atmospheric pollution histories, data analysis has involved:

(i) the presentation of proxy pollution concentration-depth profiles,
(ii) investigation of statistical relationships between the pollution proxies,
(iii) estimation of trace metal enrichment factors and
(iv) transformation of data to flux profiles.

SECTION B: RESULTS

This section of the thesis presents the sediment records obtained from urban pond sites throughout the lower Mersey region (LMR), namely, Daresbury Delph Pond, Windmill Hill, Dogs Kennel Clump and Oglet. Primarily the suitability of these selected urban ponds as long-term air pollution archives are detailed via site descriptions, lake and catchment morphology data, and site histories (Chapter 4). Textural sediment properties and isotope chronologies of the retrieved urban sediment cores are presented to demonstrate the integrity of these ponds to yield intact, reliable sediment columns, from which a datable proxy air pollution record can be obtained (Chapter 5). Proxy pollution data derived from the urban ponds are then presented as concentration-depth profiles and statistical relationships identified between the sediment characteristics within each core are detailed (Chapter 6). Local proxy pollution trends are also presented as flux profiles, demonstrating the supply of trace metals and magnetic grains to the ponds over time (Chapter 7). A cross-regional pollution record for the LMR is also reconstructed via collaboration of the proxy pollution profiles obtained from the four urban ponds (Chapter 8).

4. CHAPTER FOUR: IDENTIFIED SUITABLE URBAN PONDS

4.1. Chapter overview

Site descriptions, catchment analyses and site histories are provided for four urban ponds in and surrounding Halton, which have been identified as, potentially, suitable to yield reliable and intact records of recent (<100 years) of environmental change.

4.2. Introduction

Small urban ponds at Daresbury Delph (National Grid Reference: SJ 357366, 381975), Windmill Hill (SJ 355288, 382666), Oglet (SJ 343491, 381845) and Dogs Kennel Clump (SJ 346344, 382105) (Figure 4.1) were identified as 'high potential' sites for yielding long-term air pollution records, due to their location, age, size, high lake-to-catchment ratios and history of minimal sediment disturbance. Located within and immediately east of Runcorn, ponds at Windmill Hill and Daresbury Delph will have received atmospheric pollution fallout from a combination of sources within the urbanised setting; such as, nearby major roadways, as well as pollutants from industrial sites in Widnes and Runcorn, transported by prevailing north westerly winds. As sources of pollution from south Merseyside are likely to contribute to the pollution experienced in Halton, ponds at Dogs Kennel (northeast Halton) and Oglet (south Merseyside) were also selected, enabling the identification of a potential cross-regional air pollution signal for the lower Mersey region (LMR). OG and DKC are located in the northwest LMR, and DDP and WH in the southeast LMR (Figure 4.1).

All of the studied pond sites are small (lake areas: 192 - 1650 m^2; maximum water depth: 2-3 m) anthropogenic ponds, located within urban settlements. Their locations, size, negligible catchments and, therefore, high lake-to-catchment ratios make them suitable sedimentary archives for urban air pollution histories (Table 4.1) as their morphologies allow reasonable confidence that the primary inorganic sedimentary contribution to the ponds is atmospherically-derived (Section 1.4.5.). The following site descriptions detail the present day and historical morphological features, environmental settings and documented management histories of each site.

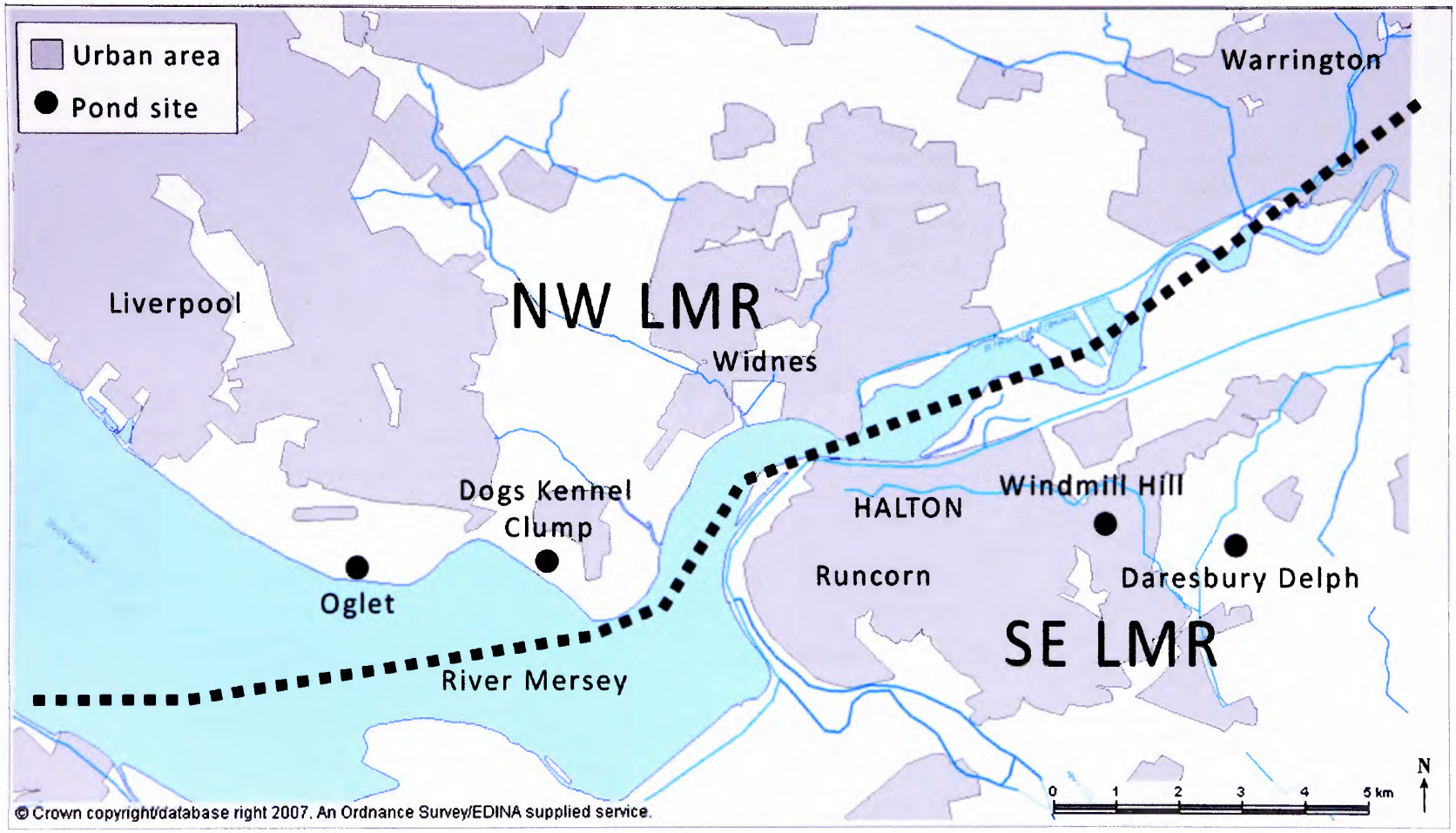

Figure 4.1: Location of investigated pond sites: Oglet, Dogs Kennel Clump, Windmill Hill and Daresbury Delph. Division of the northwest and southeast lower Mersey region is also shown (NW LMR and SE LMR, respectively). Reproduced from the 2007 Ordnance Survey Strategi 1:925915 map with the permission of Ordnance Survey on behalf of The Controller of Her Majesty's Stationery Office © Crown Copyright Edge Hill University, Ormskirk, Lancashire licence number: ED100020392.

Table 4.1: Location and morphology of studied pond sites.

Site	Lake morphology										
	National Grid Reference	Lake area (m^2)	Maximum water depth (m)	Mean water depth (m)	Lake volume (m^3)	Altitude (m) AOD at water surface	Possible extended catchment area (m^2)	Immediate catchment area (m^2)	Lake-to-catchment ratio*	Date of core collection	Collected cores (codes)
Daresbury Delph Pond (DDP)	SJ 357366, 381975	768 (0.0768 ha)	2	1.5	1125	55	~39240 (3.9204 ha)	1088 (0.1088 ha)	1:1.417	09/03/2005	ADD1, ADD2, ADD3, BDD1, BDD2, BDD3
Windmill Hill Pond (WH)	SJ 355288, 382666	256 (0.0256 ha)	2	1.5	384	45	~7875 (0.7875 ha)	450 (0.0450 ha)	1:1.758	09/03/2005	WH1, WH2, WH3
Dogs Kennel Clump Pond (DKC)	SJ 346344, 382105	1650 (0.1650 ha)	3	1.75	2887.5	15	~78400 (7.8400 ha)	2025 (0.2050 ha)	1:1.227	08/09/2000	DK1
Oglet Pond (OG)	SJ 343491, 381845	192 (0.0192 ha)	3	1.75	336	19.2	~960 (0.0960 ha)	256 (0.0256 ha)	1:1.333	08/09/2000	OG 1

* Calculated using immediate lake catchment boundary and lake area.

4.3. Daresbury Delph Pond

Table 4.2: Site description, lake morphology and site history of Daresbury Delph Pond.

Site Location and description	Daresbury Delph, located within the village of Daresbury, is situated immediately east of the urbanised town of Runcorn (Figure 4.2), <4 km from industries at Astmoor (SJ 353630, 383290) and <8 km at Weston (SJ 349726, 381646). There are a series of small marl pits that were created pre-19th century set on agricultural land, which have since been filled with water and used as ponds (SJ 357366, 381968). These ponds currently form part of the Daresbury Business Park complex, which is privately managed. The pond sites are adjacent to a dual carriage way (A56) and motorway (M56). The sediments from two of these basins have been investigated named 'ADD' and 'BDD' (Figure 4.3 B). The management history of the site was investigated via consultation with the present land manager (Mr Bill Hardman) and ecologist at Halton Borough Council (Mr Paul Oldfield), which revealed that of the series of ponds, the larger southwest pond (circled in Figure 4.2) had not been disturbed, unlike the other smaller five ponds which had been desilted. Therefore, this pond, named Daresbury Delph Pond (for the purpose of this study) was selected for further investigation (Plate 4.1).
Lake morphology and catchment	Daresbury Delph Pond (DDP) has a surface area of ~768 m^2, with a maximum water depth of 2 m. The 'ADD' and 'BDD' basins make up the hourglass-shaped Daresbury Delph Pond (Figure 4.3 B). Individually the 'ADD' and 'BDD' basins have surface areas of ~458 m^2 and ~310 m^2, respectively. The pond has an overflow drain, which is presently blocked and the immediate catchment area is defined by the steep vegetated margins of the pond. The bedrock of the site is comprised of Tarporley Sandstone (Sherwood Sandstone Group). The surrounding area comprises of the business park complex and agricultural fields. The extended catchment of the pond is determined by roads, urban development and topography. At 55 m altitude (AOD (Above Ordnance Datum) at water surface), the pond may, potentially, receive catchment run-off from the adjacent agricultural field, which inclines to 60 m (AOD).
Site history	The existence of the ponds date back to at least the mid-19th century, with the ponds apparent on the 1844 tithe map (Figure 4.4 A), which clearly shows the ADD and BDD ponds. The ponds appear 'connected' in the 1882 map, possibly due to a rise in water height (Figure 4.4.B). There appears to have been minimal change in size and shape of the ponds since the mid-19th century; reaffirming that there has been minimal disturbance at this site. Change has occurred within the surrounding area, with the development of Daresbury Business Park complex (SJ 357135, 381578), which originally existed as 'Oaklands Lodge', and developed into 'Lord Daresbury Hotel' during the 1970s and more recently into the business park, which is continually being developed. The section of the M56 motorway adjacent (<700 m to the south) to the pond site (SJ 357279, 381324) was opened between 1971 and 1975; and nearby (1 km to the north) Daresbury Laboratories (SJ 357469, 383091) was constructed in the early 1960s.

Plate 4.1: Daresbury Delph Pond (SJ 357361, 381975) facing north-west, 09/03/2005.

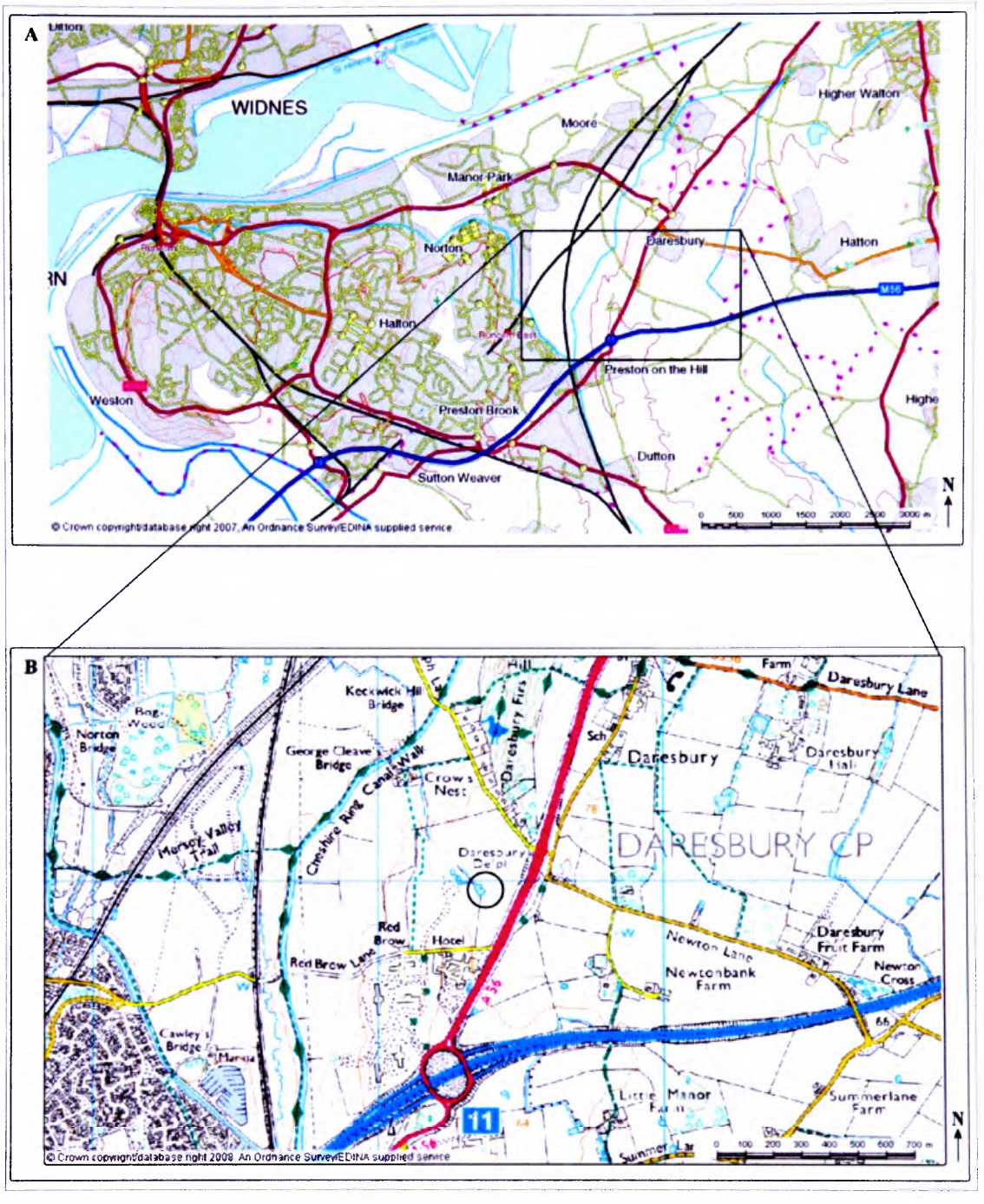

Figure 4.2: Location of Daresbury Delph Ponds (circled) (SJ 357366, 381968), Runcorn 1:146298 (A) and 1:11574 (B). Reproduced from the 2007 Ordnance Survey 1:50 000 Raster 1:146298 (A) and 1:25 000 Raster 1:11574 (B) maps with the permission of Ordnance Survey on behalf of The Controller of Her Majesty's Stationery Office © Crown Copyright Edge Hill University, Ormskirk, Lancashire licence number: ED100020392.

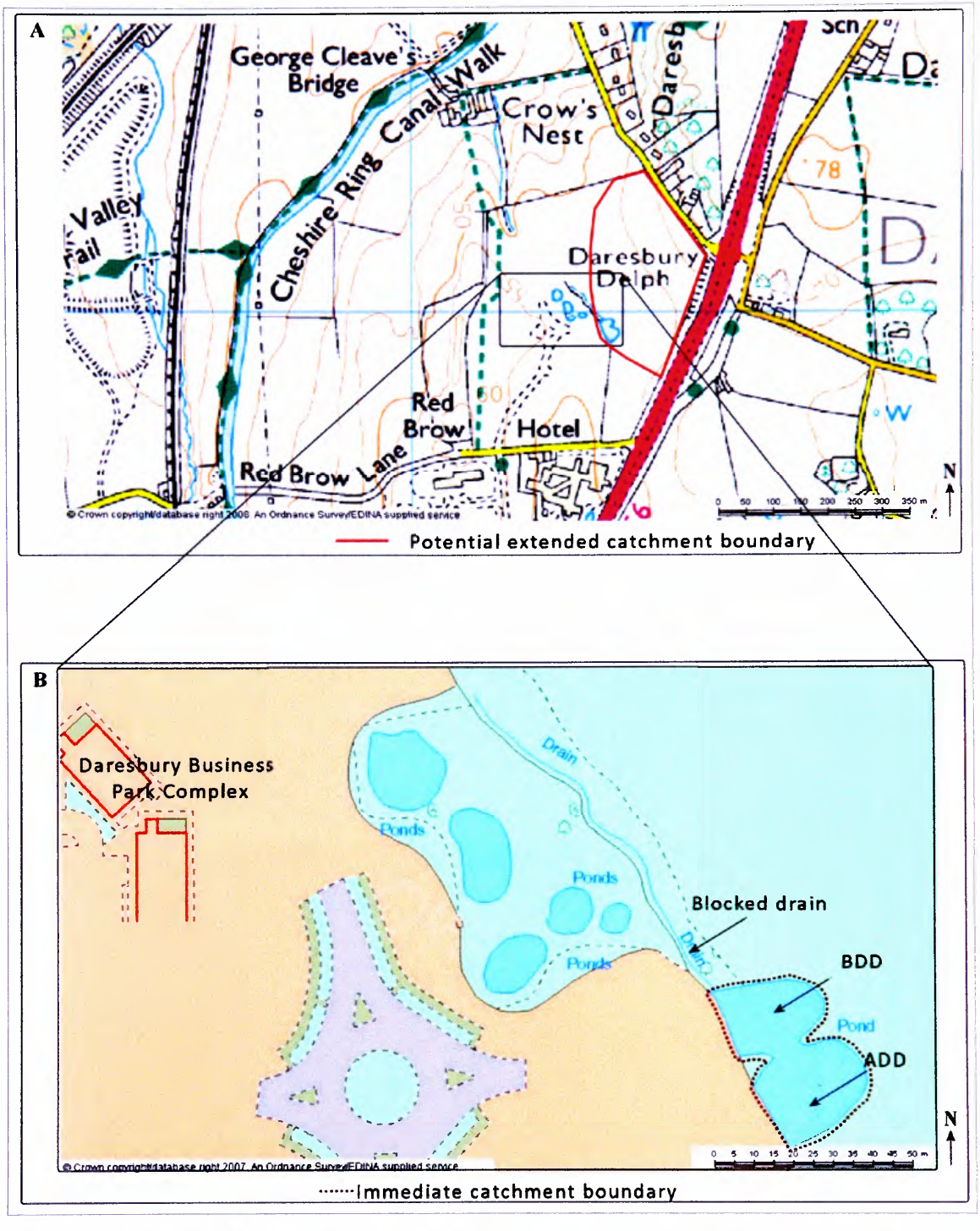

Figure 4.3: Catchment and surrounding environment of Daresbury Delph Pond (SJ 357361, 381975) 1:5787(A) and 1:1319 (B). Reproduced from the 2007 Ordnance Survey 1:25 000 Raster 1:5787 (A) and MasterMap 1:1319 (B) maps with the permission of Ordnance Survey on behalf of The Controller of Her Majesty's Stationery Office © Crown Copyright Edge Hill University, Ormskirk, Lancashire licence number: ED100020392.

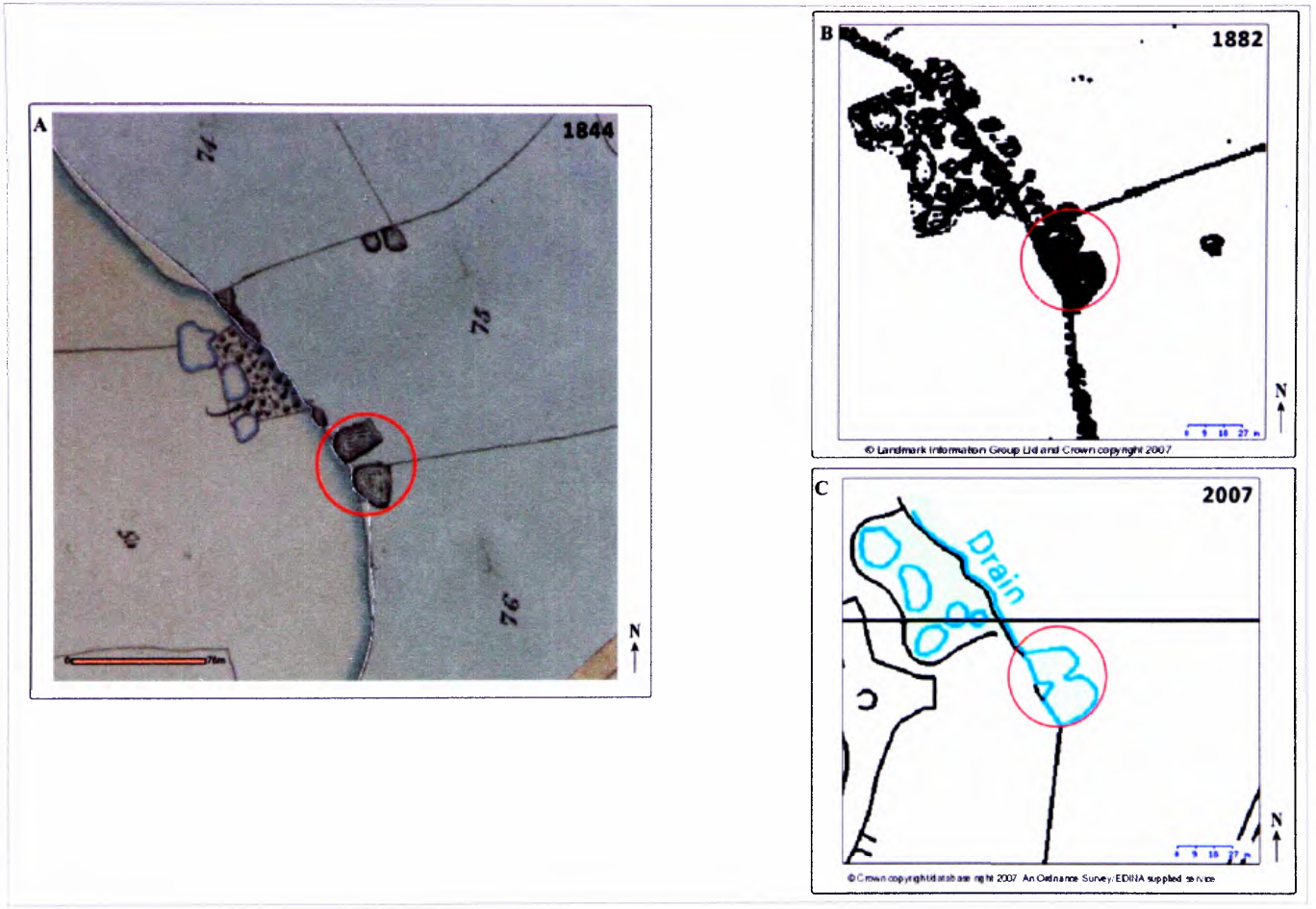

Figure 4.4: Historic views of Daresbury Delph Ponds (SJ 357366, 381968): 1844 (A), 1882 (B) and 2007 (C). Reproduced tithe 1:2400 map from Cheshire County Council http://www.cheshire.gov.uk/tithemaps (A) and the 2007 Ordnance Survey first edition 1882 County Series 1:10560 (B) and contemporary street view (C) maps with the permission of Ordnance Survey on behalf of The Controller of Her Majesty's Stationery Office © Crown Copyright Edge Hill University, Ormskirk, Lancashire licence number: ED100020392.

4.4. Windmill Hill Pond

Table 4.3: Site description, lake morphology and site history of Windmill Hill Pond.

Site Location and description	Windmill Hill Pond (SJ 355288, 382666) is located within a woodland site managed by the Woodland Trust, inside the urban district of Norton, Halton (Figure 4.5). The woodland (22.82 ha) extends north-south along a prominent Helsby Sandstone Formation escarpment, with the bedrock of the pond site comprising of Tarporley siltstone. The woodland is surrounded by residential areas that form part of Runcorn 'New Town', built post-1970, east of the former 'Old Town'. The pond is adjacent to a busy road and is <2 km from industries at Astmoor (SJ 353630, 383290) and <6 km at Weston (SJ 349726, 381646). The woodland site is currently used for recreation and the pond (Plate 4.2) has been used for fly-tipping large domestic items (such as shopping trolleys and bicycles).
Lake morphology and catchment	This small pond (surface area: 256 m^2, ~2 m maximum water depth) is at an altitude of 45 m (AOD at water surface). The steep sided margins of the pond indicate that the inorganic lake input is predominantly from the atmosphere and within this immediate catchment (Figure 4.6 B). The pond may also receive a negligible input from the extended catchment (Figure 4.6 A), which is defined by the footpaths that divide the woodland. Of the four ponds that exist within the woodland, the two north east ponds are dried up (noted on field visit 09/03/2005), although appear to hold water on the OS maps (Figure 4.6). These ponds are, therefore, deemed as unsuitable for investigation, as they may have a blurred environmental signal from inconsistent sediment accumulation from periodic drying.
Site history	The Woodland Trust have no records of any work being carried out on Windmill Hill Pond [Tim Kirwin *Pers. Comm*]; however, the larger pond, in to which it drains, was desilted in 1997 [Paul Oldfield *Pers. Comm.*]. Several quarry faces within the woodland suggest that Windmill Hill Pond is an anthropogenic quarry pit that has been filled with water. Tithe maps date the pond back to at least 1844 (Figure 4.7 A), when the woodland formed part of the Norton Priory Estate. Since this time, there has been minimal change to the size and shape of the pond (Figure 4.7). Historical maps reveal the site has remained as woodland over the last 200 years. In contrast, the surrounding environment has become urbanised due to the New Town development.

Plate 4.2: Windmill Hill Pond (SJ 355288, 382666) facing southeast, 09/03/2005.

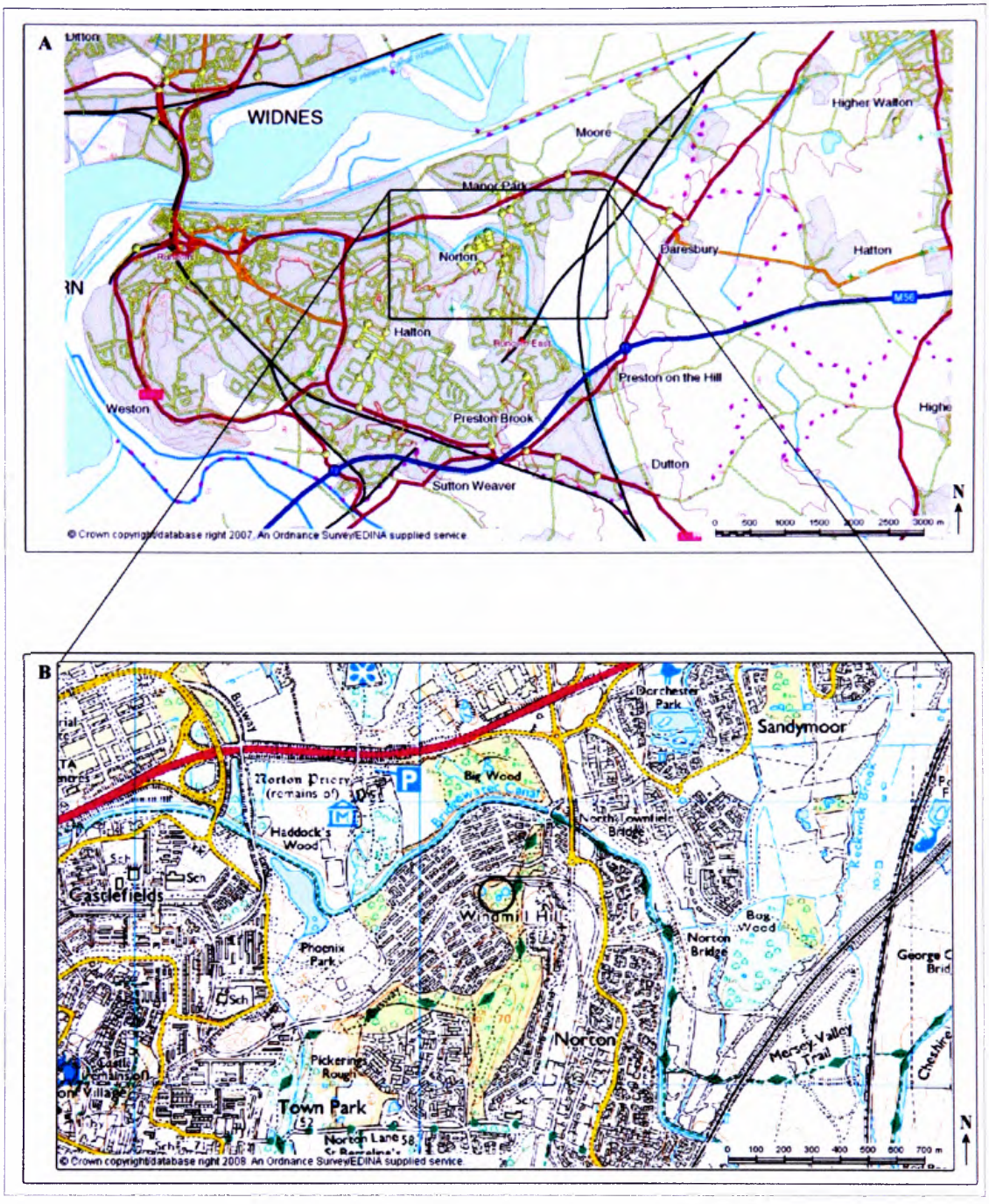

Figure 4.5: Location of Windmill Hill Pond (circled) (SJ 355288, 382666), Runcorn 1:146298 (A) and 1:11574 (B). Reproduced from the 2007(A) and 2008 (B) Ordnance Survey 1:50 000 Raster 1:146298 (A) and 1:25 000 Raster 1:11574 (B) maps with the permission of Ordnance Survey on behalf of The Controller of Her Majesty's Stationery Office © Crown Copyright Edge Hill University, Ormskirk, Lancashire licence number: ED100020392.

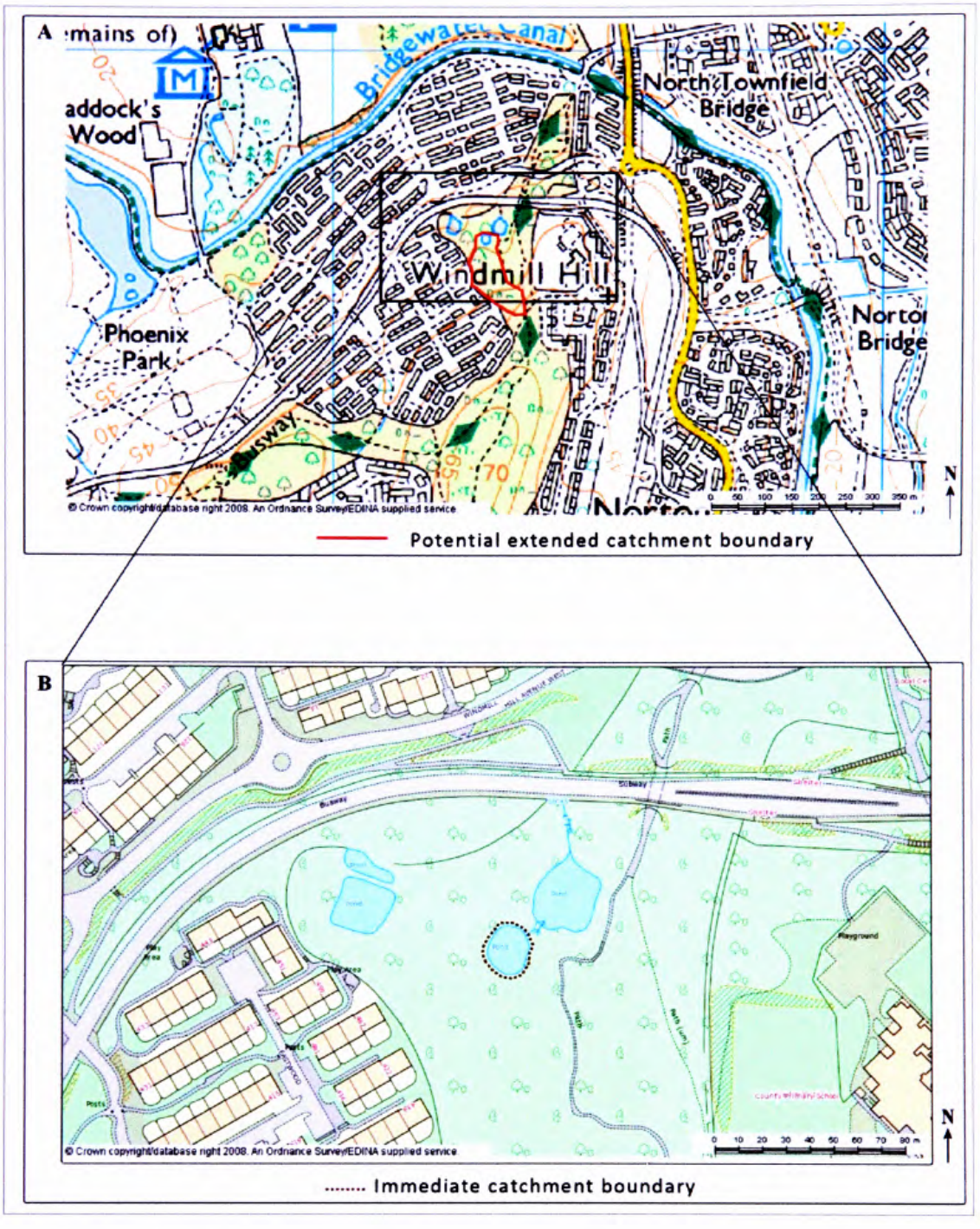

Figure 4.6: Surrounding environment and catchment of Windmill Hill Pond (SJ 355288, 382666) 1:5787 (A) and 1:1319 (B). Reproduced from the 2008 Ordnance Survey 1:25 000 Raster 1:5787 (A) and MasterMap 1:1319 (B) maps with the permission of Ordnance Survey on behalf of The Controller of Her Majesty's Stationery Office © Crown Copyright Edge Hill University, Ormskirk, Lancashire licence number: ED100020392.

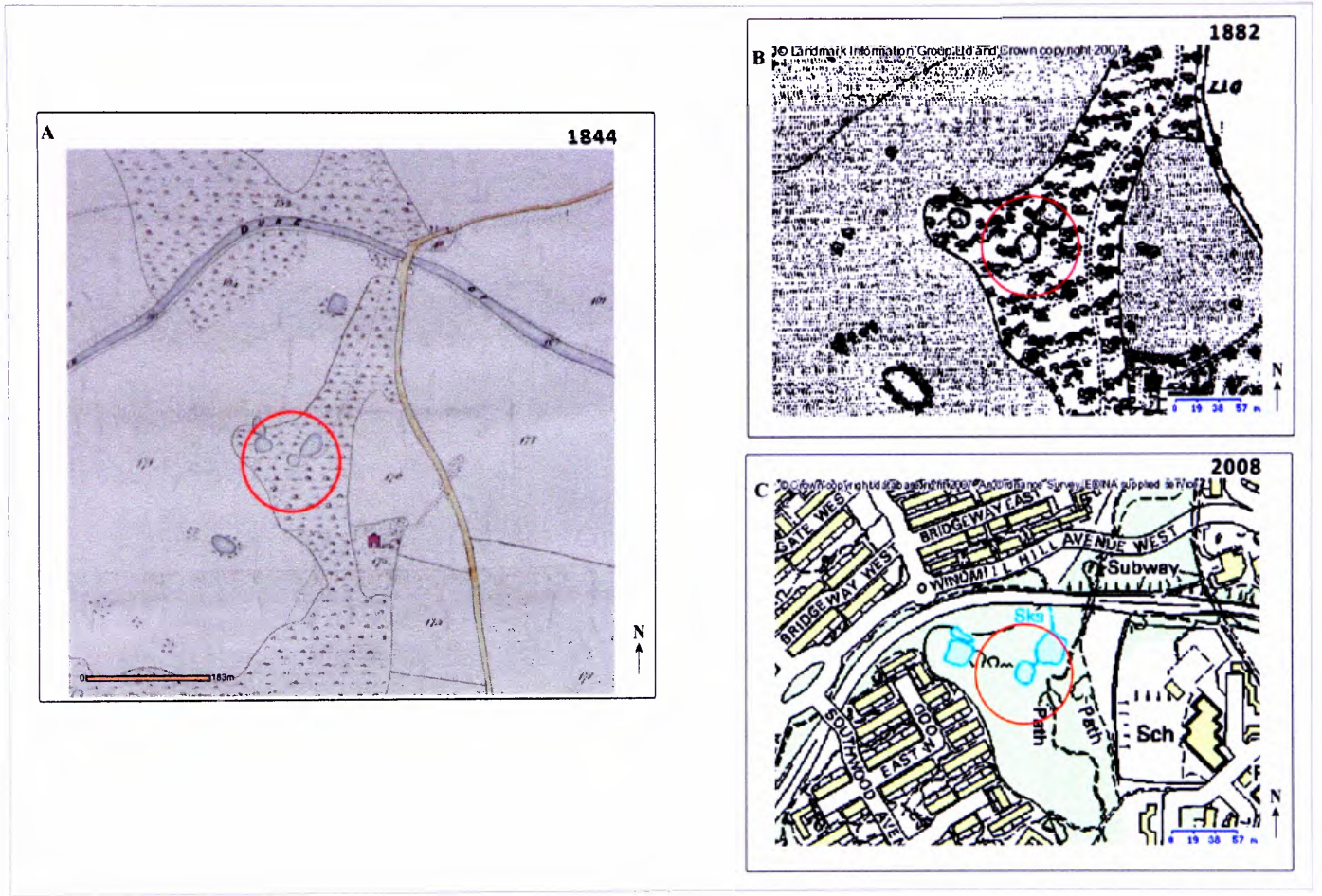

Figure 4.7: Historic views of Windmill Hill Pond (SJ 355288, 382666): 1844 (A), 1882 (B) 2008 (C). Reproduced tithe 1:2400 map from Cheshire County Council http://www.cheshire.gov.uk/tithemaps (A) and the 2008 Ordnance Survey first edition 1882 County Series 1:10560 (B) and contemporary street view (C) maps with the permission of Ordnance Survey on behalf of The Controller of Her Majesty's Stationery Office © Crown Copyright Edge Hill University, Ormskirk, Lancashire licence number: ED100020392.

4.5. Dogs Kennel Clump Pond

Table 4.4: Site description, lake morphology and site history of Dogs Kennel Clump Pond.

Site Location and description	Dogs Kennel Clump Pond (SJ 346344, 382105) is located within the village of Hale, Halton, on private farmland (Home Farm), ~5 km west of Widnes (SJ 350920, 384325) (Figure 4.8). Less than 3 km northwest of Hale village is an industrial site including chemical and pharmaceutical industries, a motor car production works (SJ 344532, 3840) and <4 km industrial works at Halewood (SJ 343435, 384608). Also nearby (<3 km west) is Liverpool John Lennon International Airport (SJ 343149, 382644), originally 'Speke Airport', which opened in 1933.
Lake morphology and catchment	This small (1650 m^2 lake area, 3 m maximum water depth) agricultural pond is a closed system, with no drainage outflows, and is located within a low-lying (15 m AOD at water surface) flat relief. The potential input from the extended catchment (Figure 4.9 A) is therefore negligible, with the main contribution of inorganic sedimentary input to the lake coming from the atmosphere and the immediate surrounding catchment, defined by the steep, vegetated margins of the pond (Figure 4.9 B). The geology of the site comprises of Shirdley Hill Sand Formation deposits overlying Chester Pebble Beds Formation bedrock.
Site history	Originally a marl pit, the pond has experienced minimal change in size and shape (Figure 4.10) and the present land owner (Mr Harrison) had no records of any work carried out on the pond. The area surrounding the pond has experienced no notable change and Hale village has remained a small village since the mid-19th century, unlike Widnes (<5 km east) and the nearby city of Liverpool (<8 km northwest) that have undergone major expansion since the Industrial Revolution.

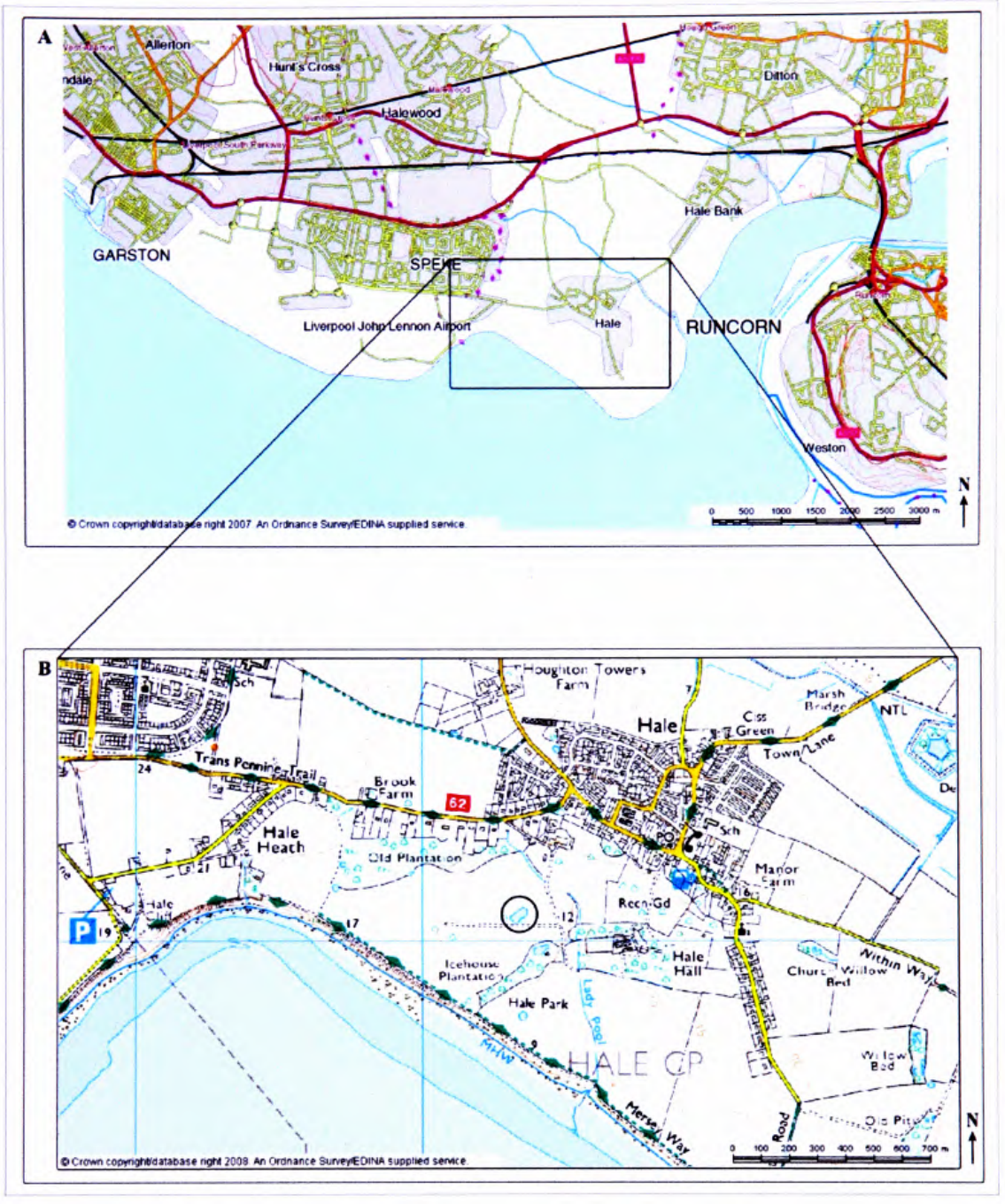

Figure 4.8: Location of Dogs Kennel Clump Pond (circled) (SJ 346344, 382105), Halton 1:46298 (A) and 1:11574 (B). Reproduced from the 2007(A) and 2008 (B) Ordnance Survey 1:50 000 Raster 1:146298 (A) and 1:25 000 Raster 1:11574 (B) maps with the permission of Ordnance Survey on behalf of The Controller of Her Majesty's Stationery Office © Crown Copyright Edge Hill University, Ormskirk, Lancashire licence number: ED100020392.

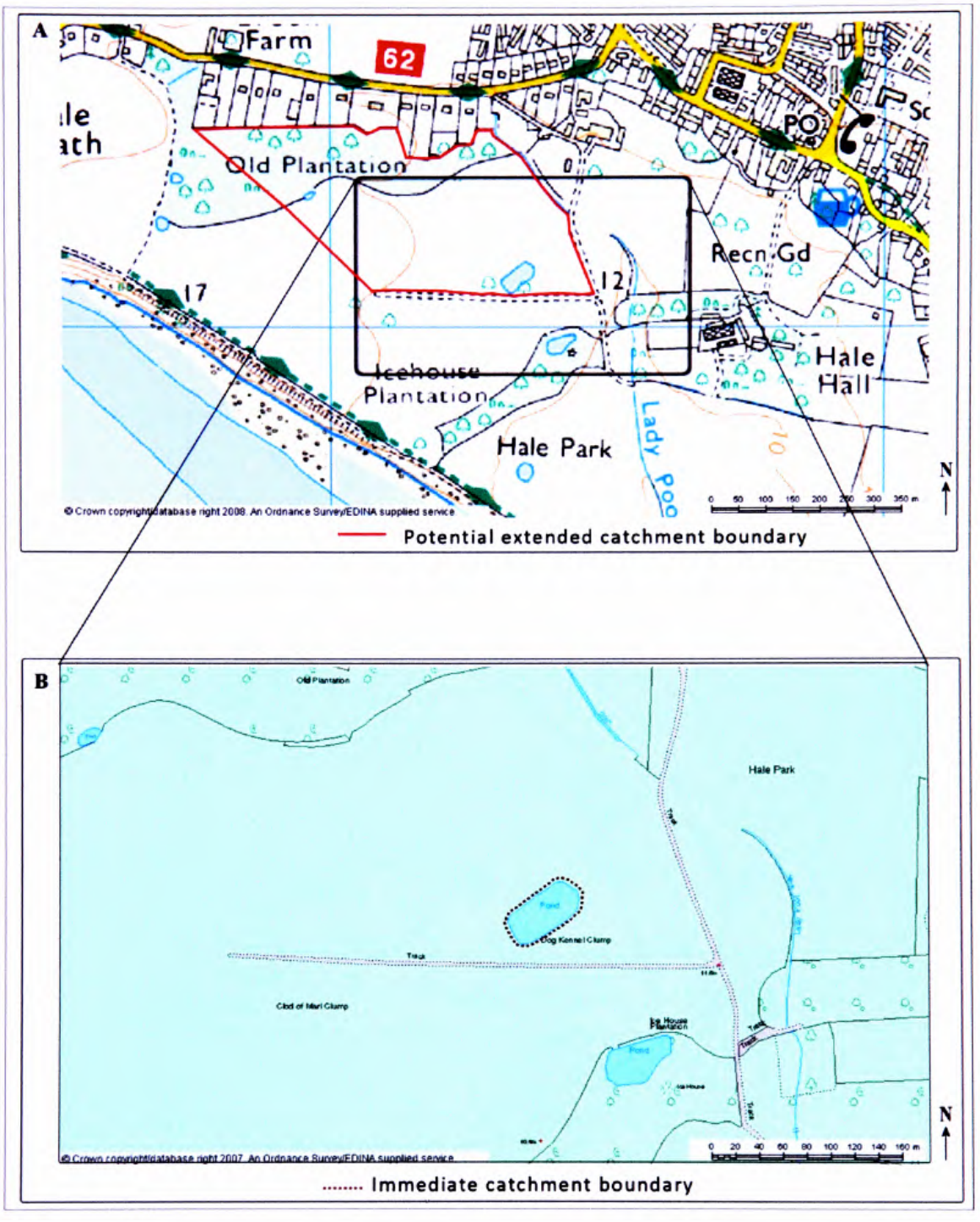

Figure 4.9: Surrounding environment and catchment of Dogs Kennel Clump Pond (SJ 346344, 382105) 1:5787 (A) and 1:2639 (B). Reproduced from the 2008 Ordnance Survey 1:25 000 Raster 1:5787 (A) and MasterMap 1:1319 (B) maps with the permission of Ordnance Survey on behalf of The Controller of Her Majesty's Stationery Office © Crown Copyright Edge Hill University, Ormskirk, Lancashire licence number: ED100020392.

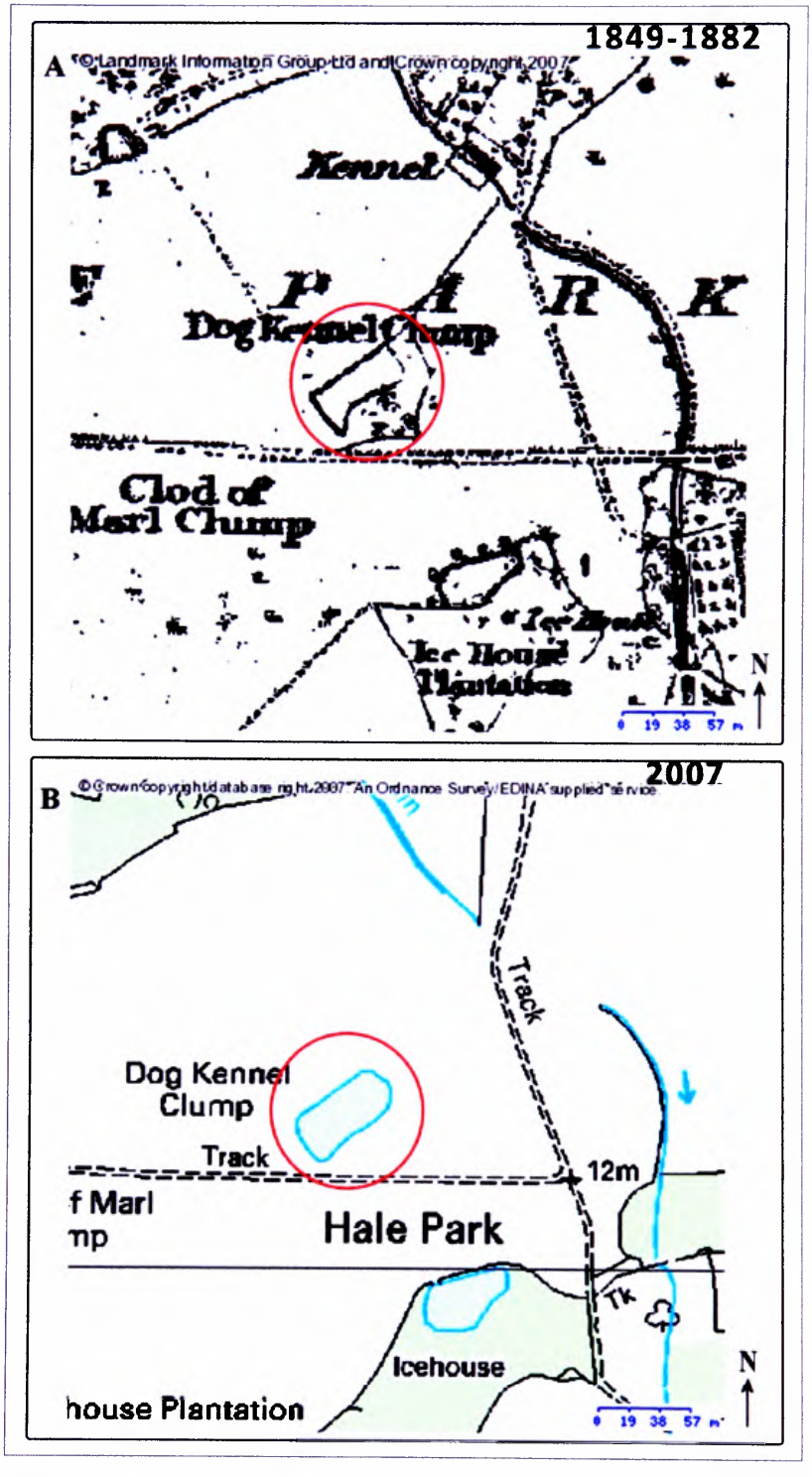

Figure 4.10: Historic views of Dogs Kennel Clump Pond (SJ 346344, 382105): 1849-1882 (A) and 2007 (B). Reproduced 2007 Ordnance Survey first edition 1882 County Series 1:10560 (A) and contemporary street view (B) maps with the permission of Ordnance Survey on behalf of The Controller of Her Majesty's Stationery Office © Crown Copyright Edge Hill University, Ormskirk, Lancashire licence number: ED100020392.

4.6. Oglet Pond

Table 4.5: Site description, lake morphology and site history of Oglet Pond.

Site Location and description	Oglet Pond (SJ 343491, 381845) is located on private agricultural fields in south Merseyside within 2.5 km east of the estate at Speke Hall (SJ 341882, 382568) and is 2 km west of Dogs Kennel Clump Pond. The site is <2.8 km northeast from industries at Halewood (SJ 343435, 384608) and <1 km east from Liverpool John Lennon International Airport (SJ 344532, 384001) (Figure 4.11). The geology of the area comprises of Chester Pebble Beds Formation, overlain with till.
Lake morphology and catchment	Oglet is the smallest of the investigated ponds (lake area: 192 m^2, maximum water depth: 3 m) and its catchment is defined by steep sided lake margins and a small wooded area that surrounds the pond (Figure 4.12 B). A track running east-west, north of the pond and the low lying (19.2 m AOD at water surface) flat topography of the surrounding area, suggests that there is negligible input from outside this extended catchment (Figure 4.12 A).
Site history	The pond, originally a marl pit, is evident on the 1781 (Addison's Map) and 1st edition OS map (1849-1882). The pond lies on old agricultural field boundaries dividing 'Wood End' and 'Wood Croft' (Figure 4.13 A). The historic views of the pond show that the shape of the pond has changed slightly between 1781 (Figure 4 13 A) and 1849 (Figure 4 13 B); however, there is no notable change since 1849 (Figure 4.13 C). A second pond, south of Oglet, evident in the 1781 and 1849 maps, has silted up. The present land owner (Mr John Williams) has no records of any work being carried out at the site and believes the pond to be undisturbed.

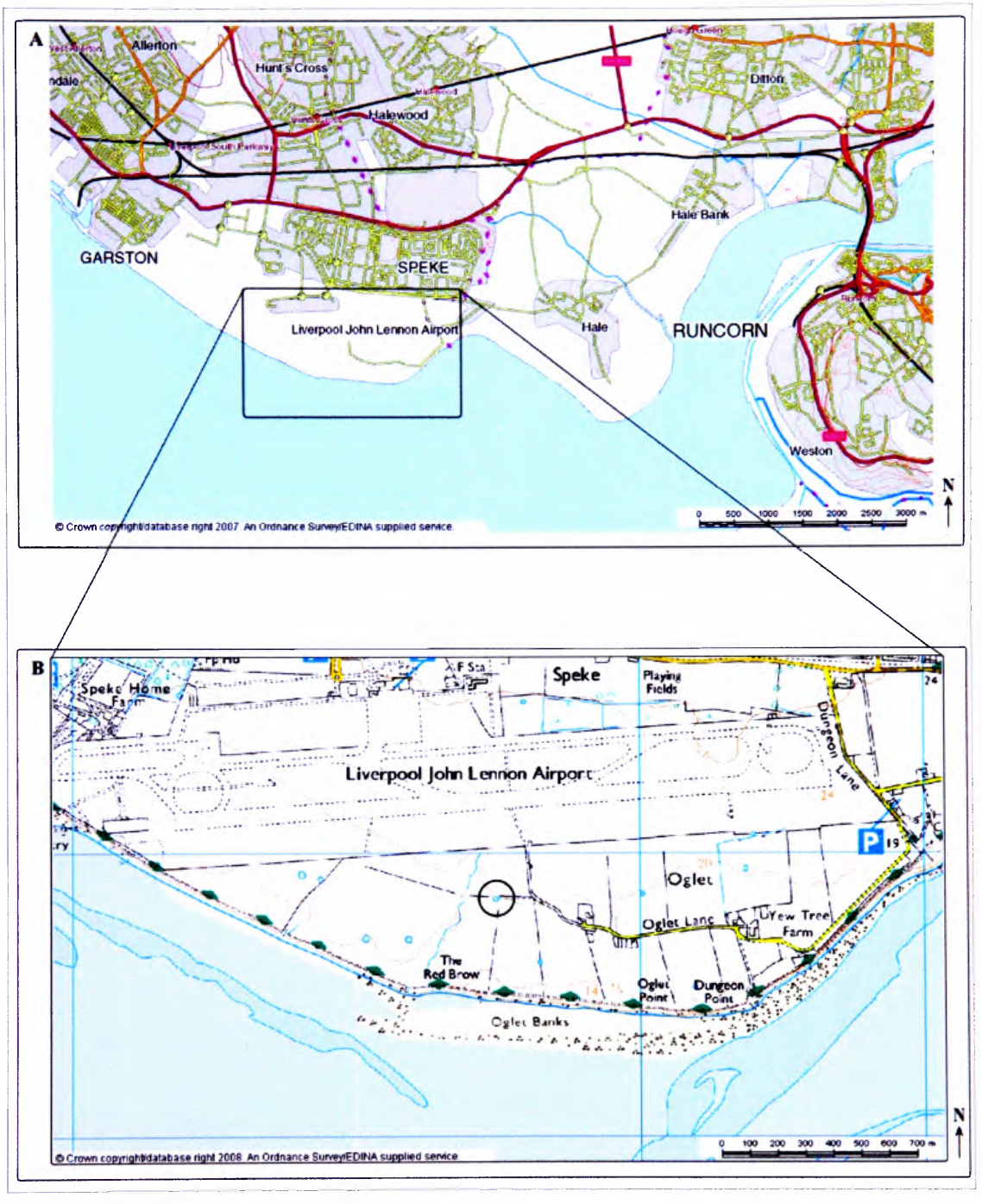

Figure 4.11: Location of Oglet Pond (circled) (SJ 343491, 381845), south Merseyside 1:146298 (A) and 1:11574 (B). Reproduced from the 2007(A) and 2008 (B) Ordnance Survey 1:50 000 Raster 1:146298 (A) and 1:25 000 Raster 1:11574 (B) maps with the permission of Ordnance Survey on behalf of The Controller of Her Majesty's Stationery Office © Crown Copyright Edge Hill University, Ormskirk, Lancashire licence number: ED100020392.

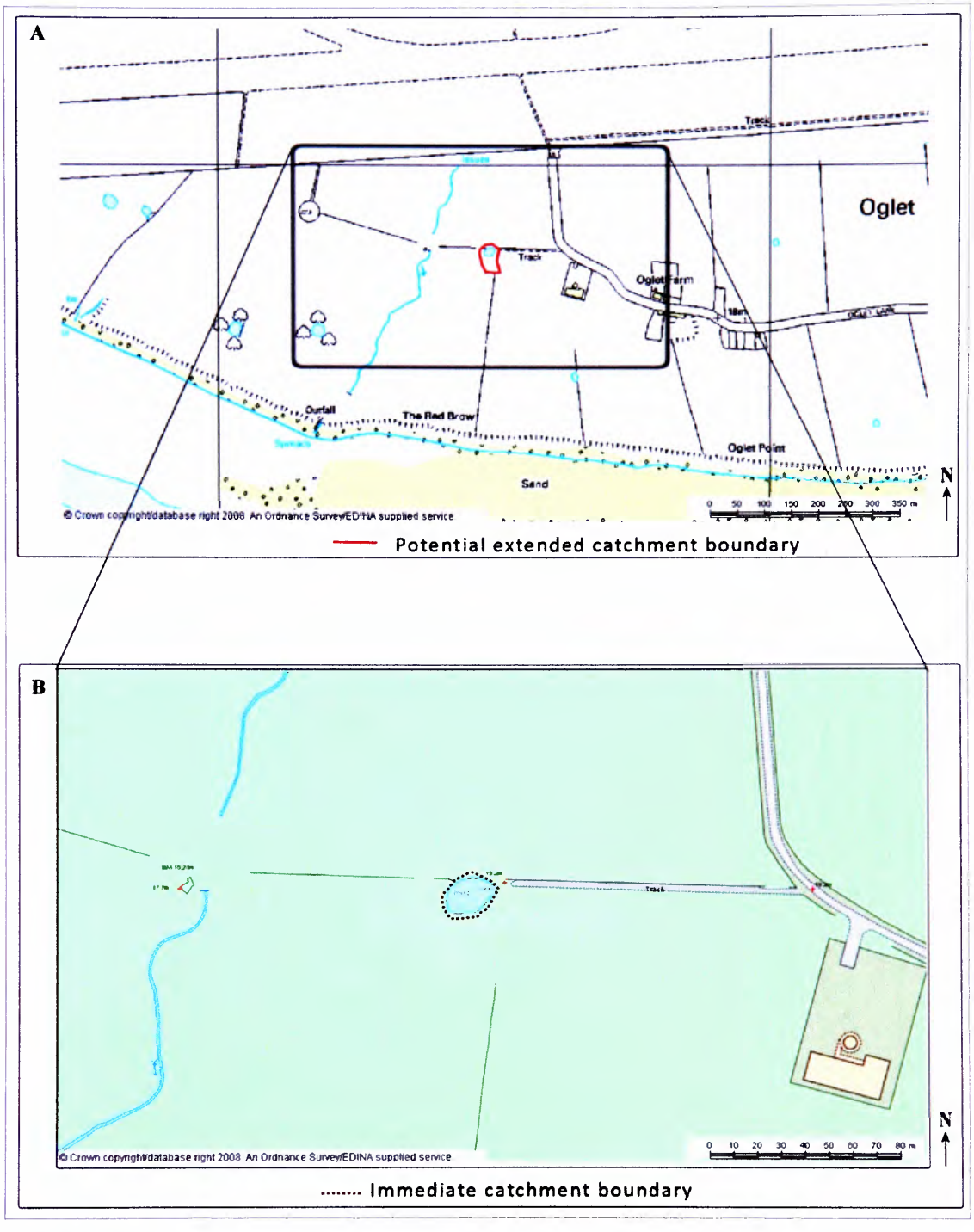

Figure 4.12: Surrounding environment and catchment of Oglet Pond (SJ 343491, 381845) 1:5787 (A) and 1:1319 (B). Reproduced from the 2008 Ordnance Survey 1:25 000 Raster 1:5787 (A) and MasterMap 1:1319 (B) maps with the permission of Ordnance Survey on behalf of The Controller of Her Majesty's Stationery Office © Crown Copyright Edge Hill University, Ormskirk, Lancashire licence number: ED100020392.

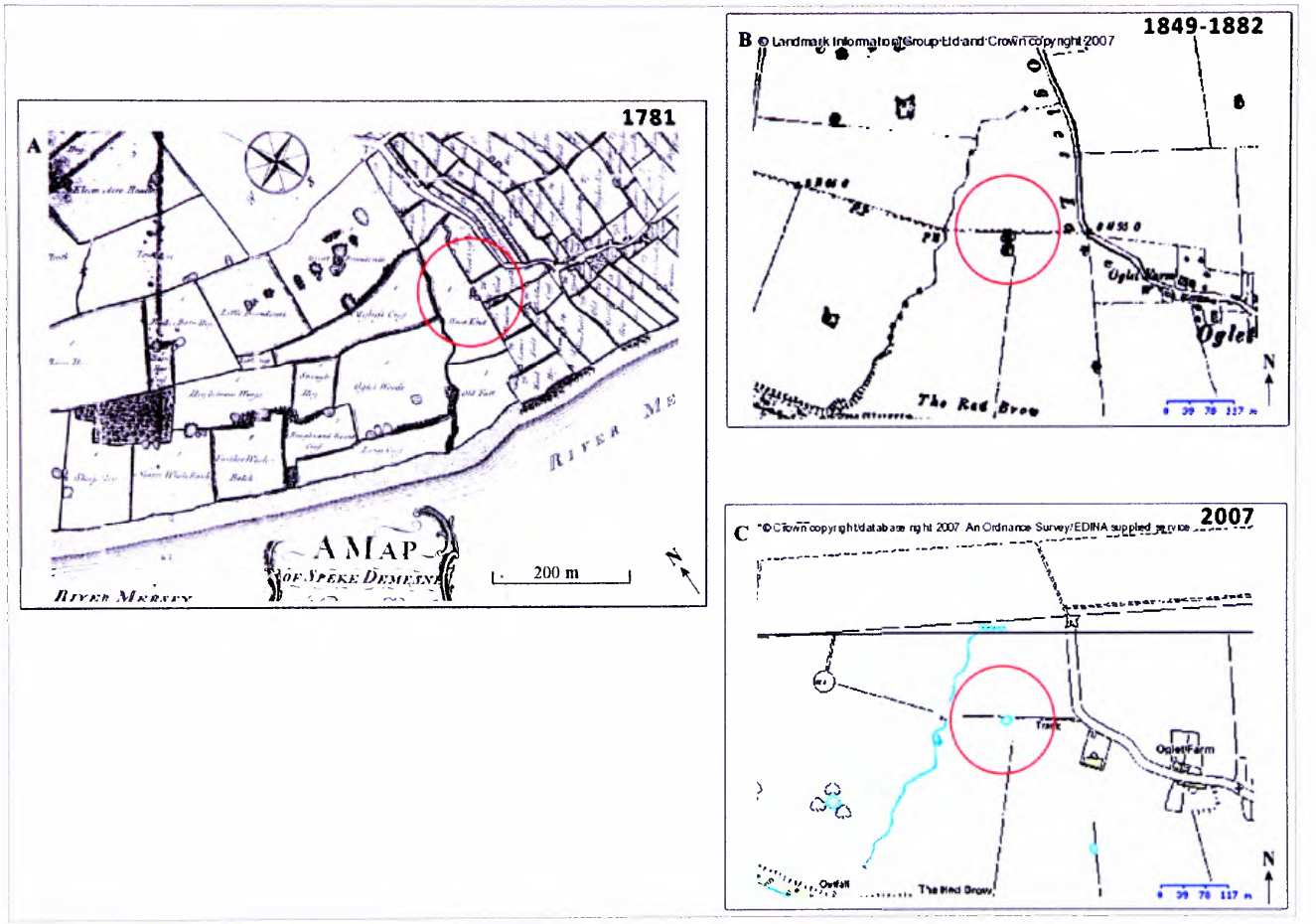

Figure 4.13: Historic view of Oglet Pond (SJ 343491, 381845): 1781 Addison's Map of Speke (A) 1849- 1882 (B) and 2007 (C). Reproduced Addison's map from Cheshire County Council (A) and 2007 Ordnance Survey first edition 1882 County Series 1:10560 (B) and contemporary street view (C) maps with the permission of Ordnance Survey on behalf of The Controller of Her Majesty's Stationery Office © Crown Copyright Edge Hill University, Ormskirk, Lancashire licence number: ED100020392.

4.7. Chapter summary

Four urban ponds in and surrounding Halton, have been identified as suitable sites of investigation:

(i) Daresbury Delph Pond, Halton

(ii) Windmill Hill Pond, Halton

(iii) Dogs Kennel Clump Pond, Halton and

(iv)Oglet Pond, south Merseyside.

These ponds meet the criteria, set out in Section 3.3, for which there is potential for yielding intact and reliable sediment archives of environmental change. Favourable characteristics, such as location and longevity within the urban landscape, histories of minimal site disturbance and high lake-to-catchment ratios, demonstrate the suitability of these ponds to be utilised in reconstructing a 150-year cross-regional air pollution history for the LMR.

5. CHAPTER FIVE: RETRIEVED URBAN SEDIMENT STRATIGRAPHIES

5.1. Chapter overview

This chapter presents sediment stratigraphies obtained from Daresbury Delph, Windmill Hill, Dogs Kennel Clump and Oglet ponds. The correlation of multiple cores collected from Daresbury Delph Pond is also detailed, along with basic sediment descriptions, and textural properties of the 'master cores' collected from each site. Chronologies and calculated sediment accumulation rates are also presented.

5.2. Introduction

Sediment stratigraphies retrieved from four urban pond sites, Daresbury Delph, Windmill Hill, Dogs Kennel Clump and Oglet, are presented. In order to reconstruct proxy air pollution histories from urban ponds it is important to first establish the integrity of the sediment archive to yield intact, reliable and datable sediment records. Primarily, the reproducibility of undisturbed sediment columns from an urban pond is explored by the correlation of multiple cores from Daresbury Delph Pond. The urban pond sediment stratigraphies are further investigated by characterisation of the sediment cores via visual inspection, particle size distributions, sediment densities and the proportion of organic matter to the sedimentary matrix. Sediment sequences that extend to pre-industrial times, with high-resolution and accurate depth-time profiles are essential for the reconstruction of reliable sediment records of temporal air pollution characteristics. Chronologies obtained from radioisotope dating are, therefore, also presented to assess the suitability of urban ponds as long-term (>200-year) sediment archives.

5.3. Urban core correlation: Daresbury Delph Pond

Multiple cores were collected from Daresbury Delph Pond (DDP). BDD1, BDD2 and BDD3 cores were retrieved from the northern section of the pond; whilst ADD1 and ADD2 were collected from the southern section (Figure 4.1). Although these two sections can be treated as separate ponds, they are grouped under 'DDP' and their sediment characteristics are presented to demonstrate the reproducibility of reliable sediment stratigraphies from urban ponds.

Basic sediment descriptions are provided for BDD1, BDD2, BDD3, ADD1 and ADD2 (Figure 5.1). The longest column of sediment retrieved from DDP was the BDD1 core (51 cm), the top 40.5 cm of which is comprised of detritus organic mud. At 40.5 to 41 cm there is a distinguishable layer of woody material and from 41.5 cm to 51 cm a change in composition occurs, with a visibly increased contribution of sand grains. As sand does not typically comprise autochthonous material, this section of the core, potentially, represents a layer of sediment infill that was probably deposited immediately after the pond was constructed. Shorter stratigraphies of detritus organic mud are observed for BDD2 (29 cm) BDD3 (33.5 cm) ADD1 (23.5 cm) and ADD2 (35.5 cm).

As the sediment descriptions reveal no distinguishable layers between the five cores, intra-site 'visual correlations'* have been assessed by identifying parallels in down-core variations of magnetic susceptibility (χ_{LF}) [Thompson *et al.*, 1975] (Figure 5.2). There appear to be similarities between the five cores, with four main closely paralleled features (Table 5.1).

* Here the term 'visual correlation' is used to describe parallels between intra-site cores, opposed to its statistical term.

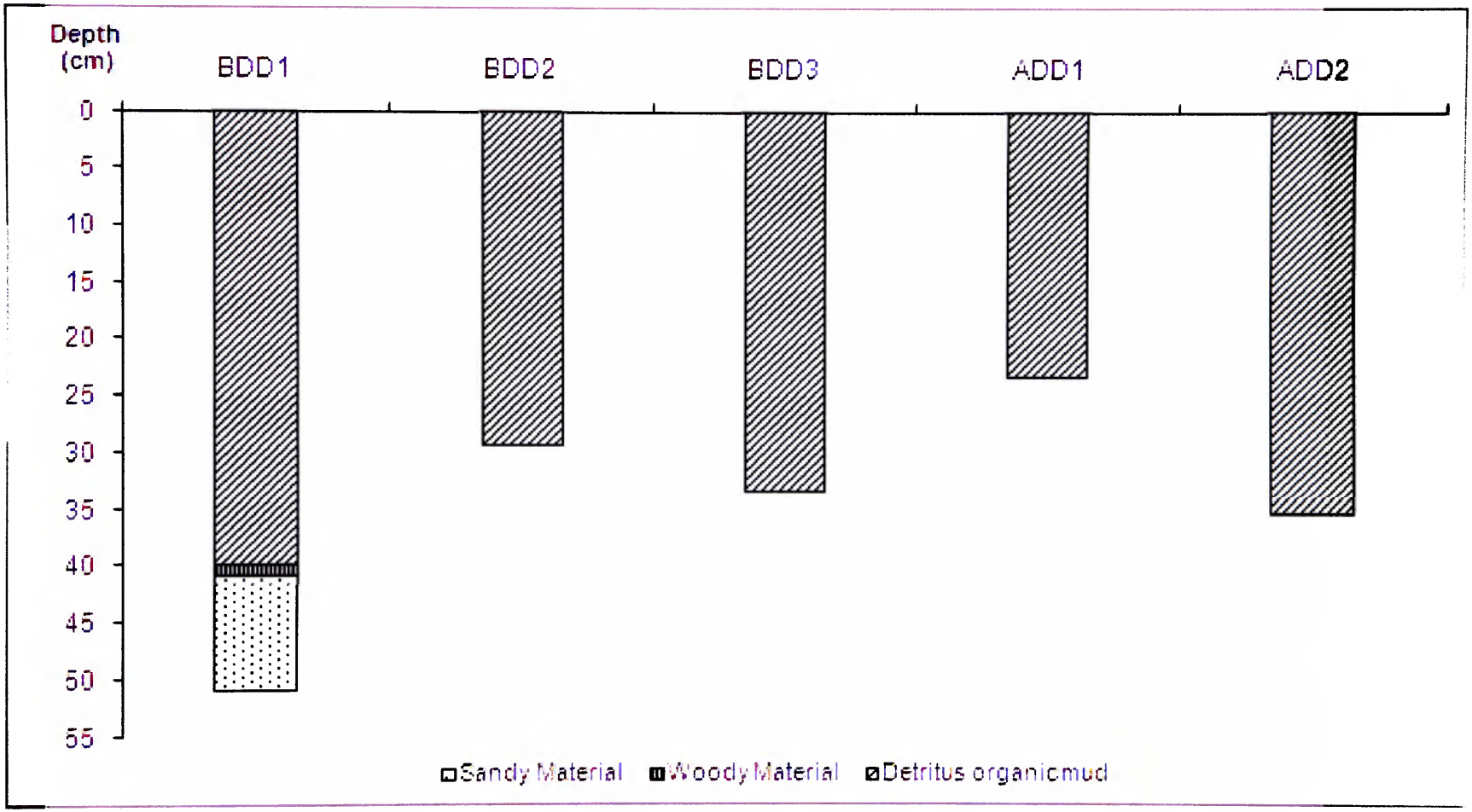

Figure 5.1: Basic sediment descriptions for the five cores collected from Daresbury Delph Pond: BDD1, BDD2, BDD3 ADD1 and ADD2.

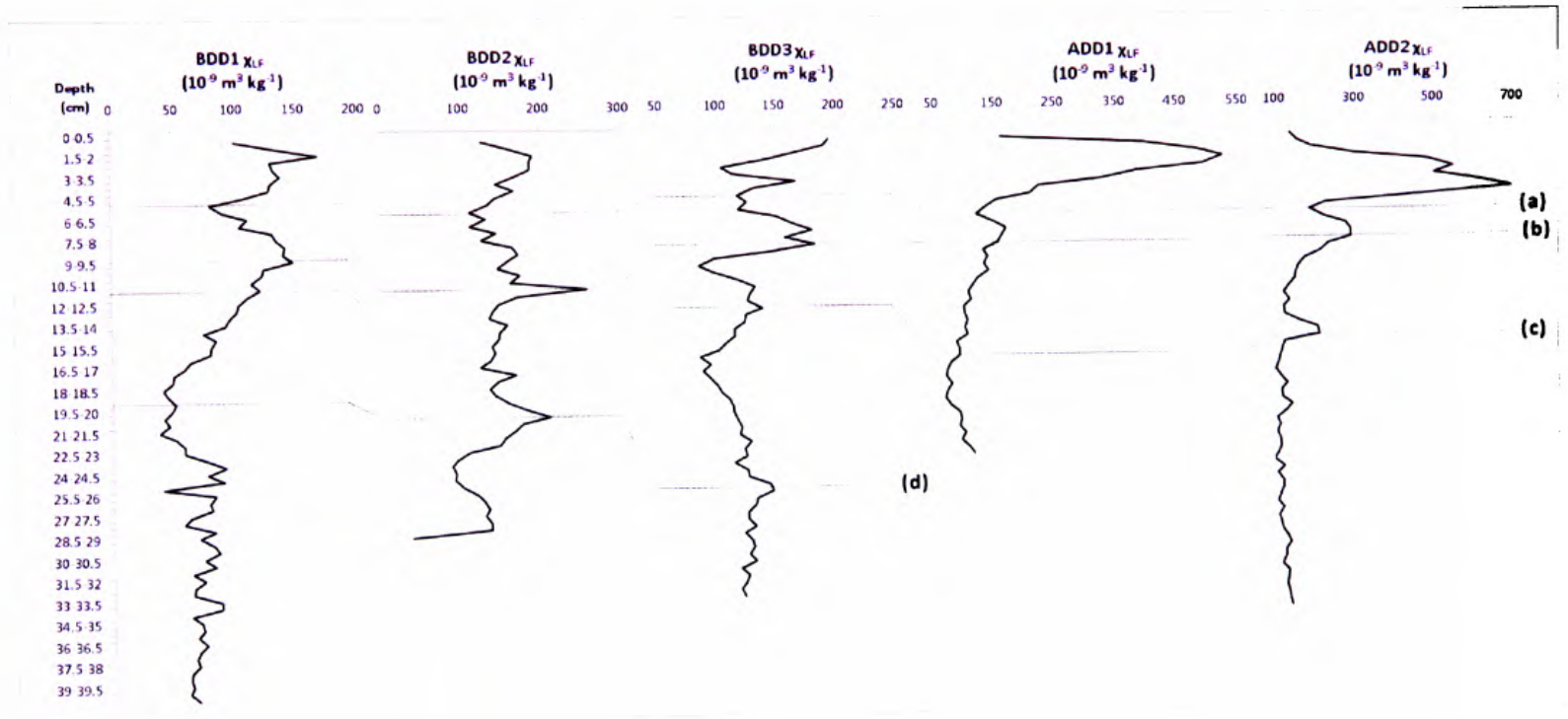

Figure 5.2: χ_{LF} profiles for the Daresbury Delph Pond cores: BDD1, BDD2, BDD3, ADD1 and ADD2 with highlighted correlating features (corresponding to Table 5.1).

Table 5.1: Correlating magnetic concentration (χ_{LF}) features observed in the Daresbury Delph Pond cores (corresponding to Figure 5.2).

Feature	Depth of feature in Daresbury Delph profiles (cm)					Description of χ_{LF} profiles
	BDD1	BDD2	BDD3	ADD1	ADD2	
(a)	5-5.5	5.5-6	4-4.5	6-6.5	6-6.5	Notable decrease in χ_{LF}, which occurs after prominent high values in the most recent section of the cores.
(b)	9-9.5	11-11.5	8-8.5	8-8.5	8-8.5	Second prominent peak mirrored throughout the cores.
(c)	11-11.5	13.5-14	12.5-13	14-14.5	15-15.5	Notable peak; of relatively lower magnetic concentration than feature (b) and peaks observed between the sediment surface and feature (a).
(d)	19-19.5	20-20.5	25.5-26			Marked increases in BDD1, BDD2 and BDD3; however trends in ADD1 and ADD2 are less pronounced with depth.

5.4. Sediment stratigraphies retrieved from urban ponds

Sediment stratigraphies of master cores obtained from the four investigated sites: Daresbury Delph Pond (BDD1), Windmill Hill (WH3), Dogs Kennel Clump (DKC) and Oglet (OG) are presented (Figure 5.3). In addition to the 40.5 cm sediment column of detritus organic mud (BDD1) obtained from DDP, a 44 cm sediment stratigraphy was retrieved from DKC, comprised of uniform sediment, characterised as detritus organic mud, with a 3 cm layer of woody material occurring from 29 to 32 cm. Shorter sediment stratigraphies were also obtained from WH and OG, respectively, comprised of 23.5 cm and 19.5 cm of detritus organic mud. Distinct clay layers are observed in the WH (23.5 to 25.5 cm) and OG (19.5 to 21.5 cm) cores, distinguished by a notable pale grey colour, which, potentially, represents the artificial linings of the ponds. There are no other visibly distinguishable features observed within the sediment stratigraphies.

The textural properties for each site are revealed via down-core organic matter (OM) percentages, dry bulk density values, particle size distributions and median particle sizes (Figures 5.4, 5.5, 5.6 and 5.7, Tables 5.2, 5.3, 5.4 and 5.5).

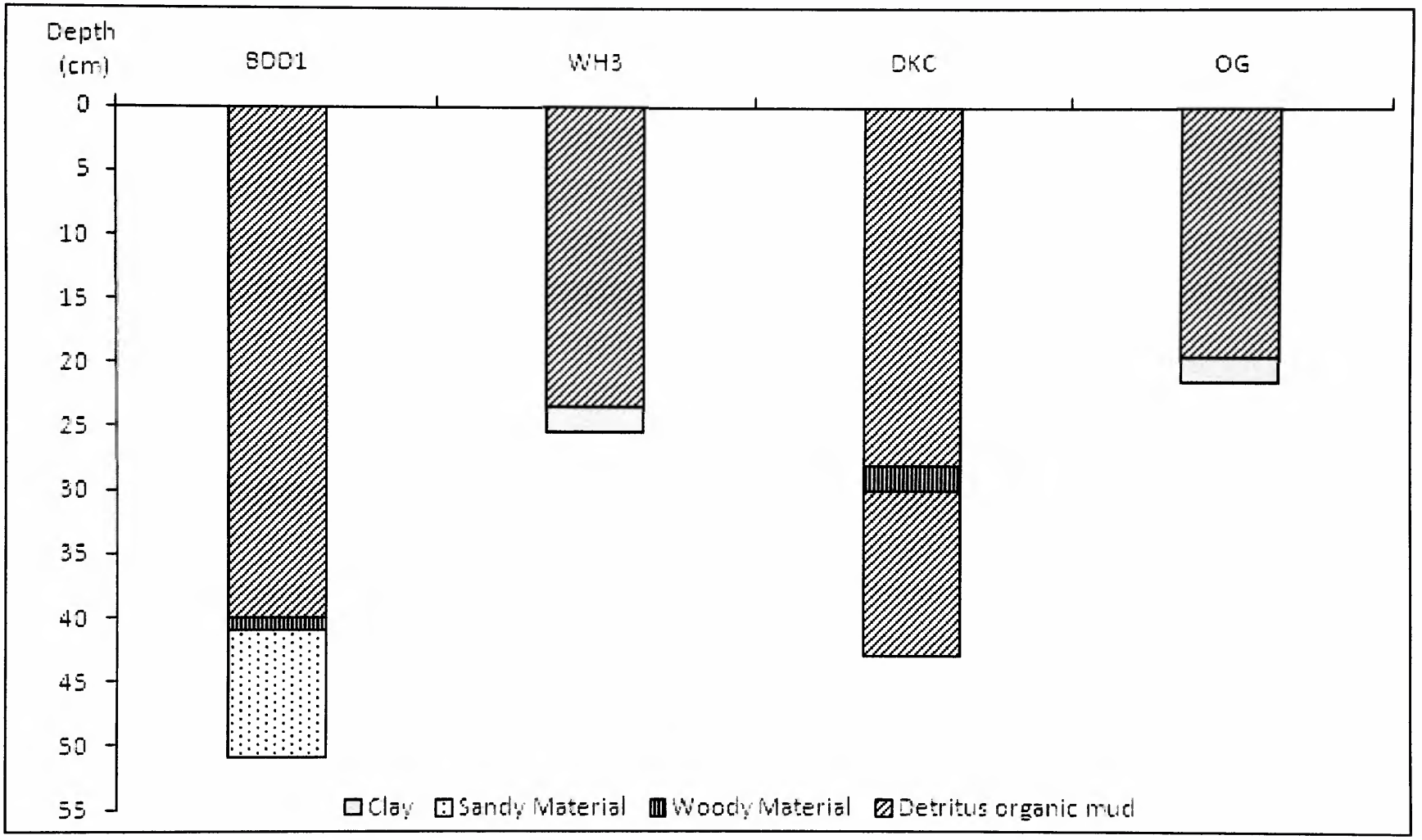

Figure 5.3: Sediment descriptions of cores collected from Daresbury Delph (BDD1), Windmill Hill (WH3), Dogs Kennel Clump (DKC) and Oglet (OG) ponds.

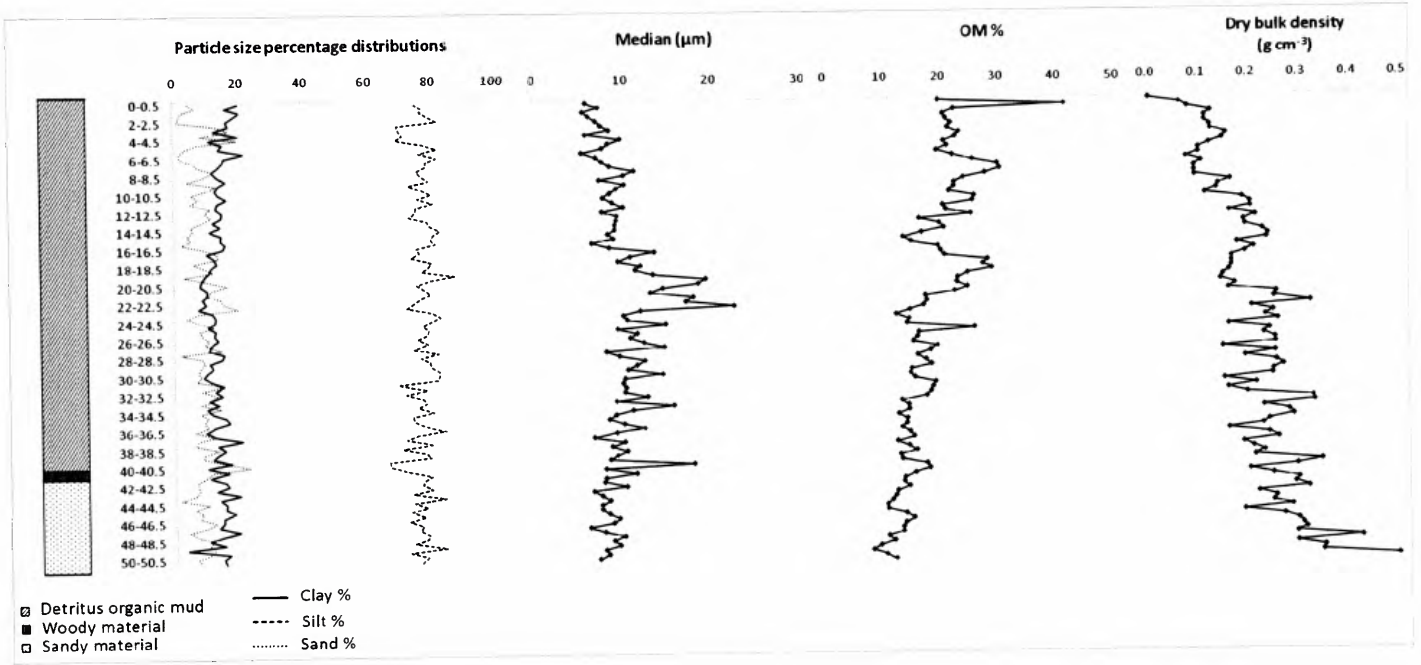

Figure 5.4: Sediment description and textural properties for BDD1 (corresponding to Table 5.2).

Table 5.2: Textural properties of BDD1 core (corresponding to Figure 5.4).

Core	Textural description
BDD1	Percentage particle size distributions range from 3.42 to 21.69% for clay, 1.16 to 22.95% for sand, and 67 to 87.68 % for silt. This demonstrates that overall the sediment column is primarily composed of silt sized particles (2 - 63 µm) with lower contributions of sand (> 63 µm) and clay (< 2 µm) fractions. The identified sediment infill layer that occurs from 40.5 to 51 cm is highlighted by low organic content and high dry bulk density values. BDD1 demonstrates a mean OM% of 19.742%, with values ranging from 12.45% to 41.66%. There is a notable shift at 20-20.5 cm from higher dry bulk densities (0.2-0.5 g cm^3) in the lower section of the core (20-20.5 to 40-40.5 cm), to relatively lower density sediment (< 0.25 g cm^3) above 20.5 cm, with a steady decrease in density to the sediment surface. Overall, OM % increases from the base of the core to the sediment surface, with relatively low OM % values (~10-25%) occurring from 23-24 cm to the base of the core. Above 23 cm there is an increase in OM % with prominent peaks at 18.5 to 19 cm (29.12%), 7-7.5 cm (30.12%) and 0.5-1 cm (41.66%). The clay component appears to steadily increase from 7.96% at 20-20.5 cm to 20.50% at 0-0.5 cm, with values between ~15-20% above 20 cm. The median particle diameter profile demonstrates an apparent shift from >10 µm below 16 cm, to <10 µm in sediment above this depth.

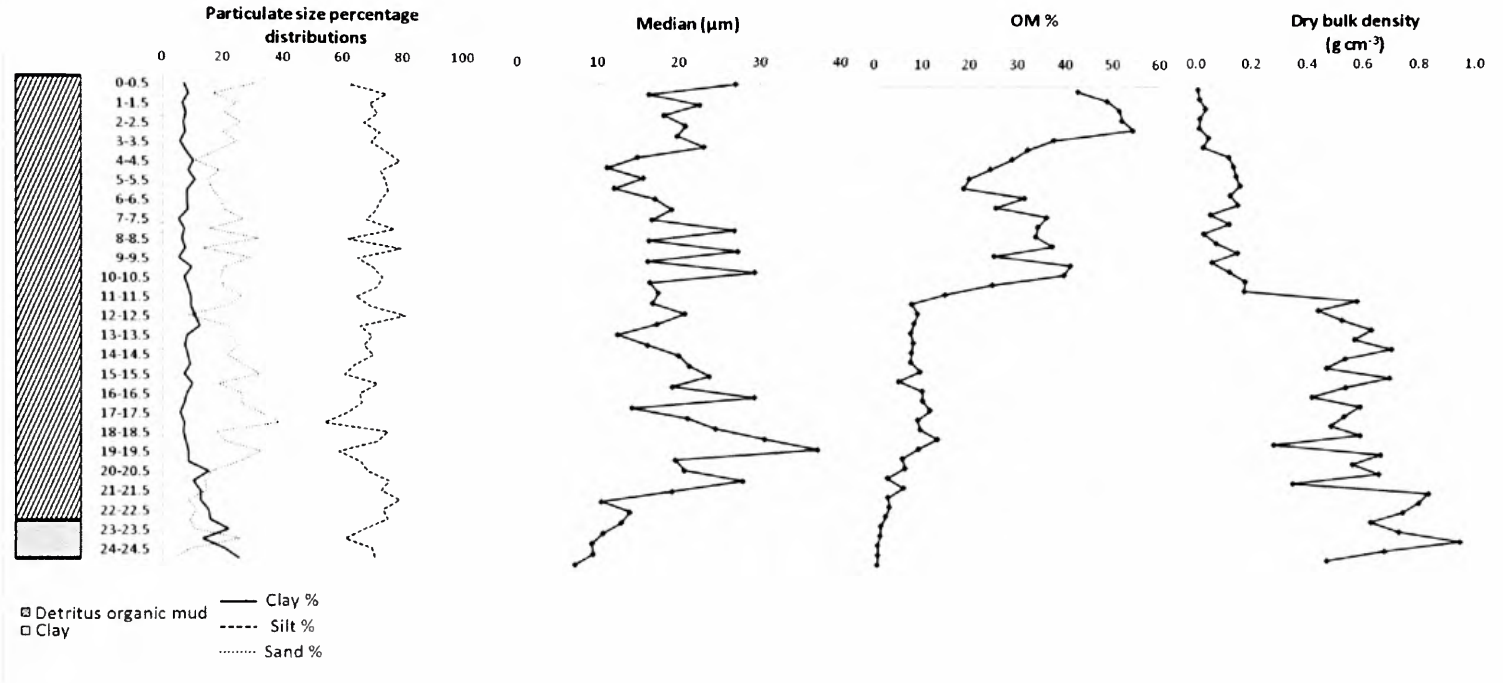

Figure 5.5: Sediment description and textural properties for WH3 (corresponding to Table 5.3).

Table 5.3: Textural properties of WH core (corresponding to Figure 5.5).

Core	Textural description
WH3	The textural properties of WH3 reveal the sediment column is primarily comprised of silt sized particles (54.03-80.99%), with smaller contributions of clay (5.20-21.85%) and sand (8.25-38.71%). The WH3 core exhibits relatively low OM values (~<10%) and high dry bulk densities (mean of 0.55 g cm^{-3}) in the lower 11 cm of the core. A distinct shift from this inorganic, high density material to lesser density organic deposits occurs throughout the upper 11 cm of the core, with observed OM 30-40% and dry bulk density 0.1 g cm^{-3}values in the section. The basal section of the core, below 20-20.5 cm, demonstrates a relatively increased contribution of clay and silt-sized particles. Median and sand particle distribution profiles identify comparatively coarser assemblages from 19-19.5 to 15-15.5 cm, 9-9.5 to 7-7.5 cm and in the upper 3.5 cm of the core.

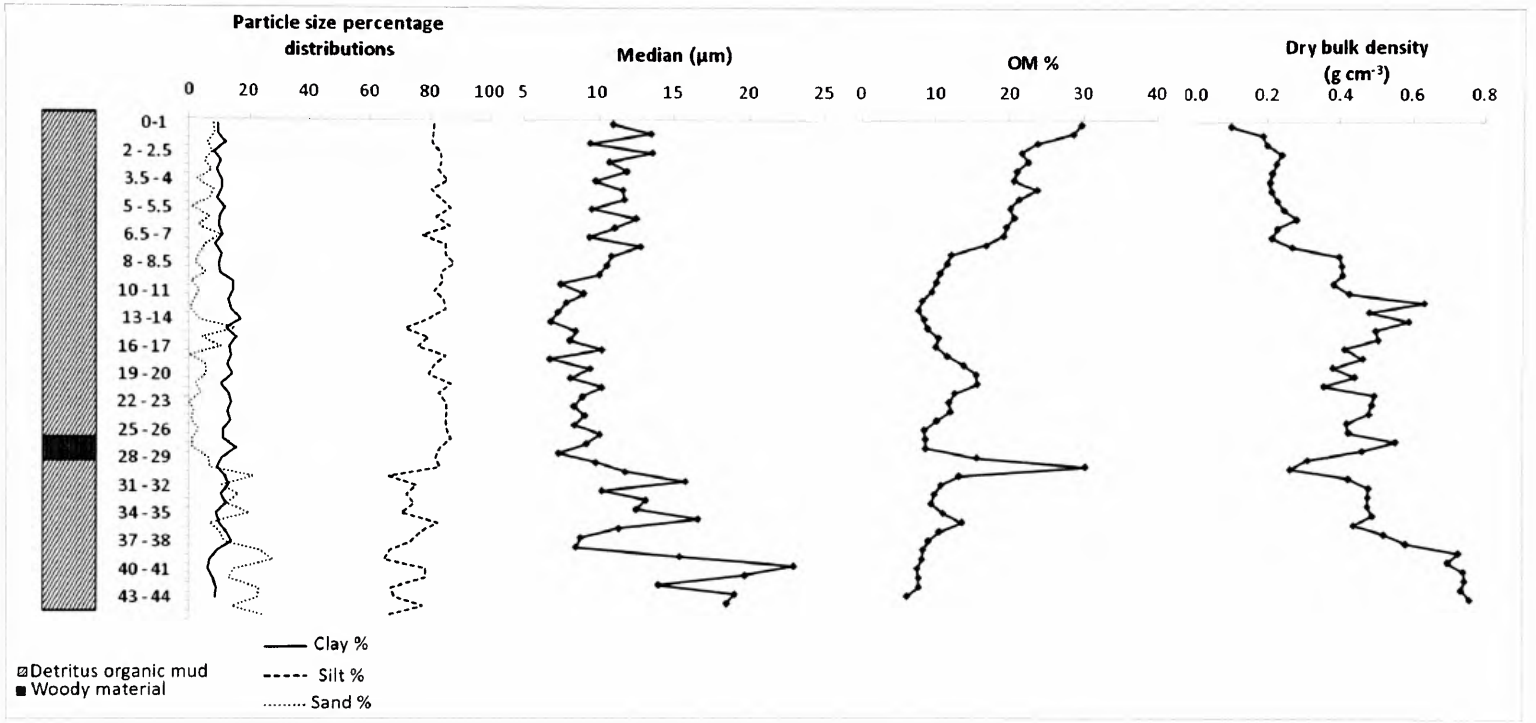

Figure 5.6: Sediment description and textural properties for DKC (corresponding to Table 5.4).

Table 5.4: Textural properties of DKC core (corresponding to Figure 5.6).

Core	Textural description
DKC	Figure 5.6 reveals the DKC core is dominated by silt-sized (2-63 µm) particles (64.66-87.93%), with a dominating inorganic component indicated by OM values from 6.33 to 30.41%. A shift to finer particle size assemblages occurs in the upper 29 cm of the core, revealed by a decrease in sand and a corresponding increase in silt, with relatively constant silt values ranging from 77.50 to 87.93%. Also a notable decrease in the clay fraction (8.39-12.58%) occurs from 8.5 to 0 cm. Textural properties of DKC also reveal an increase in OM and decrease in DBD corresponding to the identified layer of woody material. Below this layer, the sediment column is characterised by higher density inorganic sediment with relatively coarser particle size assemblages, demonstrated by higher sand-sized particles (21.39-28.15%). Lower density, organic sediment occurs above the woody layer, with a steady increase in OM and a decrease in dry bulk density to the sediment surface.

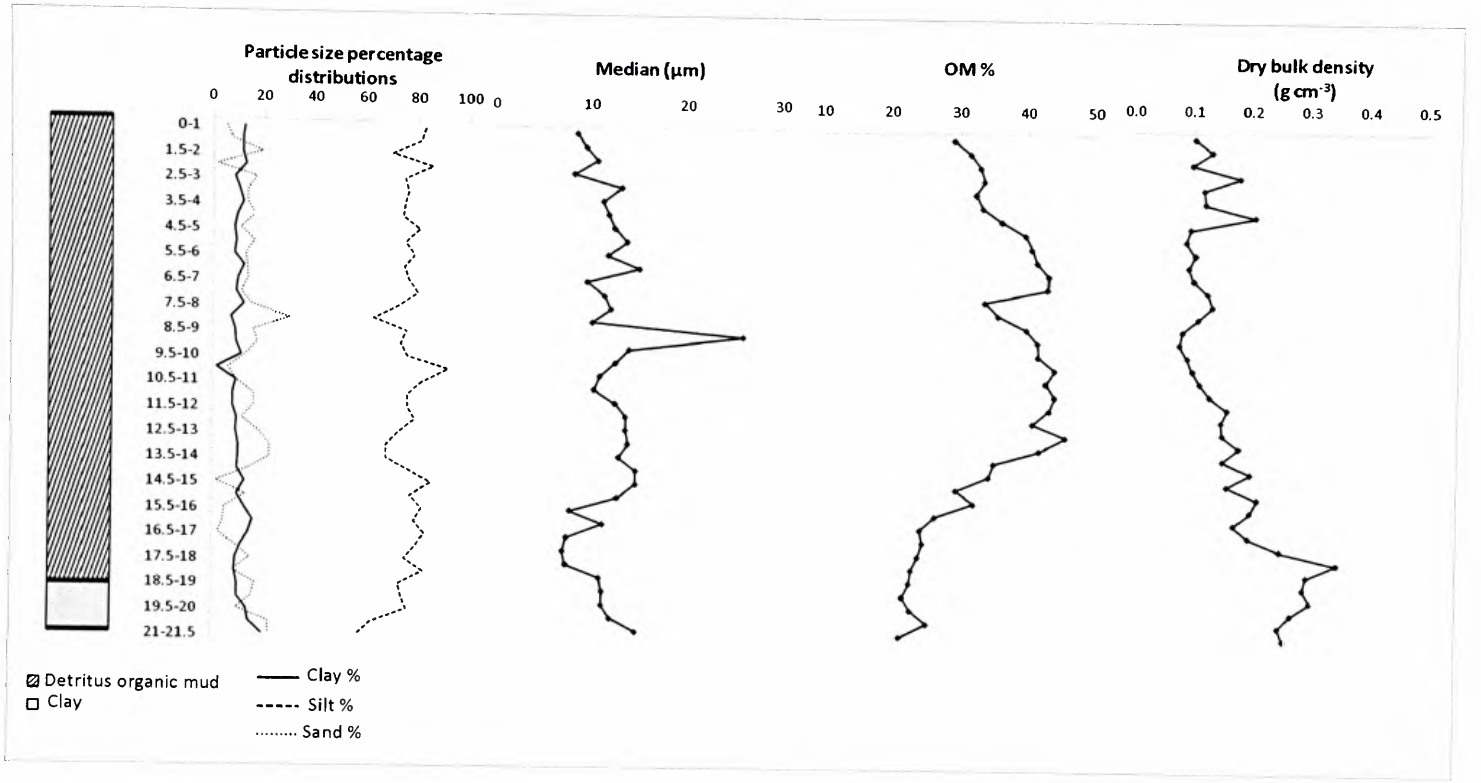

Figure 5.7: Sediment description and textural properties for OG (corresponding to Table 5.5).

Table 5.5: Textural properties of OG core (corresponding to Figure 5.7).

Core	Textural description
OG	Textural properties of OG (Figure 5.7) demonstrate the sediment column is predominantly composed of silt sized particles (62.96 - 92.37%) with smaller size distributions exhibited by sand (1.61 - 30.05%) and clay (1.64 - 15.77%) fractions. Sediment below 14.5 cm exhibits a finer particle size assemblage, demonstrated by relatively low median data. Above 9.5 cm clay-sized particles demonstrate a slightly increasing trend to the top of the core. High bulk density (~0.2-0.35 g cm^{-3}) and less organic (~<30%) sediment occurs below 14.5-15 cm. Above this depth lies less compact, lesser density (~<0.2 g cm^{-3}) sediment, with higher organic content (~>30%). OM rapidly increases from 14.5 cm with maximum peaks occurring at 11.5-12 (46.09%) to 9-9.5 cm (44.39%). A notable decrease in OM occurs at 6.5-7 cm and from 4-4.5 cm to the surface.

5.5. Urban sediment chronologies

5.5.1. Daresbury Delph Pond

The ^{210}Pb chronology for BDD1, calculated using the CRS dating model, is presented (Figure 5.8). Also shown is the ^{137}Cs-derived date of 1963, determined by a well resolved peak at 7-8 cm, reflecting the 1963 fallout maximum from nuclear weapons testing (Appendix D1). The ^{210}Pb inventory of the core corresponds to a mean ^{210}Pb supply of 14 Bq m^{-1} y^{-1}, less than 25% of the estimated atmospheric flux (~60 Bq m^{-2} y^{-1}), possibly due to poor retention of fallout radionuclides by the pond [Appendix D1]. ^{210}Pb dates were obtainable for 12.5 cm of the core, producing a chronology that extends to 1922 (Table 5.6). A polynomial trend line, used to extrapolate the ^{210}Pb chronology for sediment below 12.5 cm, suggests an age of ~482 years (1528) for the basal sediment layer.

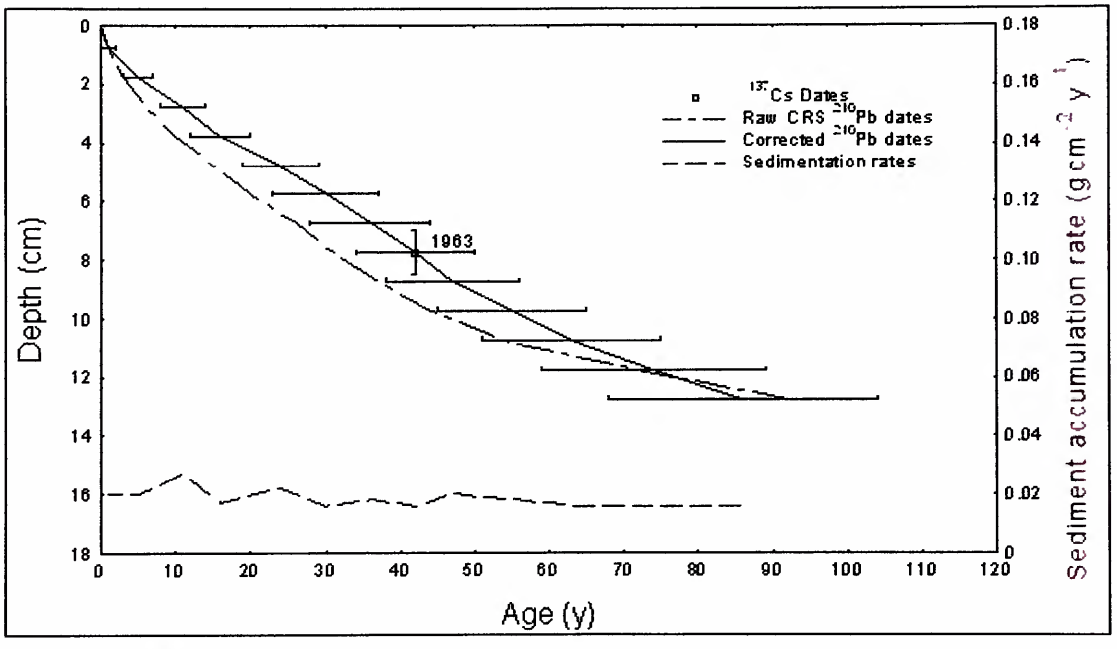

Figure 5.8: ^{210}Pb chronology data for BDD1: Radiometric chronology of Daresbury Delph Pond core BDD1 showing the CRS model ^{210}Pb dates together with the 1963 depth determined from the ^{137}Cs stratigraphy. Also shown are the corrected CRS model ^{210}Pb dates and sedimentation rates calculated using the 1963 ^{137}Cs date as a reference level.

Sedimentation accumulation rates vary throughout the BDD1 core from a maximum of 0.025 g cm^{-2} y^{-1} (2.5-3 cm) to 0.001 g cm^{-2} y^{-1} (36.5 -37 cm) (Table 5.6), with a mean sedimentation accumulation rate of 0.018 g cm^{-2} y^{-1}. Generally there is a shift to higher sedimentation delivery (>0.015 g cm^{-2} y^{-1}) in ~post-1867 sediment (0 to 17.5-18 cm), with lower rates (<0.02 g cm^{-2} y^{-1}) observed below this depth. Sedimentation rates (cm y^{-1}) reveal an increase in the supply of sediment to the pond post-1950 (mean of 0.0196 cm y^{-1}), with the highest sedimentation rates experienced from 1989 to 2005 (mean of 0.0214

cm y^{-1}). Lower sedimentation rates are observed below 14 cm (~1909) ranging from 0.021 cm y^{-1}, to 0.05 cm y^{-1} at the basal sediment interval (40-40.5 cm).

Table 5.6: ^{210}Pb derived and extrapolated (indicated by italics) dates, age and sediment accumulation rates for BDD1.

Depth (cm)	Cumulative dry mass (g cm^{-2})	Date AD	Age (years)	Sediment accumulation rate (g cm^{-2} y^{-1})	Sedimentation rate (cm y^{-1})
0.50	0.01	2005	0	0.020	0.340
0.75	0.04	2004	1	0.020	0.320
1.25	0.09	2002	3	0.020	0.265
1.75	0.14	2000	5	0.021	0.215
2.25	0.2	1997	8	0.024	0.195
2.75	0.26	1995	10	0.025	0.180
3.25	0.32	1992	13	0.022	0.165
3.75	0.39	1989	16	0.019	0.155
4.25	0.47	1985	20	0.020	0.145
4.75	0.54	1981	24	0.021	0.145
5.25	0.6	1978	27	0.019	0.155
5.75	0.66	1975	30	0.018	0.165
6.25	0.71	1972	33	0.017	0.170
6.75	0.76	1969	36	0.017	0.170
7.25	0.81	1966	39	0.017	0.170
7.75	0.85	1963	42	0.017	0.170
8.25	0.9	1961	44	0.018	0.165
8.75	0.96	1958	47	0.019	0.150
9.25	1.04	1954	51	0.019	0.135
9.75	1.11	1950	55	0.018	0.125
10.25	1.17	1946	59	0.017	0.115
10.75	1.25	1942	63	0.017	0.105
11.25	1.34	1937	68	0.016	0.095
11.75	1.44	1931	74	0.016	0.090
12.25	1.53	1925	80	0.016	0.085
12.75	*1.61*	*1921*	*83*	*0.050*	*0.290*
13.25	*1.72*	*1918*	*86*	*0.052*	*0.299*
13.75	*1.82*	*1914*	*91*	*0.021*	*0.103*
14.25	*1.92*	*1909*	*96*	*0.021*	*0.105*
14.75	*2.04*	*1904*	*101*	*0.022*	*0.103*
15.25	*2.16*	*1899*	*105*	*0.024*	*0.101*
15.75	*2.28*	*1894*	*110*	*0.024*	*0.099*
16.25	*2.37*	*1889*	*116*	*0.021*	*0.097*
16.75	*2.48*	*1884*	*121*	*0.019*	*0.095*
17.25	*2.57*	*1878*	*126*	*0.019*	*0.094*
17.75	*2.66*	*1873*	*132*	*0.017*	*0.092*
18.25	*2.75*	*1867*	*137*	*0.015*	*0.090*
18.75	*2.83*	*1862*	*143*	*0.015*	*0.089*
19.25	*2.91*	*1856*	*149*	*0.015*	*0.087*
19.75	*2.99*	*1850*	*154*	*0.014*	*0.086*
20.25	*3.06*	*1844*	*160*	*0.013*	*0.085*
25.25	*4.22*	*1780*	*225*	*0.015*	*0.073*
30.25	*5.41*	*1706*	*299*	*0.017*	*0.064*
35.25	*6.64*	*1622*	*383*	*0.016*	*0.057*
40.25	*7.82*	*1528*	*476*	*0.014*	*0.051*

5.5.2. Windmill Hill Pond

The ^{210}Pb chronology for WH3, obtained using the CRS dating model (Appleby *et al.*, 1978), is presented graphically in Figure 5.9. Total ^{210}Pb activity appears to reach equilibrium with the supporting ^{226}Ra at ~11 cm depth (Appendix D2), allowing a ^{210}Pb-derived chronology extending to a date of 1955 to be obtained (Table 5.7). The ^{137}Cs 1963 fallout maximum peak is not distinctive in the WH3 core. However, notable increases in the artificial isotope at 8.25 cm has been used as an estimate (Figure 5.9), which demonstrates good agreement with the ^{210}Pb-derived depth for this date. This demonstrates confidence in the chronology obtained for the post-1955 sediment for WH3. ^{210}Pb activity is undetectable in the denser sediment (below ~11 cm). The chronology below this depth was estimated using a polynomial extrapolation of ^{210}Pb data, which dates the basal sediment layer (23.25 cm) to ~1893 (Appendix D2).

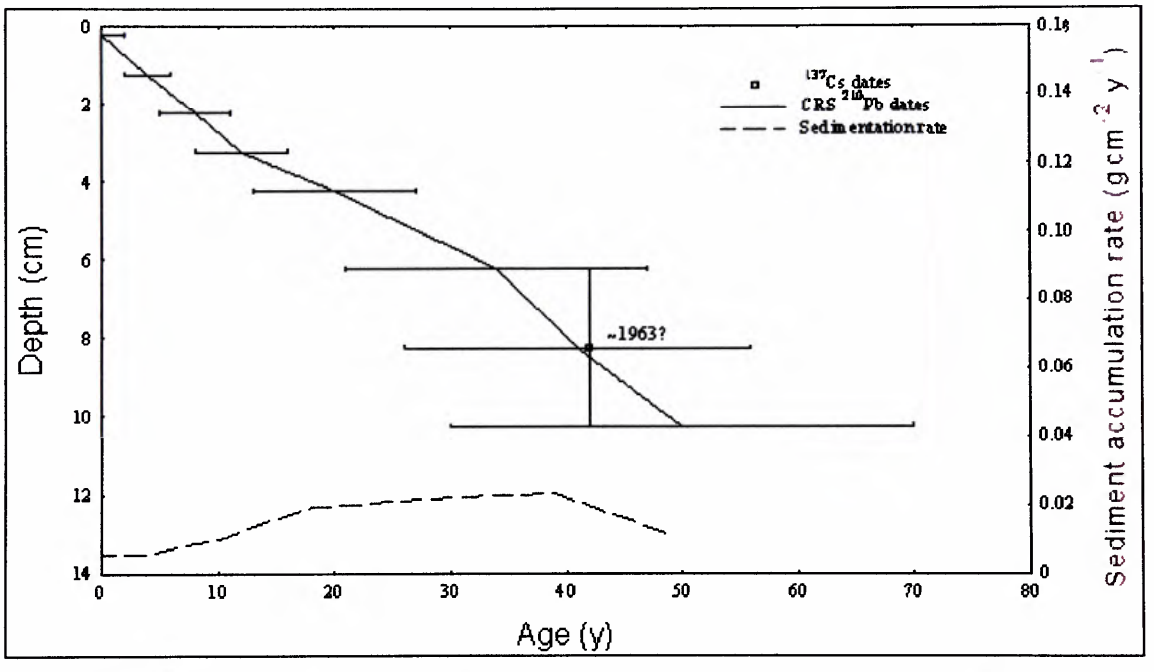

Figure 5.9: ^{210}Pb chronology data for WH3: Radiometric chronology of Windmill Hill Pond core (WH3) showing the CRS model ^{210}Pb dates together with the 1963 depth determined from the ^{137}Cs stratigraphy. Also shown are the corrected CRS model ^{210}Pb dates and sedimentation rates calculated using the 1963 ^{137}Cs date as a reference level.

Sedimentation accumulation rates for WH3 (Table 5.7) demonstrate a period of increased sediment accumulation from the late 1950s to the late 1970s (9 to 5 cm), with a mean sediment supply rate of ~0.023 g cm^{-2} y^{-1} (or 0.20 cm y^{-1}). Lower sedimentation occurs in post-1990 sediment (~3.5 cm to 0 cm) with low dry mass sediment accumulation rates of <0.010 g cm^{-2} y^{-1}. A prominent decline in sediment supply occurs post-1955 (0 to 11 cm) with sediment characteristics of high OM content (Figure 5.3).

Table 5.7: ^{210}Pb derived and extrapolated (indicated by italics) dates, age and sediment accumulation rates for WH3.

Depth (cm)	Cumulative dry mass (g cm^{-2})	Date AD	Age (years)	Sediment accumulation rate (g cm^{-2} y^{-1})	Sedimentation rate (cm y^{-1})
0.25	0	2005	0	0.006	0.380
0.75	0.01	2003	2	0.006	0.250
1.25	0.02	2001	4	0.005	0.250
1.75	0.03	1999	6	0.007	0.250
2.25	0.05	1997	8	0.008	0.250
2.75	0.06	1995	10	0.009	0.250
3.25	0.08	1993	12	0.010	0.170
3.75	0.14	1989	16	0.015	0.130
4.25	0.19	1985	20	0.019	0.140
4.75	0.26	1982	23	0.020	0.140
5.25	0.33	1978	27	0.021	0.140
5.75	0.41	1975	30	0.022	0.140
6.25	0.48	1971	34	0.022	0.170
6.75	0.52	1969	36	0.023	0.250
7.25	0.57	1967	38	0.023	0.330
7.75	0.61	1966	39	0.023	0.330
8.25	0.65	1964	41	0.023	0.200
8.75	0.71	1961	44	0.020	0.200
9.25	0.77	1959	46	0.017	0.250
9.75	0.83	1957	48	0.014	0.250
10.25	0.89	1955	50	0.011	0.250
10.75	*0.98*	*1951*	*54*	*0.023*	*0.126*
11.25	*1.27*	*1949*	*56*	*0.118*	*0.202*
11.75	*1.49*	*1946*	*59*	*0.090*	*0.203*
12.25	*1.76*	*1944*	*61*	*0.108*	*0.204*
12.75	*2.08*	*1941*	*64*	*0.131*	*0.206*
13.25	*2.37*	*1939*	*66*	*0.119*	*0.207*
13.75	*2.72*	*1936*	*69*	*0.147*	*0.208*
14.25	*2.99*	*1934*	*71*	*0.113*	*0.209*
14.75	*3.23*	*1932*	*73*	*0.100*	*0.211*
15.25	*3.58*	*1929*	*76*	*0.149*	*0.212*
15.75	*3.85*	*1927*	*78*	*0.116*	*0.213*
16.25	*4.06*	*1925*	*80*	*0.091*	*0.214*
16.75	*4.36*	*1922*	*83*	*0.129*	*0.216*
17.25	*4.63*	*1920*	*85*	*0.117*	*0.217*
17.75	*4.88*	*1918*	*87*	*0.107*	*0.218*
18.25	*5.17*	*1915*	*90*	*0.131*	*0.220*
18.75	*5.32*	*1913*	*92*	*0.063*	*0.221*
19.25	*5.65*	*1911*	*94*	*0.149*	*0.222*
19.75	*5.94*	*1909*	*96*	*0.127*	*0.224*
20.25	*6.27*	*1906*	*99*	*0.149*	*0.225*
20.75	*6.45*	*1904*	*101*	*0.081*	*0.227*
21.25	*6.87*	*1902*	*103*	*0.192*	*0.228*
21.75	*7.27*	*1900*	*105*	*0.185*	*0.230*
22.25	*7.64*	*1898*	*107*	*0.173*	*0.231*
22.75	*7.96*	*1896*	*109*	*0.147*	*0.233*
23.25	*8.32*	*1893*	*112*	*0.172*	*0.234*

5.5.3. Dogs Kennel Clump Pond

Figure 5.10 and Table 5.8 present the ^{210}Pb-derived chronology for DKC (Appendix D2). The core demonstrates irregularity in ^{210}Pb activity with low unsupported ^{210}Pb concentrations in sediment below 4.25 cm. Despite this, the ^{210}Pb derived dates calculated from the CRS dating model are consistent with the estimated 1963 ^{137}Cs date, identified by a well resolved peak at 6.25 cm attributed to nuclear weapons testing at this time. Dating of sediment below 4.25 cm was corrected using the ^{137}Cs 1963 date as a reference level, for which a high-resolution chronology of 45 years was attainable for 10.5 cm of the core. A linear extrapolation[†] of these data extends the chronology to ~1874 (126 years) for the basal sediment layer (45.5 cm).

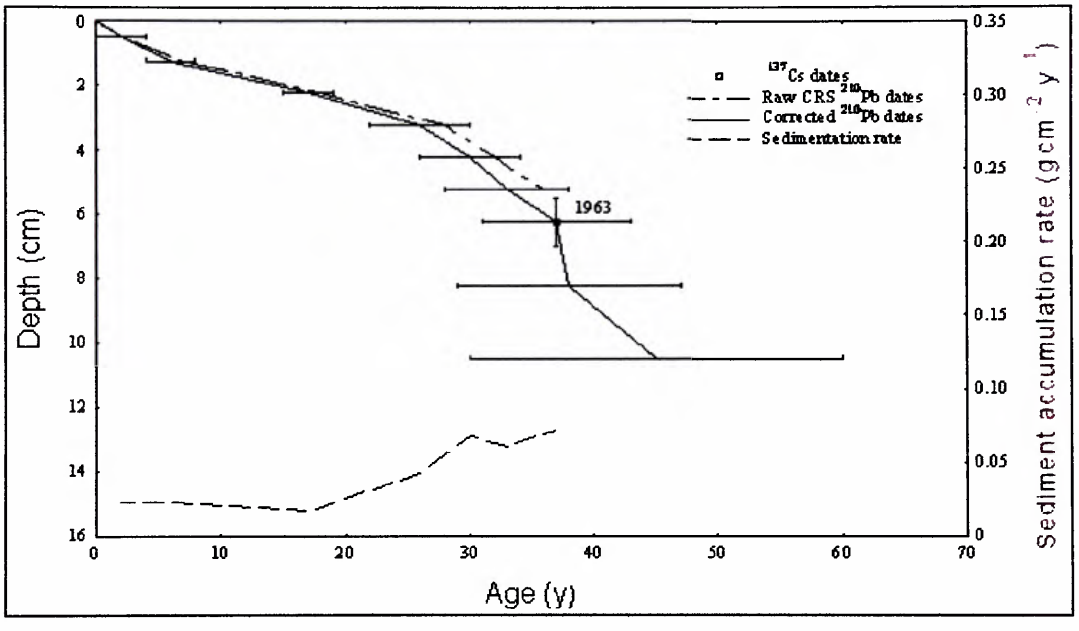

Figure 5.10: ^{210}Pb chronology data for DKC: Radiometric chronology of Dogs Kennel Clump Pond core DKC showing the CRS model ^{210}Pb dates together with the 1963 depth determined from the ^{137}Cs stratigraphy. Also shown are the corrected CRS model ^{210}Pb dates and sedimentation rates calculated using the 1963 ^{137}Cs date as a reference level.

Sedimentation rates vary throughout the DKC core (Table 5.8). The extrapolated, pre~1955, section of the core (10.5 to 45.5 cm) demonstrates a mean sedimentation rate of 0.43 cm y^{-1} or 0.232 g cm^{-2} y^{-1}. There appears to be rapid sediment accumulation from the late 1950s through to the 1970s (9.25 cm to 4.25 cm), which ranges from 0.29 to 0.67 cm y^{-1} (or 0.068 to 0.522 g cm^{-2} y^{-1}), particularly notable from 1960 to 1963. The post-1970

[†] Linear not polynomial extrapolation used due to abrupt shift of rapid accumulation event from ~1950-1970, which prevented construction of a polynomial trend line.

sediment (3.75 to 0 cm) exhibits lower, relatively uniform sedimentation rates, with mean values of 0.022 g cm^{-2} y^{-1} or 0.13 cm y^{-1}.

Table 5.8: ^{210}Pb derived and extrapolated (indicated by italics) dates, age and sediment accumulation rates for DKC.

Depth (cm)	Cumulative dry mass (g cm^{-2})	Date AD	Age (years)	Sediment accumulation rate (g cm^{-2} y^{-1})	Sedimentation rate (cm y^{-1})
0.50	0.04	1998	2	0.023	0.210
1.25	0.11	1994	6	0.023	0.130
1.75	0.10	1988	12	0.020	0.120
2.25	0.10	1983	17	0.017	0.100
2.75	0.12	1979	21	0.030	0.130
3.25	0.11	1974	26	0.042	0.150
3.75	0.10	1972	28	0.055	0.200
4.25	0.11	1970	30	0.068	0.290
4.75	0.11	1969	31	0.065	0.290
5.25	0.12	1967	33	0.061	0.290
5.75	0.13	1965	35	0.066	0.330
6.25	0.13	1963	37	0.072	0.400
6.75	0.15	1963	37	0.185	0.670
7.25	0.15	1962	38	0.500	0.297
7.75	0.15	1962	38	0.410	0.670
8.25	0.15	1962	38	0.522	0.670
8.75	0.20	1960	40	0.438	0.500
9.50	0.30	1958	42	0.311	0.250
10.50	*0.41*	*1955*	*45*	*0.142*	*0.140*
11.50	*0.64*	*1953*	*47*	*0.325*	*0.510*
12.50	*0.48*	*1951*	*49*	*0.207*	*0.429*
13.50	*0.59*	*1948*	*52*	*0.254*	*0.429*
14.50	*0.50*	*1946*	*54*	*0.215*	*0.429*
15.50	*0.51*	*1944*	*56*	*0.218*	*0.429*
16.50	*0.41*	*1941*	*59*	*0.178*	*0.429*
17.50	*0.47*	*1939*	*61*	*0.200*	*0.429*
18.50	*0.38*	*1937*	*63*	*0.164*	*0.429*
19.50	*0.44*	*1934*	*66*	*0.190*	*0.429*
20.50	*0.36*	*1932*	*68*	*0.154*	*0.429*
21.50	*0.50*	*1930*	*70*	*0.213*	*0.429*
22.50	*0.49*	*1927*	*73*	*0.211*	*0.429*
23.50	*0.48*	*1925*	*75*	*0.207*	*0.429*
24.50	*0.42*	*1923*	*77*	*0.181*	*0.429*
25.50	*0.43*	*1920*	*80*	*0.183*	*0.429*
26.50	*0.56*	*1918*	*82*	*0.239*	*0.429*
27.50	*0.46*	*1916*	*84*	*0.199*	*0.429*
28.50	*0.31*	*1913*	*87*	*0.134*	*0.429*
29.50	*7.09*	*1911*	*89*	*0.114*	*0.429*
30.50	*7.52*	*1909*	*91*	*0.183*	*0.429*
31.50	*8.00*	*1906*	*94*	*0.207*	*0.429*
32.50	*8.48*	*1904*	*96*	*0.206*	*0.429*
33.50	*8.96*	*1902*	*98*	*0.206*	*0.429*
34.50	*9.45*	*1899*	*101*	*0.211*	*0.429*
35.50	*9.89*	*1897*	*103*	*0.189*	*0.429*
36.50	*10.42*	*1895*	*105*	*0.225*	*0.429*
37.50	*11.00*	*1892*	*108*	*0.251*	*0.429*
45.50	*17.17*	*1874*	*126*	*0.398*	*0.429*

5.5.4. Oglet Pond

The ^{210}Pb chronology for OG is presented (Figure 5.11, Table 5.9 and Appendix D2). The OG core has an irregular ^{210}Pb record with no clear equilibrium depth. Unsupported ^{210}Pb concentrations are relatively constant in the upper 12.5 cm of the core, below which concentrations fall abruptly and reach low detection levels in the basal sediment layers. The ^{210}Pb chronology, achieved using the CRS model, is further supported by the ^{137}Cs fall out record, which places the 1963 maximum, identified by an abrupt increase in ^{137}Cs at 12.25 cm, in good agreement with the ^{210}Pb chronology. The earliest achievable ^{210}Pb date for the core is 1951 (at 14.25 cm), providing a high-resolution 50-year stratigraphy. Extrapolation of these dates, using a polynomial trend line, extends the chronology of the core to ~86 years, with a date of 1914 obtained for the basal sediment layer (19.25 cm).

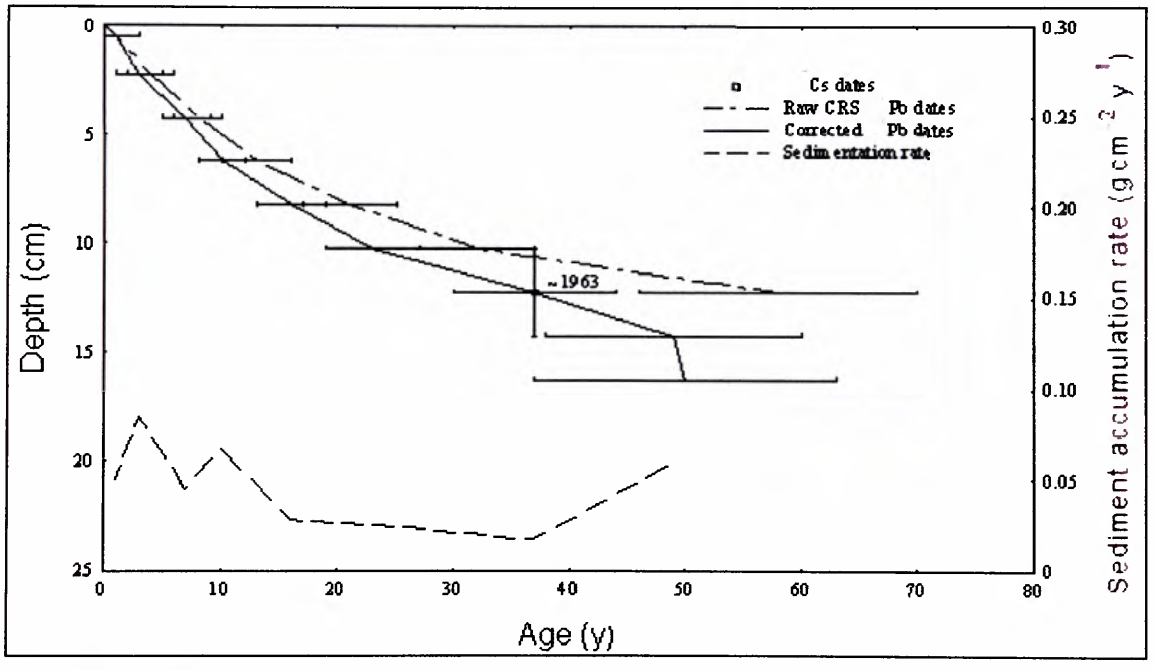

Figure 5.11: ^{210}Pb chronology data for OG: Radiometric chronology of Oglet Pond core OG showing the CRS model ^{210}Pb dates together with the 1963 depth determined from the ^{137}Cs stratigraphy. Also shown are the corrected CRS model ^{210}Pb dates and sedimentation rates calculated using the 1963 ^{137}Cs date as a reference level.

Sedimentation rate profiles for OG (Table 5.9) reveal periods of rapid sediment accumulation between 1949-1950 (13.75-14.75 cm) highlighted by a mean sedimentation rate of 0.0553 g cm^{-2} y^{-1} (or 0.257 cm y^{-1}), and post-1990 (0-6.25 cm), which exhibits a mean sedimentation rate of 0.0712 g cm^{-2} y^{-1} (or 0.605 cm y^{-1}). A relatively long period (~40 years) of slower, uniform sediment accumulation occurs between these times,

denoted by a mean sedimentation rate of 0.025 g cm^{-2} y^{-1} (or 0.20 cm y^{-1}). Low mean sedimentation rates (0.0301 g cm^{-2} y^{-1} or 0.116 cm y^{-1}) are also observed in the extrapolated pre-1950 sediment.

Table 5.9: ^{210}Pb derived and extrapolated (indicated by italics) dates, age and sediment accumulation rates for OG.

Depth (cm)	Cumulative dry mass (g cm^{-2})	Date AD	Age (years)	Sediment accumulation rate (g cm^{-2} y^{-1})	Sedimentation rate (cm y^{-1})
0.50	0.05	1999	1	0.069	0.580
1.25	0.14	1998	2	0.087	0.750
1.75	0.20	1997	3	0.096	0.750
2.25	0.26	1997	3	0.089	0.670
2.75	0.33	1996	4	0.093	0.670
3.25	0.41	1995	5	0.073	0.500
3.75	0.48	1994	6	0.067	0.500
4.25	0.55	1993	7	0.045	0.500
4.75	0.60	1992	8	0.050	0.670
5.25	0.65	1991	9	0.056	0.670
5.75	0.70	1991	9	0.062	0.500
6.25	0.75	1990	10	0.067	0.500
6.75	0.81	1988	12	0.057	0.330
7.25	0.86	1987	13	0.047	0.330
7.75	0.92	1985	15	0.038	0.330
8.25	0.98	1984	16	0.028	0.330
8.75	1.03	1982	18	0.027	0.330
9.25	1.08	1981	19	0.026	0.290
9.75	1.12	1979	21	0.026	0.220
10.25	1.17	1977	23	0.025	0.180
10.75	1.24	1973	27	0.023	0.150
11.25	1.31	1970	30	0.021	0.140
11.75	1.39	1966	34	0.019	0.150
12.25	1.46	1963	37	0.017	0.150
12.75	1.55	1960	40	0.028	0.170
13.25	1.64	1957	43	0.038	0.170
13.75	1.72	1954	46	0.049	0.220
14.25	1.81	1951	49	0.060	0.290
14.75	*1.92*	*1949*	*51*	*0.057*	*0.265*
15.25	*2.02*	*1946*	*54*	*0.030*	*0.146*
15.75	*2.11*	*1942*	*58*	*0.025*	*0.141*
16.25	*2.21*	*1938*	*62*	*0.027*	*0.136*
16.75	*2.34*	*1935*	*65*	*0.034*	*0.132*
17.25	*2.51*	*1931*	*69*	*0.045*	*0.128*
17.75	*2.66*	*1927*	*73*	*0.037*	*0.125*
18.25	*2.81*	*1923*	*77*	*0.036*	*0.121*
18.75	*2.96*	*1918*	*82*	*0.036*	*0.118*
19.25	*3.10*	*1914*	*86*	*0.031*	*0.115*

5.6. Chapter summary

Sediment stratigraphies retrieved from four urban ponds demonstrate:

- Columns of detritus organic mud, visually identified in the four urban sediment stratigraphies extending to 19.5 cm in the Oglet core, to 44 cm in the Dogs Kennel Clump core.
- Textural properties reveal the sediment stratigraphies from DDP, WH, DKC and OG are mainly comprised of inorganic material, dominated by silt-sized particle distributions.
- χ_{LF} profiles of five sediment cores collected from Daresbury Delph Pond reveal several similar key features allowing a visual assessment of intra-site 'core correlation[‡]' within an urban pond.
- Sediment stratigraphies obtained from Daresbury Delph Pond, Windmill Hill, Dogs Kennel Clump and Oglet all demonstrate a shift from relatively high density sediment in the lower sections of the cores, to lesser density sediments towards the sediment surface.
- ^{210}Pb chronologies were obtainable for the four urban ponds. Extrapolation of these ^{210}Pb data highlight a range of time scales represented by each site. Daresbury Delph pond exhibits a chronology extending to ~1528; whereas, Dogs Kennel Clump and Windmill Hill provide chronologies dating back to the start of the 20th century, and OG provides a high resolution chronology from ~1914.

A summary of the textural properties and chronologies of DDP, WH3, DKC and OG are presented in Table 5.10.

[‡] Here the term 'core correlation' refers to similar features visually identified within the sediment stratigraphies, rather than a statistical application.

Table 5.10: Summary data of sediment stratigraphies retrieved from Daresbury Delph, Windmill Hill, Dogs Kennel Clump and Oglet ponds.

Pond site (core code)	Depth of sediment archive (cm)	OM range (%)	Clay range (%)	Silt range (%)	Sand range (%)	^{210}Pb Chronology (date)	Extrapolated basal date	Mean supply of ^{210}Pb to the lake (Bq m^{-2} y^{-1})
Daresbury Delph (BDD1)	40.5	12.455 – 41.657	5.37 – 21.69	47.44 – 87.68	1.16 – 47.19	2005 – 1922	~1528	14
Windmill Hill (WH3)	23.5	1.368 – 54.313	5.20 – 21.85	54.03 – 80.99	8.25 – 38.71	2005 – 1955	~1893	8
Dogs Kennel Clump (DKC)	44	6.328 – 30.406	6.34 – 17.36	64.66 – 87.93	0.16 – 28.15	2001 – 1958	~1874	16
Oglet (OG)	19.5	21.858 – 46.090	1.64 – 15.77	62.96 – 92.37	1.61 – 30.05	2001 – 1951	~1914	16

6. CHAPTER SIX: PROXY POLLUTION CONCENTRATION PROFILES FROM URBAN PONDS

6.1. Chapter overview

Proxy pollution data from each urban pond are presented, in turn, for Daresbury Delph (Section 6.3.), Windmill Hill (Section 6.4.), Dogs Kennel Clump (Section 6.5.) and Oglet (Section 6.6.). Mineral magnetic, trace metal and (where applicable) SCP data are shown as concentration-depth profiles; whereby, down-core trends in concentration are displayed alongside corresponding ^{210}Pb-derived and extrapolated (indicated by ~) dates. Particle size distributions of particulates <10 μm and median particle sizes are also included. For convenience, trends in the concentration-depth profiles are described chronologically, from the base of the sediment core (oldest sediment) to the sediment-surface. Also statistical correlations between the concentration data are provided for each site.

6.2. Introduction

Local proxy pollution signals recorded in Daresbury Delph (DDP), Windmill Hill (WH), Dogs Kennel Clump (DKC) and Oglet (OG) ponds are presented (Sections 6.3., 6.4., 6.5. and 6.6., respectively). Concentration-depth profiles for a range of environmental proxies demonstrate down-core variations in particulate pollution characteristics:

- Magnetic properties: magnetic concentration parameters (χ_{LF}, SIRM, χ_{ARM}, HARD.$_{300mT}$ and SOFT.$_{20mT}$) demonstrate down-core variations in the concentration of magnetic grains. Magnetic ratios (χ_{FD}%, S-RATIO, χ_{ARM}/SIRM, SIRM/χ_{LF} and SIRM/ARM) are used to characterise down-core variations in the mineralogy and grain size of the magnetic signal.
- <10 μm particle size distributions: <10 μm, <2.5 μm and <1 μm, important respiratory and particulate pollution size boundaries, are provided.
- Trace metal concentrations: typical, anthropogenic trace metals (pollution tracers) Pb, Zn, Cu, S and Br are included for all sites, along with Cl, Ni and Cr concentrations where data are sufficient.
- Spheroidal carbonaceous particulates: SCP concentration profiles are presented for DDP only, detailing the down-core variations in these unambiguous indicators of pollution particulates.

Due to the site-specific nature of sediment records obtained from urban ponds [Charlesworth and Lees, 1997, 2001], the stratigraphies from each site have been visually assessed to identify down-core 'divisions' relating to magnetic, trace metal, particle size and, where applicable, SCP properties in the DDP, WH, DKC and OG cores. These 'phases' in the sediment records are superimposed over the proxy pollution profiles to aid description of these trends. These site-specific zones also aid the interpretation of localised signals recorded at each pond (Chapter 10). Also, statistical correlations identified between these proxy pollution concentrations and environmental variables (clay, silt, sand, organic matter) are tabulated for each pond site.

6.3. Local pollution signal recorded in Daresbury Delph Pond

Four phases have been identified from visual inspection of proxy pollution trends in the master core 'BDD1' from DDP (Table 6.1) to aid description and interpretation of down-core variations in magnetic properties, trace metal concentrations, particle size distributions and SCP concentrations.

Table 6.1: Down-core phases identified in BDD1.

Phase	Depth/Date	Proxy pollution trend
DDiv	Post-1978 (5.5 to 0 cm)	An overall decline in proxy pollution concentrations, with a distinct shift to a finer pollution signature.
DDiii	1900 to 1978 (15.5 to 5.5 cm)	Further proxy pollution enhancement with prominent peaks in this phase.
DDii	~1832 to 1900 (21.5 to 15.5 cm)	Initial increases in proxy pollution concentrations.
DDi	~pre-1832 (40.5 to 21.5 cm)	Relatively low proxy pollution characteristics.

6.3.1. Magnetic characteristics: BDD1

Figure 6.1 presents down-core trends in concentration-dependent parameters for BDD1, which are described in Table 6.2. χ_{LF} values range from a minimum* of 38.879 10^{-9} m^3 kg^{-1} to a maximum of 169.556 10^{-9} m^3 kg^{-1}, with a mean of 85.138 10^{-9} m^3 kg^{-1} which, when compared to published values of environmental materials, correspond to sedimentary and metamorphic rocks, paramagnetic minerals, canted antiferromagnetic minerals and topsoils [Dearing, 1999(a)]. Close parallels are exhibited between the χ_{LF}, SIRM and $SOFT_{-20mT}$ profiles, highlighting similar contributions of coarse ferrimagnetic minerals and

* A very low negative χ_{LF} value of -863.309 (10^{-9}) at the very top section of the core (0-0.5 cm) has been omitted from this range due to the potential diamagnetic effect of water in this sample interval, representing the sediment-water interface.

remanence-carrying minerals to the magnetic signal. Also, $HARD_{-300mT}$ and χ_{ARM} demonstrate similar profiles. Four main phases in magnetic concentration are identified (Table 6.2), which reveal key magnetic phases in the BDD1 core:

- DDi: Relatively low and noisy ~pre-1832 magnetic concentration signals, with a ~1787 to 1807 $SOFT_{-20mT}$, $HARD_{-300mT}$ and SIRM peak.
- DDii: A clear increasing trend in magnetic concentration with initial enhancement ~post-1832, which continues throughout the 19th century with a relatively small magnetic concentration peak observed at ~1856. A further enhancement in the magnetic signal occurs post-1900; whereby, 'hard' magnetic minerals contribute to the magnetic record and there is an increase in SP grains. Increases in the concentration of coarse ferrimagnetic minerals also occur, with notable peaks at ~1918 to 1921 and 1942. A steady increase in magnetic concentration continues throughout the 20th century. Mid-20th century coarse ferrimagnetic concentration peaks occur between 1954 and 1963.
- DDiii: Concentration of coarse ferrimagnetic grains decreases throughout the 1970s, with a decline in magnetic concentration particularly notable at 1978.
- DDiv: Magnetic concentrations increase, characterised by a shift to fine (SSD) ferrimagnetic grains and 'hard' magnetic minerals, highlighted by a distinct 'hard' contribution to the magnetic record.

Down-core trends in χ_{FD}%, S-RATIO, SIRM/χ_{LF}, χ_{ARM}/SIRM and SIRM/ARM are shown (Figure 6.2) and described (Table 6.2). Divisions DDi to DDiv are superimposed over the graphs to allow comparison with observed trends in magnetic concentration (Figure 6.1 and Table 6.2). However, as these magnetic parameter ratios demonstrate *contributions* of magnetic grain size and not actual *concentrations*, relative trends in these indicators are described for the whole core (Table 6.3) and divisions referred to where appropriate.

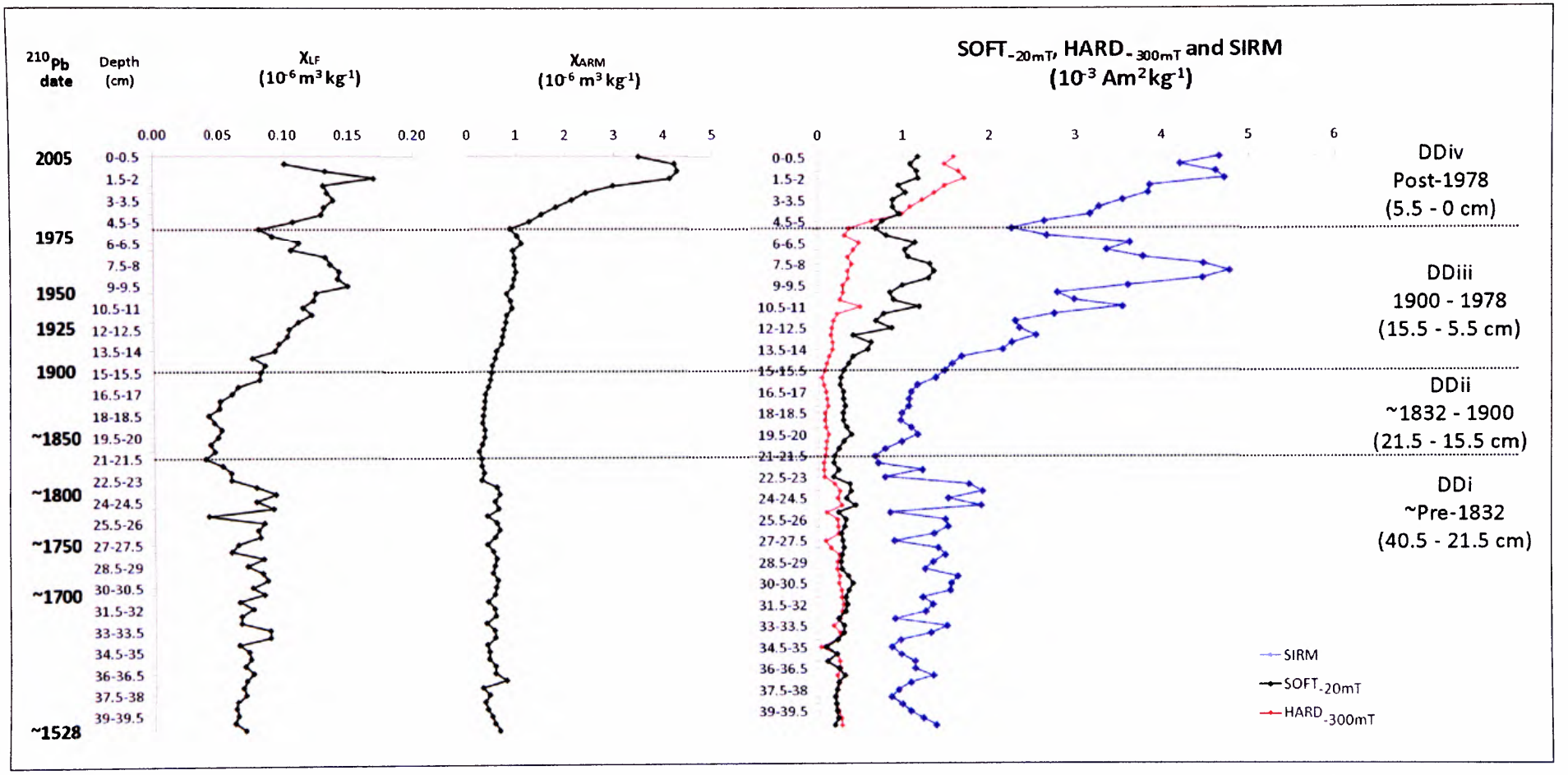

Figure 6.1: Magnetic concentration profiles for BDD1: χ_{LF}, χ_{ARM}, $SOFT_{-20mT}$, $HARD_{-300mT}$ and SIRM with superimposed phases DDi to DDiv (corresponding to Table 6.2). ~indicates extrapolated date.

Table 6.2: Down-core magnetic concentration trends in BDD1, relating to phases DDi to DDiv (corresponding to Figure 6.1).

Phase	Depth/Date	Magnetic concentration trends
DDiv	Post-1978 (5.5 to 0 cm)	A sharp decline in SIRM, $SOFT_{-20mT}$ and χ_{LF} occurs at 1978 (5-5.5 cm) with subsequent magnetic concentration increases and a recent (2000) prominent peak, whereby, maximum χ_{LF} ($169.56\ 10^{-9}\ m^3\ kg^{-1}$) and high SRIM and $SOFT_{-20mT}$ values are reached. A prominent shift in χ_{ARM} occurs in the post-1978 sediment with maximum values ($4.223\ 10^{-6}\ m^3\ kg^{-1}$) exhibited at 0.5-1 cm (2002). Also, the $HARD_{-300mT}$ profile indicates higher amounts of canted antiferromagnetic minerals/fine ferrimagnetic grains contribute to the magnetic signal post-1978. These χ_{ARM} and $HARD_{-300mT}$ increases are not proportional to the increases observed in SIRM, χ_{LF} and $SOFT_{-20mT}$, highlighting a relatively finer magnetic signal.
DDiii	1900 to 1978 (15.5 to 5.5 cm)	Further enhancement of the magnetic record occurs post-1900, with a steadily increasing trend, reaching mid-20th century peaks at ~1963. A contribution of 'hard' magnetic grains post-1900 is demonstrated in the $HARD_{-300mT}$ profile. χ_{ARM} and $HARD_{-300mT}$ values steadily increase throughout this phase, with a notable 'hard' peak at 1942 (10.5-11 cm). Magnetically 'soft' peak are evident at: • ~1918 to 1921 (12.5 to 23.5 cm), • 1942 (10.5-11 cm) and • 1958 to 1963 (7.5 to 9 cm). High χ_{LF} concentrations are observed at 1954 and maximum SIRM ($4.779\ 10^{-3}\ Am^2\ kg^{-1}$) and $SOFT_{-20mT}$ ($1.345\ 10^{-3}\ Am^2\ kg^{-1}$) at 1963 (8-8.5 cm).
DDii	~1832 to 1900 (21.5 to 15.5 cm)	SIRM, χ_{LF} and $SOFT_{-20mT}$ profiles exhibit an increasing trend in magnetic concentration, which starts at ~1832, highlighting an enhancement in coarse ferrimagnetic magnetic grains. The χ_{ARM} values show a fine (potentially, SSD) magnetic component contributing to the magnetic signal from ~20 cm (~post-1844). $HARD_{-300mT}$ demonstrates a contribution of 'hard' magnetic grains post-1900 (at 15.5 cm). $SOFT_{-20mT}$, SIRM, χ_{LF} peaks are observed at ~1856 (19-19.5 cm).
DDi	~pre-1832 (40.5 to 21.5 cm)	The base of the sediment record is characterised by relatively low and noisy χ_{LF}, SIRM, χ_{ARM}, $SOFT_{-20mT}$ and $HARD_{-300mT}$ signals. Minimum SIRM ($0.779\ 10^{-3}\ Am^2\ kg^{-1}$) and χ_{LF} ($387.879\ 10^{-9}\ m^3\ kg^{-1}$) values occur at 21-21.5 cm (~1832). Also, $SOFT_{-20mT}$ exhibits a steadily increasing trend.

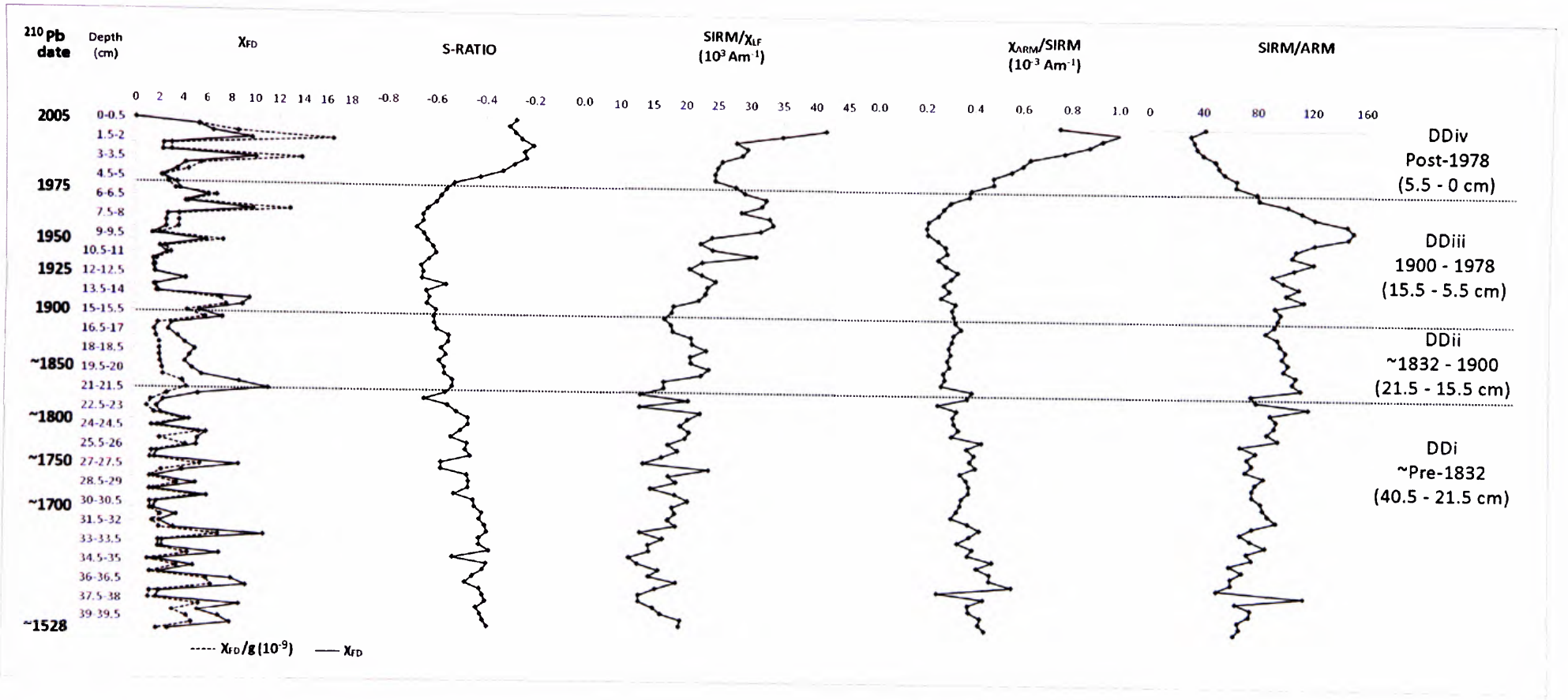

Figure 6.2: Magnetic ratio profiles for BDD1: χ_{FD}, S-RATIO, SIRM/χ_{LF}, χ_{ARM}/SIRM, and SIRM/ARM with superimposed phases DDi to DDiv (corresponding to Table 6.3). ~indicates extrapolated date.

Table 6.3: Description and interpretation of down-core trends in magnetic ratios for BDD1, (corresponding to Figure 6.2).

Magnetic ratio	Description and interpretation
$\chi_{FD}\%$	The majority of $\chi_{FD\%}$ values lie between 2-5% indicative of the presence of SSD/SP grains, with samples >5% revealing a significant SP component, typically associated with topsoil. However, only in two samples, 21-21.5 cm (11.111%) and 32.5-33 cm (10.81%), do SP grains dominate, determined from >10% values [Dearing *et al.*, 1996]. The χ_{FD}/g profile also highlights the contribution of SP grains and demonstrates a clearer down-core trend with higher χ_{FD}/g differences in 16 cm to 0 cm suggesting that a SP component is contributing to the ~post-1900 section of the core (phases DDii, DDiii and DDiv).
S-RATIO	The observed post-1978 'hard' magnetic component (Figure 6.1 and Table 6.1) is also demonstrated by the S-RATIO profile that clearly shows a shift in the magnetic signal at 5-5.5 cm (phase DDiv) of <-0.3, indicative of hard magnetic behaviour (i.e. haematite) [Robinson, 1986].
SIRM/ARM	SIRM/ARM demonstrates relatively constant ratios (~50-100) from the base of the core until ~21 cm (~1838) (phase DDi). From this depth to 5-5.5 cm SIRM/ARM values steadily increase, suggesting a coarsening of the magnetic assemblage, with a peak value of 152.168 at 8-8.5 cm (1961) (phases DDii, DDiii and DDiv). This mirrors the $SOFT_{-20mT}$ profile peak, which suggests a coarse soft magnetic signal between 21 and 5.5 cm (~1838 to 1975). SIRM/ARM values drop dramatically from 5.5 cm to 0 cm (phase DDiv), indicating a shift to finer magnetic grains (potentially in the SSD range).
χ_{ARM}/SIRM	The shift in grain size from 5.5 cm (observed in the SIRM/ARM profile) is also enhanced by a sharp increase in χ_{ARM}/SIRM ratios for this section of the core (phase DDiv), further implying a finer magnetic component in the post-1975 sediment, supported by the χ_{ARM} and $HARD_{-300mT}$ profiles (Figure 6.1, Table 6.2).
SIRM/χ_{LF}	SIRM/χ_{LF} values[†] range from 11.949 to 41.565 10^3 Am^{-1}, which Thompson *et al.*, [1980] suggest is indicative of magnetite, which typically ranges from 1.5 to 50 kA/m, opposed to haematite[‡]. However, this relationship is complicated by mixed mineral assemblages such as lake sediments. The SIRM/χ_{LF} profiles does not identify a significant SP component, typical of ratios < 0.01 kA/m [Thompson *et al.*, 1980], however, the enhanced 'hard' contribution to the core, demonstrated by $HARD_{-300mT}$ (Figure 6.1) and shifts in SIRM/ARM and χ_{ARM}/SIRM (Figure 6.2) in post-1978 (0 to 5 cm) sediments, suggest a source of fine magnetite (possibly SSD, small amount of SP, or grains on the SSD/SP boundary) [Thompson *et al.*, 1980]. Overall, the increases in high SIRM/χ_{LF} ratios highlight an increase in fine-grained magnetic minerals post-1900 (15.5 to 0 cm) (phases DDiii and DDiv).

[†] These values in 10^3 are equivalent to kilo amperes per meter (kA/m).

[‡] A haematite component would indicate values >200 kA m.

The dominance of SSD grains (0.7-0.07 μm) identified in the post-1978 section of the BDD1 core (phase DDiv), as indicated by pronounced increases of χ_{ARM} and HARD.$_{300mT}$ (Figure 6.1) and corresponding decreases in SIRM/ARM (Figure 6.2), can be further investigated by applying magnetic data to a series of bi-plots. To identify 'true' SSD dominated samples in the BDD1 core, according to criteria set out by Oldfield [1994], χ_{ARM}/SIRM versus χ_{FD}% has been plotted (Figure 6.3). Oldfield [1994] reports magnetic grains including and below the SSD boundary exhibit χ_{FD} >2% and >80 ($10^{-5}Am^{-1}$) χ_{ARM}/SIRM values. The plot reveals samples dominated by SSD grains occur within the top 2.5 cm of the BDD1 core (within phase DDiv).

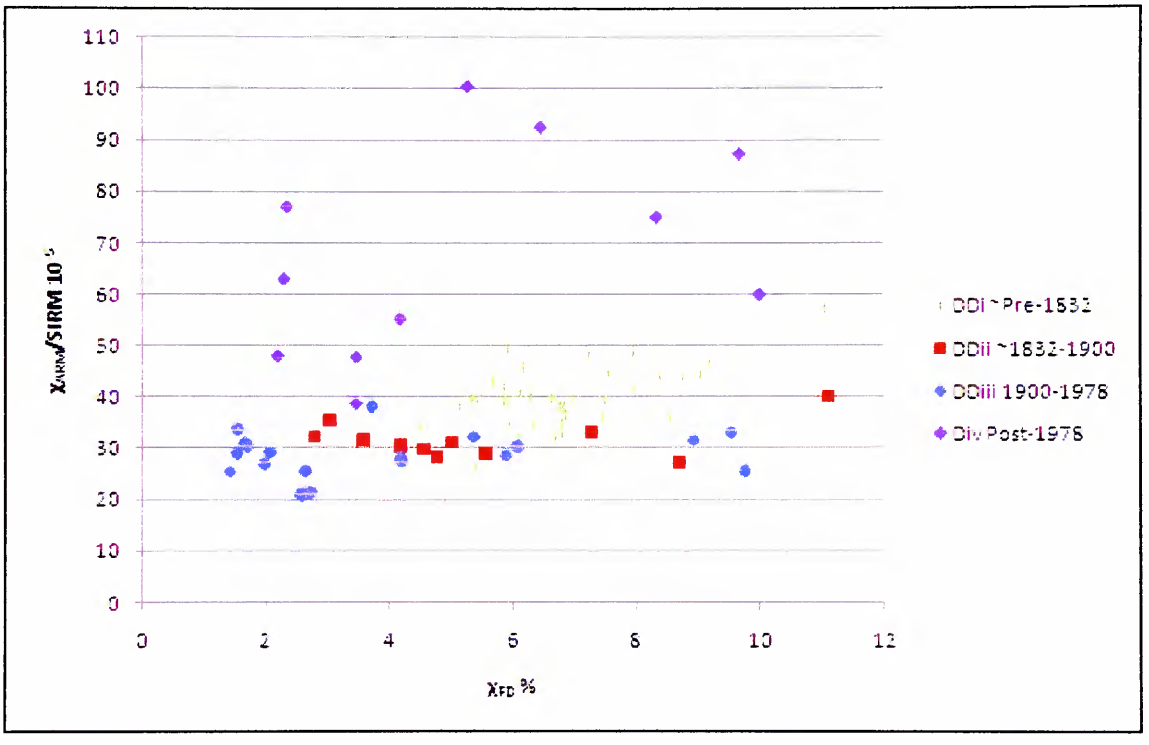

Figure 6.3: χ_{ARM}/SIRM (10^{-5} Am^{-1}) versus χ_{FD}% plots for BDD1 to identify SSD dominated samples, after Oldfield [1994]. Samples are plotted within phases DDi to DDiv.

These true SSD samples have been applied to Oldfield's [2007] bi-logarithmic plot of χ_{ARM}/χ_{FD} versus χ_{ARM}/χ_{LF} (Figure 6.4) to discriminate the potential source of these fine ferrimagnetic grains[§]. The template displays two main envelopes, the 'bacterial' group with the higher quotients, comprised of Adriatic sediments and Irish Sea saltmarsh samples that via TEM prove to be dominated by SSD bacterial magnetite. The 'soil source' group, exhibiting lower quotients, represent a range of soils and catchment sediments mainly

[§] Oldfield highlights potential problems of using this template where paramagnetic or diamagnetic minerals make a significant contribution.

dominated by finer SP grains. Also included are values for recent sediments dominated by SSD grains from small lakes in northwest England, published by Oldfield [1999, 2007], which generally fall between these two envelopes. Superimposed on to this template are the identified SSD (~<0.1 μm) ferrimagnetic grains in the BDD1 core. The BDD1 samples plot between the 'bacterial' and 'soil/catchment' envelopes (Figure 6.4), similar to the Brothers Water, Blelham and Ponsonby Tarn lake sediments [Oldfield, 1999; Oldfield and Wu, 2000]. This suggests the selected BDD1 samples have a high SSD-to-SP ratio and, therefore, the shift to a fine ferrimagnetic grain size in this recent part of the core is not attributed to a SP signal, typical of a soil or catchment-derived source, nor due to a solely bacterial-derived source of magnetite.

Oldfield and Wu [2000] suggest bacterial magnetosomes may have a notable effect on the magnetic properties of the SSD Brothers Water samples, which demonstrate an increased importance of SSD ferrimagnetic grains in ~post-1950 sediment. Oldfield attributes this enhanced SSD signal to either increased magnetosome production since 1950, and/or the dissolution of magnetosomes through time [Oldfieldand Wu, 2000]. The shift to SSD ferrimagnetic grains also occurs in recent sediment of the Daresbury Delph core. However, these samples do not exhibit χ_{ARM}/SIRM values in excess of ~2 (10^{-3}) mA, which Oldfield attributes to magnetosome-dominated samples [Oldfield, 1999].

Figure 6.5 presents (SIRM-IRM_{20mT})/SIRM versus SIRM/ARM for BDD1 [after Oldfield, 1990]. These parameters are sensitive to coarse ferrimagnetic grains. Oldfield [2007] reports a trend towards increases in both of these parameters as indicating a general increase in concentration of ferrimagnetic grains. Therefore, samples that plot in the bottom left of the graph are relatively fine compared to samples which plot in the top right. Work by Oldfield *et al.*, [1985], Hunt *et al.*, [1984] and Hunt [1986] use SIRM/ARM increases as a response to increased concentration of anthropogenic particles in sediments, because, as stated by Oldfield *et al.*, [1985], low ARM-to-SIRM ratios are common in all anthropogenic PM studied so far.

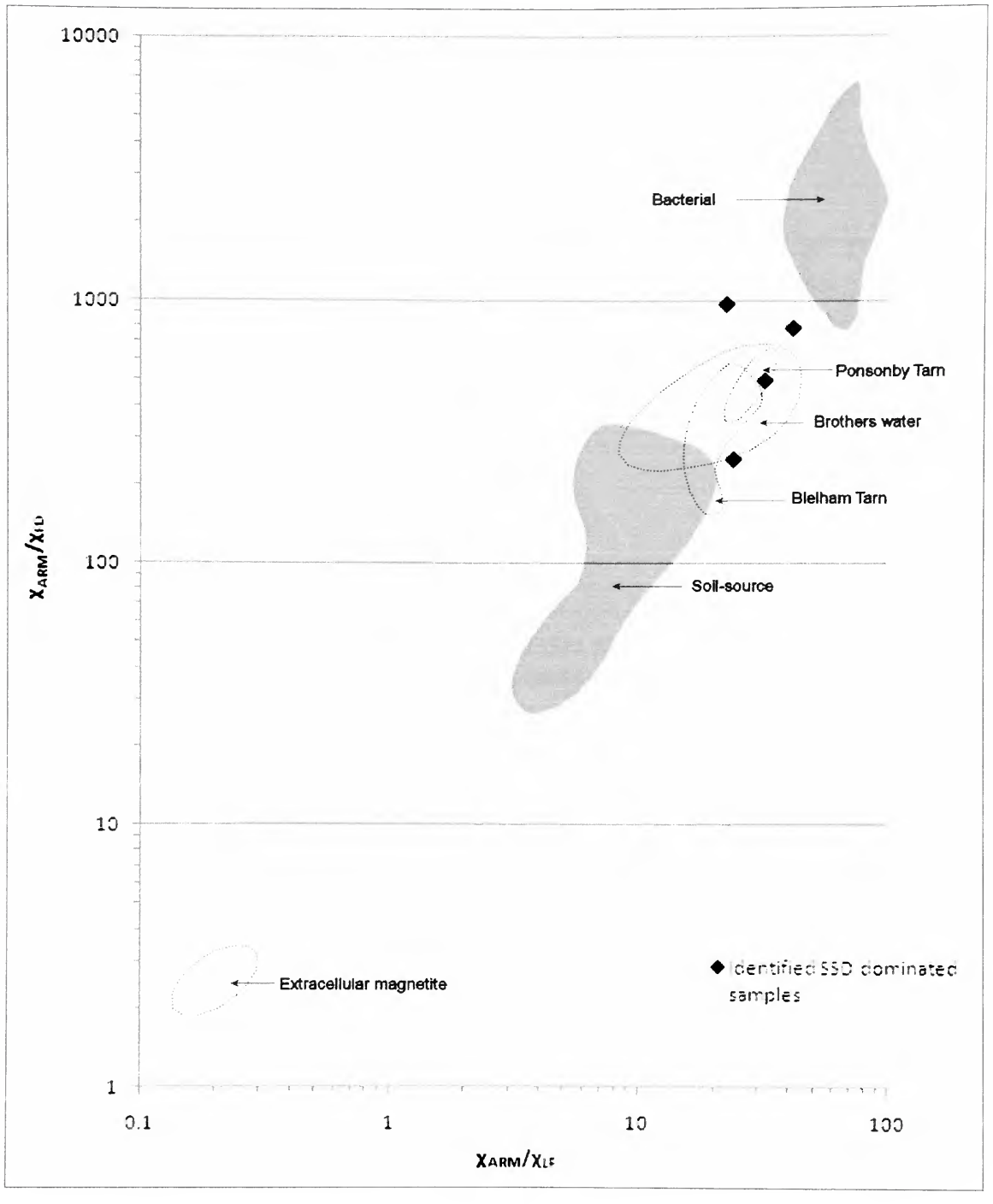

Figure 6.4: Bi-logarithmic scatter plot of χ_{ARM}/χ_{FD} versus χ_{ARM}/χ_{LF} to determine sources of fine grained magnetite for BDD1. The identified SSD dominated samples 0 to 2.5 cm (within phase DDiv) are plotted according to Oldfield [2007], superimposed over published envelopes for bacterial and soil/catchment derived fine grained magnetite [Oldfield, 1994, 2007]. Also the values for small lakes in NW England: Blelham Tarn, Brothers water and Ponsonby Tarn [Oldfield, 1994, 1999, 2007] are included.

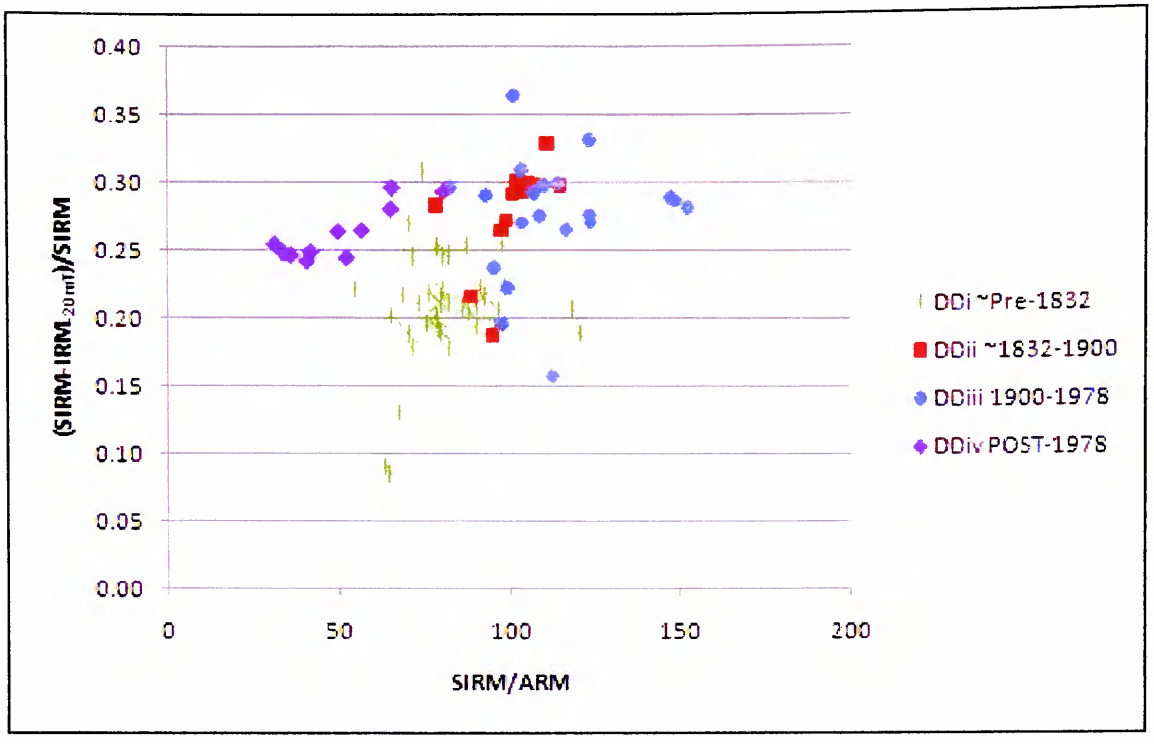

Figure 6.5: Plot of SIRM-IRM_{20mT}/SIRM versus SIRM/ARM for BDD1 after Oldfield [1990] showing down-core phases (DDi to DDiv) to assess variations in magnetic grain size within the sediment column.

Figure 6.5 presents SIRM-IRM_{20mT}/SIRM versus SIRM/ARM data for the down-core phases DDi (~pre-1832), DDii (~1832 to 1900), DDiii (1900 to1978) and DDiv (post-1978) of the BDD1 core. The template reveals:

- DDi: pre-1832 sediment is characterised by a relatively fine-grained magnetic signal;
- DDii: 1932-1900 sediment demonstrates a shift to coarser grains;
- DDiii: 1900-1978 sediment displays a relatively coarse magnetic signature; and
- DDiv: Post-1978 sediment, although exhibits very similar (SIRM-IRM_{20mT})/SIRM values to DDii and DDiii, has a clear fine-grained magnetic signal, with samples plotting in the upper left section of the graph.

6.3.2. <10 μm particle size distributions: BDD1

Figure 6.6 displays the particle size contributions to the sediment column of the respiratory size boundaries of PM_{10} (<10 μm) $PM_{2.5}$ (<2.5 μm) and PM_1 (<1 μm). Median data are included to demonstrate how average particle size varies down-core and to correct for the potential presence of relatively large organic material in the samples which may affect mean values. The divisions DDi to DDiv are overlain to aid description of particle size

trends. Overall, there is an increase in relatively fine particles post-1900, compared to relatively coarse pre-1900 data, as demonstrated by the median particle size profile which exhibits a shift to <10 μm. Also, there is a further increase in fine (<10 μm) particulates post-1978 (Table 6.4). These 20th century increases in particles <10 μm (a proxy for PM_{10}) may indicate post-1900 enhancement of PM_{10} pollution.

6.3.3. Trace metal concentrations: BDD1

Down-core Pb, Zn, Cu, S and Br concentrations are presented (Figure 6.7). The profiles exhibit closely paralleled trends (Table 6.5), corresponding to the down-core divisions for BDD1.

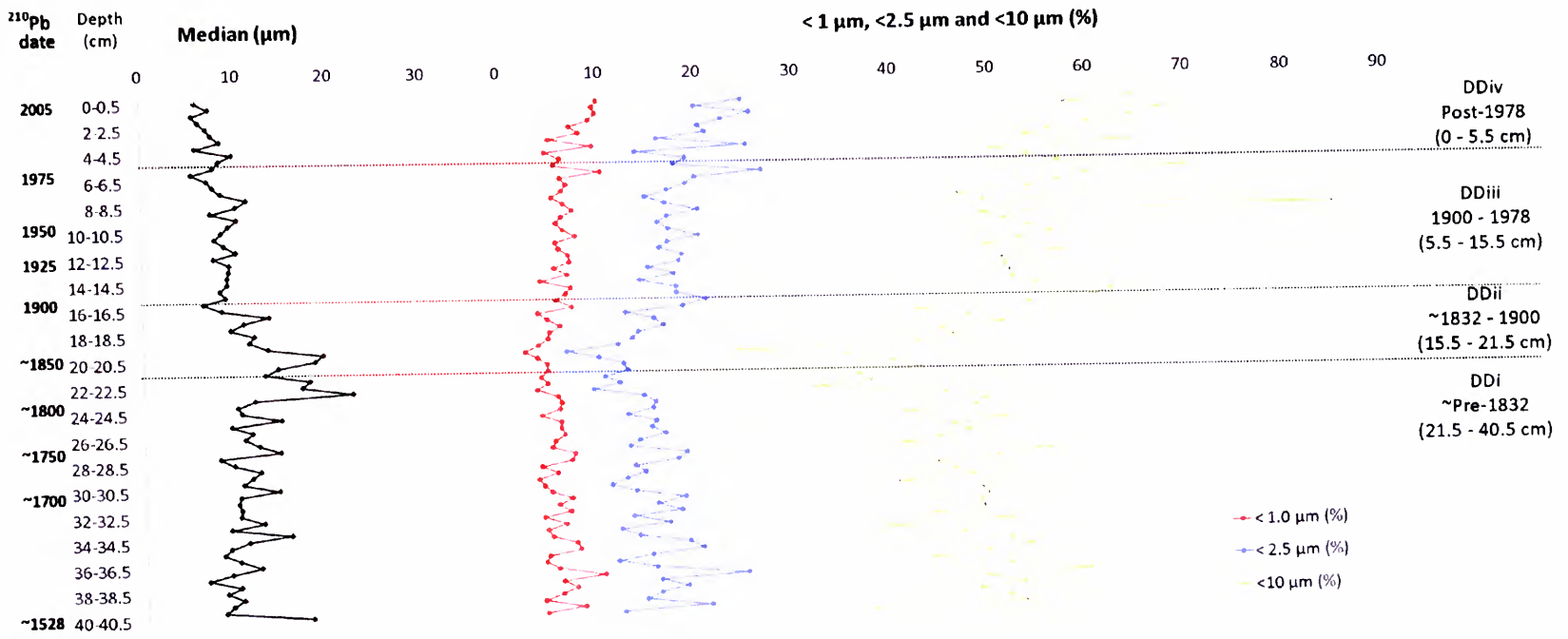

Figure 6.6: Median particulate size and percentage distributions for fractions <1 µm, <2.5 µm and <10 µm for BDD1 with superimposed phases DDi to DDiv (corresponding to Table 6.4).

Table 6.4: Down-core particle size variations in BDD1, relating to divisions DDi to DDiv (corresponding to Figure 6.6).

Phase	Depth/Date	Particle size trends
DDiv	Post-1978 (5.5 to 0 cm)	A further increase in relatively finer sediment demonstrated by increases in <10 µm, <2.5 µm and <1 µm particulates.
DDiii	1900-1978 (15.5 to 5.5 cm)	A shift to finer assemblages is observed from the start of the 20th century throughout this phase, indicated by a decrease in median particle size to <10 µm and corresponding increases in <10 µm, <2.5 µm and <1 µm particles.
DDii	~1832 to 1900 (21.5 to 15.5 cm)	A distinct coarse signal is observed in this phase, with a notable median peak at ~1850 (19.5-20 cm) and corresponding decreases in particles <10 µm.
DDi	~pre-1832 (40.5 to 21.5 cm)	Relatively coarse signal highlighted by comparatively lower <10 µm values.

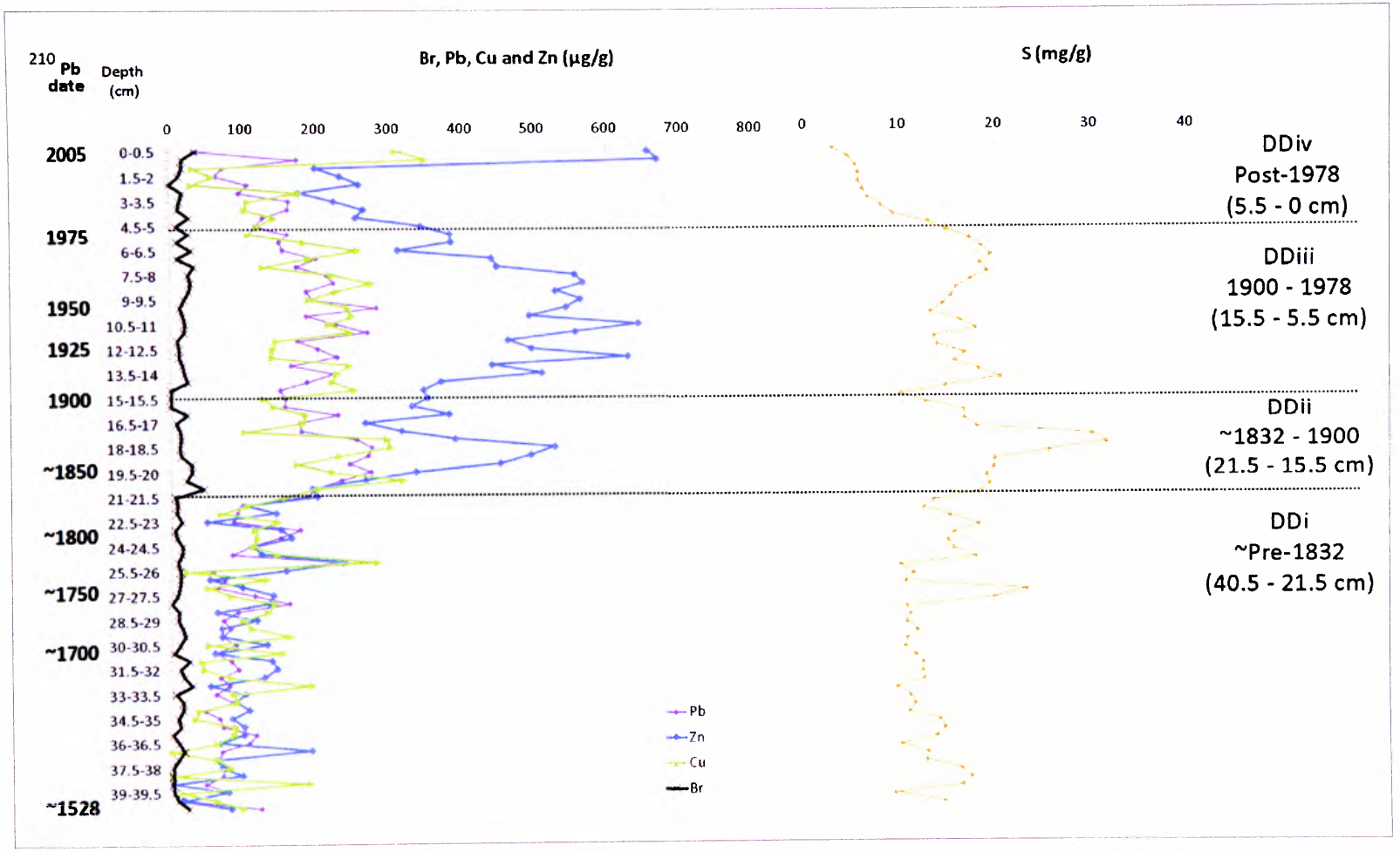

Figure 6.7: Down-core Br, Pb, Cu, Zn, and S concentration profiles for BDD1 with superimposed phases DDi to DDiv (corresponding to Table 6.5).

Table 6.5: Down-core Br, Pb, Cu, Zn and S concentration trends in BDD1, relating to phases DDi to DDiv (corresponding to Figure 6.7).

Phase	Depth/Date	Trace metal concentration trend
DDiv	Post-1978 (5.5 to 0 cm)	Pb, Zn, Cu, S and Br concentrations exhibit an overall decrease throughout this phase; however, fluctuations and smaller peaks occur, particularly a Zn peak at 1975 to 1978 (6 to 5 cm) and Pb at 1989 to 1992 (4 to 3 cm). S declines steadily declines post-1978 to reach a minimum value at the sediment-surface (3.154 mg/g).
DDiii	1900 to 1978 (15.5 to 5.5 cm)	Overall, Pb, Zn, Cu and S values generally increase throughout the 20th century with smaller peaks occurring between ~1909 and 1921 (12.5-13 and 14-14.5 cm), ~1937 (11-11.5 cm) and 1961 to 1963 (7.5 to 8.5 cm). Maximum Pb concentrations are exhibited at 1950 (9.5-10 cm) and remain relatively high throughout the 1960s, until notable declines post-1972 (6.5 to 0 cm).
DDii	~1832 to 1900 (21.5 to 15.5 cm)	Further pronounced enrichment of the Pb, Zn, S and Cu profiles occur from ~21.5 cm, in ~post-1832 sediment. This is highlighted by closely paralleled Pb, S, Zn and Cu peaks between ~1850 and 1873 (20.5 cm and ~17.5 cm), whereby, maximum S (31.817 mg/g), and high Pb (274.871 µg/g), Cu (318.803 µg/g) and Zn (527.286 µg/g) concentrations are reached. Br also exhibits enhancement ~post-1832, with maximum values (44.446 µg/g) observed from ~1850-1860 (~18 to 20 cm). Br values decline to zero during ~1894-1904 (14 to 16 cm) and then quickly recover to relatively high 20th century values. A decrease in the Zn, Cu and S occurs from ~1880 to 1900, with a corresponding reduction in Pb during the 1890s.
DDi	~Pre-1832 (40.5 to 21 cm)	Characterised by relatively low ~pre-1832 Pb, Zn, Cu, S and Br concentrations. From the basal sediment layer to 26.5 cm (~pre-1766) minimum Pb (17.919 µg/g) and zero Zn and Cu values occur. Increased Zn, Pb and Cu concentrations are observed post-1766, with peaks from 25.5 to 23 cm, corresponding to 1780 to 1807. Earlier, mid-18th century S and Pb peaks are apparent at ~1751 (27-27.5 cm).

6.3.4. SCPs: BDD1

Figure 6.8 demonstrates down-core trends in the total number of SCP counts (per dry sediment) and for SCP size fractions: 10-30 μm, 3-10 μm and 1-3 μm in the BDD1 core summarised in Table 6.6. As SCPs are unambiguous indicators of anthropogenic, combustion-derived particulates, they are commonly used to assess trends in the consumption of fossil fuel.

SCPs were identified at the basal layer of the sediment stratigraphy, with comparatively low values of ~<20 counts in pre-1832 sediment (20.50 to 40.5 cm, phase DDi). The SCP values begin to increase at 20.5-21 cm (~1838), potentially, indicating the start of the SCP record (phase DDii). The SCP profile exhibits a sharp increase in concentration at 14-14.5 cm (1909) with peaks occurring from the start of the 20th century, notably at 12.5-13 cm (1921) and 10.5-11 cm (1942) (phase DDiii). Maximum SCP concentration in the core is observed at 7.5-8 cm, corresponding to a ^{210}Pb date of 1963 (phase DDiii). Values decline in phase DDiv, with a recent increase at 0.5-1 cm (2004).

The SCP size divisions exhibit similar trends to the total SCP profile, with increased concentrations occurring at ~20.5-21 cm (1838). Close parallels in pronounced SCP concentrations occur in all SCP profiles at ~12.5 to 13.5 cm (1914 to 1921), 10.5-11cm (1942). Maximum SCP concentrations for all size ranges occur at 7.5-8 cm (1963). An overall decline in SCPs occur post-1975 with relatively smaller peaks observed throughout the profiles at 1995 and increases at 2004 in SCPs 3-10 μm and 1-3 μm. Of the total SCPs counted the majority of SCPs fall in the 3-10 μm size boundary, followed by 10-30 μm then 1-3. Values for SCPs >30 μm are comparatively low and SCPs <1 μm are only notable in the very recent section of the core 2 to 0 cm (post-2004)**.

** Unable to provide data for SCPs <1 μm due to higher magnification required to accurately count these ultrafine particles.

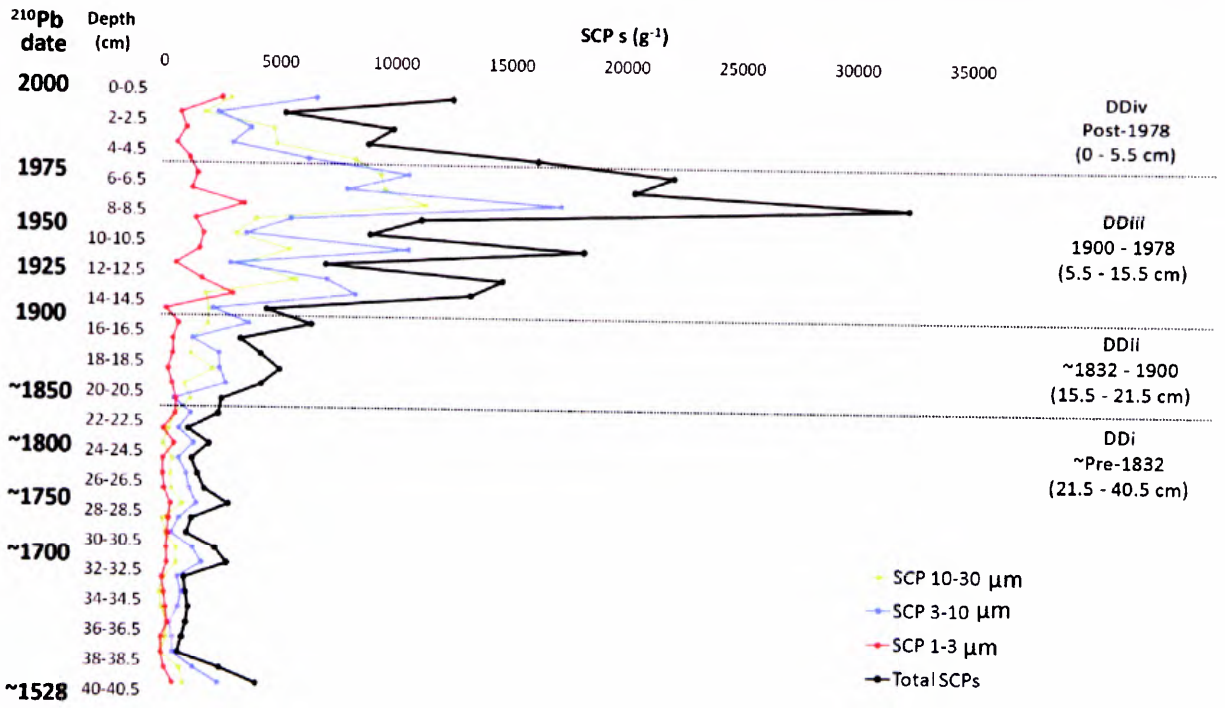

Figure 6.8: SCP counts 10-30 µm, 3-10 µm, 1-3 µm and total SCPs for BDD1 with superimposed phases DDi to DDiv (corresponding to Table 6.6).

Table 6.6: Down-core SCP concentration trends in BDD1, relating to phases DDi to DDiv (corresponding to Figure 6.8).

Phase	Depth/Date	Trace metal concentration trend
DDiv	Post-1978 (5.5 to 0 cm)	Decline in SCP concentrations.
DDiii	1900 to 1978(15.5 to 5.5 cm)	Prominent enhancement in the SCP record post-1900. Maximum SCP concentrations are reached at 1963.
DDii	~1832 to 1900 (21.5 to 15.5 cm)	Increase in SCPs post~1838, highlighting the start of the SCP record. Steadily increasing trends are observed.
DDi	~Pre-1832 (40.5 to 21 cm)	Relatively low SCP counts.

6.3.5. Statistical relationships: BDD1

Table 6.7 presents a correlation coefficient matrix for the concentration-dependent magnetic parameters, anthropogenic trace metals, organic matter (OM) and SCPs for BDD1, highlighting statistical relationships between the sediment characteristics.

Strong positive correlations are observed between OM and the magnetic parameters SIRM ($R=0.631$; $p<0.001$; $n=81$) and $SOFT_{-20mT}$ ($R=0.525$; $p<0.001$; $n=81$), as well as the trace metals Cu ($R=0.613$; $p<0.001$; $n=81$), Pb ($R=0.727$; $p<0.001$; $n=81$), Zn ($R=0.745$; $p<0.001$; $n=81$) and Br ($R=0.554$; $p<0.001$; $n=81$). Also, strong positive correlations are exhibited between OM and 'total SCPs' ($R=0.725$; $p<0.001$; $n=81$) as well as the SCP size fractions (Table 6.7).

SCPs demonstrate strong positive correlations with the concentration-dependent magnetic parameters χ_{LF} ($R=0.557$; $p<0.001$; $n=81$), SIRM ($R=0.697$; $p<0.001$; $n=81$), χ_{ARM} ($R=0.534$; $p<0.001$; $n=81$), $SOFT_{-20mT}$ ($R=0.711$; $p<0.001$; $n=81$) and $HARD_{-300mT}$ ($R=0.625$; $p<0.001$; $n=81$). These magnetic and trace metal relationships with 'total' SCP count are also mirrored by the SCP size fractions 10-30 μm, 3-10 μm and 1-3 μm (Table 6.7). Strong positive correlations are also observed between SCPs and the typically anthropogenic trace metals Zn ($R=0.790$; $p<0.001$; $n=81$), Pb ($R=0.614$; $p<0.001$; $n=81$), and Cu ($R=0.507$; $p<0.001$; $n=81$)[††].

[††] Also a particularly strong relationship with the SCPs is exhibited by Ca ($R=0.777$ $p<0.001$; $n=81$), a trace metal that is both naturally abundant with some industrial sources.

Table 6.7: Selected correlation coefficients of OM and SCP data for BDD1. R values accompanied by p value expressed as *** =p<0.001, ** =p<0.01, and * =p<0.05; n=81.

	OM	Total SCPs	SCP 10-30 µm	SCP 3-10 µm	SCP 1-3 µm
OM	1.00				
Total SCPs	0.725***	1.00			
SCP 10-30 µm	0.741***	0.953***	1.00		
SCP 3-10 µm	0.641***	0.958***	0.877***	1.00	
SCP 1-3 µm	0.613***	0.877***	0.761***	0.806***	1.00
χ_{LF}		0.557***	0.562***	0.555***	0.541***
χ_{ARM}	0.251*	0.534***	0.533***	0.515***	0.541***
SIRM	0.631***	0.697***	0.660***	0.678***	0.644***
SOFT$_{.20mT}$	0.525***	0.711***	0.683***	0.700***	0.628***
HARD$_{.300mT}$		0.589***	0.578***	0.575***	0.564***
S	0.383***				
Cu	0.613***	0.507***	0.491**	0.473**	0.419**
Pb	0.727***	0.614***	0.597***	0.564***	0.588***
Zn	0.745***	0.790***	0.757***	0.750***	0.707***
Br	0.554***				

Although S and Br do not exhibit significant relationships with SCPs (Table 6.7), they demonstrate significant correlations with Pb, Zn and Cu, and strong inter-trace metal correlations are observed between the anthropogenic trace metal group (Table 6.8). These metals also demonstrate negative correlations with the typically minerogenic trace metals K and Si (Table 6.8). No relationships exist between SCPs and the typically natural/minerogenic trace elements Al, Ti, Si, K, Fe, and Mn. Strong significant inter-element correlations are exhibited within this 'natural' trace metal group; notably between Fe and Mn (R=0.520; p<0.001; n=81), and K and Ti (R=0.789; p<0.001; n=81) (Table 6.8). Al exhibits no significant relationships with the other environmental variables.

Table 6.8: Correlation coefficient matrix of selected trace metals for BDD1. R values accompanied by p value expressed as *** =p<0.001, ** =p<0.01, and * =p<0.05; n=81.

	Si	Al	Ti	Ca	K	Fe	Mn	S	Cu	Pb	Zn	Br
Si	1.00											
Al		1.00										
Ti			1.00									
Ca	-0.773***			1.00								
K		0.261*	0.798***		1.00							
Fe	-0.418***			0.368***	0.249*	1.00						
Mn	-0.274*					0.520***	1.00					
S			-0.415***		-0.596***			1.00				
Cu	-0.361***			0.443***	-0.400***			0.492***	1.00			
Pb	-0.434***			0.596***	-0.419***			0.670***	0.672***	1.00		
Zn	-0.650***			0.758***	-0.324**			0.341**	0.606***	0.750***	1.00	
Br	-0.403***			0.405***	-0.282*				0.426***	0.330**	0.428***	1.00

Statistically significant relationships are also observed between the 'anthropogenic' trace metal group and the concentration-dependent magnetic parameters (Table 6.9). Particularly strong positive correlations are observed between Zn and SIRM ($R=0.545$; $p<0.001$; $n=81$) and $SOFT_{-20mT}$ ($R=0.681$; $p<0.001$; $n=81$) (Table 6.9). Br exhibits weaker relationships with these magnetic parameters and demonstrates a weak correlation with $HARD_{-300mT}$ ($R=0.303$; $p<0.01$; $n=81$). Cu exhibits weak positive relationships with SIRM and $SOFT_{-20mT}$, and Pb only demonstrates a statistically significant weak correlation with $SOFT_{-20mT}$. Inversely, S exhibits significant negative correlations with χ_{LF}, χ_{ARM} and SIRM (Table 6.9). The typically minerogenic trace metals Ca, K, and Ti also exhibit strong positive correlations with the concentration dependent parameters; also Fe and Mn display positive correlations with $HARD_{-300mT}$ only. Inversely, Si demonstrates negative correlations with magnetic concentration data (Table 6.9). Strong positive inter-magnetic parameter correlations are also exhibited between χ_{ARM}, SIRM, $SOFT_{-20mT}$ and $HARD_{-300mT}$; however, χ_{LF} does not exhibit significant relationship with the other magnetic properties (Table 6.9).

Table 6.9: Selected correlation coefficients of magnetic parameters for BDD1. R values accompanied by p value expressed as *** =p<0.001, ** =p<0.01, and * =p<0.05; n=81.

	χ_{LF}	χ_{ARM}	SIRM	$SOFT_{-20mT}$	$HARD_{-300mT}$	SIRM/ ARM	χ_{ARM}/ SIRM	SIRM/ χ_{LF}
χ_{LF}	1.00							
χ_{ARM}		1.00						
SIRM		0.930***	1.00					
$SOFT_{-20mT}$		0.849***	0.961***	1.00				
$HARD_{-300mT}$		0.815***	0.725***	0.635***	1.00			
SIRM/ARM				0.227*	-0.266*	1.00		
χ_{ARM}/SIRM		0.517***	0.433***	0.383***	0.477***	-0.544 ***	1.00	
SIRM/χ_{LF}		0.652***	0.748***	0.809***	0.483***	0.289**	0.292**	1.00
Si	-0.419 ***	-0.573 ***	-0.584 ***	-0.620 ***	-0.516 ***		-0.407 ***	-0.654 ***
Al								
Ti	0.571***	0.439***	0.444***	0.355***	0.323**			
Ca	0.539***	0.593***	0.666***	0.755***	0.429***		0.398***	0.811***
K	0.437***	0.393***	0.301**		0.431***	-0.498 ***	0.328**	
Fe					0.370***			0.301**
Mn					0.339**		0.323*	
S	-0.305 **	-0.367 ***	-0.252*		-0.430 ***	0.618***	-0.539 ***	
Cu			0.234*	0.382***		0.491***		0.382***
Pb				0.333**		0.578***		0.545***
Zn	0.341**	0.398***	0.545***	0.681***		0.472***		0.663***
Br		0.288**	0.332**	0.415***	0.303**	0.267*		0.393***

Particle size relationships are identified (Table 6.10). Positive correlations are observed between the clay fraction and χ_{LF} (R=0.410; p<0.001; n=81), SIRM (R=0.467; p<0.001; n=81), χ_{ARM} (R=0.485; p<0.001; n=81), $SOFT_{-20mT}$ (R=0.418; p<0.001; n=81) and $HARD_{.300mT}$ (R=0.406; p<0.001; n=81). These parameters also exhibit positive correlations with the <10 μm size fractions and negative correlations with the sand-sized fraction. Table 6.10 reveals weak positive correlations between Ca, K and Fe and the fine (<10 μm) size ranges and weak negative correlations between the fine fractions and S and Si. Positive correlations are observed between the SCPs and the clay and <10μm size fractions.

Table 6.10: Correlation coefficients of selected particle sizes for BDD1. R values accompanied by p value expressed as *** =p<0.001, ** =p<0.01, and * =p<0.05; n=81.

	Clay	Silt	Sand	<10 μm	<2.5 μm	<1 μm
Clay	1.00					
Silt		1.00				
Sand	-0.464***	-0.745***	1.00			
<10 μm	0.560***		-0.292**	1.00		
<2.5 μm	0.439***			0.909***	1.00	
<1 μm	0.341**			0.802***	0.937***	1.00
χ_{LF}	0.410***		-0.288**	0.531***	0.463***	0.433***
χ_{ARM}	0.485***		-0.333**	0.604***	0.556***	0.502***
SIRM	0.467***		-0.391***	0.562***	0.475***	0.427***
$SOFT_{-20mT}$	0.418***		-0.404***	0.501***	0.415***	0.362***
$HARD_{.300mT}$	0.406***		-0.221*	0.505***	0.510***	0.472***
SIRM/ARM					-0.238*	-0.265*
χ_{ARM}/SIRM	0.376***			0.361***	0.328**	0.322**
SIRM/χ_{LF}	0.312**		-0.244*	0.325**	0.242*	
Si	-0.491***		0.244*	-0.580***	-0.487***	-0.365***
Al						
Ti			0.260*	0.255*		
Ca	0.345**		-0.259*	0.506***	0.421***	0.289**
K	0.238*			0.347***	0.346**	0.351**
Fe				0.280*	0.340**	0.296**
Mn	0.284**					
S	-0.260*			-0.246*	-0.218*	-0.247*
Cu						
Pb						
Zn	0.260*		-0.244*	0.334**	0.235*	
Br						
Total SCPs	0.591***			0.446**		
SCP 10-30	0.531***			0.472**		
SCP 3-10	0.592***			0.437**		
SCP 1-3	0.516***			0.401**		

6.4. Local pollution signal recorded in Windmill Hill Pond

Visual assessment of proxy pollution characteristics (most notably, trace metals and magnetic properties), has revealed key features within the WH3 core sediments, which have been used to divide the core into phases to aid description and interpretation of proxy pollution profiles (Table 6.11).

Table 6.11: Down-core phases identified in WH3.

Phase	Depth/Age	Proxy pollution trend
WHiv	Post-1993 (3.5 to 0 cm)	Decline in magnetic concentration coinciding with inversely increasing trace metals.
WHiii	1949 to 1993 (11.5 to 3.5 cm)	Further magnetic and trace metal increases, and prominent magnetic peaks.
WHii	~1906 to 1949 (20 to 11.5 cm)	Enhancement in proxy pollution concentrations.
WHi	~Pre-1906 (23 to 20.5 cm)	Relatively low proxy pollution characteristics.

6.4.1. Magnetic characteristics: WH3

Down-core trends in the magnetic concentration-dependent magnetic parameters are presented for WH3 (Figures 6.9 A and 6.9 B). χ_{LF} values range from -259.067 10^{-9} m^3 kg^{-1} to 7560.878 10^{-9} m^3 kg^{-1}, with a mean of 907.138 10^{-9} m^3 kg^{-1}. Compared to published values [Dearing, 1999(a)], these data correspond to measurements for a range of environmental materials including diamagnetic minerals, sedimentary and metamorphic rocks, paramagnetic minerals, igneous rocks, topsoils, burned soils and antiferromagnetic minerals. Close parallels are exhibited between χ_{LF}, SIRM, χ_{ARM}, $SOFT_{-20mT}$ and $HARD._{300mT}$, (Figure 6.9A) and the main temporal phases in magnetic concentration are detailed in Table 6.12. Very prominent magnetic peaks are exhibited at 10-10.5 cm (1955) and 11-11.5 cm (1949) (Figure 6.9 A). When these data samples are omitted (Figure 6.9 B), magnetic concentration trends can be better assessed.

Down-core variations in magnetic interparameter ratios are also presented (Figure 6.10), described and interpreted (Table 6.13). Down-core divisions for WH3 are superimposed over the profiles for these magnetic parameter ratios (Figure 6.10), which demonstrate magnetic grain size assemblages, rather than actual concentrations.

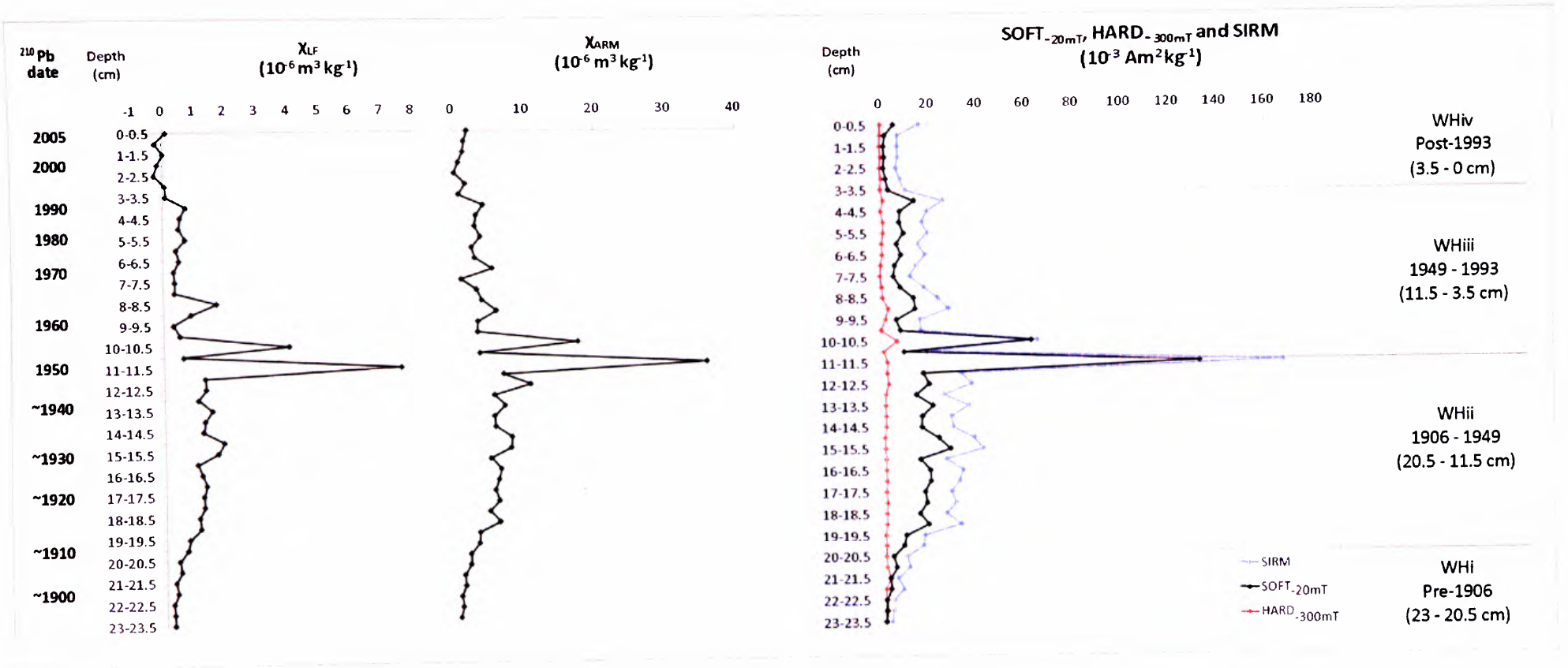

Figure 6.9A: Magnetic concentration profiles for WH3: χ_{LF}, χ_{ARM}, $SOFT_{-20mT}$, $HARD_{-300mT}$ and SIRM with superimposed phases WHi to WHiv (corresponding to Table 6.12).

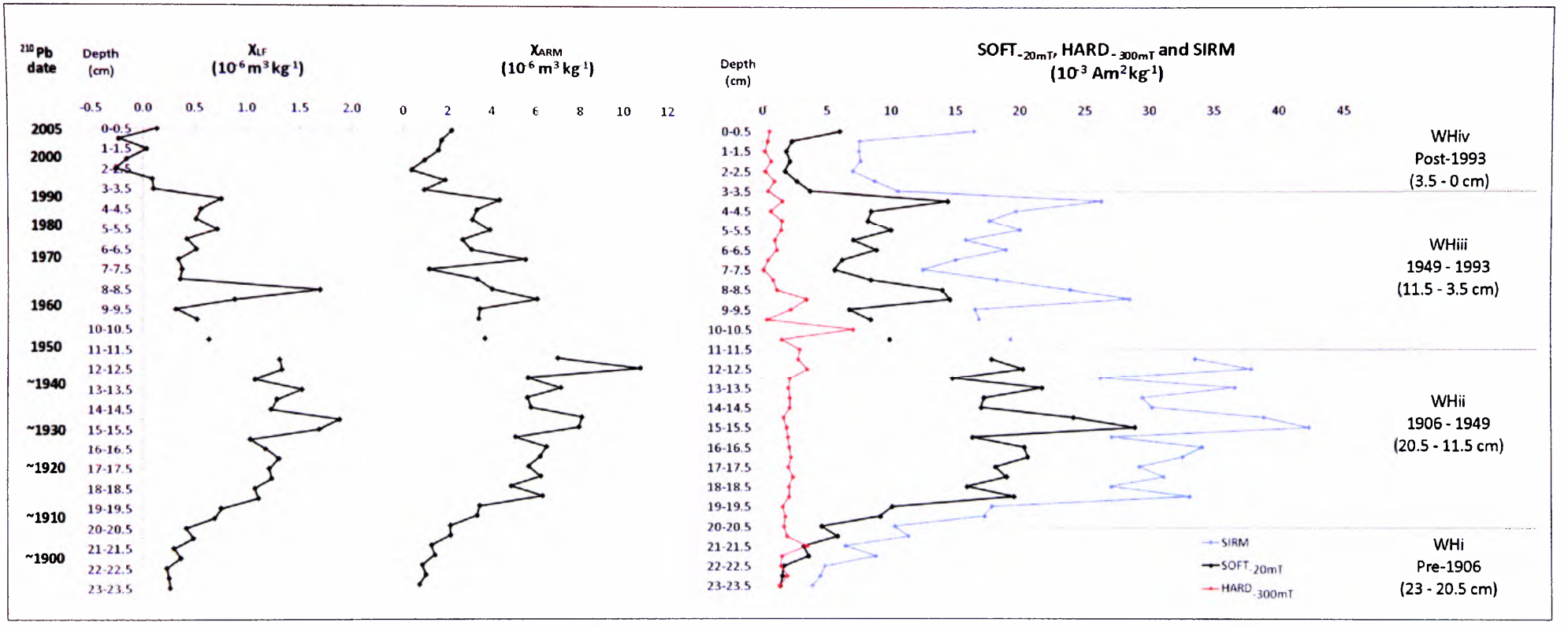

Figure 6.9B: Magnetic concentration profiles for WH3: χ_{LF}, χ_{ARM}, $SOFT_{-20mT}$, $HARD_{-300mT}$ and SIRM with superimposed phases WHi to WHiv (corresponding to Table 6.11). SIRM and $SOFT_{-20mT}$ data for sediment samples 10-10.5 cm and 11-11.5 cm are omitted due to high values obtained, therefore, demonstrating less variation in the profiles, allowing assessment of trends.

Table 6.12: Down-core magnetic concentration trends for WH3 relating to divisions WHit to WHiv (corresponding to Figure 6.9A and 6.9B).

Phase	Depth/Date	Magnetic concentration trend
WHiv	Post-1993 (3.5 to 0 cm)	Negative χ_{LF} values occur in post-1993 sediment, indicating a dominating diamagnetic contribution. This may reflect the relatively high (>40%) organic matter content observed in the top 3.5 cm of the core (Figure 5.5, Section 5.4.) and diamagnetic behaviour associated with organic material and moisture. SIRM and χ_{ARM} also exhibit decreases in this phase, with a slight enhancement in the magnetic signal at the sediment surface. Post-1993 $SOFT_{.20mT}$ values notably decline and $HARD_{.300mT}$ values steadily continue to decline to the sediment surface.
WHiii	1949 to 1993 (11.5 to 3.5 cm)	Prominent increases in magnetic concentration are exhibited between ~1949 and 1957 (11 to 9.5 cm) for χ_{LF}, SIRM and χ_{ARM}. χ_{LF} increases from relatively low values (<1 10^{-6} m^3 kg^{-1}) in ~pre-1949 sediment, to a maximum value of 7.561 10^{-6} m^3 kg^{-1}. Maximum concentrations are mirrored in the χ_{LF}, SIRM and χ_{ARM} profiles at ~1949 (11-11.5 cm), with a closely paralleled smaller peak occurring at 1955 (10-10.5 cm). Prominent maximum $SOFT_{.20mT}$ values (132.832 10^{-3} Am^2 kg^{-1}) occur at 1949 (11-11.5 cm) highlighting a steady increase in the contribution of MD ferrimagnetic minerals to the pond. Increased contributions of 'hard' magnetic minerals indicated by maximum $HARD_{.300mT}$ values (7.066 10^{-3} Am^2 kg^{-1}) are exhibited at 1955 (10-10.5 cm). Post-1957 magnetic concentrations decline to values lower than ~pre-1949 (phase WHii); however, a distinct peak is observed at 1964 (8-8.5 cm) and values subsequently steadily increase reaching a recent peak at 1989 (3.5-4 cm), after which values decline.
WHii	~1906 to 1949 (20 to 11.5 cm)	χ_{LF}, SIRM, χ_{ARM} and $SOFT_{.20mT}$ values notably increase from ~20 cm (~1906) and continue to steadily increase throughout the 20th century, with a notable peak at ~1929-1932 (14.5-15 cm) and smaller concentration increases between ~1940 to 1946 (13 to 11.5 cm). $HARD_{.300mT}$ also increases steadily throughout this phase.
WHi	~pre-1906 (23 to 20.5 cm)	Relatively low χ_{LF}, SIRM, χ_{ARM} and $SOFT_{.20mT}$ concentrations are exhibited; however, high, consistent $HARD_{.300mT}$ values (>1.357 10^{-3} Am^2 kg^{-1}) are observed from the base of the core to 14.5-15 cm, highlighting an antiferromagnetic contribution to the magnetic signal ~pre-1906.

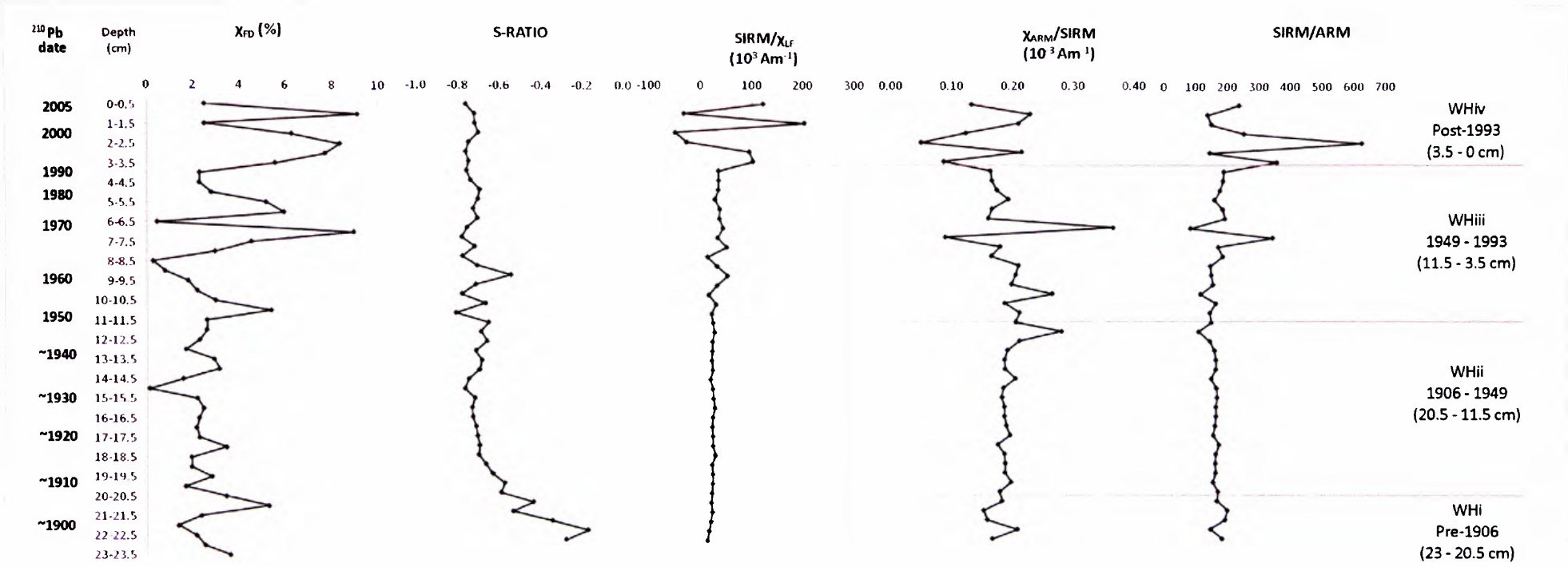

Figure 6.10: Magnetic ratio profiles for WH3: χ_{FD}, S-RATIO, SIRM/χ_{LF}, χ_{ARM}/SIRM and SIRM/ARM with superimposed phases WHi to WHiv (corresponding to Table 6.13).

Table 6.13: Description and interpretation of magnetic ratios for WH3 (corresponding to Figure 6.15).

Magnetic ratio	Description and interpretation
χ_{FD}	The majority of χ_{FD} values lie between 2-5%, highlighting a dominance of SSD (0.7-0.07 μm) in these samples. However, an increase in finer SP grains (<0.05 μm) occurs in the top 6.5 cm of the core, with several samples exhibiting χ_{FD} values >5%, indicative of a significant SP contribution. SP grains are so small they do not hold a remanence, therefore an increased contribution of these fine grains in post-1989 sediment is reflected by corresponding reduced SIRM values from 4 to 0 cm. This potentially suggests an increased contribution of <0.05 μm grains, potentially soil/catchment-derived, to the lake post-1989 (phase WHiv).
S-RATIO	S-RATIO values -0.6 to -0.2 in ~pre-1906 sediment highlights an antiferromagnetic contribution to the magnetic signal (phase WHi). The majority of S-RATIOs in ~post-1906 sediment lie between -0.6 to -0.8, revealing a dominance of MD ferrimagnetic grains.
SIRM/ARM	SIRM/ARM values are relatively consistent throughout the core, however, notable peaks occur at 7-7.5 cm (1967), 3-3.5 cm (1993) and 2-2,5 cm (1997), indicative of a higher contribution of coarse magnetic grains at these times.
SIRM/χ_{LF}	SIRM/χ_{LF} values range from 15.461 10^3 Am^{-1} to 53.231 10^3 Am^{-1} in pre-1989 sediment (23.5 to 4 cm), which Thompson *et al.*, [1980] and Maher *et al.*, [1999] report is indicative of magnetite. The SIRM/χ_{LF} profile also indicates a gradual shift from coarse grained magnetite in the lower section of the core (10 to 23.5 cm) to finer magnetite grain size from 10 to 3.5 cm (1955 to 1989 (phase WHiii)). A noisy post-1989 profile is exhibited, with values ranging from 202.704 10^3 Am^{-1}, indicative of haematite [Thompson *et al.*, 1980], to negative ratios attributed to the negative χ_{LF} values obtained in this recent section; however, the post-1989 SIRM. χ_{LF} trend is disrupted by negative χ_{LF} values (phase WHiv).
χ_{ARM}/SIRM	χ_{ARM}/SIRM values range from 0.050 to 0.367 10^{-3} Am^{-1} which, with χ_{FD} values <9.091%, excludes the dominance of the magnetic signal by soil-derived magnetite, typically characterised by χ_{FD} values >8% and χ_{ARM}/SIRM ratios between 0.5-1.8 10^{-3} Am^{-1}. These values do not reflect a contributing source of magnetosomes to the magnetic signal, which are typical of χ_{ARM}/SIRM values in excess of ~2 10^{-3} Am^{-1} [Oldfield, 1999]. Also the presence of samples dominated by SSD grains within the core is undetected, recognised using criteria set out by Oldfield, [1994] of χ_{ARM}/SIRM values >0.8 10^{-3} Am^{-1} with corresponding <2% χ_{FD} data. The χ_{ARM}/SIRM profile demonstrates relatively consistent values from the base of the core, until an increase at 12-12.5 to 8.5-9 cm, highlighting an increase in fine magnetic grains from ~1944-1961. A noisy χ_{ARM}/SIRM signal in the upper 7 cm of the core suggests a more mixed magnetic grain size assemblage post-1967.

The down-core trends in magnetic characteristics demonstrate a gradual reduction in the dominating grain size, reflected in the WH divisions:

- WHi: Relatively low ~pre-1906 magnetic concentrations, characterised by a notable 'hard' magnetic component.
- WHii: From ~1906 there is a notable enhancement of the magnetic signal, with steadily increasing magnetic concentrations throughout the 20th century and distinct concentration peaks at ~1929 to 1932 and ~1940 to 1946.
- WHiii: Prominent magnetic peaks are observed from 1949 to 1957. From 1957 magnetic concentrations steadily decline, however a notable peak is evident at 1964. A fine-grained magnetic signature is observed from 1955 to 1989, with a potential increase of SP post-1989.
- WHiv: Magnetic concentrations continue to decline post-1993.

6.4.2. <10 μm particle size distributions: WH3

Respiratory particle size range and median distributions are presented (Figure 6.11), which reveal a higher contribution of particles <10 μm (26.39-60.34%), compared to <2.5 μm (6.69-26.11%) and <1 μm (2.39-11.06%) that exhibit increases values in sediment below 19.5 cm (~pre-1911, phase WHi). Distributions for these particle size ranges are relatively constant in sediment above 16 cm (post-1925), with notable increases at 1975 to 1985 (5.5 to 4 cm) and 1941 to 1957 (13 to 9 cm). Decreases in particles <10 μm occur from 1959-1967 (9 to 7 cm) and post-1993 (3.5 to 0 cm, phase WHiv), mirrored in all three profiles. Only the <10 μm size range exhibits an increase at the sediment surface.

6.4.3. Trace metal concentrations: WH3

The typically anthropogenic-derived trace metals, Pb Zn, Cu, Br and S (Figure 6.12) overall exhibit closely paralleled trends, described according to the divisions identified in WH3 (Table 6.14).

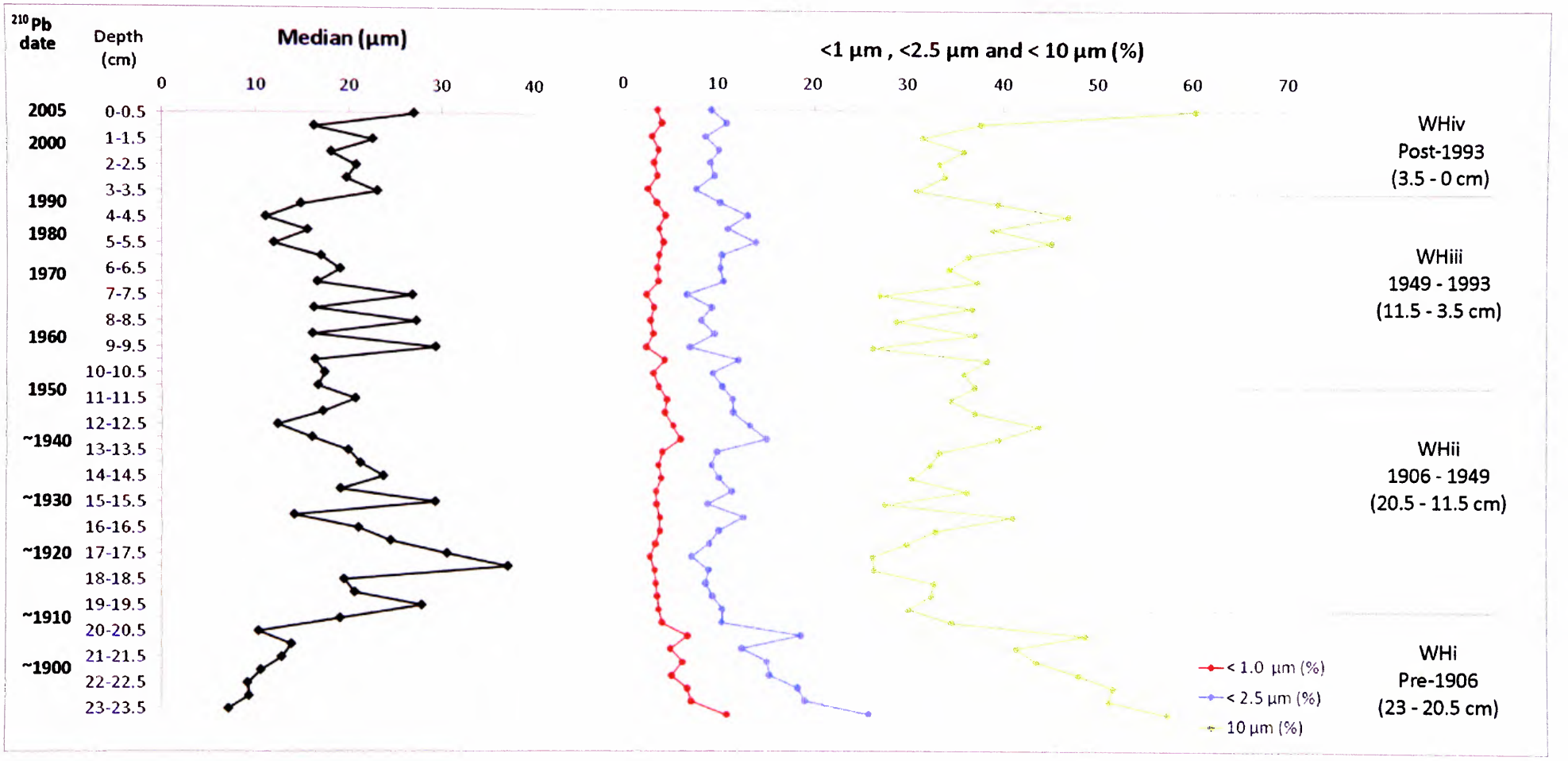

Figure 6.11: Median particulate size and percentage distributions for size fractions <1 µm, <2.5 µm and <10 µm for WH3 with superimposed phases WHi to WHiv.

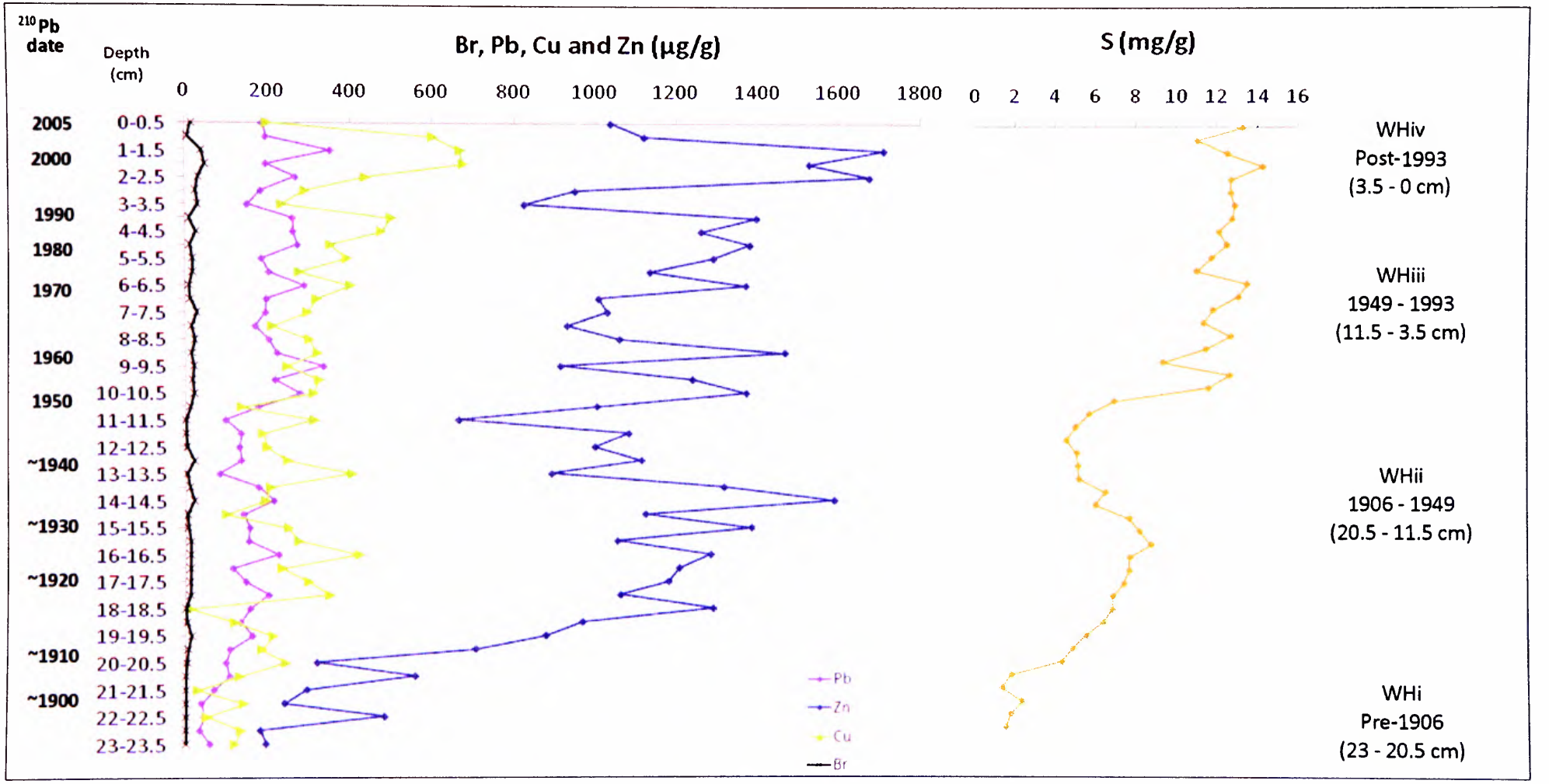

Figure 6.12: Down-core Br, Pb, Cu, Zn and S concentration profiles for WH3 with superimposed phases WHi to WHiv (corresponding to Table 6.14).

Table 6.14: Down-core Br, Pb, Cu, Zn and S concentration trends for WH3, relating to divisions WHi to WHiv (corresponding to Figure 6.12).

Phase	Depth/Age	Trace metal concentration trend
WHiv	Post-1993 (3.5 to 0 cm)	A recent concentration increase from 1997 to 2001 is observed for Pb and Zn, whereby maximum values are reached (351.074 μg/g and 1709.340 μg/g, respectively) and is particularly prominent in the Cu (maximum of 674.597 μg/g) and Br (maximum of 48.999 μg/g) profiles. Also maximum S concentrations (14.285 mg/g) are observed at 1999 (1.5-2 cm).
WHiii	1949 to 1993 (11.5 to 3.5 cm)	Pb, S and Br exhibit a second distinct elevation in the upper 10.5 cm (post-1955) of the core. S values increase to exceed 6.966 mg/g in post-1955 sediment, with a relatively small peak occurring at 8-8.5 cm (1964). This post-1955 shift is not as prominent in the Zn or Cu core; however, concentrations are notably higher. Distinct mid-20th century Pb and Zn peaks occur between 1955 and 1961. Cu and Br demonstrate an overall steady increase in concentration throughout the post-1949 sediment, mirroring the Pb and Zn trends. Distinct increases in Pb, Zn and Cu occur between 1989-1971 (6.5-3.5 cm), mirrored less prominently in the Br and S profiles.
WHii	~1906-1949 (20.5 to 11.5 cm)	A distinct enhancement in anthropogenic trace metals concentrations is observed ~post-1906. This elevation is particularly evident in the Zn profile, whereby, values increase from <600 μg/g in pre-1906 sediment to reach 129.239 μg/g at ~1915 (18-18.5 cm). Pb also exhibits a prominent shift, from lower values (<60.851 μg/g) in ~pre-1906, to exceed 108.557 μg/g in ~post-1906 sediment. A period of high Pb concentration from 19 to 17.5 cm (~1909 to ~1918). This increase is also clearly demonstrated by the S profile, which displays <2.396 mg/g ~pre-1900 values, compared to >4.390 mg/g throughout the rest of the core (~post-1900). ~Post-1906 trace metal enhancement is sustained, with steadily increasing values throughout the first quarter of the 20th century. Prominent peaks in Pb, Cu and S are observed at 16-16.5 cm (~1925), 15-15.5 cm (~1929) and a slightly later peak, particularly distinct in the Zn, Pb and Br profiles, at 14-14.5 cm (~1934). However, this later peak is diminished in the Cu and S profiles. A relatively smaller concentration peak is observed between ~1939 to 1949 (~13 to 11 cm) for Pb, Zn, and S.
WHi	~Pre-1906 (23 to 20.5 cm)	Relatively low ~pre-1906 Pb, Zn, Cu, S and Br concentrations observed in sediment below 20 cm.

Original concentration profiles exhibit a prominent increase in trace metal concentrations post-1955 in the WH3 core. This corresponds with an increase in organic content in post-1955 sediment (10.5 to 0 cm) (Section 5.4, Figure 5.5). Therefore, trace metal data for WH have been normalised for inorganic content[‡‡], which reveal less pronounced post-1955 trace metal increases (Figure 6.13); whereas, similar pre-1955 values are obtained for the lower section of the core (below 10.5 cm). This may suggest a higher organic-derived contribution of trace metals in post-1955 sediments. Zn and Cu concentrations corrected for inorganic content demonstrate an overall decrease post-1955; Pb and Br exhibit values consistent with pre-1955 data; and only S displays an increase post-1955 (Table 6.15). The increasing trends in these trace metals are mirrored in both the original and inorganic corrected trace metal concentration profiles (Figure 6.18).

[‡‡] Total trace metal concentration divided by inorganic content.

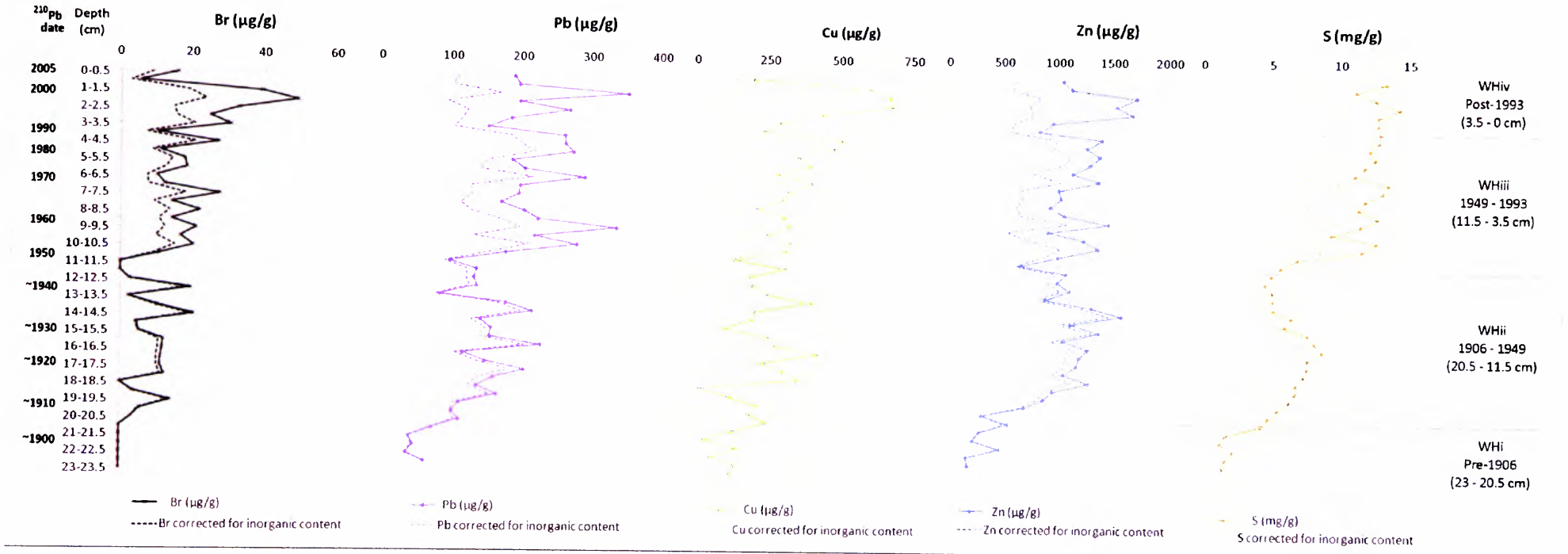

Figure 6.13: Trace metal concentrations (µg/g) (solid line) and trace metal concentrations corrected for inorganic content (dotted line) for WH3, with superimposed phases WHi to WHiv (corresponding to Table 6.15).

Table 6.15: Post-1955 Br, Pb, Cu, Zn and S concentrations trends for WH3 when corrected for inorganic content (corresponding to Figure 6.18).

Trace metal	Post-1955 trend when corrected for inorganic content
Br	Br demonstrates consistent values post-1955 when corrected for inorganic content. Br peaks are observed from 1955 to 1985 (10.5 to 4 cm), 1993 (3-3.5 cm) and 1999 (1.5-2 cm).
Pb	Pb increases post-1955 are less pronounced when corrected for inorganic content. Pb elevations are, however, observed from 1955 to 1959 (10.5 to 9cm), at 1971 (6-6.5 cm) and during the 1980s (5 to 3.5 cm), with maximum Pb peak occurring at 1982. Post-1989 decreases in Pb are exhibited.
Cu	Cu values decrease post-1955 when corrected for inorganic content. Observed increases are exhibited from 1971 to 1989 (6-6.5 to 3.5-4 cm) and decreases occur throughout the 1990s, with further increases from 1999 to 2003 (2 to 0.5 cm). Maximum Cu in the inorganic profile is observed at 1925.
Zn	Zn demonstrates an overall decline throughout the post-1955 sediment. However, increases are exhibited at 1955 (10-10.5 cm), 1961 (8.5-9 cm) and 1971 to 1989 (6.5 to 3.5 cm). Lower post-1989 values are also observed and the maximum Zn concentration when corrected for inorganic content occurs at 1934.
S	S demonstrates an increase in concentration post-1955 (10.5 to 0 cm). S values gradually increase reaching maximum peaks at 1971 (6-6.5cm) and high values are sustained until 1982 (4.5-5 cm), after which, values steadily decline.

6.4.4. Statistical relationships:WH3

Two distinct groups of trace metals, broadly grouped as 'anthropogenic' (Table 6.16) and 'natural' (Table 6.17) are recognised via common characteristics revealed by correlation coefficients. The typically anthropogenic trace metals exhibit strong positive correlations with OM: S ($R=0.892$; $p<0.001$; $n=46$), Cu ($R=0.605$; $p<0.001$; $n=46$), Pb ($R=0.753$; $p<0.001$; $n=46$), Zn ($R=0.497$; $p<0.001$; $n=46$) and Br ($R=0.724$; $p<0.001$; $n=46$) (Table 6.16). Inversely, clay exhibits strong negative correlations with this group: Pb ($R=-0.513$; $p<0.001$; $n=46$), Br ($R=-0.544$; $p<0.001$; $n=46$), S ($R=-0.577$; $p<0.001$; $n=46$) and Zn ($R=-0.432$; $p<0.01$; $n=46$).

Strong positive relationships are also identified between these trace metals, with particularly strong relationships between Pb and Zn, Cu, S and Br. The 'anthropogenic' group also displays negative relationships with the 'naturally-derived' trace metals (e.g. Al, Ti and Si). Statistical correlations are not identified between the anthropogenic group and the magnetic parameters, only Zn weakly correlates with SIRM ($R=0.327$; $p<0.05$; $n=46$) and $SOFT_{-20mT}$ ($R=0.324$; $p<0.05$; $n=46$).

Table 6.16: Selected correlation coefficients of Pb, Zn, Cu, S and Br for WH3. R values accompanied by p value expressed as ** ($p<0.01$) and *** ($p<0.001$); $n=46$.

	Pb	Zn	Cu	S	Br
Pb	1.00				
Zn	0.741***	1.00			
Cu	0.670***	0.537***	1.00		
S	0.781***	0.573***	0.676***	1.00	
Br	0.710***	0.486***		0.742***	1.00
OM	0.753***	0.497***	0.605***	0.892***	0.724***
Clay	-0.513***	-0.432**		-0.577***	-0.544***
χ_{LF}					
SIRM		0.327*			
χ_{ARM}					
$SOFT_{-20mT}$		0.324*			
$HARD_{-300mT}$	-0.340*		-0.353*	-0.610***	-0.462***
Si	-0.635***	-0.362*	-0.595***	-0.770***	-0.586***
Al	-0.397**		-0.413**	-0.533***	-0.401**
Ti	-0.745***	-0.453***	-0.628***	-0.855***	-0.712***
Ca				0.340*	
K	-0.771***	-0.499***	-0.676***	-0.855***	-0.725***
Fe	-0.747***	-0.469***	-0.590***	-0.855***	-0.730***
Mn	-0.585***	-0.435***	-0.552***	-0.621***	-0.727***

Si, Al, Ti, Ca, K, Fe and Mn exhibit similar attributes and, therefore, have been grouped as 'natural' trace elements due to their common association with minerogenic and natural sources, further supported by negative correlations observed with the anthropogenic trace metals (Table 6.17). This group demonstrates strong positive correlations with clay and strong negative correlations with OM (Table 6.17).

Table 6.17: Selected correlation coefficients of Si, Al, Ti, Ca, K, Fe and Mn for WH3. R values accompanied by p value expressed as * ($p<0.05$), ** ($p<0.01$) and *** ($p<0.001$); n=46.

	Si	Al	Ti	Ca	K	Fe	Mn
Si	1.00						
Al	0.745***	1.00					
Ti	0.922***	0.706***	1.00				
Ca	0.539***	0.571***	0.522***	1.00			
K	0.892***	0.739***	0.961***	0.438***	1.00		
Fe	0.779***	0.660***	0.909***	0.501***	0.915***	1.00	
Mn	0.727***	0.714***	0.798***	0.480***	0.826***	0.760***	1.00
OM	-0.817***	-0.663***	-0.901***	-0.447**	-0.921***	-0.957***	-0.735***
Clay	0.479***	0.387**	0.574***		0.582***	0.596***	0.479***
χ_{LF}	0.382**	0.361*	0.388**	0.693***		0.368*	
SIRM				0.707***			
χ_{ARM}				0.670***			
$SOFT_{-20mT}$				0.700***			
$HARD_{-300mT}$	0.5330***	0.458***	0.566***	0.621***	0.522***	0.582***	0.454***

Strong positive relationships are exhibited between the concentration-dependent magnetic parameters χ_{LF}, χ_{ARM}, SIRM and $SOFT_{-20mT}$, with weaker relationships observed between these magnetic parameters and $HARD_{-300mT}$ (Table 6.18).

Table 6.18: Correlation coefficient matrix of the concentration-dependent magnetic parameters for WH3. R values accompanied by p value expressed as * ($p<0.05$), ** ($p<0.01$) and *** ($p<0.001$); n=46.

	χ_{LF}	SIRM	χ_{ARM}	$SOFT_{-20mT}$	$HARD_{-300mT}$
χ_{LF}	1.00				
SIRM	0.935***	1.00			
χ_{ARM}	0.909***	0.960***	1.00		
$SOFT_{-20mT}$	0.943***	0.994***	0.960***	1.00	
$HARD_{-300mT}$	0.670***	0.610***	0.652***	0.609***	1.00

6.5. Local pollution signal recorded in Dogs Kennel Clump Pond

Assessment of the proxy pollution profiles from DKC reveal four main down-core divisions in sediment characteristics (Table 6.19), which have been applied to aid description and interpretation of results.

Table 6.19: Down-core phases identified in DKC.

Phase	Depth/Date	Proxy pollution trend
DKiv	Post-1974 (3.5 to 0 cm)	Overall a reduction in coarse magnetic grains, Pb, Zn, Cu and S, which coincides with increases in Ni, Cr and Br. Characteristic of a fine magnetic signature.
DKiii	1962-1974 (8.5 to 3.5 cm)	Further proxy pollution increases (with notable magnetic, Pb, Zn, Cu and S peaks).
DKii	~1913 to 1962 (28 to 8.5 cm)	Proxy pollution enhancement.
DKi	~pre-1913 (44 to 18 cm)	Relatively low proxy pollution characteristics.

6.5.1. Magnetic characteristics: DKC

Magnetic profiles for concentration-dependent parameters are presented for DKC (Figure 6.14). Down-core variations in magnetic concentration are identified (Table 6.20). The range in χ_{LF} values of 85.266 to 1045.355 10^{-9} m^3 kg^{-1}, compared to published data for various environmental materials including topsoils, igneous rocks, canted antiferromagnetic minerals, metamorphic rocks, paramagnetic minerals and sedimentary rocks [Dearing, 1999(a)].

Magnetic behaviour and grain size assemblages are further explored via down core trends in magnetic ratios (Figure 6.15, Tables 6.21 and 6.22). The changing contributions of dominating grain sizes (coarse/fine) to the magnetic signal are highlighted by the SIRM/χ_{LF}, SIRM/ARM and χ_{ARM}/SIRM profiles (Figure 6.15 and Table 6.22). Shifts in magnetic grain size assemblages correspond to divisions DKi to DKiv (Table 6.21).

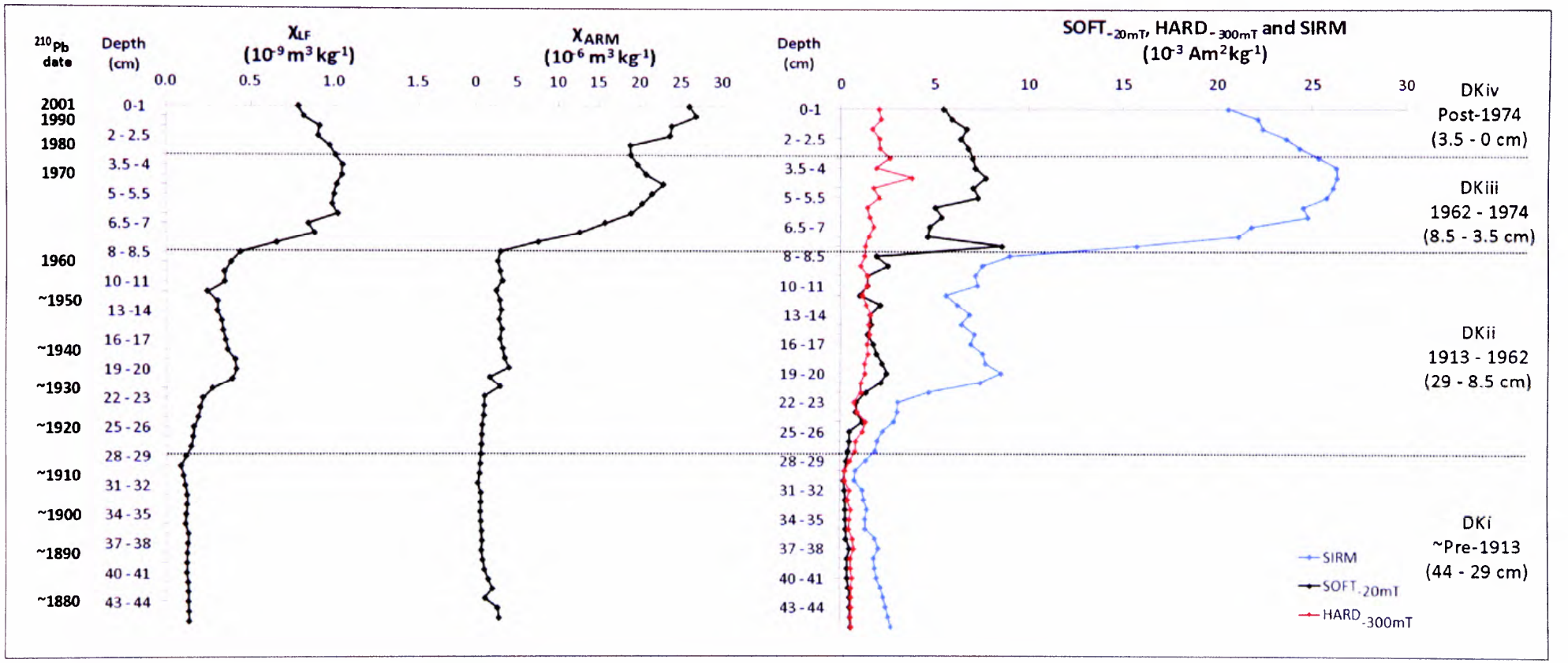

Figure 6.14: Magnetic concentration profiles for DKC: χ_{LF}, χ_{ARM}, $SOFT_{-20mT}$, $HARD_{-300mT}$ and SIRM, with superimposed phases DKi to DKiv (corresponding to Table 6.20).

Table 6.20: Down-core magnetic concentration trends in DKC, relating to phases DKi to DKiv (corresponding to Figure 6.14).

Phase	Depth/Date	Description of magnetic concentration trend
DKiv	Post-1974 (3.5 to 0 cm)	χ_{LF} and SIRM values are reduced post-1974 (3.5-0 cm); however, χ_{ARM} values notably increase post-1979 (2.5 to 0 cm) to reach a maximum value (26.796 10^{-3} Am^2 kg^{-1}) at 1994 (1-1.5 cm). This increase in χ_{ARM} reveals an increased contribution of finer, potentially SSD (0.7-0.07 μm) magnetic grains in the post-1979 section of the core. $HARD_{.300mT}$ and $SOFT_{.20mT}$ values gradually decrease post-1974 (3.5 to 0 cm), however, remain notably higher than pre-1962 values.
DKiii	1962 to 1974 (8.5 to 3.5 cm)	Further, more pronounced, increases in χ_{LF}, SIRM and χ_{ARM} are exhibited post-1962, whereby maximum values are reached for χ_{LF} (1045.36 10^{-9} m^3 kg^{-1}) at 1974 (3-3.5 cm) and SIRM (26.343 10^{-3} Am^2 kg^{-1}) at 1970 (4-4.5 cm). χ_{ARM} demonstrates a distinct peak (22.801 10^{-6} m^3 kg^{-1}) at 1970 (4-4.5 cm). $SOFT_{.20mT}$ values exhibit a pronounced peak at 1962 (7.5-8 cm). The $HARD_{.300mT}$ profile exhibits a more gradual increase post-1962, until values reach a maximum at 4-4.5 cm (1970).
DKii	~1913 to 1962 (28 to 8.5 cm)	A corresponding enhancement in χ_{LF}, SIRM and χ_{ARM} occurs ~post-1913, with a distinct shift to higher magnetic concentrations at 21-22 cm (1930). Values steadily decline from 1930 to 1955 (22 to 9 cm), with values ranging from 214.890 to 407.45 10^{-9} m^3 kg^{-1} for χ_{LF}, 2.629 to 3.922 10^{-6} m^3 kg^{-1} for χ_{ARM} and 4.714 to 8.565 10^{-3} Am^2 kg^{-1} for SIRM. Steady increases in $SOFT_{.20mT}$ and $HARD_{.300mT}$ are exhibited post-1913, reflecting increased concentrations of 'hard' and 'soft' magnetic grains, with notable peaks in the $HARD_{.300mT}$ profile at ~1923 (24-25 cm) ~1948 (13-14 cm) and 1958 (9-10 cm); and peaks in the $SOFT_{.20mT}$ profile at ~1923 (24-25 cm), ~1934 (19-20 cm), ~1951 (12-13 cm) and 1960 (8.5-9 cm).
DKi	~Pre-1913 (46 to 28 cm)	Relatively low magnetic concentrations are exhibited from the base of the core to 28-29 cm (~pre-1913) for χ_{LF} (<134.27 10^{-9} m^3 kg^{-1}), SIRM (< 2.711 10^{-3} Am^2 kg^{-1}) and χ_{ARM} (<2589 10^{-6} m^3 kg^{-1}). Relatively low $HARD_{.300mT}$ and $SOFT_{.20mT}$ pre-1913 values.

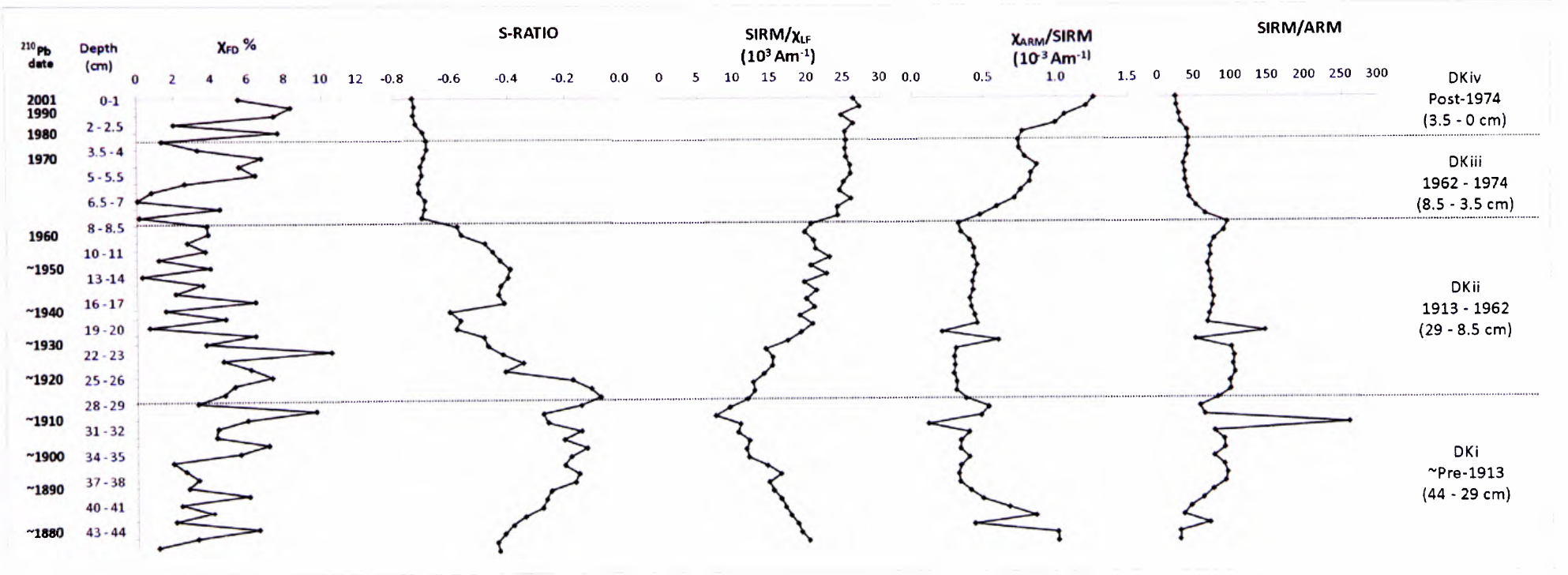

Figure 6.15: Magnetic ratio profiles for DKC: χ_{FD}%, S-RATIO, SIRM/χ_{LF}, χ_{ARM}/SIRM and SIRM/ARM with superimposed phases DKi to DKiv (corresponding to Tables 6.21 and 6.22).

Table 6.21: Down-core divisions in magnetic grain size assemblages for DKC, (corresponding to Figure 6.15).

Phase	Depth/Date	Description of magnetic grain size
DKiv	Post-1974 (3.5 to 0 cm)	Notable increase in χ_{ARM}/SIRM from 2.5 cm to the sediment-surface (post-1983), and further SP increases.
DKiii	1962 to 1974 (8.5 to 3.5 cm)	SIRM/χ_{LF} and χ_{ARM}/SIRM values increase further. The SIRM/ARM profile mirrors this post-1962 increase in fine magnetic grains, with ratios exhibiting a gradual decline. χ_{FD}% and, therefore, SP grains increase in this phase.
DKii	1913 to 1962 (28 to 8.5 cm)	SIRM/χ_{LF} ratios reveal a gradual shift to a relatively fine magnetic signal, particularly notable at 19-20 cm (~1934), which is evident, but less pronounced, in the χ_{ARM}/SIRM profile. SIRM/ARM further supports this with a decrease in values at ~ 1934.
DKi	~Pre-1913 46 to 28 cm)	SIRM/χ_{LF} and χ_{ARM}/SIRM ratios are relatively low, demonstrating an overall decrease from the base of the core (~1874) until 28-29 cm (~1913). Inversely, SIRM/ARM ratios increase throughout this lower section of the core, highlighting a gradual coarsening of the magnetic signal.

Table 6.22: Description and interpretation of magnetic ratios for DKC, (corresponding to Figure 6.15).

Magnetic parameter	Description of magnetic ratios
χ_{FD}%	Down-core trends of $\chi_{FD\%}$ reveal the changing contribution of SP magnetic grains (<0.05 μm), typically attributed to a soil-derived magnetic component, throughout the core. χ_{FD}% values 5-10% indicate a significant SP contribution from ~1899 to 1932 (34-35 cm to 21-20 cm), and also in post-1967 sediment (5.5 to 0 cm). SP grains do not significantly contribute to the remainder of the core, which χ_{FD} values highlight, is dominated by SSD ferrimagnetic minerals with a potential small contribution of SP grains (χ_{FD} 2-5%). Few (<5) samples appear to be dominated by MD magnetic grains (χ_{FD} <2%).
S-RATIO	~Pre-1913 (phase DKi) S-RATIO values (-0.3 to 0) characterise this phase as magnetically 'hard', highlighting a potential canted antiferromagnetic and/or fine grained ferrimagnetic contribution. From 1913 to 1962 (29 to 8.5 cm) S-RATIO values demonstrate a 'soft' magnetic signal, with the majority of samples exhibiting S-RATIOs -0.4 to -0.6, indicative of fine ferrimagnetic grains. A more pronounced enhancement of 'hard' and 'soft' minerals occurs post-1962 (8.5 to 0 cm). Also S-RATIO values (-0.6 to -0.8), highlight a dominating coarse ferrimagnetic component in the upper 8.5 cm of the core (phases DKii and DKiv).
SIRM/χ_{LF}	SIRM/χ_{LF} values range from 7.464 to 27.174 10^{3} Am^{-1}, which Maher and Thompson [1999] attribute to magnetite.
χ_{ARM}/SIRM	χ_{ARM}/SIRM values 0.5-1 10^{-3} Am^{-1} in the DKC core highlight secondary, soil-derived ferrimagnetic grains, however, χ_{FD} values <8% do not support this [Oldfield, 1999]. The range of χ_{ARM}/SIRM values (0.120 to 1.262 10^{-3} Am^{-1}) also discounts a dominating contribution of bacterial magnetite to the magnetic signal, which Oldfield [1999] attributes to values >2 10^{-3} Am^{-1}.

To assess if the pronounced χ_{ARM} increases in the upper section of the DKC (Figure 6.14.) reflect a true SSD contribution to the post-1962 magnetic signal, data have been applied to a χ_{ARM}/SIRM versus χ_{FD}% bi-plot according to Oldfield [1994] (Figure 6.16). Samples with corresponding >80 10^{-5} Am^{-1} χ_{ARM}/SIRM ratios and >2 χ_{FD}% values are indicative of SSD (0.7-0.07 μm) dominated material [Oldfield, 1994]. Samples that meet these criteria occur within the top 6 cm of the core (post-1963), as well as two samples at the base of the core.

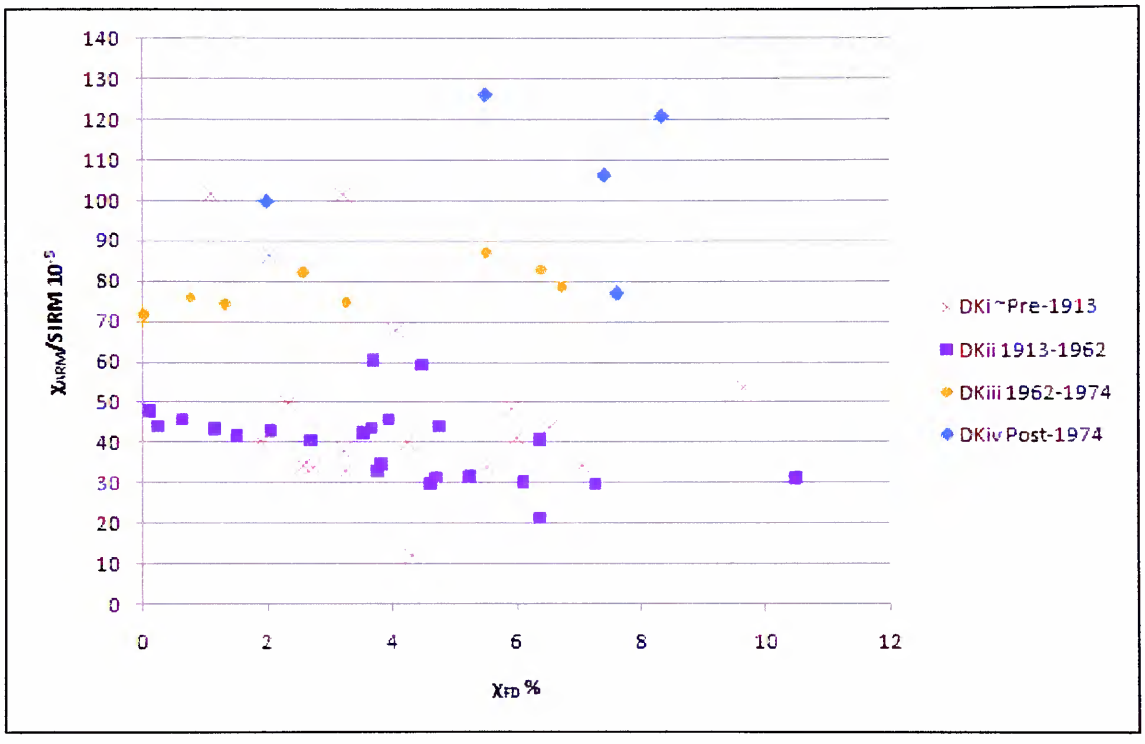

Figure 6.16: χ_{ARM}/SIRM (10^{-5} Am^{-1}) versus χ_{FD}% plots for DKC to identify SSD dominated samples, after Oldfield, [1994]. Samples are plotted within phases DKi to DKiv.

The post-1963 SSD dominated samples have been applied to Oldfield's [2007] bi-logarithmic plot of χ_{ARM}/χ_{FD} versus χ_{ARM}/χ_{LF}, to determine the source of these fine magnetic grains (Figure 6.17). Similar to the DDP samples (Figure 6.4), the DKC samples plot between the soil and bacterial-derived envelopes. This suggests that these SSD grains are not typical of a bacterial or detritus magnetic signature.

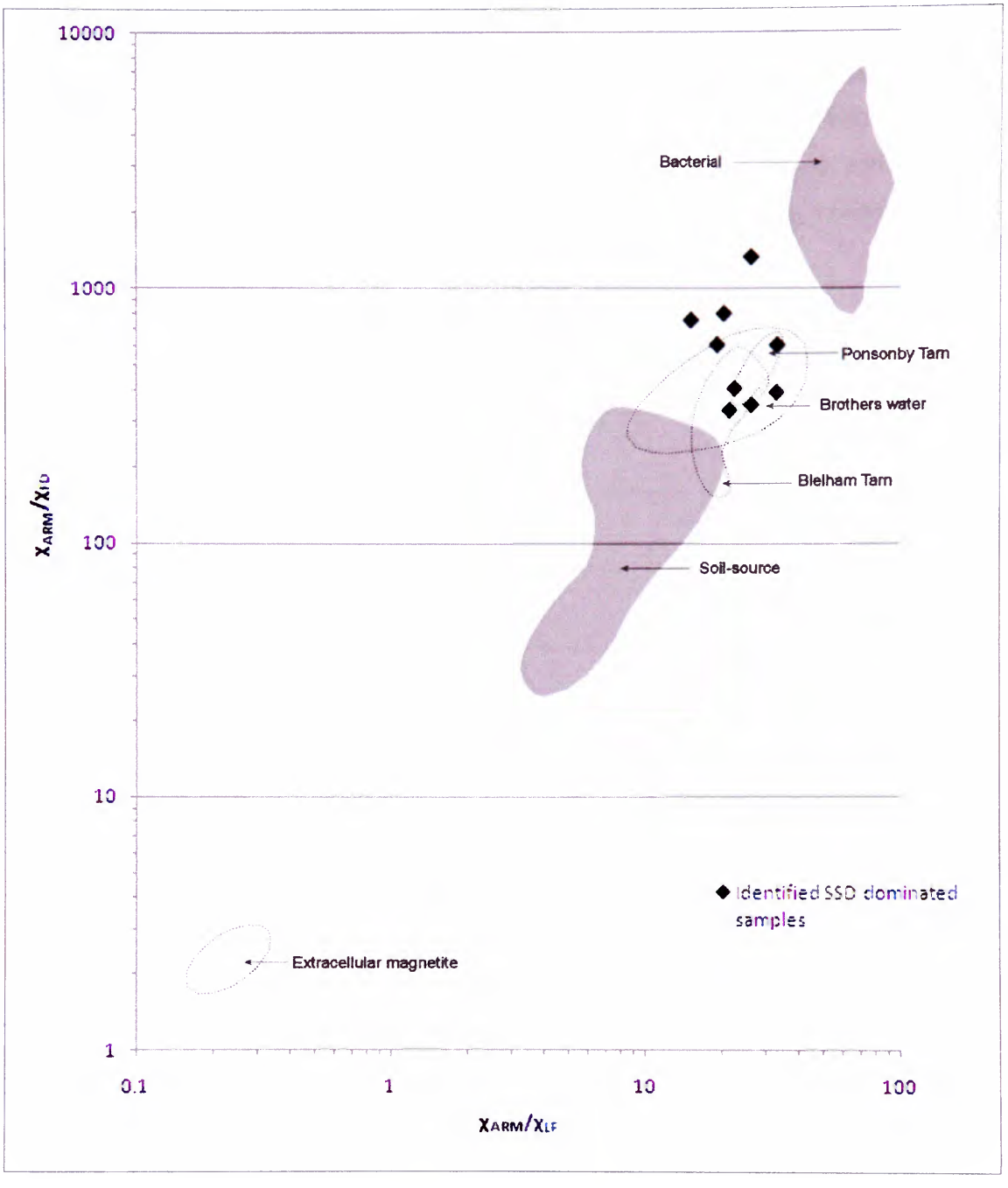

Figure 6.17: Bi-logarithmic scatter plot of χ_{ARM}/χ_{FD} versus χ_{ARM}/χ_{LF} to determine sources of fine grained magnetite for DKC. The identified SSD dominated samples 8.5 to 0 cm (within phase DKiii and DKiv) are plotted according to Oldfield [2007], superimposed over published envelopes for bacterial and soil/catchment derived fine grained magnetite [Oldfield, 1994, 2007]. Also the values for small lakes in NW England: Blelham Tarn, Brothers Water and Ponsonby Tarn [Oldfield, 1994, 1999, 2007] are included.

Figure 6.18 presents SIRM-IRM$_{20mT}$ /SIRM versus SIRM/ARM data for DKC [after Oldfield, 1990]. Data are plotted in down-core division (DKi to DKiv) to assess variations in magnetic grain size within the sediment column. The plot identifies a distinct shift in magnetic characteristics in the post-1962 sediment (phases DKiii and DKiv), with samples, particularly post-1965, plotting to the left of the graph, further supporting a relatively finer magnetic signature.

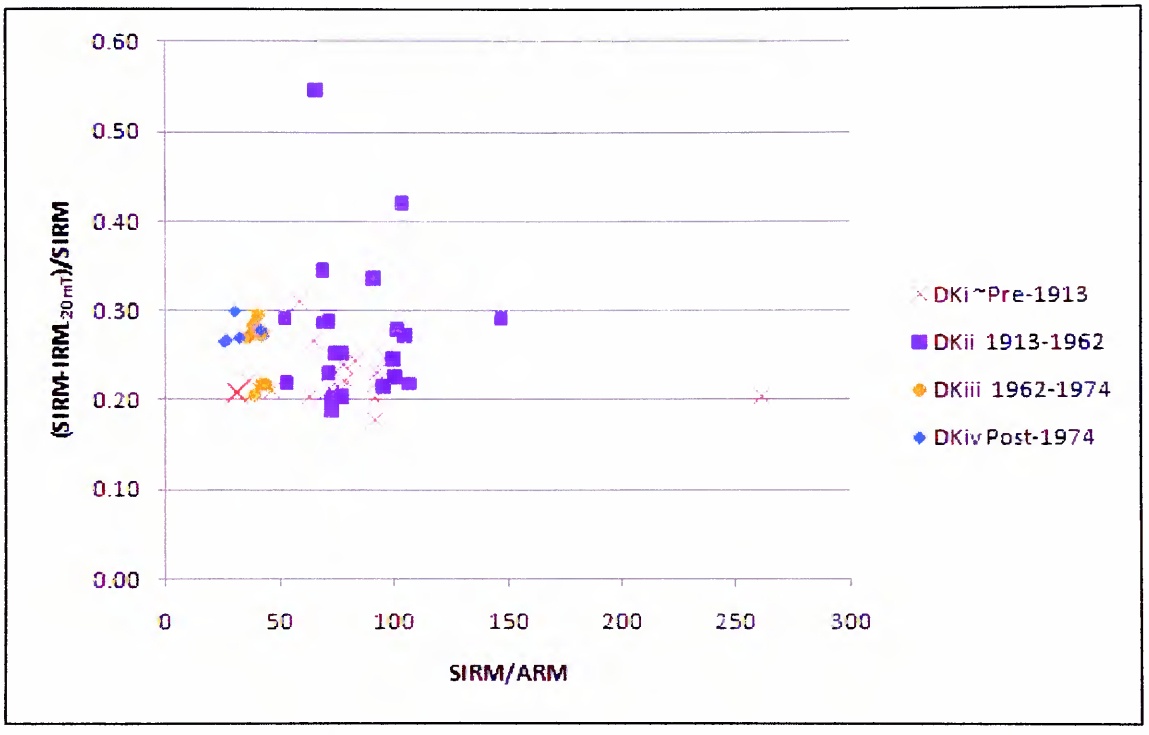

Figure 6.18: Plot of SIRM-IRM$_{20mT}$/SIRM versus SIRM/ARM for DKC after Oldfield [1990] showing down-core phases (DKi to DKiv) to assess variations in magnetic grain size within the sediment column.

6.5.2. <10 µm particle size distributions: DKC

Down-core trends in the particle size distributions of the respiratory size boundaries <10 µm, <2.5 µm and <1 µm and median particle sizes are shown (Figure 6.19). Particles <10 µm exhibit relatively low, however, steadily increasing trends from the base of the core to 28 cm (~pre-1913, phase DKi). This corresponds with relatively high ~pre-1913 median values. A shift to finer particles occurs post-1913 (phase DKii) indicated by reduced median values and distinct <10 µm, <2.5 µm and <1 µm particle size distribution increases. Post-1962 (phases DKiii and DKiv), a coarsening of the sediment occurs revealed by increasing median data and corresponding decreases in <10 µm particulates.

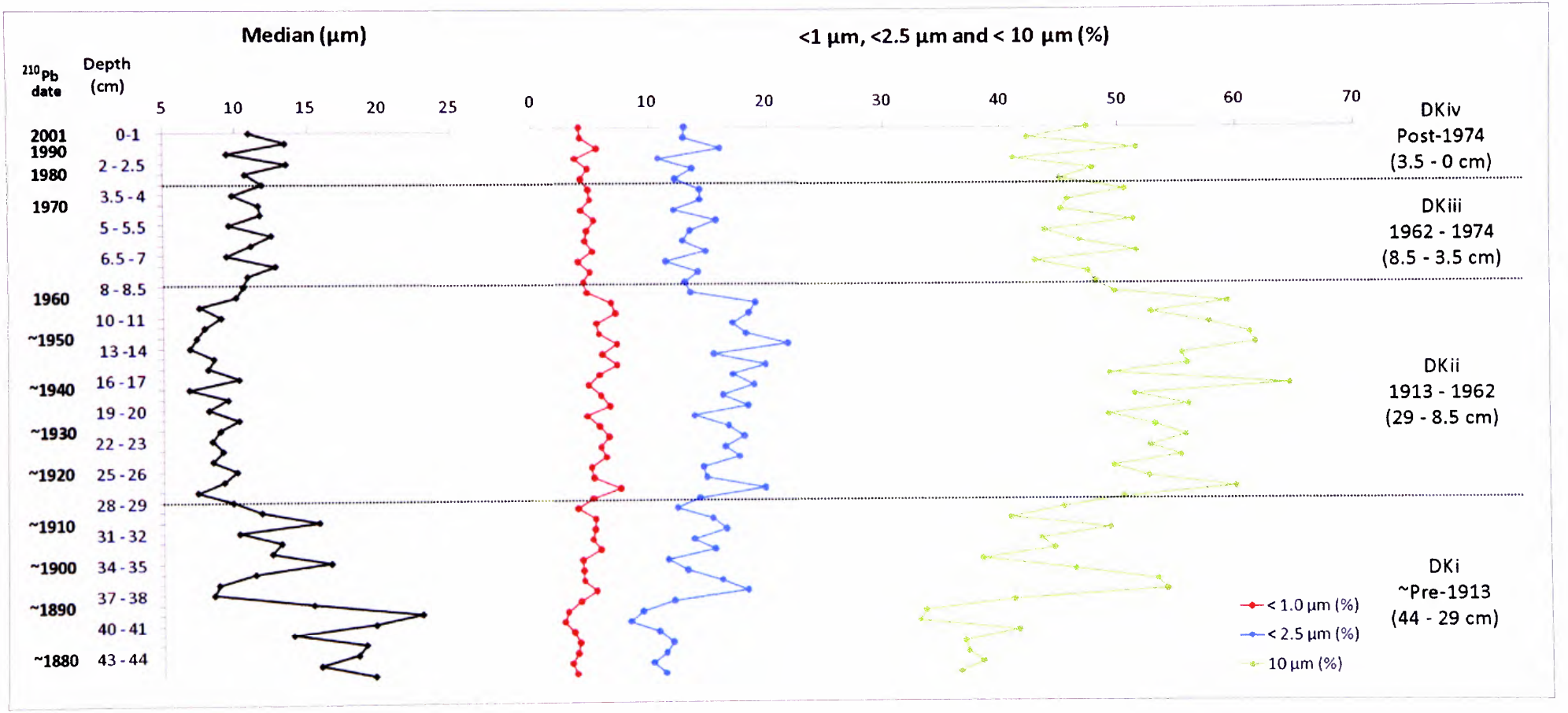

Figure 6.19: Median particle size profile and percentage distributions for respiratory size fractions <1 µm, <2.5 µm and <10 µm for DKC with superimposed phases DKi to DKiv.

6.5.3. Trace metal concentrations: DKC

Pb, Zn Cu, S, Br, Cr and Ni (Figure 6.20, Table 6.23) are presented. Unlike DDP and WH, Cr and Ni concentrations are notably high and, therefore, displayed. Cu values are also presented, despite several zero values throughout the core, to demonstrate the periods of noteworthy Cu concentrations. Trends are also summarised according to down-core phases in the DKC core (Tables 6.23). Also, detailed descriptions of individual trace metal trends are provided (Table 6.24).

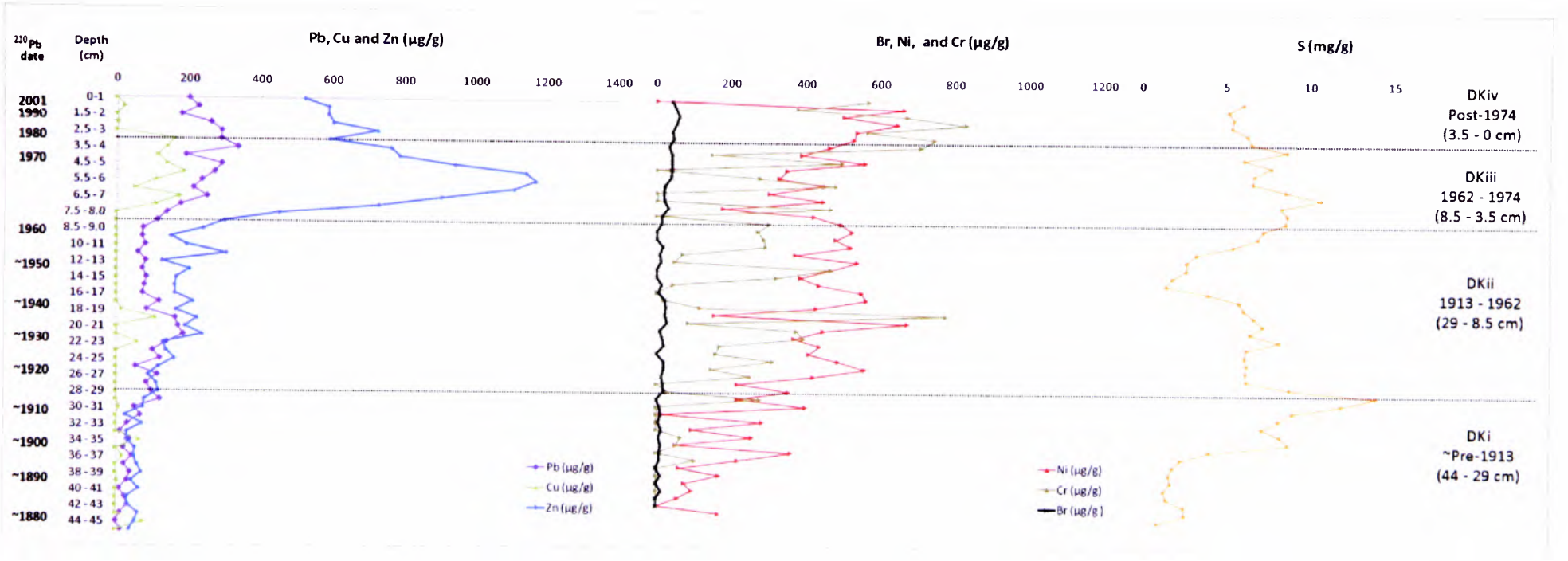

Figure 6.20: Down-core Pb, Cu, Zn, Br, Ni, Cr and S concentration profiles for DKC with superimposed phases DKi to DKiv (corresponding to Tables 6.23 and 6.24).

Table 6.23: Down-core Pb, Cu, Zn, Br, Ni, Cr and S concentration trends in DKC relating to divisions (DKi to DKiv) in DKC (corresponding to Figure 6.20).

Phase	Time/ Depth	Trace metal concentration trends
DKiv	Post-1974 (3.5 to 0 cm)	Zn, Pb, S and Cu exhibit an overall decline. Further Ni, Cr and Br increases, with maximum concentrations reached in this phase.
DKiii	1962 to 1974 (8.5 to 3.5 cm)	Prominent Cu, S, Zn and Pb enhancement with Ni, Cr and Br increases. Maximum Zn, Cu and Pb peaks are exhibited.
DKii	1913 to 1962 (28 to 8.5 cm)	Elevated Zn, Pb, Cr, and Ni concentrations. A sharp decrease in S occurs, however, relatively high S values are sustained throughout the 1930s, corresponding with a distinct Pb peak and Cu increases at this time, followed by a further decline in S at 1944. Zn steadily increases.
DKi	~Pre-1913 (46 to 28 cm)	Relatively low ~pre-1913 Pb, Zn, Cu, Ni, Cr and Br with increases starting from the early 1900s for these metals S, however, exhibits relatively high values during this phase with a notable earlier increase from ~1897 (35-36 cm). Maximum S peak is observed at ~1911 (29-30 cm).

Table 6.24: Trace metal concentration trends for DKC (corresponding to Figure 6.20).

Trace metal	Concentration trends
Pb	Pb exhibits relatively low concentration values ~pre-1900 (<44.291) with a marked elevation from 1904, whereby values steadily increase throughout the 20th century, exhibiting a period of elevated concentration from ~1911-1918 (30 to 26 cm) and reaching a notable peak of 184.114 µg/g at ~1930 (21-22 cm). Subsequently, Pb values decrease and are relatively constant until a small peak at 1955 (10-11 cm). A pronounced enhancement of Pb to the sediment record is evident in post-1955 sediment (above 10 cm). Pb concentrations are particularly enhanced from 1963 to 1979 (7 to 2.5 cm) with maximum Pb levels (333.256 µg/g) experienced in 1972 (3.5-4 cm). Post-1980 Pb levels steadily decline, 10 years later than the observed decrease in Zn at 1970, with a small recent Pb peak observed in 1994 (1-1.5 cm).
Zn	Closely paralleled trends are observed between Zn and Pb. Zn demonstrates relatively low (<71.169 µg/g) concentrations in pre-~1900 sediment (below 30 cm). Values increase ~post-1900, and continue to rise throughout the 20th century with a notable elevation from 1930 (21-22 cm), whereby, values exceed 200 µg/g and exhibit a notable peak (302.318 µg/g) at 1955 (11-12 cm), which is sustained until ~1960 (9 cm). Zn concentrations then demonstrate an abrupt substantial increase in post-1960 sediment, with maximum Zn values (1164.329 µg/g) experienced at 1965 (5.5-6 cm). Pronounced concentrations (>1000 µg/g) are experienced from 1963-1967, after which, values steadily decline from 783.178 µg/g at 1970 (4-4.5 cm), reaching 519.294 µg/g at the sediment surface. These post-1970 values remain comparatively higher than the pre-1960 concentrations, with a smaller peak observed at 1979 (2.5-3 cm).
Cu	The Cu profile is sporadic with several zero concentration values interrupted by notably increased Cu concentrations at ~1870 (44-45 cm), 1899 (33-34 cm), 1934 (19-20 cm) and 1927 (22-23 cm). Cu enhancement occurs post-1960 and is sustained until 1974, whereby, values range from 4.9626 to 185.307 µg/g. The maximum Cu concentration in the core is observed at 1967 (5-5.5 cm).
S	Compared to Zn and Pb, the S profile displays a slightly earlier increase from relatively low concentrations (<2.637 mg/g) in the oldest section of the core, with values sharply increasing at 1897 (35-36 cm) to 38.799 mg/g. This enhancement continues throughout the first half of the 20th century, with maximum S concentration (13.993 mg/g) experienced in ~1911 (29-30 cm), until a sharp decline occurs from 1939 (17-18 cm), whereby, values drop to 1.468 mg/g. S concentrations steadily increase from 1944 (15-16 cm) with enhanced values from 1958 (9-10 cm), similar to those observed from ~1897 to 1939. Mid-20th century S peaks are experienced at 1963 (6.5-7 cm), and 1972 (3.5-4 cm). The pronounced post-1960 increases exhibited by Pb and Zn are not mirrored in the S profile, which exhibits an overall reduction post-1960.
Ni	Ni demonstrates relatively low concentrations (<362.553 µg/g) in sediments below 33-34 cm (~pre-1902). Ni values steadily increase ~post-1900 with a period of notable enhancement from ~1916 to 1930, with maximum Ni concentrations (675.326 µg/g) reached at ~1930 (21-22 cm). An abrupt decline occurs at ~1932 (~20 cm), despite which, values remain relatively constant throughout the 20th century, until 1958 (9-10 cm). A second notable decrease occurs at 1962 (7.5-8 cm), with post-1960 sediment exhibiting a steadily increasing Ni trend, with notable peaks at 1969 (4-4.5 cm), 1983 (2-2.5 cm) and 1994 (1-1.5 cm). Ni concentration decreases sharply at the sediment-surface.
Cr	Cr concentrations display increases from relatively low ~pre-1906 (32 to 46 cm) values (<104.321 µg/g). Values steadily increases from~1913 (28-29 cm) to a peak (777.268 µg/g) at ~1932 (20-21 cm). Subsequently values sharply decline at 1939 (17-18 cm). A peak is observed at 1946 (14-15 cm), with consistent values from 1952 to 1962. A noisier Cr signal is exhibited from ~1960 to 1970; however, post-1979 Cr values exhibit a distinct increase, reaching maximum concentrations (828.010 µg/g) at 2-2.5 cm (1983).
Br	Low ~pre-1909 Br values (<12.301 µg/g) are observed in sediment below ~30 cm. Br steadily increases above this depth with a period of notable concentration increase from ~1930-1937. (22 to 18 cm). Br concentrations decline ~post-1937, with low values exhibited until ~1960 (8.5-9 cm), whereby, values abruptly increase and continue to rise throughout post-1960 sediment. Notable peaks are observed at 1962 (7.5-8 cm), 1965-1970 (6-4 cm), with maximum Br values (58.656 µg/g) occurring at 1988 (1.5-2 cm). The Br profile also exhibits a decrease at the sediment surface.

6.5.4. Statistical relationships: DKC

Correlation coefficients for DKC identify three main groups of trace metals, according to common attributes:

(i) Zn, Pb, Br, Cu, Ni and Cr (Table 6.25);
(ii) Al, Si, K, and Ti (Table 6.26); and
(iii) Fe, Mn and Ca (Table 6.27).

Anthropogenic trace metals Pb, Zn, Cu, S, Br, Cr and Ni (group i) demonstrate strong positive correlations with magnetic concentration parameters, OM and the silt fraction (Table 6.25). Pb and Zn demonstrate particularly strong correlations with these variables. Good agreement is exhibited between the anthropogenic metals indicated by strong positive inter-trace metal correlations. Pb, Zn, Cu and Br exhibit very strong positive correlations with the concentration-depended magnetic parameters χ_{LF}, χ_{ARM}, SIRM, SOFT.$_{20mT}$ and HARD.$_{300mT}$, Particularly notable are relationships between Zn and: χ_{LF} ($R=0.922$; $p<0.001$; $n=54$), SIRM ($R=0.909$; $p<0.001$; $n=54$), χ_{ARM} ($R=0.847$; $p<0.001$; $n=54$), SOFT.$_{20mT}$ ($R=0.908$; $p<0.001$; $n=54$), HARD.$_{300mT}$ ($R=0.858$; $p<0.001$; $n=54$); and Pb and: χ_{LF} ($R=0.815$; $p<0.001$; $n=54$), SIRM ($R=0.784$; $p<0.001$; $n=54$), χ_{ARM} ($R=0.709$; $p<0.001$; $n=54$), SOFT.$_{20mT}$ ($R=0.785$; $p<0.001$; $n=54$), HARD.$_{300mT}$ ($R=0.757$; $p<0.001$; $n=54$). The sand size fraction also exhibits strong negative correlations with Pb ($R=-0.475$; $p<0.001$; $n=54$) and Zn ($R=-0.456$; $p<0.001$; $n=54$) (Table 6.25).

Table 6.25: Selected correlation coefficients of Pb, Zn, Cu, S, Br, Cr and Ni for DKC. R values accompanied by p value expressed as * ($p<0.05$), ** ($p<0.01$) and *** ($p<0.001$); $n=54$.

	Pb	Zn	Cu	S	Br	Cr	Ni
OM%	0.823***	0.677***	0.350**	0.561***	0.764***	0.523***	0.376**
Silt	0.587***	0.549***		0.399**	0.390**	0.457***	0.501***
Pb	1.00						
Zn	0.871***	1.00					
Cu	0.342*	0.337*	1.00				
S	0.383**			1.00			
Br	0.781***	0.705***		0.310*	1.00		
Cr	0.657***	0.560***			0.507***	1.00	
Ni	0.534***	0.530***			0.380**	0.571***	1.00
χ_{LF}	0.815***	0.922***	0.359**		0.637***	0.533***	0.545***
SIRM	0.784***	0.909***	0.380**		0.613***	0.514***	0.508***
χ_{ARM}	0.709***	0.847***	0.348**		0.570***	0.432***	0.461***
SOFT.$_{20mT}$	0.785***	0.908***	0.384**		0.608***	0.518***	0.501***
HARD.$_{300mT}$	0.757***	0.858***			0.544***	0.561***	0.616***

Al, Si, K (group ii), Fe, Mn and Ca (group iii) have been grouped as 'naturally-derived' trace metals due to the widely regarded natural origins of these elements. Common characteristics between Al, Si and K (Table 6.26), include strong negative correlations with OM, the silt fraction, magnetic concentration parameters and the 'anthropogenic' trace metal group. This, potentially, highlights a common origin for these typical minerogenic trace metals (Table 6.26). Inversely, particularly strong negative correlations are exhibited between the magnetic concentration parameters and Si, and weaker negative relationships observed with Al and K (Table 6.26). Ti does not exhibit significant relationships with the anthropogenic trace metal group or OM; however, Ti demonstrates strong positive correlations with silt (R=0.459; p<0.001; n=54) and K (R=0.814; p<0.001; n=54) (Table 6.26).

Table 6.26: Selected correlation coefficients of Al, Si, and K for DKC. R values accompanied by p value expressed as * (p<0.05), ** (p<0.01) and *** (p<0.001); n=54.

	Al	Si	K	Ti
Al	1.00			
Si	0.614***	1.00		
K	0.498***	0.434***	1.00	
Ti	0.292*		0.814***	1.00
OM	-0.829***	-0.570***	-0.614***	0.459***
Silt	N/A	-0.394**	N/A	0.459***
χ_{LF}	-0.414**	-0.606***	-0.332*	
SIRM	-0.420**	-0.593***	-0.375**	
χ_{ARM}	-0.416**	-0.573***	-0.436***	
$SOFT_{-20mT}$	-0.418**	-0.581***	-0.384***	
$HARD_{-300mT}$	-0.427***	-0.629***		
Pb	-0.503***	-0.762***	-0.432**	
Zn	-0.424***	--0.629***	-0.326*	
Cu			-0.467***	
S		-0.366**		
Br	-0.451***	-0.616***	-0.535***	
Ni	-0.340*	-0.469***		0.380**
Cr		-0.557***		

Fe, Mn and Ca (group iii) exhibit different characteristics from group ii. Common attributes include strong positive correlations between these trace metals and the concentration-dependent magnetic parameters, the anthropogenic trace metals (group i), OM and the silt fraction. Negative correlations are also observed between Fe, Mn, Ca and Sr and group ii (Table 6.27). Strong positive correlations are observed between OM and Ca (R=0.840; p,0.001; n=54), Fe (R=0.512; p<0.001; n=54) and Mn (R=0.525; p<0.001; n=54). Also, negative correlations are exhibited between the sand fraction and Fe (R=-0.540; p<0.001; n=54), and Mn (R=-0.527; p<0.001; n=54), whereas silt exhibits strong positive correlations with these trace metals (Table 6.27).

Table 6.27: Selected correlation coefficients of Fe, Mn and Ca for DKC. R values accompanied by p value expressed as * ($p<0.05$), ** ($p<0.01$) and *** ($p<0.001$); n=54.

	Fe	Mn	Ca
Fe	1.00		
Mn	0.719***	1.00	
Ca	0.334*	0.532***	1.00
OM	0.512***	0.525***	0.840***
Silt	0.547***	0.479***	0.321**
χ_{LF}	0.660***	0.671***	0.484***
SIRM	0.628***	0.647***	0.476***
χ_{ARM}	0.597***	0.632***	0.425***
$SOFT_{-20mT}$	0.627***	0.634***	0.468***
$HARD_{-300mT}$	0.709***	0.755***	0.388**
Si (group ii)	-0.704***	-0.694***	-0.701***
Al	-0.486***	-0.431***	-0.567***
K			-0.670***
Pb (group i)	0.714***	0.631***	0.701***
Zn	0.757***	0.720***	0.549***
Cu			0.379**
S	0.314*		0.532***
Br	0.502***	0.442***	0.742***
Ni	0.5554***	0.706***	
Cr	0.640***	0.360**	0.397**

Strong positive correlations are observed between the magnetic concentration parameters (Table 6.28). OM exhibits strong positive significant correlations with the magnetic parameters χ_{LF}, (R=0.580; $p<0.001$; n=54), χ_{ARM} (R=0.525; $p<0.001$; n=54), SIRM (R=0.571; $p<0.001$; n=54), $SOFT_{-20mT}$ (R=0.565; $p<0.001$; n=54) and $HARD_{-300mT}$ (R=0.511; $p<0.001$; n=54). The silt sized fraction also appears to govern the magnetic signal with strong positive correlations observed between silt and χ_{LF} (R=0.502; $p<0.001$; n=54), SIRM (R=0.461 $p<0.001$; n=54), $SOFT_{-20mT}$ (R=0.462 $p<0.001$; n=54), $HARD_{-300mT}$ (R=0.410 $p<0.001$; n=54) and χ_{ARM} (r=0.315 p:<0.01; n=54). Also, negative correlations are demonstrated between sand and: χ_{LF} , $SOFT_{-20mT}$ and $HARD_{-300mT}$ (Table 6.28).

Table 6.28: Selected correlation coefficients of the concentration-dependent magnetic parameters for DKC. R values accompanied by p value expressed as * ($p<0.05$), ** ($p<0.01$) and *** ($p<0.001$); n=54.

	χ_{LF}	SIRM	χ_{ARM}	$SOFT_{-20mT}$	$HARD_{-300mT}$
χ_{LF}	1.00				
SIRM	0.989***	1.00			
χ_{ARM}	0.929***	0.954***	1.00		
$SOFT_{-20mT}$	0.988***	0.997***	0.950***	1.00	
$HARD_{-300mT}$	0.916***	0.913***	0.900***	0.906***	1.00
OM%	0.580***	0.571***	0.525***	0.565***	0.511***
Clay %					
Silt %	0.502***	0.461***	0.315*	0.462***	0.410**
Sand %	-0.415**	-0.370**		-0.362**	-0.401**

6.6. Local pollution signal recorded in Oglet Pond

Four main down-core divisions are identified in the OG stratigraphy (Table 6.29), which are superimposed on the proxy pollution concentration profiles to aid description of trends and interpretation.

Table 6.29: Down-core phases identified in OG.

Phase	Time/ Depth	Proxy pollution trend
OGiv	Post-1991 (6 to 0 cm)	Further magnetic increases, characteristic of a relatively fine magnetic signature and overall reduction in trace metals.
OGiii	1973 to 1991 (11 to 6 cm)	Proxy pollution concentrations decline, but remain higher than phase OGi.
OGii	1949 to 1973 (15 to 11 cm)	Increases and prominent peaks in magnetic and trace metal concentrations.
OGi	Pre-1949 (19.5 to 15 cm)	Relatively low proxy pollution trends.

6.6.1. Magnetic characteristics: OG

Down-core χ_{LF}, SIRM, χ_{ARM}, $SOFT_{-20mT}$ and $HARD_{-300mT}$ profiles are presented (Figure 6.21) and described (Table 6.30) for OG. χ_{LF} values range from 98.266 to 1363.225 10^{-9} m^3 kg^{-1}. These data correspond to published values for a range of environmental materials including metamorphic rocks, igneous rocks, paramagnetic minerals, canted antiferromagnetic minerals, topsoils and burned soils [Dearing, 1999(a)]. Close parallels are identified between the concentration profiles, most notably, between χ_{LF}, SIRM and $SOFT_{-20mT}$; and $HARD_{-300mT}$ trends mirror the χ_{ARM} profile.

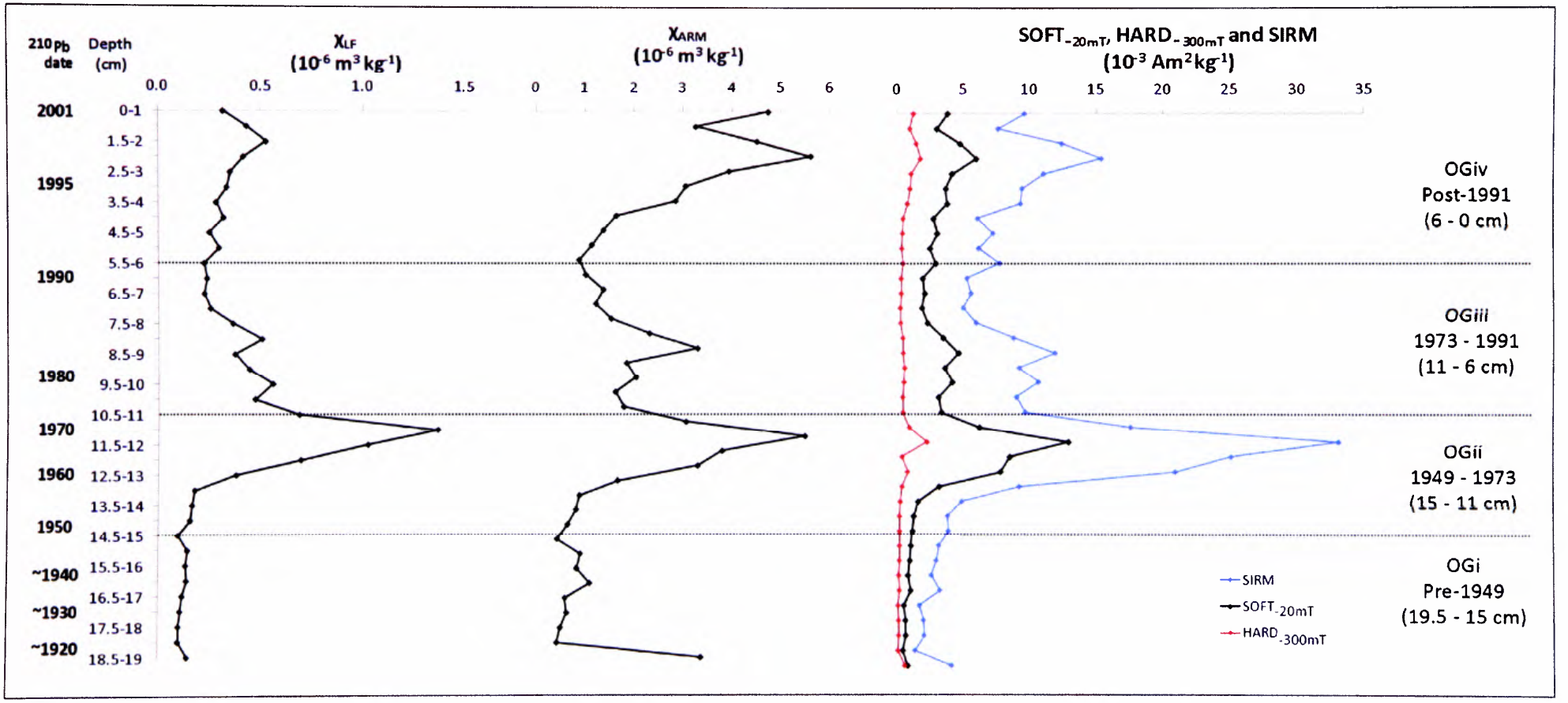

Figure 6.21: Magnetic concentration profiles for OG: χ_{LF}, , χ_{ARM}, $SOFT_{-20mT}$, $HARD_{-300mT}$ and SIRM with superimposed phases OGi to OGiv (corresponding to Table 6.30).

Table 6.30: Down-core magnetic concentration trends in OG relating to phases OGi to OGiv (corresponding to Figure 6.21).

Phase	Depth/Date	Trace metal concentration trends
OGiv	Post-1991 (6 to 0 cm)	A recent increase in magnetic grains occurs post-1991, with gradually increasing trends observed in the SIRM, χ_{LF} and SOFT.$_{20mT}$ profiles, which exhibit distinct peaks at ~1996-1997 (~2 cm). χ_{ARM} and HARD.$_{300mT}$ exhibit proportionally higher post-1991 increases compared to SIRM, χ_{LF} and SOFT.$_{20mT}$, highlighting an increase in finer ferrimagnetic magnetic grains to the post-1991 signal. Maximum χ_{ARM} values occur at 1997 (2-2.5 cm) and sustained high χ_{ARM} values continue to the top of the core. Magnetic concentration decreases at the sediment-surface.
OGiii	1973 to 1991 (11 to 6 cm)	Throughout 1977 to 1981 (10 to 9 cm) magnetic concentration values decline, however, remain higher than pre-1954 data. A second notable concentration peak is observed for χ_{LF}, SIRM and χ_{ARM} at 1982 (8.5-9 cm), with lower subsequent values and an overall decrease in magnetic concentration until 1991 (5-5.5 cm). Smaller peaks in HARD.$_{300mT}$ and SOFT.$_{20mT}$ also occur from 1979 to 1982 (10 to 8.5 cm), with subsequent lower values throughout the 1980s.
OGii	1949 to 1973 (15 to 11 cm)	Prominent increases in magnetic concentration occur from 1954, with maximum χ_{LF} (1363.22 10^{-9} m^3 kg^{-1}) and SIRM (33.26410^{-3} Am^2 kg^{-1}) values reached at 1966 (11.5-12 cm), with corresponding high χ_{ARM} values (5.500 10^{-6} m^3 kg^{-1}) at this depth. Notable enhancement of 'soft' and 'hard' magnetic minerals mirror this trend with maximum SOFT.$_{20mT}$ (13.021 10^{-3} m^3 kg^{-1}) and HARD.$_{300mT}$ (2.325 10^{-3} m^3 kg^{-1}) values occurring from 1966 (11-11.5 cm) to 1960 (12.5-13 cm).
OGi	Pre-1949 (19.5 to 15 cm)	Relatively low concentrations of magnetic grains observed in pre-1954 sediment (13.5 to 19.5 cm), for χ_{LF} (<179.04 10^{-9} m^3 kg^{-1}), SIRM (<4.954 10^{-3} Am^2 kg^{-1}), χ_{ARM} (<1.089 10^{-6} m^3 kg^{-1}), SOFT.$_{20mT}$ (<1.66110^{-3} m^3 kg^{-1}) and HARD.$_{300mT}$ (<0.614 10^{-3} m^3 kg^{-1}). Notably high χ_{ARM} and HARD.$_{300mT}$ values observed at 19-19.5 cm, highlighting a fine magnetic signature, which may represent the start of an artificial clay lining, identified below 19.5 cm (Figure 5.4).

Down-core interparameter magnetic ratios are presented (Figure 6.22) and detailed (Table 6.31) which, combined with the concentration parameters, magnetically characterise the four divisions in the OG core:

- OGi (pre-1949): Relatively low magnetic concentrations, with a notable ferrimagnetic/hard component at 19.5 cm, potentially reflecting the start of the identified artificial clay lining.
- OGii (1949 to 1973): Elevated magnetic concentrations occur post-1954, with pronounced peaks from 1960-1966.
- OGiii (1973 to 1991): Subsequently, magnetic values decline throughout the 1970s and 1980s; however, values remain notably higher than pre-1949 (OGi). Also a notable peak occurs at 1982.
- OGiv (post-1991): Magnetic concentration increases, characterised by a relatively finer (potentially SSD) ferrimagnetic signal.

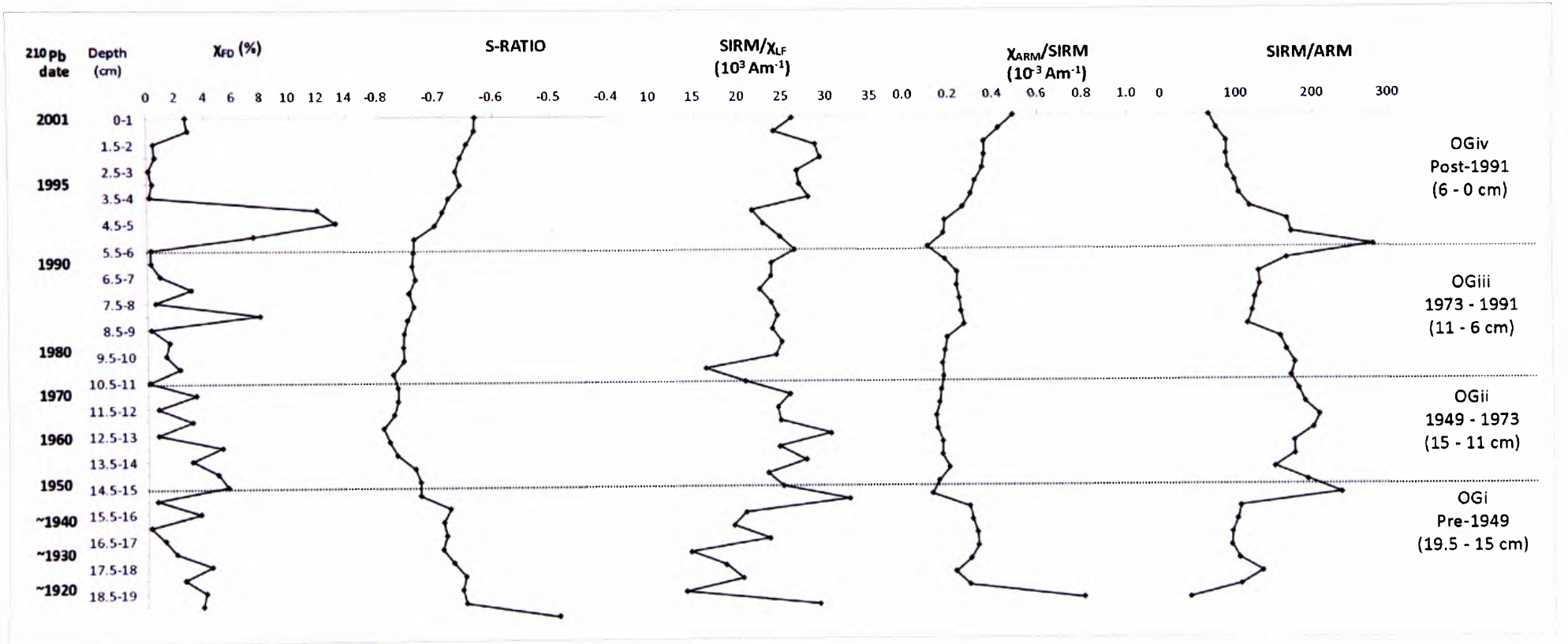

Figure 6.22: Magnetic ratio profiles for OG: χ_{FD}%, S-RATIO, SIRM/χ_{LF}, χ_{ARM}/SIRM and SIRM/ARM with superimposed phases OGi to OGiv (corresponding to Table 6.31).

Table 6.31: Description and interpretation of magnetic ratios for OG (corresponding to Figure 6.22).

Magnetic ratio	Description of trend
χ_{FD}%	The χ_{FD}% profile reveals a significant presence of SP (<0.05 μm) grains to the magnetic signal at 1984 (8-8.5 cm) highlighted by values >5%. Also, χ_{FD} values >10% observed from 1992-1993 (4-4.5 to 5-5.5 cm) reveal a dominating contribution of SP grains to these samples. The majority of χ_{FD} values are <5%, which highlights an insignificant contribution of SP grains to the remainder of the core.
S-RATIO	The S-RATIO profile indicates a consistent magnetic mineralogy with values -0.6 to -0.8 throughout the upper 19 cm of the core, indicative of coarse (MD) ferrimagnetic behaviour. At 19-19.5 cm values increase to >-0.6, reflecting a finer magnetic component, further supported by the χ_{ARM} profile (Figure 6.21), potentially, indicative of the start of the clay lining. A gradual increase in S-RATIOs from 12-12.5 cm highlights a potential increase in finer magnetic grains to the signal throughout post-1963 sediment.
SIRM/χ_{LF}, χ_{ARM}/SIRM and SIRM/ARM (grain size signals)	The gradual increase in SIRM/χ_{LF} values post-1992 (5 to 0 cm) further supports a shift from relatively coarse to finer ferrimagnetic grains (phase OGiv). This is also reflected in the χ_{ARM}/SIRM profile, which exhibits a distinct increase post-1993 (4.5 to 0 cm), and the SIRM/ARM profile, whereby, values decrease in this phase (OGiv). Also relatively higher SIRM/ARM ratios highlight a notable coarse magnetic signature in sediment from ~1946-1981 (15.5 to 9 cm) and at 1991 (5-5.5 cm) (OGiv).
SIRM/χ_{LF}, χ_{ARM}/SIRM (mineralogy signatures)	SIRM/χ_{LF} values range form 14.013 to 32.475 10^{3} Am^{-1}, indicative of magnetite [Thompson *et al.*, 1980]. The upper 19 cm of the core (phases OGii, OGiii and OGiv) demonstrates χ_{ARM}/SIRM values <0.4 which, combined with overall χ_{FD} values <6%, suggest the magnetite-type behaviour of the magnetic signal is not soil derived [Oldfield, 1999]. Also, low χ_{ARM}/SIRM ratios do not highlight a bacterial magnetosome contribution to the magnetic signal, typically attributed to χ_{ARM}/SIRM values >2 10^{-3} mA [Oldfield, 1999].

To investigate the contribution of SSD grains to the sediment column, χ_{ARM}/SIRM versus χ_{FD}% values are plotted according to Oldfield, [1994] (Figure 6.23). The plot reveals that there are no SSD dominated samples within the OG core, as data do not meet criteria set out by Oldfield, [1994] (χ_{FD} values >2% and χ_{ARM}/SIRM ratios >80 10^{-5}), to identify true SSD behaviour.

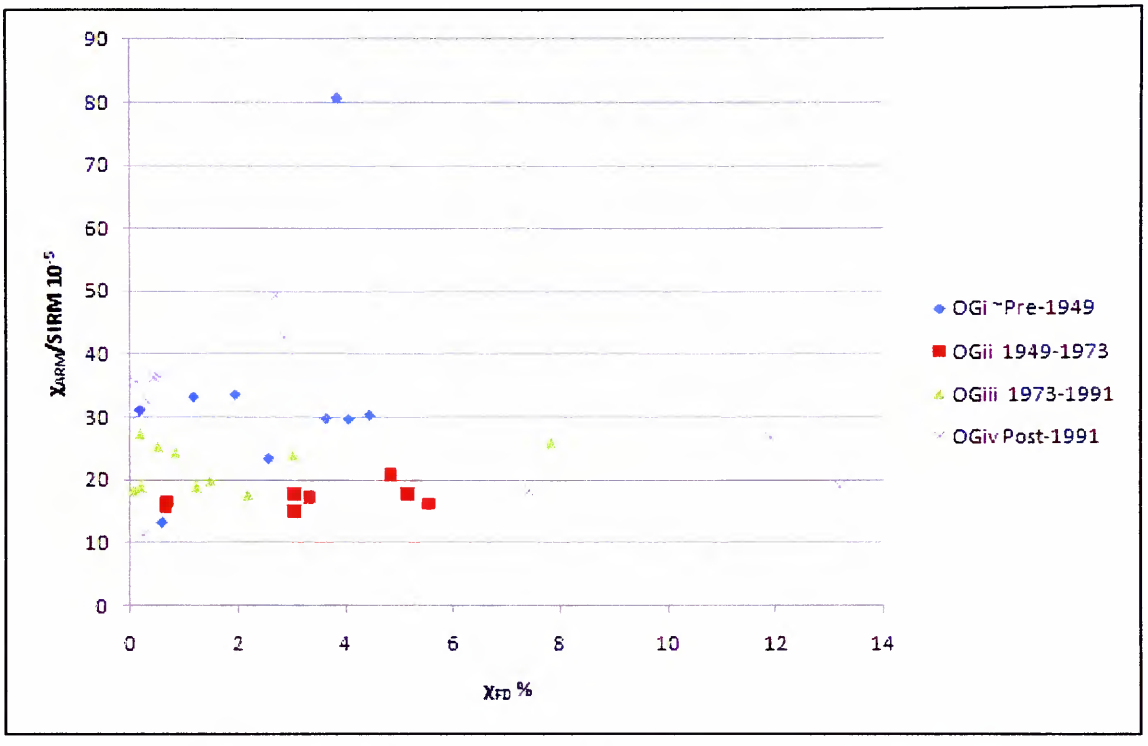

Figure 6.23: χ_{ARM}/SIRM (10^{-5} Am^{-1}) versus χ_{FD}% plots for OG to identify SSD dominated samples, after Oldfield [1994].

OG samples have also been divided into down-core phases (OGi to OGiv) and applied to Oldfield's [1990] bi-plot to determine temporal variations in magnetic grain sizes (Figure 6.24). The graph shows post-1973 samples (phases OGiii and OGiv) plot to the left of the 1949-1973 samples (phase OGii), highlighting a shift from a relatively coarse pre-1973 signal (phases OGi and OGii) to finer magnetic grains post-1973.

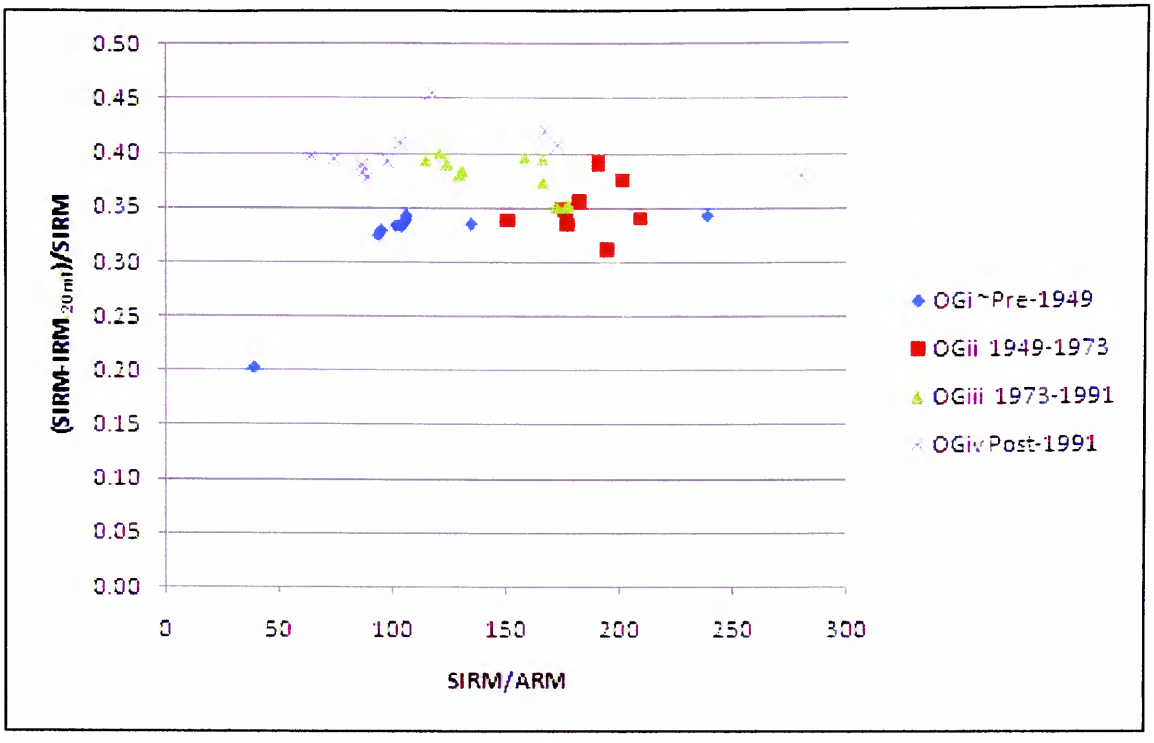

Figure 6.24: Plot of SIRM-IRM_{20mT}/SIRM versus SIRM/ARM for OG after Oldfield [1990] showing down-core phases (OGi to OGiv) to assess variations in magnetic grain size within the sediment column.

6.6.2. <10 µm particle size distributions: OG

Down-core size distributions of particulates <10 µm (Figure 6.25) demonstrate a relatively finer sediment pre-1949 (phase OGi), which is reflected by corresponding decreases in median size. Median values increase post-1949 (phases OGii, OGiii and OGiv). The particle size distributions also show a gradual increase in <10 µm, <2.5 µm and <1 µm particulates post-1991 (phase OGiv).

6.6.3. Trace metal concentrations: OG

Down-core trends in concentrations of Zn, Pb, Cu, S, Br, Cl and Ni are presented (Figure 6.26 and Table 6.33). Similar trends are exhibited, revealing down-core variations in trace metals. Detailed descriptions of individual trace metal trends are also included (Table 6.33).

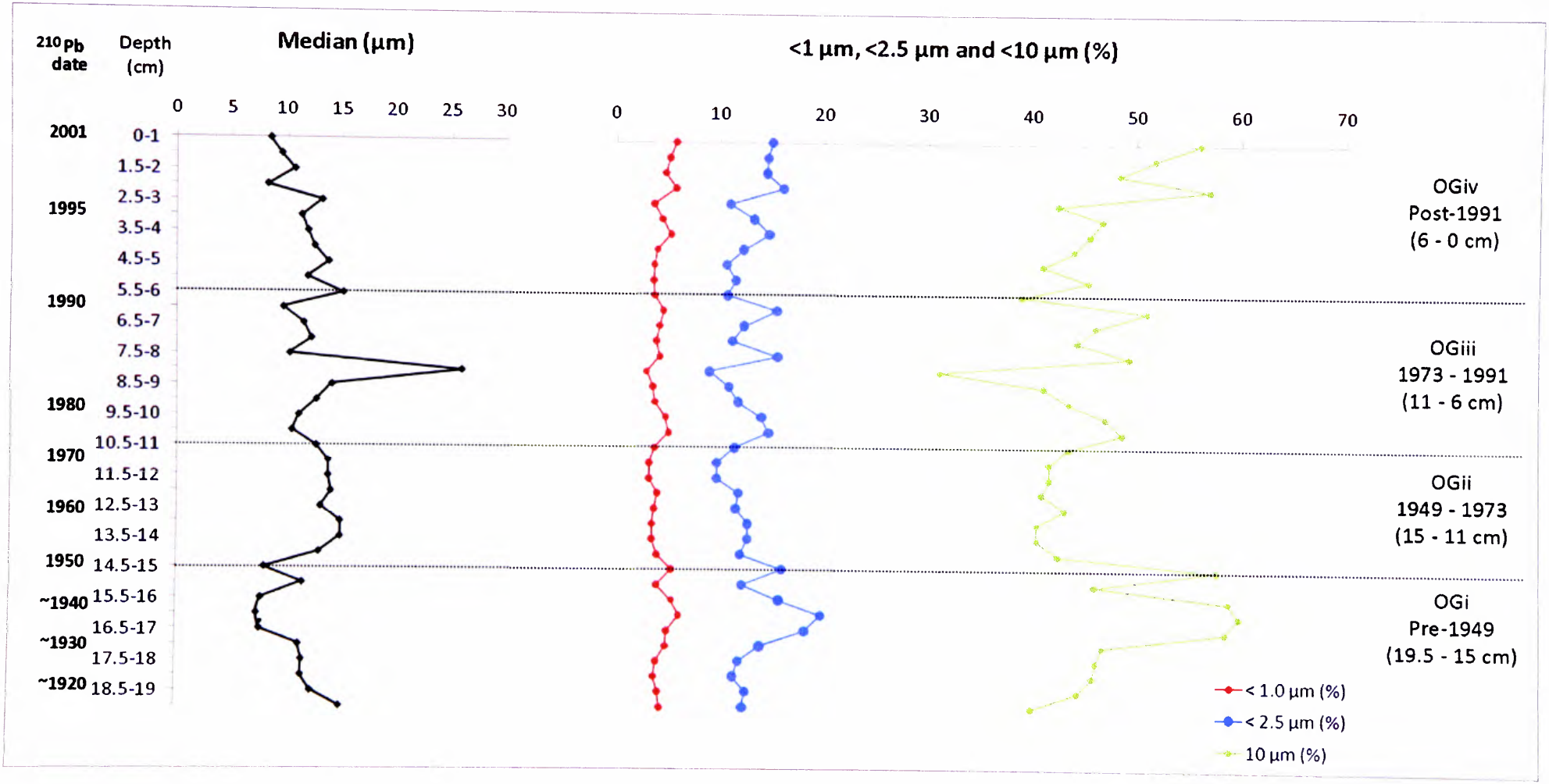

Figure 6.25: Median particle size and percentage distributions for respiratory size fractions <1 µm, <2.5 µm and <10 µm for OG with superimposed phases OG to OGiv.

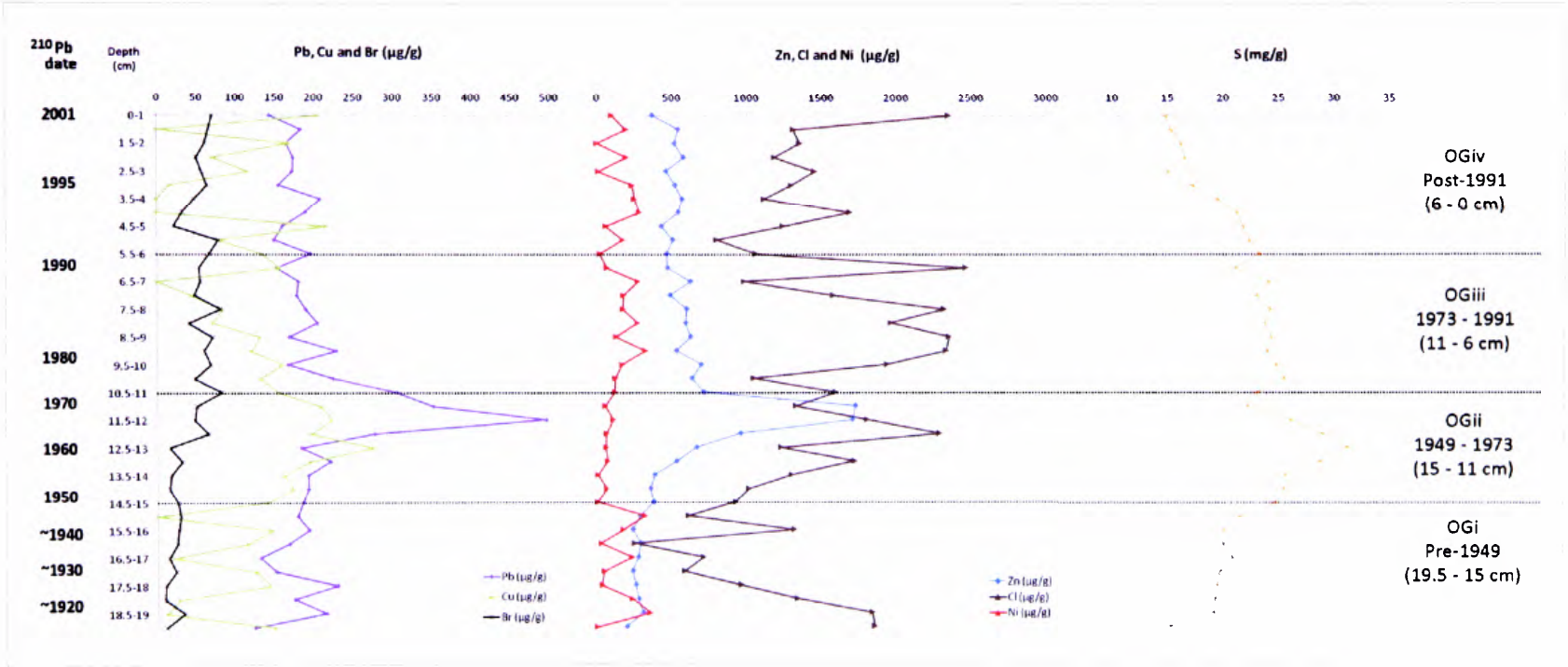

Figure 6.26: Down-core Pb, Cu, Br, Zn, Cl, Ni and S concentration profiles for OG with superimposed phases OGi to OGiv (corresponding to Tables 6.32 and 6.33).

Table 6.32: Down-core Pb, Cu, Br, Zn, Cl, Ni and S concentration trends in OG, relating to phases OGi to OGiv (corresponding to Figure 6.26).

Phase	Depth/Date	Pb, Zn, Cu and S concentration trends
OGiv	Post-1991 (6 to 0 cm)	Recent, smaller increases in Zn, Pb and S, with subsequent reductions and decreases sediment-surface concentrations during the late 1990s. Prominent Cu, Cl and Br increases with high sediment surface concentrations. Ni demonstrates an overall decline.
OGiii	1973 to 1991 (11 to 6 cm)	Overall decrease in Zn, Pb, S and Cu concentrations throughout the 1970s and 1980s; however, Ni, Br and Cl exhibit high concentrations.
OGii	1949 to 1973 (15 to 11 cm)	Pronounced Cu, Cl and S peaks at ~1960 with a slightly later and very prominent peaks in Pb and Zn from 1966-1970. Low Ni and Br values.
OGi	Pre-1949 (19.5 to 15 cm)	Relatively low, steadily increasing Zn, Cu, Br, Cl and S concentrations with distinct peaks at ~1942 in Cu, ~1918 to 1937 in Pb and ~1927 in Ni.

Table 6.33: Trace metal concentration trends for OG (corresponding to Figure 6.26).

Trace metal	Concentration trends
Pb	Pb exhibits distinct peaks in the lower section of the core, from ~1918 to 1937 (19 to 17.5 cm). Pb concentration increases gradually from ~1942 (15.5-16 cm) to reach a peak (219.934 µg/g) at 1957 (13-13.5 cm). However, a more prominent Pb enhancement occurs post-1960, with a pronounced peak (495.634 µg/g) at 1966 (11.5-12 cm) and sustained high values until a decrease at 1977 (10-10.5 cm). Values subsequently decline (<227.535 µg/g) post-1977, and overall, continue to decline to the sediment-surface (143.403 µg/g). However, there are smaller peaks at 1981 (9-9.5 cm), 1984 (8-8.5 cm), 1991 (5.5-6 cm), 1994 (3.5-4 cm) and a small near surface increase at 1998 (1-1.5 cm).
Zn	Zn exhibits a distinct shift from relatively low pre-1954 (below 13.5-14 cm) concentrations (<374.374 µg/g) to notably enhanced post-1954 values. Maximum Zn concentrations are observed between 1970-1966 (11 and 12 cm); whereby, values reach 1726.768 µg/g, highlighting a marked increase Zn. Post-1970 Zn values decline to <692.872 µg/g, however, remain notably higher than pre-1954 concentrations. Overall, Zn values decline throughout the post-1970 sediment, however, smaller peaks are observed at 1979 (9.5-10 cm), 1982 to 1985 (9 to-7.5 cm), 1988 (6.5-7 cm), 1994 (3.5-4 cm) and 1997-1998 (1-2.5cm).
Cu	Cu demonstrates relatively low values (<145.790 µg/g) in ~pre-1950 sediment (15-19.5 cm), and exhibits two distinct peaks in this lower phase at ~1942 (15.5-16 cm) and ~1927 (17.5-18 cm). Above 14.5 cm Cu concentrations are notably enhanced, reaching maximum Cu concentrations (275.601 µg/g) at 1960 (12.5-13 cm), which coincides with peak S concentrations at this time. This enhancement of Cu is sustained throughout the 1960s into the 1970s, with values decreasing from 1979 (9.5-10 cm) to 1988 (6.5-7 cm). Pronounced Cu peaks are observed post-1990, with periods of notable enhancement 1990 to 1993 (6.5 to 4.5 cm) and 1996 to 1997 (3 to 1.5 cm), and sediment surface enrichment.
S	S exhibits relatively low (<21.107 mg/g) concentrations in the lower section of the core below 15.5 cm (~1914 to 1946), with a small peak occurring in this phase at ~1935 (16.5-17 cm). S concentration increases sharply ~post-1950, to reach maximum concentration (31.386 mg/g) at 1960 (12.5-13 cm). Subsequent values decline at 1970 (11-11.5 cm); however, values then increase at 10-10.5 cm (1977) and remain consistent ranging from 25.601 mg/g at this depth, decreasing slightly to 23.209 mg/g at 1991 (5.5-6 cm). S values decline more rapidly in post-1991 sediment, with notable decreases from post-1993 (4-4.5 cm), with a small recent increase in post-1997 sediment.
Br	Br exhibits relatively low pre-1949 concentrations. From 1951 (14 cm) there is a distinct elevation in Br, whereby, values increase from <34.297 µg/g to 65.032 µg/g (at 12-12.5 cm). This increase is sustained in the post-1959 sediment, with notable Br peak at 1973 (10.5-11 cm), 1979 to 1982 (10 to 8.5 cm), 1985 (7.5-8 cm) and 1991 (5-5.5 cm). Br values decline during the early 1990s and high sediment-surface concentrations are observed.
Cl	Cl demonstrates low concentrations pre-1949. A distinct Cl increase occurs from ~1951 (14 cm), with notable peaks occurring at 1963 (12-12.5 cm), 1981 to 1985 (7.5 to 9 cm) and 1990 (6-6.5 cm). A sharp decline in Cl concentration occurs during the early 1990s, after which, values steadily increase to reach high sediment-surface concentrations.
Ni	Unlike Pb, Zn, Cu, S, Br and Cl, Ni exhibits relatively high concentration values in the lower section of the core ~pre-1942 (19.5 to 15.5 cm). This may highlight relatively higher contribution of Ni in pre-1949 sediment compared to the other typically pollution-derived trace metals at this time. Lower Ni values are observed, however, between 1946 and 1963 (15.5 to 12 cm), values are <106.881 µg/g. From 1963, Ni concentrations steadily increase to reach a maximum value (320.159 µg/g) at 9.5-10 cm (1979). Elevated Ni concentrations are sustained until 1987 (7-7.5 cm), after which, levels sharply reduce to 18.901 µg/g (6-6.6 cm). Subsequent values increase abruptly with a period of notable Ni increase from 1993-1994 (4.5 to 3.5 cm) with a post-1994 decline.

6.6.4. Statistical relationships: OG

Negative correlations are observed between OM and the clay sized fraction (R=-0.519; p<0.001; n=38). OM demonstrates significant strong positive correlations with the magnetic parameters χ_{LF} (R=0.722; p<0.001; n=38), SIRM (R=0.651; p<0.001; n=38), $SOFT_{-20mT}$ (R=0.708; p<0.001; n=38), $HARD_{.300mT}$ (R=0.458; p<0.01; n=38) and χ_{ARM} (R=0.380; p<0.05; n=38). Associations are also identified between OM and the 'typically anthropogenic' trace metals, with particularly strong relationships with Zn (R=0.803; p<0.001; n=38) and Br (R=0.614; p<0.001; n=38); with weaker correlations for Pb, Cl and S (Table 6.34). S, Pb and Zn demonstrate weak negative correlations with the clay fraction.

The 'anthropogenic' trace metal group exhibit strong positive correlations with the magnetic concentration parameters, and negative correlations with the, typically, minerogenic elements (such as Al, Si and Ti) (Table 6.34). Strong significant inter-element relationships are also identified between Pb, Zn and S; and Br Zn and Cl. Ni exhibits insignificant relationships with the other trace metals, magnetic parameters or OM.

Table 6.34: Selected correlation coefficients of Pb, Zn, S, Cu, Br and Cl for OG. R values accompanied by p value expressed as * (p<0.05), ** (p<0.01) and *** (p<0.001); n=38.

	Pb	Zn	Cu	S	Br	Cl	Ni
Pb	1.00						
Zn	0.437**	1.00					
Cu			1.00				
S	0.468**	0.493**	0.410*	1.00			
Br		0.594***			1.00		
Cl		0.361*			0.424**	1.00	
Ni			-0.685***				1.00
OM	0.394*	0.803***		0.543***	0.614***	0.424***	
χ_{LF}		0.853***	0.440**	0.336*	0.542***	0.405*	
SIRM		0.807***	0.395*		0.574***	0.407*	
χ_{ARM}		0.600***			0.461**	0.483**	
$SOFT_{-20mT}$		0.847***	0.388*	0.326*	0.556***	0.385*	
$HARD_{.300mT}$		0.604***			0.509***	0.375*	
Ti	-0.444**	-0.714***		-0.660***	-0.453**	-0.429**	
Si		-0.787***		-0.480*	-0.643***	-0.511***	
Al		-0.366*					

The minerogenic trace elements Si, Al, Ti, Ca, K, Fe and Mn have been grouped according to common characteristics revealed from the correlation coefficients (Table 6.35). This group of trace metals demonstrate strong significant negative correlations with OM. Strong positive correlations exist for Si, Al, and Ti, with the clay sized fraction (<2 μm), and weaker associations for Ca and Fe. Overall, this group of metals also exhibits a negative

correlation with the magnetic concentration parameters and with the 'anthropogenic' trace metal group, in particular Zn.

Fe and Mn demonstrate relatively weaker negative correlations with OM, and insignificant significant relationships with the magnetic parameters or the anthropogenic trace metals. However, Fe and Mn do exhibit significant positive correlations with Al, Si, Ti and K (Table 6.35). Si, Ti, Ca and K demonstrate negative correlations with the magnetic concentration parameters (Table 6.35).

Table 6.35: Selected correlation coefficients of Si, Al, Ti, Ca, K , Fe and Mn for OG. R values accompanied by p value expressed as * ($p<0.05$), ** ($p<0.01$) and *** ($p<0.001$); n=38.

	Si	Al	Ti	Ca	K	Fe	Mn
Si	1.00						
Al	0.510***	1.00					
Ti	0.877***	0.491**	1.00				
Ca			0.564***	1.00			
K	0.846***	0.524***	0.892***	0.675***	1.00		
Fe	0.477**	0.507***	0.424**		0.355*	1.00	
Mn	0.428**	0.354*	0.480**		0.418**	0.366*	1.00
Pb			-0.444**	-0.486**	-0.427**		
Zn	-0.787***	-0.366*	-0.714***	-0.499****	-0.788***		
Cu				-0.469**			
S	-0.408**		-0.660**	-0.889***	-0.695***		
Br	-0.643***		-0.453**		-0.509***	-0.335*	-0.375*
Cl	-0.571***		-0.429**				
Ni							
OM	-0.918***	-0.490**	-0.891***	-0.527***	-0.934***	-0.473**	-0.425**
Clay	0.544***	0.494***	0.604***	0.351*	0.610***	0.446**	
χ_{LF}	-0.686***	N/A	-0.561***	-0.439**	-0.687***		
SIRM	-0.624***		-0.461**	-0.356*	-0.602***		
χ_{ARM}	-0.451**						
SOFT$_{20mT}$	-0.658***		-0.530***	-0.448**	-0.669***		
HARD$_{300mT}$	-0.505***				-0.367*		

Strong significant positive relationships are exhibited between the concentration dependent parameters χ_{LF}, SIRM, χ_{ARM}, SOFT$_{-20mT}$ and HARD$_{-300mT}$, demonstrating associations between the deposition of ferrimagnetic (χ_{LF}), remanence carrying (SIRM), fine ferrimagnetic (χ_{ARM}), coarse ferrimagnetic (SOFT$_{-20mT}$) and antiferromagnetic (HARD$_{-300mT}$) magnetic minerals (Table 6.36).

Table 6.36: Correlation coefficient matrix of the concentration-dependent magnetic parameters for OG. R values accompanied by p value expressed as * ($p<0.05$), ** ($p<0.01$) and *** ($p<0.001$); n=38.

	χ_{LF}	SIRM	χ_{ARM}	$SOFT_{-20mT}$	$HARD_{-300mT}$
χ_{LF}	1.00				
SIRM	0.824***	1.00			
χ_{ARM}		0.874***	1.00		
$SOFT_{-20mT}$	0.986***	0.986***	0.819***	1.00	
$HARD_{-300mT}$	0.956***	0.583***	0.920***	0.829***	1.00

6.7. Chapter summary

Proxy pollution records have been reconstructed from Daresbury Delph, Windmill Hill, Dogs Kennel Clump and Oglet ponds, via down-core trends in magnetic properties, trace metals, SCPs, and percentage distributions of particulates <10 μm. Down-core phases are identified for each site complimented by isotope chronologies, which reveal local proxy pollution 'signals'.

Daresbury Delph pond provides a >250-year history of variations in the concentration of SCPs, magnetic minerals and trace metals. Notable trace metal enhancement is exhibited from 1780 to 1807. SCP and magnetic enhancement occurs ~post-1832, coinciding with further trace metal elevation. Proxy pollution concentrations continue to increase throughout the 20th century. Several distinct peaks are observed, notably between 1910-1921, mid-1930, and during the 1950s and 1960s. Post-1960 there is an overall decline in trace metal and magnetic concentrations and SCPs decline post-1985. A post-1975 shift to a relatively fine magnetic signal is mirrored by corresponding increases in <1 μm and < 2.5 μm particulates.

Windmill Hill Pond demonstrates a post-1906 trace metal elevation, with a slightly later magnetic enhancement ~post-1913. Increases in magnetic and trace metal concentrations occur throughout the 20th century. A notable ~1925 Pb, Cu and S peak occurs and increased magnetic concentrations are observed from ~1929 to 1932, with corresponding trace metal increases at ~1929 and 1934. Also, a ~1940 to1946 magnetic concentration peak, mirrored by ~1939 to 1949 Pb, Zn and S increases are exhibited, with maximum magnetic concentrations from ~1949 to 1955. Post-1955 magnetic decreases coincide with inversely increasing trace metal trends. Further trace metal enhancement occurs, reaching maximum 1997 to 2001 concentrations.

Dogs Kennel Clump pond exhibits ~post-1900 increases in trace metal concentrations with slightly later magnetic elevation from ~1913. A notable magnetic concentration peak occurs at ~1923. Further trace metal enhancement occurs during the ~1930s, with sustained high values throughout the 1940s and 1950s. DKC exhibits a pronounced post-1960 magnetic and trace metal enhancement, followed by post-1970 decline in magnetic concentration, Zn and S. However, Pb, Br, Cr and Ni, continue to increase post-1970.

Oglet Pond demonstrates a ~80-year sediment history. Pb, Cu, S and Ni increases occur from ~1918; however, ~pre-1950 magnetic, Zn and Br concentrations are relatively low. A pronounced 1960-66 maximum magnetic peak occurs, which is mirrored by maximum S, Cu and Cl concentrations at 1960, and later maximum Pb and Zn peaks from 1966 to 1970. Post-1970 there is a decrease in trace metals (Zn, Pb, S and Cu) and a relatively small 1990-93 trace metal peak. Br, Cl and Ni, however, exhibit sustained high post-1970 values. Magnetic concentration decrease during the 1970s and 1980s; however, a magnetic peak is observed at 1982 and post-1991 the magnetic record demonstrates a relatively fine signal.

7. CHAPTER SEVEN: URBAN FLUX PROFILES

7.1. Chapter overview

Magnetic and trace metal flux profiles are presented in turn for Daresbury Delph, Windmill Hill, Dogs Kennel Clump and Oglet ponds. As the DDP sediment stratigraphy extends to a time of low-scale industrial activity, prior to the intensification of industry during the Industrial Revolution (i.e. pre-1800), the anthropogenic contribution to trace metal flux are determined for this site. Site-specific, down-core phases applied in Chapter 6 are superimposed over the flux profiles to aid description of flux trends and comparison between flux and concentration patterns.

7.2. Introduction

Original concentration data have been normalised by sediment accumulation rates (g cm^{-2} y^{-1}) to assess the temporal supply of magnetic grains (Section 3.6.8.1.), trace metals (Section 3.6.8.2.) and SCPs (Section 3.6.8.3.) to the urban ponds, producing flux profiles. These profiles provide a 'real time' accumulation of metals and magnetic grains to each pond, allowing an assessment of depositional histories and accounting for potential influences of changing sediment delivery to the pond. Selected Pb, Zn Cu and S flux profiles are presented to demonstrate deposition of anthropogenic trace metals. Magnetic flux profiles are shown for SIRM, $SOFT_{-20mT}$ and $HARD_{-300mT}$. These parameters have been selected as they reflect the 'total' supply of magnetic grains (SIRM), as well as 'hard' ($HARD_{-300mT}$) and 'soft' ($SOFT_{-20mT}$) contributions [Oldfield, 1990]. The supply of SCPs to DDP are included, however, SCP data are only available for this site, due to time constraints. Also, the anthropogenic contribution to total trace metal deposition histories are calculated for DDP (Section 3.6.8.2.), using pre-1800 normalisations for background/natural metal inputs. As the sediment stratigraphies for WH, DKC and OG do not extend to pre-1800, assessment of anthropogenic components to the trace metal flux record are prevented.

7.3. Daresbury Delph Pond

Magnetic flux profiles for the BDD1 core (Figure 7.1) mirror trends observed in the original magnetic concentration profiles (Figure 6.1). SIRM and $SOFT_{-20mT}$ flux profiles are closely paralleled and demonstrate a dominating 'soft' magnetic component to the sediment record. An increase in magnetic flux from ~1832, corresponds to the notable

increase observed in the SCP record (Figure 6.13). A period of elevated magnetic flux occurs between ~1780 and 1800. These pre-1832 increases (Phase DDi) are, however, relatively small when compared to post-1832 values.

SIRM and $SOFT_{-20mT}$ exhibit an overall increase of remanence carrying minerals and coarse (MD) ferrimagnetic grains, respectively, from ~1832 (Phase DDii) to the sediment-surface. Periods of elevated SIRM and $SOFT_{-20mT}$ occur between ~1910 and 1920; 1954 and 1963; and a further increase in supply of magnetic grains post-1980 (Phase DDiv), reaching maximum flux from 1992 to present day. The $HARD_{-300mT}$ flux profile also mirrors these trends; however, it demonstrates a later, ~post-1900 increase. This reveals an enhancement in the contribution of antiferromagnetic grains (and or SSD ferrimagnetic grains) to the pond, which steadily increases from ~1900 (Phase DDiii). Further enhancement of 'hard' minerals in the magnetic record occur post-1978 (Phase DDiv) with proportionately higher increases than those observed post-1980 for SIRM and $SOFT_{-20mT}$.

Pb, Zn, Cu and S flux profiles are presented for BDD1 (Figure 7.2) with trends for each trace metal noted (Table 7.2). By normalising the total flux by mean trace metal concentration in ~pre-1800 sediment, representing a time of pre-intensified industrial activity, natural/background trace metal inputs can be assessed and, therefore, trends in the anthropogenic supply of trace metals to the lake can be established (Figure 7.2).

Zn, Pb, S and Cu display clear marked increases in total flux from ~1832, highlighting a potential anthropogenic source, in contrast to the relatively low total flux values observed in the ~pre-1832 sediment (Phase DDi). This corresponds to pronounced increases observed in the SCP (Figure 7.3), SIRM and $SOFT_{-20mT}$ (Figure 7.1) flux profiles at this time. This is further supported by the marked increase in anthropogenic trace metal flux in the ~post-1832 sediment. S, Pb and Cu also exhibit earlier increases at 1751, 1780 and 1807 with corresponding smaller peaks in Zn. However, these ~pre-1832 peaks are relatively small, in comparison with the ~post-1832 elevation in total and anthropogenic flux. The marked increase in trace metals from ~1780 may also contribute to the enhancement of the magnetic signal observed at this time (Figure 7.1), further supporting an anthropogenic component to the magnetic signature.

Generally, there is minor variation in the trends between the 'total' and estimated anthropogenic flux profiles for Zn, Pb, Cu and S (Figure 7.2), which suggests deposition of these trace metals is not governed by natural inputs. The profiles highlight a pronounced increased in Pb, Zn and S between 1850 and 1867; whereby, maximum S supply is

observed (1867) (Phase DDii). Very high Cu and Zn flux occurs from ~1900-1920, Pb demonstrates ~50 years of sustained high flux from 1900 to the mid-20th century (1958) and maximum Pb supply is reached at 1950 (Phase DDiii). S, Zn and Cu also exhibit elevated total and anthropogenic flux throughout the 20th century (Phase DDiii). High Cu and Zn values are sustained into the early 1960s, and S exhibits particularly high flux values from 1969 to 1975 (Phase DDiii). Overall, reductions in S, Zn, Cu and Pb occur after these peaks to present day, however smaller peaks are observed for Pb at 1978 and 1992; Cu at 1972, 1985, 1995 and 2005; Zn from 1972 to 1985 and at 2005 (Phase DDiv). S demonstrates a steady decline post-1975 (Phase DDiv).

Flux profiles of total SCPs, SCPs 10-30 μm, SCPs 3-10 μm and SCPs 1-3 μm are presented (Figure 7.4, Table 7.4). All SCP profiles demonstrate relatively low ~pre-1832 values Phase DDi). Total SCPs start to steadily increase post-1838 (Phase DDii). A steady increase in the supply of SCPs 10-30 μm and 1-3 μm occurs from ~1800 and SCPs 3-10 μm exhibit later, ~post-1832 increases. A pronounced increase in SCPs occurs in all profiles post-1894, demonstrating a distinct SCP enhancement into the 20th century (Phase DDiii). SCP flux values post-1900 (Phases DDiii and DDiv) are notably higher than pre-1900 (Phases DDi and DDii), and relatively high values are sustained throughout the 20th century.

Maximum flux of SCPS 1-3 μm occurs at 1914, reflected by a prominent increase in SCPs 10-30 μm and 3- 10 μm at this time. SCP values continue to increase throughout the first half of the 20th century, reaching maximum peak at 1963 for total SCPs and SCPs 3-10 μm (Phase DDiii). Larger SCPs (10-30 μm) display maximum flux at 1981. SCPs 3-10 μm and 10-30 μm decline post-1981, with an earlier decline observed for SCPs 1-3 μm, post-1963; however, this size range also demonstrates recent post-1995 increases (Phase DDiv).

The DDP flux profiles highlight corresponding features between the supply of SCPs, magnetic grains and trace metals to the pond within the divisions of the BDD1 core (Figure 7.5 and Table 7.5).

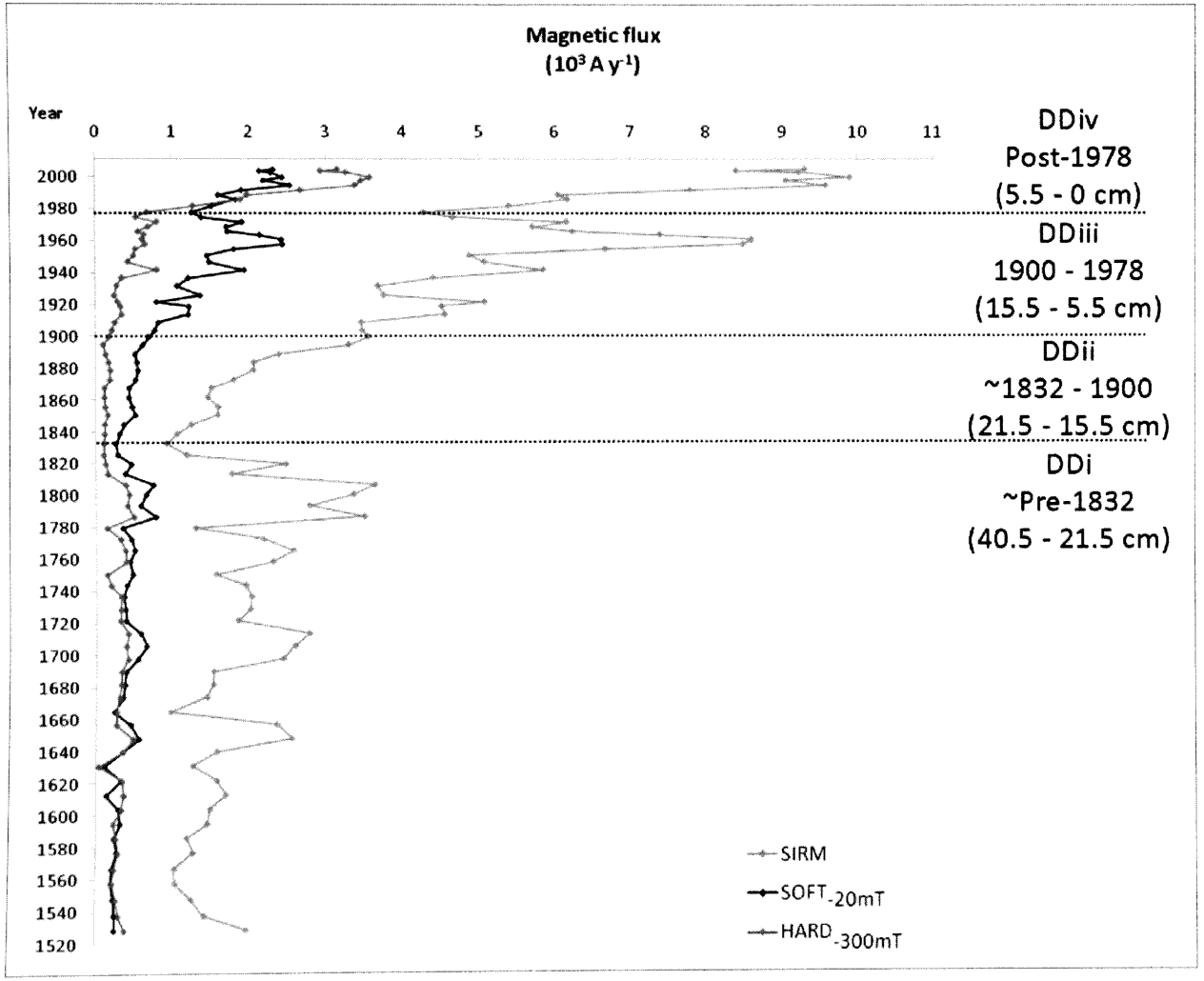

Figure 7.1: Magnetic flux profiles for BDD1: $HARD_{.300mT}$, $SOFT_{.20mT}$ and SIRM with superimposed phases DDi to DDiv (corresponding to Table 7.1).

Table 7.1: Magnetic flux trends in BDD1 relating to down-core divisions DDi to DDiv (corresponding to Figure 7.1).

Phase	Timescale	Description of trend
DDiv	Post-1978	Prominent magnetic elevation with an increased contribution of 'hard' magnetic minerals.
DDiii	1900 to 1978	Further enhancement throughout the 20th century with a reduction in SIRM and $SOFT_{.20mT}$ at 1978.
DDii	1832 to 1900	Increase in magnetic flux starts at ~1832 continuing throughout this phase.
DDi	~Pre-1832	Relatively low magnetic flux with a period of magnetic elevation from ~1780 to ~1800.

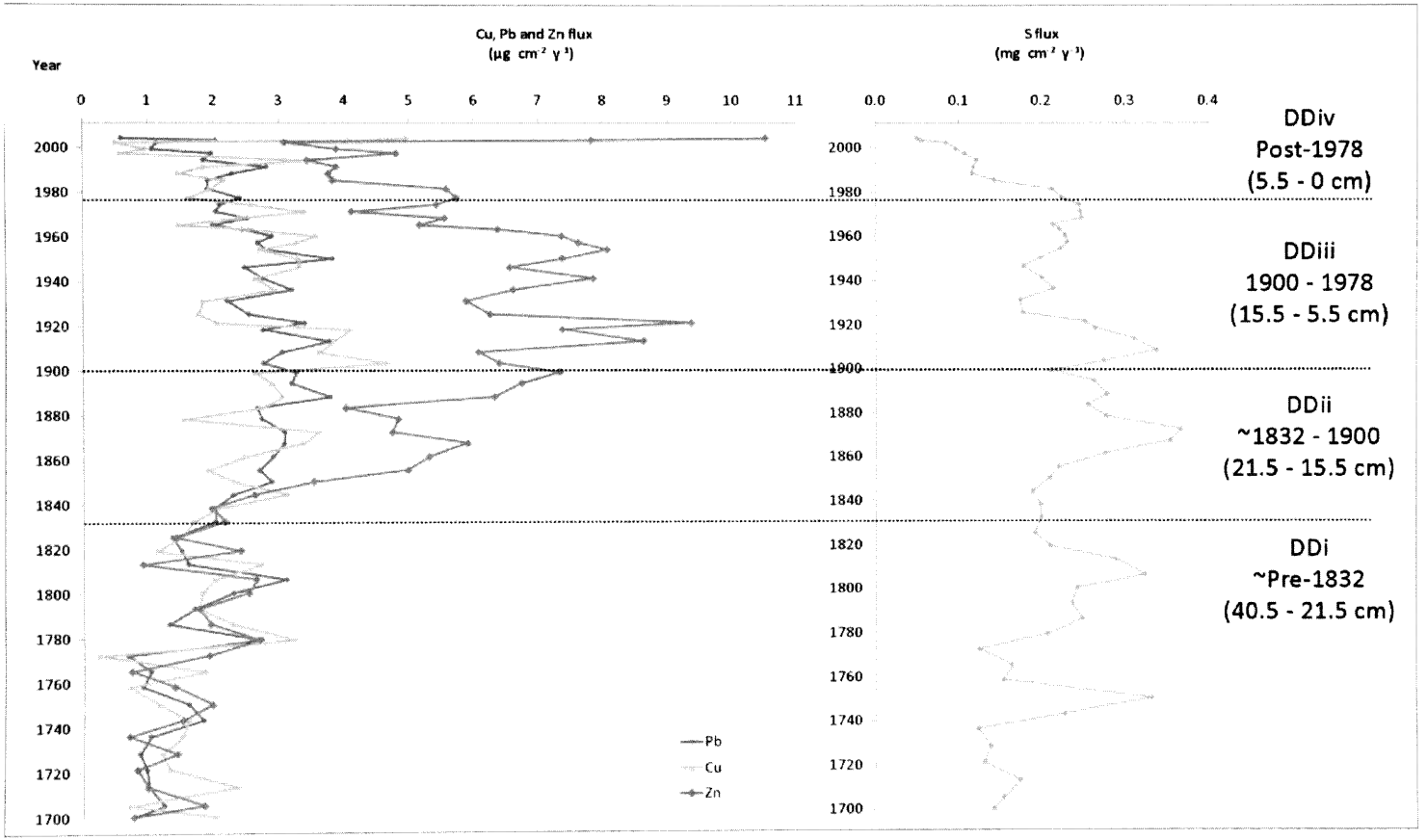

Figure 7.2: Total Pb Zn, Cu and S flux profiles for BDD1 with superimposed phases DDi to DDiv (Corresponding to Table 7.2).

Table 7.2: Pb, Zn, Cu and S flux trends in BDD1 relating to down-core divisions DDi to DDiv (corresponding to Figure 7.2).

Phase	Timescale	Description of trend
DDiv	Post-1978	Steady reductions in S mirrored by overall reductions in Pb, Zn and Cu.
DDiii	1900 to 1978	Further trace metal increases occur post-1900, sustained throughout this phase, reaching mid-20th century peaks.
DDii	1832 to 1900	Pb, Cu and Zn enhancement, with prominent Zn elevation. S exhibits further increases.
DDi	~Pre-1832	Period of relatively low Pb, Cu and Zn, however, S values are relatively high in this phase, from ~1850 to ~1867.

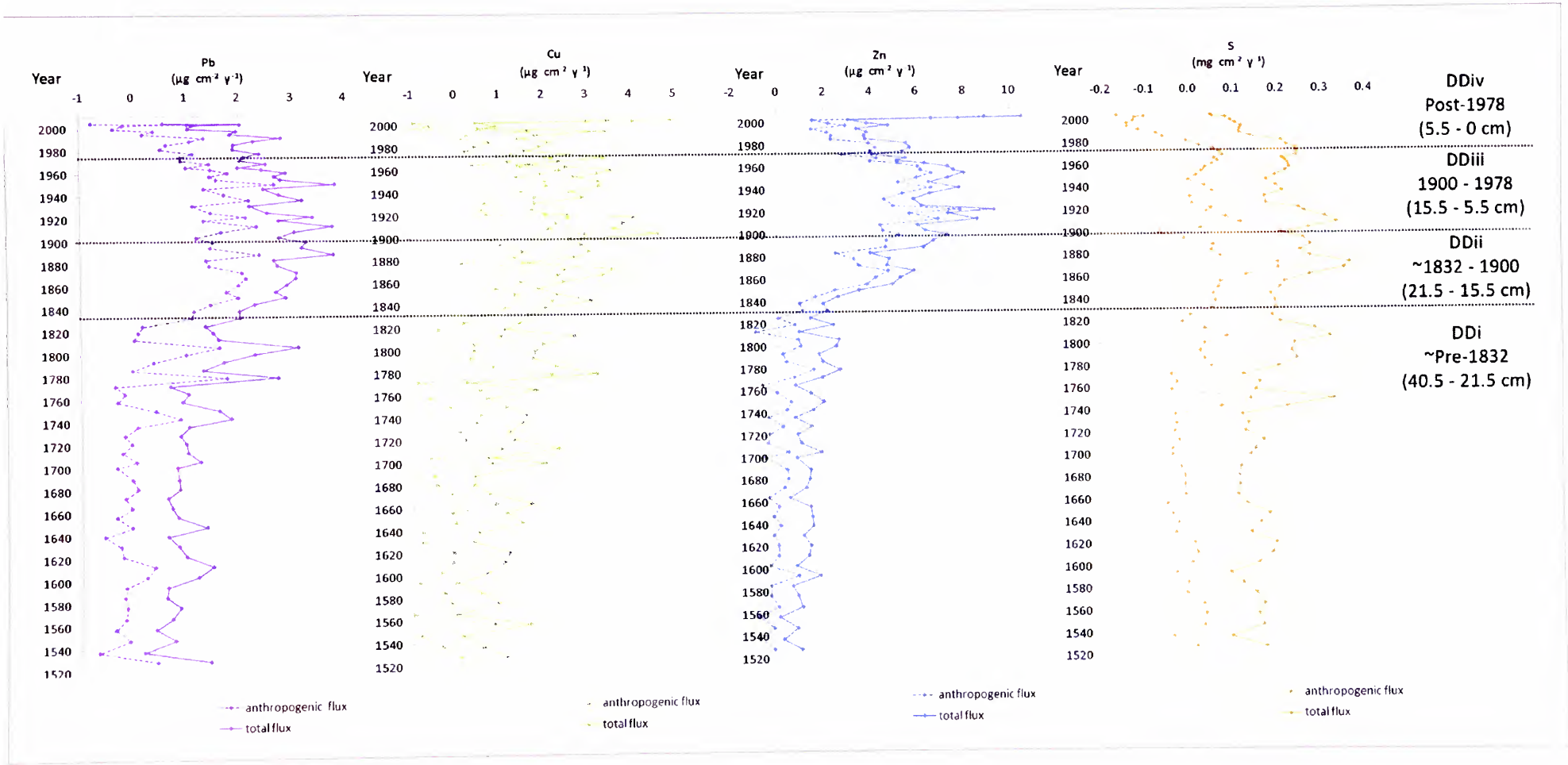

Figure 7.3: Total and anthropogenic Pb Zn, Cu and S flux profiles for BDD1 with superimposed phases DDi to DDiv (Corresponding to Table 7.3).

Table 7.3: Pb, Zn, Cu and S flux trends in BDD1 (corresponding to Figure 7.2).

Trace metal	Flux trend
Pb	An increase in Pb is observed at ~1744 and between 1785 and 1810. However, a notable enhancement of Pb occurs from ~1832 with increased Pb supply at ~1850 and ~1867. High values are sustained throughout the 19th century, into the 20th century with peaks at ~1889 to 1899, ~1914 to 1921 and ~1937 to 1958; reaching maximum flux at 1950, after which, Pb declines, with smaller peaks observed at 1978 and 1992.
Cu	Cu flux values demonstrate an early peak at ~1785 to 1815, with a marked enhancement from ~1838. Cu levels are particularly elevated from ~1878 to 1838, with a notable increase between 1904 and 1918. The Cu profile also exhibits a prominent increase from 1937 to 1961, after which, values decline and smaller peaks at 1972, 1985 and 1995 occur, with elevated 2005 levels.
Zn	Marked increases in total and anthropogenic flux occur from ~1832. Post-1856 demonstrates the earliest, most notable Zn enhancement, with sustained high values until ~1867. This is followed by a further Zn increase post-1900. Notably high values are exhibited from 1914 to 1925, and from 1937 to 1963. Zn declines post-1966, however, smaller Zn increases are observed from 1972 to 1985, with maximum 2005 values.
S	Notable peaks in supply of S are observed at ~1750 and between ~1780 and 1820, with a notable peak at 1807. Values markedly increase from ~1826 until maximum values at ~1873, after which, values decline until flux increases at 1909, with a S peak at 1937 and from 1969 to 1975. This increase continues until 1981. S supply subsequently reduces sharply and reaches low present day values.

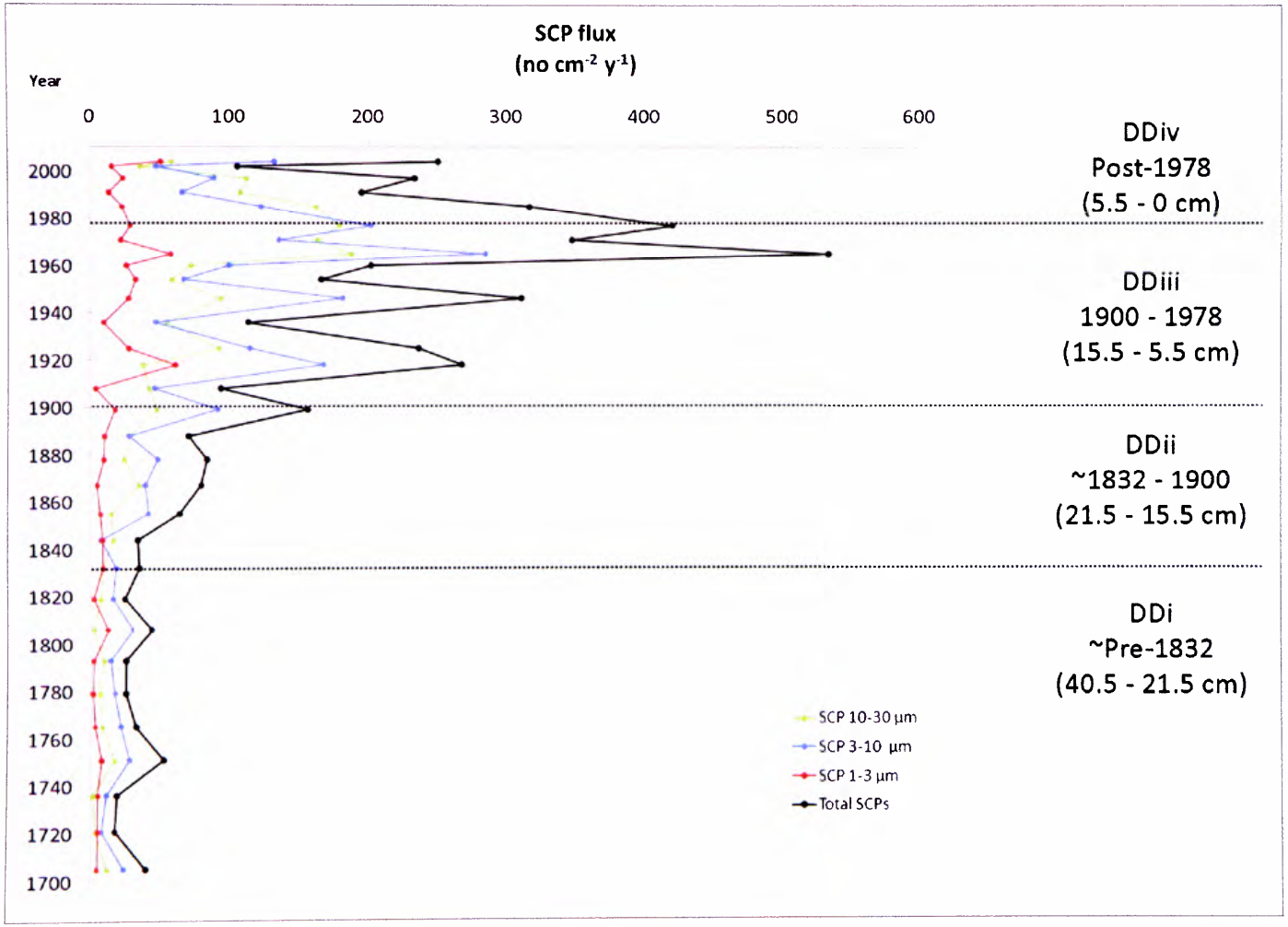

Figure 7.4: SCP flux profiles for BDD1: Total SCPs, SCPs 10-30 µm, SCPs 3-10 µm and SCPs 1-3 µm (no. cm^{-2} y^{-1}) with superimposed phases DDi to DDiv.

Table 7.4: SCP flux trends in BDD1 relating to down-core divisions DDi to DDiv (corresponding to Figure 7.4).

Phase	Timescale	Description of trend
DDiv	Post-1978	Maximum peak in SCPs 10-30 µm at 1981. Overall reductions un SCPs during this phase with a recent post-1995 increase.
DDiii	1900 to 1978	Pronounced SCP enhancement during the 20th century with maximum peak at 1963 for total SCPs and SCPs 3-10 µm.
DDii	1832 to 1900	Initial increase in SCPs from ~1838.
DDi	~Pre-1832	Relatively low SCP values.

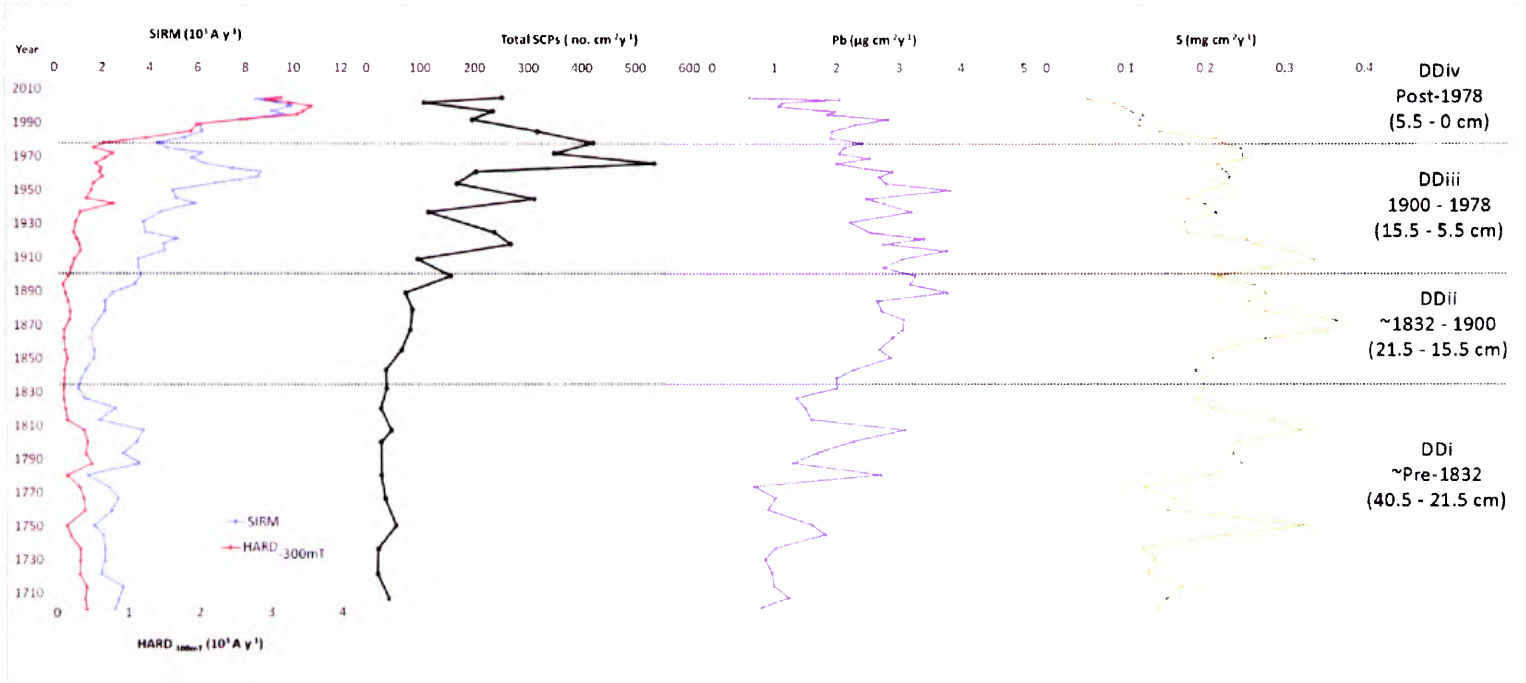

Figure 7.5: Proxy pollution profiles post-1700 for BDD1: Magnetic, total SCP, Pb and S with superimposed phases DDi to DDiv (corresponding to Table 7.5).

Table 7.5: Summary of proxy pollution flux trends in BDD1, relating to down-core phases DDi to DDiv (corresponding to Figure 7.5).

Phase	Timescale	Flux trends
DDiv	Post-1978:	S steadily declines to present day and Zn, Cu and Pb exhibit overall reductions. Maximum SCPs 10-30 µm flux at 1981. Increase in SCPs 1-3 µm post-1995. Increase in supply of magnetic grains (SIRM flux) post-1980, characteristic of a fine-grained signal revealed by $HARD_{300mT}$ profile.
DDiii	1900 to 1978:	Further post-1900 metal, magnetic and SCP increases. 1914 to 1921 Pb, Cu, and Zn peaks mirrored by SCPs 1-3 µm maximum. Trace metal peak at 1937, followed by mid-20th century increases: Pb at 1950 to 1958; Cu at 1961; Zn at 1963; S from 1969-1975, maximum SCP flux at 1963; and 1954 to 1963magnetic increases.
DDii	1830 to 1900:	Pb, Cu, Zn, S, magnetic and SCP enhancement post-1832. Prominent trace metal increases from 1850-1880, particularly notable in the Pb and S profile. Decline in trace metal flux from ~1880-1900.
DDi	Pre-1832:	Overall low pre-1830 trace metal, magnetic and SCP values. Pb and S peak at ~1751; Pb and S increases from 1780-1810.

7.4. Windmill Hill

Magnetic flux data profiles for WH3 are presented (Figure 7.6A) and summarised (Table 7.6). $HARD_{-300mT}$, $SOFT_{-20mT}$ and SIRM flux profiles exhibit a distinct reduction post-1951. The pre-1951 phase demonstrates a gradual increase in the supply of 'soft' and remanence-carrying magnetic minerals from ~1893 to ~1929; whereas, the supply of 'hard' magnetic minerals is relatively constant throughout this phase. An overall decrease occurs from 1939 to 1941, followed by increases, particularly notable in the SIRM and $SOFT_{-20mT}$ profile at 1949, and from 1944 to 1949 in the $HARD_{-300mT}$ profile. The magnetic record appears to be dominated by soft minerals throughout the core.

Magnetic flux data are calculated by multiplying magnetic concentration data by sediment accumulation rates. Sediment accumulation rates for WH3 are notably lower in the upper 10 cm of the core, due to low density sediment, which may explain the pronounced magnetic reduction from 1951. Post-1951 flux data (presented separately, Figure 7.6B) demonstrate an overall steady decline from 1951 to present day. Periods of increased magnetic flux occur from 1961 to 1964 and from 1978 to 1989. A sharp reduction in supply of magnetic grains to the lake occur post-1993.

Pb, Zn, Cu and S flux profiles are presented (Figure 7.7) with summarised trends (Table 7.7). A shift from increased metal deposition pre-1951, to depleted metal supply post-1951, is notable. Close parallels are exhibited between Pb, Zn, Cu and S (Table 7.7), which also reflect trends observed in the magnetic flux profiles (Figure 7.3). The distinct peak in magnetic flux at 1944 to 1949 is only mirrored by the Cu flux profile, potentially, suggesting a pollution event from a site-specific Cu emitting pollution source.

Low metal flux is exhibited in pre-1906 sediment (Phase WHi), with a gradually increasing supply of metals to the lake post-1906 (WHii). Periods of maximum Zn deposition occur between 1927 and 1934, Pb reaches maximum supply at 1934, S at 1929 and Cu from 1939 to 1949 (Phase WHiii). Following these peaks, trace metals decline to notably lower post-1955 values (Phases WHiii and WHiv). Despite this reduction, there are periods of increased metal deposition during the mid-20^{th} century (~1959 to 1967) and during the 1980s (1978 to 1985) (Phase Whiii); however, the supply of metals post-1993 is further reduced (Phase WHiv).

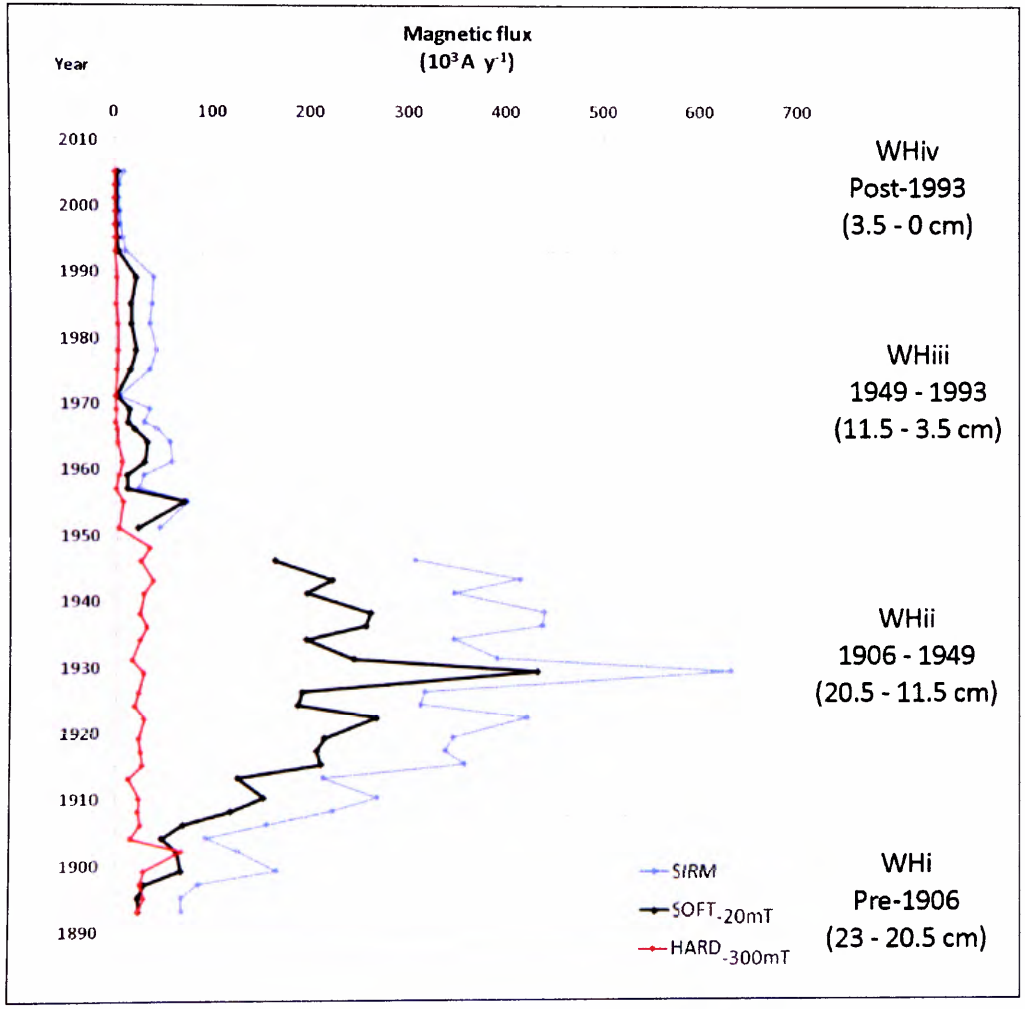

Table 7.6: Magnetic flux trends for WH3, relating to down-core divisions WHi to WHiv (corresponding to Figures 7.6A and 7.6B).

Phase	Time scale	Description of flux trend
WHiv	Post-1993	Notable decline in supply of magnetic grains.
WHiii	1949 to 1993	Maximum magnetic flux, notably higher for remanence carrying magnetic minerals and coarse ferrimagnetic minerals, opposed to canted antiferromagnetic and or fine ferrimagnetic grains, from 1944-1949. Sharp decline in magnetic flux post-1955, however, two distinct increases in the supply of magnetic grains from 1961-1964 and 1978-1990.
WHii	1906 to1949	Consistently high 'hard' (antiferromagnetic and or fine ferrimagnetic grains) minerals supplied to the lake throughout this phase, with gradually increasing remanence-carrying and coarse ferrimagnetic grains throughout the 20th century, with a peak in magnetic flux at 1929. An overall decline in supply of magnetic grains occurs post-1929 to 1944.
WHi	Pre-1906	Relatively low SIRM and $SOFT_{-20mT}$ flux and high values of $HARD_{-300mT}$

Figure 7.6A: Magnetic flux profiles for WH3: $HARD_{-300mT}$, $SOFT_{-20mT}$ and SIRM with superimposed phases WHi to WHiv (corresponding to Table 7.6). Sample 11-11.5 cm (1949) omitted due to prominent peak.

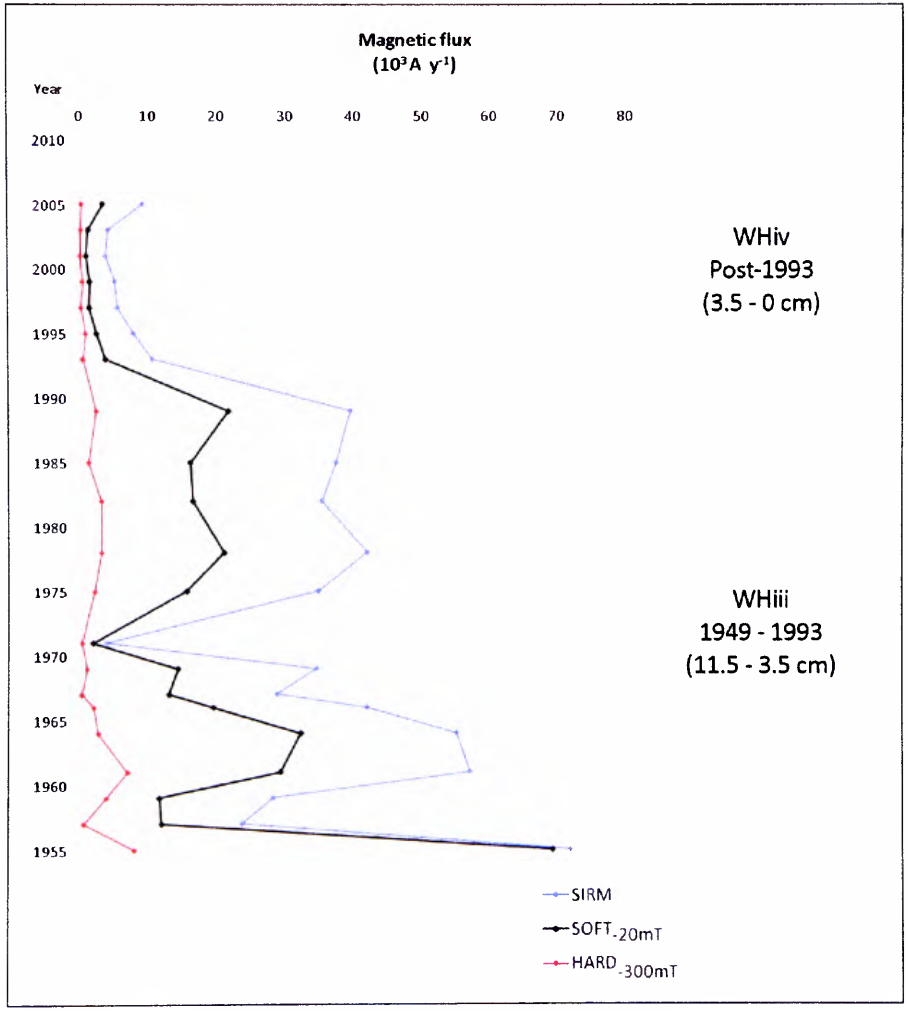

Figure 7.6B: Magnetic flux profiles for WH3 post-1955: $HARD_{-300mT}$, $SOFT_{-20mT}$ and SIRM with superimposed phases WHiii and WHiv (corresponding to Table 7.6).

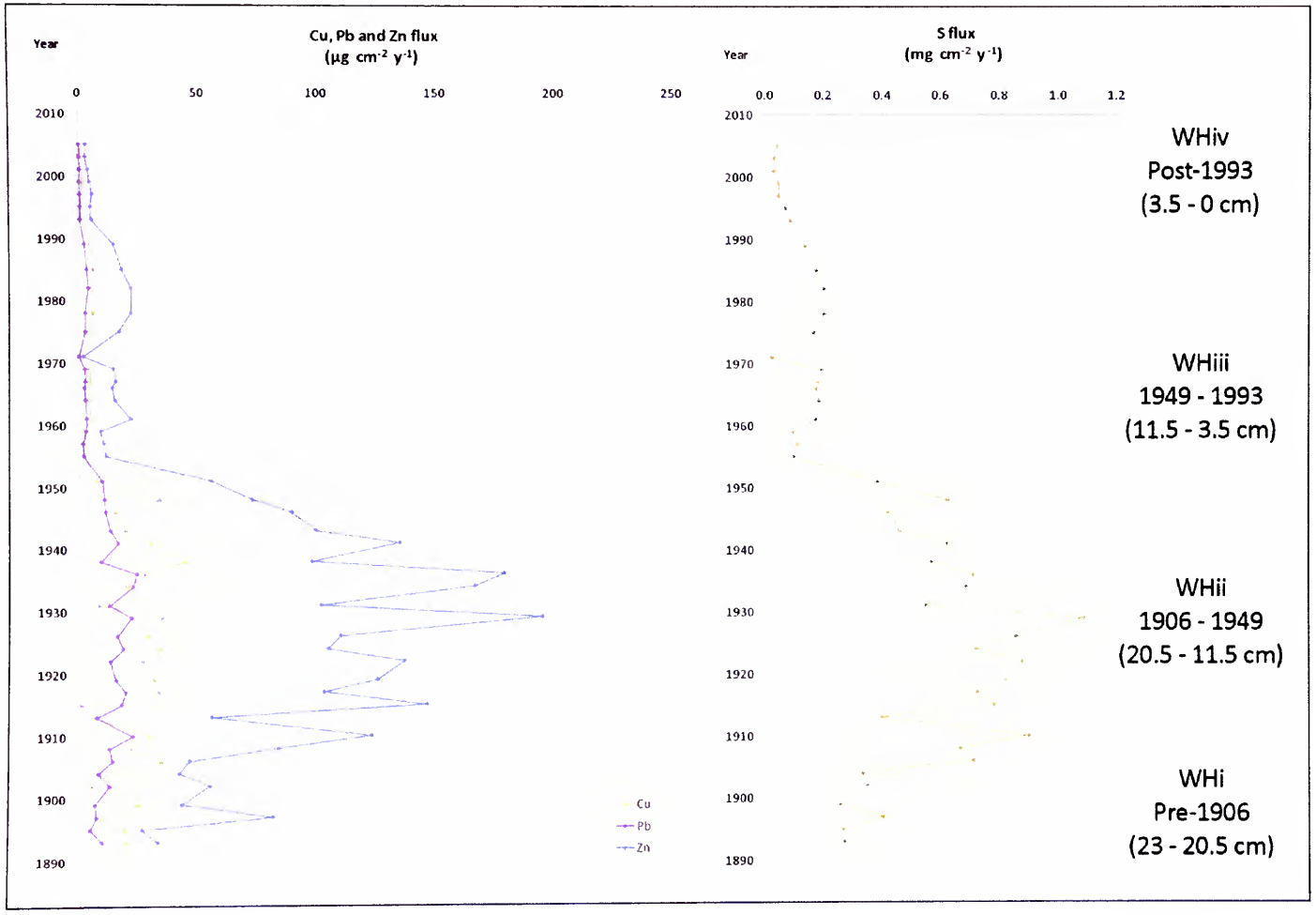

Figure 7.7: Total Pb, Zn, Cu and S flux profiles for WH3 with superimposed phases WHi to WHiv (corresponding to Table 7.7).

Table 7.7: Trace metal flux trends for WH3, relating to down-core divisions WHi to WHiv (corresponding to Figure 7.7).

Phase	Time scale	Description of metal flux trend
WHiv	Post-1993	Sharp decrease in metal flux.
WHiii	1949 to 1993	High Cu and S observed at 1949. Prominent trace metal decline post-1955, with periods of increased metal supply from 1959 to 1967 and 1978 to 1985.
WHii	1906 to1949	Overall increase in metal flux from start of the 20th century with maximum Pb, Cu, Zn and S flux occurring from 1929 to 1936.
WHi	Pre-1906	Relatively low metal flux.

7.5. Dogs Kennel Clump

Flux profiles for the magnetic parameters SIRM, $SOFT_{-20mT}$ and $HARD_{-300mT}$ (Figure 7.8 and Table 7.8) reveal trends in the supply of magnetic minerals to the DKC pond over time:

- DKi ~pre-1913: A gradual decrease in relatively low $SOFT_{-20mT}$, $HARD_{-300mT}$ and SIRM flux data from the base of the core (~1874) to ~1909, highlights a low and decreasing supply of magnetic grains to the pond during this period.
- DKii 1913 to 1962: From 1913, SIRM and $SOFT_{-20mT}$ flux profiles demonstrate an increase in the deposition of ferrimagnetic (coarse) and remanence-carrying minerals, until a distinct peak is reached at ~1934. The $HARD_{-300mT}$ flux profile exhibits a notable period of enhancement in the supply of canted antiferromagnetic grains and or fine (SSD) ferrimagnetic grains to the lake from ~1916 to ~1934. A notable decrease in magnetic flux occurs from 1937 to 1939, after which, the supply of magnetic grains steeply increases throughout the 1940s, and the mid-20th century, with notable periods of enhancement from the late 1940s to 1953. Pronounced peaks of maximum flux are exhibited at 1962 in the $SOFT_{-20mT}$, $HARD_{-300mT}$ and SIRM flux profiles.
- DKiii 1962 to 1974: A smaller flux peak is observed at 1969-1970, followed by post-1970 decreases.
- DKiv post-1974: Further reductions occur. Increases in 'hard' magnetic minerals identified in the concentration profiles (Section 6.5.1., Figure 6.14) are not reflected in the $HARD_{-300mT}$ flux profile.

Flux data for Pb, Zn and S (Figure 7.9 and Table 7.9) are presented for DKC. The reconstruction of a Cu flux profile is perturbed due to negative Cu concentration data. Close parallels are observed between the trace metal deposition profiles.

- DKi pre-1913: Relatively low Zn and Pb flux data exhibited from ~1874 to ~1913. S exhibits relatively low ~pre-1890 values, however, a notable enhancement in S deposition occurs from ~1897, with a period of increases S supply from ~1899 to 1909.
- DKii 1913 to 1962: Slightly later than S, enhancement in Zn and Pb occurs ~post-1913. Overall, trace metal flux increases throughout the 20th century, and

four distinct peaks are identified, which show similarities with the features identified in the magnetic flux profiles:

  - S and Pb flux peaks at ~1918;
  - period of increased Pb Zn and S flux from ~1930 to ~1934;
  - increased flux during 1948 to 1953, particularly prominent in the Zn flux profile, with relatively smaller peaks observed for Pb and S; and
  - prominent 1960 to 1963 flux peak, displaying maximum Zn, Pb and S flux values.

- DKiii 1962 to 1974: Trace metal flux profiles exhibit prominent decreases. A relatively small flux peak is observed at 1972 in the S and Pb flux profiles.
- DKiv post-1974: Further reductions in trace metals continue to present day.

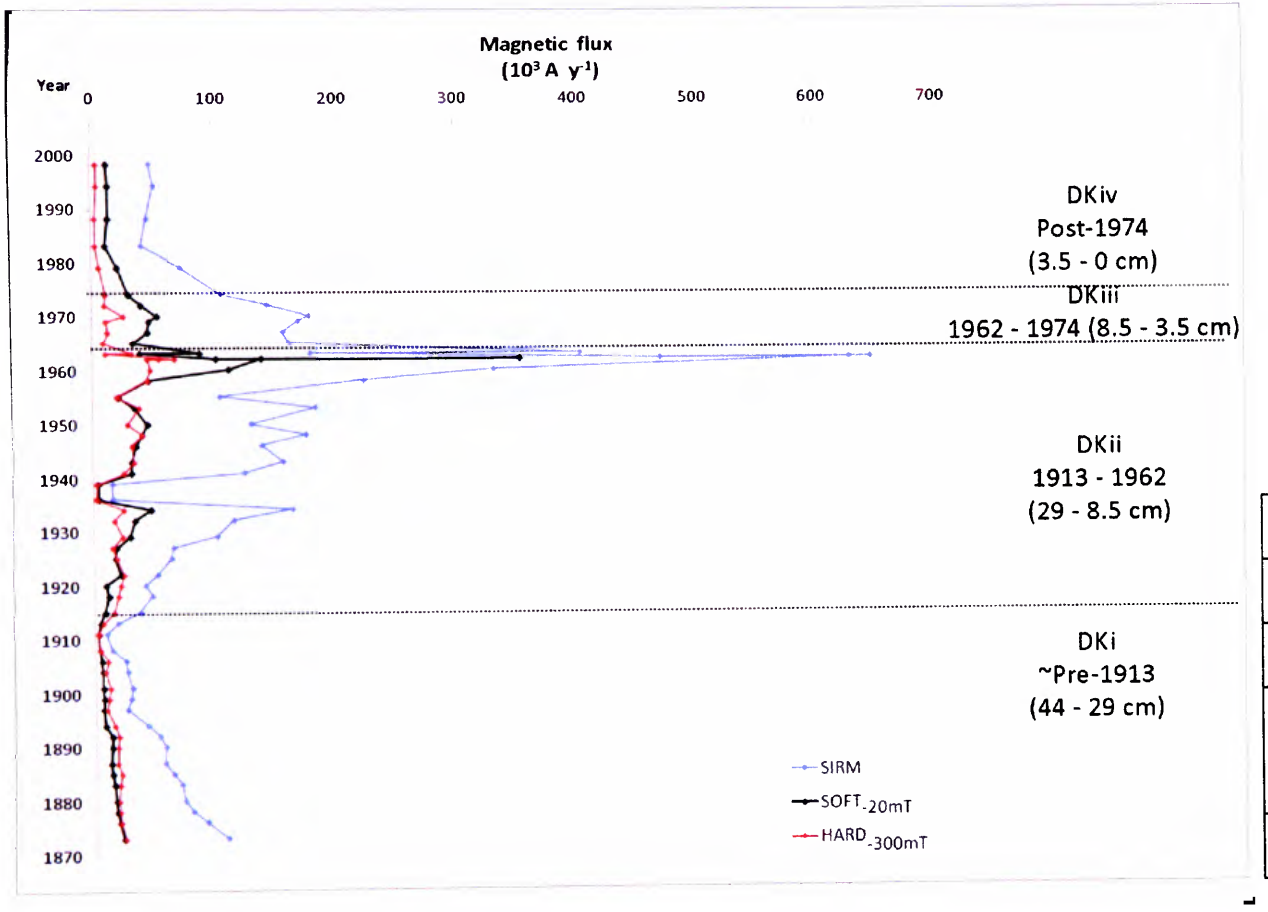

Table 7.8: Magnetic flux trends for DKC, relating to down-core divisions DKi to DKiv (corresponding to Figure 7.8).

Phase	Time scale	Description of magnetic flux trend
DKiv	Post-1974	Further reduction in magnetic flux.
DKiii	1962 to 1974	Lower magnetic flux compared to phase DKii, with a 1969 to 1970 magnetic peak.
DKii	1913 to 1962	Increase in supply of magnetic grains from 1913 to 1934, with further increases post-1940 and prominent 1962 peaks.
DKi	~Pre-1913	Relatively low magnetic flux.

Figure 7.8: Magnetic flux profiles for DKC: $HARD_{-300mT}$, $SOFT_{-20mT}$ and SIRM with superimposed phases DKi to DKiv (corresponding to Table 7.8).

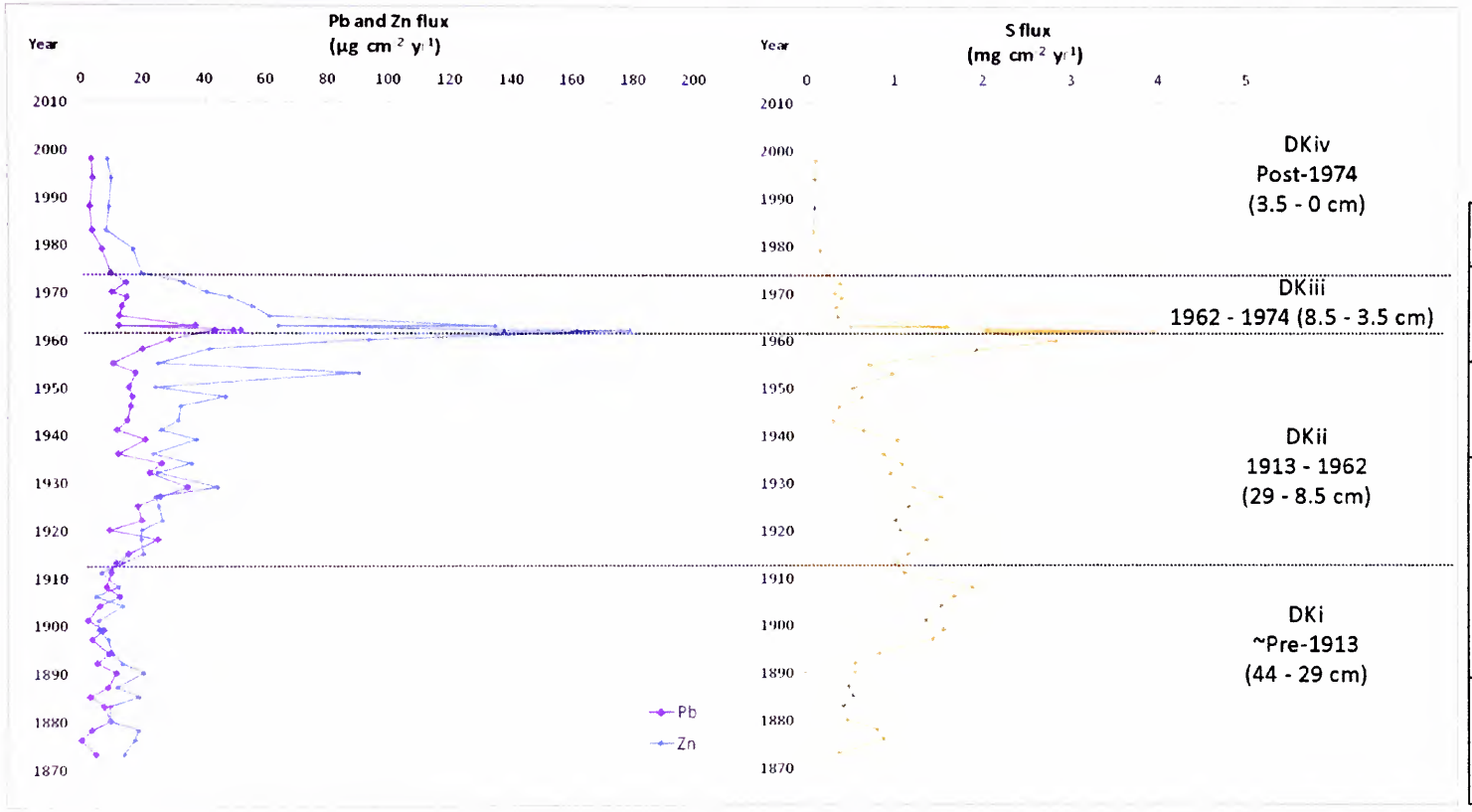

Figure 7.9: Total Pb, Zn and S flux profiles for DKC with superimposed phases DKi to DKiv (corresponding to Table 7.9).

Table 7.9: Trace metal flux trends for DKC, relating to down-core divisions DKi to DKiv (corresponding to Figure 7.9).

Phase	Time scale	Description of metal flux trend
DKiv	Post-1974	Further trace metal decreases, continuing to present day.
DKiii	1962 to 1974	Prominent reduction in trace metals post-1963.
DKii	1913 to 1962	Pb and Zn elevation with metal increases throughout the 20th century with peaks at ~1930 to 1934, ~1948 to 1953 and pronounced 1960 to 1963 values.
DKi	~Pre-1913	Relatively low trace metal flux with increases from ~1899 to 1909.

7.6. Oglet

Down-core zones in OG applied to concentration/depth profiles (Chapter 6) are superimposed on the flux profiles to aid comparison between concentration and flux data. However, conversion of concentration data to flux reveals the influence of changing sedimentation rates on the proxy pollution record. Flux profiles do not mirror concentration trends and, therefore, phase 'OGiii' is divided into 'OGiiiA' and 'OGiiiB' and superimposed on the flux profiles.

Magnetic flux profiles are presented (Figure 7.10 and Table 7.10). The OG magnetic record is dominated by 'soft' magnetic minerals with a lower contribution of 'hard' grains. Peaks in magnetic flux correspond to increases exhibited by the original magnetic concentration data (Figures 6.22), however, the trends are not closely mirrored. For example, the 1960 to 1970 enhancement is less pronounced in the flux profiles compared to the concentration profiles; whereas, the post-1993 increases in magnetic flux are more prominent compared to the concentration trends.

The Zn, Pb, S and Cu flux profiles (Figure 7.11) demonstrate the supply of metals to the Oglet pond over time and, therefore, reveal increased post-1980 trends, which are not apparent in the original concentration profiles (Figure 6.27), due to a post-1980 shift to higher sediment accumulation rates. Close parallels are exhibited between the trace metal flux profiles (Figure 7.11, Table 7.11).

The main features in the OG trace metal flux profiles are:

- 1949 to 1951 Pb, S, Cu and Zn peak;
- 1970 to 1966 Pb and Zn peak, not mirrored in the Cu or S profiles;
- prominent trace metal increases post-1985 (OGiiiB); and
- further, post-1991 Pb, Zn, Cu and S increases (OGiiiA), highlighting a recent, and continually increasing supply of trace metals to the OG pond post-1980.

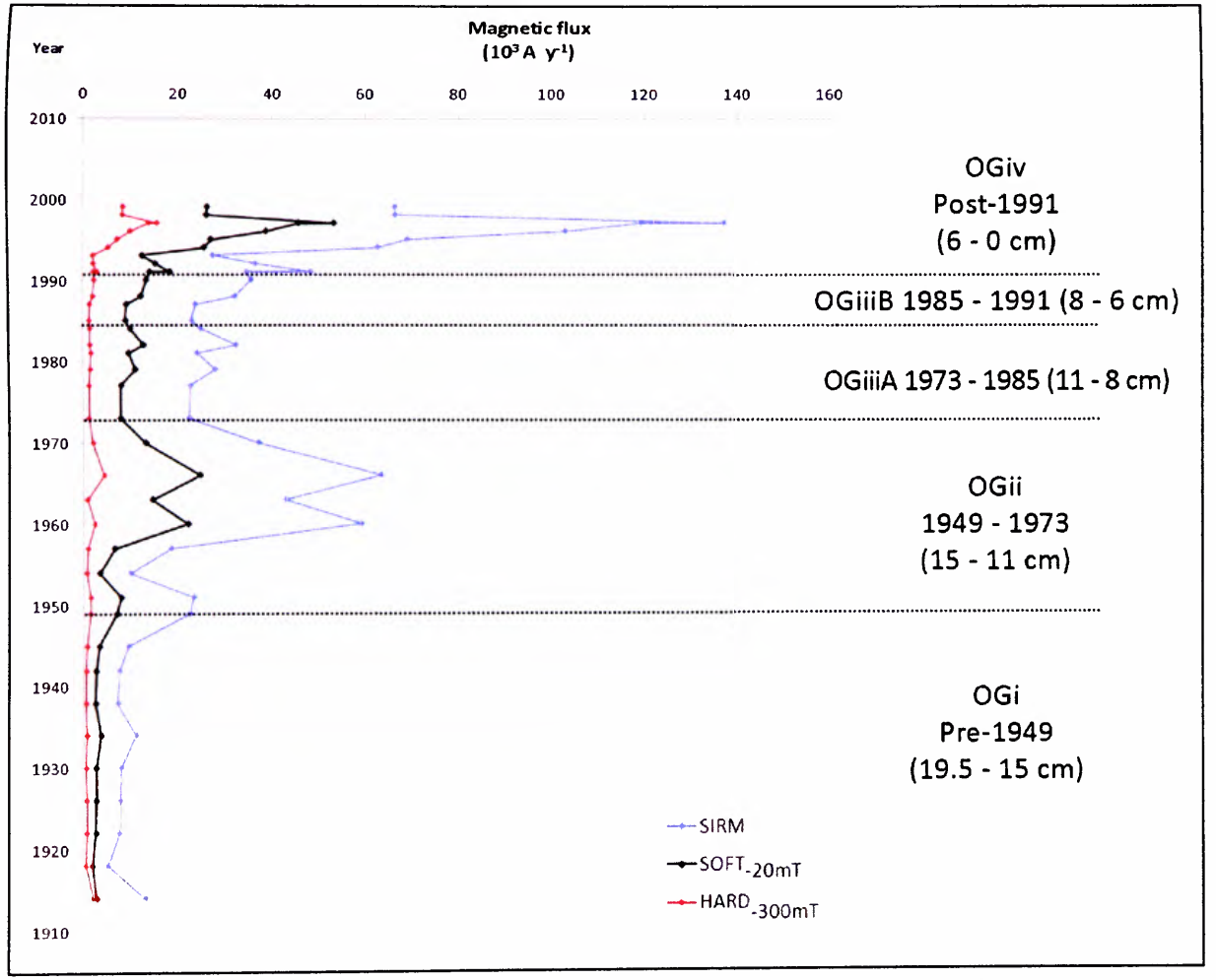

Figure 7.10: Magnetic flux profiles for OG: $HARD_{-300mT}$, $SOFT_{-20mT}$ and SIRM with superimposed phases OGi to OGiv (corresponding to Table 7.10).

Table 7.10: Magnetic flux trends for OG, relating to down-core divisions OGi to OGiv (corresponding to Figure 7.10).

Phase	Timescale	Description of trends
OGiv	Post-1991	A second, more recent, increase in supply of magnetic grains to the lake occurs post-1994; whereby, maximum values are reached at 1997, followed by a decrease in flux at the sediment-surface
OGiiiB	1985 to 1991	Increase in magnetic flux during the late 1980s and early 1990s.
OGiiiA	1973 to 1985	Relatively lower flux values occur throughout the 1970s with a subsequent small flux peak, less pronounced in the $HARD_{-300mT}$ profile, from 1979 to 1982.
OGii	1949 to 1973	Increase in the supply of magnetic grains to the lake post-1949, with distinct enhancement from 1960 to 1970
OGi	Pre-1949	Relatively low magnetic flux.

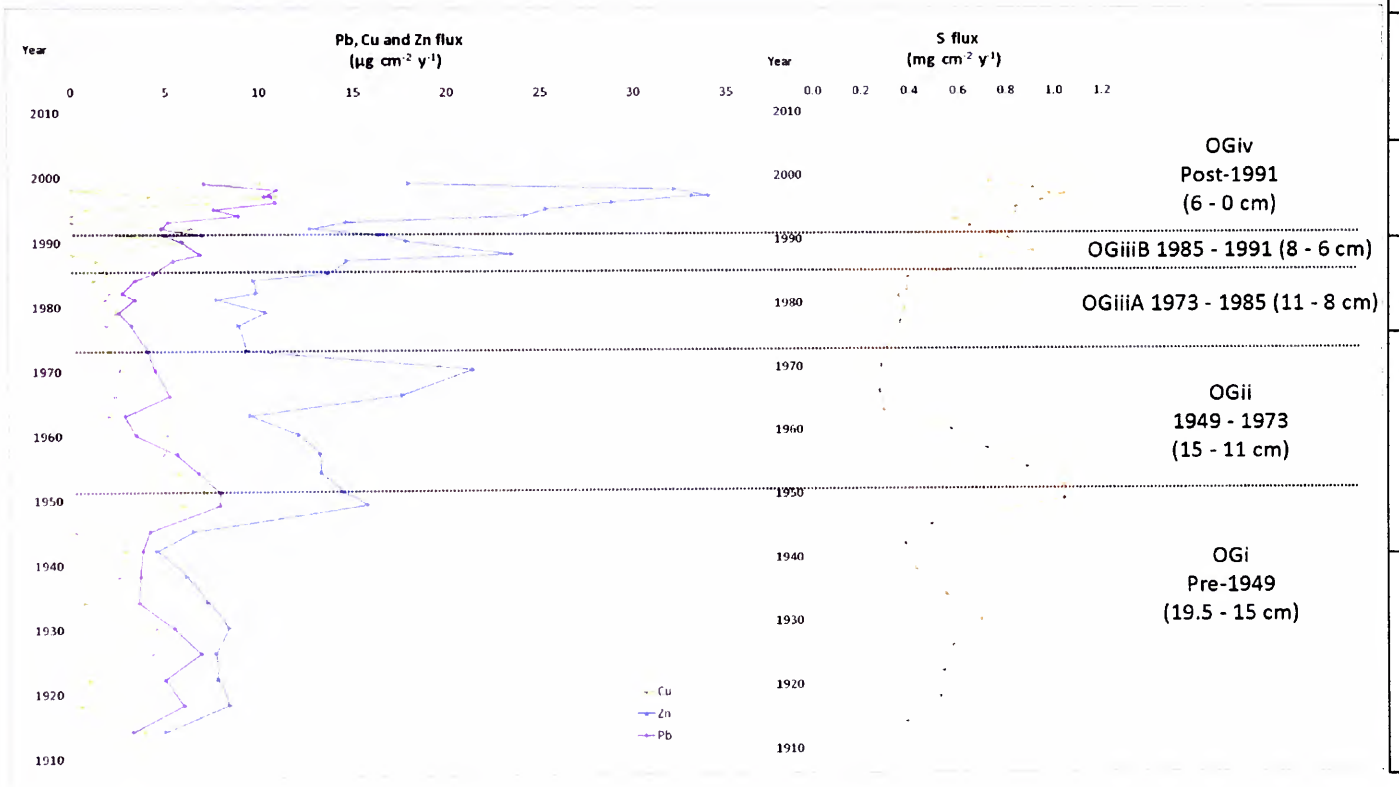

Figure 7.11: Total Pb, Zn, Cu and S flux profiles for OG with superimposed phases OGi to OGiv (corresponding to Table 7.11).

Table 7.11: Pb, Zn, Cu and S flux trends in OG relating to down-core divisions OGi to OGiv (corresponding to Figure 7.11).

Phase	Time scale	Description of metal flux trend
OGiv	Post-1991	Further increase in the supply of trace metals post-1991, with maximum flux values reached in this recent peak.
OGiiiB	1985 to 1991	Prominent trace metal increases from ~1985 to 1990.
OGiiiA	1973 to 1985	The supply of Zn and Pb declines, continuing into the 1980s
OGii	1949 to 1973	Distinct Pb, S, Cu and Zn peaks at 1949-1951. S and Cu decreases throughout the 1960s and 1970s; however, Zn exhibits an increase post-1960 with a peak at 1970, mirrored by Pb increases throughout the 1960s.
OGi	Pre-1949	Relatively low pre-1946 Zn and Cu. Pb, S and Br demonstrate relatively high pre-1949 trends with a notable increase from 1927-1931. A notable enhancement in trace metals occur post-1946.

7.7. Chapter summary

Urban flux profiles demonstrate the temporal supply of trace metals and magnetic grains to Daresbury Delph, Windmill Hill, Dogs Kennel Clump and Oglet ponds. Daresbury Delph Pond exhibits a depositional history spanning >250 years, revealing the anthropogenic component of 'total' trace metal flux via normalisation by pre-1800 values. Close parallels are observed between 'total' and 'anthropogenic' flux profiles in the DDP core. As pre-1800 data are not available for DKC, WH or OG ponds, due to younger stratigraphies retrieved from these sites, anthropogenic corrections are not applied to the flux profiles from these ponds; however, WH, OG and DKC, exhibit high-resolution post-1900 deposition histories. Trends in SIRM, $HARD_{-300mT}$, $SOFT_{-20mT}$, Pb, Zn, Cu and S were presented and described for all sites, accompanied by SCP flux profiles from DDP.

DDP demonstrates trace metal enhancement from ~1780 to ~1807, with corresponding magnetic and trace metal elevation ~post-1832. Trace metal and magnetic flux values increase throughout the 20th century with observed metal flux peaks at ~1910 to 1920, an increase in trace metals throughout the 1930s to the 1960s and a prominent magnetic flux increase from 1954 to 1963. Pb, Cu and Zn flux decline post-1960, S declines post-1980. Pb and magnetic flux values increase post-1992.

WH exhibits increasing magnetic flux values from 1904, with maximum magnetic flux values reached during the mid-20th century. Trace metals also increase from the early 20th century, reaching maximum flux peaks from 1929 to 1936. Trace metal flux declines ~post-1940 with a slightly later post-1950 decrease in magnetic flux. Further post-1990 magnetic and trace metal flux declines are also noted.

Trace metal and magnetic enhancement occurs ~post-1913 in the DKC profile, which exhibits peaks during the 1930s and from 1948 to 1953 and 1960 to 1963. Post-1963 trace metal and magnetic flux decreases are observed.

OG exhibits relatively low ~pre-1946 Cu, Zn and magnetic flux values, with higher S and Pb values observed. Notable trace metal increases occur post-1949, with observed peaks from 1949-1951, and sustained high values until 1960. Magnetic flux profiles demonstrate a distinct magnetic enhancement from 1960 to 1966. Trace metal flux declines post-1960, with a slightly later decrease in magnetic flux, post-1970. Increases in the supply of magnetic grains and trace metals to the pond are observed post-1985, with maximum post-1994 trace metal and magnetic flux values.

8. CHAPTER EIGHT: CROSS-REGIONAL POLLUTION PROFILES

8.1. Chapter Overview

A cross-regional pollution signal for the lower Mersey region (LMR) is presented, constructed from 'local' urban pollution profiles obtained from DDP, WH, DKC and OG.

8.2. Introduction

By combining local pollution signals recorded in the DDP, WH, DKC and OG ponds, a cross-regional signal for the LMR, which encompasses the borough of Halton, can be reconstructed (Figure 8.1). OG and DKC provide archives for the northwest LMR, whereas, the pollution archives obtained from Windmill Hill are representative of pollution experienced in Runcorn, and Daresbury Delph captures the pollution signal for the southeast LMR. As well as spatial variation between the sites, the temporal range of sediment records captured at each pond also varies. The LMR cross-regional signal is comprised of post-1750 data obtained from DDP, representing the longest time period achieved in the urban stratigraphies; complimented by high-resolution archives of the 20th century from WH and DKC. Also, OG provides a high-resolution 80-year history, which is particularly detailed in post-1980 sediment (Figure 8.1).

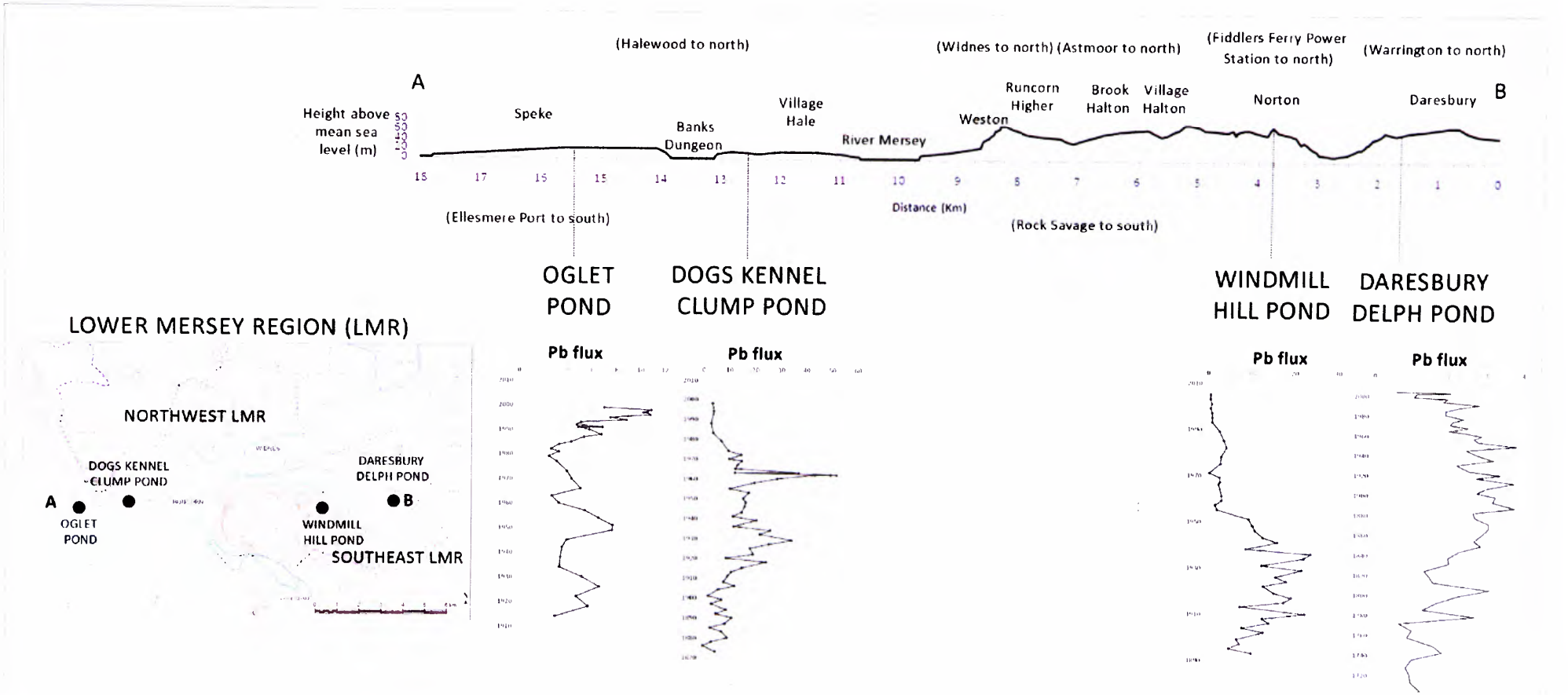

Figure 8.1: Topographical cross-section of the lower Mersey region, from A: Speke (SJ 342100, 382000) to B: Daresbury (SJ 359000, 382000) highlighting locations of the urban ponds: Daresbury Delph, Windmill Hill, Dogs Kennel Clump and Oglet. Pb flux profiles for each site are presented, accompanied by the time scale each stratigraphy represents, to demonstrate how the local signals form a cross-regional history. Map inset shows location of pond sites and points A and B of transect. Reproduced from the 2007 Ordnance Survey Strategi 1:925915 map with the permission of Ordnance Survey on behalf of The Controller of Her Majesty's Stationery Office © Crown Copyright Edge Hill University, Ormskirk, Lancashire licence number: ED100020392.

Magnetic concentration profiles obtained from the four urban pond sites, are shown (Figures 8.2 and 8.3). However, due to the different environmental histories of the four ponds, and varying sedimentation accumulation rates, trace metal and magnetic flux profiles are presented to infer a depositional history of pollution throughout the LMR. Flux profiles are displayed:

(i) on the same scale axis to assess how flux values range across the LMR (Figures 8.6, 8.12, 8.13, 8.14 and 8.15) and

(ii) as individual site profiles, presented alongside each other, in order of location across the LMR (west to east) to demonstrate the changing deposition patterns at each site, due to variation in flux values recorded at the four sites (Figures 8.5A, 8.5B, 8.8, 8.9, 8.10 and 8.11).

Superimposed over the graphs are divisions of the cross-regional signal. The site-specific zones applied in Chapters 6 and 7 are not included, in order to assess *regional*, rather than *local* pollution histories. The cross-regional phases (Ri to Rv) have been applied after careful consideration of the four local proxy pollution signals obtained from DDP, WH, DKC and OG, which have been combined to provide evidence for pollution deposition across the LMR (Table 8.1).

Table 8.1: Phases of proxy pollution characteristics identified in the cross-regional signal for the LMR.

Phase	Timescale	Proxy pollution trends
Rv	Post-1980	Phase highlighted in the DDP and OG profiles, which demonstrate post-1980 increases in pollution proxies.
Riv	1950 to 1980	Further proxy pollution increases at DDP, DKC and OG, with corresponding shifts in the sediment record at WH.
Riii	1900 to 1950	A period of magnetic and trace metal elevation, a corresponding regional feature exhibited by DDP, WH, DKC and OG.
Rii	1830 to 1900	A phase of initial proxy pollution increases recorded in DDP.
Ri	~pre-1830	Representing relatively low proxy pollution levels, identified in the extensive (i.e. post-1700) DDP sediment record.

8.3. Cross-regional proxy pollution concentration characteristics

The cross-regional magnetic concentration signal is presented via χ_{LF} (Figure 8.2) and χ_{ARM} profiles (Figure 8.3) on a linear date axis to demonstrate concentration of total ferrimagnetic and fine ferrimagnetic grains, from DDP, WH, DKC and OG. The main regional features are detailed in Table 8.2. Increases in magnetic concentration occur from 1900 in the DKC, WH and DDP profiles, with a steadily increasing trends continuing throughout the first half of the 20th century, exhibited in all four ponds. Mid-20th century

peaks are also mirrored between the sites, with prominent χ_{LF} peaks at 1958 in the DDP core, 1949 in WH, 1963 in DKC and at 1966 exhibited by OG. Subsequent declines occur, however, DDP and OG demonstrate increases post-1975 and post-1980, respectively.

Figures 8.2 and 8.3 also demonstrate how the magnetisation of sediments varies between the four sites. Lower magnetic concentrations are exhibited by DDP, compared to OG, WH and DKC. WH exhibits the highest concentrations of ferrimagnetic grains in phase Riii (1900-1950). Post-1950, (phases Riv and Rv), magnetic concentration declines at WH, and DKC exhibits the highest magnetic concentration values of the four sites in this phase.

The cross-regional χ_{ARM} profiles highlight a steady increase in fine (SSD) ferrimagnetic gains post-1900, as revealed by DDP. Further enhancement in the contribution of fine magnetic grains to the regional signal is observed post-1978 at DDP, mirrored by χ_{ARM} increases, proportionately higher than χ_{LF} increases, at DKC and OG post-1980 (phase Rv). However, the presence of a fine-grained magnetic signal is not as distinct in the WH profile, which exhibits very similar χ_{LF} and χ_{ARM} trends. The pronounced χ_{ARM} elevation exhibited by DKC highlights a notable contribution of SSD grains at this site post-1980.

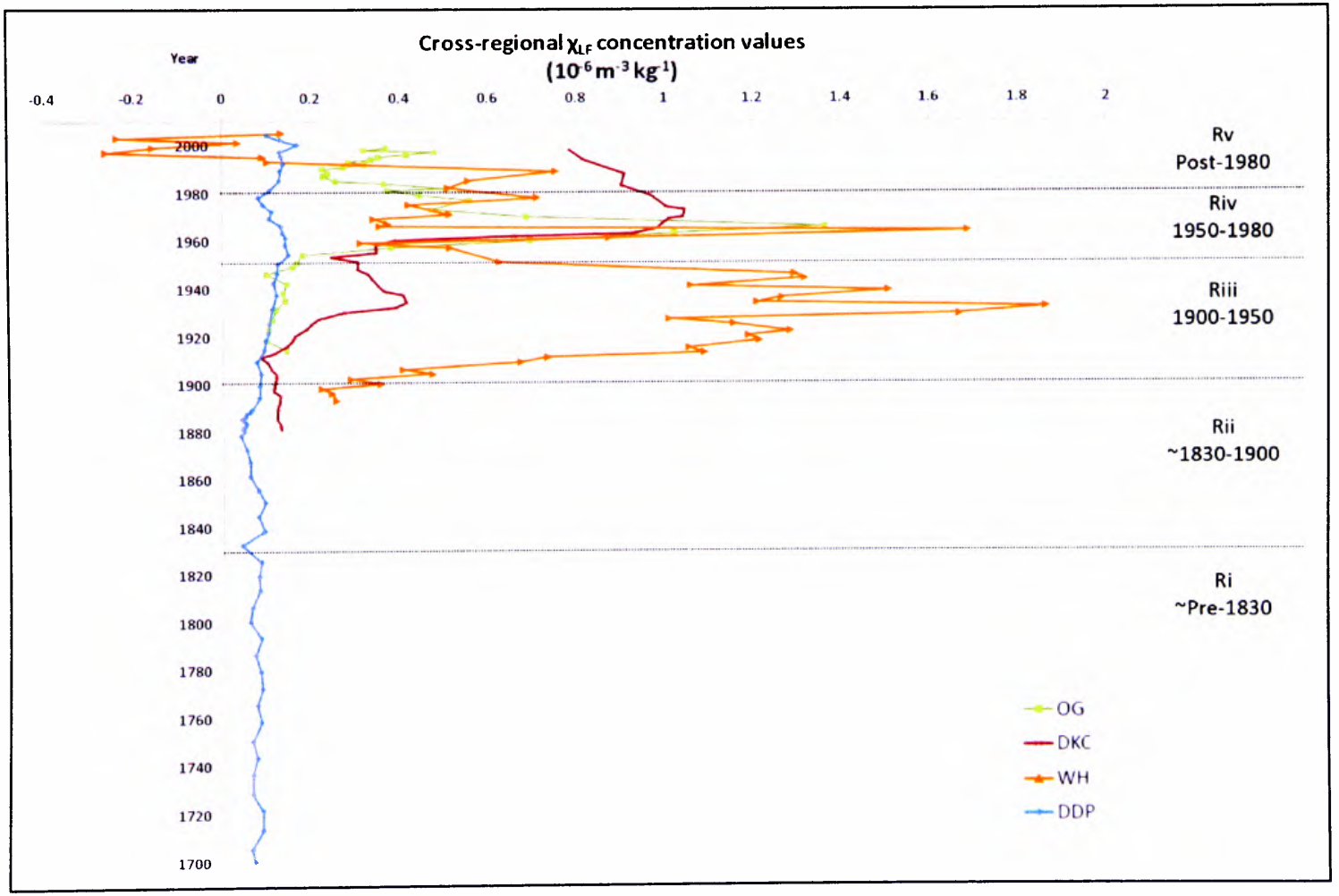

Figure 8.2: Cross-regional χ_{LF} concentration signal: Down-core profiles from OG, DKC, WH and DDP with superimposed regional phases Ri to Rv (corresponding to Table 8.2).

Table 8.2: Cross-regional χ_{LF} concentration signal relating to regional phases Ri to Rv (corresponding to Figure 8.2).

Phase	Timescale	Description of magnetic concentration trend
Rv	Post-1980	OG exhibits a high-resolution signal for the 1980s, which demonstrates a distinct peak at 1982, after which χ_{LF} declines. This is also reflected in the DKC core. OG and DDP profiles exhibit post-1990 increases, with distinct peaks at 1997 and 1995, respectively. DKC and WH χ_{LF} values, however, decline post-1990. A prominent 2002 χ_{LF} peak is also exhibited in the DDP core.
Riv	1950 to 1980	Prominent peaks from 1960 to 1972 in the OG profile, 1962 to 1972 in the DKC profile, and at 1964 for WH. DDP exhibits a decrease in magnetic concentration throughout the 1960s; however, values are still notably high until 1969. Post-1970 decreases in χ_{LF} occur in the OG and DDP profiles. This trend is not mirrored in the WH profile and high post-1970 DKC concentrations are sustained. However, corresponding magnetic concentration peaks are observed at 1977 in the OG profile, 1978 in WH, also DDP exhibits a peak at 1975.
Riii	1900 to 1950	Post-1900 there is a further enhancement in the magnetic signal, whereby steep increases are exhibited by the DDP core. DKC and WH cores contribute to the regional signal post-1900, displaying relatively low and steadily increasing values. A steep increase in magnetic concentration occurs post-1920 in the DDP, DKC and WH cores, which coincides with the contribution of the OG profile to the regional signal, which demonstrates a steadily increasing trend. A clear peak in magnetic concentration is evident in the DKC core from 1932 to 1937, mirrored in the WH core as a distinct peak at 1932. Mid-20th century increases are exhibited throughout the four profiles. In WH a distinct magnetic peak occurs from 1949 to 1957. DDP also exhibits a prominent peak at 1954. DKC and OG demonstrate increases in χ_{LF} from 1955 and 1954 respectively.
Rii	~1830 to 1900	Magnetic increases occur from ~1832, which steadily increase throughout this phase at DDP.
Ri	~Pre-1830	A small peak from ~1793 to 1807 is observed, following relatively low ~pre-1800 magnetic concentration data exhibited by DDP. Magnetic concentration decreases until an increase in χ_{LF} at ~1832.

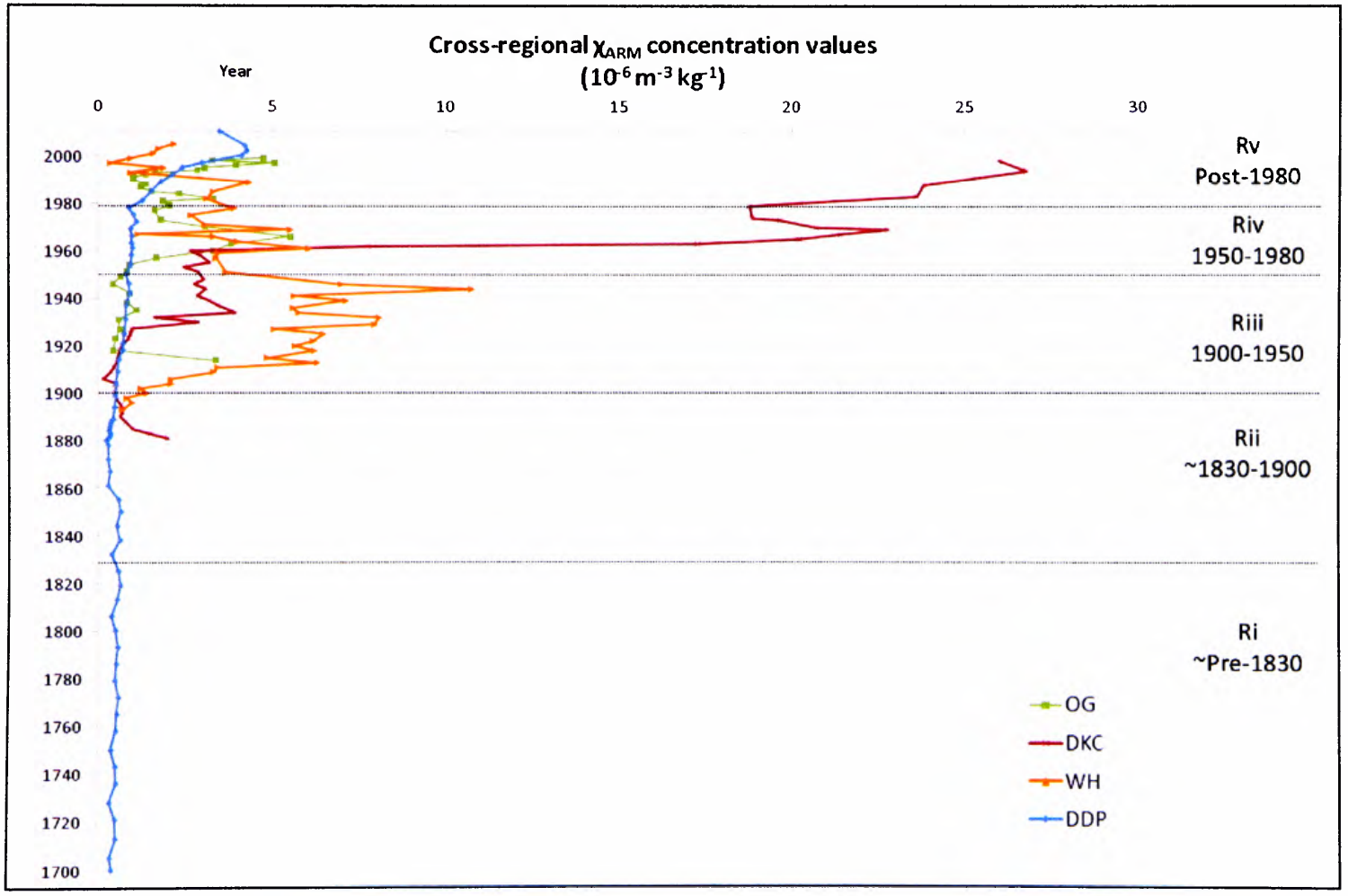

Figure 8.3: Cross-regional χ_{ARM} concentration signal: Down-core profiles from OG, DKC, WH and DDP with superimposed regional phases Ri to Rv.

Inter-site comparison of the recorded minimum, maximum and mean χ_{LF} and trace metal concentrations (Table 8.3 and Figure 8.4) reveals higher Pb, S and Br concentrations experienced in the OG core, with higher Ni concentrations also experienced at OG, compared to DKC. Ni concentrations are only notably high in the OG and DKC profile. This suggests higher Ni values are experienced in the northwest LMR, opposed to the southeast LMR. Copper concentrations are not detectable for the majority of samples in the DKC core (highlighted as zero values). Higher Zn and Cu concentrations are exhibited at WH, which also exhibits the highest χ_{LF} values, due to the observed pronounced 1949 peak. Figure 8.4 reveals similar mean Pb concentrations (139.946 to 198.171 µg/g) exhibited throughout the region. Relatively low Zn and Br values are recorded in the DDP sediments, compared to the other sites. Pb and Cu values are consistent with the other sites and mean S concentrations at the DDP site are higher than at WH and DKC.

Table 8.3: Mean, minimum and maximum χ_{LF}, Pb, Zn, Cu, S, Br and Ni concentrations recorded in OG, DKC, WH and DDP (* indicates several zero values recorded throughout the core).

Pollution proxy		OG Value	Year	DKC Value	Year	WH Value	Year	DDP* Value	Year
χ_{LF} (10^{-9} m^3 kg^{-1})	Mean	349.62		486.241		907.138		88.028	
	Minimum	98.266	1949	85.266	1913	-259.367	1997	-863.309	2005
	Maximum	1363.225	1970	1045.355	1974	7560.878	1949	169.556	2000
Pb (µg/g)	Mean	198.171		139.946		163.722		148.565	
	Minimum	123.153	1914	10.016	1876	6.746	1904	37.138	1538 (~pre-1744)
	Maximum	495.634	1970	333.256	1972	351.074	1989	282.273	1950
Zn (µg/g)	Mean	538.737		365.588		1037.961		292.147	
	Minimum	195.191	1935	23.678	1906	183.409	1898	48.334	1729
	Maximum	1726.768	1966	1164.329	1965	1709.340	1939	670.671	2004
Cu (µg/g)	Mean	112.666		20.502		227.496		157.195	
	Minimum	0.000	1944	0.000	*	12.710	1920	21.288	1736
	Maximum	275.601	1960	185.307	1967	674.597	1929	351.387	2004
S (mg/g)	Mean	21.935		6.744		8.512		14.629	
	Minimum	14.805	1996	1.486	1847	1.425	1893	3.1154	2005
	Maximum	31.368	1960	13.993	1911	14.285	1978	31.817	1867
Br (µg/g)	Mean	44.058		20.817		12.736		14.867	
	Minimum	9.688	1923	0.000	*	0.000	*	0.000	*
	Maximum	82.388	1973	58.656	1988	48.999	2003	44.446	1838
Ni (µg/g)	Mean	135.063		428.07		*		*	
	Minimum	0.000	*	11.880	1847	*		*	
	Maximum	352.400	1914	675.326	1930	*		*	

* Includes pre-1900 values.

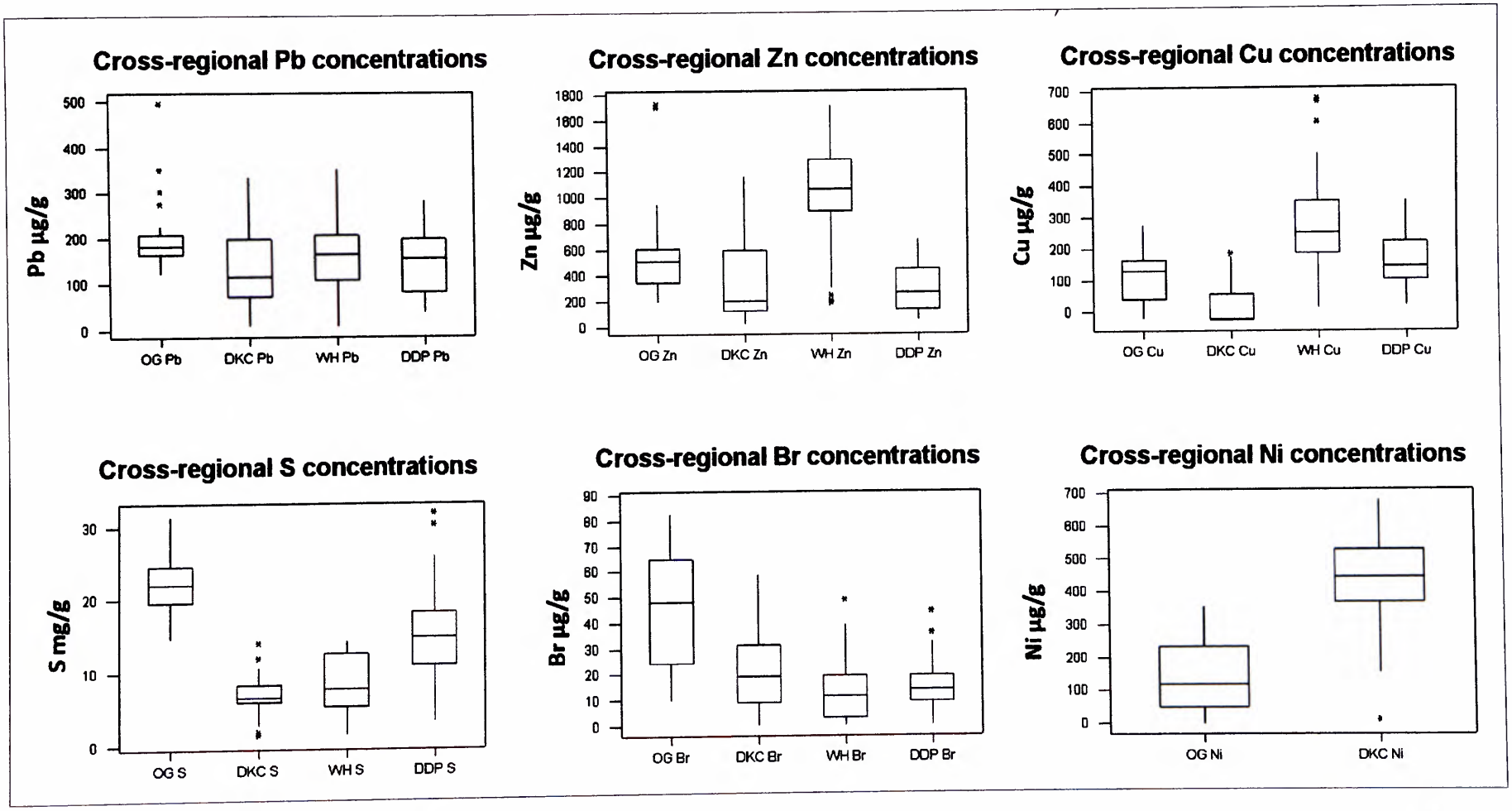

Figure 8.4: Cross-regional Pb, Zn, Cu, S, Br and Ni concentrations recorded in OG (n=38), DKC (n=42), WH (n=50) and DDP (n=70) sediments presented as box and whisker plots (* indicates outlier).

8.4. Cross-regional proxy pollution flux signal

Trace metal and magnetic flux profiles, obtained from the four urban ponds within the LMR, provide an assessment of the deposition of pollution at each pond over time. The pre-1900 magnetic and trace metal flux signal is represented in the BDD1 core (from DDP), highlighting the pollution signal recorded in the southeast LMR; however, flux data from WH, DKC and OG ponds contribute to the 20th century signal, providing a spatial dimension to the historical deposition of pollution across the LMR.

A post-1700 depositional signal of total magnetic grains is shown via SIRM flux profiles from OG, DKC, WH and DDP (Figure 8.5A and Table 8.4). A high-resolution, post-1900 depositional history of magnetic grains in the LMR is also presented to assess 20th century trends (Figures 8.5B, 8.6 and Table 8.4).

DDP exhibits the lowest magnetic flux values of the four sites (Figure 8.6). WH demonstrates the highest magnetic flux values throughout phase Riii (1900 to 1950), however post-1950, magnetic flux at WH decreases, and the highest flux values are recorded at DKC. Post-1980 declines occur at DKC and WH, with the highest post-1980 (phase Rv) flux values exhibited at OG, which highlight a recent increasing trend (Figure 8.6).

Lead, Zn, Cu and S flux profiles obtained from DDP are presented with superimposed regional phases (Ri to Rv) to demonstrate the supply of trace metals in Halton since the 18th century (Figure 8.7, Table 8.5). Due to the variability in flux values recorded at each site, Pb (Figure 8.8 and Table 8.6), Zn (Figure 8.9 and Table 8.7), Cu (Figure 8.10 and Table 8.8) and S (Figure 8.11 and Table 8.9) flux trends are presented on individual axis to show how deposition of these metals has changed at each site. The cross-regional Cu flux signal is comprised of data from DDP, WH and OG only, as calculation of Cu flux for the DKC profile is perturbed due to zero Cu concentration values. Cross-regional post-1900 trace metal flux profiles are also presented (with superimposed phases Riii to Rv) to demonstrate the spatial and temporal variability of Pb (Figure 8.12), Zn (Figure 8.13), Cu (Figure 8.14) and S (Figure 8.15) deposited across the LMR.

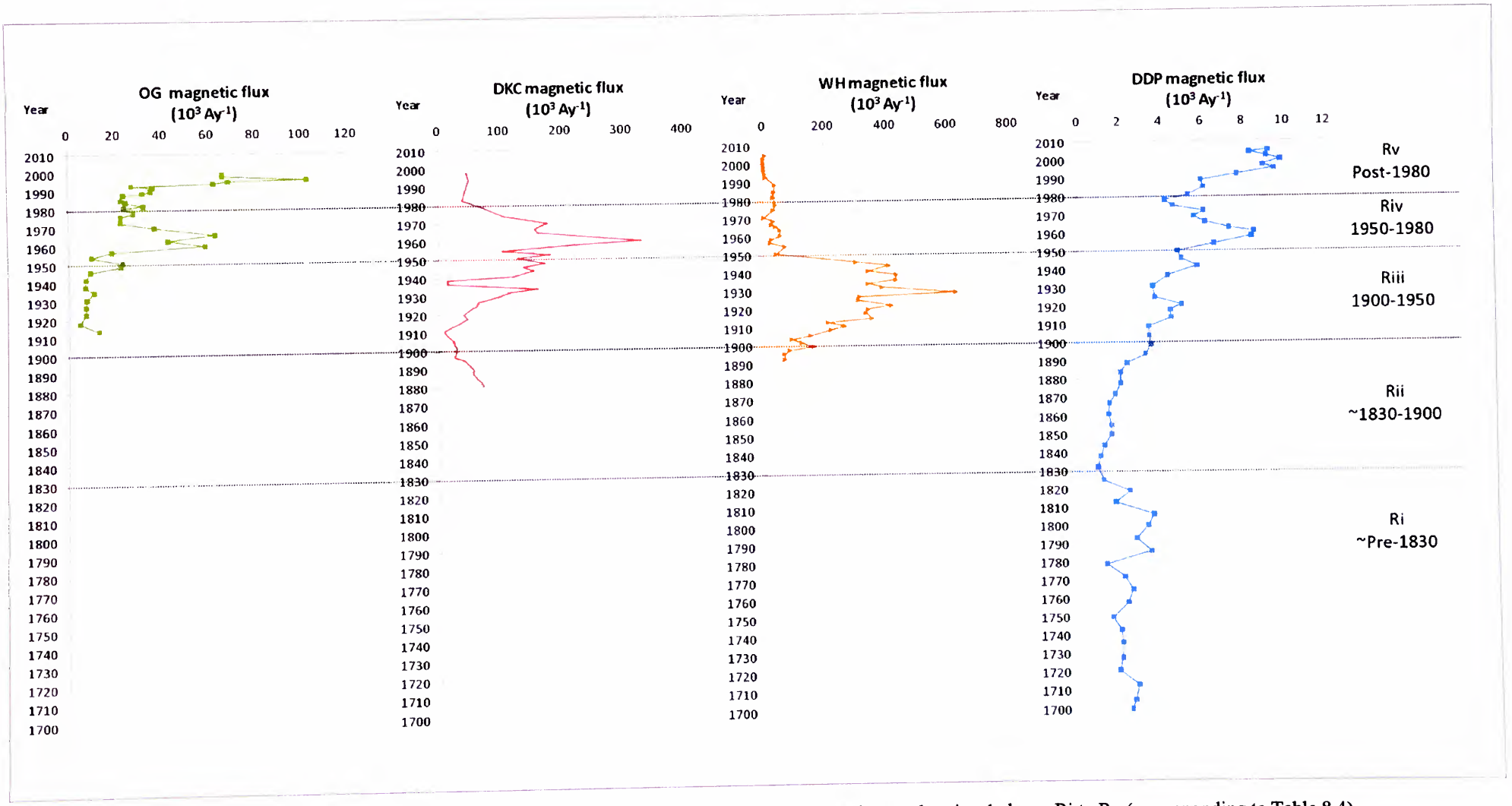

Figure 8.5A: Post-1700 cross-regional magnetic (SIRM) profiles from OG, DKC, WH and DDP with superimposed regional phases Ri to Rv (corresponding to Table 8.4).

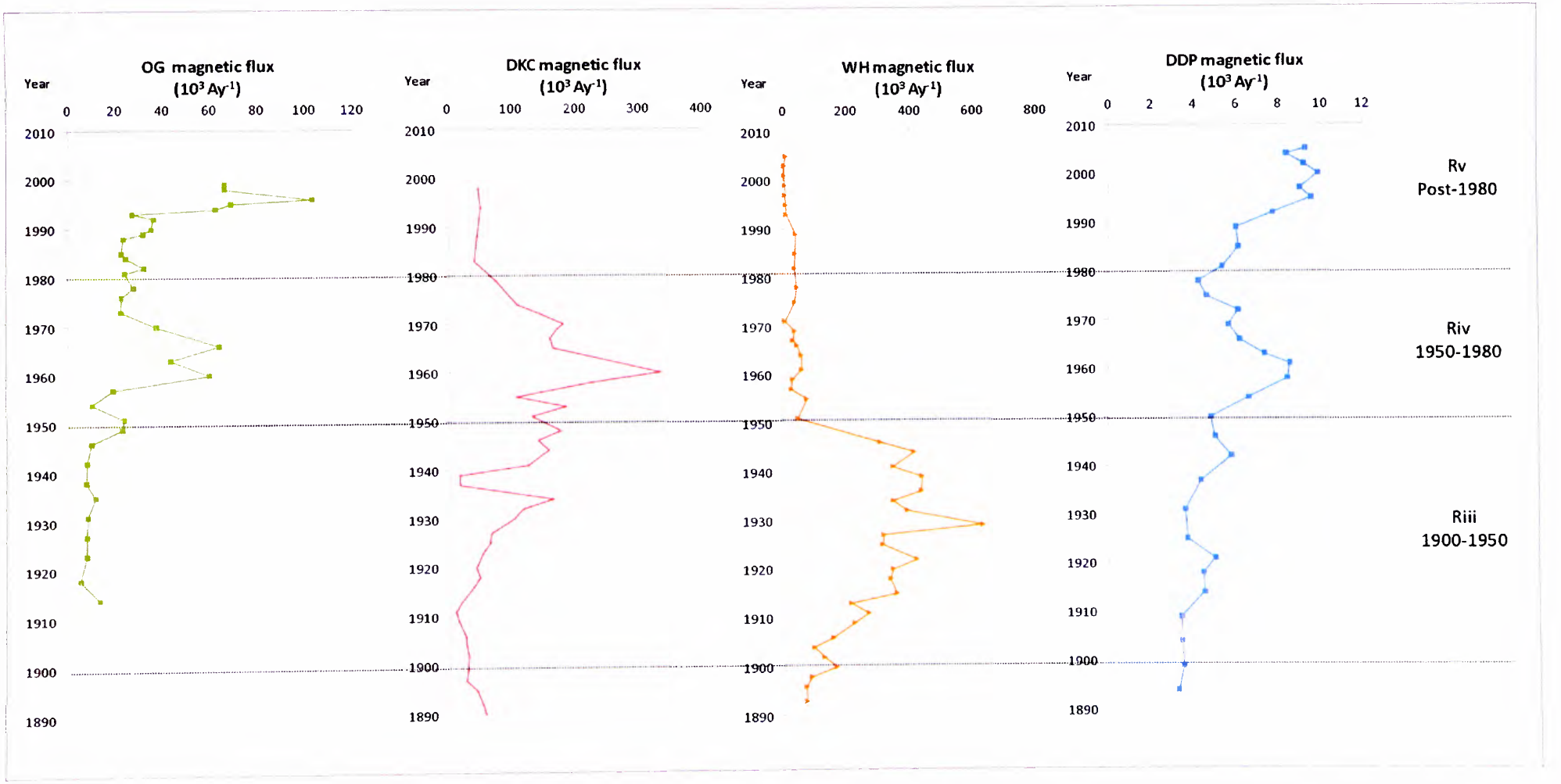

Figure 8.5B: Post-1900 cross-regional magnetic (SIRM) flux: Flux profiles from OG, DKC, WH and DDP with superimposed regional phases Riii to Rv (corresponding to Table 8.4).

Table 8.4: Cross regional magnetic signal relating to regional phases Ri to Rv (corresponding to Figures 8.5A and 8.5B).

Phase	Timescale	Description of trend
Rv	Post-1980	DDP and OG demonstrate an increase in magnetic grains to the signal post-1980 with prominent peaks at 1985 (DDP) and 1982 (OG). Also, further magnetic enhancement is observed post-1990 with maximum OG and DDP SIRM exhibited post-1995. This post-1980 signal is characteristic of finer magnetic grains, demonstrated by an increase in $HARD_{-300mT}$ in the OG and DDP profiles. WH and DKC, however, demonstrate a steady reduction in magnetic flux.
Riv	1950 to 1980	Post-1955 SIRM flux exhibits a prominent reduction in WH. Maximum SIRM occurs in the DKC profile at 1962, with a corresponding OG peak at 1960, and a prominent DDP peak at 1958 to 1960. Later peaks are also observed at 1966 in the OG core, 1969 in the DKC core and 1972 in the DDP profile. Magnetic flux decreases post-1970 at all four sites.
Riii	1900 to 1950	The supply of magnetic grains to the region is further enhanced post-1900, with prominent SIRM flux increases observed throughout the DDP, WH and DKC profiles at this time. WH and DKC exhibit a clear SIRM increase from ~1910. Periods of high SIRM flux are mirrored throughout the profiles during ~1910-1920: from 1914 to 1921 (DDP), 1915 to 1922 (WH), and post-1918 (DKC). Magnetic flux continues to increase throughout the 1930s and 1940s with distinct peaks mirrored in the DKC and OG profiles at 1935 and 1934, respectively. Corresponding SIRM peaks are also identified at 1942 in the DDP, and 1944 in the WH and DKC profiles. Also OG demonstrates a pronounced 1949 to 1951 peak; whereby, maximum SIRM values are reached. This is also reflected in the WH profile, by maximum 1949 SIRM flux values.
Rii	~1830 to 1900	Start of increasing magnetic flux from ~1832; which steadily increases throughout the 19th century.
Ri	~Pre-1830	Relatively low magnetic flux with elevated SIRM from ~1780 to 1800, as demonstrated by the DDP profile.

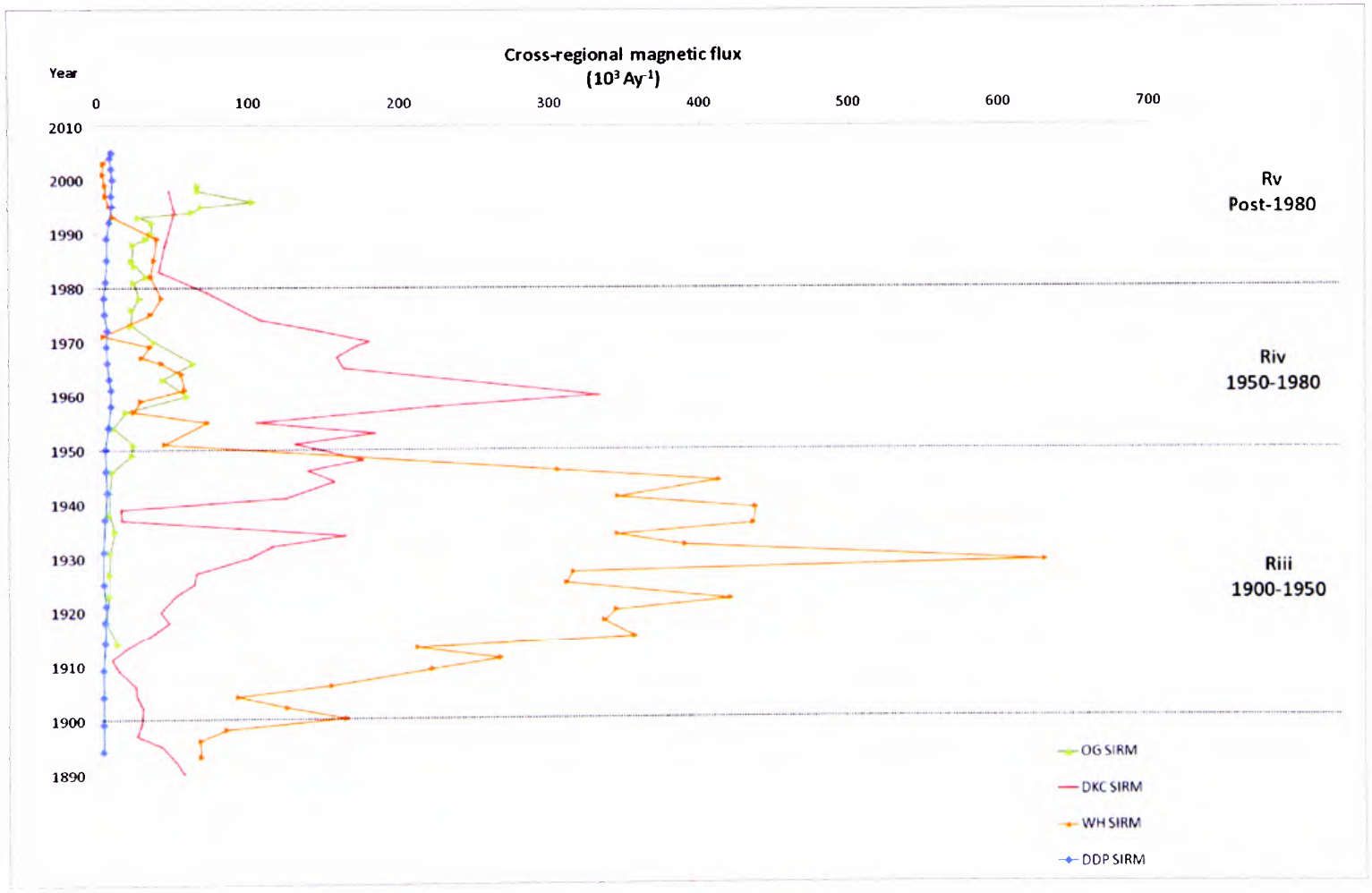

Figure 8.6: Post-1900 cross-regional variation of magnetic (SIRM) flux with superimposed regional phases Riii to Rv.

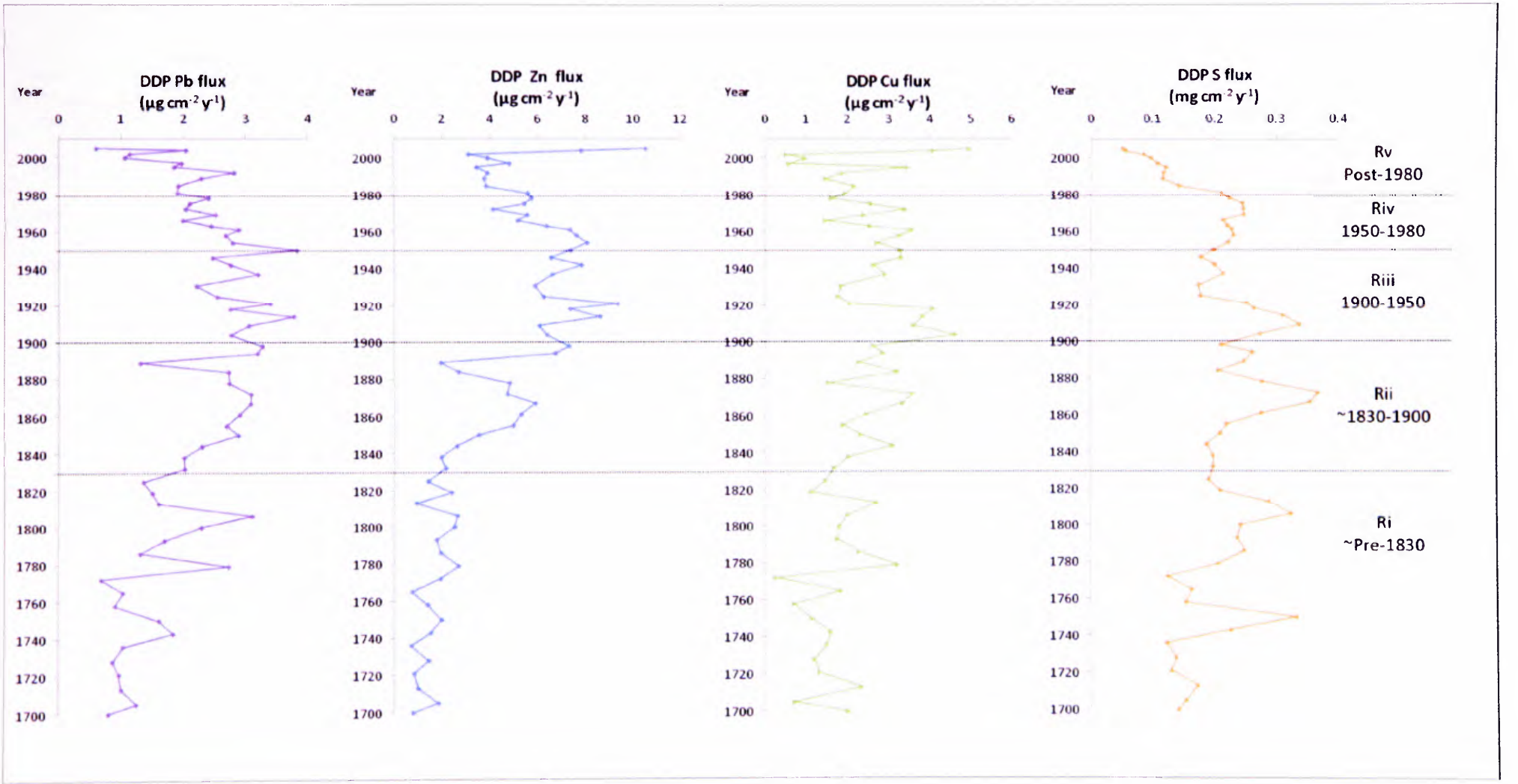

Figure 8.7: Post-1700 Pb, Zn, Cu and S flux profiles from DDP with superimposed regional phases Ri to Rv (corresponding to Table 8.5).

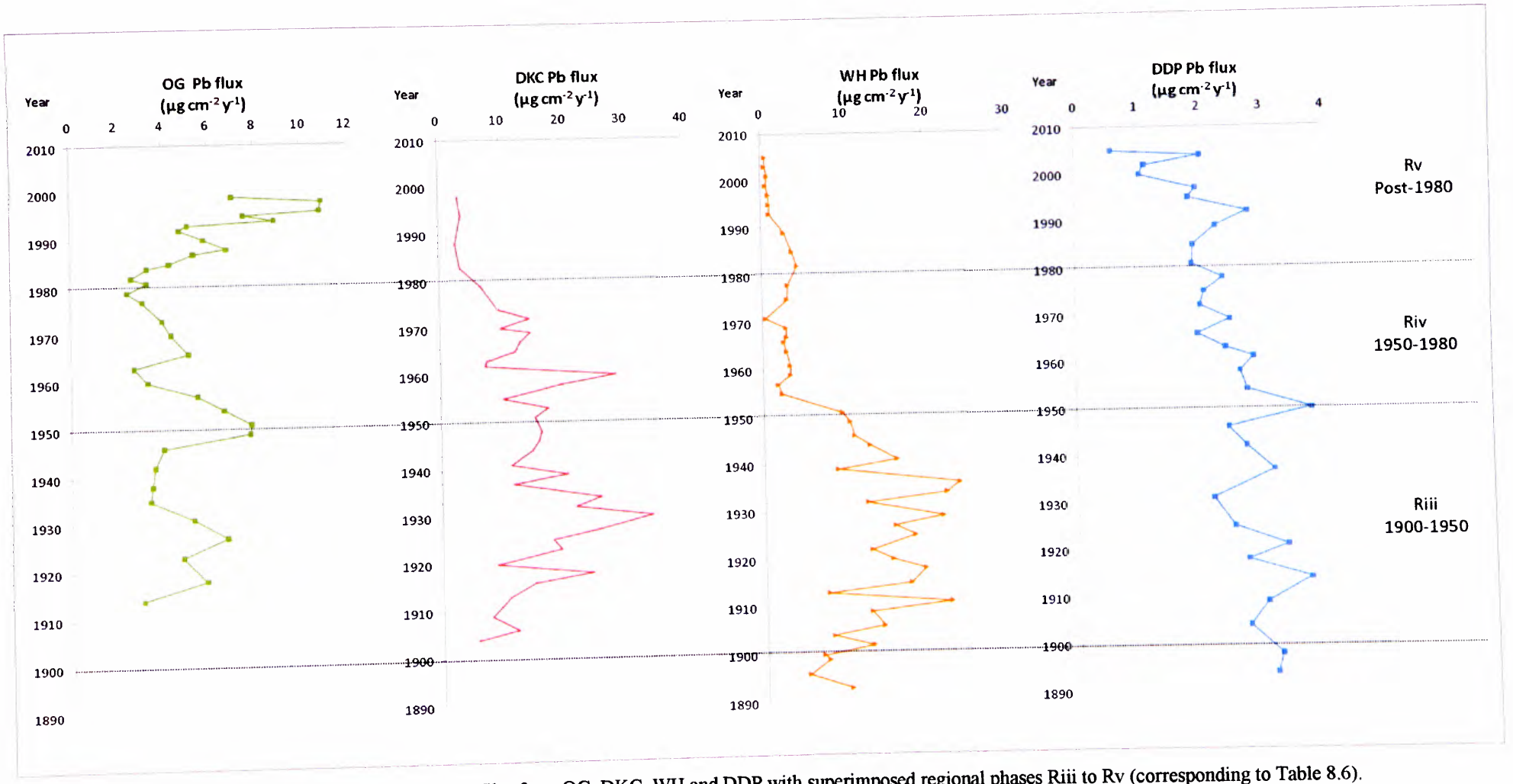

Figure 8.8: Cross-regional Pb signal post-1900: Pb flux profiles from OG, DKC, WH and DDP with superimposed regional phases Riii to Rv (corresponding to Table 8.6).

Table 8.5: Cross-regional trace metal signal 1700 to 1900 relating to regional phases Ri to Rii (corresponding to Figure 8.6).

Phase	Timescale	Description of trend
Rii	1830 to 1900	Pb supply increases ~post-1832, and a pronounced enhancement post-1889 in the DDP profile. A clear enhancement in Zn flux occurs post-1856 in the DDP profile, with a distinct Zn peak at 1867, and further Zn enhancement post-1889. Cu values are elevated from 1844 with a peak at 1873. Further S enhancement occurs from 1867 to 1873, reaching maximum S flux values in the DPP profile. A relatively small S peak is observed at 1889.
Ri	~Pre-1830	Relatively low Pb, Zn and Cu values. A peak in Pb flux occurs from ~1780 to 1807. A period of increased Cu flux occurs from 1780 to 1813. S displays early increases from 1787, with a prominent peak observed at 1807.

Table 8.6: Cross-regional Pb signal post-1900 relating to regional phases Riii to Rv (corresponding to Figure 8.8).

Phase	Timescale	Description of trend
Rv	Post-1980	Pb declines at DKC and WH; however, Pb increases at 1992 at DDP and post-1980 increases at OG which continue post-1990 and maximum supply at 1996.
Riv	1950 to 1980	Pb peaks noted at 1962 in DKC, 1966 to 1973 in OG, 1959 to 1967 in WH and 1960 and 1969 at DDP, with an overall reduction post-1970 across the region.
Riii	1900 to 1950	DDP exhibits sustained high Pb in this phase. Pb increases are observed at 1911 at WH and 1918 at DKC, with a corresponding Pb peak at 1914 at DDP. Maximum Pb flux in the WH profile occurs from 1929 to 1936, with peaks observed at DKC from 1930 to 1934, and 1927 at OG, and 1937 at DDP. Mid-20th century Pb peaks are also observed throughout the region. OG exhibits a pronounced 1949 to 1951 peak; DKC exhibits an increase in Pb from 1946 to 1953; in the WH profile from 1941 to 1951; and DDP demonstrates maximum Pb flux at 1950.

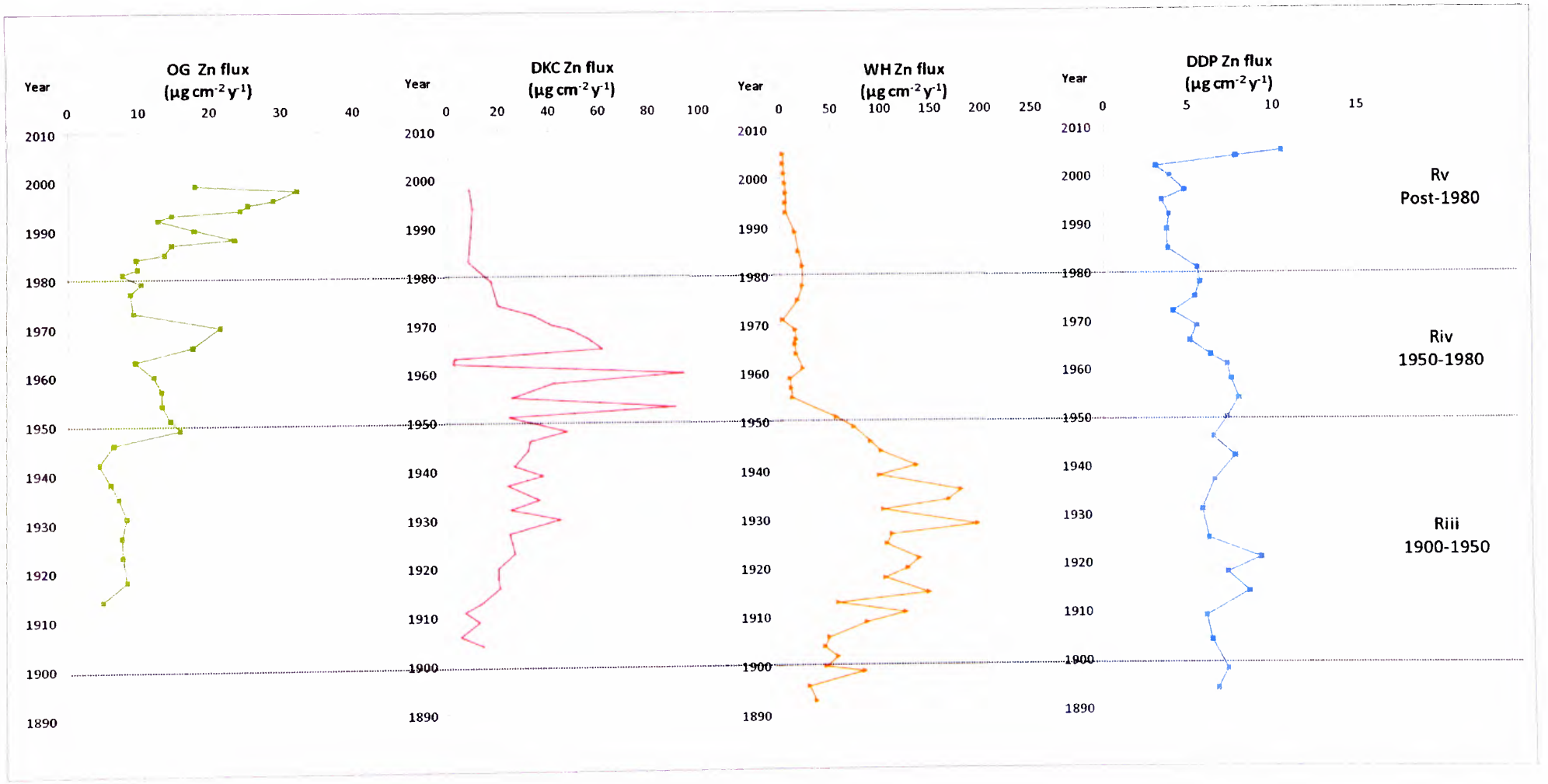

Figure 8.9: Cross-regional Zn signal post-1900: Zn flux profiles from OG, DKC, WH and DDP with superimposed regional phases Riii to Rv (corresponding to Table 8.7).

Table 8.7: Cross regional Zn signal post-1900 relating to regional phases Riii to Rv (corresponding to Figure 8.9).

Phase	Timescale	Description of trend
Rv	Post-1980	Prominent Zn increases occur post-1988 at OG, with maximum Zn flux at 1997. This is reflected at DDP by a distinct peak at 1997, with maximum Zn flux at 2005. DKC and WH , however, exhibit a continued Zn decline.
Riv	1950 to 1980	Mid-1950 peaks are observed at DKC (1953) and DDP (1954). DDP and WH exhibit post-1955 Zn reductions, pronounced in the WH profile. DKC, however, demonstrates an increase post-1955 with prominent early 1960 Zn peaks, whereby maximum Zn flux values are reached. Although relatively lower than pre-1955 values, there are periods of Zn enhancement in the WH profile from 1961 to 1967. Increases are also observed during the late 1970s, with peaks at 1978 in DDP and WH, and at 1979 in the DKC profile. OG demonstrates a continual Zn increase post-1950, with a pronounced peak at 1970.
Riii	1900 to 1950	DDP demonstrates prominent Zn enhancement during the 20th century when compared with pre-1900 values (phases Ri and Rii). Zn increases occur post-1911 at WH, with a distinct 1922 peak. This is reflected at DDP, by 1914 to 1921 increases. Also, post-1916 Zn increases are observed at DKC. Closely paralleled Zn peaks are identified at 1929, 1930 and 1931, respectively, at WH, DKC and OG. Sustained high Zn values are observed until 1939 at DKC and 1941 at WH signal, which corresponds with a 1942 Zn at DDP. Also, OG and DKC exhibit closely paralleled Zn peaks at 1949 and 1948, respectively, marking a notable Zn enhancement at OG.

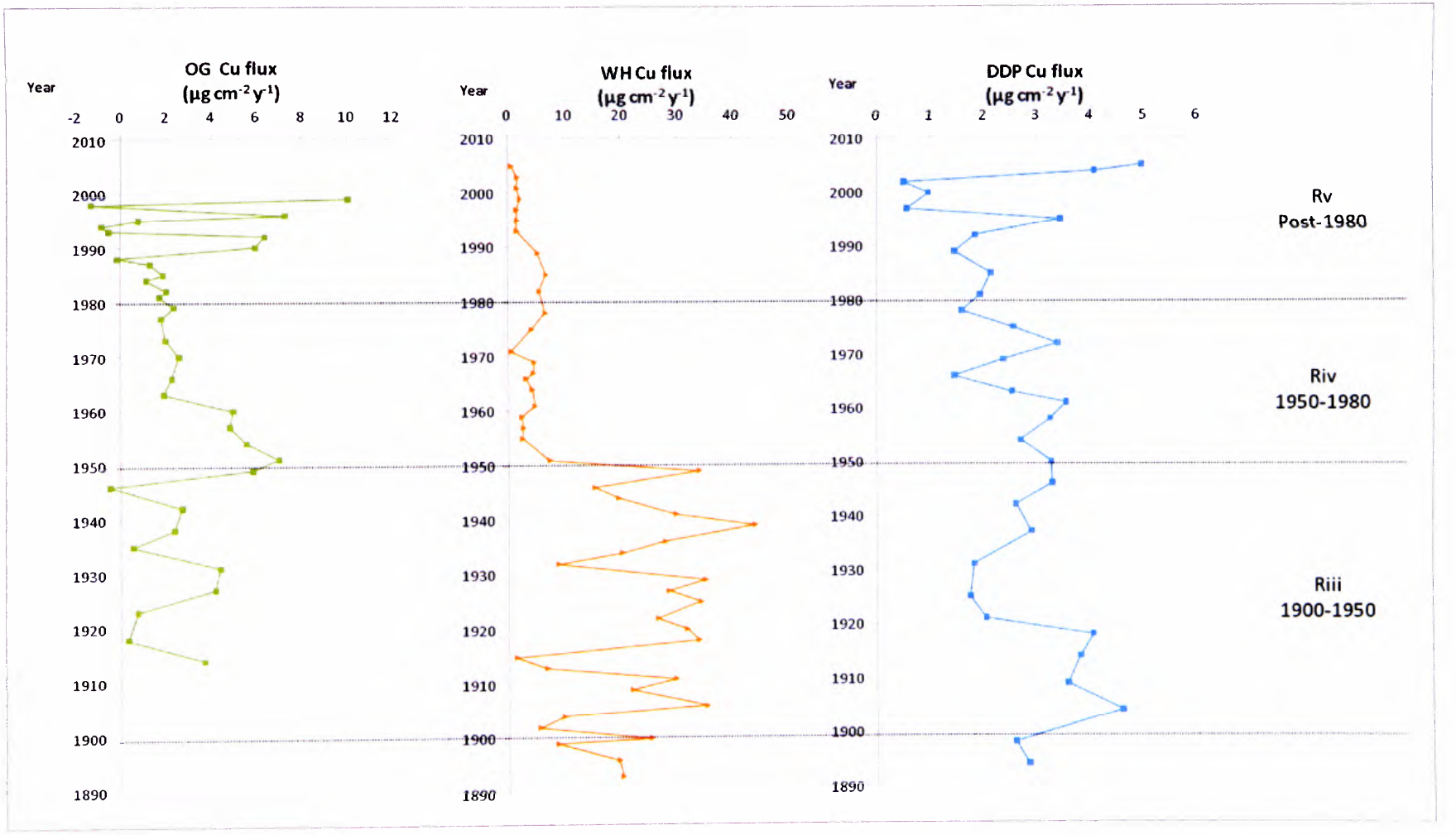

Figure 8.10: Cross-regional Cu signal post-1900: Cu flux profiles from OG, DKC, WH and DDP with superimposed regional phases Riii to Rv (corresponding to Table 8.8).

Table 8.8: Cross-regional Cu signal post-1900 relating to regional phases Riii to Rv (corresponding to Figure 8.10).

Phase	Timescale	Description of trend
Rv	Post-1980	A period of Cu enhancement from 1978 to 1989 occurs at WH, after which there is a further decline, with a small increase at 1997. Cu also increases during the 1980s at DDP, with peaks at 1985, 1995 and maximum Cu supply at 2005. More prominent increases are observed post-1990, at OG with maximum Cu flux at 1997.
Riv	1950 to 1980	Post-1949, Cu declines at WH, with relatively smaller increases from 1961 to 1967. Later, post-1970, Cu declines occur at DDP, after prominent peaks at 1961 and 1972. OG demonstrates a period of Cu enhancement from 1951 to 1960, post-1960 Cu values decline, however, values are higher than phase Riii.
Riii	1900 to 1950	Cu enhancement post-1904, with sustained high values until 1918, as demonstrated at DDP profile. WH exhibits a prominent Cu increase from 1906 to 1911, and 1918 to 1929. OG exhibits an increase in Cu flux from 1927, with a period of high values sustained until 1931. Cu peaks are also identified at 1939 and 1949 in the WH profile mirrored at 1937 and 1950 in the DDP signal. Also, OG exhibits an increased period of Cu from 1938 to 1942.

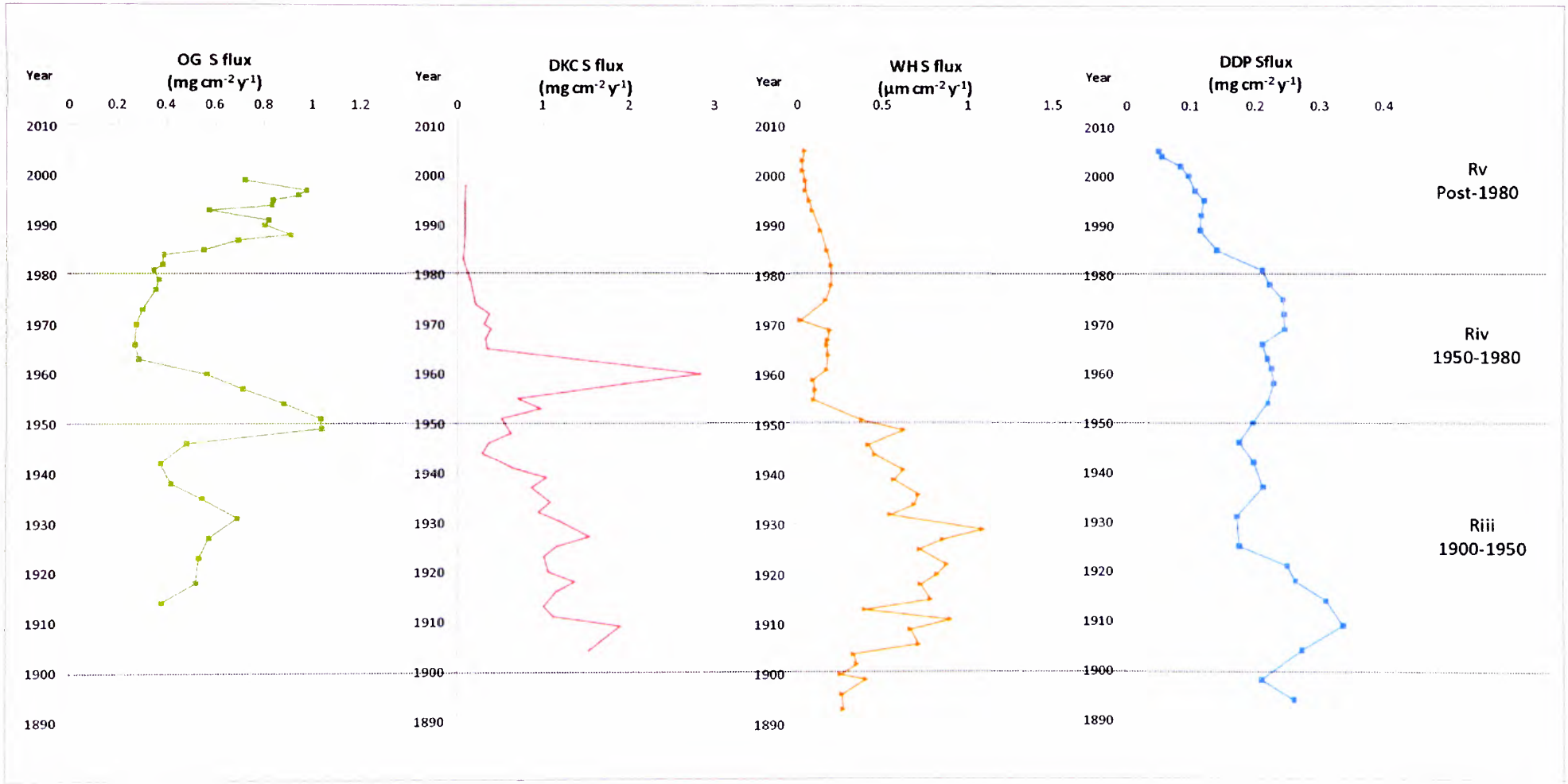

Figure 8.11: Cross-regional S signal post-1900: S flux profiles from OG, DKC, WH and DDP with superimposed regional phases Riii to RV (corresponding to Table 8.9).

Table 8.9: Cross-regional S signal post-1900 relating to regional phases Riii to Rv (corresponding to Figure 8.11).

Phase	Timescale	Description of trend
Rv	Post-1980	Prominent reductions in DDP, which steadily decline throughout this phase, also reflected in the DKC and WH profiles. Inversely, prominent S increases are observed at OG post-1985, with maximum flux at 1997.
Riv	1950 to 1980	S values are lower than pre-1949 at WH; however, increases are observed at 1961 to 1967 and from 1978 to 1982. DKC and OG exhibit prominent S increases post-1949, with a very pronounced 1949 to 1951 OG peak. DKC displays a later S peak from 1960 to 1962, after which, values notably decline.
Riii	1900 to 1950	DDP exhibits high S values from the start of the 20th century to ~1920. This is reflected in the WH profile which exhibits a clear S enhancement post-1906, with a steep increase in S throughout the 1910s and 1920s, followed by a maximum WH S flux peak at 1929. DKC also demonstrates enhancement in S at this time, with distinct peaks at 1909, 1918 and 1927. OG exhibits a period of S enhancement from 1918 to 1931. Post-1929 S decreases are exhibited in the WH profile, however, a peak at 1934 occurs, reflected in the DDP profile at 1937.

Inter-site comparisons of post-1900 Pb (Figure 8.12), Zn (Figure 8.13), Cu (Figure 8.14) and S (Figure 8.15) flux values demonstrate that there is both spatial and temporal variability in the supply of trace metals across the LMR. Flux data recorded at DDP is low when compared to WH, DKC and OG, for all trace metals and magnetic flux (Figure 8.6). Highest flux values are recorded at varying sites throughout the cross- regional temporal phases:

- Riii 1900 to 1950: WH exhibits notably higher magnetic and Zn flux when compared to DDP, DKC and OG. Pb values are similar at WH and DKC in this phase (~6 - 25 $\mu g\ cm^{-2}\ y^{-1}$). Also, the highest deposition of S is recorded at DKC.
- Riv 1950 to 1980: Flux values are reduced at WH post-1950. Zn, Pb and S deposition is highest at DKC.
- Rv post-1980: trace metal flux values at WH, DKC and DDP exhibit a corresponding reduction in this phase and demonstrate similar values. However, OG, inversely, exhibits an increasing trend post-1980, with deposition of S, Pb and Zn highest at OG in this recent phase. Post-1980 OG trace metal flux values are generally lower than values recorded in phases Riv and Rii at DKC and WH.

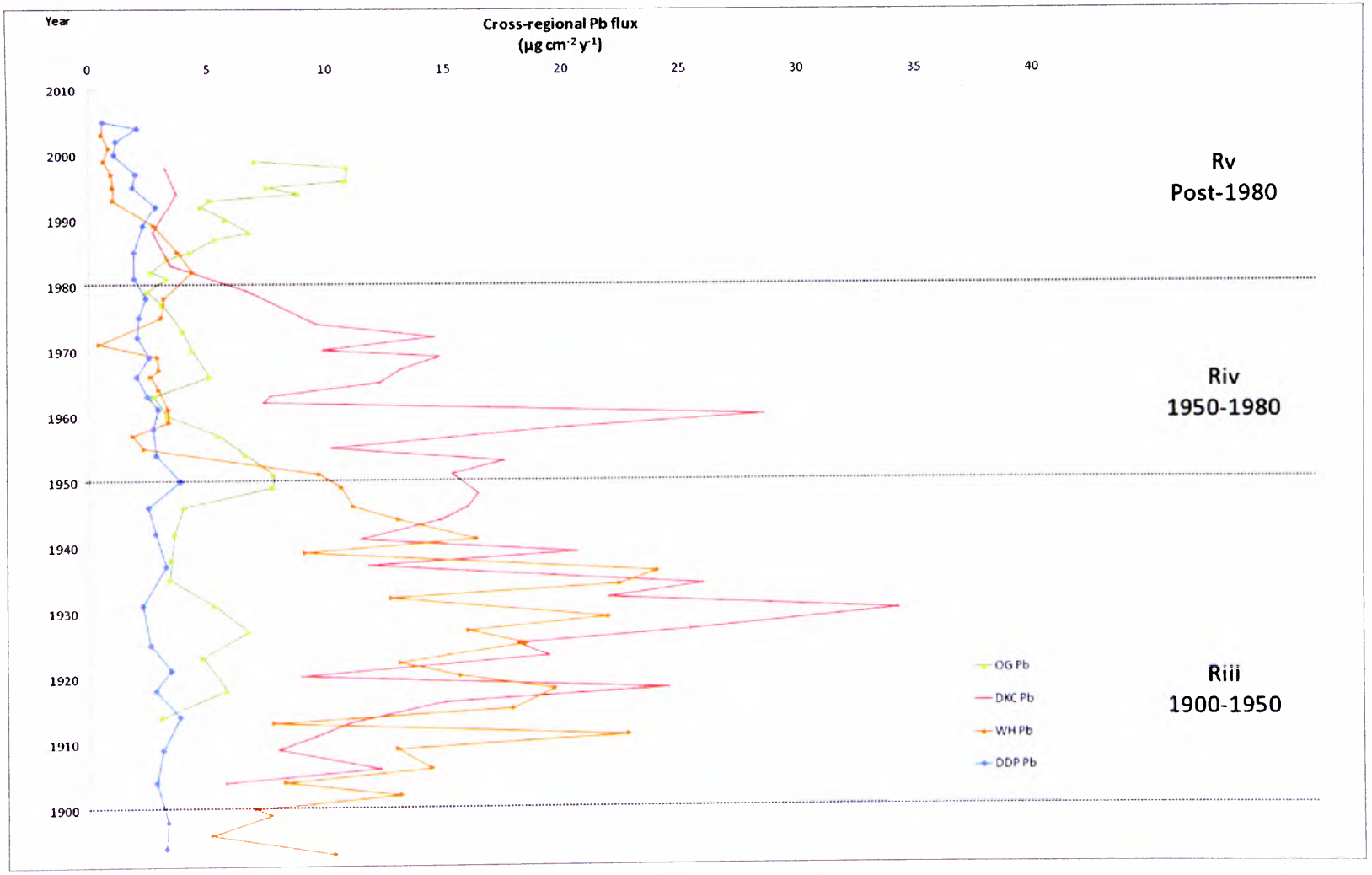

Figure 8.12: Post-1900 cross-regional variation of Pb flux with superimposed regional phases Riii to Rv.

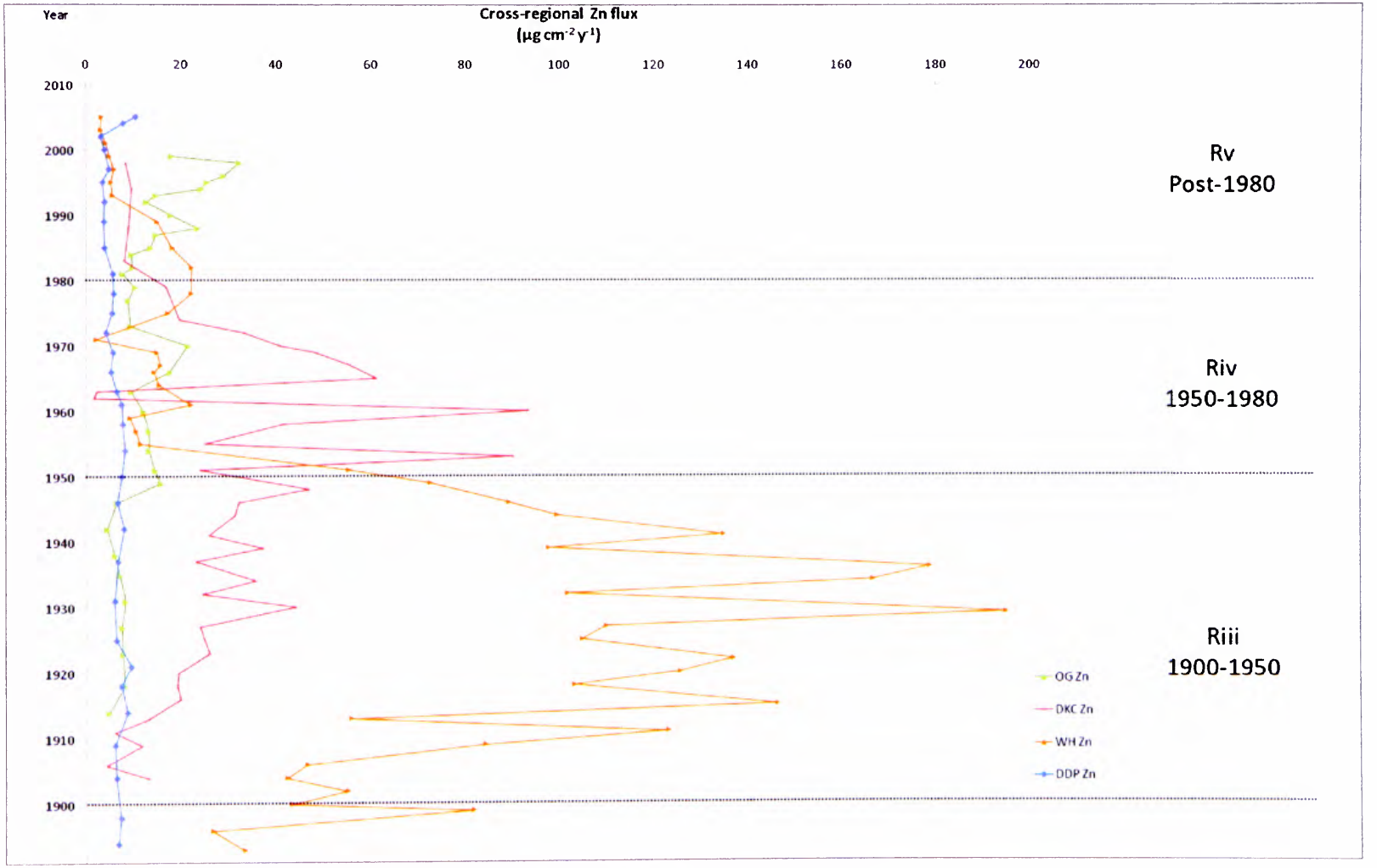

Figure 8.13: Post-1900 cross-regional variation of Zn flux with superimposed regional phases Riii to Rv.

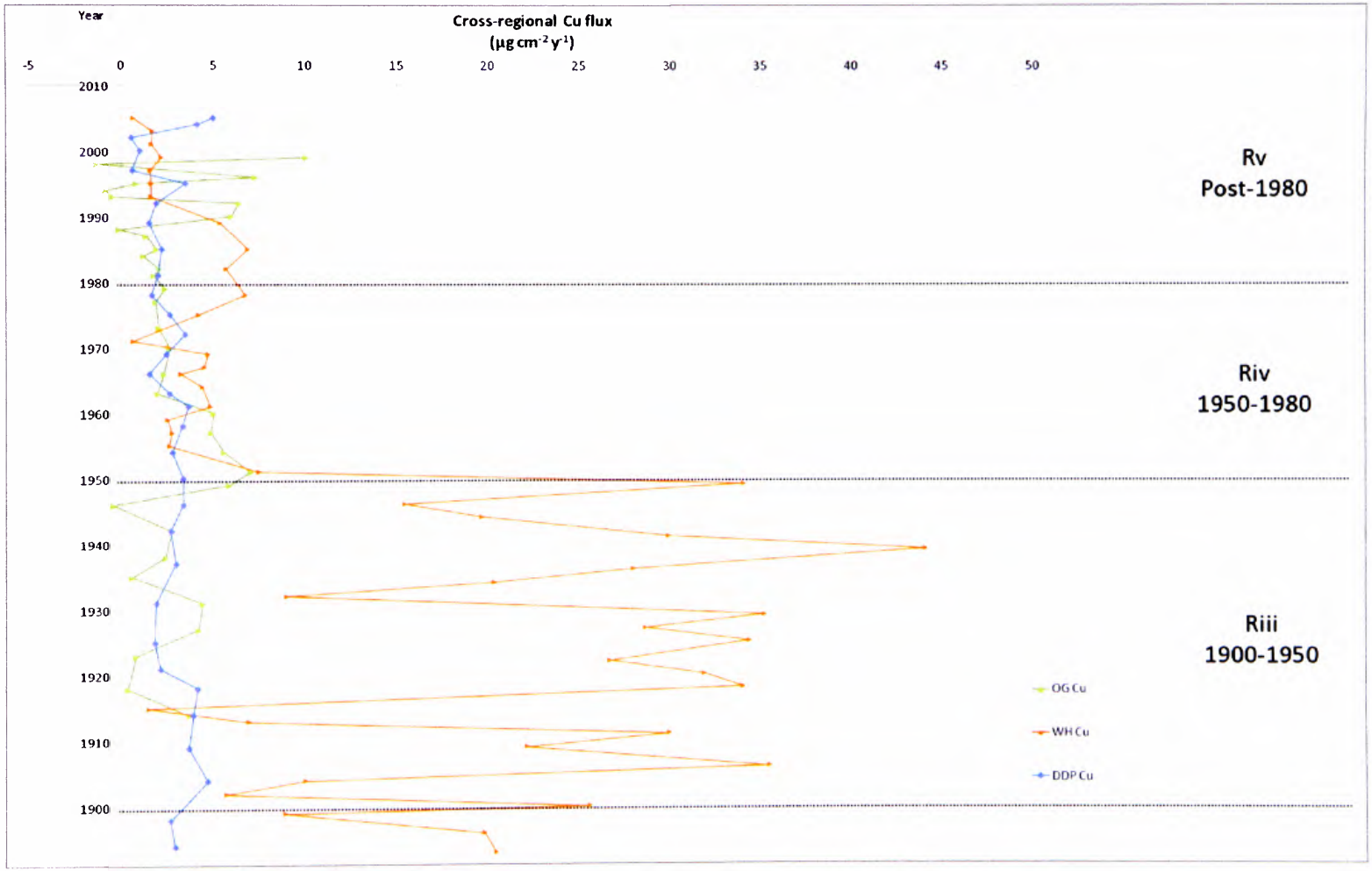

Figure 8.14: Post-1900 cross-regional variation of Cu flux with superimposed regional phases Riii to Rv.

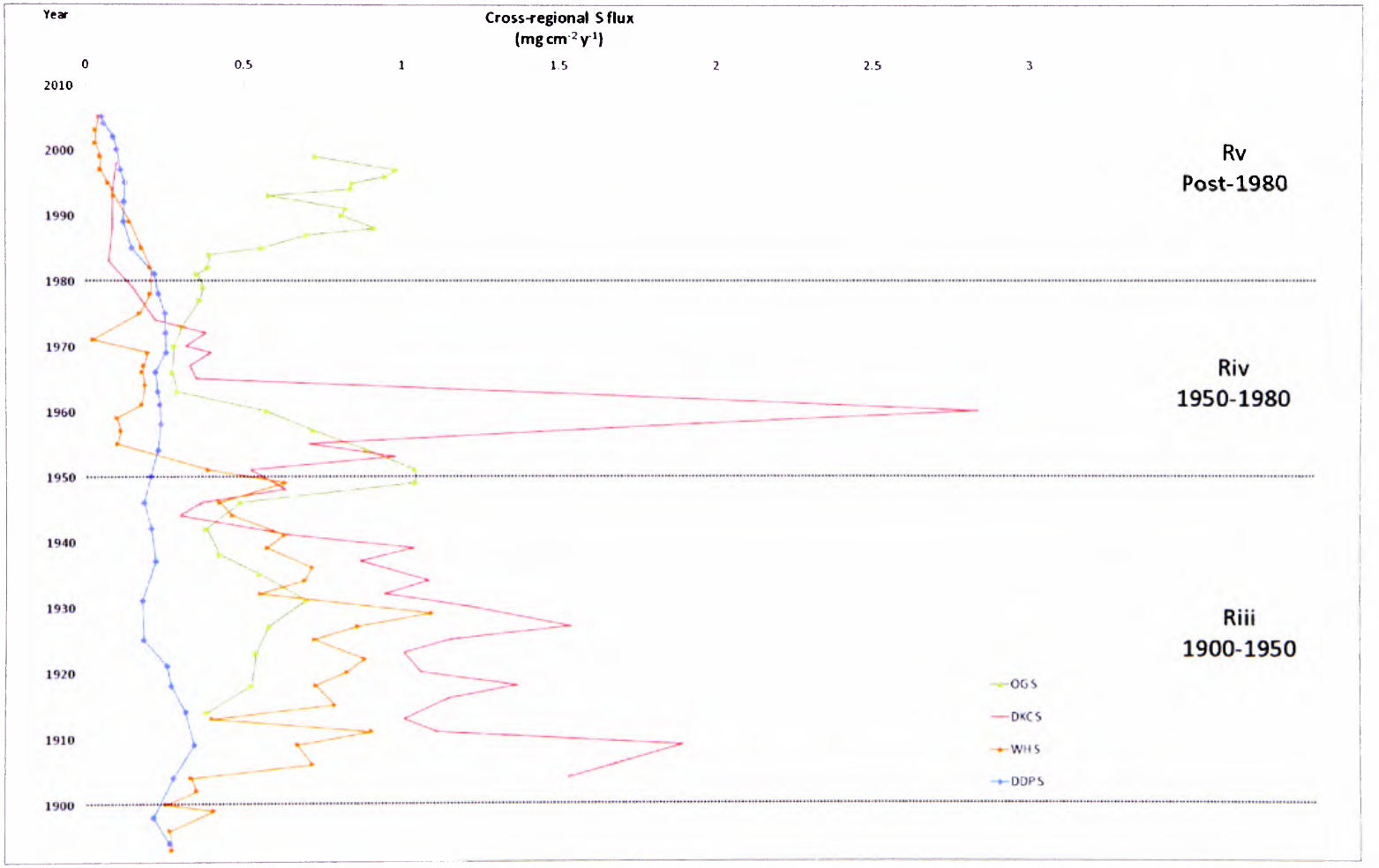

Figure 8.15: Post-1900 cross-regional variation of S flux with superimposed regional phases Riii to Rv.

The regional phases identified within the cross-regional signal reveal spatial and historical trends in the deposition of magnetic minerals and trace metals throughout the LMR.

- Ri Pre-1830:

The earliest notable enhancement in the proxy pollution record, observed in the DDP core, occurs at ~1751, with a distinct S peak at this time. Also, distinct SIRM, Pb, Cu and S increases are exhibited between ~1780 and 1807. However, throughout this phase the proxy pollution profiles demonstrate relatively low values.

- Rii: ~1830 to 1900:

DDP demonstrates a ~post-1832 magnetic, Pb, Cu, S and Br enhancement, with a slightly later, post-1856, Zn increase. A steady increase in magnetic grains occurs post-1830; however, a more pronounced increase between 1850 and 1880 is observed in the trace metal flux profiles, with maximum S flux values observed in the DDP profile at 1873. Subsequent to this increase, a decline in S and Cu occurs from ~1880 to 1900.

- Riii: 1900 to 1950:

Trace metal and magnetic elevation occurs from ~1900 in the DDP profile, at which time DKC and WH ponds receive the regional signal. This post-1900 increase is reflected in the three cores, with further corresponding increases observed from 1910:

- 1914 to 1921 Pb, Zn and SIRM increases, 1904 to 1921 Cu increases, and 1909 to 1918 S peaks demonstrated in the DDP profile. Relatively higher Pb and Zn flux observed at this time in the DDP profile.
- 1911 to 1929 Pb, Zn, and SIRM increases in the WH profile. Maximum S and increased Cu flux occurs from 1906 to 1922.
- Post-1918 Pb, Zn S and SIRM increases exhibited by the DKC profile.

OG also demonstrates increases in trace metal flux at the start of its record (1914):

- 1918 to 1931 Pb, Zn, S, 1927 to 1931 Cu increase in the OG profile; however, this enhancement is not reflected in the magnetic flux.

All pond sites exhibit an overall steady increase in trace metal and magnetic flux throughout the fist half of the 20th century. Although undetected in the OG flux profiles,

DKC, WH and DDP exhibit corresponding notable increases during the 1930s, observed at:

- 1937 Pb, Zn, S and SIRM increase, 1942 SIRM peak and post-1946 Cu increase in the DDP profile;
- 1939 to 1949 Cu and S increases, and 1934 to 1941 Pb, Zn and SIRM increases in the WH profile, reaching maximum trace metal and magnetic flux values at 1949; and
- 1930 to 1939 Pb, Zn, S and SIRM increases in the DKC profile.

OG exhibits a prominent enhancement in magnetic and trace metal flux from 1940, with continuing increases observed throughout the urban ponds, most notably, sustained high flux throughout the 1940s and 1950s in the DDP profile, for example maximum Pb flux at 1950. Also, 1946-53 Pb, Zn, S and SIRM peaks are exhibited by DKC; while WH exhibits a prominent magnetic peak at 1949, mirrored by particularly high Cu values.

- Riv: 1950 to 1980:

WH demonstrates a reduction in pollution flux post-1951, particularly notable in the magnetic flux profiles. However, DDP, DKC and OG exhibit further post-1950 increases in trace metal and magnetic flux with distinct mid-20th century peaks:

- 1958 to 1961 SIRM peak, maximum 1958 Pb peak and 1963 Zn peak in the DDP profile.
- 1960 to 1962 maximum trace metal and magnetic peak prominent in the DKC profile.
- 1951 to 1960 Cu peak, 1960 to 1966 SIRM peak, and 1966 Pb and Zn peak in the OG profile.

The DKC and OG ponds demonstrate pollution enhancement which continues into the 1970s, potentially, highlighting a pollution signature for the northwest LMR, as this is not reflected in the DDP or WH cores. DDP exhibits an overall decline in proxy pollution flux post-1970, later than the post-1951 reductions observed in the WH pond. Although flux values are lower post-1949 in the WH core, increasing proxy pollution trends are observed from 1956 to 1967. A prominent reduction in trace metal and magnetic flux occurs in the DKC pond post-1970, mirrored by reductions in OG flux trends during the 1970s and overall continuing declines in the WH and DDP ponds.

- Rv post-1980:

Sulphur exhibits the most distinct decline, with steady reductions post-1980 in the WH and DDP cores and post-1970 in the DKC profile, continuing to present day. Despite reductions in trace metals, the DDP core exhibits a post-1980 increase in SIRM, with proportionately higher $HARD_{300mT}$ flux trends, highlighting a post-1975 increase in fine magnetic grains to the lake. Post-1990 increases in Pb, Zn and Cu in the DDP profile, with maximum SIRM flux post-1995. The OG core demonstrates pronounced increases in trace metal and magnetic flux post-1980, with further pronounced increases post-1990. Maximum trace metal and magnetic flux values are reached in the OG core post-1990. This recent enhancement is not reflected in the other pond sites.

8.5. Chapter summary

A cross-regional deposition history of Pb, Zn, Cu, S and magnetic grains in four urban ponds, Oglet, Dogs Kennel Clump, Windmill Hill and Daresbury Delph, is presented. A >250-year history of proxy pollution trends detail concentration and flux profiles from sites across the LMR. Pre-1900 proxy pollution trends are revealed via Daresbury Delph Pond, and high-resolution post-1900 records are demonstrated via Oglet, Windmill Hill and Dogs Kennel Clump Ponds.

The DDP flux profiles reveal an increase in trace metals and magnetic grains in the borough occurring from 1780 to 1807. A more pronounced enhancement occurs post-1832, with further enhancement post-1900. The high-resolution post-1900 signal gathered from DDP, DKC, WH and OG reveals corresponding notable increases in trace metal flux values throughout the borough from 1910 to 1920. Increases in magnetic and trace metal flux continue throughout the first half of the 20th century, with notable peaks identified during the 1920s, mid-1930s and 1940s. Distinct mid-20th century magnetic and trace metal peaks are mirrored throughout the four urban pond sites during the 1950s and 1960s.

Overall, the four urban ponds exhibit a reduction in trace metals post-1970. This decline continues to present day in the DKC and WH profiles; however, post-1980 trace metal and magnetic increases are observed at the DDP and OG sites, characteristics of a finer-grained magnetic signal. A pronounced post-1980 trace metal enhancement is also observed in the OG core, not reflected in the other urban pond sites. This cross-regional signal, therefore highlights variations in the depositional histories of magnetic grains and trace metals throughout the LMR.

SECTION C: DISCUSSION AND CONCLUSIONS

This third section of the thesis explores the temporal air pollution stories captured by urban ponds in Halton. Initially, the integrity of small, manmade ponds to yield reliable and intact sediment records is assessed. The contributions of anthropogenic-to-natural inputs are also investigated to allow confidence that the temporal patterns of proxy pollution deposition are derived from the atmosphere (Chapter 9).

Local air pollution histories recorded in the urban pond sediments are then interpreted from each site in turn (Chapter 10). These local impacts of urbanisation are further highlighted via comparison of the urban pond records with regional (UK) trends in pollution deposition obtained from remote lakes. Comparison of local air pollution records from the lower Mersey region (LMR) with other urban stratigraphies highlights the importance of urban ponds as sedimentary archives of urbanisation (Chapter 10).

A cross-regional pollution signal for the LMR is also explored by combining the local pollution signals from DDP, OG, DKC, and WH. Variations in the history of pollution deposition throughout the borough are discussed. This cross-regional signal is further explored using other available sedimentary evidence in south Merseyside, notably a local air pollution signal from Speke Hall Lake (Chapter 11). The main conclusions from this work, the implications of a cross-regional signal for the LMR and suggestions of future work is also included (Chapter 12).

9. CHAPTER NINE: INTEGRITY OF URBAN PONDS AS AIR POLLUTION ARCHIVES

9.1. Chapter Overview

The suitability of urban ponds to yield reliable sediment records of air pollution is assessed in this chapter. The identification of suitable urban pond sites, intra-site core correlation and the integrity of sediment chronologies, are discussed to explore the ability to extract intact sediment stratigraphies from urban ponds. The supply of sediment to urban ponds and contributions of anthropogenic and natural inputs, allows further assessment of the capture of an accurate air pollution signal recorded within the ponds.

9.2. Introduction

Urban ponds are not widely used in palaeolimnology. However, their central location within urban environments means they receive atmospheric particulate emissions from urban activities and, therefore, are important sedimentary archives of air pollution [Worsley, *et al.*, 2006; Van Metre and Callender, 1997]. To ensure reliable air pollution histories are obtained, the integrity of the ponds to produce intact sediment records of pollutants derived from the atmosphere requires exploration. Initial identification of suitable pond sites, intra-site core correlation* and the reconstruction of isotope chronologies are assessed to determine the reliability of the sediment sequences extracted from the urban ponds from which environmental histories are inferred. Relative contributions of natural and anthropogenic inputs are then assessed to determine if records of proxy atmospheric pollution or catchment material have been captured. Confidence that the sediment record reflects temporal patterns in the deposition of air pollution is essential, in order to interpret local pollution signals at each site.

9.3. Identification of suitable urban ponds

The site descriptions, catchment analyses and site histories of the four urban ponds: DDP, WH, DKC and OG (Chapter 4) demonstrate the identification of suitable ponds (criteria set out in Section 3.3.) within and surrounding the borough of Halton. Unlike the majority of palaeolimnological studies which utilise sediments from large, natural, rural lakes; the

* Core correlation is used in this chapter to describe similar features within different sediment cores, as termed by Thompson *et al.*, 1975, rather than its statistical meaning.

nature of sediments from manmade urban ponds and their catchments has required extensive investigation to enable confidence in the sequences derived from cores. Exploration of maps spanning from the present day to tithe publications (mid-19th century) allowed an initial establishment of the age of these urban ponds, as well as the identification of physical changes in the size and shape of the ponds, indicative of catchment development and, therefore, potential sediment disruption. Although results are presented for four urban sites, hundreds of ponds in south Merseyside and north Cheshire were initially investigated (Appendix A, Table A1).

Documentation of management histories varied at each site. No documentary histories were available for DKC or OG; however, assurance that their sediments had not undergone recent (~50-year) disruption (e.g. dredging) was provided by landowners. Staff at Halton Borough Council, however, had a more detailed account of work carried out on pond sites under their management (WH), and other local private ponds (DDP). The risk of undocumented sediment disturbance at all four sites has been reduced due to the achievement of ^{210}Pb chronologies.

A limitation of using small ponds is the potential restriction of multiple core extraction. To obtain complete sediment cores often required multiple attempts at some sites and, therefore, some disruption of the pond sediments occurred. Due to their small basins, cores were retrieved from central basin positions, thus restricting multiple core extraction and, therefore, limiting future extraction. Also, very recent (post-2004) urban development adjacent to DDP prevents future core retrieval due to considerable catchment disturbance.

9.4. Core correlation within an urban pond

Reproducibility of sediment stratigraphies from within an urban pond is demonstrated by the intra-site core correlations observed within DDP. The five sediment cores extracted from the pond exhibit paralleled magnetic (χ_{LF} and SIRM) peaks and troughs of similar values, (Figure 5.2 and Table 5.1) [Charlesworth and Lees, 2001]. These visual correlations demonstrate the same environmental history has been recorded throughout the pond with minimal catchment disturbance. The morphology of DDP can be divided into two separate, smaller basins (ADD and BDD), which appear as one pond due to water level (Section 4.3., Figure 4.3). The χ_{LF} profiles from DDP reveal distinct elevated peaks in the ADD basin post-1975 (ranging from ~250 to 700 10^{-9} m^3 kg^{-1}), higher than maximum values recorded in BDD (Figure 5.2). A potential explanation for this higher magnetisation

may be due to the closer proximity of the ADD basin to the adjacent A56 roadway (<120 m), compared to BDD (<140 m) (Figure 4.3). The potential contribution of roadside particulates to DDP is further explored in the following chapter (Section 10.3.3.), however, the magnetic signature of vehicular particulates and their deposition near roadways (i.e. close to source) [Hoffman *et al.*, 1999] coupled with this post-1975 increase in magnetisation at ADD, which coincides with the construction of the adjacent roadways, may suggest a vehicular-derived magnetic source. This highlights that although similar magnetic trends have been retrieved, a higher concentration of magnetic grains is experienced at ADD, possibly reflecting deposition of vehicular particulates. The closely paralleled magnetic signatures of the two basins highlights inter-site correlation of magnetic records between two adjacent basins, as well as intra-site correlation within the pond.

9.5. ^{210}Pb chronologies and sedimentation rates

The ^{210}Pb and ^{137}Cs chronologies from DDP, WH, DKC and OG ponds highlight the successful application of isotope dating in urban pond sediments, supporting previous work by Worsley *et al.*, [2006], whereby, a ^{210}Pb chronology extending to 1881 was achieved from Speke Hall Lake (SH) in urban south Merseyside. Sediment disturbance would prevent the reconstruction of a ^{210}Pb chronology, as demonstrated in an urban pond by Charlesworth and Lees [2001]. Isotope chronologies obtained, therefore, provide further confidence in the undisturbed sequences of the sediment stratigraphies. The interpretation of the urban sediment chronologies in south Merseyside and north Cheshire do, however, require some caution, due to an observed deficiency in ^{210}Pb and ^{137}Cs isotopes retained by the five urban pond sites. However, similarities between the ^{210}Pb and ^{137}Cs profiles, allows confidence in the chronologies (Appendix D1 and D2).

The isotope chronology for DDP is further supported by the SCP profile, commonly used to date sediment cores using three typical features (Table 9.1 and Figure 9.1):

A. The start of the SCP record (1830s to mid-19th century) [Rose *et al.*, 1995];
B. Rapid increase in SCP concentrations (mid-20th century) [Rose *et al.*, 1999(b); Yang *et al.*, 2001(a)]; and
C. Near-surface concentration peaks (1970-1980) [Rose *et al.*, 1995; Rose *et al.*, 1999(b); Merilänien *et al.*, 2003].

The DDP profile exhibits a clear increase in total SCPs from ~1830 (Feature A), however, the presence of SCPs in the core pre-dates this enhancement, which may highlight a source of SCPs, potentially from low-scale industrial combustion activities, extending to the start of the sediment stratigraphy at ~1528. Rose *et al.*, [1999(b)] describes the start of the SCP record as the initial presence of SCP, with no prior SCP counts, the pre-1830 detection of SCPs may be due to core smearing, the movement of sediment with high SCP concentrations to lower levels during core extraction or extrusion [Rose *et* al., 1999(b)]. However, it is possible that the relatively late dates of Rose's sites are due to their rural / upland locations. The earlier SCP concentrations in the DDP profile may reflect deposition of SCPs close to source from early, localised industrial activities.

Feature A at DDP demonstrates similarities with the SCP dates for this feature at other UK sites. An earlier 1920, opposed to national 1940-1960 [Rose *et al.*, 1995] rapid increase is observed at DDP. Also, a relatively earlier, 1963, SCP maximum is exhibited in the DDP core, compared to later, 1970s-80s peak observed elsewhere in the UK [Rose *et al.*, 1995]. These variations, from the national features, in the DDP sediments may be due to localised impacts (further explored in Section 10.7.3.).

Table 9.1: ^{210}Pb dates for the three SCP dating features (A: the start of the SCP record; B: rapid increases in SCP concentration; and C: maximum peak) recorded in lake sediment cores (taken between 1986-92) from UK lakes published by Rose *et al.*, [1995] * indicates an extrapolated date.

Site	A:Start of SCP record	B: Rapid increase	C: Concentration peak (+/- 2)
North Scotland			
Loch Coire nan Arr	1830s	1960s	1974
Loch na Larach	1860s	1960s	1976
Long Loch of Dunnet Head	1860s	1960s	1975
Lochnagar	1860s	1960s	1977
Loch Ness	1870s	1960s	1978
Loch Uisage	1860s*	1950s	1975
Mean	1850s	1960s	1976
Wales			
Llyn Conwy	1850s	1960s	1975
Llyn Cwm Mynach	1840s/50s	Late 1950s	1980
Llyn Glas	1850s	Late 1940s	1976
Llyn Irddyn	1860s	Late 1950s	1980
Llyn Ilagi	1850s	1940s	1978
Mean	1850s	1950s	1978
Ireland			
Lough Maam	1910s	1970s	1981
Lough Maumwee	1880s	1970s	1981
Lough Muck	1850s	1940s	1982
Lough Veagh	1890s	1950s	1982
Mean	1880s	1960s	1981
Southern Scotland and northern England			
Burnmoor Tarn	1840s/50s	1950s	1978
Round Loch of Glenhead	1870s	1940s	1979
Scoat Tarn	1840s/50s	1950s	1975
Mean	1850s	1950s	1977
Southern England			
Hampstead Heath Pond	Pre-1920s	1950s	1969
Northwest England			
Daresbury Delph Pond	~1830 *	~1920s	1963

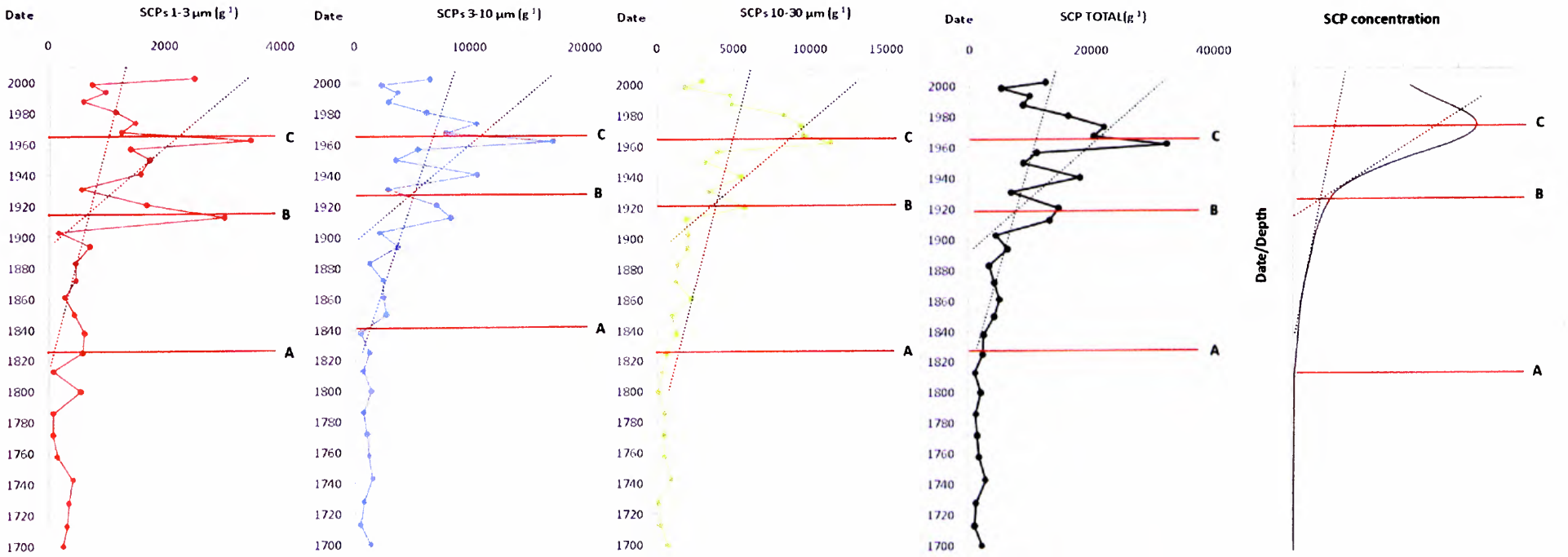

Figure 9.1: SCP concentrations from DDP (presented on a linear date axis) alongside a schematic figure of a typical SCP profile highlighting the three common features used in sediment core dating. A: the start of the SCP record; B: rapid increases in SCP concentration; and C: maximum SCP peak [adapted from Rose, 2001].

Sulphur is not, typically, used in palaeolimnology as a feature for inter-site core correlation, however, linear S concentration profiles demonstrate distinct close parallels post-1800 between the DDP and SHL sites (Figure 9.2). The closely matched ^{210}Pb dates assigned to these main peaks and troughs between SHL and DDP, potentially, further support the accuracy of the isotope chronologies. Due to these apparent corresponding features, S profiles may, potentially, be used as dating profiles in these urban ponds and lakes in the same way as SCP patterns. S concentrations are an overall indicator of industrialisation in post-1900 sediments due to the release of SO_2 into the atmosphere from fossil fuel combustion [Eimers *et al.*, 2006]. Due to the known coal combustion trends in the UK, corresponding to the SCP dating features, S concentrations are expected to rise, initially, during the Industrial Revolution, increase throughout the mid-20th century due to energy demands and, subsequently, decrease due to the introduction of Clean Air Acts post-1956. As urban ponds are likely to be heavily impacted by industrialisation, this may highlight a viable method of validating inter-site chronologies where sedimentation rates have minimal influence on the sediment record. As sediment accumulation rates vary with time at DKC, WH and OG, an assessment of correlating S concentration features with SHL is problematic.

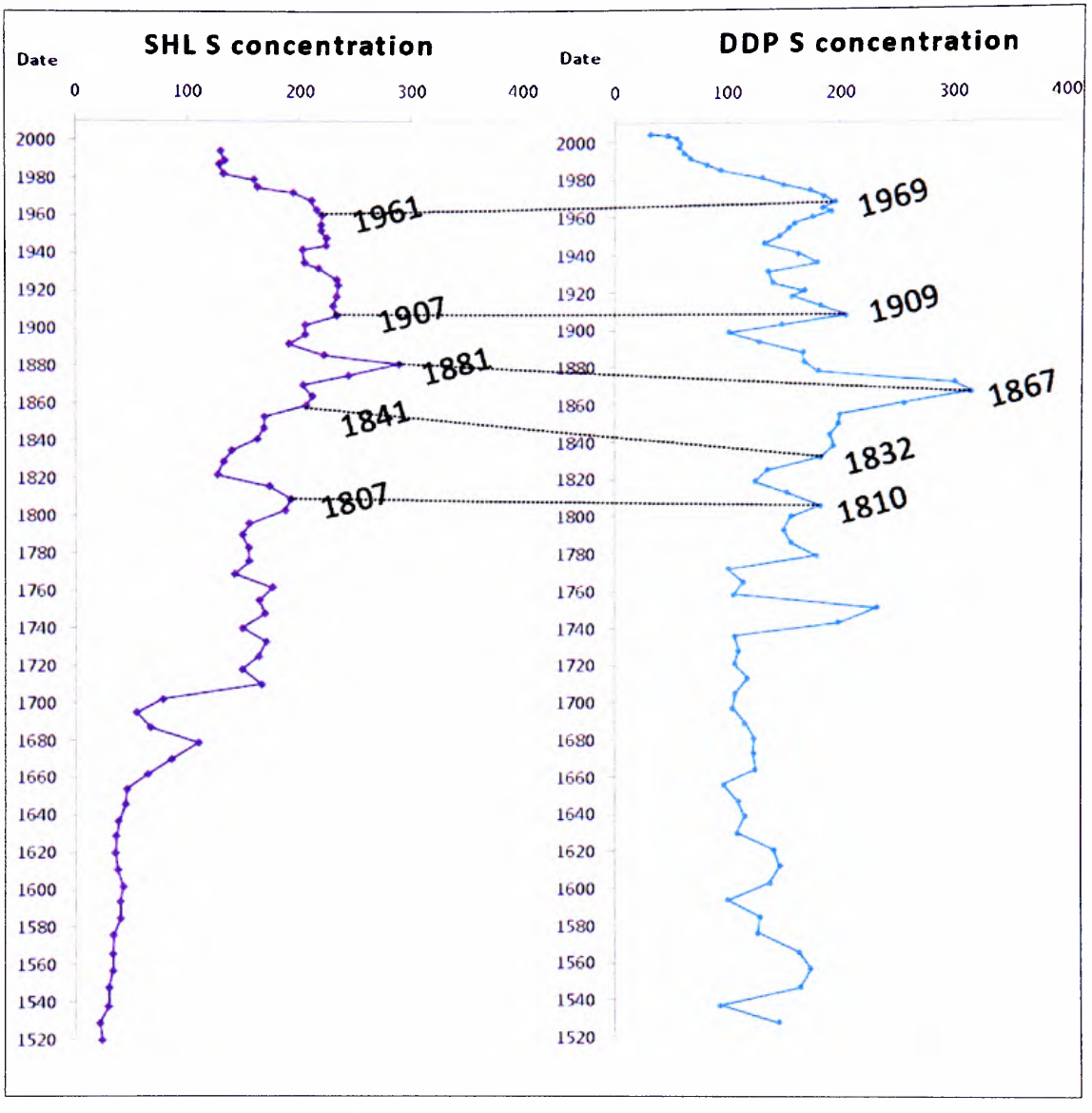

Figure 9.2: Correlating S features and assigned ^{210}Pb dates observed between Speke Hall Lake (SHL) [Worsley *et al.*, 2006] and Daresbury Delph Pond (DDP).

The high-resolution chronologies obtained from the four ponds (Section 5.5) allow sediment accumulation rates to be calculated at each site. Sedimentation rates vary between each of the investigated sites (Table 9.2). Van Metre and Callender [1997] state that sedimentation rates for most rural lakes vary from 0.05 to 10 mm y^{-1} (0.005 to 1 cm y^{-1}) [Oliver *et al.*, 1989; Sanders *et al.*, 1992], and higher rates are observed in man-made reservoirs, ranging from 10 to 200 mm y^{-1} (1 to 20 cm y^{-1}) [Van Metre and Callender, 1997]. Sediment rates (cm y^{-1}) presented for DDP, WH, DKC, OG and SHL (Table 9.2) correspond to the typical sedimentation rate for rural sites, with higher maximum sedimentation rates observed at DKC and OG. Urban ponds and lakes, however, receive sediment differently to rural lakes. Charlesworth and Lees [2001] highlight the problem of

catchment disturbance when using urban stratigraphies, and identified a lack of intra-site time synchronous horizons in two urban lakes in Coventry. Charlesworth and Lees [2001] attribute this to a sporadic delivery of sediment in urban lakes, opposed to a continuous supply characteristic of rural lakes. However, this may be ruled out in the LMR ponds because of the ^{210}Pb chronologies obtained, which would not be possible if disturbed (Section 9.5.).

Table 9.2: Sedimentation accumulation rates at DDP, DKC, WH, OG and SHL.

Site	Sediment accumulation rate g cm^{-2} y^{-1}			Sedimentation rate cm y^{-1}		
	Maximum	Minimum	Mean	Maximum	Minimum	Mean
DDP	0.052	0.011	0.018	0.340	0.051	0.107
WH	0.192	0.002	0.075	0.380	0.126	0.219
DKC	0.522	0.017	0.203	0.670	0.100	0.391
OG	0.096	0.017	0.046	0.750	0.115	0.328
SHL	0.019	0.011	0.014	0.210	0.090	0.129

All of the investigated pond sites in the LMR demonstrate rapid increases in sedimentation rates during the mid to late 20th century. This may reflect potential site specific changes within the catchments and/or increased atmospheric pollution inputs due to urban developments [Meriläinen *et al.*, 2003]. The catchments of these investigated ponds are negligible, defined by built-up, vegetated margins of the pond; therefore, the contribution of sediment from land surrounding the site is expected to be very small. This is further supported by χ_{FD}% values which, although highlight an SP contribution, typical of topsoil, do not show a dominance of a magnetic soil signature within the four urban ponds.

Charlesworth and Foster [1999] highlight an increase in sedimentation rates in an urban lake due to atmospheric fallout from vehicular emissions, which they report is a viable source of sediment to urban lakes with negligible catchment areas, due to an increase in vehicular emissions from 30 (10^3) tonnes in 1970 to 70 (10^3) by 1990 [Quality of Urban Air Group 1993]. Thus, combined with industrial emissions, this anthropogenic input to lakes from the atmosphere may reflect the increases in sediment rates observed in the urban ponds, which are, potentially heavily impacted by atmospheric fallout due to their high lake-to-catchment ratios.

DDP exhibits a steadily increasing trend in sedimentation post-1860, with higher depositional rates post-1950, which may reflect the general urbanisation of the surrounding area. The inclined agricultural field adjacent to the DDP pond may provide a negligible input to the lake, potentially, affected by agricultural practices; and the development of the

surrounding roadways, which form the boundaries of the extended catchment, may also have influenced sediment delivery.

Due to limited evidence for disturbance within the catchment, atmospheric input may be responsible for increased sediment delivery at DKC and OG. These ponds are closed systems with vegetated (woodland) margins. The expansion of the John Lennon International airport and increased air travel activity may have impacted the adjacent (<1 km) OG pond, further explored in Section 10.6.5. Also, increases in sediment accumulation at DKC and OG coincide with a considerable urban development at nearby Halewood (<4 km from DKC and <3 km from OG) during the 1950s and 1960s, further highlighting the potential contribution of air pollution particulates to sediment accumulation rates.

A notable shift in the contribution of sediment to WH is observed post-1951; whereby, sedimentation rates increase, with a higher supply of organic material (from <10% pre-1951 to 30-40% post-1951). A corresponding reduction in dry bulk density may reflect a reduction in compaction in this recent post-1951 section (Figure 5.6, Section 5.4.). Potential causes for increased organic sediment accumulation at this site may include:

(i) An increased supply of leaf matter to the lake basin from the surrounding woodland.

(ii) The covering of tarmac and concrete within the urban catchment [Charlesworth and Foster, 1999]. For example, the footpaths that surround the WH pond, may have been 'improved' with concrete and tarmac and, therefore, reducing an inorganic catchment/soil-derived signal.

(iii) Changing hydraulic conditions. For example, a reduction in drainage efficiency due to the blockage of the overflow drain that links WH with an adjacent larger pond. This may have caused a shift in organic contributions to the lake, with higher organic fractions accumulating, due to suspended material not being delivered to the adjacent pond [Foster *et al.*, 1990; Charlesworth and Foster, 1999].

(iv) Changing atmospheric deposition. Atmospheric fallout of inorganic pollution may have locally reduced due to the closure of nearby (~<2 km) tanneries, which coincides with an increase in anthropogenic organic compounds, produced as by-products by the organic chemical industry. This may impact this site due to the extensive amount of organic chemical production and release of a range of organic substances throughout the borough (Table 2.1, Section 2.4.1.).

Also, post-1949 increased growth of the woodland which surrounds the pond may have resulted in trees acting as particulate traps, due to the known adsorption of pollution on the surface of tree leaves [Matzka and Maher, 1999; Hansech *et al.*, 2003; Moreno *et al.*, 2003; Power *et al.*, 2006, 2009]. This may explain reduction in post-1949 magnetic (Figure 7.5) and trace metal flux (Figure 7.7). Due to this change in depositional conditions post-1951 at the WH site, the extrapolation of dates pre-1951 should be regarded with some caution.

9.6. Post depositional changes to the magnetic and trace metal records

Origins of magnetic grains in the urban pond sediments can be broadly divided into: (i) allogenic processes, the transportation of grains to the lake via aeolian or fluvial processes, which includes direct atmospheric fallout of pollution particulates; and (ii) authigenic processes, the formation within or on the surface of the lake sediments via bacterial magnetosomes, authigenic iron sulphide or reductive diagenesis [Dearing, 1999(a)]. There is potential for magnetic grains to undergo post-depositional changes as a consequence of reducing environments within lakes [King and Channell, 1991; Verosub and Roberts, 1995; Dekkers, 1997]. The magnetic record is influenced by the naturally occurring reactions relating to the decomposition of organic matter in sedimentary environments [Verosub and Roberts, 1995]. The urban ponds demonstrate a constant supply of organic sediment and under these conditions, biogenic magnetite can form [Verosub and Roberts, 1995]. The identification of bacterial magnetite within the four urban ponds is dealt with (Chapter 6), where SSD grains dominate, and magnetic properties suggest the potential for a bacterial source impacting the magnetic signal.

Samples identified as dominated by SSD grains, in the recent sediments of DDP and DKC, is further explored using Oldfield's [2007] bi-logarithmic template (Section 6.3.1., Figure 6.4, Section 6.5.1. and Figure 6.17, respectively), which suggests two instances of fine (SSD) ferrimagnetic grains in lakes: in soil and magnetosome dominated samples (Section 6.3.1.). However, another potential source of SSD ferrimagnetic grains in the sediments of urban ponds, not included in Oldfield's [2007] template (Figure 6.4 and Figure 6.17) could arise from atmospherically-derived particulates.

Anthropogenic derived magnetic spherules are widely characterised as ferrimagnetic and antiferromagnetic MD (>10 μm) and PSD grains (~>1 μm) [Hunt *et al.*, 1984; Oldfield *et al.*, 1985; Hunt, 1986; Yang *et al.*, 1997; Petrovský and Ellwood, 1999; Evans and Heller, 2003]. However, several authors report the significance of anthropogenic ferrimagnetic

grains <1 μm in urban sediments, which fall into the SSD and, potentially, SP boundaries. For example, Muxworthy *et al.*, [2001, 2003] report a SSD magnetite-type phase, attributed to vehicular pollution, in urban dusts with mean grain sizes of 0.2-0.5 μm and <0.1 μm. Also, Xie *et al.*, [2001] report a potential anthropogenic SP component in contemporary urban dust. This is further supported by known significant submicron particulate size ranges for diesel exhaust PM (<1 μm) [Morawska *et* al., 1998], oil fly ash (<0.7 μm), coal fly ash (0.2-10 μm) [Mamane *et* al., 1986] and a range of fine (<2.5 μm) and ultra fine (<0.1 μm) pollution sources of PM [McElroy *et al.*, 1982; Phalen, 2002], highlighting a potential anthropogenic source of SSD magnetic grains.

The early work by Oldfield *et al.*, [1985] and Hunt *et al.*, [1984], distinguishing the anthropogenic sources of magnetic grains via mineral magnetic properties, compared atmospheric dust samples collected using meshes, which do not efficiently capture particulates <1 μm [Hunt *et al.*, 1984; Oldfield *et al.*, 1985; Hunt, 1986]. Fly ash and vehicular particulates were captured using a four-stage cascade impactor, which Hunt [1985] reports as having a 50% efficiency and cut-off diameters of 7, 3, 2 and 1.1 μm. These samples may, therefore, not be efficiently representative of atmospheric dusts <1 μm, which fall into the SSD size boundary[†] (~<1 μm), resulting in the magnetic properties of PM_1 not being fully realised. This may, therefore, effect the magnetic characterisation of the investigated polluted dusts, for example, the high SIRM/ARM ratios exhibited. Thus, the use of magnetic properties as proxies of anthropogenic SSD ferrimagnetic grains is limited, resulting in high ARM values being solely attributed to soil-derived (SP) inputs[‡].

The potential contribution of <1 μm (SSD) magnetic grains to pollution-derived signals is of importance in this work, especially due to the post-1975 shifts to fine grains in DDP and DKC, and the relatively finer magnetic signal post-1989 at WH and post-1990 at OG; combined with the noted suitability of ARM as a proxy for PM_1 pollution of contemporary urban dusts [Power *et al.*, 2009; Yang *et al.*, 2010]. Muxworthy *et al.*, [2001, 2002] report a potential anthropogenic magnetic component of urban street dusts, characteristic of 0.1-0.7 μm. A fine-grained, 0.2-5 μm magnetic fraction of urban dust, attributed to exhaust particulates is also reported by Matzka and Maher [1999]. This is further supported by the accepted trimodal size distributions of anthropogenic PM, which can display coarse, fine

[†] Although individual fine magnetic spheres can form agglomerates of coarse PM [Morwaska *et al.*, 1999], the magnetic properties of PM_1 may not have been fully explored.

[‡] Oldfield *et al.*, [1983] states that 'viscous grains are common in soils, we have never found a large viscous component in any of the domestic fossil fuel combustion particulates'.

and sub-micron particle size peaks [Phalen, 2002] and the long-range transportation of fine (<1 μm) industrial magnetic grains [Yang *et al.*, 1997].

The magnetic signal can also be influenced by the authigenic formation of gregite due to reductive dissolution of ferrimagnetic grains, typically, occurring in slowly accumulating (<0.5 mm y^{-1}) lakes [Oldfield *et al.*, 1992; Verosub and Roberts, 1995; Dekkers, 1997; Dearing, 1999(a); Snowball and Torii, 1999]. Criteria (i to vi) set out by Dearing [1999(a)] were used to identify the presence of gregite and effects of dissolution in then urban pond sediments:

(i) correlation of Mn and Fe with χ_{LF}, χ_{ARM} or SIRM;
(ii) high χ_{ARM}/SIRM values;
(iii) SIRM/χ_{LF} values >40 k Am^{-1};
(iv) lack of correlation between ferrimagnetic grains and 'hard' grains;
(v) very low/zero magnetic concentrations; and
(vi) lack of intra-site core correlation.

Correlations between SIRM, χ_{LF} and χ_{ARM} with Mn and Fe (i) were only identified in DKC; however, stronger correlations identified between the magnetic concentration parameters and Pb and Zn, highlight a dominating anthropogenic source of magnetic grains. Also, increases in χ_{ARM}/SIRM trends (ii) observed in the DKC and DDP profiles in the most recent section of the sediments, highlighting a potential shift to a finer grained magnetic signal. However, SIRM/χ_{LF} values (iii) do not signify a dominance of gregite at any of the sites. Also, criteria iv to vi are not identified in the urban pond sediment records, apart from low and negative χ_{LF} values, exhibited by WH, which may reflect a diamagnetic effect on the magnetic record due to the observed OM increases.

Post-depositional mobility of trace metals in lake sediments is also a factor that may blur the proxy pollution record. Opposing Pb and Zn trends observed in an urban lake in Wales, highlights the potential of Zn mobility within the lake sediment column [Blake *et al.*, 2007]. SCPs are, however, immobile in lake sediments [Rose, 2001]. Therefore, the strong positive correlations between trace metals and SCPs observed in the DDP core suggest a lack of mobility. Also, near surface Cu and Zn maxima, as observed at DDP, is a phenomenon which is sometimes observed in lake sediments [Tylmann, 2005] and is attributed to the diffusion of metals and processes of exchange between sediment and near-bottom water [Boyle, 2001]. Surface maximums are, therefore, interpreted with caution

due to active characteristics of the sediment surface layer and associated biogeochemical processes and diagenesis [Tylmann, 2005].

9.7. Catchment/ soil derived contributions to the sediment record

Increased sedimentation rates are a potential indicator of erosion episodes and, therefore, the supply of catchment derived material to lakes [Dearing *et al.*, 1998]. Foster *et al.*, [1991] demonstrates the importance of flux profiles, reflecting sedimentation rates due to erosion within lake catchments. Supply of trace metals, SCPs and magnetic grains to the urban ponds are presented as flux profiles (Chapter 7, discussed in Chapter 10). Flux conversions essentially correct for variations in sedimentation rates. Normalisation of proxy pollution data in this way is important, due to the observed temporal variations of sediment delivery in the urban ponds.

Due to their negligible catchment size it is likely that atmospheric input, as opposed to the input of catchment soils, is the dominating contribution to the magnetic records in the urban ponds [Oldfield and Richardson, 1990(a)]. This is further supported by very few sediment samples exhibiting a dominance of SP grains in the four ponds, a magnetic characteristic of topsoils, signified by χ_{FD} values exceeding 10%. However, for most of the urban cores, χ_{FD} values highlight a contribution of SP grains. The application of SP grains as a magnetic signature for soil inputs may be complicated in urban sediments, due to the potential for anthropogenic magnetic particulates to contribute to this SP (<0.05 μm) size range. Particulates of this size are widely reported in studies analysing size characteristics of urban PM [McElroy *et* al., 1982; Morawska *et al.*, 1998; Phalen, 2002] and the potential for SP grains to contribute to urban street dust is also reported [Xie *et al.*, 1999(b)].

The closely paralleled synchronous trends in trace metal profiles, within each pond suggest an atmospheric signal, rather than a catchment derived source, which as Yang and Rose [2004] suggest, would be characterised by peaks occurring at differing time scales/depth of sediment core because of separation of trace metals after deposition within the catchment and subsequent deposition to the lake at varying times.

Minerogenic trace elements (Al, Si, Ti, Zr) have also been used as tracers for catchment/ soil derived material [Mackereth 1966; Van Metre and Callender, 1997]. Varying trends are observed between typically anthropogenic trace metals and minerogenic trace elements at all four pond sites, suggesting the trace metal record is not governed by soil inputs. Strong positive relationships identified, in the DDP site, between magnetic concentration

parameters (SIRM, χ_{LF} and χ_{ARM}) and Ti, Ca and K, potentially, indicate a detrital contribution to the magnetic record. χ_{FD}% in the DDP sediment record are 2-5%, which does not suggest a dominating topsoil input.

The use of trace metal enrichment factors, calculations of anthropogenic enrichment of trace metals in sediments using Al and Ti normalisations (Section 3.6.5.) have been used to further assess the effects of anthropogenic trace metals to the urban ponds. Pb enrichment factors (EF) are presented for BDD1 (Figure 9.3), revealing normalisations of the total Pb concentrations with basic Al and Ti corrections as well as pre-1800 pollution tracer-to-passive tracer ratio normalisations using Al (EF Pb:Al) and Ti (EF Pb:Ti) [Tylmann, 2005]. The EF profiles, overall, strongly resemble trends in original Pb concentration profiles (also presented for visual comparison), which highlight minimal diluting influence of the minerogenic component in the trace metal record. Although pre-1800 data are not available for DKC, WH and OG, perturbing normalisations using natural/pre-industrial contributions of Pb, normalisations using Ti concentrations reveal corresponding trends to the original Pb concentration profiles (Figure 9. 4) This suggests anthropogenic deposition overrides potential effects from soil/catchment inputs [Rose *et al.*, 1999(b)].

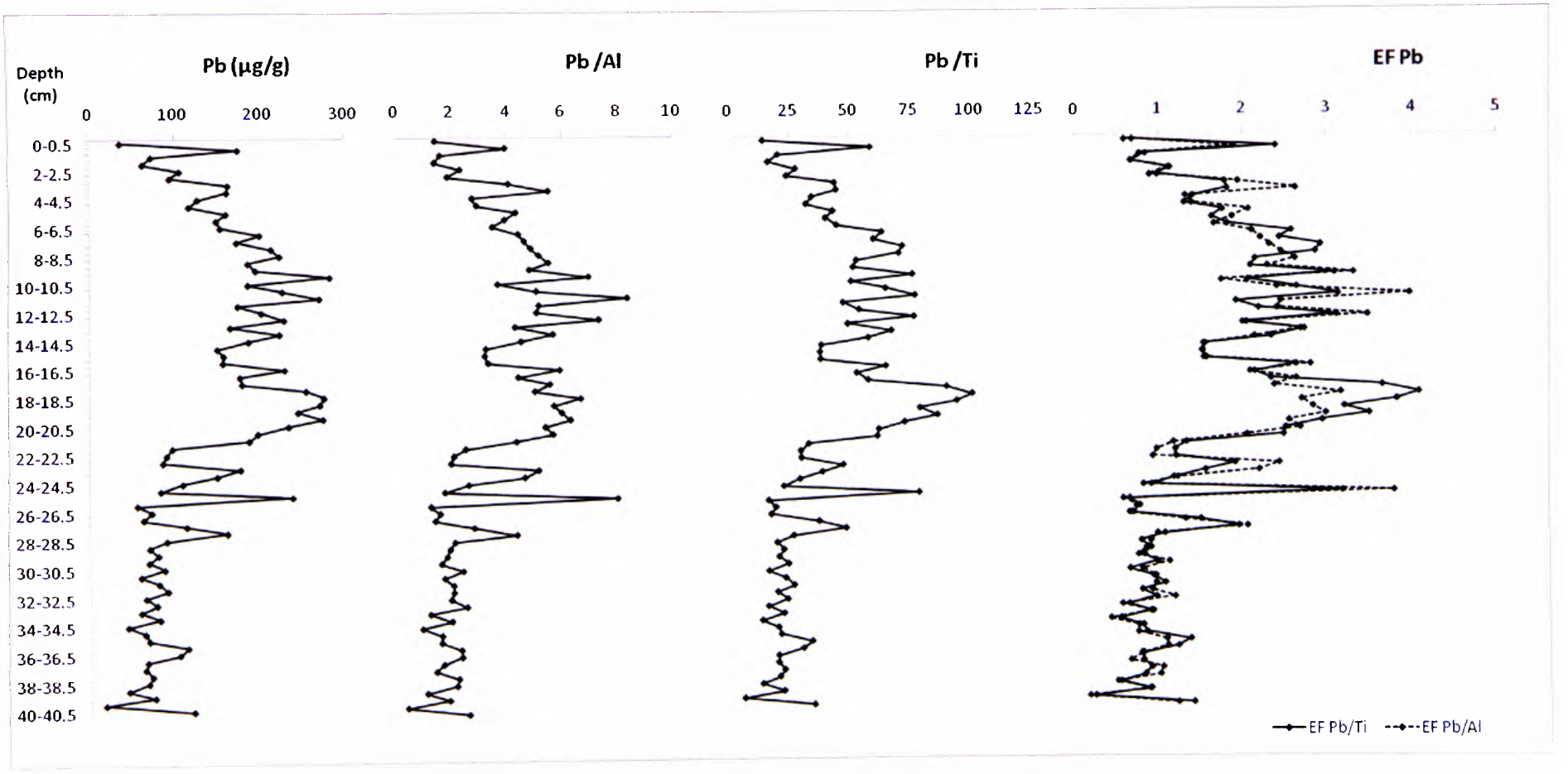

Figure 9.3: Original Pb concentration profiles with normalisation of Pb using Pb:Ti (10^3), Pb:Al (10^3) and EF Pb for BDD1.

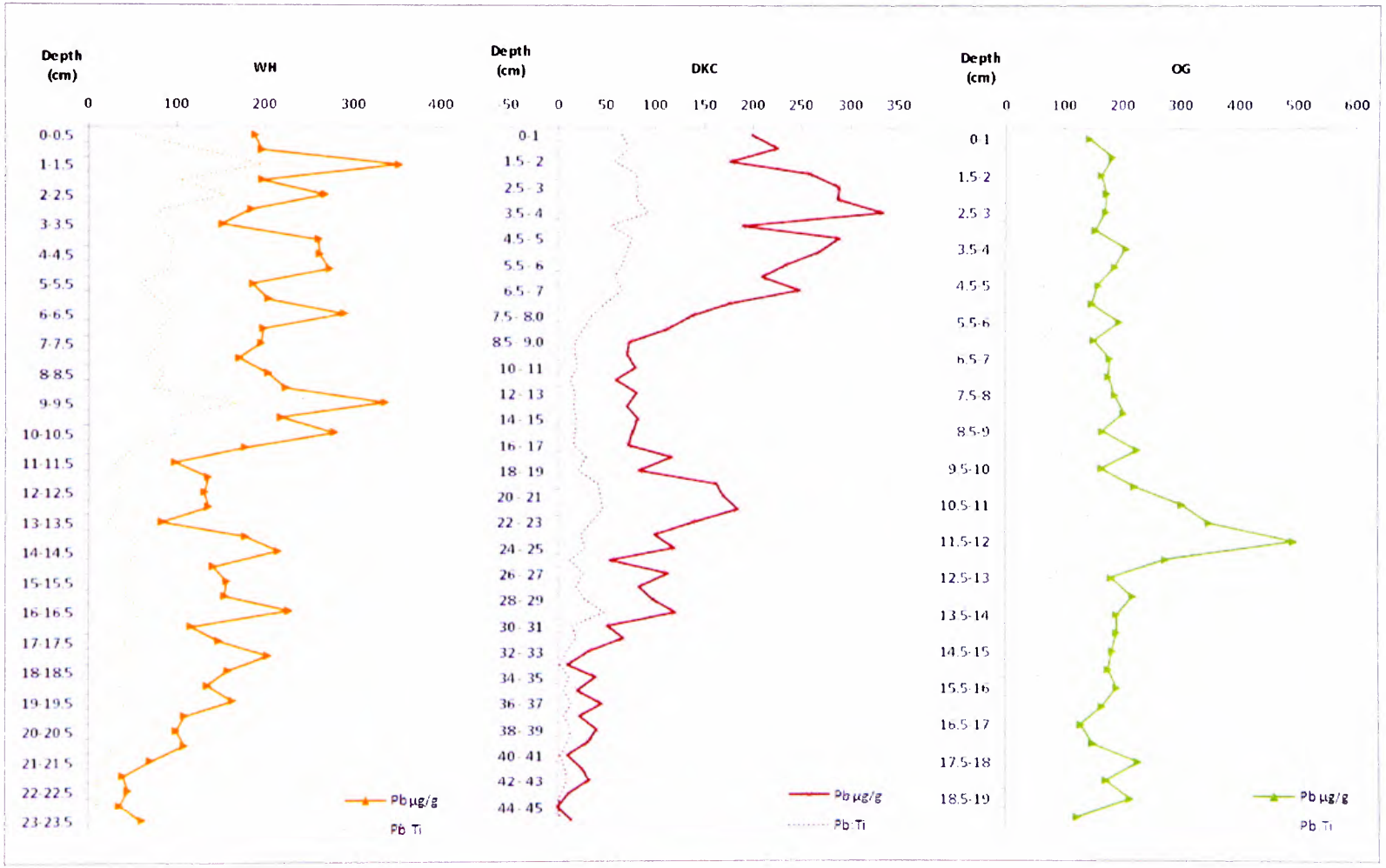

Figure 9.4: Pb:Ti, ratios and original Pb concentration profiles for DKC, WH and OG ponds.

9.8. Anthropogenic contributions to the sediment record

The main components of industrial pollution are the volatile compounds NO_X, NH_X, SO_X and O_3. When deposited in lake sediments these volatile compounds may be chemically reduced and ozone will remain a gas and no residue will remain in the sediment. Therefore, proxy pollution characteristics such as magnetic properties and trace metals (Pb, Zn, Cu and S) are used to infer pollution deposition. Magnetic records from lake sediments dominated by pollution particles are either from lakes close to urban areas, or from small upland catchments where fluvial inputs are low [Dearing *et al.*, 1998]. In these lakes the magnetic signal is dominated by fly ash from coal burning and metalliferous dusts [Locke and Bertine, 1986; McLean, 1991; Dearing *et al.*, 1998; Worsley *et al.*, 2006]. The central location of the urban ponds investigated in the LMR, combined with their small catchment sizes, suggest atmospheric fallout of particulates from surrounding emission sources heavily influences the sediment record. Enrichment factors (Figures 9.3 and 9.4) support the evidence for a sediment signature dominated by anthropogenically generated particles, opposed to catchment material, recorded at DDP, DKC, WH and OG.

SCPs are unambiguous indicators of anthropogenic particulates, most notably derived from the combustion of fossil fuels [Rose *et al.*, 1999(a)]. Therefore, strong significant relationships between SCPs and magnetic parameters and trace metals observed in the DDP pond (Table 6.7, Section 6.3.5.) highlight:

(i) The reliability of an urban pond (DDP) in capturing a depositional history of atmospheric particulate pollution within its sediments.
(ii) The magnetic record, is derived from atmospheric inputs rather than the catchment and; therefore,
(iii) The use of magnetic concentration parameters as suitable proxies for anthropogenic particulates.
(iv) The use of trace metals as reliable proxies of pollution deposition.
(v) The trace metal and magnetic signals in the other urban ponds (WH, DKC and OG) are highly likely to have been derived from anthropogenic sources.

Potential origins of environmental signals within the sediment records can be further explored via correlations between sediment characteristics [Heit *et al.*, 1981].

- Magnetic and trace metal associations:

In DDP and WH sediments, magnetic-trace metal associations are observed between Zn and SIRM. A lack of association between other trace metals and magnetic concentration parameters in the WH core may be due to a disruption in the magnetic signal due to diamagnetic values recorded in the recent sediments. Higher correlations with SIRM, as opposed to χ_{LF}, and trace metals have also been observed by Georgeaud *et al.*, [1997], who suggest paramagnetic minerals contribute to the χ_{LF} signal, while ferromagnetic minerals contribute to both χ_{LF} and SIRM values. This, potentially, highlights the suitability of SIRM, over χ_{LF} as a proxy for pollution deposition. Strong positive correlations between the typically natural elements, in particular Fe, and magnetic parameters are exhibited in the DKC sediment record. However, relatively higher associations are observed between the magnetic properties and Pb and Zn. This further highlights the division of the magnetic fraction between a weakly magnetic source of natural origin, associated with Fe, compared to a strongly magnetic fraction derived from anthropogenic sources, associated with Pb and Zn [Georgeaud *et al.*, 1997].

Despite closely paralleled trace metal and magnetic concentration profiles, a lack of a statistical association between the other magnetic parameters and the anthropogenic trace metal group is exhibited by WH and DDP. Charlesworth and Lees [1997] identified a lack of correlation between magnetic parameters and trace metal concentrations in the finer fraction (<63 μm) of urban dusts and urban lake sediments, further supported by principle component analysis (PCA), which they attribute to chemical and physical changes to urban sediment during transport and deposition throughout the urban environment. Charlesworth and Lees [1997, 1999(a)] suggest that due to complex mixing processes of pollutants during transport, pollution particulates found in the sedimentary matrix of urban lakes undergo transformations, from their original deposition in street dusts to their eventual deposition in urban lakes. Charlesworth and Lees [1997, 1999(b)] suggest this may, potentially, complicate trace metal and magnetic relationships, and affect the use of magnetic properties as a surrogate for trace metal pollution, which has been widely recognised in urban sediments [Strzyszcz, 1993; Hunt *et al.*, 1984].

Strong correlations between magnetic concentration parameters and trace metals in the sediments of DKC and OG, however, support Jennett *et al.*, [1980] who suggest that due to the complexity of urban pond processes, trace metal behaviour may be ecosystem specific and influenced by local catchment patterns of industrialisation and, therefore, may

potentially make the findings by Charlesworth and Lees [1997] non-transferable to other urban ponds [Charlesworth and Lees, 1997]. Also, Georgeaud *et al.*, [1997] identified strong associations between magnetic parameters and anthropogenic trace metals in a large urban lake (155.5 km^2) in southern France. Georgeaud *et al.*, [1997] suggest associations between magnetic parameters and trace metals in lake sediments occur from:

(i) co-precipitation of metal pollution during magnetic genesis from combustion processes;
(ii) subsequent adsorption of metals on magnetic grains; and
(iii) co-genesis of magnetite and metals without real physical links.

- The organic fraction of sediments and the anthropogenic signal:

Strong correlations observed between anthropogenic trace metals and OM at all four urban pond sites highlight a governing of the metal signal by the organic fraction of the sediment column. OM has a well-known affinity for trace metals identified in sediment cores [Renberg, 1986; Vesley *et al.*, 1993; Boyle *et al.*, 1998; Boyle, 2001; Yang and Rose, 2005]. Trace metals deposited in lakes either bind to sediment particulates in the lake water, accumulate in particulate form or become bound to organic matter [Renberg, 1986]. Authigenic organic matter and allochthonous soil organic fraction make up OM in lake sediments [Boyle, 2004], which play an important role in the distribution of trace metals during burial and diagenesis [El Bilali *et al.*, 2002; Huang and Lin, 2003].

Humic minerals can scavenge metal ions in lake sediments due to metal-organic binding systems [Coker, 1995; Plater *et al.*, 1998]. Trace metals absorb and/or adsorb to OM, which may explain the trace metal enhancement within the OM fraction of urban ponds. Upon sedimentation, trace metals partition themselves among various binding substrates within the sediments, e.g. iron and manganese oxides and organics [Lewis and McIntosh, 1989; Nriagu and Coker, 1980; Dissanayake, 1983]. As humic material has a potential association with Fe and Mn, this may explain the positive associations between the anthropogenic metal group and Fe and Mn in DKC (Table 6.21, Section 6.5.4.).

At WH (Table 6.13), DKC (Table 6.20) and OG (Table 6.27), negative correlations are observed between OM and the minerogenic elements, whereas no associations are exhibited at DDP, further highlighting the role of the organic fraction and the capture of anthropogenic trace metals. OM associations with magnetic concentration parameters

(DDP (Table 6.4), DKC (Table 6.44) and OG (Section 6.6.5.)) and SCPs (DDP (Table 6.4)) are also observed. This may reflect the trapping of pollution particulates within the organic fraction, deposition of SCPs alongside the accumulation of organic matter within the basin, or an indirect association between SCPs and OM, due to the observed correlations between SCPs and trace metals which, in turn, are associated with OM.

- Particle size relationships:

Particle size relationships are identified in the DDP core, highlighting a fine-grained signature of the magnetic and SCP signal, due to their positive association with the clay fraction, particle distributions <10 μm and negative correlations with sand (Table 6.7). However, the trace metals do not exhibit significant associations with a particular size fraction. No particle size relationships were identified in the WH sediments. In the DKC sediments, the silt fraction appears to govern Pb, S and Zn concentrations, which also exhibits positive correlations with Fe and Mn (Table 6.27), potentially, reflecting the importance of the organic fraction as Fe and Mn are associated with humic substances Blake *et al.*, 2007] and demonstrated negative association with the minerogenic elements. Also, the clay fraction appears to govern the minerogenic component of sediments in the OG pond.

- Inter-trace metal/element groups:

Due to similar characteristics and, potentially, common sources, revealed by statistical analyses, trace metal concentrations in the urban ponds can be grouped into anthropogenic and natural classifications (Figure 9.5). A general division between pollution derived and naturally occurring elements is observed at all four urban ponds. Anthropogenic trace metals, overall, show an association with the organic fraction, magnetic concentration parameters and in the DDP sediments, with SCPs. Strong positive correlations observed between the anthropogenic metals, further enhances a common source. Inter-elemental relationships are also identified between the natural elements, again suggesting they are derived from a similar source (Figure 9.5). Furthermore, negative correlations between the anthropogenic and natural element groups, support a distinction of depositional histories between the groups (Figure 9.5). The similar trace metal, magnetic and OM relationships, identified in the sediments of all four ponds, also highlights similar depositional conditions within the urban basins.

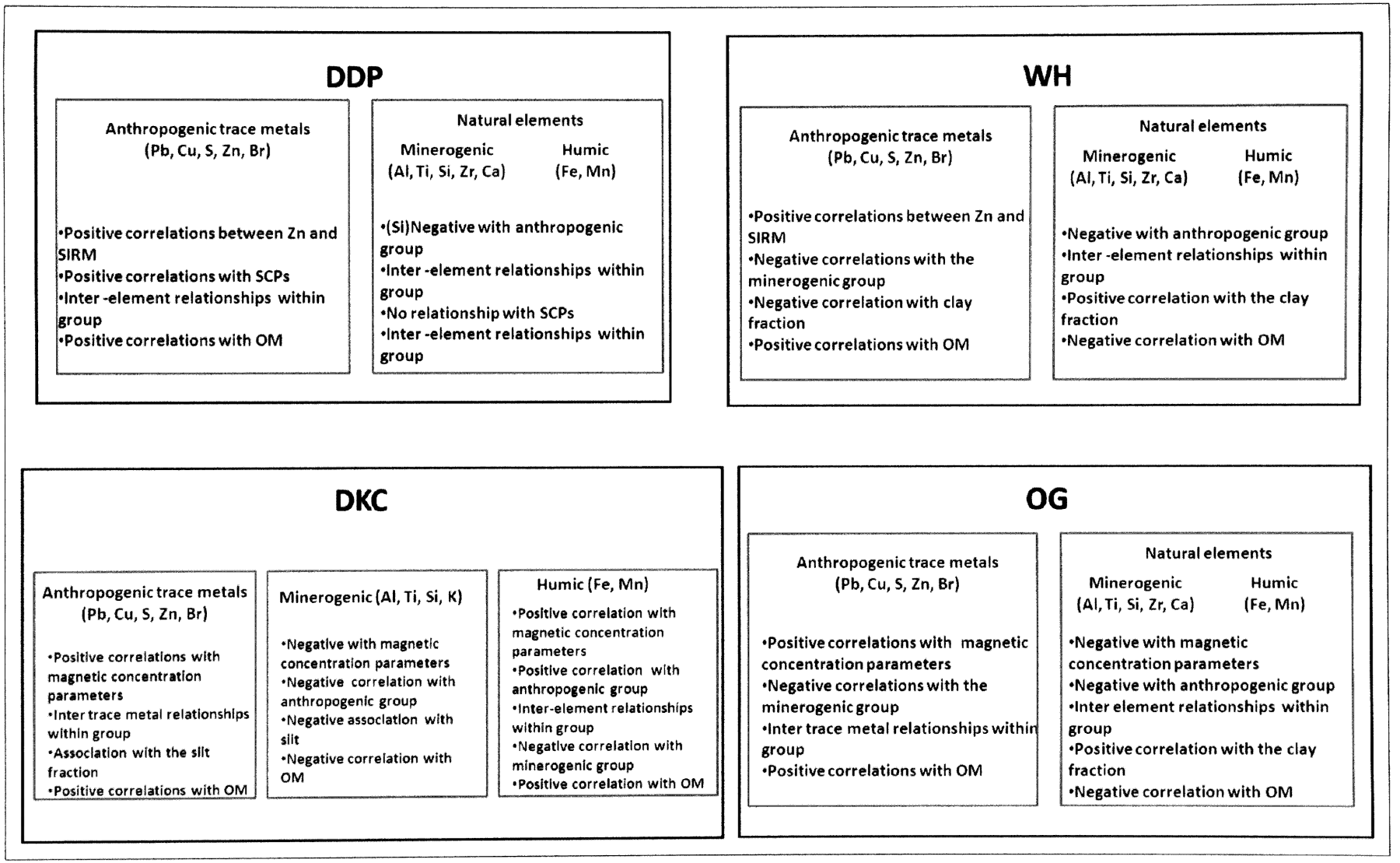

Figure 9.5: Potential trace metal groups and their characteristics identified in the urban pond sediments.

The stratigraphy obtained from DDP extends to pre-industrial times, allowing normalisations of background/natural inputs using pre-industrial (i.e. pre-1800) data; therefore, separating natural from anthropogenic fractions. The anthropogenic supply of trace metals can therefore be further explored via a range of normalisations including:

(i) trace metal inventories,
(ii) cultural enrichment factors and
(iii) anthropogenic flux profiles.

- Trace metal inventories:

Total and anthropogenic Pb, Zn, Cu and S inventories in the sediments of DDP are presented for the down-core phases identified at DDP (DDi to DDiv) (Table 9.3). 'Total' inventories are the sum of total trace metal concentrations multiplied by sediment per unit area for a given time period, and 'anthropogenic' inventories are an estimate of the anthropogenic contribution to the total inventory, normalised for background (pre-1800) trace metal concentrations (Section 3.6.7.). Therefore, the trace metal inventories allow an assessment of the total and anthropogenic supply of a particular trace metal for a certain time period [Yang and Rose, 2005].

Table 9.3: Total and anthropogenic ('anthro') pollution inventories for BDD1 [after Yang and Rose, 2005].

Trace metal	**DDiv: Post-1978**		**DDiii: 1900-1978**		**DDii 1832-1900**		**DDi Pre-1832 (1832-1700)**	
	Total	*Anthro*	Total	*Anthro*	Total	*Anthro*	Total	*Anthro*
Pb (μg cm^2)	73.744	*23.039*	285.191	*163.900*	254.432	*153.101*	217.189	*30.205*
Zn (μg cm^2)	174.211	*114.799*	697.968	*555.850*	413.627	*294.894*	243.577	*23.052*
Cu (μg cm^2)	70.935	*16.706*	302.061	*172.326*	234.840	*126.454*	243.172	*54.337*
S (mg cm^2)	5.022	*-2.978*	23.891	*4.754*	23.302	*7.315*	30.554	*1.210*

Minimum total inventories for Pb, Zn, Cu and S occur post-1978 (DDiv), lower than pre-1832 (DDi) values. Anthropogenic inventories or Pb, Cu and S are also lowest in this phase. S demonstrates negative anthropogenic inventory values, possibly highlighting a reduction in S below pre-1832 levels. These relatively low total and anthropogenic inventories post-1978 reflect the overall decline in trace metals observed in the concentration (Figure 6.7) and flux profiles for DDP (Figure 7.2).

Total and anthropogenic inventories are highest for Pb, Zn and Cu from 1900-1978 (DDiii) indicating a considerable anthropogenic input during this phase. Highest anthropogenic S contributions occur from 1832-1900 (DDii) and total S pre-1832 (DDi). This possibly reveals an early (pre-1832) anthropogenic contribution of S to the DDP record.

This highlights the deposition of trace metals is not uniform. Maximum anthropogenic S inventories form 1832-1900 (DDii), potentially, reflect the Industrial Revolution and associated coal combustion; whereas the highest Zn, Pb and Cu anthropogenic inventories occur post 1900 (DDiii) suggesting a 20th century source of these trace metals influencing the sediment record.

Ratios of these anthropogenic-to-total inventories (Table 9.4) reveal anthropogenic contributions of trace metals increase post-1832 (DDii). Zn demonstrates a notable increase in anthropogenic fraction post-1900, with ~80% of Zn concentrations highlighted as anthropogenic from 1900-1978 (DDiii). Pb and Cu also demonstrate relatively high anthropogenic contributions (~60% and 54%, respectively) in this phase. These inventories also reveal the anthropogenic contributions of Pb (52%), Zn (72%) and Cu (48%) in post-1800 sediment. S, however, exhibits low anthropogenic-to-natural ratios, which may reveal a catchment source of S, or may highlight relatively high pre-1800 S levels.

Table 9.4: Anthropogenic-to-total trace metal inventory ratios for DDP (* post-1978 anthropogenic S fraction calculation is prevented due to zero values).

Trace metal	DDiv Post-1978	DDiii 1900-1978	DDii 1832-1900	DDi Pre-1832 (1832-1700)	Total (post-1800)
Pb	0.312	0.575	0.602	0.139	0.523
Zn	0.659	0.796	0.713	0.095	0.717
Cu	0.235	0.571	0.538	0.223	0.484
S	*	0.199	0.314	0.040	0.165

- Cultural enrichment factors:

The anthropogenic component of Pb, Zn, Cu and S in the DDP sediment samples is explored via Cultural Enrichment Factors (CEFs) (Table 9.5) for each ~post-1800 depth interval. CEFs, applied by Heit *et* al., [1981] are ratios of trace metal concentration-to-constant baseline (pre-1800) values and, therefore, identify elevated levels of trace metals beyond natural/background values (Section 3.6.6.). CEF ratios: <1 and ~1 indicates no significant anthropogenic contribution, 1-2 suggests some evidence of anthropogenic input and >2 highlights greater anthropogenic contributions [Heit *et al.*, 1981] (Section 3.6.6.).

Zn demonstrates the highest CEF ratios (maximum of 6.8) compared to maximum ratios exhibited by Pb (3.3), Cu (3.9) and S (2.4). The maximum Zn CEF occurs at the sediment-surface[§], however, Zn demonstrates elevated (>2) CEFs throughout the core from 1844 (20-20.5 cm), with particularly high values (>4) occurring between 1914 and 1969 (6.5 to 14.5 cm). Elevated Pb and Cu CEFs (>2) are observed from 1832 and 1838 respectively, which continue until 1889 for Pb and 1873 for Cu. Pb demonstrates particularly high (>3) values between 1850 and 1873, which corresponds to elevated Zn, Cu and S at this time. Pb also exhibits CEFs >2 from 1909 to 1969, however CEFs decline to <2, highlighting a reduction in anthropogenic contribution post-1969. Also Cu displays relatively high (>2) CEF values from 1937-1975, which then decrease to <2 in post-1975 sediment. S demonstrates relatively low (1-2) CEF ratios throughout the core, with values declining to <1 from 1981 to present day, indicating no significant anthropogenic contribution.

[§] High Zn CEFs in 0-1 cm may be due to migration, or may be due to surface enrichment.

Table 9.5: Cultural Enrichment Factors (CEFs) for DDP post 1800 according to Heit *et al.*, [1981]. CEF <1 showing no significant anthropogenic input (not highlighted), CEF 1-2 (highlighted orange) and CEF >2 (highlighted red) demonstrate significant anthropogenic contribution.

Depth (cm)	Age	Pb CEF	Zn CEF	Cu CEF	S CEF
0-0.5	2005	0.4	6.6	3.4	0.2
0.5-1	2004	2.1	6.8	3.9	0.4
1-1.5	2002	0.9	2.0	0.4	0.4
1.5-2	2000	0.8	2.4	0.6	0.4
2-2.5	1997	1.3	2.6	0.3	0.4
2.5-3	1995	1.1	1.8	2.0	0.5
3-3.5	1992	1.9	2.3	1.2	0.5
3.5-4	1989	1.9	2.7	1.2	0.6
4-4.5	1985	1.5	2.6	1.6	0.7
4.5-5	1981	1.4	3.5	1.3	1.0
5-5.5	1978	1.9	3.9	1.2	1.1
5.5-6	1975	1.8	3.9	2.0	1.3
6-6.5	1972	1.8	3.2	2.9	1.4
6.5-7	1969	2.4	4.5	2.1	1.5
7-7.5	1966	2.0	4.5	1.4	1.4
7.5-8	1963	2.5	5.6	2.5	1.4
8-8.5	1961	2.6	5.7	3.1	1.3
8.5-9	1958	2.2	5.3	2.5	1.2
9-9.5	1954	2.3	5.7	2.1	1.2
9.5-10	1950	3.3	5.5	2.7	1.1
10-10.5	1946	2.2	5.0	2.8	1.0
10.5-11	1942	2.7	6.5	2.4	1.2
11-11.5	1937	3.2	5.6	2.7	1.4
11.5-12	1931	2.1	4.7	1.6	1.0
12-12.5	1925	2.4	5.0	1.6	1.1
12.5-13	1921	2.7	6.4	1.5	1.3
13-13.5	1918	2.0	4.5	2.7	1.2
13.5-14	1914	2.6	5.1	2.5	1.4
14-14.5	1909	2.2	3.7	2.4	1.6
14.5-15	1904	1.8	3.5	2.8	1.1
15-15.5	1899	1.9	3.6	1.4	0.8
15.5-16	1894	1.8	3.3	1.6	1.0
16-16.5	1889	2.7	3.9	2.0	1.3
16.5-17	1884	2.1	2.7	2.0	1.3
17-17.5	1878	2.1	3.2	1.1	1.4
17.5-18	1873	3.0	3.9	3.3	2.3
18-18.5	1867	3.3	5.3	3.3	2.4
18.5-19	1862	3.2	5.0	2.5	1.9
19-19.5	1856	2.9	4.6	1.9	1.5
19.5-20	1850	3.2	3.4	2.5	1.5
20-20.5	1844	2.8	2.7	3.5	1.4
20.5-21	1838	2.3	1.9	2.2	1.5
21-21.5	1832	2.2	2.0	1.7	1.4
21.5-22	1826	1.1	1.0	1.2	1.0
22-22.5	1820	1.1	1.4	0.7	0.9
22.5-23	1813	1.0	0.5	1.6	1.2
23-23.5	1807	2.1	1.5	1.3	1.4
23.5-40.5	Pre -1800 mean	1.0	1.0	1.0	1.0

- Anthropogenic flux fractions:

The conversion of concentration data to flux profiles allows a 'real-time' accumulation of pollution proxies to be assessed (Chapter 7). Total and anthropogenic Zn, Pb (Figure 9.6), Cu and S (Figure 9.7) flux for DDP are presented. Pre-1800 Ti normalisations, a passive tracer after Norton *et al.*, [1992] and natural corrections using pre-1800 Pb and Zn data after Vesléy *et al.*, [1993] (Section 3.6.8.2.) demonstrates an overriding anthropogenic contribution of Pb, Zn, Cu and S to total trace metal flux (Figure 9.3), reflected by mirrored total and anthropogenic flux trends. This further supports the dominance of an anthropogenic, opposed to natural, trace metal signal recorded in the DDP sediments.

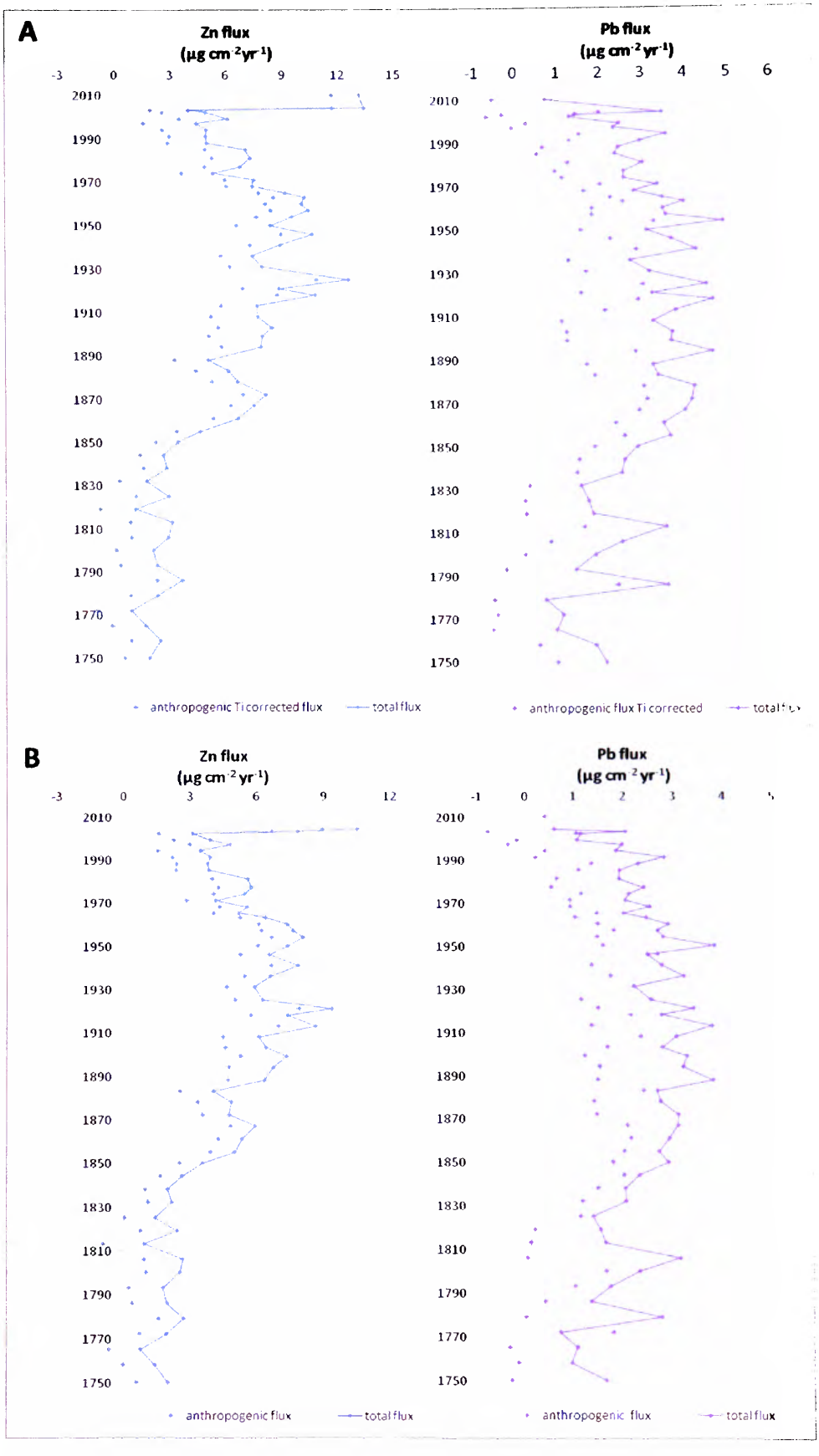

Figure 9.6: Total and anthropogenic fractions of Pb and Zn flux for DDP. A: Total and anthropogenic flux normalised via pre-1800 Ti inputs [after Norton *et al.*, 1992]; B: Total and anthropogenic flux normalised via pre-1800 trace metal contributions [after Vesléy *et al.*, 1993].

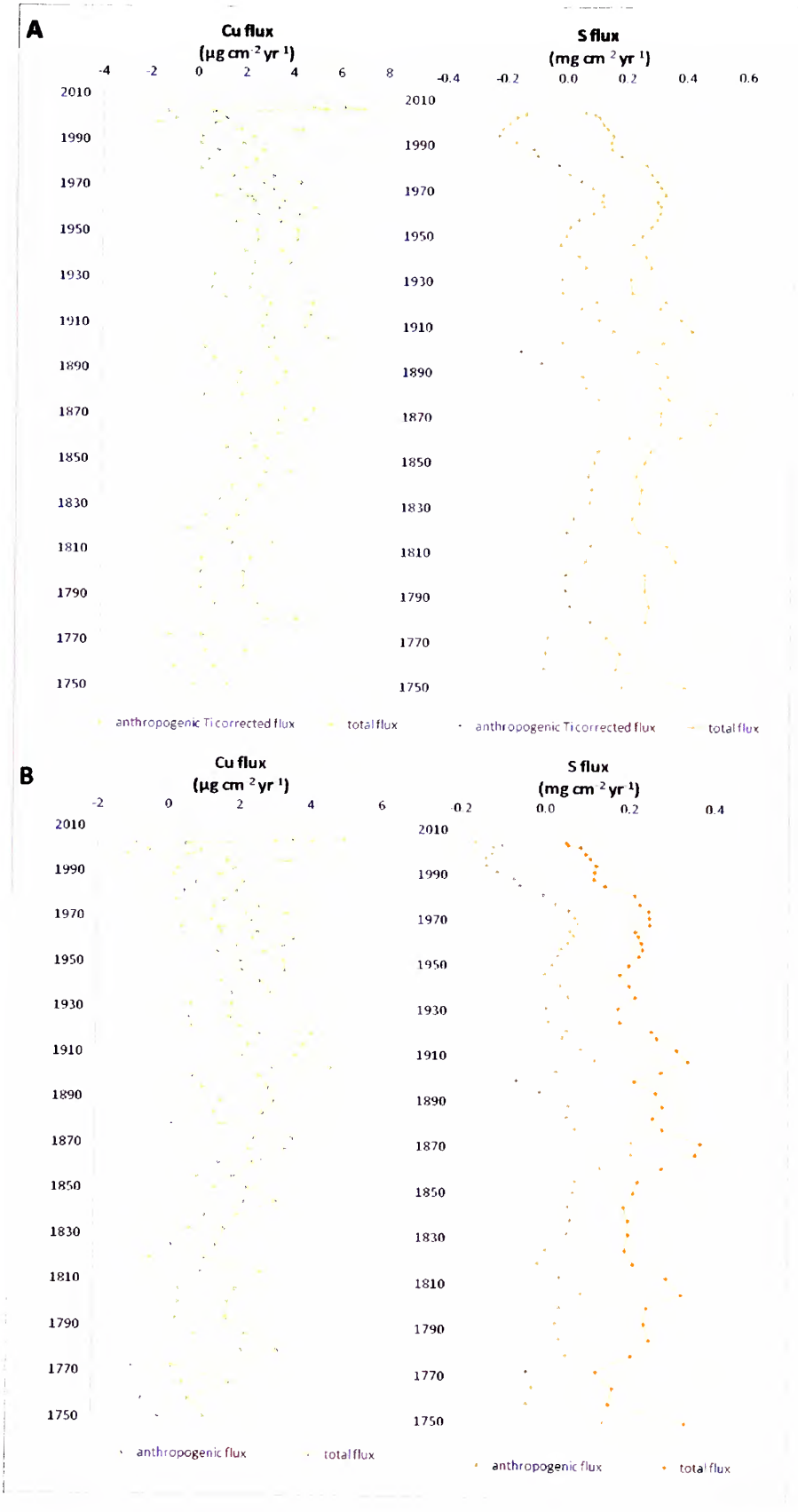

Figure 9.7: Total and anthropogenic fractions of Cu and S flux for DDP. A: Total and anthropogenic flux normalised via pre-1800 Ti inputs [after Norton *et al.*, 1992]; B: Total and anthropogenic flux normalised via pre-1800 trace metal contributions [after Vesléy *et al.*, 1992].

9.9. Chapter Summary

Intra-site core correlation, demonstrated by DDP, highlights the retrieval of reproducible sediment records from an urban pond. The reconstruction of ^{210}Pb histories from all sites further supports the retrieval of undisturbed sediment sequences. Assessment of potential post-depositional changes to the magnetic and trace metal record, combined with a review of contributions to the sediments from the atmosphere and catchment, highlight an overriding atmospheric anthropogenic signal revealed in the sediments of the urban ponds.

10. CHAPTER TEN: LOCAL AIR POLLUTION HISTORIES IN THE LOWER MERSEY REGION.

10.1. Chapter Overview

Local pollution histories recorded in the sediments of the four urban ponds, Daresbury Delph, Windmill Hill, Dogs Kennel Clump and Oglet, are interpreted in turn. Each pond provides a site specific history of pollution deposition, attributed to surrounding industrial and urban development within the LMR. The localised signature of these urban air pollution trends are highlighted via comparison with the published regional, background air pollution signal for the UK and Europe, derived from the sediments of large remote lakes. Further comparison of the local pollution histories obtained in the LMR with pollution depositional histories obtained from other urban lakes and ponds, highlights the importance of small manmade urban ponds as archives of localised pollution impacts.

10.2. Introduction

Daresbury Delph, Windmill Hill, Dogs Kennel Clump and Oglet ponds have captured a complex mixture of anthropogenic particulates, from surrounding industrial, domestic and transport activities, within their sediments. Due to their high lake-to-catchment ratios, the primary inorganic inputs of the investigated ponds are atmospherically-derived (Chapter 9), therefore, recording local, site specific air pollution signals, which reflect the industrial and transport activities unique to the LMR. Down-core phases identified at each site are superimposed over selected proxy pollution flux profiles from each site to aid interpretation of local air pollution records. Documented urban events within the LMR (Figure 10.1 and Table 10.1) are used to interpret these air pollution histories.

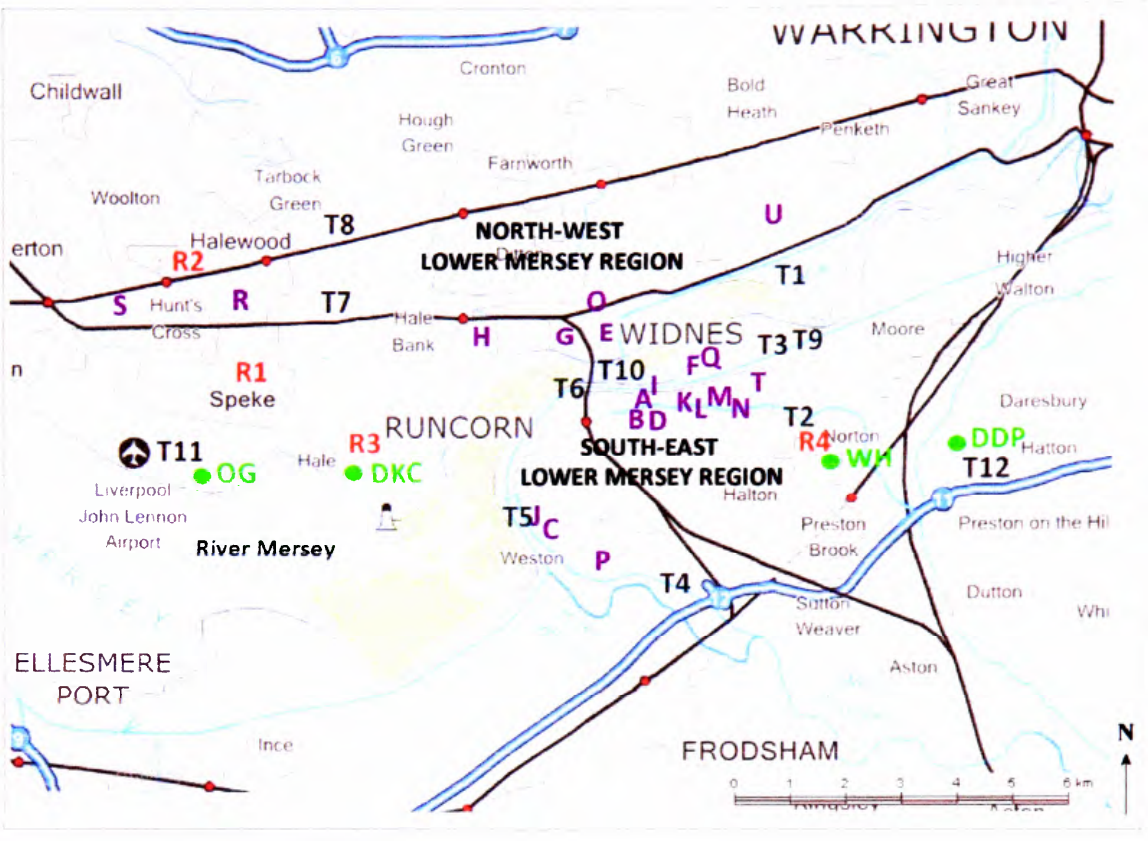

Figure 10.1: Location of selected transport, residential and industrial sites in the LMR, corresponding to urban events mentioned throughout Chapter 10, corresponding to Table 10.1.

Table 10.1: Key to transport, residential and industrial sites located in Figure 10.1.

Code	Site	Date of occurrence
A	Johnson's works	1803
B	Hazlehurst's works	1818
C	Kennedy and Maguire works	1834
D	Rook and Hunter	1834
E	Gossage works	1847
F	Wigg's works	1850
G	Works at Widnes Marsh	1866
H	Works at Ditton Road	1870
I	Runcorn Soap and Alkali Co.	1890s
J	Castner-Kellner	1896
K	Highfield Tannery	~1850
L	Puritan Tannery	~1850
M	Camden Tannery	~1900
N	Astmoor Tannery	~1900
O	ICI plastics and polymers	1929
P	Rocksavage, Weston	1930s
Q	Randle works	1930s
R	Halewood industrial site	1950s
S	Halewood industrial site	1960s
T	Astmoor industrial site	1960s
U	Fiddlers Ferry power station	1973

Code	Site	Date of occurrence
T1	Sankey Canal	1757
T2	Bridgewater Canal	1776
T3	Old Quay Canal	1803
T4	Weaver Canal	1807
T5	Weston Canal	1807
T6	Runcorn Gap Railway	1831
T7	Cheshire Lines railway	~mid-19th century
T8	Liverpool North Extension Lines railway	1880
T9	Manchester Ship Canal	1894
T10	Transporter Bridge	1905
T11	John Lennon International Airport (originally Speke Airport)	1930
T12	M56 motorway	1975
R1	Speke residential estate	1950s
R2	Halewood residential estate	1950s
R3	Hale Village	medieval
R4	Windmill Hill residential estate	1970s

10.3. Local pollution history from Daresbury Delph Pond

Daresbury Delph Pond provides a high-resolution >300-year air pollution history, the oldest stratigraphy of the four ponds investigated. Detailed variations in trace metals, magnetic characteristics and SCPs demonstrate distinct temporal phases in pollution trends, relating to the history of industry and urbanisation in Runcorn and the LMR (Figure 10.2). Temporal phases identified in the sediment records, which are discussed in turn, reflect:

- DDi pre-1832: early industrial activity in the LMR (10.3.1.);
- DDii 1832 to 1900: the Industrial Revolution and Leblanc chemical production (10.3.2.);
- DDiii 1900 to 1978: population increases and industrial expansion during the 20th century and subsequent air quality legislations during the late 20th century (10.3.3.); and
- DDiv post-1978: modern industrial processes, transport activities and stringent air pollution controls (10.3.4.).

Down-core magnetic, trace metal and SCP flux profiles from DDP are presented alongside a timeline of the LMR (Figure 10.2) with superimposed down-core phases (DDi to DDiv), to demonstrate how sediment records reflect local industrial pollution, vehicular emissions and air quality legislations.

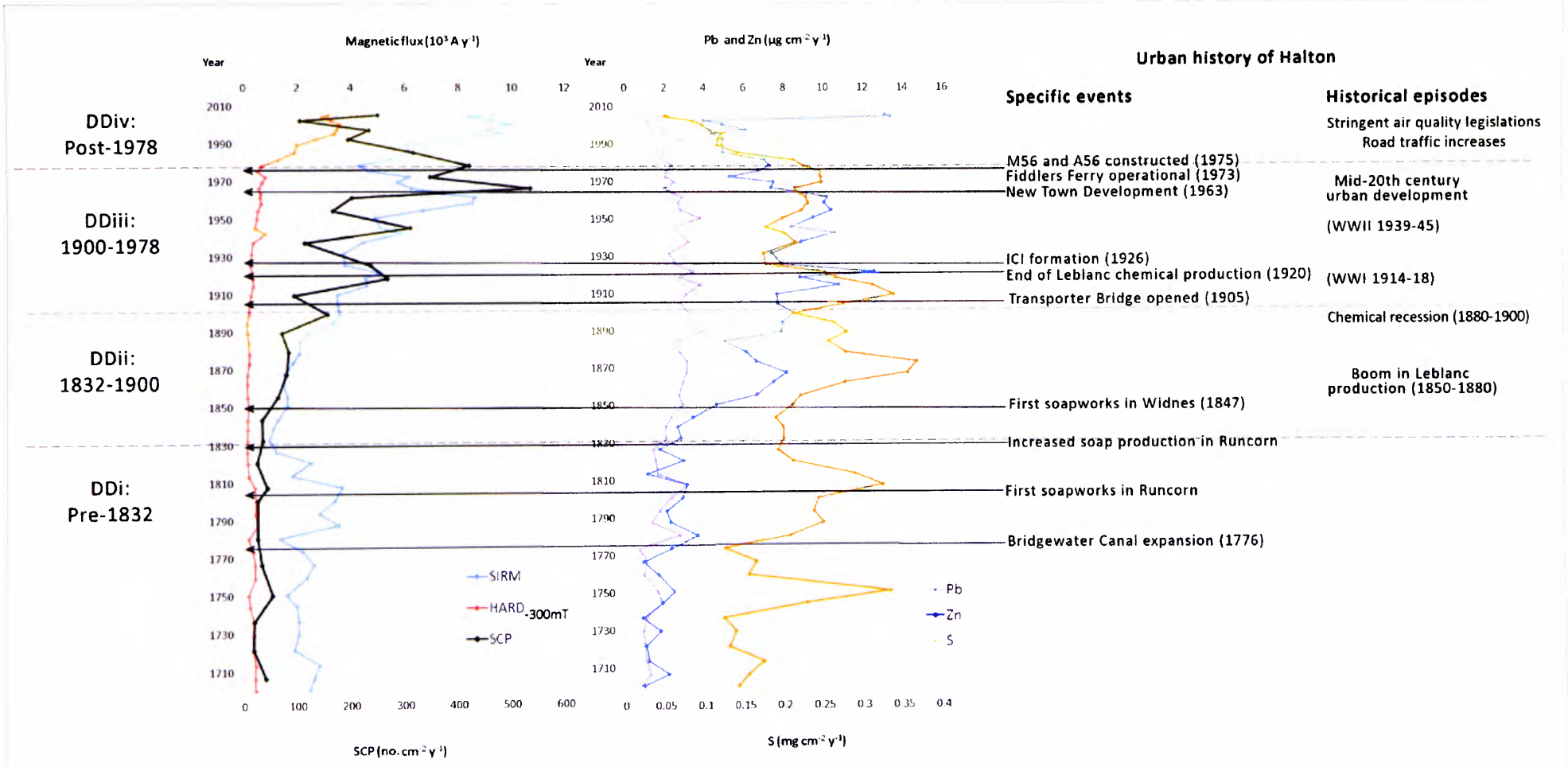

Figure 10.2: Magnetic (SIRM (10^3 A y^{-1}) and $HARD_{-300mT}$ (10^3 A y^{-1})), total SCP (no cm^{-2} y^{-1}), Pb (µg cm^{-2} y^{-1}), Zn (µg cm^{-2} y^{-1}) and S (mg cm^{-2} y^{-1}) flux profiles for DDP, with superimposed phases DDi to DDiv, highlighting corresponding urban events which may explain trends.

10.3.1. DDi ~pre-1830: early industrial pollution signal

The identified relatively low magnetic, SCP and trace metal concentrations and flux in ~pre-1832 sediment reflects low pollution levels prior to the intensification of industry in Runcorn that occurred during the 19th century. The 'noisy' pre-1832 SIRM and χ_{LF} signal may reflect trends in the deposition of combustion particulates from localised early industry during the 18th century. The pre-1832 SIRM and χ_{LF} signal may also be influenced by a fine-grained, potentially, soil-derived catchment signal contributing to the lake at this time, as the $SOFT_{-20mT}$ profile, indicative of coarse (~>1 μm) ferrimagnetic grains, demonstrates a relatively lower, steadily increasing trend. Relatively finer pre-1832 magnetic assemblages are also identified in the SIRM/ARM and χ_{ARM}/SIRM profiles (Figure 6.2) and Oldfield's, [1990] plot (Figure 6.5). As low-scale early industrial processes were occurring in the LMR at this time, this fine grained magnetic signal may be dominated by a natural (i.e. soil-derived), rather than anthropogenic source.

The earliest notable increases in trace metals in the DDP profile occur at 1751, with peaks in Pb and S concentration and flux, however, corresponding SCP and magnetic peaks are not observed. This early Pb and S signal may reflect low-scale local early industrial activity and coal combustion; however, Runcorn was a minor port until improvements in transport links (e.g. canal expansions) to the town during the late 18th century [Runcorn and District Historic Society, n.d.]. Therefore, this may, potentially, highlight a Pb and S signal from industrial activity at Liverpool, which was a more established urban centre at this time.

Overall, increases in proxy pollution concentrations and flux directly coincide with improvements in transport links in Runcorn and Widnes. Improved access to Runcorn subsequently resulted in establishment and expansion of industrial activity in the area. The observed post-1766 Pb, Zn, Cu and S increases, prominent trace metal peaks from 1780 to 1807, and corresponding small magnetic concentration peak at ~1793 to 1807, may coincide with an increase in industrial activity post-1770 in Runcorn, brought about by the expansion of the Bridgewater Canal in 1776, the linking of Runcorn with Warrington via the Old Quay Canal in 1803 and Weston Point with the Weaver Navigation via Weston Canal in 1807 [Runcorn and District Historical Society, n.d.] (Figure 10.1). These improved transport links, to the previously by-passed town, consequently, increased barge and shipping repair in Runcorn, expanded Runcorn as a port and resulted in the growth of new industries [Runcorn and District Historical Society, n.d.], for example, the first

soapworks (Johnson's) along the Bridgewater Canal in 1803 (Figure 10.1). The steadily increasing proxy pollution concentration trends during the early 19th century may, therefore, reflect an increase in pollution experienced in the LMR from establishing industries in Runcorn.

10.3.2. DDii 1830 to 1900: the Industrial Revolution and Leblanc chemical production in the LMR

Three main features are identified in the proxy pollution profiles throughout the 19th century (DDii):

a) post-1832 trace metal, SCP and magnetic enhancement;
b) 1850 to 1880 trace metal peak, most notably increased supply of Pb and S; and
c) decline in Cu and S from 1880 to 1900.

Potentially, these trends correspond to initial industrial activity in Runcorn and, possibly, a later (~post-1850) pollution signal from Widnes, as industries established and, subsequently, expanded throughout the borough during the 19th century.

- (a) Post-1830 industrial development

The clear enhancement in the SCP, magnetic and trace metal concentration (Figures 6.1, 6.7 and 6.8) and flux profiles (Figures 7.1, 7.2 and 7.3) from ~1832 indicate a distinct increase in pollution experienced in Halton, which steadily increases throughout the 19th century. This reflects a period of industrial intensification in Runcorn, due to the opening of the Runcorn Gap Railway in 1831, which led to an expansion of industry in Runcorn. In 1834 the first soapworks (Kennedy and Maguire) in Weston was constructed and a further chemical works (Rooke and Hunter) at Halton Lane opened (Figure 10.1). Also, an increase in soap production at the already established Hazelhurst's and Johnson's works on the Bridgewater Canal in Runcorn, occurred during the 1830s [Barker and Harris, 1959] (Figure 10.1). This prominent elevation in trace metals, magnetic grains and SCPs may predominantly reflect industrial activity at these soapwork sites during the 1830s. Other existing industries at this time included tanneries, shipyards, quarries, a steam mill, brewery and an acid works, slate works and timber yard [Pigot and Co., 1834], which may have also contributed to the pollution signal.

- (b) 1850 to 1880: Boom in Leblanc chemical production in Halton

A boom in chemical trade during the mid-19th century is reflected by notable trace metal peaks from ~1850 to 1873 (Figures 10.2 and7.2). Observed maximum S and very high Pb concentrations in the DDP core at this time (Figure 6.7) may reflect outputs from the early chemical industry, which was dominated by the Leblanc process. Leblanc production was a wasteful method; whereby, salt, limestone and sulphuric acid were heated in Pb chambers to produce alkali. High volumes of coal were combusted in the process, resulting in smoke emissions being a persistent nuisance in Halton [Warren, 1980]. The Leblanc process may have been a significant source of S and Pb to the environment at this time, as well as trace metals associated with coal combustion, for example Zn and Cu [Swain, 1995] (Figure 1.6, Section 1.4.3.2.), contributing to peaks in Pb and S during this phase. The Cl concentration and flux profiles obtained from BDD1 (Appendix E, Figure E1) also exhibits a prominent increase from 1832 to 1873, which may represent the expelling of hydrochloric acid gas from tall chimneys in the Leblanc production [Dingle, 1982], further highlighting the Leblanc process as a primary pollution source during this phase.

The 1850-1873 trace metal peaks may also reflect the opening of new Leblanc works, at Astmoor Saltmarsh (e.g. Wiggs works; Figure 10.1) in 1850, and a boom in alkali trade from 1861 to 1875 [Rintoul, 1984], by increases of soap production increasing by at least a third at the Johnson and Hazlehurst soapwork sites in Runcorn between 1832 to 1874 (Table 10.2) [Rintoul, 1984].

Table 10.2: Soap production figures for Johnson and Hazelhurst soap works in Runcorn in 1832 and 1874, adapted from Rintoul [1984].

Works	Soap production 1832 (tons)	Soap production 1874 (tons)
Johnson	1500	2000
Hazlehurst	910	1260

Furthermore, the DDP record may also incorporate a pollution signal from Widnes. The onset of industry occurred in Widnes from 1847, with a boom in chemical trade in the town at 1855 and the construction of 22 Leblanc works between 1847 and 1884 [Warren, 1980] (Figure 2.8). This period of outstanding development in Widnes is indicated by the increases in rateable values of Widnes and Ditton from 1841 to 1875 (Table 10.3). In 1872, the Leblanc chemical industry dominated industrial activity in Widnes, with 24 of the 35 industrial plants in Widnes being chemical works [Warren, 1980]. These works may,

therefore, have also contributed to the high pollution trends observed in the DDP sediment record between ~1850-73.

Table 10.3: Rateable values of Widnes and Ditton from 1841 to 1871 [Warren, 1980].

Year	1841	1851	1861	1871
Rateable value (£)	6,236	8,134	21,846	86,114
Change from 1841 (%)		30%	250%	1,281%

Cu increases in the DDP core throughout this phase, most notably at 1844 and from 1867 to 1873, may not only reflect the combustion of coal extensively used by the early chemical industry, but may also indicate increased releases of Cu to the environment from associated industries, such as Cu smelting. Involving the extraction of pyrites for use in the Leblanc process [Rintoul, 1984], Cu smelting also emits associated heavy metals such as Zn, Pb and Ni into the atmosphere [Alloway and Ayeres, 1997]. Cu smelting was carried out from 1847 in Widnes at the town's first soap works (Gossage), constructed along the Sankey Canal at Woodend [Warren, 1980; HBC, 1991] (Figure 10.1), which may be represented by the observed ~1844 Cu peak. This peak 'ties' the sediment records to the documentary record of this Cu smelter opening in 1847, supporting the ^{210}Pb dates. A Cu works was also constructed during the late 1860s at Weston (Runcorn Soap and Alkali Co.) [Rintoul, 1984] and a further three Cu works were established in Ditton and Widnes from 1870 to 1874 [Warren, 1980], which may explain increased levels of Cu experienced in Halton post-1844 identified in the DDP core.

The steadily increasing proxy pollution trends throughout the 19th century may also reflect population increases in Runcorn during the 1900s related to the growth of industry (Table 10.4). A decrease in population of 3,109 people, from 1891 to 1901 was due to a recession in chemical trade and, therefore, migration of workers out of the town. The increasing population in the borough will have also contributed to increased pollution emissions from domestic coal combustion.

Table 10.4: Population figures for Runcorn during the 19th century [Runcorn and District Historical Society, n.d.]. *1664 population data is an estimate for Runcorn and Widnes [Cheshire County Council and English Heritage (2003) Cheshire Historic Towns Survey: Runcorn and Halton Archaeological Assessment].

Year	1664*	1801	1821	1841	1861	1881	1891	1901
Population	305 to 375	1,474	3,103	6,957	10,063	15,133	20,050	16,941
Population change from 1664		334%	813%	1,947%	2,860%	4,351%	5,797%	4,883%

- (c) 1880-1900 Recession in chemical trade

The observed decline in S and Cu from ~1880-1900, and reductions in Pb and Zn during the 1880s and 1890s, respectively, in the DDP profile may correspond to an international recession in the Leblanc chemical trade during the 1880s and 1890s, due to Slovay and electrolytic chemical processes superseding Leblanc methods [Warren, 1980]. Figure 10.3 demonstrates the British export of alkali from 1850 to 1905, which exhibits a decrease post-1880, with a notable reduction post-1890, mirroring S and Cu trends. Leblanc works declined in Widnes during the 1880s [Warren, 1980] with a recession in chemical trade during the 1890s. Three main alkali works existed in Runcorn during the 1890s and one works at Weston. Also, closure of the United Alkali Company works in Runcorn, formed in the 1890s via the merger of Leblanc manufacturers, occurred during the 1900s. This period of relatively low S may, therefore, reflect a reduction in Leblanc production in Halton during the recession.

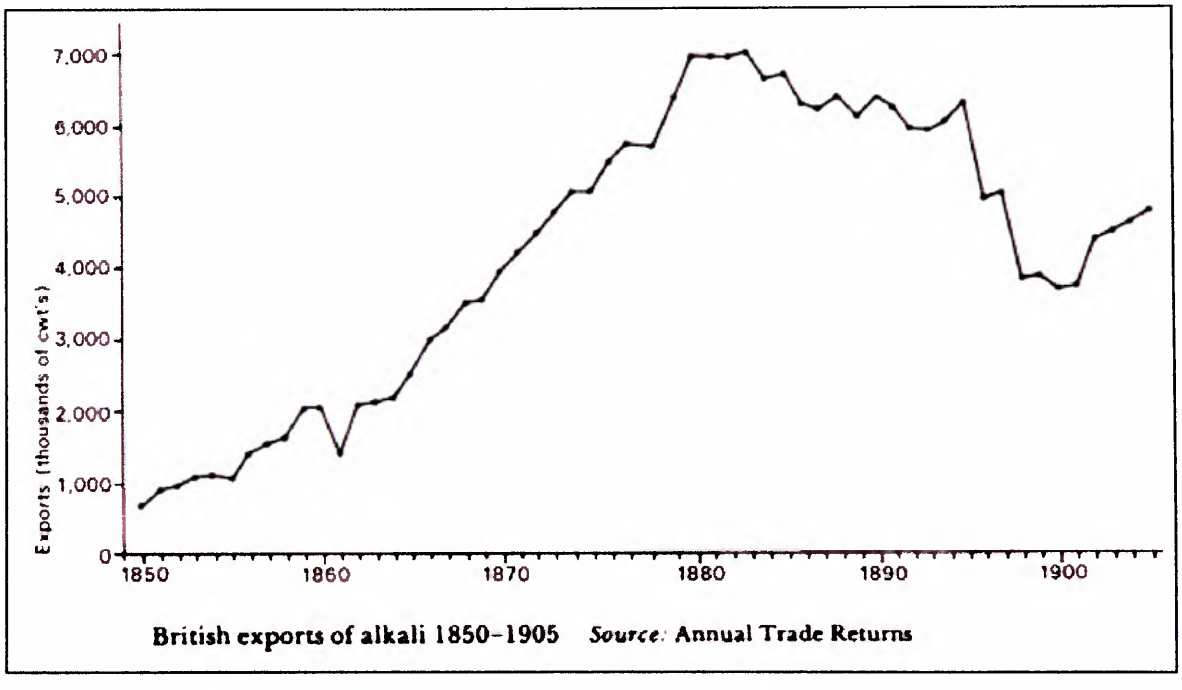

Figure 10.3: British exports of alkali from 1850 to 1905 [Warren, 1980].

However, the SIRM and SCP profiles continue to steadily increase at the end of the 19th century, into the 20th century. This represents an overall increase in pollution particulates during this phase, potentially, due to shifts in production within the chemical industry, for example the development of the Castner-Kellner works in Runcorn in 1896, which

required increased electricity generation; and increase in number of domestic coal fires and train (steam) transport.

10.3.3. DDiii 1900 to 1978: 20th century urban signal

The main temporal pollution features highlighted in the DDP core during the 20th century include:

a) further trace metal, magnetic and distinct SCP increases from 1900, characterised by a finer magnetic signal;
b) 1909 to 1921 proxy pollution peak;
c) late 1930/early 1940 proxy pollution peak;
d) mid-20th century increases; and
e) post-1963 declines.

It becomes more difficult to tease out specific industrial events, corresponding to the proxy pollution trends post-1900, due to the complexity of the urban signal during the 20th century. An increase in various substances released from industrial emissions due to the phasing out of the Leblanc process and shifts in production methods (i.e. electrolysis and Slovay process), combined with the introduction of organic chemicals and, therefore, expansion of manufactured products, complicates the pond's industrial signal. Also, as the population of Halton increased throughout the 20th century (Figure 10.4), domestic coal burning presents a further important contributing environmental burden, as well as pollutants from transport activities, particularly post-1960 as the Halton population increased due to the New Town Development (Figure 10.4).

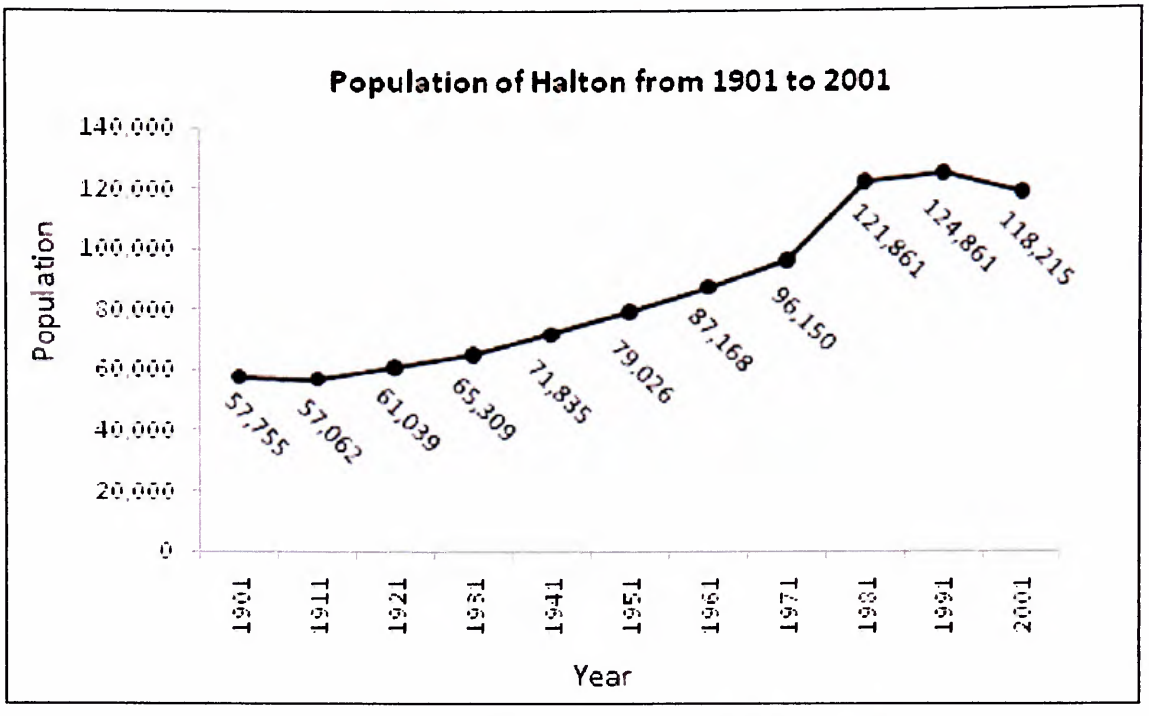

Figure 10.4: Population data for Halton from 1901 to 2001 [Phillipots and Cohen, 2004].

- (a) Further pollution increases from the start of the 20th century:

Post-1900 trace metal increases and enhancement of the SCP and magnetic concentration record signify a distinct increase in pollution, characteristic of a finer signal (Figure 10.2), as indicated by an increase in SP sized (~<0.005 μm) magnetic grains (Figure 6.2), an increase in 'hard' magnetic minerals (Figure 6.1) and shifts to <10 μm median particle diameters (Figure 6.6). This may reflect the recovery of the chemical industry during the 20th century after the late 19th century recession and the shift to new industrial production methods. For example, the construction of the Castner-Kellner works at Weston in 1896, introducing electrolysis of brine using mercury cell technology in Halton. The pollution signal may be further enhanced by the construction of the Transporter Bridge, opened in 1905 [Runcorn and District Historical Society, n.d.], improving transport links between Runcorn and Widnes. Also, the completion of the Manchester Ship Canal in 1894 resulted in a narrowing of industries in Runcorn as the town became less important as a dock. The main industries were tanning, chemicals, soap and stone at this time [Runcorn and District Historical Society, n.d.].

- (b) 1909 to 1921 proxy pollution peak:

The corresponding 1918-21 magnetic concentration peak, 1909-21 trace metal concentration peaks, 1914-21 SCP peak, and maximum flux of SCPs in the size range 1-3 μm, coincide with wartime (WW1 1914-18) demands on the chemical industry in Halton. It is speculated that production at the Castner-Kellner plant at Weston Point (under Brunner Mond Co.) may also contribute to this observed peak, as WWI sustained chlorine production, used as a war gas, at the plant from 1914 into the 1920s [Rintoul, 1984]. The end of Leblanc chemical production, signified by closures in Leblanc works during the 1920s and 1930s and the cease of production at Castner-Kellner works from 1926 to 1931 [Rintoul, 1984] is, potentially, reflected in the local pollution signal by decreases in proxy pollution trends after the observed WWI peak.

- (c) Late 1930/early 1940 peak:

Trace metal peaks occur at 1937 with a slightly later SCP and magnetic concentration peak at 1942. This may reflect further wartime (WWII: 1939-1945) pressures put on chemical industries in Widnes and Runcorn, important national manufacturing centres, at which time plants were operating to capacity [Hardie, 1950]. Also, the Rocksavage plant (Weston) and Randel works (adjacent to Wiggs at Astmoor) were constructed in the late 1930s [Rintoul, 1984] and new processes were established, particularly in Widnes during the 1930s, with the production of organic chemicals.

- (d) Mid-20th century peaks:

The observed steadily increasing pollution trends accumulating throughout the first half of the 20th century may reflect the domination and expansion of the chemical industry in Runcorn and Widnes. The 'modern' production of inorganic and a range of organic chemicals in Runcorn and Widnes required increased capacity from the power stations at West End (Widnes) and Weston Point (Castner-Kellner) to supply the chemical factories [Hardie, 1950]. Also, as industry further developed and population increased, domestic coal combustion in the borough may be an attribute of the observed increasing pollution trend.

Despite the phasing out of the Leblanc process, a potential primary source of Pb pre-1920, Pb has increased since the start of the 20th century and reaches an observed maximum Pb concentration and flux peak at 1950/58. Potential Pb sources during the mid-20th century

may include industrial emissions, the release of Pb due to coal combustion (domestic and industrial) and the consumption of leaded petrol for vehicle use. High Zn concentrations and flux sustained from 1925 to 1963 highlights a modern (20th century) Zn source, as values are notably higher than pre-1900 levels. Zn emissions may, potentially, be derived from a modern industrial process, such as the application of Zn to car paint as a rust inhibitor and its use in plastic manufacture (Table 1.7, Section 1.4.3.2.). These industrial processes were introduced in the area with the formation of ICI, in 1926, and the establishment of industries at Halewood during the 1950s.

High trace metal and magnetic concentrations and flux also occur from 1958 to 1963, and parallel maximum total SCP trends at 1963 (Figure 10.1). This suggests a maximum supply of anthropogenic particulates at this time. This may reflect a period of rapid expansion of the chemical industry in Halton due to the New Town Development, in 1963, and domination of industry by ICI and an expansion of manufactured chemicals, especially organic chemicals, during the 1960s, as well as the environmental burdens of an increasing population, most notably domestic coal combustion and increased energy demands. Despite the introduction of the Clean Air Acts in 1956, which introduced smoke control areas and prohibited 'dark smoke' from chimneys and brought about a shift in domestic fuel consumption, it is not until after the mid-1960s that there is a decline in the proxy pollution trends.

- (e) Post-1963 proxy pollution decline:

Overall, decreases in trace metal and SCPs post-1963 (Figures 10.1, 6.7 and 7.3) highlight a decline in pollution, which may be a result of the Clean Air Acts, initially introduced in 1956 and reinforced by several subsequent legislations throughout the late 20th century (Table 1.13, Section 1.5.2.). The Clean Air Acts of 1956 and 1968, were implemented to reduce smoke emissions and applied to both industrial activities and the domestic combustion of coal. These smoke restrictions are reflected in the trace metal profiles, particularly in the S profile, which exhibits a steady decrease from 1975 to present day; potentially, a direct consequence of these legislations. Also, the increased use of plastics, led to a demise in tanneries in Halton during the 1950s and 1960s. For example, Astmoor and Camden Tanneries closed in 1964 [Runcorn and District Historical Society, n.d.], which may also contribute to the observed decrease in pollution.

High S concentrations are, however, sustained from 1969 to 1975 (Figure 6.7), which may reflect emissions from Fiddlers Ferry power station (SJ 354374, 386387) that was operational post-1969. The nearby (<5 km) power plant is coal-fired and, therefore, potentially a significant source of SO_2 in the area. Despite the 1956 Clean Air Act it is not until 1975 that S concentrations decline. The gradual decline may, however, be due to subsequent legislations such as the 1974 Control of Pollution Act, which reduced the amounts of S in fuel oil and later (1988) EC Directives (88/609/EEC) that limited the release of sulphur dioxide from power stations and large combustion industrial plants. The S profile also highlights comparatively less S in the atmosphere post-1975, than the 1850-1873 period of maximum S concentration. Smoke was a persistent problem associated with the Leblanc chemical industry in Halton during this time, therefore, the S profile suggests air quality has improved post-1975 in Halton.

Unlike S, fluctuating post-1960 trends are observed in the Pb, Zn, Cu and Br profiles (Figures 6.7 and 7.2), which exhibit an overall decline. This decrease in proxy pollution trends may also reflect a decline in chemical output, an increase in unemployment and industrial closures during the 1970s and 80s, which occurred despite the New Town Development in the 1960s [HBC, 1991] and improved industrial emissions controls. The fluctuating trace metal trends and increases in magnetic concentrations and flux post-1960 may be due to an enhancement in the urban pollution signal because of the establishment of housing in Runcorn at Castlefields, Halton Brook, Southgate, Palacefields, Brookfield, Murdishaw and Windmill Hill; attracting 33,500 new residents between 1964 and 1979 [Runcorn and District Historical Society, n.d.] and, subsequent, environmental burdens due to population increases, such as increased energy demands (e.g. Fiddlers Ferry power station) and vehicular pollution.

After the 1950s Pb maximum, relatively high Pb levels are sustained throughout the 1960s and notably decline post-1972 (Figures 10.1, 6.7 and 7.2), which may also reflect an improvement in air quality post-Clean Air Acts. However, at this time, the amount of road traffic increased in the UK from 180 billion passenger kilometres in 1952 to 414 billion passenger kilometres in 1975 [Department of Transport, 2008]. Therefore, vehicular emissions will have been an important mobile source of Pb in the atmosphere post-1950. The 1978 EC Directive (78/611/EEC) and the Motor Fuel legislation (1981), limited the maximum permissible lead content of petrol, and unleaded petrol was introduced in 1985 (EC Directive 85/210/EEC). Despite these acts to reduce Pb emissions, BDD1 exhibits a

Pb increase from 1989 to 1992. This may reflect a local increase of road traffic in Runcorn, which nationally increased (to 581 billion passenger km) in 1989 [Department of Transport, 2008] and the continued use of leaded fuel by vehicles which pre-dated the introduction of unleaded petrol. Also, diesel engine road vehicles, which have increased in the UK since the 1950s [MacDonald-Wallis and Young, 2007], release Pb and other trace metals (Cd, Zn, Cr) into the atmosphere [Dwivedi *et al.*, 2006]. Vehicular pollution is, therefore, an important modern source of Pb in the environment, as transport is responsible for 78% of Pb emissions to air compared to 18% from industry [UK Emissions Inventory Team, 2007]. Also, modern industrial emissions have higher capture efficiencies of pollutants, due to technological advances and stringent air quality standards. Although trace metals decline post-1975, there is a sustained high deposition of particulates, revealed by a high supply of anthropogenic particulates (SCPs) to DDP from 1963 to 1981.

10.3.4. DDiv post-1978: fine grained magnetic signal: a potential vehicular source

The distinct shift in the magnetic signal post-1975 to a finer, SSD (~<0.7 to 0.07 μm) magnetic signature identified in the BDD1 core (Figures 6.1, 6.2, 6.3, 6.4 and 6.5), coincides with the construction of the M56 motorway and A56 dual carriageway that opened between 1971 and 1975, which is within 700 m of DDP. Also, since the national increasing trends in vehicular use throughout the 20th century, a potential significant source of this increased contribution of fine magnetic grains could potentially be from vehicular emissions. Indeed, Charlesworth and Foster [1999] report an increase in sedimentation rates in an urban lake due to atmospheric fallout from vehicular emissions, which they report is a viable sediment source to urban lakes with negligible catchments, due to an increase in vehicular emissions from 30 (10^3) tonnes in 1970 to 70 (10^3) tonnes by 1990 [Quality of Urban Air Group, 1993]. This could be the case at DDP.

The overall, steadily increasing trends in ferrimagnetic grain size throughout the core is disrupted in the post-1975 sediment; whereby, there is a prominent enhancement in χ_{ARM} (Figure 6.1) and $HARD_{-300mT}$ magnetic flux (Figure 7.1). As the Daresbury Delph Pond has a small catchment, located within an urban environment, this fine-grained signal may be anthropogenic, rather than from a soil or bacterial source (Section 9.6). A shift to fine-grained magnetite in the post-1975 sediment is characteristic of particulates produced from high temperature combustion processes and vehicular exhaust particulates [Mamane *et al.*, 1986; Morawska *et al.*, 1998].

10.4. Local pollution history from Windmill Hill Pond

The WH sediment stratigraphy provides a high-resolution ^{210}Pb chronology dated to 1955, allowing extrapolation to 1893, detailing a history of pollution deposition throughout the 20th century in Runcorn. The prominent shift to notably lower inorganic sediment accumulation ~post-1951 observed in the WH3 core, due to low dry bulk density values and an increased supply of OM, results in prominent variations between concentration and flux profiles for this site post-1951.

The local air pollution signal from WH is presented using selected SIRM, Pb, Zn, Cu and S flux profiles (Figure 10.5), with superimposed phases WHi to WHiv, with a corresponding timeline of urban activity in the LMR. Interpretation of the local air pollution signal for WH is divided into these down-core divisions:

- WHi ~Pre-1906: low proxy pollution levels (Section 10.4.1.),
- WHii ~1906 to 1949: industrial expansion and population increases (Section 10.4.2.),
- WHiii 1949 to 1993: industrial shifts and New Town Development (Section 10.4.3.) and
- WHiv Post-1993: air quality legislations (Section 10.4.4.).

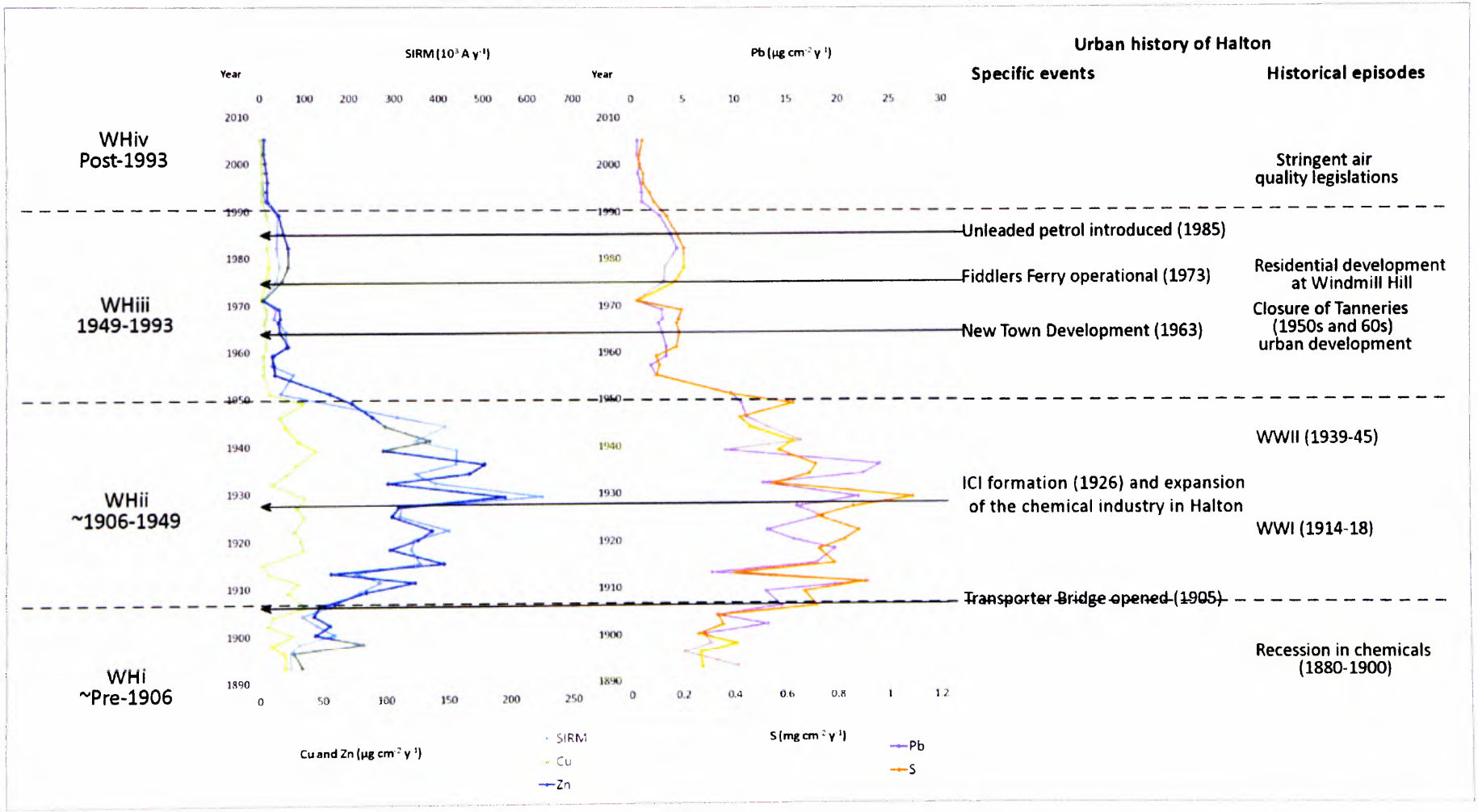

Figure 10.5: Magnetic (SIRM (10^3 A y^{-1})), Pb (µg cm^{-2} y^{-1}), Zn (µg cm^{-2} y^{-1}), Cu (µg cm^{-2} y^{-1}) and S (mg cm^{-2} y^{-1}) flux profiles for WH, with superimposed phases WHi to WHiv, highlighting corresponding urban events which may explain trends.

10.4.1. WHi ~pre-1906: low proxy pollution levels

Low pre-1906 proxy pollution trends, potentially, reflect the end of the recession in the Leblanc chemical industry from 1880 to 1900 as indicated in the DDP Cu and S profiles (Figure 10.5), or highlights comparatively low pre-1900 proxy pollution trends prior to 20th century increases.

10.4.2. WHii 1906 to 1949: industrial expansion and population increases

Pollution enhancement post-1906 (Figures 10.5, 6.9B, 6.12, 7.5A and 7.6) may reflect the growth of industry in Runcorn, aided by the opening of the Transporter Bridge in 1905, combined with the introduction of electrolysis production in Runcorn from 1896 at the nearby Castner-Kellner works in Weston (Figure 10.1). The steadily increasing trends in trace metals and magnetic grains may also reflect the shift to organic, as well as inorganic, chemical production in the area, resulting in expanding industrial activity throughout the 20th century and wartime (WWI: 1914-18) demands on industry in Halton. Highfield, Camden, Puritan and Astmoor tanneries in Runcorn may also contribute to the pollution signal at WH at this time. Further contributing to the observed increasing pollution experienced ~post-1906 may be the increasing population of Runcorn (Figure 10.4) and associated domestic coal burning. This complexity of urban pollution emissions within Runcorn may be important factors impacting the WH pond during the 20th century.

From ~1939, Pb, Zn, S and Br exhibit a gradual decrease in concentration and flux; however, a high Cu peak is observed from ~1939 to 1949, which corresponds with maximum, and very high, magnetic concentration and flux values observed at ~1949 (Figure 6.9A) (omitted from figure 10.5). This may relate to a localised pollution episode; whereby, high levels of Cu were released, potentially, from a copper works or a particular industrial process operating at this time. To date such an incident is not in the public domain.

10.4.3. WHiii 1949 to 1993: industrial shifts and New Town Development

Due to the prominent shifts in dry bulk density and organic content post-1949 (Section 5.5.2.) in the WH core, trace metal concentrations corrected for inorganic content (Figure 6.13), opposed to original concentration data (Figure 6.12), will be primarily used to infer an environmental history at this site. Also, these trace metal concentration profiles tell different stories post-1949 from the flux profiles (Table 10.5). This suggests trace metal

concentrations are influenced by the varying inorganic sedimentation rates observed, unlike the pre-1949 data. The decrease in magnetic concentration (Figure 6.9A) and flux (Figure 7.5B) post-1955 may be due to relatively higher organic content recorded in the post-1949 sediment, which may be diluting the magnetic signal in this phase.

Table 10.5. Summary of post-1949 trends in concentration and flux profiles in the WH core.

Phase	Concentration trend	Flux trend
1949 to 1993 (WHiii)	Original trace metal concentrations increase post-1951; however, are less pronounced when corrected for inorganic sediment mass, with only S exhibiting post-1949 increases. Magnetic concentrations, however, exhibit a prominent decrease post-1949. Trace metal increases are further observed between 1971 and 1989, with corresponding increases in magnetic concentrations, although values relatively lower than pre-1955, from 1964 to 1989.	Decreases in trace metal and magnetic flux occur post-1949, with a more prominent reduction observed in the magnetic flux profiles. Increases in trace metal flux are observed at 1949-1969 and 1978-1985; and also in the magnetic flux profiles at 1961 to 1964 and 1978 to 1989.
Post-1993 (WHiv)	Post-1993 magnetic concentrations decline, however inversely, trace metal concentrations increase from 1997 to 2001.	Low trace metal and magnetic flux values are observed post-1993.

Trace metal concentrations corrected for inorganic content demonstrate a prominent decline post-1949. This prominent post-1949 reduction in magnetic and trace metal flux may be influenced by a reduced industrial output, due to the closure of tanneries in Runcorn throughout the 1950s and 60s. There were four major tanneries operating in Runcorn prior to this time: Astmoor (SJ 353716, 382892), Highfield (SJ 352485, 382958), Puritan (SJ 352358, 382892) and Camden (SJ 352358, 382669) [Runcorn and District Historical Society, n.d.] (Figure 10.1).

The tanneries required sufficient power generation for the heating of animal skins to produce leather and, therefore, relied on coal combustion; for example, Highfield Tannery used coal until 1947, when replaced by oil-fired burners [Runcorn and District Historical Society, n.d.]. These tanneries closed during the 1950s and 1960s due to the introduction of plastics, the manufacture of which increased the release of organic pollutants. The demise of these, nearby, tanneries (Camden <4 km, Highfield <3 km, Puritan <3 km and Astmoor <2 km), may have impacted WH pond. The introduction of the Clean Air Act (1956) may also contribute to the reduction in the pollution experienced post-1951 in the WH core. Interpretation of this shift is, however, potentially complicated by the observed increase in OM delivery to the pond (Section 9.5).

S demonstrates sustained high values from 1955 until 1982 (Figure 10.5). Post-1940 Pb, Zn and Cu flux values are relatively lower than pre-1949, however increasing trends are observed from 1959 to 1969 and 1978 to 1985, with corresponding SIRM increases from 1961-64 and 1978-89 (Figure 10.5). This enhancement may be due to the New Town Development that occurred in Runcorn (~1963); whereby, lighter industries (e.g. warehouses) were introduced at Astmoor (SJ 353676, 383260) < 1.5 km of WH pond (Figure 10.6). Proxy pollution increases throughout the 1970s and 1980s may be due to residential expansion, also part of the New Town Development. For example, the nearby (<60 m west and <100 m north) Windmill Hill housing estate (Figure 10.7). Also, Fiddlers Ferry power station (Figure 10.1) was operational post-1973, and may have been an important source of S and other trace metals in Runcorn during the 1970s and 1980s (prior to stringent air quality controls).

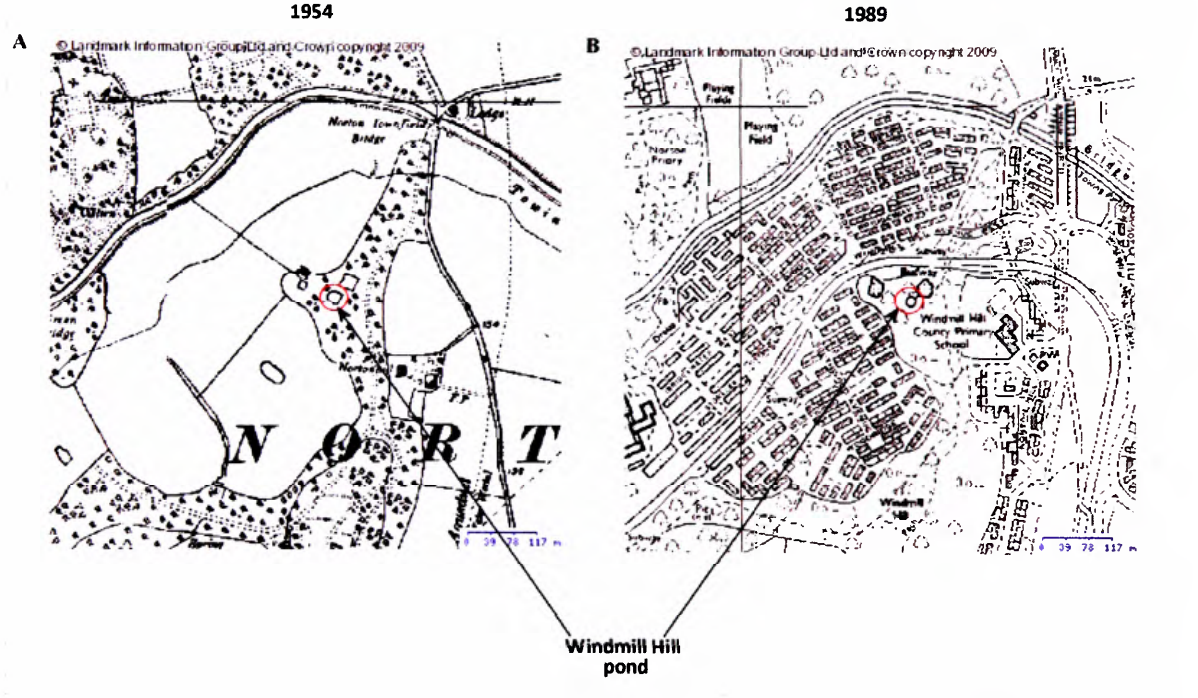

Figure 10.6: Windmill Hill, pre- and post-residential development. Reproduced from the 2008 Ordnance Survey second revision 1959-1982 County Series 1:10560 (A) and 1989 Ordnance Survey 1:10000 (B) maps with the permission of Ordnance Survey on behalf of The Controller of Her Majesty's Stationery Office © Crown Copyright Edge Hill University, Ormskirk, Lancashire licence number: ED100020392.

10.4.4. WHiv Post-1993: air quality legislations

Low trace metal and magnetic profiles (Figure 10.5) reflect a decline in pollution post-1993. S exhibits a gradual decline post-1982, which may be explained by stringent standards set by the air quality legislations. For example, the 1989 Air Quality Standards regulations, which limited guide values for SO_2, suspended particulates and Pb in air and reinforced by a series of EC Directives and the Environmental Protection Act (1990), highlighting an improvement in air quality.

10.5. Local pollution history from Dogs Kennel Clump Pond

The DKC ^{210}Pb stratigraphy dates to 1955 and extrapolates back to 1874 (Section 5.2.3.), providing a high-resolution change of pollution characteristics during the 20th century. Situated in the north-west LMR (Figure 10.1), geographically to the west of DDP and WH, a different pollution signal has been obtained. Down-core SIRM, Pb, Zn, and S flux trends identified in the DKC are interpreted relating to surrounding urbanisation and industrial activity in the LMR (Figure 10.7):

- DKi pre-1913: low proxy pollution levels (10.5.1.),
- DKii 1913-1962: industrial recovery and population increases (10.5.2.),
- DKiii 1962-1974: urban expansion at Halewood (10.5.3.) and
- DKiv post-1974: air quality legislations (10.5.4.).

The adjacent village of Hale has not undergone significant urban development since the onset of industry in Halton; therefore, the shifts in pollution are mainly attributed to nearby industrial activities at Halewood, Widnes and Runcorn which are likely to impact DKC (Figure 10.1).

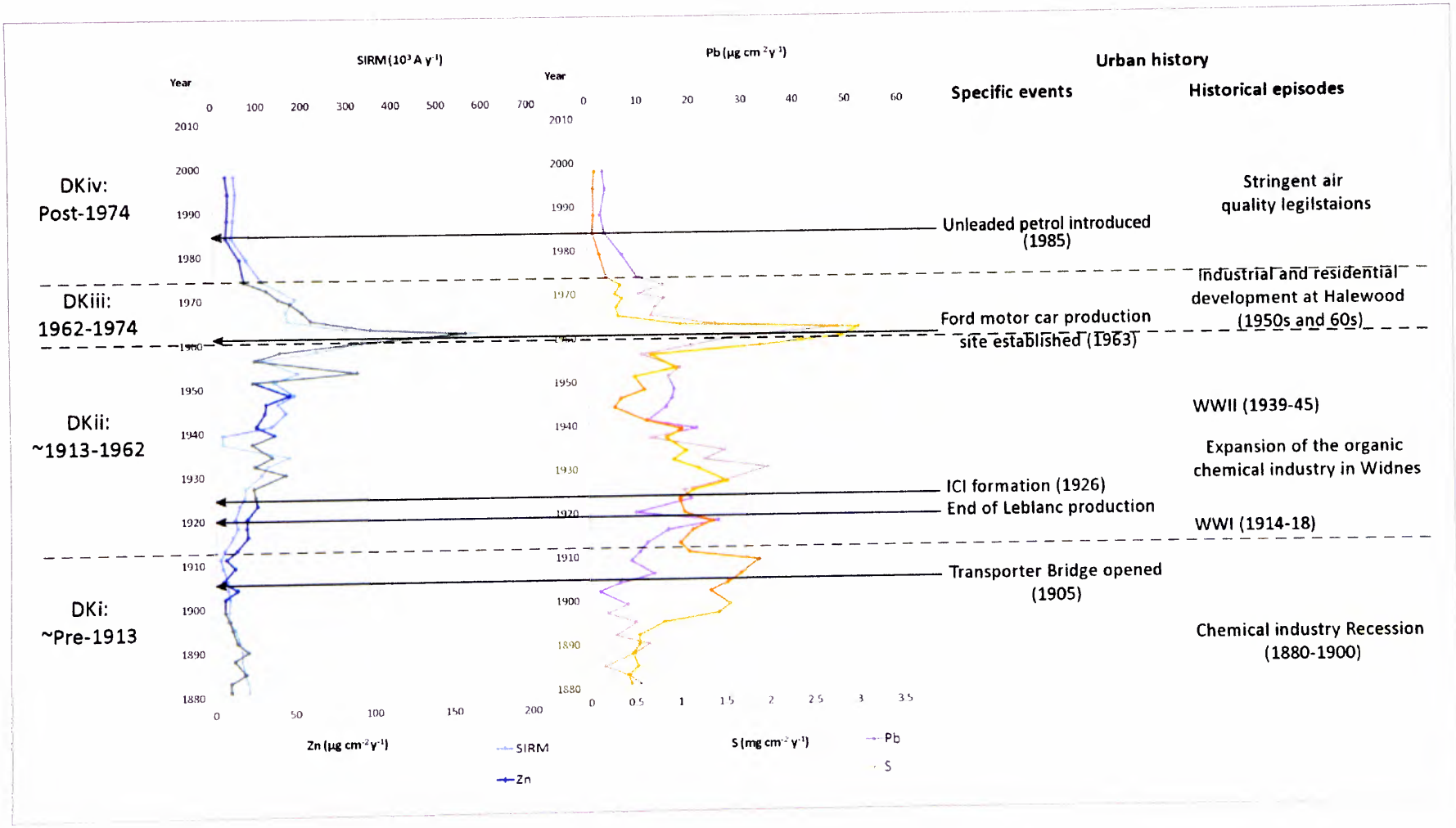

Figure 10.7: Magnetic (SIRM (10^3 A y^{-1})), Pb (µg cm^{-2} y^{-1}), Zn (µg cm^{-2} y^{-1}) and S (mg cm^{-2} y^{-1}) flux profiles for DKC, with superimposed phases DKi to DKiv, highlighting corresponding urban events which may explain trends.

10.5.1. DKi pre-1913: low pollution levels

Low pre-1900 trends in flux (Figures 10.7, 7.8 and 7.9) and concentration of trace metals (Figure 6.20) and ferrimagnetic grains (Figure 6.14) may represent the recession in Leblanc chemical production in Runcorn and Widnes from 1880-1900, which is also reflected at DDP and WH. The 'hard' magnetic behaviour identified in this phase may also highlight a fine-grained magnetic signal, possibly signifying the start of a potential artificial clay lining of the pond. At this time, the Cheshire Lines and Liverpool North Extension Lines Railways (extending west to east across Halewood) (Figure 10.1), constructed in the mid-19th century, may be an important source of pollution.

10.5.2. DKii 1900 to 1962: industrial recovery and population increases

The steadily increasing proxy pollution trends from 1913, demonstrated by gradual increases in magnetic concentration (Figure 6.14) and flux (Figure 7.8), particularly fine ferrimagnetic grains and trace metals (Figure 7.8), may mark wartime (1914-18) demands on industry in Halton, supported by an observed peak in trace metals at ~1918 (Figure 10.6). The overall post-1900 pollution increases in the DKC sediment record may reflect the expansion of the chemical industry in Runcorn and Widnes throughout the 20th century due to the opening of the Transporter Bridge in 1905 (Figure 10.1) and the introduction of organic chemicals and new chemical production techniques, such as electrolysis, in the region. The increasing population of Halton (Figure 10.4) may also contribute to the pollution signal due to the domestic combustion of coal, an important source of S and other trace metals released into the atmosphere.

Continuing pollution increases into the 1920s and 1930s may reflect the specialisation of the chemical industry in Widnes which, with the ICI merger of 1926, resulted in various inorganic and organic chemical production methods operating in Halton and, therefore, industrial emissions. The observed 1940s and 1950s pollution increases may reflect a localised pollution signal due to the establishment of industries at Halewood (SJ 342994, 384134) (Figure 10.1) during the mid-20th century, which included pharmaceutical production factories, chemical works, foundries, varnish and colour works, a bio-chemicals factory, chemical factories and concrete works.

The 1948-1953 trace metal flux peak is relatively more prominent in the Zn profile, (and Ni, and Cr (Appendix E Figure E2) when compared to S and Pb (Figure 7.9). This may highlight a reduction in S and Pb at this time, or may indicate increases in Zn, Ni and Cr

emissions, it is speculated, from new industrial sources at Halewood. Industrial activity at Halewood is likely to be a significant source of pollutants post-1950 impacting the DKC pond as pre-1950 these sites did not exist, and the nearest industrial sites to DKC pond were at Widnes and Runcorn. Therefore DKC, potentially captures a localised pollution record, influenced by nearby urban development post-1960.

10.5.3. DKiii 1962 to 1974: urban expansion at Halewood

Maximum trace metal and magnetic flux occurs in the DKC core from 1960-1963, highlighting a period of notable pollution (Figure 10.7). Coinciding with this maximum flux in proxy pollution is the establishment of the Ford Motor car production site at Halewood (SJ 344542, 384063), presently owned by Jaguar, which was completed in 1963. The site also includes a combustion plant providing steam and hot water for space heating and process heating [Knowsley PCT, 2008], which currently emits PM and SO_2 to air [Environment Agency, 2005]. It is speculated this local industrial development may be responsible for this high pollution peak.

The 1960-63 peak may also incorporate a pollution signal from the urban population of Halewood (Figure 10.7), which expanded post-1950 (Figure 10.1). Pre-1950 Halewood's population was ~1,000, however, during the 1950s and 1960s, housing estates were created at Speke (SJ 344500, 383416) and Halewood (SJ 344689, 385077) (Figure 10.1) to accommodate large shifts in the population from Liverpool, resulting in a ten-fold increase of the population of Halewood [Knowsley Metropolitan Borough Council, 1998]. Relatively high proxy pollution trends sustained throughout the 1960s may reflect a combined effect of production at the Ford site, the expansion of chemical products produced in Halewood and Halton and population increases occurring at this time.

10.5.4. DKiv Post-1974: air quality legislations

The observed decreases in trace metals and magnetic flux post-1974 (Figure 10.7), and further reductions post-1980 may reflect increasingly stringent air quality legalisations established post-1956, improved industrial emissions controls, introduction of unleaded petrol (1985) and shift in domestic fuel combustion from coal to gas and electricity. Also, increases of fine ferrimagnetic grains, as indicated by χ_{ARM} profile (Figure 6.14, Section 6.5.1), post-1974 highlights a modern fine-grained magnetic signature, potentially, signifying a shift to a relatively finer pollution signal, as identified in the DDP profile (Section 10.3.3).

10.6. Local pollution history from Oglet Pond

Sediment stratigraphy obtained from OG pond provides high-resolution trends in air pollution post-1914, with a particularly high-resolution history of recent environmental change post-1980. The local pollution history for OG pond is interpreted via the site specific phases:

- OGi pre-1949: low proxy pollution levels (10.6.1.);
- OGii 1949 to 1973: urban development at Halewood (10.6.2.);
- OGiiiA 1973 to 1985: air quality legislations (10.6.3.); and
- OGiiiB 1985 to 1991 and OGiv post-1991: a potential aviation signal (10.6.4.).

These phases, superimposed over selected SIRM Pb, Zn, Cu and S proxy pollution flux profiles from OG (Figure 10.8) are interpreted via industrial and urban developments that have occurred throughout the LMR, most notably the Halewood industrial estate and the John Lennon International Airport.

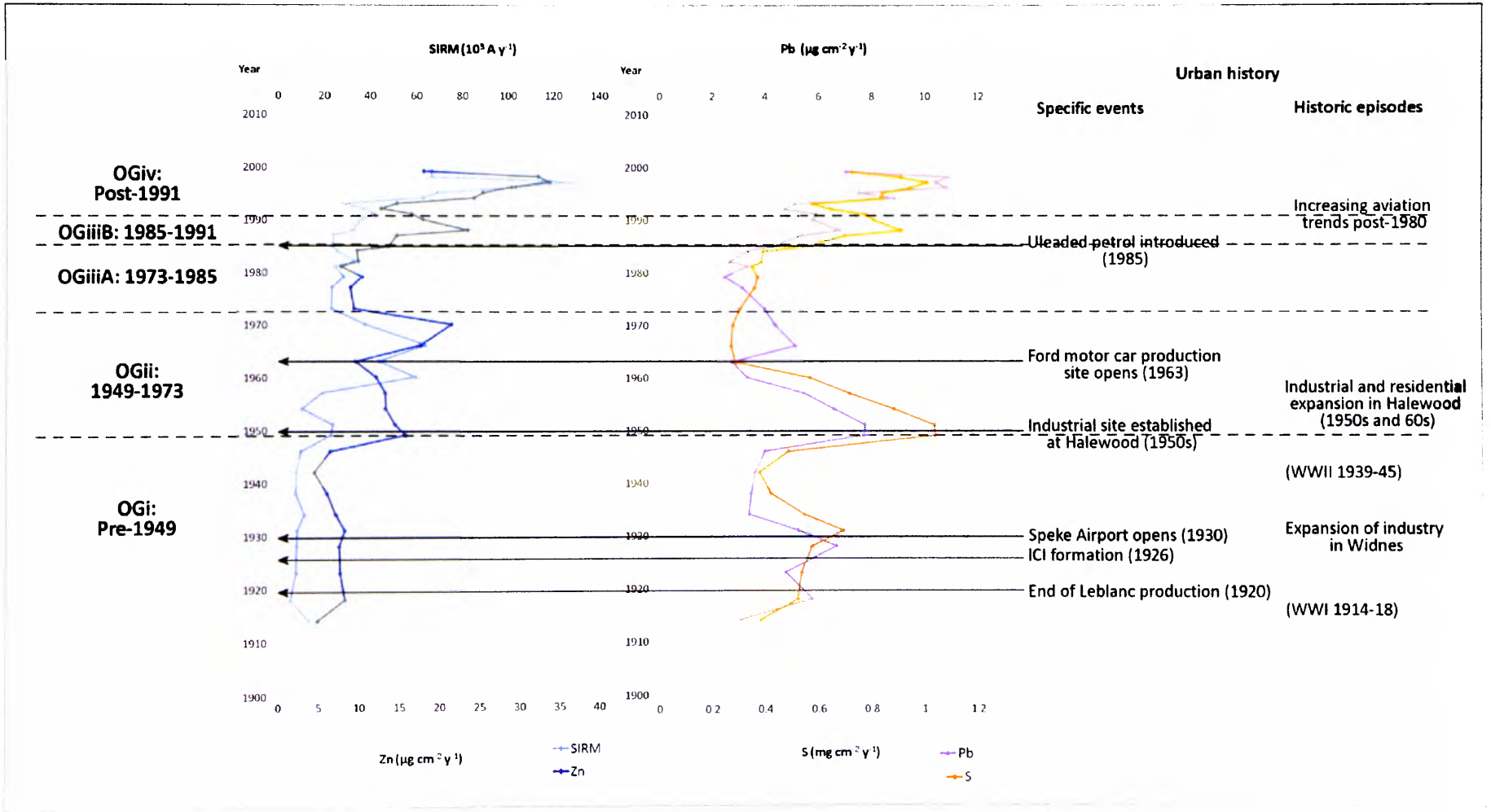

Figure 10.8: Magnetic (SIRM (10^3 A y^{-1})), Pb (µg cm^{-2} y^{-1}), Zn (µg cm^{-2} y^{-1}), Cu (µg cm^{-2} y^{-1}) and S (mg cm^{-2} y^{-1}) flux profiles for OG, with superimposed phases OGi to OGiv, highlighting corresponding urban events which may explain trends.

10.6.1. OGi pre-1949: low proxy pollution levels

The pre-1949 signal demonstrates relatively low magnetic, Zn and Cu trends (Figure 7.11). At this time there was minimal urban development within the Speke and Halewood area, which surrounds the pond, and it was not until the 1950s that industrial sites were established at Halewood (SJ 342994, 384134) (Figure 10.1). However, OG exhibits relatively high Pb and S flux from 1927 to 1931 (Figure 7.11), which highlights a source of these trace metals impacting the lake at this time. This coincides with the opening of Speke Airport (SJ 343149, 382664) in the 1930s, which may have been an important source of these trace metals from the combustion of aviation fuel, or may reflect an industrial signal due to extensive industrial processes operating in nearby Widnes (~6 km) and Runcorn (~6 km), in particular, the expansion of chemical production due to the ICI merger in 1926.

10.6.2. 1949-1960: Urban development at Halewood

A distinct enhancement in the proxy pollution record post-1949 is highlighted by increases in the supply of magnetic grains to the lake from 1949, magnetic concentration increases post-1954 and subsequent maximum magnetic concentrations at 1966, coupled with trace metal concentration and flux peaks from 1949-51, which are sustained until 1960. This may reflect the establishment of the Halewood industrial site (SJ 342994, 384134) <3 km north of the OG pond (Figure 10.1). Works established at this site included pharmaceutical production factories, chemical works, foundries, varnish and colour works, bio-chemicals factory, organic and inorganic chemical factories and concrete works, introducing new pollutant sources to the surrounding area. Emissions from these industrial sources and traffic to and from these plants, may explain the prominent increases in Zn and Cu, which were relatively low pre-1949, also reflected in the DKC sediment record. A housing estate at Speke (SJ 344406, 383218) (Figure 10.1) was constructed during the 1950s <1 km of the OG site, and subsequent increase in population will have also resulted in an increase in pollution due to a rise in vehicular emissions and increased energy demands.

Sulphur and Cu trends decrease post-1960; however, magnetic flux increases and high Zn and Pb values are sustained throughout the 1960s until 1970 (Figure 10.8), which is also reflected in the DKC profile (Figure 10.7). This may reflect further industrial development at Halewood, with the construction of the Ford motor car production site (SJ 344542, 384063) and expansion of housing estates throughout the area, leading to further population increases in Halewood. Also, it is speculated, the observed post-1963 increased

contribution of fine magnetic grains (Figure 6.21) may be due to industrial emissions occurring at this time. For example, the combustion plant at Halewood associated with the car production site.

10.6.3. OGiiiA 1973 to 1985: air quality legislations

Trace metal and magnetic flux decreases during the 1970s (Figures 10.8, 7.10 and 7.11), and corresponding declines in magnetic, Pb, S, Zn and Cu concentrations (Figure 6.26), highlight a reduction in pollution at this time, which may reflect air quality legislations and improved emission controls from industrial activity and vehicular pollution, for example, via the Clean Air Act (1968), 1970 EC Directive (70/220/EEC), 1972 EC Directive (72/306/EEC) and subsequent legislations.

10.6.4. OGiiiB and OGiv post-1985: a potential aviation signal

The observed increase in sediment accumulation rates from 1985 (Section 5.5.4) results in a 'dilution' of the post-1985 trace metal concentration profiles, as a shorter time period is represented by the sediment intervals. However, when original concentration data (Figure 6.21 and 6.26) are converted into flux profiles (Figures 7.10 and 7.11), the 'real-time' accumulation of trace metals to the OG pond over time can be assessed, which demonstrates a prominent pollution enhancement from 1985 to 1999. Distinct magnetic, S, Pb, Zn and Cu flux increases are exhibited post-1985, with further pronounced proxy pollution enhancement post-1990. The post-1985 signal is also characterised by an increase in SP grains (χ_{FD}% values, Figure 6.22) and fine (SSD) ferrimagnetic grains (χ_{ARM} profile, Figure 6.21), which coincides with an increase in <10 μm and <2.5 μm particulate distributions (Figure 6.24) and $HARD_{-300mT}$ flux values (Figure 7.10).

As a result of the Clean Air Act introduced in 1956 and subsequent legislations, there are stringent standards on the releases of trace metals from industrial and vehicular sources. This is especially true for Pb, which is one of eight pollutants closely monitored by the National Air Quality Strategy [DEFRA, 2007]. Due to known detrimental health effects, Pb has been 'phased out' in ambient air (EC Directive 85/884/EEC, Air Quality Standards Regulations 1989, The Environment Act 1995), via reduction in industrial processes (Environmental Protection Act 1990) and vehicular emissions (EC Directive 78/611/EEC, The Motor Fuel Regulation 1981) with the introduction of unleaded petrol in 1985 (EC Directive 85/210/EEC). Therefore, an increase in trace metals, particularly Pb, post-1980 is unexpected and highlights a potential local, rather than regional, source.

Despite the phasing out of Pb use in industrial processes and gradual decline of Pb in motor car petrol, a potential source of Pb in the environment is from aviation fuels [Ebbinghaus and Wiesen, 2001]. Pb additives (tetra-ethyl lead) are still applied to Aviation Fuel (also known as Avgas or Aviation Gasoline) to achieve high-octane fuel for general aircraft with piston engines [Ebbinghaus and Wiesen, 2001; US EPA, 2008] and, therefore, is an important source of Pb and other trace metals, including sulphur, in the environment. Aviation Turbine Fuel (known in the USA as 'jet fuel') is a second type of fuel, similar to diesel, used to power jet (turbine) engine aircrafts which, unlike Aviation Fuel, does not have Pb added to it [US EPA, 2008]. Limited literature is published regarding the composition of jet engine particles (referred to as JEPs), however, there is evidence that Aviation Turbine Fuel also emits a range of trace metals, including Pb, to the atmosphere [Boyle, 1996].

Observed pronounced increase in trace metals post-1980 in the OG core, and further post-1990 increases, are not reflected in the DDP, WH or DKC cores, further supporting a site-specific source of pollution impacting the OG site. As the pond is located <1 km of John Lennon International Airport and <300 m from the runway (Figure 10.9) it may receive emissions from the take-off and/or landing activity of aeroplanes; whereby, more fuel is combusted due to higher energy demands and, therefore, higher pollution deposition is expected adjacent to airports [Boyle, 1996].

The airport, originally 'Speke Airport', opened in the 1930s, and, therefore, may represent an important pollution source since this time; however, the pronounced proxy pollution increases post-1985 may be explained by recent trends in aviation travel. Figure 10.10 demonstrates the gradual increase in air travel from 1950 in the UK. Prominent increases in freight weight, terminal passengers, and take off and landing activity occur post-1980. Trends in UK terminal passengers exhibit an increase post-1980 from <57,823,000 to ~102,418,000 in 1990, reaching ~235,139,000 in 2006 [Department of Transport, 2008]. Figure 10.10 demonstrates the closely paralleled post-1980 trends in take off and landing activity in the UK with the recorded Pb flux profile obtained from OG pond. The Pb flux appears to mirror the aviation trends very closely ~post-1975 (Figure 10.10), potentially, highlighting a dominating aviation pollution signal in the post-1975 OG sediment. The Pb profile most interestingly mirrors the prominent increase in aviation activity post-1980, and further increases in air travel post-1990 (Figure 10.11).

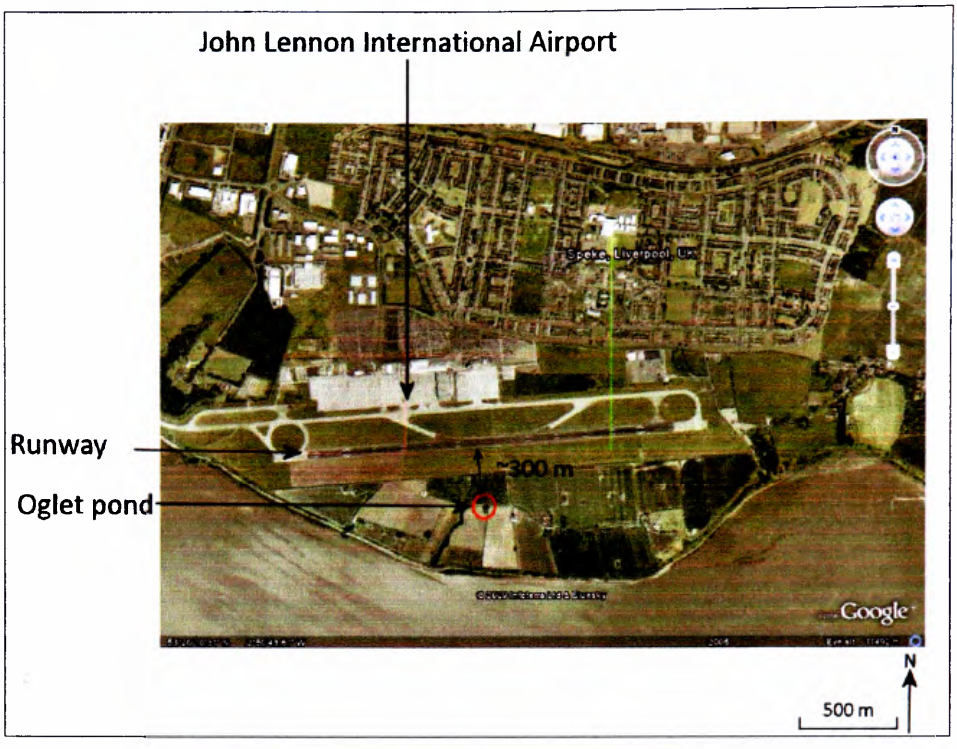

Figure 10.9: Satellite image of Oglet pond showing its location adjacent to runway at John Lennon International Airport (SJ 343491, 381845) [Google earth].

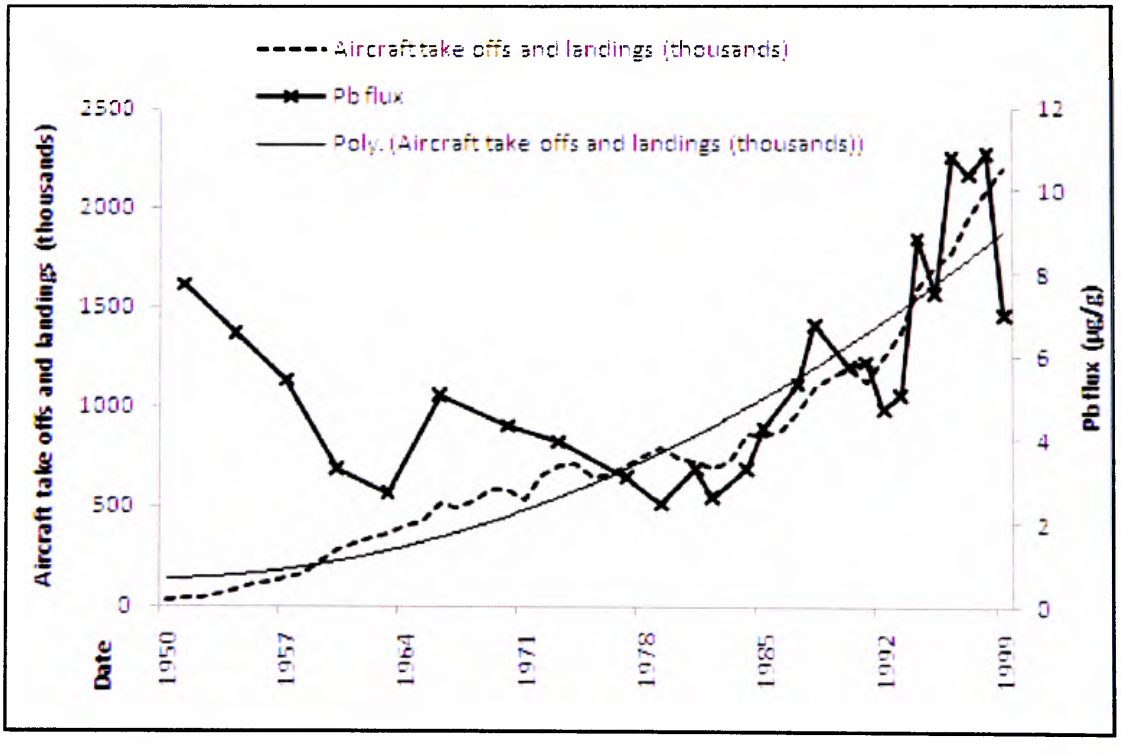

Figure 10.10: Activity at civil aerodromes (UK) 1950-1999. Air transport movements: aircraft landings or take-offs (thousands) and polynomial trend line [collated from Historical Annual Airport Tables produced by the Civil Aviation Authority http://www.caa.co.uk] compared with Pb flux (10^2 µg cm^{-2} y^{-1}) from OG pond (corrected for inorganic sediment accumulation).

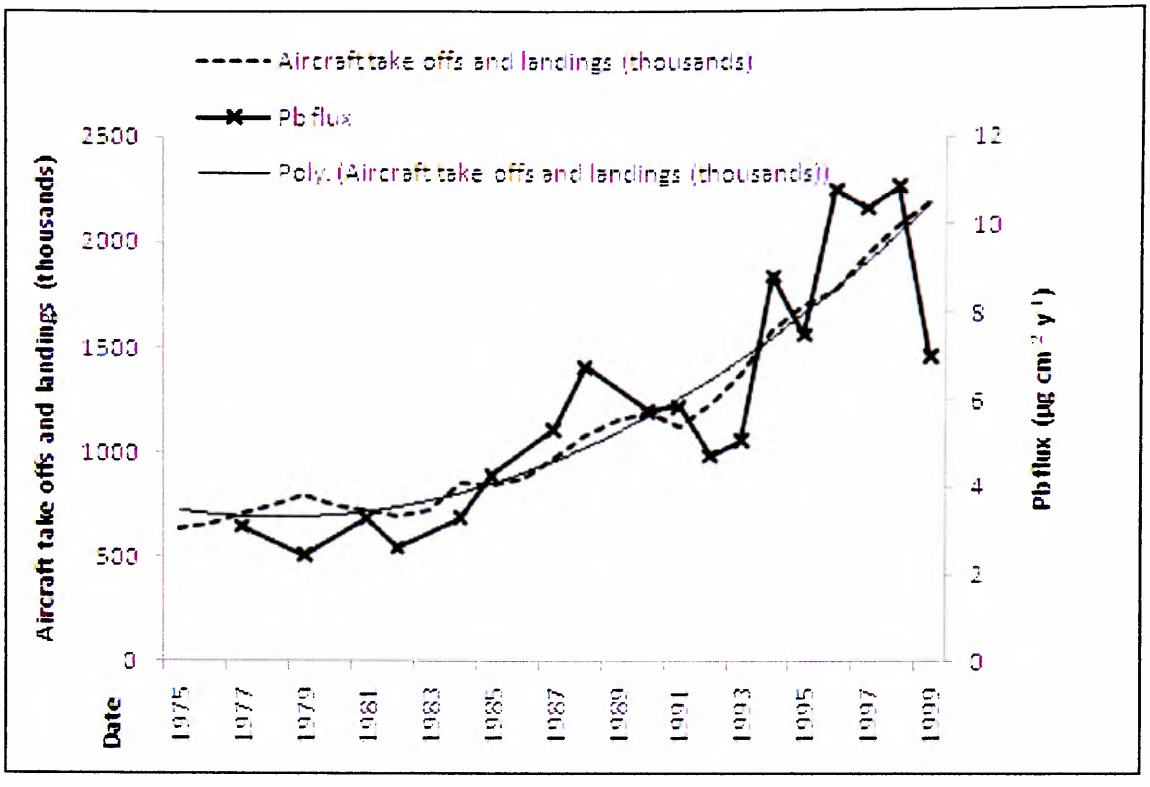

Figure 10.11: Activity at civil aerodromes (UK) 1975-1999: Air transport movements: aircraft landings or take-offs (thousands) and polynomial trend line [collated from Historical Annual Airport Tables produced by the Civil Aviation Authority http://www.caa.co.uk/statistics] compared with Pb flux (10^2 µg cm^{-2} y^{-1}) from OG pond (corrected for inorganic sediment accumulation).

Data are also available for the number of terminal passengers at John Lennon International Airport from 1986 to 2008 (Figure 10.12) [Civil Aviation Authority] which reflects the observed national trends post-1986. When these data are compared with the Pb flux profile from OG pond, visual similarities can be identified (Figure 10.12). In particular, there are close parallels between Pb flux and terminal passenger trends from 1986 to 1994, a 'dip' in passengers at 1995, coinciding with a decrease in Pb flux and steadily increasing post-1995 passenger and Pb flux trends. The only apparent discrepancy is the low Pb flux at 1999 obtained from the sediment surface which may be affected by processes at the water-sediment interface.

Work on particulate emissions from jet engines by Boyle [1996] reports emissions of not only Pb, but associated trace metals (e.g. Zn and Cu), which may explain the observed increases in all trace metals post-1980. Furthermore, Boyle [1996] discovered the majority of JEPs were <1 µm, indicating a fine-grained signature of aviation particulates. The observed increases in SP, χ_{ARM} and <1 µm contributions post-1980 in the OG core further supports the presence of an aviation signature recorded by the OG pond. Prominent post-

1990 increases may also reflect increased energy demands during take-offs and landings, which uses a third more energy than during flight. Although capture efficiencies of aircraft emissions may have improved, the observed increase in air travel, may result in an overall elevation in aviation pollution.

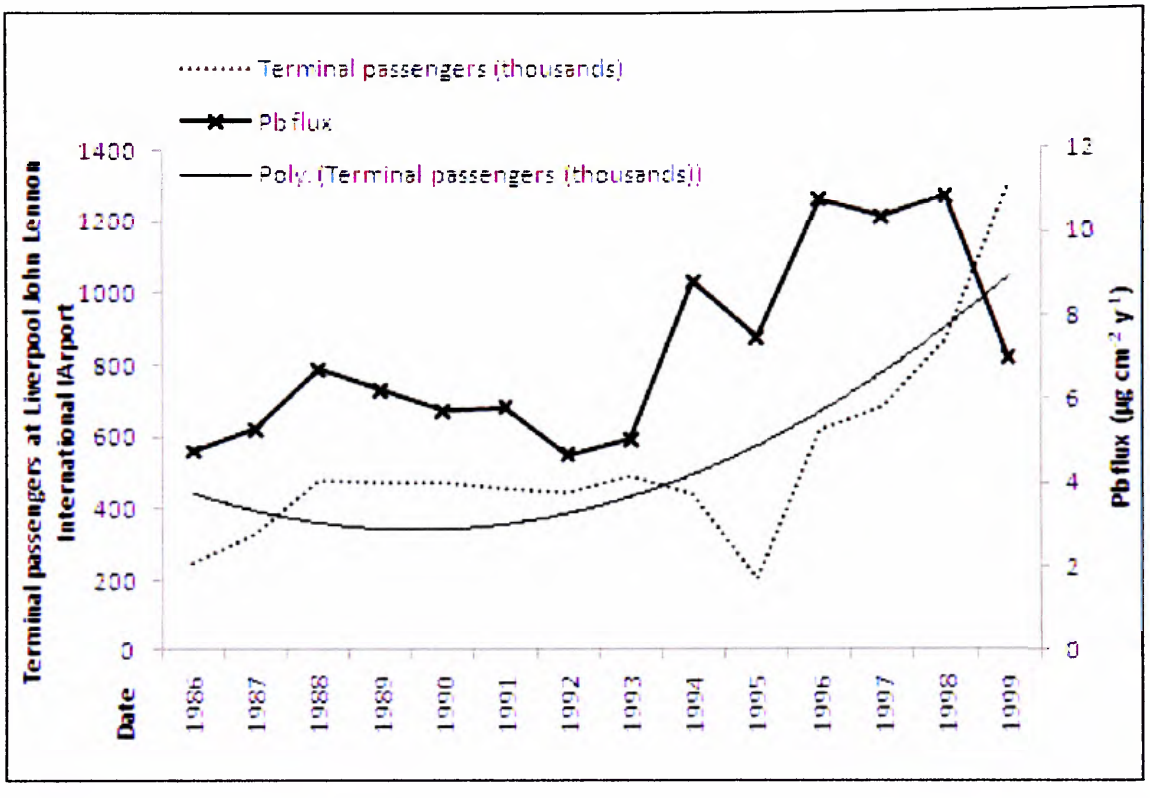

Figure 10.12: Trend of terminal passengers at Liverpool John Lennon Airport from 1986 to 1999 and polynomial trend line [collated from Historical Annual Airport Tables produced by the Civil Aviation Authority http://www.caa.co.uk] compared with Pb flux (corrected for inorganic sediment accumulation).

This possible aviation signal record at OG, which is <300 m from the runway is not mirrored in the DKC record, which is ~3 km from the airport. This may indicate very localised deposition of airport emissions. It is also important to note that air pollution from the airport may not solely derive form aircrafts. Maintenance equipment, facilities and fuel depots on the ground, as well as heavy road traffic generated by visitors and workers contribute to pollution emissions at airports [Whitelegg and Williams, 2000]. A possible aviation pollution signal is also highlighted by Graney and Eriksen [2004], who report a nearby airport as a potential source of anthropogenic Pb, from combusted aviation fuel residues, recorded in a rural lake (Stella Ireland), in Broome County, USA.

10.7. Local versus regional pollution records from lakes

DDP (Figure 10.2), WH (Figure 10.5), DKC (figure 10.7), and OG (10.8) ponds have captured site specific records of pollution influenced by the urban history of the surrounding area. They allow an assessment of long-term pollution experienced in an urban environment, providing an alternative to reliance upon background air pollution signals retrieved from remote, rural lakes as the main sedimentary archives of environmental change. The majority of rural lake sediment stratigraphies provide an important, but relatively basic, history of air pollution in comparison with urban ponds, where a general enhancement of SCPs, magnetic grains and trace metals are observed post-19th century [Oldfield *et al.*, 1983; Yang and Rose, 2005; Oliveira *et al.*, 2009].

For some rural lakes, which have large catchments-to-lake ratios, the identification of an atmospheric pollution record is perturbed due to relatively higher catchment-derived inputs. Therefore, human impacts are interpreted as erosion histories due to land use changes, rather than the enhanced magnetic or trace metal concentrations due to industrial emissions. Yang *et al.*, [2002] studied a 'small' (9.8 ha) mountain lake Lochnagar in Scotland, and estimated that 90% of the total Pb to the lake was derived from the large catchment (92 ha), opposed to atmospheric fallout. Although atmospheric deposition of particulates will contribute to the UK rural lake sediment record, in some studies, the air pollution signal is obscured by erosion episodes within the catchment [Appleby *et* al., 1985; David *et al.*, 1998; Jordan *et al.*, 2002; Oldfield *et al.*, 2003; Yeloff *et al.*, 2005]. This highlights the importance of calculating background and natural inputs to the lake.

The urban ponds studied in the LMR have large lake-to-catchment ratios. Therefore, due to their negligible catchment sizes, the primary inorganic input is derived from the atmosphere. The trace metal enrichment factors from DDP, calculated using Al and Ti normalisations and by teasing out pre-industrial (pre-1800), natural Pb concentrations and flux (Section 9.7.), show that the trace metal signal is dominated by anthropogenic sources. This highlights a potential advantage of using small (<1 ha) urban ponds to infer air pollution histories, due to their minimal catchment effect on the sediment record.

Some large rural lake studies show intra-lake spatial variations of pollution deposition [Grayson and Plater, 2009]. However, as the LMR ponds are very small (<0.2 ha), this limits the spatial variation of sediment stratigraphies obtained within the same pond (Section 9.4.), making them sensitive to environmental change, and by determining air

pollution histories from several small ponds, intra-urban spatial variations in depositional histories can also be assessed.

10.7.1. The rural-urban pollution deposition gradient

Local pollution histories retrieved from urban ponds provide an important, urban dimension to the deposition of pollution experienced within the UK, due to the rural-urban deposition gradient [Foster and Charlesworth, 1996; Chalmers *et al.*, 2007]. Spatial and temporal variations in pollution deposition in lakes, rivers and ponds in New England, USA, identified a rural-urban gradient [Chalmers *et al.*, 2007] with higher deposition rates in urban environments, gradually decreasing to lower values at rural sites. This is further supported by Graney and Eriksen [2004], who report increased deposition of trace metals in an urban storm water pond compared to suburban and rural lakes throughout Broome County, USA, highlighting the weak anthropogenic signal recorded in rural ponds.

In the UK, Foster and Charlesworth [1996] identified higher trace metal deposition within urban areas, compared to rural sites and suggest trace metals are not transported far from their source, further highlighting the importance of using urban ponds as archives of urban pollution. Higher levels of Zn contamination were also identified in two urban UK lakes in Coventry, when compared with rural lakes in north Warwickshire and the Isle of Scilly, which have no direct pollution sources [Foster *et al.*, 1991]. Also, Yang and Rose [2005] identified heavier trace metal contamination in rural UK lakes in sites closer to pollution sources, further supporting a fallout gradient, even within the rural environment.

10.7.2. The background air pollution signal for the UK from the sediments of remote rural lakes

Due to the remote nature of the pollution signal observed in rural lakes, the interpretation of pollution enhancement, via proxy magnetic and trace metal trends, is very generalised, mainly attributed to post-19th century global industrial emissions. Oldfield *et al.*, [1983] report a magnetic enhancement ~post-1913 in a glacial kettle lake in rural south Cheshire, corresponding to the main increase in magnetic spherule flux observed in peat surfaces in north Europe ascribed to national fossil fuel combustion [Oldfield, 1981]. Thirty-nine cores from 32 UK lake sites, investigated by Oldfield and Richardson [1990(a)], revealed a magnetic enhancement in 70% of the sites, from the early-to-mid-19th century, continuing to present day, with a notable steep increase ~post-1940. Oldfield and Richardson

[1990(a)] suggest this magnetic enhancement is due to industrial particulate emissions. This is also supported by Yeloff *et al.*, [2005], who report a post-1840 magnetic increase in a south Pennine reservoir, West Yorkshire, UK, accredited to a general rise in air pollution.

Trace metal pollution enhancement, due to industrialisation, has been reported in UK rural lakes [Farmer *et al.*, 1996; Yang *et al.*, 2002; Yang and Rose, 2005; Grayson and Plater, 2009]. This also includes peat burning and metal mining over several millennia in the UK [Mighall *et* al., 2002; Meharg and Killham, 2003; Yang and Rose, 2005]. Renberg *et al.*, [2001] present a global Pb record spanning 2000 BC to 2000 AD, from European sediments, with two distinct Pb increases at ~100 BC to 200 AD, ascribed to Pb production during the Roman period, and at 1000-1200 AD, reflecting medieval increases in Pb production and metal smelting. Post-1850 records from lakes in Sweden and peat bogs in Switzerland demonstrate a post-1900 Pb enhancement, with a ~1970 peak and subsequent decline [Renberg *et al.*, 2001]. Temporal patterns of trace metal deposition in the UK were investigated by Yang and Rose [2005] using five rural UK lakes ranging in size from 5.7 to 114 ha (lake area) and from 13 to 26 m maximum water depth. Yang and Rose [2005] report a pre-1860 contamination of trace metals impacting three of the remote lakes, from metal mining, and a rapid post-1860 trace metal increase reflect impacts of the Industrial Revolution.

The majority of work concerned with atmospheric pollution signals from UK and European lakes has been conducted by authors Rose and Yang [Rose, 1996; Rose *et al.*, 1996; Rose *et al.*, 1999(b); Yang *et al.*, 2001(b); Rose *et al.*, 2002]. Long-term SCP records retrieved from rural lakes provide a remote, background signal of anthropogenic-derived particulates for the UK. The majority of investigated lakes are focused in remote locations such as upland Scotland and rural Wales [Yang *et al.*, 2001(b)], which when combined with rural European lakes, enable the establishment of a background pollution signal for Europe. A distinct SCP signal for Europe is recognised due to the occurrence of three man features in the SCP record. These features are widely accepted as reliable dating events (Section 9.5.), relating to national fossil fuel combustion trends [Rose *et al.*, 1999(a)]. The UK particulate record begins to increase from the mid-19th century due to the Industrial Revolution, followed by sharp increases post WWII due to the rapid expansion of electricity production in the UK. A maximum SCP peak occurs during the 1970s-80s. Rose *et al.*, [1999(a)] suggests that the national coal and oil statistics and UK

trends in power generation explain these observed anthropogenic particulate emission trends.

10.7.3. Variations between the regional (UK) and the LMR pollution signal

The local pollution histories recorded in urban ponds override the large-scale temporal deposition patterns obtained for the UK, due their central position within the urban environment and impacts of nearby point sources [Renberg *et al.*, 2001]. The high-resolution chronologies of the urban sediment stratigraphies in the LMR also allow a more detailed interpretation of pollution deposition trends, via documented local industrial and domestic activities. Such localised impacts of industry and urban development on urban lakes are also recognised in similar urban studies [Tylmann, 2005].

Atmospheric pollution deposition at DDP appears to be influenced by localised urban impacts, due to the relatively early dates allocated to the features of the SCP profile at this site, when compared to national SCP trends (Figure 9.1, Section 9.5.). The SCP record demonstrated in the DDP stratigraphy indicates the start of the SCP record at ~1830 (feature A). Rose *et al.*, [1999(a)] describe this feature, commonly dated at 1850-60, as the initial increase in SCPs following an absence of SCPs in the stratigraphy, to coal combustion during the Industrial Revolution. Emissions at this time were expelled from low chimneys of abundant, small scale and local industrial activities and, therefore, Rose *et al.*, [1999(a)] suggest deposition of these particulates were highest near their source. This may explain the earlier SCP increase observed in the urban DDP pond (Figure 9.1) which, due to its location, is more sensitive to industrial emissions than the rural lakes, which provide the background UK signal. Also, as the start of the national SCP record pre-dates the first electric power stations in the UK, introduced during the late 19th century [Rose *et al.*, 1999(a)], a potential source of SCPs during the early 19th century in the LMR may have been from the early, low scale industrial uses of coal.

Nationally, SCP values steadily increase until a notable rapid enhancement (feature B), typically, occurring between 1940-60 [Rose *et* al., 1999(a)], which Rose *et al.*, [1999(a)] attribute to emissions from large-scale oil-fired power stations, which established at this time due to the availability of cheap fuel oil. The earlier ~post-1920 SCP increase observed in the DDP profile may reflect the shift in industrial production from Leblanc to electrolytic chemical production methods in Runcorn and Widnes, which required increased capacity of electricity generation at power stations at Weston Point and West

Bank (Widnes), to supply the chemical factories. This again, potentially, reveals a local variation from the national SCP record, relating to site specific industrial activity in Halton.

Maximum SCP peaks in the UK, typically, occur during the 1970s-80s. Despite a continued increase in energy consumption, the development of combustion technology and the replacement of small local stations with the National Grid, where more efficient power stations with taller stacks and, therefore, improved dispersion of emissions, combined with air quality legislations, resulted in the subsequent decline in SCPs following the SCP maximum peak (feature C) [Rose *et al.*, 1999(a)]. A slightly earlier, 1963 SCP maximum peak is also observed in the DDP profile, which coincides with the New Town development in Runcorn, which may further reflect the shifts in industrial activity in Runcorn and Widnes at this time. It is highly likely that the subsequent post-1963 SCP reduction may reflect the shift in power generation in Halton from Fiddlers Ferry power station which became operational post-1973. The dates of the three main SCP features in DDP are presented alongside those obtained from rural sites throughout the UK and Ireland (Table 9.1, Section 9.5.). The non-corresponding dates between the remote signal and DDP demonstrate the SCP record exhibits local variability.

10.8. Comparison of local air pollution signals in the LMR with other urban stratigraphies.

Local air pollution records obtained within the LMR are site specific to the urban environment of the borough and the surrounding industrial processes. Local pollution signals reconstructed from other urban lake and pond sediments in the UK, Europe, USA and Canada ascribe documented localised industrial and urban development events to the temporal pollution patterns obtained [Van Metre and Callender, 1997; Dauval'ter, 2004; Graney and Eriksen, 2004; Couillard *et al.*, 2008], further supporting the interpretation of the local pollution histories from DDP, WH, DKC and OG.

Clear distinctions between low pre-industrial proxy pollution data and post-Industrial Revolution enhancement is observed in a range of urban sediment stratigraphies, including urban ponds during the 19th century [Gilbertson *et al.*, 1997]. This is reflected in the DDP profile, which exhibits a clear pollution enhancement due to the documented intensification of industry in the LMR during the 1830s. In other studies, later pollution elevations are

observed, corresponding to the localised onset of industrial development revealed by 20th century records from urban lakes stratigraphies:

- A post-1920 depositional history of air pollution was revealed in a Russian urban lake by Dauval'ter [2004], who suggests maximum SCP concentrations are due to highest levels of coal production in the region during the 1970s and 1980s.
- A post-1912 history of contamination in a large American urban reservoir is presented by Van Metre and Callender [1997], who associate Pb and Zn enhancements to urbanisation within the catchment and gasoline consumption. Decreases in Pb post-1980 are explained by unleaded petrol consumption [Van Metre and Callender, 1997].
- An SCP record from a large Finish urban lake reveals an air pollution deposition history attributed to soot emissions, most notably from a nearby heavy fuel- and coal-fired power plant [Meriläinen *et al.*, 2003]. However, due to some industrial effluent discharge to the lake, the trace metal record is associated with the establishment of a sewerage system, opposed to atmospheric deposition.
- A 50-year history of trace metal deposition in a storm water pond in USA was investigated by Graney and Eriksen [2004], who detail a rise in pollution, corresponding to local industrial processes, and consumption of leaded petrol, and the subsequent fall post-1970 ascribed to the effects of Clean Air Acts [Graney and Eriksen, 2004].

The majority of studies inferring urban air pollution histories have relied on large urban lakes (Table 10.6), to provide contamination histories for an urban area. The manmade urban ponds investigated in the LMR are however relatively very small (<0.2 ha). For example, Tylmann [2005] attributes pollution enhancement in an urban lake sediment stratigraphy to local industrial activity, highlighting the valuable archives of local pollution signals obtained from small (7.5 ha) shallow (<3 m) urban lakes. However, the investigated lake (Pusty Staw) has a surface area up to three orders of magnitude higher than Oglet pond, the smallest investigated pond site in the LMR (<0.02 ha).

Small urban ponds are, however, advantageous as sinks of urban pollution. Within the UK, sediments from small urban lakes have been investigated by Charlesworth and Lees [2001], who produced post-1850 contamination histories from two urban lakes in Coventry, Swanswell Pool (lake area: 0.73 ha, catchment area: 220 ha, reduced to <1 ha by the 20th century) is of similar size and urban catchment to the ponds investigated in the

LMR, and the larger Wyken Slough (lake area 2.25 and catchment area 450 ha). Trace metal flux for two time periods are presented, from 1850 to 1954 and 1954 to 1991 [Charlesworth and Lees, 2001].

Charlesworth and Foster [1999] report higher trace metal flux rates at Swanswell Pool, due to its inner-city location, compared to Wyken Slough located on the city outskirts. Higher trace metal rates observed in the urban Coventry ponds compared to published enrichment factor values of emissions released into the environment, highlights the central position urban ponds occupy for receiving trace metal pollution [Charlesworth and Foster, 1999].

Table 10.6: Lake and catchment areas from the investigated urban ponds in the LMR compared to other investigated urban lakes sites (* morphological feature not described by author).

Author	Lake	Lake area (ha)	Max water depth (m)	Catchment area (ha)	Lake: catchment ratio	Sediment record
	Daresbury Delph Pond	0.077	2	0.1088	1:1.417	Continuous post-1700 air pollution record.
	Windmill Hill Pond	0.026	2	0.0450	1:1.758	Continuous post-1900 air pollution record.
	Dogs Kennel Clump Pond	0.165	3	0.2050	1:1.227	Continuous post-1900 air pollution record.
	Oglet Pond	0.019	3	0.026	1:1.333	Continuous post-1920 air pollution record.
Blake *et al.*, 2007	Fendrod Lake, Swansea, Wales	7	3	1400	1:200	Sediment stratigraphy not dated.
Chalmers *et al.*, 2007	Upper Mystic Lake, Boston, USA	45	*	*	*	Continuous post-1940 record used to assess remediation history of contaminated site via trace metal concentrations.
Charlesworth and Lees, 2001	Swanswell Pool, Coventry, UK	0.73	1.3	<1	1:1.370	1850-1954 and post-1954 proxy pollution comparisons using dating horizons. Reference dates used rather than isotope chronologies.
Charlesworth and Lees, 2001	Wyken Slough, Coventry, UK	2.25	0.8	450	1:200	Pre-and post-1850 proxy pollution comparisons, using reference date.
Dauval'ter, 2004	Vorkuta, Russia	44	*	*		Post-1920 continuous record of localised air pollution.
Georgeaud *et al.*, 1997	Berre Lake, France	1.555	10 m average	*		4 m sediment sequence extracted, with a C14 date of 5600 BP, however a continuous sediment record of proxy pollution characteristics not presented, instead, magnetic-trace metal associations discussed.
Meriläinen *et al.*, 2003	Urban lake, Finland	34	27	*		Continuous post-1840 record, using reference dates and Cs^{137} date (1963), revealing history of pollution effluents received by lake.
Tylmann, 2005	Pusty Staw, Poland	7.5	3	<100	1:13.333	Post-1730 continuous record of flux and concentration data, corresponding to local urban activity and sewage discharge to lake.
Van Metre and Callender, 1997	White Rock Lake, Texas, UA	440	6	25900	1:58.333	Post-1912 continuous sediment record. Shows trace metal and persistent organic pollution trends relative to water quality impacts from agricultural processes and human activity.
Worsley *et al.*, 2006	Speke Hall Lake, UK	0.309	3	0.596	1:1.927	Continuous post-1600 air pollution record with isotope chronology relating to local urban activity.

Despite investigations of the use of urban lakes and ponds to reconstruct urban air pollution histories, the only successful extrapolation of a continuous sediment chronology extending back to pre-industrial times for a small lake/pond (<1 ha surface area) in the UK is by Worsley *et al.*, [2006]. Other investigated urban lake sites provide only a post-1900 or post-1950 history, or allow a generalised comparison of pollution deposition during two time periods [Georgeaud *et al.*, 1997; Charlesworth and Lees, 1999(a), 2001].

The pollution records obtained within the LMR also demonstrate a continuous ^{210}Pb chronology, allowing a more detailed temporal assessment of pollution trends, compared to work by Charlesworth and Foster [1999]. That work makes comparisons of pre- and post-1950 trace metal flux data and, therefore, does not pick out detailed temporal trends as observed in the sediment histories from the LMR ponds. These ponds reveal maximum pollution experienced during the mid-20th century and subsequent reduction post-1970, due to air quality legislations.

The post-1700 ^{210}Pb chronology obtained from DDP further supports work by Worsley *et al.*, [2006] highlighting the suitability of urban ponds to provide a continuous ^{210}Pb chronology, encompassing pre-industrial times to present day, allowing a comparison of temporal pollution trends pre- and post- the industrial intensification. DKC, WH and OG further support the suitability of urban ponds in providing detailed datable histories of high-resolution environmental change during the 20th century.

The combination of air pollution deposition records from several small urban ponds allow a cross-regional urban signal to be investigated *within* an urban area. The cross-regional air pollution signal allows a more detailed understanding of pollution impacts across the LMR, which is heavily industrialised, encompassing a range of industrial emissions from various processes, as well as domestic and transport pollution sources. Other studies investigating lakes classified as 'urban' are only affected by a few local industrial sources, and the pollution impacts are identified within the sediment stratigraphy [Merilläinen *et al.*, 2003; Dauval'ter, 2004]. The LMR ponds, however, reveal the complex nature of pollution experienced within an urban and heavily populated area.

10.9. Chapter summary

Local depositional air pollution histories for DDP, WH, DKC and OG are presented, which reveal site-specific, localised effects of industry and urban development on their sediment records. The interpretation of the local pollution signal from each site in relation to nearby industrial processes, urban sprawl and the overall effects of air quality legislations, highlights an intra-urban variation in the temporal pollution patterns experienced within the LMR. The overriding impacts of localised emissions on the urban ponds is demonstrated when compared with the background air pollution signal for the UK, obtained from sediment stratigraphies from remote rural lakes in the UK and Europe. The importance of small manmade ponds, set within the urban environment, is further emphasised via a comparison of the data yielded by the four ponds in the LMR, with air pollution histories obtained from other urban lake sediments.

11. CHAPTER ELEVEN: THE CROSS-REGIONAL AIR POLLUTION SIGNAL FOR THE LOWER MERSEY REGION

11.1. Chapter overview

This chapter details the cross-regional air pollution depositional history for the lower Mersey region (LMR) via the combination of local pollution histories from DDP, WH, DKC and OG. The main historical trends throughout the LMR are identified, impacted by local industrial and urban activity. Comparison of the cross-regional signal with available post-1960 monitored pollution data for Halton, highlights the importance of a long-term, intra-urban pollution record. The cross-regional signal is further complimented by pollution deposition histories obtained from other urban sediment stratigraphies, obtained from the Mersey Estuary and Speke Hall Lake, allowing a detailed reconstruction of pollution deposition across the LMR from pre-industrial times to present day.

11.2. Introduction

Urban ponds in the LMR are set amongst a heavily industrialised environment which, although dominated by the chemical industry, experiences a variety of industrial processes at over twenty industrial sites across the region (Figure 2.4,Section 2.4.1.). This industrial signal is combined with domestic and vehicular/aviation pollution and a potential long-range signal from other surrounding conurbations, such as Liverpool and Ellesmere Port. The combination of the urban ponds in the LMR with the air pollution archives obtained from Speke Hall, provide the first cross-regional air pollution histories from within a conurbation. Although other studies have analysed lake sediments from within a region [Charlesworth and Lees, 2001; Graney and Eriksen, 2004], only broad differences between urban and rural sites have been made. The small size of the urban ponds investigated in the LMR, from which the cross-regional signal is constructed, allows detailed spatial patterns in temporal pollution deposition within an ~18 km urban transect (Figure 8.1, Section 8.2.).

Investigation of a cross-regional signal is important due to the spatial and temporal variations in pollution deposition throughout a conurbation, as the local air pollution histories from DDP, WH, DKC and OG highlight (Chapter 10). The cross-regional signal reveals potential intra-urban differences in impacts of industrial and urban activities within the LMR. By combining the site specific pollution histories from the four urban ponds, a spatial dimension to the depositional histories of pollution across Halton and the LMR can be assessed, allowing a retrospective assessment of urban air quality throughout the area.

11.3. The cross-regional pollution history of the LMR

High-resolution post-1900 pollution deposition histories gathered from OG, DKC, WH and DDP provide a detailed account of pollution experienced throughout the 20th century, spatially spanning the breadth of the LMR. However, the extensive industrial history of the LMR extends to the start of the 19th century. This early industrial pollution signal is picked up by the DDP pond, which provides a high-resolution post-1700 stratigraphy, allowing an assessment of pollution deposition in Runcorn throughout the 18th and 19th centuries. The cross-regional signal, therefore, depicts a history of proxy pollution characteristics spanning from pre-industrial intensification (i.e. pre-1800) to present day. The cross-regional signal can be divided into zones, identified from visual assessment of the local pollution signals to highlight key patterns of proxy pollution trends occurring throughout the LMR (Table 11.1):

- Ri ~pre-1830: pre-industrial intensification (11.3.1.),
- Rii 1830 to 1900: the Industrial Revolution (11.3.2.),
- Riii 1900 to 1950: 20th century industrial expansion and population increases (11.3.3.),
- Riv 1950 to 1980: late 20th century urban development (11.3.4.) and
- Rv post-1980: stringent air quality legislation and increased road and air travel (11.3.5.).

Table 11.1: Cross-regional phases and identified trends.

Phase	Timescale	Proxy pollution trend
Ri	~Pre-1830	Relatively low proxy pollution levels revealed at DDP.
Rii	1830 to 1900	Initial increases in proxy pollution trends from ~1830, steadily increasing throughout the 19th century identified in the DDP core.
Riii	1900 to 1950	Elevated pollution trends post-1900 identified at DDP, with corresponding enhancement at WH and DKC. Increasing pollution trends observed at all pond sites throughout this phase.
Riv	1950 to 1980	Prominent proxy pollution peaks identified at DDP, DKC and OG. WH profiles also exhibits pollution increases during this phase, despite an overall reduction.
Rv	Post-1980	A reduction in trace metal trends is observed opost-1980 at DKC, WH and DDP; however, OG exhibits prominent increases, which corresponds with an increase in fine ferrimagnetic grains identified at DDP and DKC.

These divisions are superimposed over magnetic and trace metal flux profiles from each pond to demonstrate the supply of magnetic grains, a proxy of total pollution particulates (SIRM) and fine (~<1 μm) PM ($HARD_{.300mT}$) to the LMR.

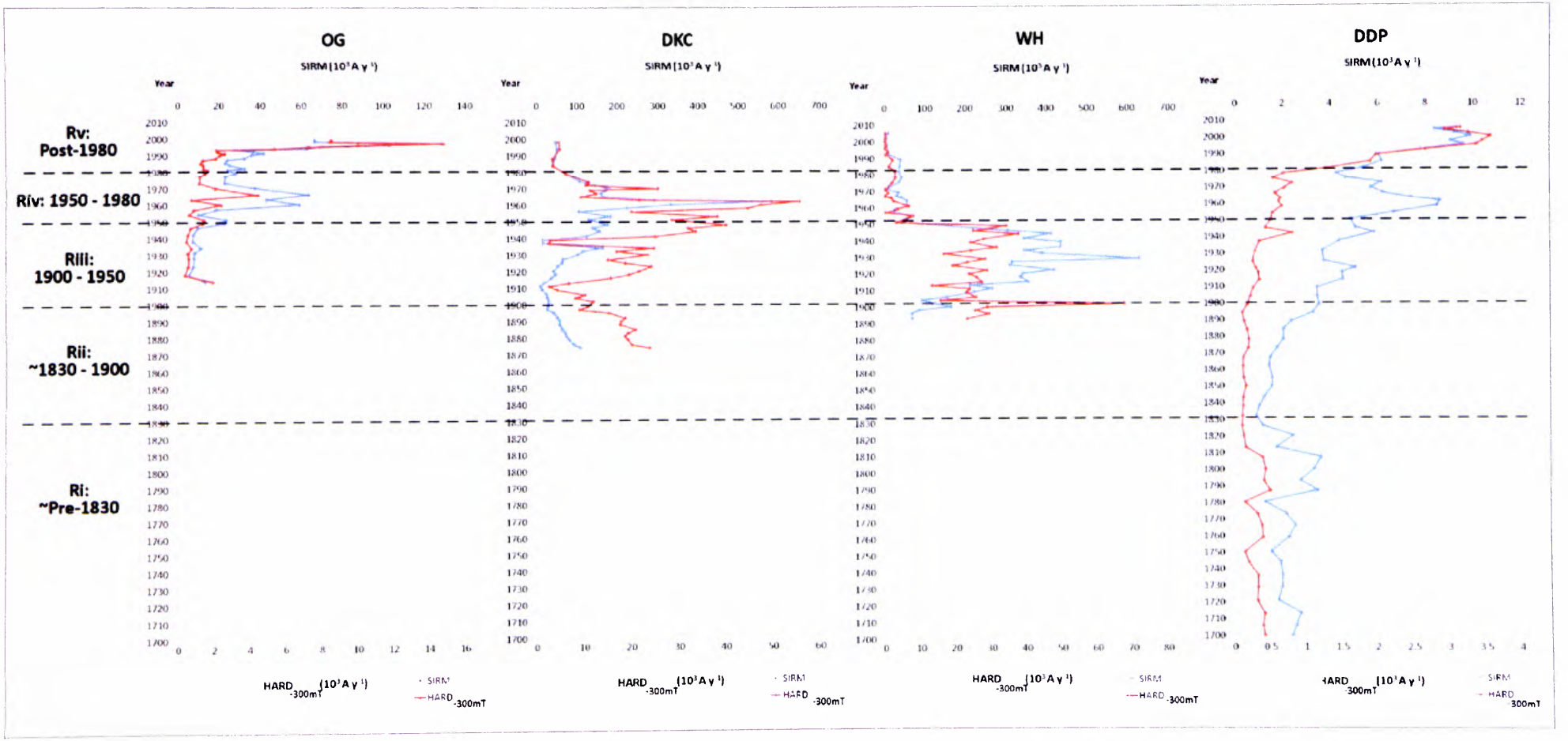

Figure11.1: Post-1700 cross-regional magnetic flux profiles (SIRM and $HARD_{-300mT}$) from OG, DKC, WH and DDP, with superimposed phases Ri to Rv.

11.3.1. Ri ~pre-1830: pre-intensification of industry in the LMR

The local contamination history reconstructed from DDP has been used to assess the pre-1900 regional deposition of pollution (Figure 11.2). Although located in the south-east of the LMR, DDP is representative of pollution experienced post-1700 in the region, due to the differing urban histories of Runcorn and Widnes. During the 1700s both Runcorn and Widnes were villages, with low-scale localised industrial activity. Industrial development occurred primarily in Runcorn during the late 18th century; however, it was not until the mid-19th century that significant growth of industry occurred in Widnes.

The relatively low pre-1830 proxy pollution flux values in the DDP core, however, represent a time of pre-intensified industry in Halton. Runcorn and Widnes were agricultural villages during the 1700s as transport routes by-passed the towns [Poole, 1906]. Pre-industrial Halton was perceived to have good air quality, compared to other nearby industrial cities (e.g. Liverpool), as Runcorn was renowned as a health resort [Vardy, 2005] which is reflected by the low pre-1830 regional pollution signal.

The earliest proxy pollution increases observed in the S profile at ~1751, potentially reflect small-scale industrial activity in Runcorn. The distinct SIRM, S and Pb peaks, from ~1780-1800 correspond with improved transport links to the town, such as the expansion of the Bridgewater Canal (1776), Old Quay Canal (1803) and Weaver Canal (1807), which in turn, resulted in a rise in quarrying, barge and ship building in Runcorn, increasing the town's importance as a port. A consequence of this was the establishment of further industry in Runcorn, for example, Johnson's soapworks in 1803 and, therefore, an increase of industrial pollution emissions. This initial industrial growth is reflected by observed S and Pb increases, and further trace metal and magnetic increases during the early 19th century.

11.3.2. Rii 1830 to 1900: the Industrial Revolution

The noted post-1832 proxy pollution enhancement, reflects marked industrial development in Halton; predominantly in Runcorn as, at this time, principle trades in Widnes included watch making, tool making, file cutting, wire drawing, farming and beer selling (documented in the 1841 Census) [Warren, 1980]. This increase corresponds with the opening of the Runcorn Gap Railway in 1831, which led to further industrial growth and, therefore, the town experienced increased pollution outputs from tanneries, shipyards and the developing chemical industries in Runcorn and Weston. The post-1830 increase may

also reflect a rise in soap production, by a third, at the existing Johnson's and Hazlehurst sites in Runcorn [Barker and Harris, 1959].

The prominent 1850-1880 Pb, Zn and S peaks reflect an episode of increased pollution in Runcorn, potentially, due to increased industrial emissions from the boom in chemical production at this time. This subsequently led to population increases from 6,957 in 1841 Runcorn to 15,133 in 1881 [Runcorn and District Historical Society], which may also be reflected in this pollution peak. The peak may also encompass significant industrial development in Widnes, with the onset of the chemical industry in 1847 and the construction of 22 Leblanc chemical sites in the town between 1847 and 1884. At this time Widnes rapidly turned into a 'chemical town':

'Houses and streets spread themselves over the open spaces around the works, and in a very few years Widnes was transformed from a pretty, sunny riverside hamlet...into a settlement of thousands of labouring men... with dingy, unfinished streets of hastily constructed houses, with works that were belching forth volumes of the most deleterious gases, and clouds of black smoke form chimneys of inadequate heights...' [Allen, 1906].

Immediate adverse air quality issues were observed due to the new chemical landscape (Section 2.4.3.), which is reflected by the pollution peak in the DDP profile. A quote by Hurter in 1888 described the urban Mersey landscape:

'It is permissible to imagine that the ashes of Sodom and Gomorrah immediately after the destruction of those wicked cities emitted no more pestiferous odours, or were more devoid over all their wide area of one single green leaf or sign of vegetation, than those twin towns of Mersey – Widnes and Runcorn.' [Warren, 1980].

Of particular environmental burden were smoke and hydrochloric acid gas emitted by Leblanc methods, which dominated chemical production in Halton from 1803 to ~1900. There are several reported accounts of devastation to the countryside and the health of chemical workers and the public during the 19th century [Warren, 1980] (Section 2.4.3.), which brought about the introduction of the Alkali Act in 1863 that aimed to curb emissions of hydrochloric acid gas from Leblanc chimneys.

The Leblanc process involved heating of salt with sulphuric acid in lead-lined chambers and was heavily reliant on coal combustion, which may explain the distinct pre-1900 industrial pollution signature, characterised by increases in SIRM (Figure 11.1) and SOFT$_{20mT}$, SCPs 10-30 μm and 3-10 μm (Section 7.3., Figure 7.3), and distinct Pb and S enhancement observed in the DDP profile post-1830.

Magnetic and SCP flux demonstrate an increase throughout the late 19th century, potentially, reflecting the shift in chemical production at this time in Halton and increased energy demands. Sulphur and Cu flux values, however, exhibit a notable decline from 1880 to 1900, reflected by Pb and Zn decreases during the late 19th century. This may represent the decline in Leblanc chemical production at this time due to a recession in the chemical trade. A corresponding reduction in proxy pollution is also observed in the DKC local pollution history, further supporting the decline in pollution at this time throughout the LMR.

11.3.3. Riii 1900 to 1950: 20th century industrial expansion and population increases

The flux profiles from DDP allow a comparison of how pollution has changed pre- and post-1900. Prominent increases in proxy pollution post-1900 exhibited by the DDP core highlights further pollution enhancement during the 20th century. Also, prominent SCP increases post-1900 further demonstrate a distinct elevation in pollution particulates from the start of the 20th century. The BDD1 core reveals a shift to a finer particle size assemblage post-1900 (Section 6.3.2., Figure 6.6) with a median particle diameter <10 μm, highlighting a finer post-1900 magnetic contribution to the sediment record. This reflects work by McLean [1991] which, via light microscopy of magnetic spherules, revealed a reduction in modal sizes of magnetic grains to <10 μm throughout the 20th century, which may be transported thousands of km from source, highlighting a potential long-range pollution signal [ApSimon *et al.*, 2001; Wu *et al.*, 2006].

Higher post-1900 Zn deposition is observed in the DDP core, highlighting a modern (20th century) source of Zn emissions. This is supported by Charlesworth and Foster [1999] who report Zn demonstrating the largest post-1950 flux increases (of all investigated trace metals) at both urban lakes investigated in Coventry; and by Graney and Eriksen [2004] who report post-1970 Zn elevations attributed to car metal plating industries. Charlesworth and Lees [1999(a)] highlight car tyre wear as important source of Zn and Cu in urban lakes, as well as industrial emissions. An increase in the supply of Pb and S occur post-1900; however, S values are relatively low compared to maximum flux values exhibited during the observed ~1850-1880 peak. This may reflect the demise of Leblanc chemical production in Halton during the start of the 20th century, indicating an association of high S output with the early chemical industry.

The contribution of WH, DKC and OG to the cross-regional signal during the 20th century allows a more broad assessment of pollution deposition across the LMR (Figure 11.3 and 11.4). A complex urban pollution signal is observed post-1900, combining the expansion of industry, population increases and domestic coal combustion. Due to the already established industrial activity and 20th century population increases observed in Halton, it becomes more speculative and difficult to 'tease out' specific events related to industrial activity [Carter, 1964; Warren, 1980]. Correlating trends between the four urban ponds may reflect regional air quality issues. The DKC and WH profiles demonstrate close parallels, from 1900 to 1950, highlighting a similar pollution story across the LMR at this time. The post-1900 DDP history is comparatively less detailed than at WH, DKC and OG due to a lower resolution of the sediment stratigraphy.

Overall, there is an increase in pollution across the LMR post-1900, which continues throughout the first half of the 20th century. Reflected in all four ponds, this highlights a correlating feature of air quality degradation. Initial post-1900 increases may reflect the recovery of the chemical industry at the start of the 20th century [Rintoul, 1984], the expansion of industry due to the introduction of new production methods that occurred in the LMR at this time [Carter, 1964; Campbell, 1971; HBC, 1991, 2005(a)] and the opening of the Transporter Bridge in 1905, connecting Runcorn and Widnes [Starkey, 1981, 1990]. Also, the completion of the Manchester Ship Canal in 1894 resulted in Runcorn becoming less important as a dock, which in turn led to less diversified industry in Halton [Jones, 1969]. At the start of the 20th century industry in Halton generally comprised of:

- expansive chemical industry in Widnes, which became predominantly concerned with the manufacturing of organic chemicals [HBC, 2005];
- electrolytic inorganic chemical production introduced at Weston (1896) due to the phasing out of Leblanc production finally ending in 1920 [Rintoul, 1984]; and
- tanneries established at the former Leblanc soapwork sites in Runcorn [Runcorn and District Historic Society, n.d.].

The observed increasing trend in pollution deposition throughout the LMR from 1900 to 1950 encompasses the demands of two world wars on industry in Runcorn and Widnes, which were important manufacturing centres in the UK. Notable increases in pollution occur throughout the LMR from~1910, reflected in DKC, WH and DDP profiles, with periods of increased pollution deposition from 1914-21 at DDP, 1911-29 at WH, and peaks

at 1918 in the DKC and OG profiles, which may reflect a WWI (1914-18) pollution signal due to increased industrial output.

Rising proxy pollution trends throughout the LMR during the 1920s and 1930s may reflect an industrial signal comprised of emissions from tanneries, and the diversifying chemical industry in Widnes and Runcorn may be due to the formation of ICI (1926). Also, population increases experienced in Halton will have resulted in heavier environmental burdens, such as domestic coal burning, which is likely to be incorporated into this signal, as a, potentially, important source of S post-1900, following on from the Industrial Revolution.

Relatively high pollution values are sustained throughout this phase, reaching mid-20th century peaks in all four ponds, which may signify urban expansion throughout the LMR. WH demonstrates a prominent magnetic flux peak at 1949, which is not mirrored in the other urban pond profiles, so, potentially, highlights a site specific pollution episode at this time. Also, OG demonstrates prominent magnetic and trace metal flux increases from 1949-51, which, it is speculated, may be due to local urban development in Halewood, which is explained in the following section.

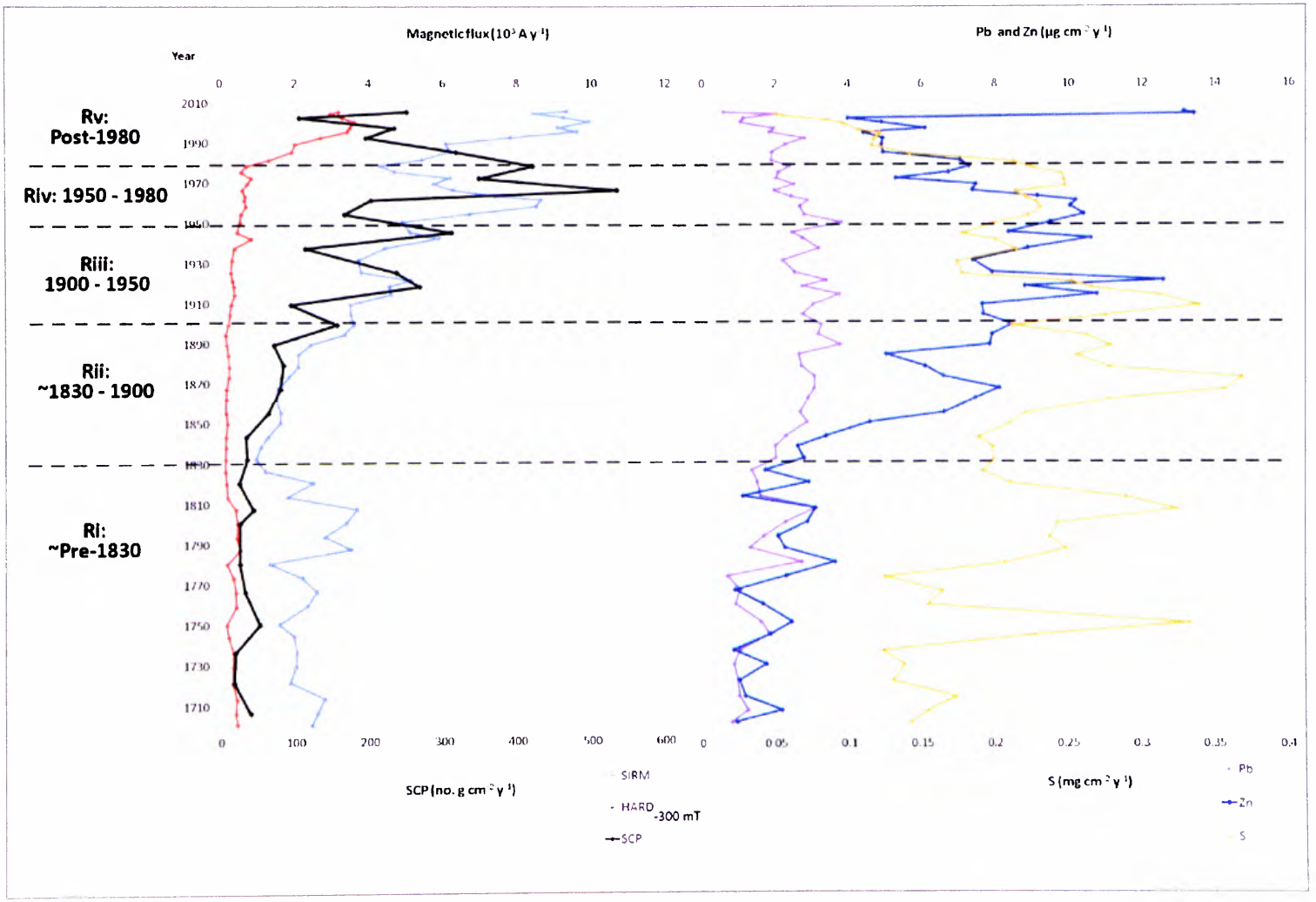

Figure 11.2: Post-1700 Magnetic (SIRM and $HARD_{-300mT}$) SCP (total), Pb, Zn and S flux signal for the LMR recorded at DDP, with superimposed regional phases Ri to Rv.

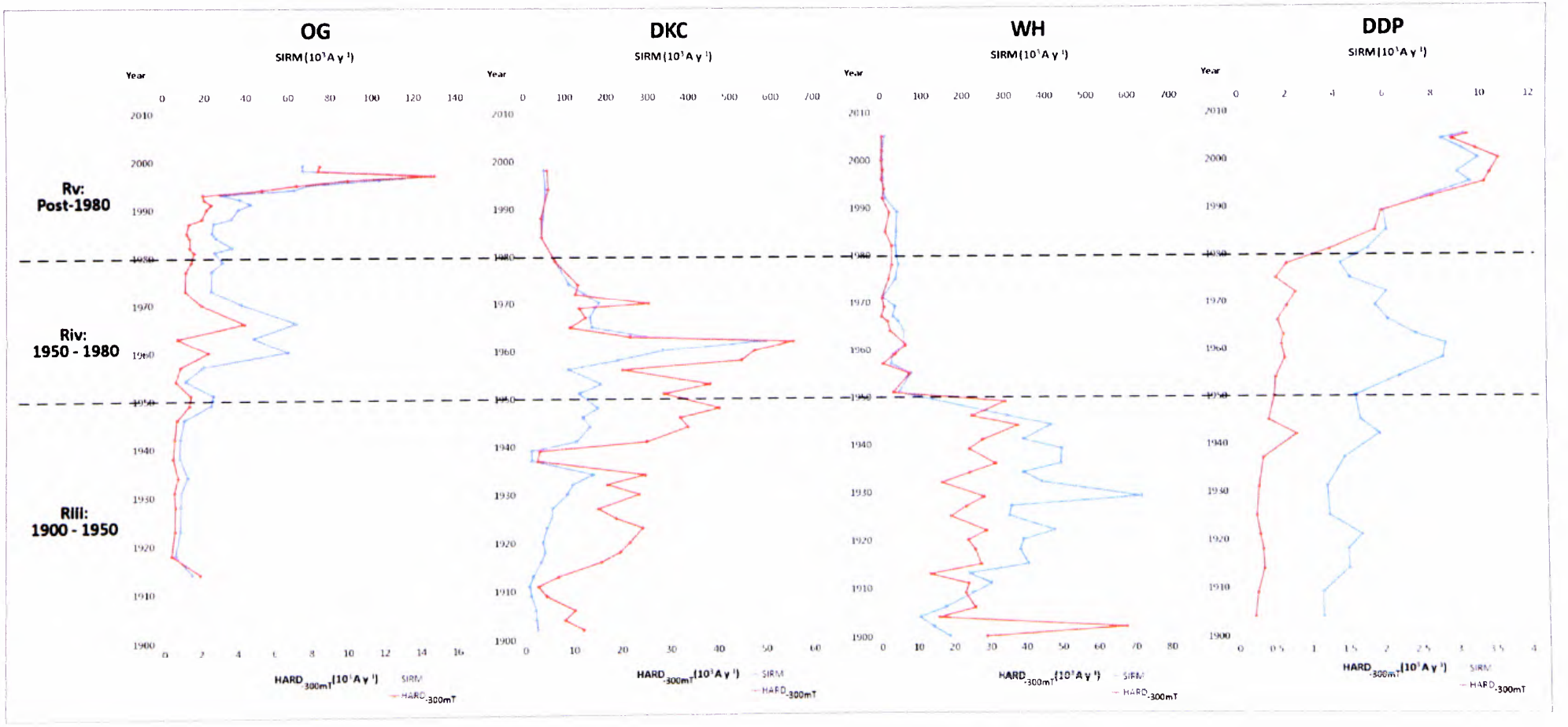

Figure 11.3: Post-1900 cross-regional magnetic flux (SIRM and $HARD_{-300mT}$ (10^3 A y^{-1})) signal for the LMR, with superimposed phases Riii to Rv.

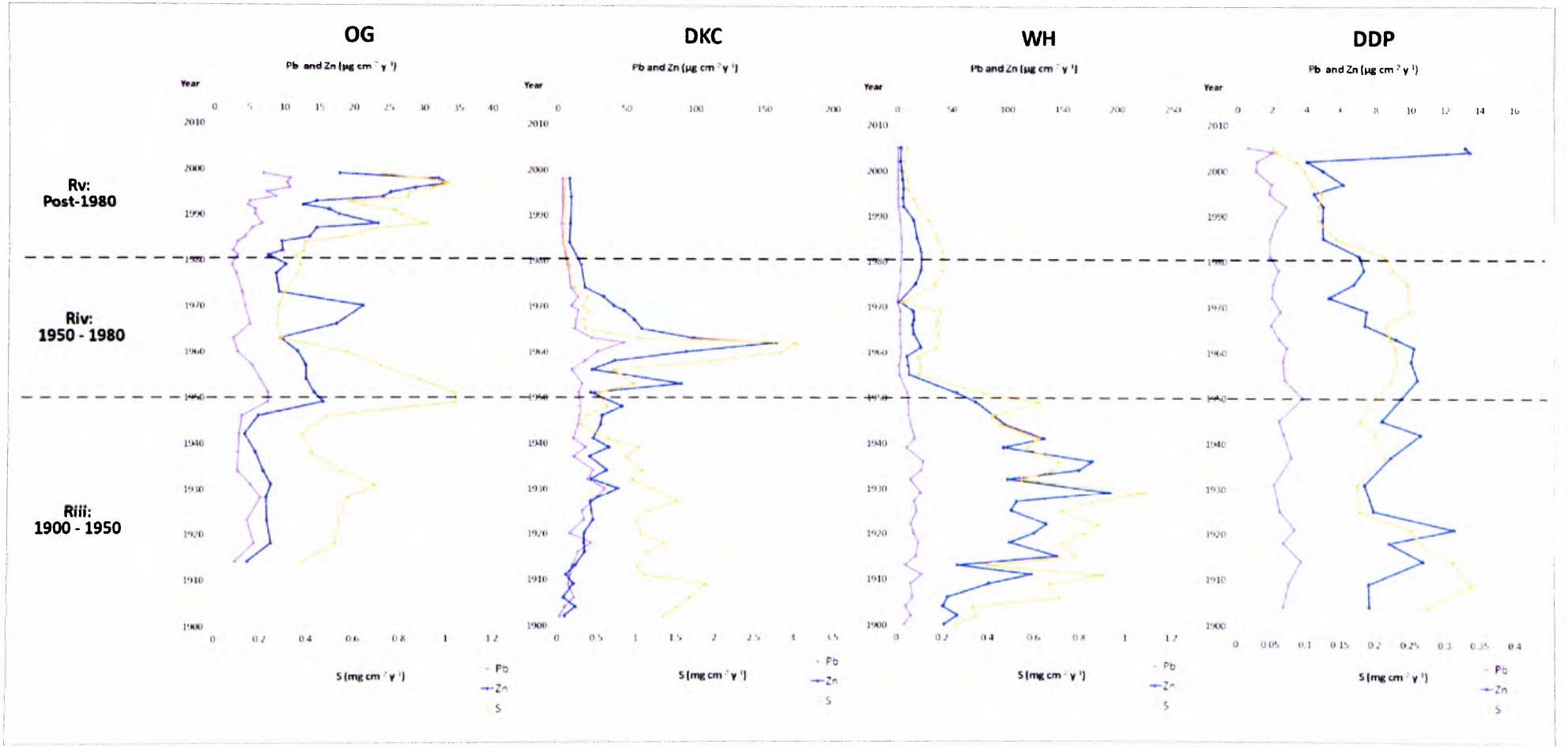

Figure 11.4: Post-1900 cross-regional Pb, Zn (µg cm^{-2} y^{-1}) and S (10^{-1} mg cm^{-2} y^{-1}) flux signal for the LMR, with superimposed phases Riii to Rv.

11.3.4. Riv 1950 to 1980: late 20th century urban development

Modern industrial processes, urban sprawl, New Town developments, increasing population trend, and transport activities, coupled with increasingly stringent air quality legislations are characteristics of the cross-regional, post-1950 urban pollution signal recorded in the LMR. Post-1950 urban sprawl throughout the area considerably influences the regional signal. Prominent mid-20th century peaks observed throughout the region demonstrate post-1950 urban development and subsequent population increases. Despite the introduction of the Clean Air Act in 1956, post-1950 increases in pollution are observed throughout the LMR.

DDP demonstrates a prominent proxy pollution increase from 1958-63 with maximum SCP flux at 1963. This suggests that the deposition of anthropogenic particulates was greatest during the early 1960s. This corresponds with the New Town Development in Runcorn and the development at Halewood, as OG and DKC also demonstrate high ~1960 magnetic and trace metal peaks. Although WH demonstrates relatively low post-1951 flux values, increases in pollution deposition are observed from 1964-1989, coinciding with the New Town development and residential development during the 1970s within Windmill Hill, a sub-district of Runcorn. At this time, vehicle particulates may be an important contributor to the urban pollution signal due to increasing trends in road transport post-1950 (Section 10.3.3., Figure 10.3), in particular, Pb emissions due to leaded petrol consumption, reflected by high Pb flux at 1950 in DDP sediments.

The post-1950 OG and DKC local pollution histories, potentially, reveal industrial impacts in the north-west of the LMR. The post-1949 increases observed in the OG pond may reflect the development of the Halewood industrial site during the 1950s, which included chemical works, pharmaceutical factories and foundries. These industrial processes are likely to have impacted the nearby DKC and OG ponds, and may, therefore, be responsible for the observed post-1950 increases. Furthermore, the expansion of the chemical industry and subsequent manufacturing of a variety of products at this site may have introduced new pollutants to the area, reflected by prominent post-1950 increases in Zn, Cu and Br exhibited in the OG and DKC cores. Also, post-1950 enhancement may be related to an increase in population in Halewood and Speke due to the construction of housing estates during the 1950s and 1960s. The prominent 1960-1963 pollution peak exhibited in the DKC core coincides with the establishment of the Ford motor car production site, marking further industrial development in Halewood. Due to these site specific urban

developments, the DKC and OG post-1950 signal may represent industrial emissions at Halewood, as prior to this the nearest industrial sites were at Widnes and Runcorn. WH and DDP demonstrate a pollution signature for the south-east of the LMR.

All sites demonstrate a reduction in trace metal deposition after these mid-20th century peaks. The overall post-1951 reduction in pollution observed in the WH pond may highlight the closure of nearby tanneries during the 1950s and 1960s. However, increased pollution experienced at WH during the 1970s and 1980s may reveal pollution impacts from the local residential development, with further, post-1990, pollution reductions influenced by more stringent air quality controls. DDP demonstrates an overall reduction in trace metals post-1963, with sustained high S and Pb values until ~1975. This may reflect the 1956 Clean Air Act, and subsequent stringent legalisations, which have reduced, for example, the use of Pb and S in fuels and industrial processes, and shifts in domestic fuel from coal to gas. This reduction in pollution is particularly notable in the S profile at DDP, which exhibits a steadily decreasing trend from 1975 to present day, with the lowest S flux exhibited in the recent sediment. This reduction is also mirrored in the DKC profile, which exhibits steadily declining pollution trends post-1970. OG also demonstrates a 1970-1980 decrease in the supply of pollutants. These S reductions may also mirror the decline in SO_2 documented in the UK [Goodwin *et al.*, 1999; UK Emissions Inventory Team, 2007], thus, reinforcing the reliably of urban pond sediments as indicators of air quality.

11.3.5. Rv post-1980: stringent air quality legislations and increased road and air travel

The OG core exhibits an increase in trace metals and magnetic flux post-1980, which is not mirrored in the other four urban ponds. This suggests that a site-specific pollution source impacted the OG pond which, due to the proximity of the pond to the runway at John Lennon International Airport is, potentially, a pollution signal from aviation activity (Section 10.6.5.). Figure 11.5 demonstrates increased post-1980 Pb deposition at OG pond compared to the other four urban ponds. This may reflect the proximity of the ponds from the airport (OG: 300 m, DKC: <3.5 km, WH: <12 km and DDP: ~14 km) revealing a gradient of decreasing Pb deposition away from the airport. Also, relatively high χ_{ARM} values recorded at DKC in this recent phase (Figure 8.3), may reveal higher deposition of fine (SSD) magnetic grains, typical of airport emissions [Boyle, 1996], being deposited away from source due greater transport distances of finer PM [ApSimon *et al.*, 2001].

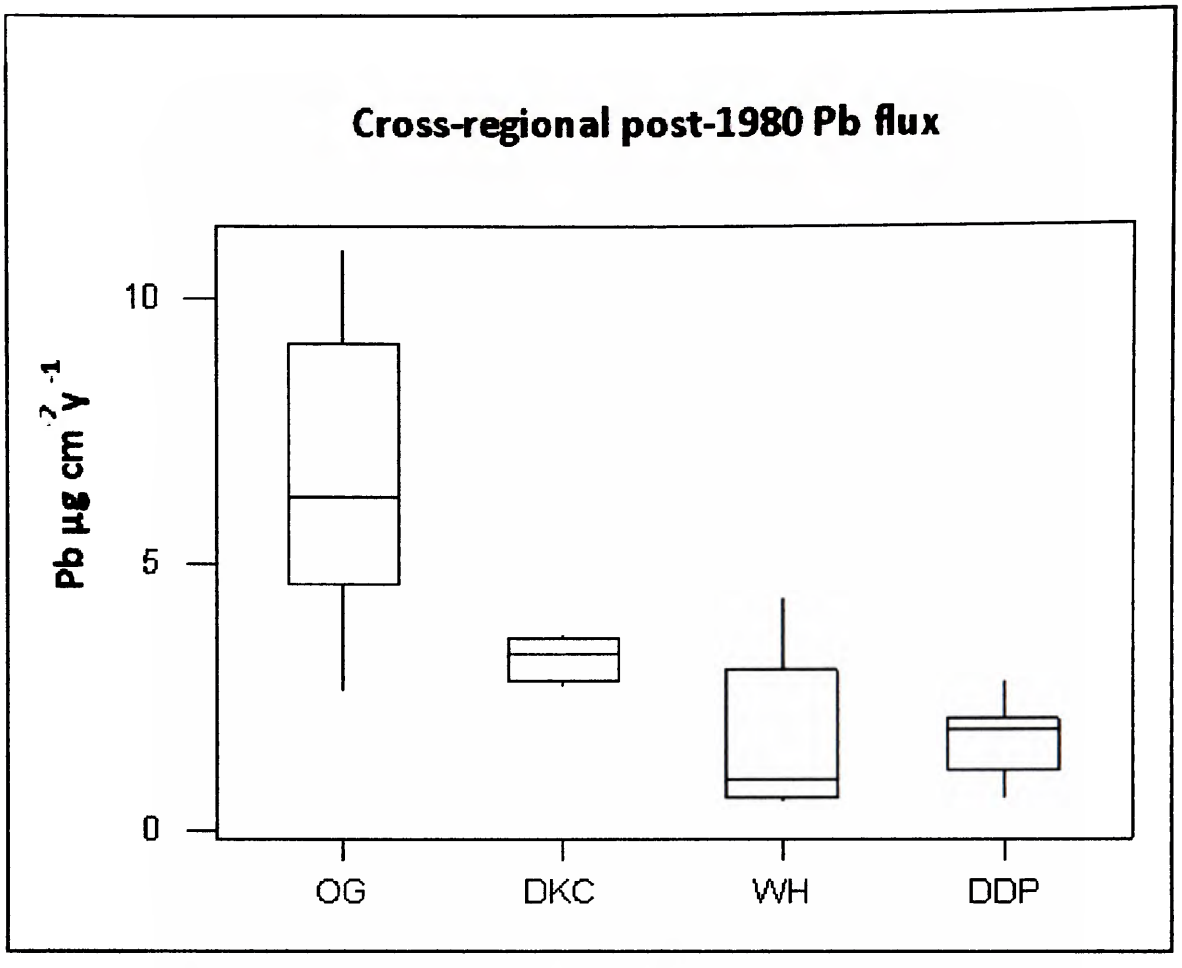

Figure 11.5: Cross-regional post-1980 deposition of Pb in the LMR. (OG n=18; DKC n= 4; WH n= 10; DDP n= 10).

The data suggest post-1980 pollution from airports, following increasing trends in air traffic, has become a significant post-1980 source of pollution, opposed to industrial emissions, at OG, and possibly DKC. The signature of the aviation transport signal is characterised by prominent increases in the deposition of trace metals and fine magnetic grains. Also, in the east of the LMR there is evidence of a post-1975 transport activity signal in the DDP profile, as SIRM and $HARD_{-300mT}$ flux increases coincide with the construction of the M56 motorway adjacent to the site. The presence of a recent fine grained magnetic signature is also detected in the DKC profile post-1974, revealed by χ_{ARM} increases at this time (Section 6.5.1., Figure 6.14).

Diesel and vehicular exhausts are the primary source of atmospheric nano- and micro-particles in urban areas [Buzea *et al.*, 2007]. Most particulates from vehicle exhausts are 20

to 130 nm* for diesel engines, and 20 to 60 nm for petrol engines. These nanoparticles comprise >90 % of diesel generated particulates [Buzea *et al.*, 2007]. The importance of these ultra-fine particulates (<0.1 μm) to the urban environment are reported [Hitchins *et al.*, 2000; Zhu *et al.*, 2002; Sioutas *et al.*, 2005].

Due to the stringent air quality legislations, post-1956 air quality is thought to have improved with the monitoring of industrial emissions and 'phasing out' of Pb use, highlighted by post-1970 trace metal declines in the DDP, DKC and WH sites. However, the potential shift to a fine-grained vehicular pollution signature post-1978 in the DDP pond, and post-1980 fine-grained aviation pollution signature with high trace metal burdens in the OG pond, may highlight the impact of transport activity emissions on post-1980 air quality. This recent pollution signal may be more harmful to health [Vedal, 1997; Oberdórster, 2000; Morawska and Zhang, 2002; Raloff, 2003; Englert, 2004; Willson *et al.*, 2005], due to the fine-grained nature of the signature and therefore, although pollution levels have reduced since the reported nuisances of the Industrial Revolution and pre-1956 Clean Air Act legislations, the cross-regional signal demonstrates a potentially more toxic pollution signature post-1980. The changing balance of industrial-to-transport emissions may reveal that the urban environment is more impacted by vehicular and air travel emissions, than pollutants from industrial stacks, as indicated by contemporary data of industrial and transport derived fractions of Pb presented in Table 11.2.

Table 11.2: Percentages of pollutant emissions from industrial and transport sources in the UK [UK Emissions Inventory Team, 2007]

Pollutant	Industrial contribution (%)	Transport activity contribution (%)
Benzene	20	67
1,2 Butadiene	13	77
Carbon monoxide (CO)	12	75
Lead (Pb)	18	78
Nitrogen oxides (NOX)	37	46
PM	59	26 (PM_{10}) 50 (black smoke)
Sulphur dioxide (SO_2)	89	2
Volatile organic compounds (VOCs)	53	29

* 1 nanometer (nm) = 0.001 μm.

11.4. The cross-regional signal versus available monitored historical pollution data

The cross-regional pollution signal allows a long-term assessment of pollution deposition throughout the LMR. Post-1960 black smoke and sulphur dioxide concentrations (available from the National Air Quality Archives) monitored by filter reflectance and acid titration, respectively, at eight sites throughout the LMR (Figure 2.6) provide only a comparatively recent 'snap shot' of recent pollution trends, for an area that has experienced releases of contaminants since the onset of industry during the early 19th century. This is particularly notable when compared to the air pollution trends extending from pre-industrial times to present day, captured by the cross-regional signal (Figure 11.6). The cross-regional pollution history, therefore, allows an assessment of:

- how pollution has changed throughout the 19th and 20th centuries;
- details air quality trends prior to the introduction of the Clean Air Act (1956); and
- effects of the Clean Air Act and subsequent, increasingly stringent, air quality legislations on pollution deposition.

Figure 11.7 presents the monitored post-1960 sulphur dioxide data alongside the cross-regional S flux profiles. Reductions in S post-1960 observed in the DDP and DKC cores mirror the declining measured SO_2 levels. Further, post-1980, reductions are also paralleled by DDP, DKC and WH. These closely paralleled trends between the regional S profile and measured SO_2 levels demonstrate the overall reduction in S experienced throughout the LMR, reinforcing the reliability of urban ponds as air pollution archives. The local, site specific, post-1980 S increase identified in the OG core, potentially derived from John Lennon International Airport, is not reflected in the historically monitored SO_2 data, highlighting spatial variations in S deposition revealed by the cross-regional signal.

Black smoke and SO_2 are pollutants associated with the combustion of coal and oil. The observed declining trends in these pollutant characteristics may, therefore, potentially reflect the reduction of both domestic and industrial coal combustion, initially brought about by the introduction of the Clean Air Act (1956). However, the monitored data does not represent the various industrial emissions experienced in the LMR. The cross-regional pollution signal demonstrates a wider range of inorganic air quality characteristics. For example, various trace metals, SCPs, magnetic particulates and particle size variations with the further potential of revealing trends in persistent organic pollutants.

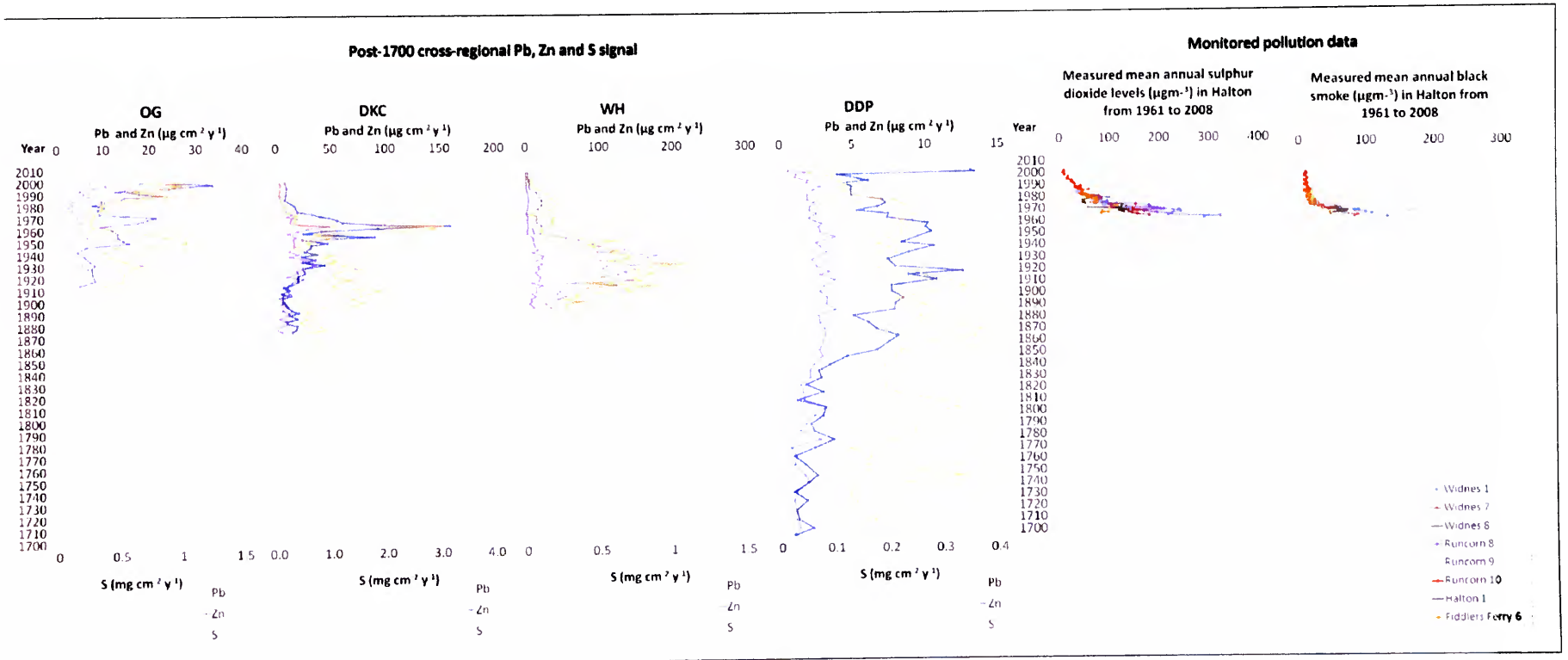

Figure 11.6: Post-1700 cross-regional Pb, Zn and S flux profiles obtained from urban ponds DDP, WH, DKC and OG, presented alongside available historical air pollution data for Halton: monitored black smoke and sulphur dioxide concentrations measured post-1960 [produced from the UK National Air Quality Archives (DEFRA) http://airquality.co.uk/smsites.php].

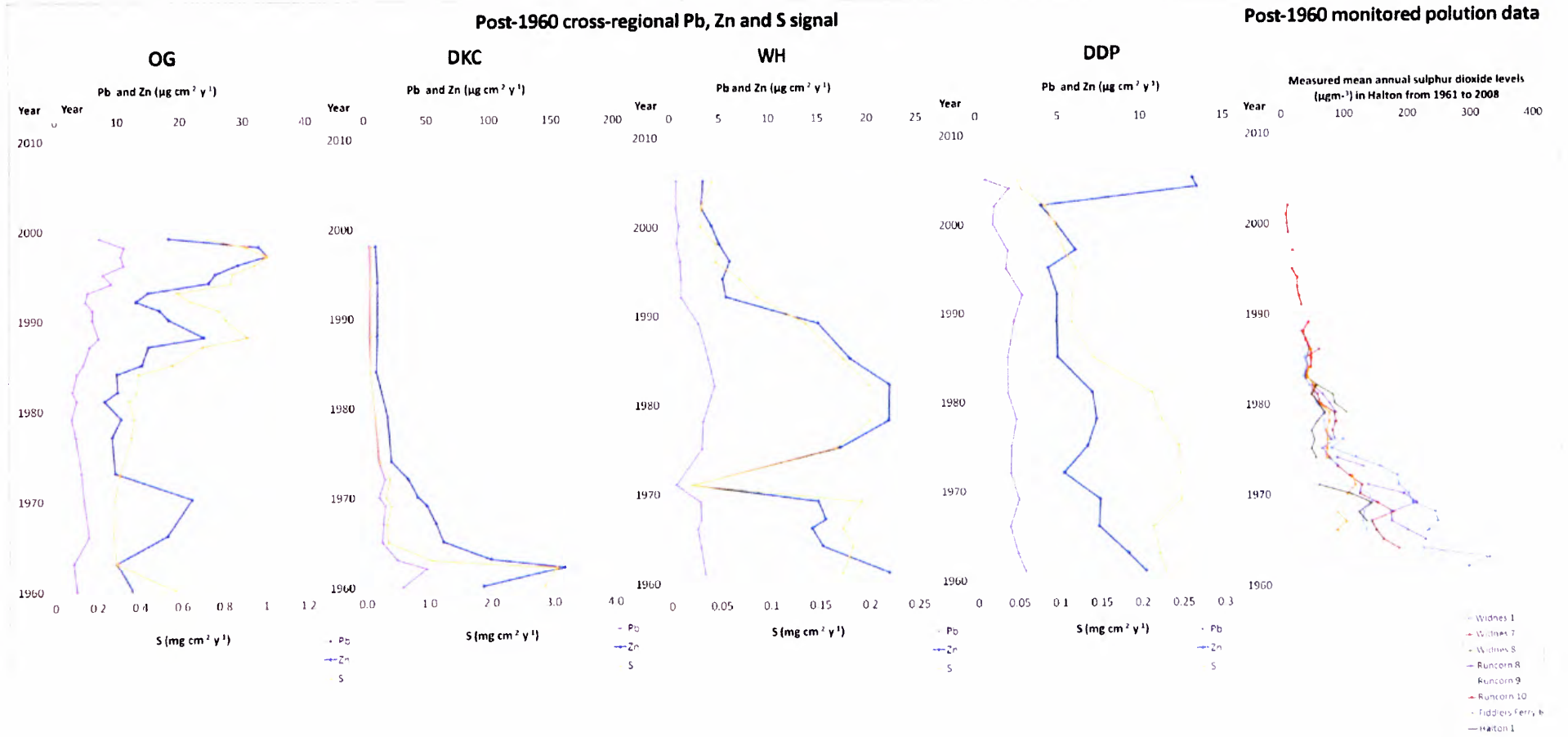

Figure 11.7: Post-1960 cross-regional Pb, Zn and S flux profiles obtained from OG, DKC, WH and DDP, presented alongside available post-1960 sulphur dioxide concentrations for Halton [produced from the UK National Air Quality Archives (DEFRA) http://airquality.co.uk/smsites.php].

11.5. Combination of the cross-regional signal with other sedimentary evidence in Merseyside

11.5.1. Estuarine sediment archives

Detailed and extended contamination histories have been reconstructed using sedimentary evidence, for example, from the Mersey Estuary. The Mersey Estuary is reported to be the most polluted in Europe [National Rivers Authority, 1995; Fox *et al.*, 1999] and its sediments have been used as archives of contamination. Harland *et al.*, [2000] provide a recent, 25-year history of trace metal concentrations in the Mersey Estuary from 1974-1998. Values obtained from a post-1974 sampling strategy of sediment samples from the estuary are published. The research is particularly focused on post-1974 reductions in mercury that have been discharged into the estuary as a by-product of chlor-alkali production, most notably from the mercury cell electrolysis plant at Weston, since 1896. Other trace metal concentrations are presented (Figure 11.8), including Pb, Zn, and Cu, which demonstrate overall post-1974 reductions. This, generally, shows good agreement with the cross-regional urban pond pollution signal, which exhibits a steady decline in trace metals post-1970 in the DDP, DKC and WH cores. However, while this is only a general comparison between two different types of data, i.e. between the urban pond flux profiles and concentration data obtained from annually collected estuarine surface sediments, it is nevertheless an important one.

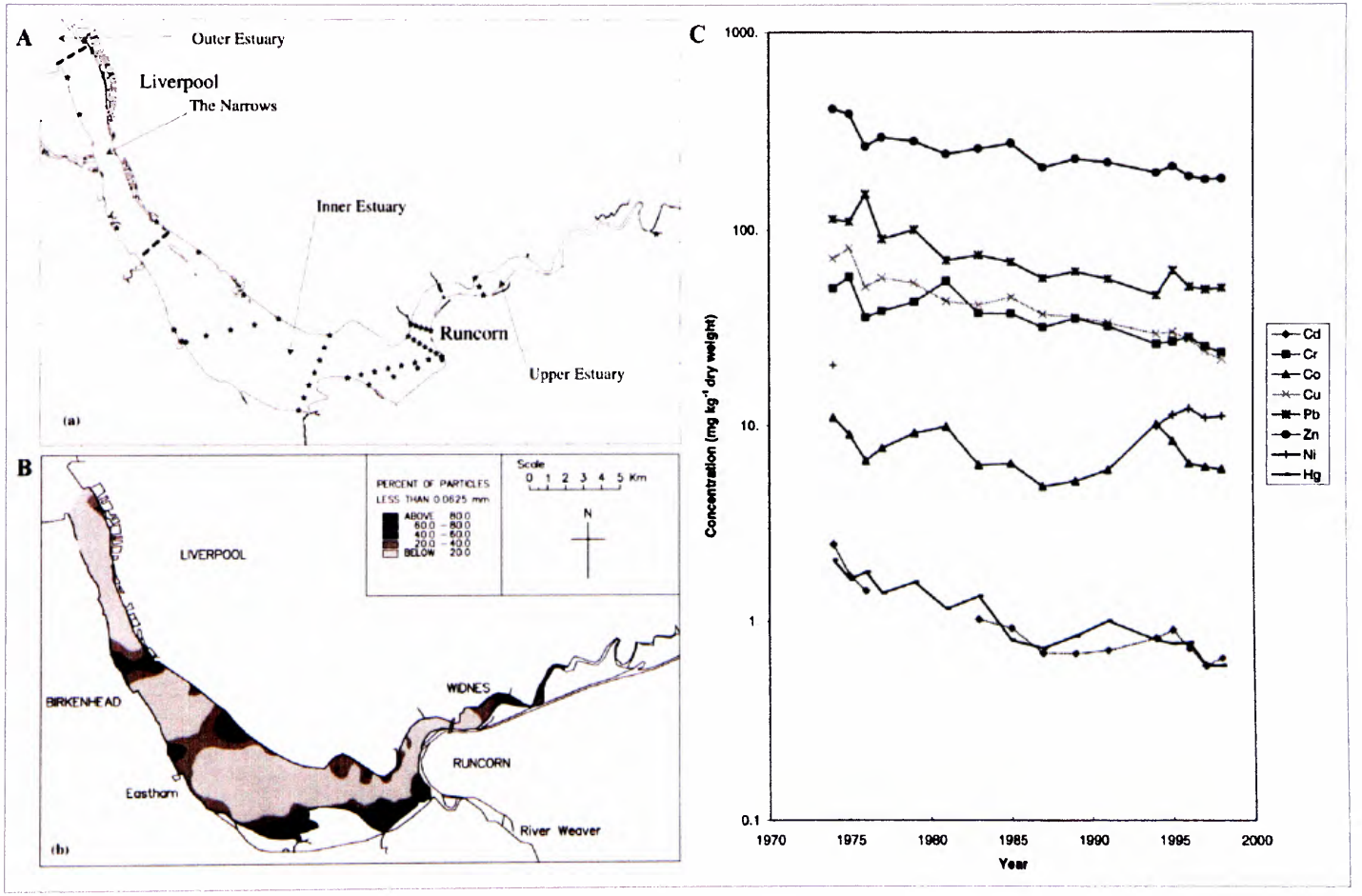

Figure 11.8: The distribution of trace metals in the sediments of the Mersey Estuary from 1974-1998 reported by Harland *et al.*, [2000]. A: map of the Mersey Estuary showing directive monitoring stations; B: map of the Mersey estuary showing distribution of silt sized particles (<63 μm); and C: mean metal concentrations (linear scale) for the Mersey Estuary normalised to 40% silt content (1974-1998) [Harland *et al.*, 2000].

Fox *et al.*, [1999] have published a continuous history of metal contamination in the Mersey Estuary using saltmarsh sediment cores, which date to 1860 (Figure 11.9). Saltmarsh cores retrieved from Widnes Warth and Ince Marsh provide 120- and 50-year archives of metal contamination, respectively. Uniform sediment accretion in the Widnes Warth core, effectively eliminates the influence of sediment accumulation on the trace metal concentrations, allowing a more reliable comparison of metal accumulation between this site and the cross-regional urban pond pollution signal; unlike the Ince core, which exhibits a shift in sediment accumulation rates post-1968.

The Widnes Warth As, Cr, Cu, Pb, Zn concentration profiles (Figure 11.9) exhibit a pronounced post-1900 metal enhancement, following relatively lower concentrations from 1880-1900 [Fox *et al.*, 1999]. This is mirrored in the regional urban pond profile that demonstrates distinct metal and magnetic increases from the start of the 20th century. Maximum peaks between 1920 to 1960 in the Widnes Warth core, and subsequent steady post-1960 reductions reflect trends observed in the DDP, DKC and WH flux profiles (Figure 11.10). However, the saltmarsh sediment records incorporate both an atmospheric contamination history as well as industrial effluent discharges, which have been released directly into the River Mersey.

Other limitations in using saltmarsh sediments as archives of air pollution include the redistribution of sediments observed in the Mersey Estuary [Harland *et al.*, 2000]; and problems with radioisotope dating in saltmarsh sediments due to releases of isotopes to water from nuclear activities, including Sellafield (nuclear power station) in Cumbria, which interrupts the natural ^{210}Pb record and the well documented artificial ^{137}Cs fallout from weapons testing. Despite this, the saltmarsh 'geochronologies' provide further evidence of industrial impacts on urban sedimentary archives, mirrored in the pollution records from the urban ponds. The use of urban pond sediments in reconstructing a cross-regional pollution history provides long-term (post-1520), temporal patterns in the deposition of atmospheric-derived particulates (Figure 11.10).

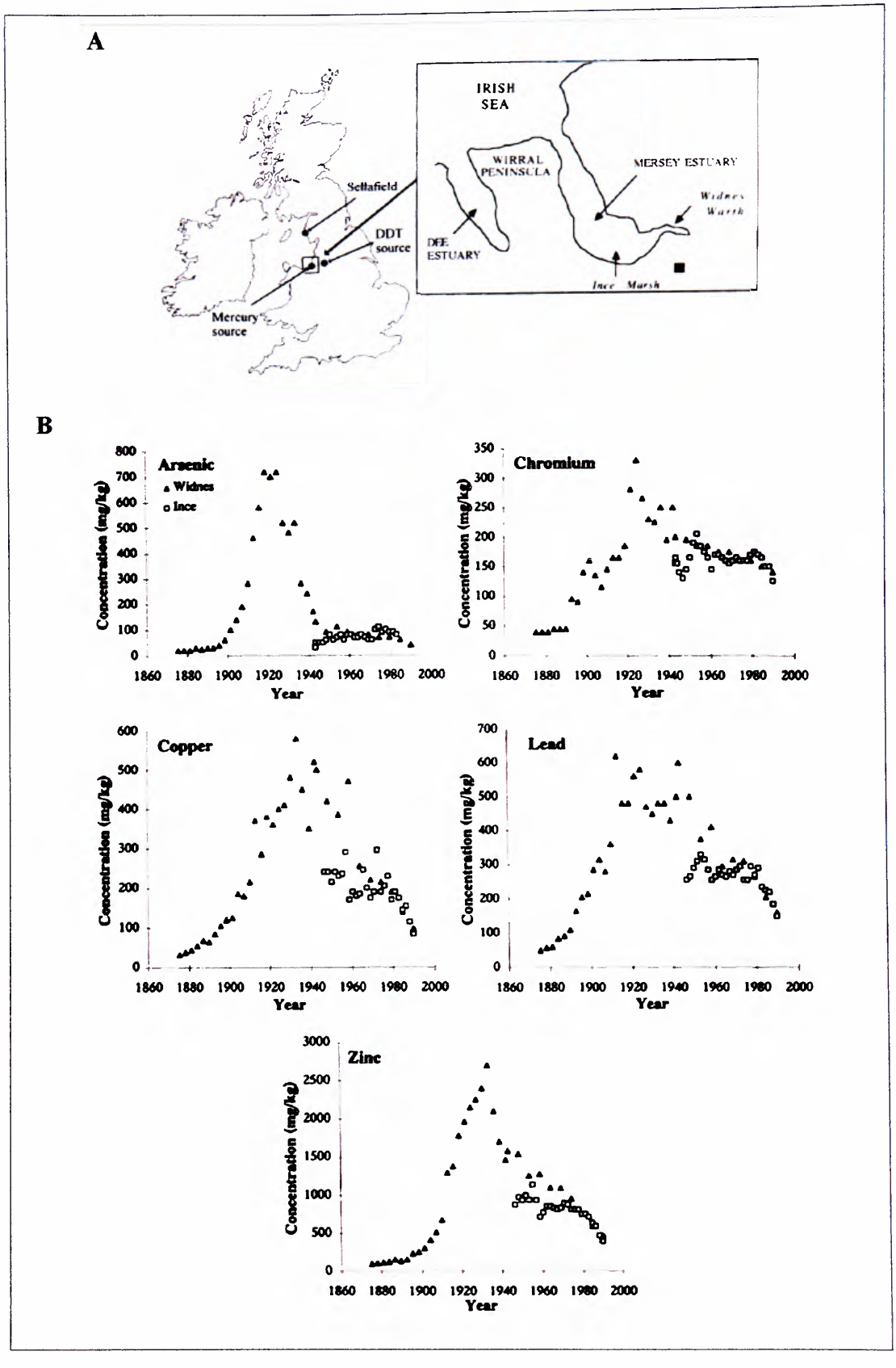

Figure 11.9: Historical contamination profiles in the Mersey Estuary reported by Fox *et al.*, 1999. A: sampling sites in the Mersey Estuary and sources of key pollutants; and B: stable metal concentrations in dated core Warth and Ince Marsh; [Fox *et al.*, 1999].

Figure 11.10: Historical Pb flux profiles from DDP post-1520 (A); and post-1880 Pb flux trends recorded in DDP (B), WH (C), DKC (D) and OG (E) ponds.

11.5.2. Sediment records from Speke Hall Lake

High-resolution air pollution histories extending to the 17th century retrieved from Speke Hall Lake (SJ 341960, 382789) (Plate 11.1) initially highlighted the potential for urban ponds as suitable sedimentary archives of particulate deposition [Worsley *et al.*, 2006]. Located within the urban region of Speke (<2 km south of Liverpool), Speke Hall Lake (SHL) (Figure 11.11) is situated <1800 m north-west of OG, within the Speke Hall estate grounds. Larger than DKC, DDP, WH and OG, SHL (3094 m^2 (0.309 ha), 3 m maximum water depth) is <800 m north-west of the runway at John Lennon International Airport, which itself was originally built in part of the Speke Hall grounds. The lake catchment is defined by the steep-sided lake margins; therefore, the lake has a high lake-to-catchment

ratio of 1:1.927. The surrounding urban area includes an adjacent light industrial estate (SJ 342571, 383201), nearby industries at Halewood including chemicals and pharmaceuticals (<1800 m; SJ 342994, 384134), and motorcar production (<2700 m; SJ 344532, 3840) and a housing estate at Speke (<1400 m; SJ 344406, 383218).

The Speke Hall Estate, constructed pre-17th century, is managed by the National Trust and has a robust documented history. The provenance of SHL, historically known as 'Higher Damme' [Nicholson, 1983], can be dated to the 18th century, as the lake appears on Addison's 1781 map (the first known map of Speke Hall) and, further back, to the late 17th century from estate records [Nicholson, 1983] detailing the site management history. The lake may have originally been a marl pit, with records of the exploitation of marl in the area, to fertilise agricultural fields, extending back to 1329 [Lumby, 1939]. The earliest records of the lake detail the provision of fish stock (1694), construction of fishing posts and work carried out on the sluice at the head of the lake (1713) [Nicholson, 1983]. The estate records reveal that the ''Higher Damme' (Speke Hall Lake) has not been dredged or desilted, therefore, despite the construction of fishing posts on the lake margins, the sediment away from the margins is undisturbed.

Plate 11.1: Speke Hall Lake (SJ 341960, 382789) 03/12/2004, facing north east.

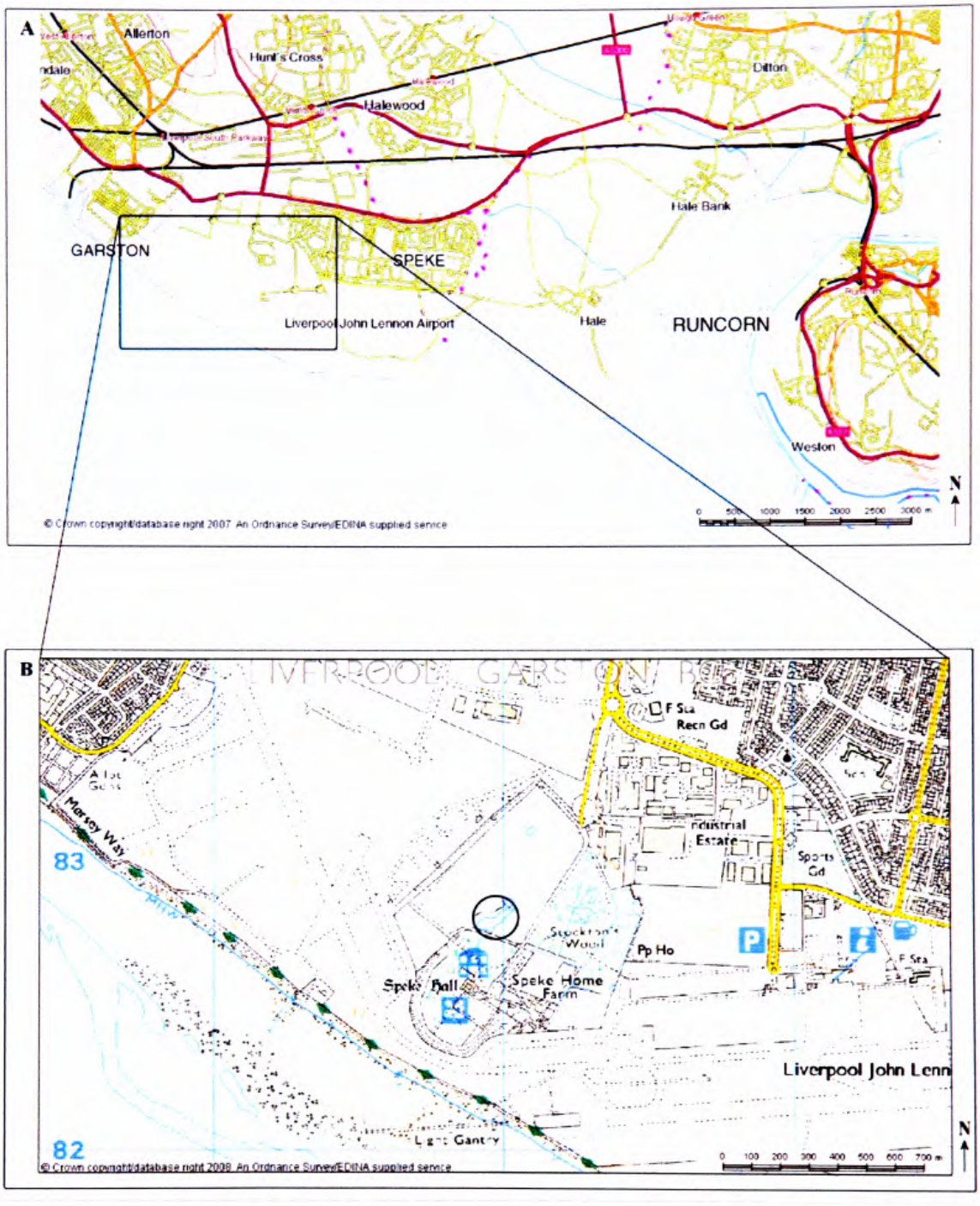

Figure 11.11: Location of Speke Hall Lake, south Merseyside 1: 146298 (A) and 1: 11574 (B). Reproduced from the 2007 Ordnance Survey 1:50 000 Raster 1:146298 (A) and 2008 1:25 000 Raster 1:11574 (B) maps with the permission of Ordnance Survey on behalf of The Controller of Her Majesty's Stationery Office © Crown Copyright Edge Hill University, Ormskirk, Lancashire licence number: ED100020392.

The well documented history of the site allows confidence in the prevalence of the site and supports the ^{210}Pb chronology obtained from the lake, which using radioisotope dating methods, extends to 1881 (Appendix D3). Polynomial extrapolation of the ^{210}Pb data extends the chronological scale to ~ 1500 for the basal sediment layer (32 cm), under which there is an artificial clay lining, and an underlying sand layer. Figure 11.12 demonstrates how the S profile obtained from SHL contributes to the spatial cross-regional pollution signal for the LMR.

SHL provides a long-term, post-1700 air pollution history for the west of the LMR, which, when assessed alongside post-1700 data from DDP, allows a long-term spatial assessment of pollution deposition from east to west across the region. Pb, S (Figure 11.13), Zn and Cu profiles (Figure 11.14) from SHL and DDP are presented. SHL exhibits trends corresponding to the main phases identified in the cross-regional signal:

- Ri ~pre-1830: pre-industrial intensification:

Relatively low pre-1840 S, Zn and Cu concentrations in the SHL core, corresponds to low pre-1830 trace metal flux and concentration values identified in DDP. These relatively low trace metal concentrations east to west of the LMR, reflect low-scale industrial activity in the LMR area at this time, before the Industrial Revolution. SHL exhibits an earlier steady increase in Pb ~post-1755, with a clear enhancement post-1816. Relatively low pre-1830 Pb values are observed in the DDP pond, with a fluctuating pre-1800 signal. This may, therefore, highlight an early source of Pb impacting the west of the region, potentially, from localised industrial activity in Liverpool, which was a developing urban centre at this time.

- Rii 1830-1900: the Industrial Revolution:

Distinct post-1841 trace metal enhancement in the SHL core and corresponding post-1832 enhancement in the DDP profiles, provide further evidence of pollution enhancement in the LMR at this time due to rapid industrial growth. Close parallels between the S profiles, indicative of coal combustion and, potentially, Leblanc chemical production are observed. Distinct S enhancement from ~1841-87, with maximum concentration at ~1887 in the SH core, mirrors ~1832-1880 S elevation and maximum S concentration at ~1873 at DDP. Sustained high Pb concentrations in the SHL core from ~1816 to 1887, further supports this Industrial Revolution signal, mirroring Pb enhancement in the east of the borough (DDP) from ~1832 to 1889.

Cu increases across the LMR occur at ~1830, revealed by distinct increases ~post-1829 at SHL, which closely parallels post-1832 Cu increases in the DDP core. High Cu values are sustained in the west of the region until 1887, and continue into the 20th century in the east of the LMR. Similar concentrations of Zn are exhibited in this phase by DDP and SHL; however, SHL demonstrates a relatively small~1829 peak, compared to a relatively more prominent Zn enhancement from ~1832-1867 at DDP. This may highlight a source of Zn, possibly from coal combustion, impacting the east of the LMR during this period of rapid industrial development.

- Riii 1900-1950: 20th century industrial expansion and population increases:

DDP and SHL demonstrate distinct Zn increases post-1914 and post-1917, respectively, with relatively higher post-1900 Zn concentrations exhibited at SHL. This indicates an enhancement of Zn across the region throughout the first half of the 20th century, particularly prominent in the west of the LMR, which may reflect the expanding chemical industry, particularly in Widnes, and shift in industrial production at this time. A potential source of Zn to the environment may be from the manufacturing of car paint, containing Zn additives, which occurred from 1910-60 in the area [Fox *et al.*, 1999].

Cu displays an overall reduction in the SHL core post-1900, highlighting a steady decrease in Cu emitted in the west of the LMR. This may reflect the closure of Leblanc chemical works, and associated industries, such as copper works which existed in Widnes. Cu trends in the DDP profiles, however, demonstrate an increase from 1904 to 1918, which may reflect a localised industrial process, operating at capacity during WWI. S and Pb increases are experienced throughout the region post-1900, marking industrial and urban expansion, wartime demands on industry and domestic coal combustion.

- Riv 1950 to 1980: late 20th century urban expansion

Zn trends continue to increase post-1950, until maximum concentrations are reached at 1961 in the SH core, reflected by high Zn levels during the 1950s and 60s at DDP. Zn subsequently decreases in both cores, indicating a reduction in Zn emissions in the LMR, reflecting air quality legislations and subsequent improvement of air quality. This is further supported by post-1981 S flux declines in the DDP, DKC and WH cores, which may reflect stringent air quality legislations that has reduced S in fuels and reduced domestic combustion of coal. Cu exhibits an overall decline throughout the LMR during the latter half of the 20th century, with notable reductions post-1953 in the SHL core and post-1961

in DDP. Pb concentrations exhibit an overall decline post-1950 in the SHL core, however, a post-1950 reduction is less prominent than the observed Zn, Cu and S declines. This recent (post-1950) Pb signal may reflect the rapid rise in road travel, experienced nationwide, and the steady Pb decline may, therefore, reflect the gradual 'phasing out' of Pb in fuel and the introduction of unleaded petrol.

- Rv post-1980: stringent air quality legislations and increased road and air travel:

Overall, reductions in Pb, S Zn and Cu are exhibited at SHL, mirroring trends observed at DDP, WH and DKC, which are likely to reflect stringent air quality legislations.

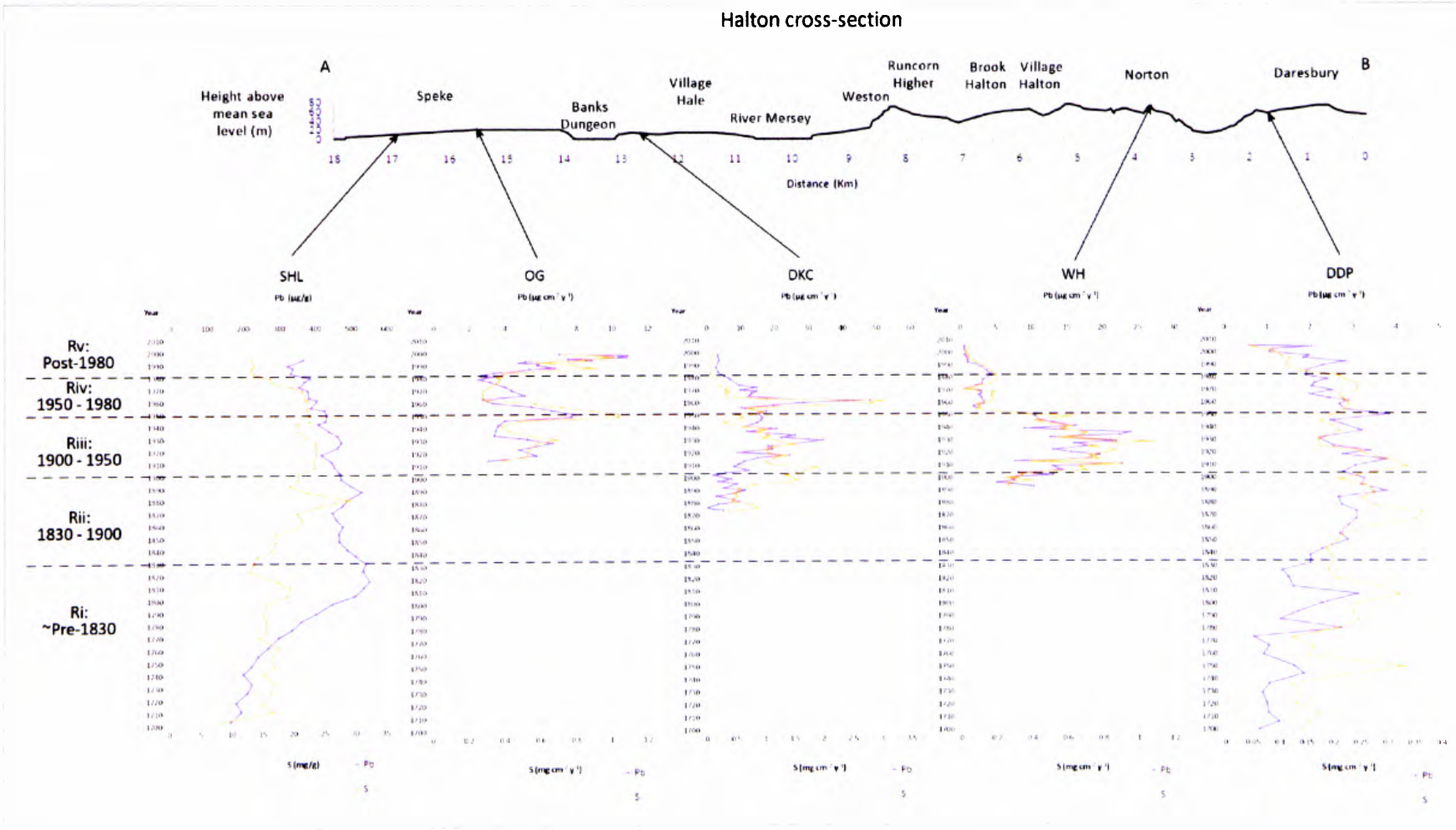

Figure 11.12: Cross-regional S concentrations and flux signals obtained from SHL, OG, DKC, WH and DDP, with cross-section (A: SJ 342100, 382000 to B: SJ 359000, 382000) across the LMR. Superimposed phases Ri to Rv highlight down-core divisions of the cross-regional proxy pollution signal.

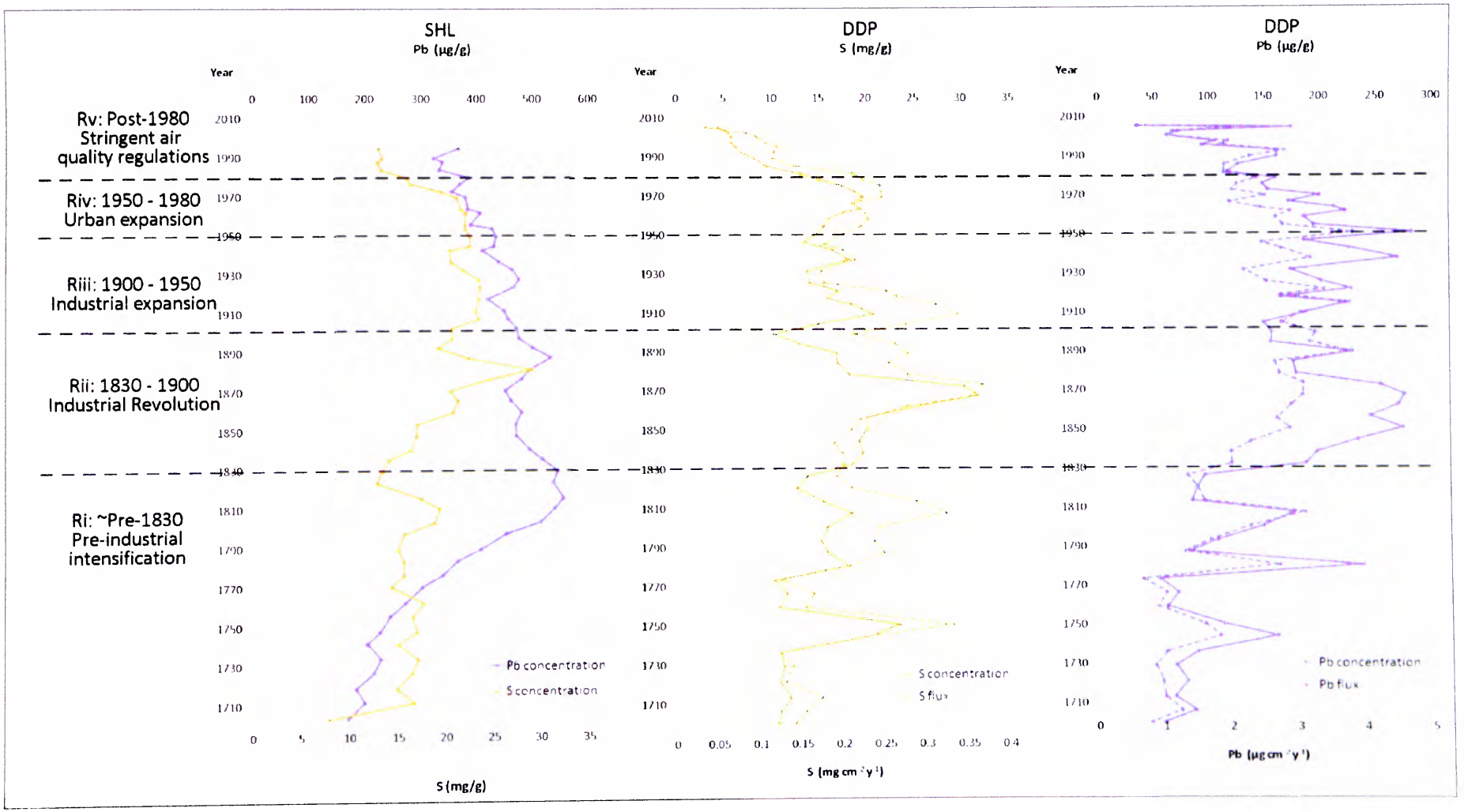

Figure 11.13: Post-1700 S and Pb linear concentration profiles from SHL and DDP, with flux data from DDP and superimposed regional phases Ri to Rv.

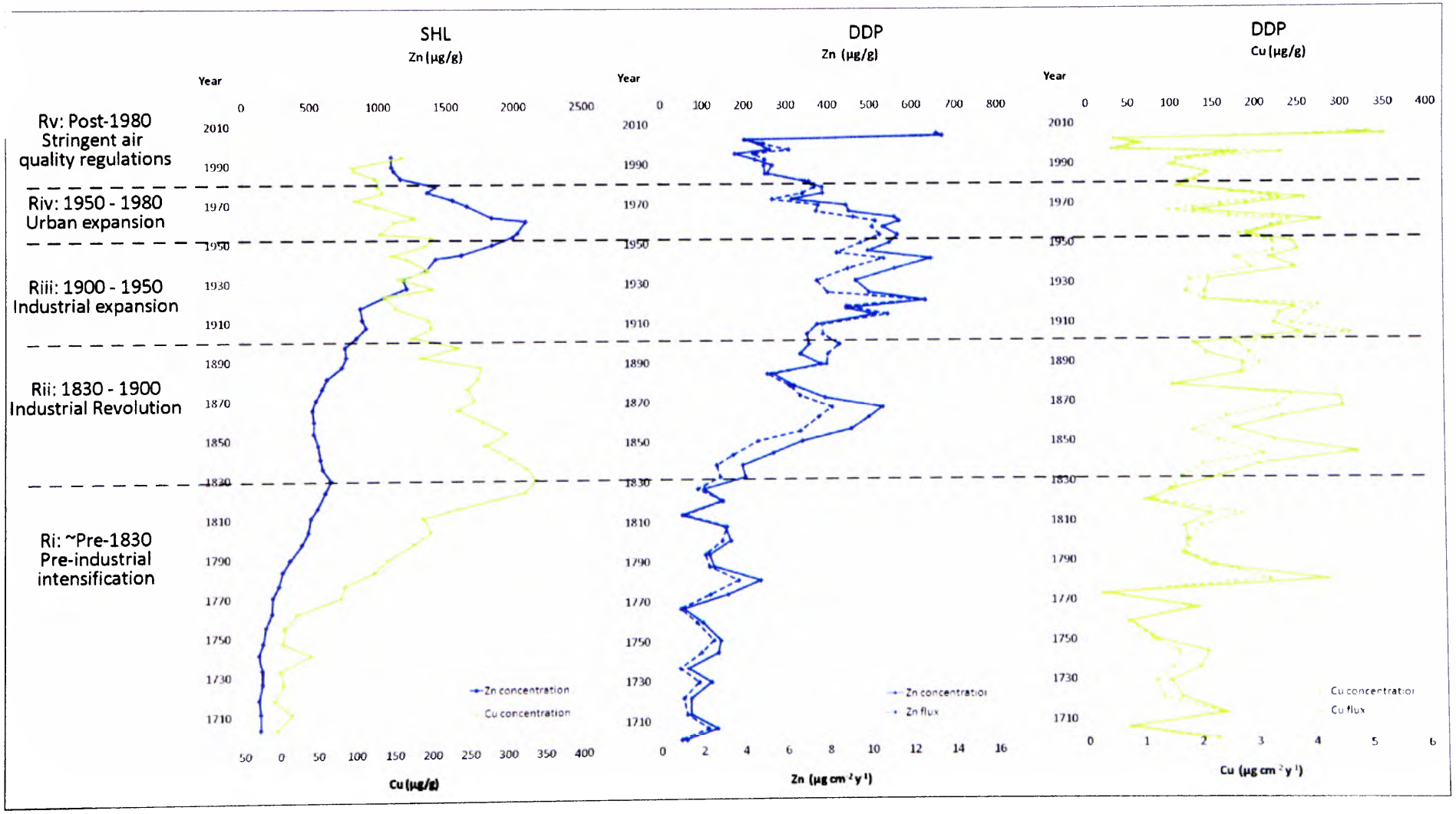

Figure 11.14: Post-1700 Zn and Cu linear concentration profiles from SHL and DDP, with flux data from DDP and superimposed regional phases Ri to Rv.

Overall, similar trends in temporal pollution deposition throughout the LMR are observed via common features identified between SHL and DDP. However, there are local, spatial variations in the post-1950 cross-regional profile, particularly between the west and east of the region; whereby, DKC and OG are, potentially, impacted by urban expansion at Halewood during the mid-20th century. The post-1870 air pollution history from SHL compliments the high-resolution local signals obtained from DKC and OG, allowing a more detailed understanding of pollution deposition throughout the 20th century in the north-west of the LMR (Figure 11.15).

Pb and S concentration peaks in the SHL core at 1881-87 represents the end of a period of intensive industrial activity in the LMR during the late 19th century. Zn, however, demonstrates relatively low pre-1900 levels, until enhancement from ~1916 to 1918, corresponding with Pb increases at this time, observed in the three pond sites, reflecting wartime demands on industries. The continual increase in Pb, S and Zn throughout the 1920s and 30s observed in the SHL, OG and DKC cores, coincide with a period of industrial specialisation in Widnes, with the formation of ICI (1926), and growth of organic chemicals, combined with population increases and, therefore, increased domestic coal combustion.

SHL, DKC and OG exhibit simultaneous increases in pollution post-1944 which may, initially, reflect wartime demands on the already established chemical industry in Widnes and Runcorn, and subsequent industrial development post-1950 at Halewood. Pb increases are observed into the 1960s, with distinct peaks at SH (1966), DKC (1962) and OG (1961). S also demonstrates high mid-20th century values, from 1944 to 1969. Zn demonstrates sustained high values into the early 1970s in the west of the LMR. This modern source of Zn may be explained by the use of Zn post-1910 as a rust inhibitor in car paints [Fox *et al.*, 1999], likely to have been manufactured in Widnes and Halewood and the galvanisation of car bodies [Barakat *et al.*, 2006], possibly at the Halewood car production site. The SHL appears to mirror the post-1950, urban expansion pollution signal from established industries and residential development at Halewood, highlighting an increase in trace metals to the environment post-1950 in the west of the LMR.

Overall, post-1980 trace metal declines in the SHL core mirror the DKC trace metal profiles, with a slight increase in Pb and S observed post-1990. The local pollution signal for OG, which demonstrates post-1980 increases, potentially, due to an aviation pollution signal, is not identified in the sediments of SHL, despite being located <800 m of the

runway at John Lennon International Airport runway. This may be explained by the high-resolution of post-1980 change detailed by the OG pollution record, compared to the low-resolution of recent change observed in the SHL profile[†].

[†] Low resolution post-1980 data in the SHL record, which may show an increase when converted to flux data.

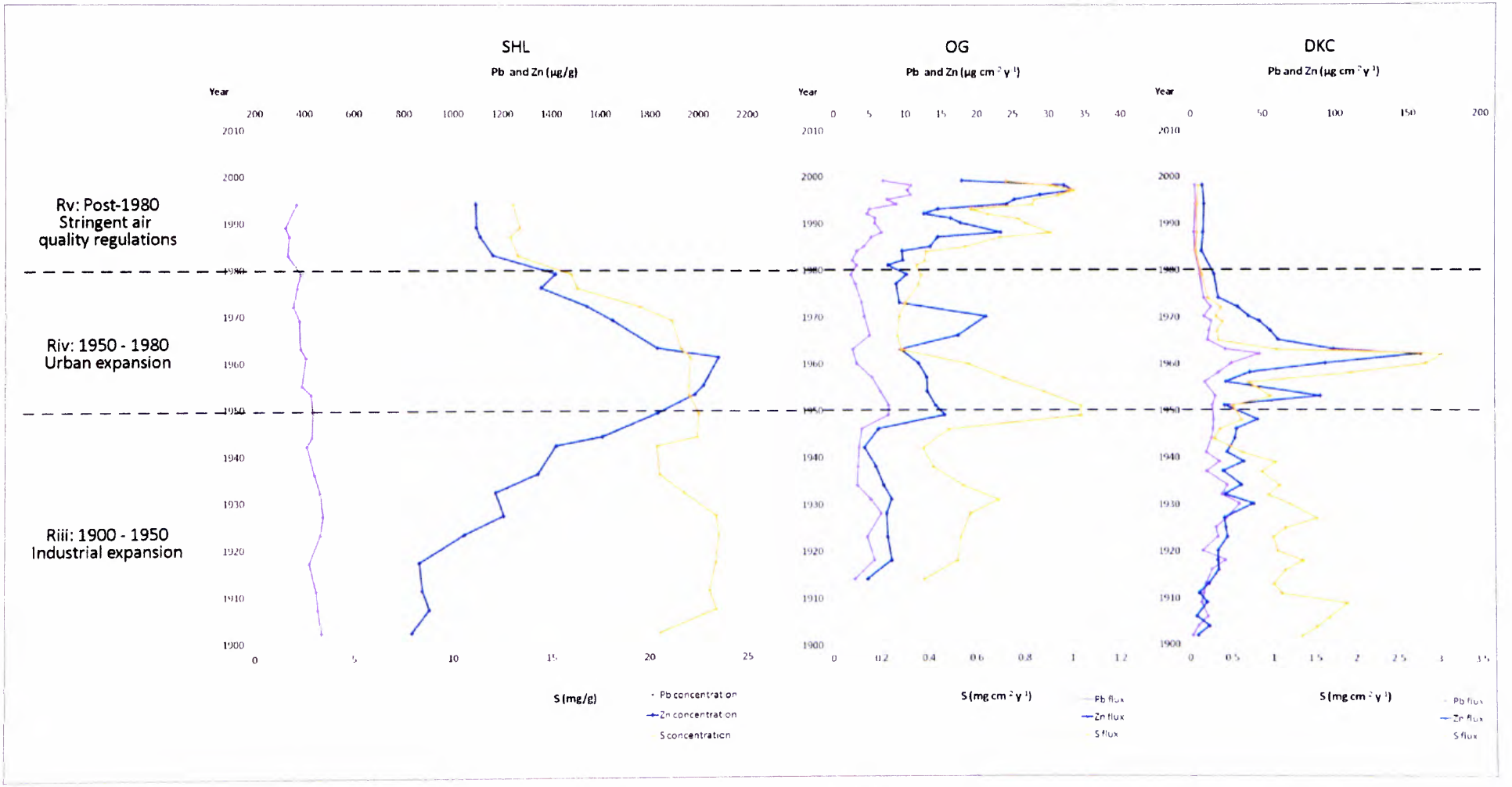

Figure 11.16: Post-1900 S, Pb and Zn signal for the north-west of the LMR via SHL, DKC and OG ponds. Linear concentration profiles are presented alongside flux trends, with superimposed regional phases Riii to Rv.

11.6. Chapter summary

A cross-regional air pollution signal for the LMR has been recognised and interpreted, which demonstrates ~300 year history of pollution deposition spatially spanning from the north-west (SHL), to the south-east of the region (DDP). The high-resolution urban sediment records allow a detailed pre-1900 local account of pollution characteristics, which span pre-industrial intensification and encompass the Industrial Revolution, therefore, allowing an assessment of pollution impacts during the establishment and expansion of industry in the LMR.

A detailed temporal and spatial air pollution history for the LMR throughout the 20th century is comprised using sediment records from DDP, WH, DKC, OG and SHL. The complexity of the post-1900 pollution signal reflects urban expansion and shifts in industrial process and chemical production methods that occurred in Halton during the 20th century. DDP, WH, DKC and OG reveal high-resolution post-1950 patterns of pollution deposition in the LMR, which demonstrates the impact of local industrial processes, urban sprawl, road and air travel.

The combination of the cross-regional pollution signal derived from the small urban ponds and lakes in the LMR, with contamination records from the Mersey Estuary further explores the long-term, large-scale cross-regional air pollution record compiled from sedimentary evidence. Furthermore, the importance of small manmade ponds to produce long-term pollution records within an urban environment is highlighted via comparison of these sedimentary data with available post-1960 pollution data for Halton.

12. CHAPTER TWELVE: CONCLUSIONS, IMPLICATIONS AND FUTURE WORK

12.1. Chapter overview

This chapter concludes the main findings of the thesis and details implications of the research, with suggestions for future work.

12.2. Introduction

Local air pollution records have been obtained from small (<1 ha), manmade ponds throughout the lower Mersey region (LMR). Sediment records from Oglet (OG), Dogs Kennel Clump (DKC), in the north-west LMR, and Windmill Hill (WH) and Daresbury Delph (DDP) ponds, in the south-east LMR, have allowed a reconstruction of changing air pollution characteristics spanning pre-intensification of industry in the area (i.e., pre-1800) to present day. Also, by combining these *local* air pollution signals, spatial, intra-urban variations in the historical deposition of particulate pollution have been assessed and a cross-regional air pollution signal has been identified.

By extending the air pollution record back beyond monitored pollution data, this work highlights the importance of urban ponds as proxy air pollution archives, providing an alternative method for long-term air pollution monitoring. Also, the changing characteristics of urban PM over time throughout the LMR, revealed by the cross-regional air pollution signal, has epidemiological benefits for understanding retrospective pollution exposure assessments for the local population. It is recommended that the historical and contemporary cross-regional signal for the LMR is further explored via additional environmental analyses of the urban pond stratigraphies and contemporary urban sediments.

12.3. Main conclusions

Based on the thesis objectives (Chapter 1) four main conclusions are gathered:

(i) Reliable records of air pollution deposition can be reconstructed from the sediments of small manmade urban ponds

Palaeolimnological studies have largely focused on using sediments from natural, rural lakes to infer environmental change; however, anthropogenic, urban ponds are increasingly being recognised as important sedimentary archives. Despite being *viewed* as having inappropriate conditions for the uniform accumulation of sediment, due to

possible fluctuating water tables, urban development within the catchment and human management (de-silting), this work shows urban ponds *can* produce intact, reliable sediment sequences of relatively high sediment accumulation. Not all urban ponds are suitable for providing long-term (>50 years) sedimentary records, however, with careful selection of pond sites via inspection of documentary evidence, historical maps and discussions with land managers, suitable ponds can be identified (Chapter 4).

Sediment records obtained from DDP, WH, DKC and OG ponds throughout the LMR demonstrate that small urban ponds can produce reliable, high-resolution, intact sedimentary evidence of air pollution deposition. Magnetic analyses (Chapter 6) and achievement of isotope chronologies (Chapter 5) allow confidence in the sediment sequence captured at each site. The robust nature of sediment records obtained from urban ponds is further demonstrated by intra-site core correlation of magnetic features within the five cores collected from the DDP basins. This highlights the reproducibility and, therefore, reliability of sediment records from urban ponds.

As urban ponds typically have very small catchments (and high lake-to-catchment ratios) the primary source of inorganic material received by the ponds is atmospherically-derived. Due to their location within the urban landscape, these ponds receive a complexity of urban particulates from surrounding industrial, domestic, vehicular and aviation sources. Enrichment factors, statistical relationships and elimination of post-depositional sediment changes reveal a dominating atmospheric-derived signal recorded in the sediments of these urban ponds, opposed to a natural/catchment signal (Chapter 9).

The anthropogenic contribution to the sediment record has been further explored using the DDP stratigraphy, which extends to pre-1800. Normalisation of pre-industrial intensification (i.e. pre-1800) trace metal values has allowed anthropogenic inputs to be separated from natural/background contributions. Furthermore, statistically significant relationships identified between SCPs, trace metals and magnetic properties further signifies the suitability of trace metals and magnetic characteristics as particulate pollution proxies and highlights a lack of trace metal mobility within the sediment column. The suitability of urban ponds as reliable archives of atmospheric pollution deposition is confirmed in this work (Chapter 9).

(ii) Urban ponds are important archives of long-term, *local* air pollution

The high-resolution sediment records captured by DDP, WH, DKC and OG demonstrate how urban ponds can produce localised air pollution histories, specific to their urban environments. DDP exhibits a high-resolution post-1700 history, revealing changing pollution characteristics spanning from times of pre-industrial intensification, encompassing the Industrial Revolution and 20th century. WH, DKC and OG exhibit high-resolution archives of pollution deposition post-1900 (Chapter 5).

These small urban ponds are highly sensitive to changes within the urban landscape, demonstrated by variations between the air pollution records from each site reflecting nearby industrial and urban activity. This makes urban ponds very important archives of air pollution experienced within the urban environment. They vary from *regional/background* air pollution records derived from rural lakes in remote locations (Chapter 10) as are site specific, reflecting the unique urban history of the LMR.

For example, pollution enhancement observed in the north-west LMR, at DKC and OG post-1950, potentially due to industrial development at Halewood during the 1950s and 1960s, whereas proxy pollution levels decline post-1950 in the south-east LMR, observed at DDP and WH, possibly reflecting the closure of tanneries near to WH (~<2 km) and shift to residential and light industrial (e.g. warehouse) urban development in Runcorn and Widnes post-1950. Also impacts from road and air travel pollution vary across the LMR, with a potential aviation pollution signal demonstrated at OG post-1980 due to close proximity to runway (<300 m) at John Lennon International Airport and vehicular signature highlighted post-1978 at DDP coinciding with construction of adjacent (~<120 m) roadways.

(iii) The cross-regional air pollution signal demonstrates post-1700 air pollution deposition across the LMR

Via the combination of local air pollution histories from DDP, WH, DKC, OG and SHL, a cross-regional air pollution signal has been reconstructed revealing spatial intra-urban variations of particulate pollution deposition within the LMR (Chapter 11). Five main cross-regional phases are identified:

a) Ri ~pre-1830: relatively low proxy pollution values highlight a time of low scale industrial activity in the LMR.

b) Rii ~1830 to 1900: DDP and SHL demonstrate an initial increase in proxy pollution values ~post-1830 and ~post-1840, respectively, marking the establishment and expansion of early industries in Runcorn. ~Post-1850 increases reflect the establishment of the early chemical (Leblanc) works in Widnes and boom in chemical trade during the 19th century in the LMR. The corresponding increases at SHL and DDP signify a time of pollution increases experienced in the LMR.

c) Riii 1900 to 1950: further pollution enhancement at SHL and DDP post-1900 is reflected at OG, DKC and WH, highlighting a cross-regional feature observed throughout the LMR. Gradually increasing pollution trends throughout the first half of the 20th century reflect a period of urban expansion in Runcorn and Widnes, with the diversification of the chemical industry due to modern chemical production as well as urban expansion, population increases and increased energy demands.

d) Riv 1950 to 1980: intra-urban variations in the cross-regional signal are observed post-1950. Closure of nearby tanneries, the introduction of the Clean Air Act (1956) and shifts from industrial expansion to residential development in Runcorn may explain pollution declines observed in the south-east LMR (at WH and DDP). However, DKC and OG reveal increased pollution deposition in the north-west LMR post-1950 into the 1960s, which may be explained by industrial developments in Halewood which occurred at this time.

e) Rv post-1980: DDP, WH and DKC exhibit trace metal reductions post-1980, which reflects increasingly stringent air quality controls, due to the 'phasing out' of trace metals in fuels and industrial processes. However, prominent trace metal increases are observed post-1980 at OG. This indicates a very localised pollution signal which, due to the close proximity (<300 m) of OG to the runway at John Lennon International Airport, may be derived from aviation activity which has increased considerably since the 1980s. Also, magnetic increases observed post-1978 at DDP, coincides with the construction of adjacent roadways, further highlighting the importance of road and air travel contributions to the cross-regional air pollution signal during this recent phase.

(iv) Historical changes in pollution characteristics across the LMR are revealed by the cross-regional air pollution signal

The cross-regional air pollution signal provides a detailed, high-resolution history of particulate pollution deposition that extends beyond monitored pollution data and the post-1960 black smoke and SO_2 concentrations which have nationally been recorded. Declining black smoke and SO_2 recorded in the LMR highlight an overall improvement in air quality, reflecting the introduction of the Clean Air Act in 1956, which reduced smoke emissions. The cross-regional air pollution records from urban ponds in the LMR not only extends our understanding of pollution trends beyond the 1960s, but also provides high-resolution historical and spatial patterns of proxy pollution characteristics via a range of trace metals, magnetic grains, SCPs and particulate sizes.

The early pollution signal (Phase Rii) is characterised by relatively high Pb and S values and a relatively coarse magnetic signature, reflecting early Leblanc chemical industrial activity in Runcorn and Widnes, which involved the heating of limestone and salts in Pb chambers to produce alkali, which also relied heavily on coal combustion. The 20th century cross-regional signal demonstrates an increased deposition of fine (~<1 μm) magnetic grains, increased trace metals and SCPs, highlighting a more complex urban air pollution signature. The replacement of Leblanc chemical production methods at the start of the 20th century, with modern technological processes (such as electrolysis) and subsequent diversification of chemical manufacture, may explain further trace metal elevations and the observed shift to a finer pollution signal post-1900 revealed by DDP (Riii). Also, higher Zn deposition in the 20th century highlights important modern sources of this trace metal, potentially from industrial processes (application of Zn in car paints). Also shifts in domestic fuel consumption from coal to electricity and gas post-Clean Air Acts (1956) may also influence pollution characteristics.

Increased petrol consumption and road travel is also possibly reflected in the cross-regional signal at DDP, which demonstrates a post-1980 pollution signature characteristic of fine magnetic grains. Reduced Pb observed post-1985 may reflect the introduction of unleaded petrol. An overall reduction in trace metals is observed post-1980, reflecting increasingly stringent air quality legislations, however, the potential aviation signal at OG highlights the importance of the airport as a source of trace metals and fine (~<1 μm) magnetic grains to the northwest LMR, with declining post-1980 Pb deposition rates observed with increased distance from the airport. Also OG and DKC

exhibit increased fine magnetic grains post-1980. Post-1980 pollution characteristics appear to be influenced by increasingly stringent air quality controls and increased road and air travel, highlighting a shift from industrial and urban expansion impacts.

12.4. Implications of the research

The local and cross-regional air pollution histories obtained from DDP, WH, DKC and OG strengthens the justification of using anthropogenic urban ponds as reliable archives of air pollution. Not only can long-term air pollution histories be reconstructed from urban ponds but, as they are so sensitive to change in the urban environment, several ponds can be investigated to infer cross-regional, spatial pollution deposition patterns. Although useful regional/background air pollution histories are produced from large, rural lakes; to extend back urban air pollution records to beyond monitored data, we have to investigate *urban* sedimentary archives and small manmade ponds are uniquely placed amongst the complex sources of pollution within the urban landscape.

Furthermore, although environmental analyses adopted in this work are widely applied to lake studies, this work highlights that urban ponds should be treated differently to rural lakes. Different pressures impact these ponds, such as heavy loadings of particulate pollution, and they have different lake-to-catchment systems. These local signals exhibit variations from the regional/background pollution records (e.g. SCPs) for Europe, due to the high sensitivity of these ponds and deposition of pollution particulates close to source. This work also further supports the use of magnetic properties and trace metals as pollution proxies.

The intra-urban variations in pollution deposition across the LMR revealed by the cross-regional air pollution history also highlights limitations in the way contemporary urban PM is monitored. Pollution monitoring stations or 'boxes' have measured useful temporal data across the UK since ~1990 as part of the Urban Air Quality Strategy; however, they are spatially limited, with usually one station assigned to an urban centre. Therefore, they do not identify spatial variations within a conurbation, and therefore, locations adjacent to roadways, industrial processes or airports may experience higher pollution loads, undetected by the monitoring boxes. This work also highlights inadequacies in using the monitored black smoke and SO_2 data when assessing long-term patterns of pollution. While S reductions observed in the cross-regional LMR signal reflect recorded SO_2 reductions, it is clear that other proxy

pollution measurements suggest changes in pollution type, such as a shift to fine particulate pollution, which is also detrimental to human health.

Although air quality is perceived to have improved since the indiscriminate releases of pollution to air during the Industrial Revolution and introduction of the Clean Air Acts, the cross-regional air pollution signal demonstrates that pollution reductions do not consistently decline throughout the LMR and although trace metals have declined at most sites, there is a shift to a finer pollution signal, likely to reflect increasing road and air travel. This has potential epidemiological implications. Long-term (life-time) exposures to air pollution are important, especially for diseases with long latency times such as cancer. Therefore, retrospective pollution exposure assessments are imperative when understanding links between the environment and health.

Due to the limited availability of historical pollution data, these novel air pollution archives in the LMR allow an understanding of how pollution characteristics have changed over time, relating to urban activities. Identifying health linkages with the environment is very complicated due to the various pathways of exposure to pollutants (i.e. from air, water, land) and the potential for synergic effects of mixtures of pollutants, as well as socio-economic factors, which also contribute to health (deprivation life style, diet and exercise). This makes it very difficult to 'tease out' environmental burdens on health. However, this work provides an important piece of a very complex puzzle in better understanding retrospective air pollution exposures in the LMR.

This work demonstrates how urban sediment records provide high-resolution air pollution histories, revealing how human activities have changed the atmospheric chemistry during the 18^{th}, 19^{th} and 20^{th} centuries. This, combined with potential applications of proxy climatic indicators (e.g. chironomids) to these urban archives, may also have potential implications for climate change modelling.

12.5. Recommendations for future work

In order to fully explore the atmospheric signal captured within the urban pond sediments, further characterisation of the sediment stratigraphies could be carried out, including SCP analyses of all cores and scanning electron microscopy, to identify morphological features of pollution particulates and further discriminate potential bacterial magnetite samples and fine pollution particulates. Analyses of different Pb

isotopes in the sediments may also reveal various anthropogenic Pb sources (industrial/vehicular/aviation). Further data analysis, such as, principle component analysis and unmixing models, may be applied to differentiate sediment (i.e. catchment/pollution) and atmospheric pollution sources (i.e. vehicular/industrial). Investigation of methods to differentiate different pollution sources ('fingerprinting') would provide useful information regarding the components that make up urban PM.

To further investigate the cross-regional air pollution signal in the LMR, mercury (Hg) trends may be explored. Hg deposition trends are of particular importance in Halton, as the only chlor alkali plant using mercury cell technology in the UK is located in Weston, Runcorn. This may also aid research by Hodgson [2005], who used historical estimates of mercury releases from Hg emitting sources to determine retrospective exposures of the pollutant to the Halton population. This work may, therefore, provide a continuous history of Hg deposition in the borough if further elemental analyses for example, inductively coupled plasma mass spectrometry (ICP-MS), which has a better detection of Hg in sediments than XRF, were applied [Boyle, 2001].

Also, analysis of the organic pollution component (e.g. persistent organic pollutants (POPs), polycyclic aromatic hydrocarbons (PAHs) and polychlorinated biphenyls (PCBs)) of the sediment records could be investigated via gas chromatography [Blais and Muir, 2001]. Generally, sediment records of organic pollutants are derived from estuarine archives; however, urban ponds would allow an assessment of atmospherically-derived organic pollution across the LMR. A cross-regional signal of organic, as well as inorganic, pollutants is of particular importance in the LMR, most notably, due to volatile organic compounds and organochlorides emitted in the region during organic chemical production. Also, benzene, a known carcinogen, is of special consideration due to its presence in petrol [Palmgren *et al.*, 2001]; therefore, investigating the cross-regional PAH signal may help to understand the importance of road vehicles as a mobile source of this pollutant in the urban environment.

Investigation of contemporary street dusts in the LMR may also be beneficial to this work in order to understand in more detail present day pollution characteristics. Spatial, contemporary urban PM data would compliment the urban pond archives, allowing a more detailed and reliable characterisation of present day pollution, potentially, inhibited in the most recent pond sediments due to the active nature of the sediment-water interface. Spatial mapping of proxy pollution characteristics across the LMR may

reveal intra-urban variations, how pollution composition varies within the borough and, therefore, population exposure to pollution particulates. Environmental analyses of surface samples from roadways, airport runways and street dusts or soils adjacent to industrial sources may provide information to 'fingerprint' emissions. Also, a methodology to collect the fine (<1 μm) component of urban dusts should be investigated to further identify and magnetically characterise this harmful fraction of urban pollution.

The cross-regional signal derived from the urban ponds has provided an account of pollution specific to the LMR, due to the unique combination of industrial processes occurring within the area (i.e. the dominance of the organic and inorganic chemical industry). Therefore, a comparison of the cross-regional signal for the LMR with local pollution signals from urban ponds in other urban centres may reveal further variations in the deposition of pollution throughout the UK. For example, how a heavily industrialised area compares with an urban centre with limited industrial activity. This may help to better understand the characteristics of pollution experienced in Halton, which may be a factor in the ill health of the Halton population.

This work also offers potential epidemiological applications, whereby, a comparison of pollution trends from the sediment archives can be made with historical health data, in order to better understand environmental health linkages. There are limitations with historical health data, due to the inconsistency of records and the variations in disease classification from present day to that of the past. However, basic historical mortality rates in Halton could be compared with, for example temporal Pb trends, in order to understand how long-term releases of pollutants may impact the health of the Halton population. Close collaboration with public health teams and health statisticians is envisaged to allow a novel, cross-disciplinary and holistic approach to assess environmental burdens on public health.

REFERENCES

ADAMSON, I.Y.R., PRIEDITIS, H., HEDGECOCK, C. & VINCENT, R. (2000) Zinc is the toxic factor in the lung response to atmospheric particulate sample. *Toxicology and Applied Pharmacology*, 166, 111-119.

AGRAWAL, Y. C., MCCAVE, I. N. & RILEY, J. B. (1991) Laser Diffraction Size Analysis. IN SYVITSKI, J.P.M. (Ed.) Principles, Methods, and Application of Particle Size Analysis. *Cambridge, Cambridge University Press.*

AHRENS, W. & STEWART, P. (2003) retrospective exposure assessment. IN NIEUWENHUIJSEN, M.J. (Ed.) Exposure assessment in occupational and environmental epidemiology. *Oxford, Oxford University Press.* pp. 341-366.

ALLEN, (1906) Some founders of the chemical industry. *Sherrat and Hughes.*

ALLEN, A.G., NEMITZ, E. SHI, J.P., HARRISON, R.M. & GREENWOOD, J.C. (2001) Size distributions of trace metals in atmospheric aerosols in the United Kingdom. *Atmospheric Environment*, 35, 4581-4591.

ALLEN, J.R.L. & RAE, J.E. (1986) Time sequence of metal pollution, Severn Estuary, southwestern UK. *Marine Pollution Bulletin*, 17, 427-431.

ALLIKSAAR, T. & PUNNING, J-M. (1998) The spatial distribution of characterised fly-ash particles and trace metals in lake sediments and catchment mosses: Estonia. *Water, Air and Soil Pollution*, 106, 219-239.

ALLOWAY, B.J & AYRES, D.C. (1997) Chemical Principles of Environmental Pollution. *London, Blackie Academic and Professional.*

AL-MEREY, R., KARAJOU, J. & ISSA, H. (2005) X-Ray fluorescence analysis of geological samples: exploring the effect of sample thickness on the accuracy of results. *Applied Radiation and Isotopes*, 62, 501-508.

AL-RAJHI, M.A., AL-SHAYER, S.M., SEAWARD, M.R.D. & EDWARDS, H.G.M. (1996) Particle size effect for heavy metal pollution analysis of atmospherically deposited dust. *Atmospheric Environment*, 30,145-153.

ANDERSON, H.R., SPIX, C., MEDINA, S., SCHOUTEN, J.P., CASTELLSAGUE, J., ROSSI, G., ZMIROU, D., TOULPUMI, G., WOJTYNIAK, B., PONKA, A., BACHAROVA, L., SCHWART, J. & KATSOUYANNI, K. (1998) Air pollution and daily admissions for chronic obstructive pulmonary disease in six European cities: results from the APHEA project. *European Respiratory Journal*, 11,992-993.

ANKER, S.A., COLHOUN, E.A., BARTON, C.E., PETERSON, M. & BARBETTI, M. (2001) Holocene vegetation and paleomagnetic history from Lake Johnston, Tasmania. *Quaternary Research*, 56, 264-274.

ANNON (1880) The sanitary state of Runcorn. *Lancet*, 24th January, 142-143.

APPELBY, P.G. & OLDFIELD, F. (1978) The calculation of lead-210 dates assuming a constant rate of supply of unsupported ^{210}Pb to the sediment. *Catena*, 5, 1-8.

APPLEBY, P.G. & OLDFIELD, F. (1979) Records of lead deposition in Lake Michigan sediments since 1800. *Environmental Science and Technology*, 13, 478-480.

APPLEBY, P.G. & OLDFIELD, F. (1982) Application of lead-210 to sedimentation studies. IN IVANOVICH, M. & HARMON, R.S. (Eds.) Uranium Series Disequilibrium. *Oxford, Oxford University Press.* pp.731-778.

APPLEBY, P.G. & OLDFIELD, F. (1983) The assessment of ^{210} Pb data from sites with varying sediment accumulation rates. *Hydrobiologia,* 103, 29-35.

APPLEBY, P.G. (1993) Forward to the lead-210 dating anniversary series. *Journal of* Paleolimnology, 9, 155-160.

APPLEBY, P.G. The role of 210Pb dating in long-term sequences. (unpublished document).

APPLEBY, P.G., DEARING, J.A. & OLDFIELD, F. (1985) Magnetic studies of erosion in a Scottish lake catchment: 1. Core chronology and correlation. *Limnology and Oceanography*, 30, 1144-1153.

APPLEBY, P.G., NOLAN, P.J., GIFFORD.D, W., GODFREY, D.W., OLDFIELD, F., ANDERSON, N.J. & BATTARBEE, R.W. (1986) ^{210} Pb dating by low background gamma counting. *Hydrobiologia,* 143, 21-27.

APSIMON, H.M., GONZALEZ DEL CAMPO, M.T. & ADAMS, H.S. (2001) Long-range transport of primary particulate matter over Europe. *Atmospheric Environment*, 35, 343-352.

AQEG (2005) *Particulate matter in the United Kingdom*, London, DEFRA.

ARIZTEGUI, D. & DOBSON, J. (1996) Magnetic investigations of framboidal gregite formation: a record of anthropogenic environmental changes in eutrophic Lake St Moritz, Switzerland. *The Holocene,* 6, 235-241.

ARIZTEGUI, D., CHONDROGIANNI, C., LAMI, A., GUILIZZONI, P. & LAFARGUE, E. (2001). Lacustrine organic matter and the Holocene paleoenvironmental record of Lake Albano (central Italy). *Journal of Paleolimnology,* 26, 283-292.

ARTIOLA, J.F. (1996) Industrial sources of pollution . IN PEPPER, I.L., GERBA, C.P. & BRUSSEAU, M.L. (Eds.) Pollution Science. *London, Academic Press*. pp. 267-277.

(ASSOCIATION OF PUBLIC HEALTH OBSERVATIONS (APHO) & DEPARTMENT OF HEALTH.) (2007) *Halton Health profile 2007.* www.nwhpo.org.uk/information [accessed 12/01/08].

AVNIMELECH, Y., MCHENRY, J.R. & ROSS, J.D. (1984) Decomposition of organic matter in lake sediments. *Environmental Science and Technology*, 18, 5-11.

BALLESTER, D., SAEZ, Z.M., ALONSO, F.M.E., TARACIDO, T.M., ORDONEZ, I.J.M., AGUINAGA, O.I., DAPN, C.A., BELLIDO, B.J., GUILLEN, P.J.J., PEREZ, B.M.J., CANADA, M.A., ARRIBAS, M.F. & PEREZ-HOYOS, S. (1999) The EMECAM project: the Spanish multicentre study on the relationship between air pollution and mortality. *Revista Española de Salud Pública*, 73, 165-175.

BANERJEE, S. K., KING, J. & MARVIN, J. (1981) A rapid method for magnetic granulometry with applications to environmental studies. *Geophysical Research Letters*, 8, 333-336.

BARKER, T.C & HARRIS, J.R. (1959) A Merseyside town in the Industrial Revolution St Helens 1750-1900. *London, Frank Cass and Co Ltd.*

BATTARBEE, R.W., APPELBY, P.G., ODELL, K. & FLOWER, R.J. (1985) ^{210}Pb dating of Scottish lake sediments, afforestation and accelerated soil erosion. *Earth Surface Processes and Landforms*, 10, 137-142.

BAZYLINSKI, D. A. (1996) Controlled biomineralization of magnetic minerals by magnetotactic bacteria. *Chemical Geology*, 132, 191-198.

BEAUDOIN, A. (2003) A comparison of two methods for estimating the organic content of sediments. *Journal of Paleolimnology*, 29, 387-390.

BECKWITH, P.R., ELLIS, J.B., REVITT, D.M. & OLDFIELD, F. (1986) heavy metal and magnetic relationships for urban source sediments. *Physics of the Earth and Planetary Interiors*, 42, 67-75.

BELL, H. & WALKER, M.J.C. (1992) Late Quaternary environmental change: Physical and human perspectives. *Essex, Longman.*

BELL, M.L., O'NEIL, M.S., CIFUENTES, L.A., BRAGA, A.L.F., GREEN, C., NWEKE, A., ROGAT, J. & SIBOID, K. (2005) Challenges and recommendations for the study of socioeconomic factors and air pollution health effects. *Environmental Science and Policy*, 8, 525-533.

BERGE, F. BRODIN, Y-W., CRONBERG, G., EL-DAOUSHY, F., HØEG, H.I., NILSSEN, J.P., RENBERG, I., SANDØY, S., TIMBERLID, A. & WIK, M. (1990) Palaeolimnological changes related to acid deposition and land-use in the catchments of two Norwegian soft-water lakes. IN THE ROYAL SOCIETY. Palaeolimnology and lake acidification. *Cambridge, University Press.* pp. 159-163.

BERQUÓ, T.S., THOMPSON, R. & PARTITI, C.S.M. (2004) Magnetic study of Brazilian peats from São Paulo state. *Geoderma*, 118, 233-234.

BERRY, A. & PLATER, A. J. (1998) Rates of tidal sedimentation from records of industrial pollution and environmental magnetism: the Tees E`stuary, north-east England. *Water, Air & Soil Pollution*, 106, 463-479.

BERTINE, K.K. & MENDECK, M.F. (1997) Industrialization in New Haven, Connecticut, as recorded in reservoir sediments. *Environmental Science and Technology*, 12, 201-207.

BHOPAL, R.S., MOFFATT, S., PLESS-MULLOLI, T., PHILLIMORE, P.R., FOY, C., DUNN, C.E. & TATE, J.A. (1998) Does living near a constellation of petrochemical, steel and other industries impair health? *Occupational and Environmental Medicine*, 55, 812-822.

BIRKS, H.J.B., JONES, V.J. & ROSE, N.L. (2004) Recent environmental change and atmospheric contamination on Svalbard as recorded in lake sediments- and introduction. *Journal of Paleolimnology*, 31, 403-410.

BJÖRCK, S., NOE-NYGAARD, N., WOLIN, J., HOUMARK-NIELSEN, M., HANSEN, H.J. & SNOWBALL, I. (2000) Eemian Lake development, hydrology and climate: a multi-stratigraphic study of the Hollerup site in Denmark. *Quaternary Science Reviews,* 19, 509-536.

BLAIS, J.M. & MUIR, D.C.G. (2001) Paleolimnological methods and applications for persistent organic pollutants. IN IN LAST, W.M. & SMOL, J.P. (Eds) Tracking environmental change using lake sediments. *London, Kluwer Academic Publishers.* pp. 271-298.

BLAKE, W.H., WALSH, R.P.D., REED, J.M., BARNSLEY, M.J. & SMITH, J. (2007) Impacts of landscape remediation on the heavy metal pollution dynamics of a lake surrounded by non-ferrous smelter waste. *Environmental Pollution,* 148, 268-280.

BLOEMENDAL, J., KING, J. W., HALL, F. R. & DOH, S. J. (1992) Rock magnetism of Late Neogene and Pleistocene deep sea sediments: relationship to sediment source, diagenetic processes and sediment lithology. *Journal of Geophysical Research,* 97, 4361-4375.

BLOEMENDAL, J., LAMB, B. & KING, J. (1988) Paleoenvironmental implications of rock-magnetic properties of the late Quaternary sediment cores from the eastern equatorial Atlantic. *Paleoceanography,* 3, 61-87.

BLOEMENDAL, J., LIU, X.M. & ROLPH, T.C. (1995) Correlation of the magnetic susceptibility stratigraphy of Chinese loess and the marine oxygen isotope record: chronological and palaeoclimatic implications. *Earth and Planetary Science Letters,* 131, 371-380.

BOFFETTA, P. (2004) Epidemiology of environmental and occupational cancer. *Oncogene,* 23, 6392-6403.

BOGGS , Jr. S. (1995) Principles of Sedimentology and Stratigraphy: Second Edition. *New Jersey, Prentice-Hall Inc.*

BOHREN, C.F. & HUFFMAN, D.F. (1998) Absorption and scattering of light by small particles. *New York, Wiley.*

BONNETT, P.J.P., APPLEBY, P.G. & OLDFIELD, F. (1988) Radionuclides in coastal and estuarine sediments from Wirral and Lancashire. *The Science of the Total Environment,* 70, 215-236.

BOONYATUMANOND, R., WATTAYAKORN, G., AMANO, A., INOUCHI, Y. & TAKADA, H. (2007) Reconstruction of pollution history of organic contaminants in the upper Gulf of Thailand by using sediment cores: first report from Tropical Asia Core (TACO) project. *Marine Pollution Bulletin,* 54, 554-565.

BOOTH, C. A. (2002) Sediment-source-linkages in the Gwendraeth Estuary, South Wales, based on mineral magnetic analysis. *Unpublished PhD Thesis, University of Wolverhampton.*

BOOTH, C. A., WALDEN, J., NEAL, A. & SMITH, J. P. (2005) Use of mineral magnetic concentration data as a particle size proxy: a case study using marine, estuarine and fluvial sediments in the Carmarthen Bay area, South Wales, UK. *Science of The Total Environment,* 347, 241-253.

BOWMAN, J.J. & HARLOCK, S. (1998) The spatial distribution of characterised fly-ash particles and trace metals in lake sediments and catchment mosses: Ireland. *Water, Air and Soil Pollution,* 106, 263-286.

BOYLE, J. (2004(b)) A comparison of two methods for estimating the organic matter content of sediments. *Journal of Palaeolimnology*, 31, 125-127.

BOYLE, J.F. (2001) Inorganic geochemical methods in palaeolimnology. IN LAST, W.M. & SMOL, J.P. (Eds.) (2001) Tracking Environmental Change using Lake Sediments: Volume 2 Physical and Geochemical Methods. *Dordrecht, The Netherlands, Kluwer Academic Publishers*. pp. 83-141.

BOYLE, J.F. (2001) Inorganic geochemical methods in palaeolimnology. IN LAST, W.M. & SMOL, J.P. (Eds.) Tracking environmental change using lake sediments. *London, Kluwer Academic Publishers*. pp. 83-141.

BOYLE, J.F. (2000) Rapid elemental analysis of sediment samples by isotope source XRF. *Journal of Palaeolimnology*, 23, 213-221.

BOYLE, J.F. (*Pers. Comm.)* Email regarding XRF sample corrections for low mass samples (22/03/2007) Liverpool University, jfb@liv.ac.uk.

BOYLE, J.F., ROSE, N.L., APPLEBY, P.G. & BIRKS, H.J.B. (2004) Recent environmental change and human impact on Svalbard: the lake-sediment geochemical record. *Journal of Paleolimnology*, 31, 515-530.

BOYLE, J.F., ROSE, N.L., BENNION, H., YANG, H. & APPLEBY, P.G. (1999) Environmental impacts in the Jianghan Plain: evidence from lake sediments. *Water, Air and Soil Pollution*, 112, 21-40.

BOYLE, K.A. (1996) Evaluating particulate emissions from jet engines: analysis of chemical and physical characteristics and potential impacts on coastal environments and human health. *Transportation Research Record*, 1517, 1-9.

BRÄNNVALL, M-L., BINDER, R., RENBERGE, I., EMTERYD, O., BARTNICKI, J. & BILLSTRÖM, K. (1999) The medieval metal industry was the cradle of modern large-scale atmospheric lead pollution in northern Europe. *Environmental Science and Technology*, 33, 4391-4395.

BRICKER, S.B. (1993) The history of Cu, Pb and Zn inputs to Narragansett Bay, Rhode Island as recorded by salt-marsh sediments. *Estuaries*, 16, 589-607.

BRUNEKREEF, B. & HOLGATE, S.T. (2002) Air pollution and health. *The Lancet*, 360, 1233-1242.

BRUNEKREEF, B., DOCKERY, D.W. & KRZYZANOWSKI, M. (1995) Epidemiologic studies on short-term effects of low levels of major ambient air pollution components. *Environmental Health Perspectives*, 103, 3-13.

BURGESS, C., CRUTCHLEY, A., CLARK, G., DAVIES, G., GATRELL, T., POOLEY, C., STELFOX, M., WATSON, N., WELSHMAN, J. & WHYATT, D. (2003) *Final report: Understanding the factors affecting health in Halton*. Lancaster University: Department of Geography and Institute for Health Research.

BUZEA, C., PACHECO, I.I. & ROBBIE, K. (2007) Nanomaterials and nanoparticles: sources and toxicity. *Biointer Phases*, 2, 18-71.

CABALLERO, M. & GUERRERO, B.O. (1998) Lake levels since about 40,000 years ago at Lake Chalco near Mexico City. *Quaternary Research,* 50, 69-79.

CACHIER, H. (1998) Carbonaceous combustion aerosol. IN HARRISON, R.M. & VAN GRIEKEN, R. (Eds.) Atmospheric Particles. *New York, Wiley.* pp. 295-348.

CAITCHEON, G. G. (1993) Sediment source tracing using environmental magnetism: a new approach with examples from Australia. *Hydrological Processes*, 7, 349-358.

CAITCHEON, G. G. (1998) The significance of various sediment magnetic mineral fractions for tracing sediment sources in Killimicat Creek. *Catena*, 32, 131-142.

CALLENDER, E., & RICE, K.C., (2000) The urban environmental gradient: anthropogenic influences on the spatial and temporal distributions of lead and zinc in sediments. *Environmental Science and Technology*, 34, 232-238.

CAMACHO-IBAR, V.F. & MCEVOY, J. (1996) Total PCBs in Liverpool Bay sediments. *Marine Environmental Research,* 41, 241-263.

CAMPBELL, W.A. (1971) The Chemical Industry. *London, Longman Group Ltd.*

CANTWELL, M.G., KING, J.W., BURGESS, R.M. & APPLEBY, P.G. (2007) Reconstruction of contaminant trends in a salt wedge estuary with sediment cores dated using a multiple proxy approach. *Marine Environmental Research*, 64, 225-46.

CARTER, D.H. (1964) Mond Division. *ICI Magazine*. pp 2-7.

CELIS, J.E., MORALES, J.R., ZAROR, C.A & INZUNZA, J.C. (2004) A study of the particulate matter PM10 composition in the atmosphere of Chillán, Chile. *Chemosphere,* 54, 541-550.

CHALMERS, A.T., VAN METRE, P.C. & CALLENDER, E. (2007) The chemical response of particle-associated contaminants in aquatic sediments to urbanization in New England, U.S.A. *Journal of Contaminant Hydrology,* 91, 4-25.

CHAN, L.S., NG, S.L., DAVIS, A.M., YIM, W.W.S. & YEUNG, C.H. (2001) Magnetic properties and heavy-metal contents of contaminated seabed sediments of Penny's Bay, Hong Kong. *Marine Pollution Bulletin,* 42, 569-583.

CHAN, L.S., YEUNG, C.H., YIM, W.W.S. &OR, O.L. (1998) Correlation between magnetic susceptibility and distribution of heavy metals in contaminated sea-floor sediments of Hong Kong harbour. *Environmental* Geology, 36, 77-86.

CHARLES, D.F., BINDFORD, M.W., FURLONG, E.T., HITES, R.A., MITCHELL, M.J., NORTON, S.A., OLDFIELD, F., PATERSON, M.J., SMOL, J.P., UUTALA, A.J., WHITE, J.R., HITEHEAD, D.R. & WISE, R.J. (1990) Paleoecological investigation of recent lake acidification in the Adirondack Mountains, N Y, *Journal of Paleolimnology*, 3, 195-211.

CHARLESWORTH, S. M. & LEES, J. A. (2001) The application of some mineral magnetic measurements and heavy metal analysis for characterising fine sediments in an urban catchment, Coventry, UK. *Journal of Applied Geophysics*, 48, 113-125.

CHARLESWORTH, S.M & LEES, J.A. (1997) The use of mineral magnetic measurements in polluted urban lakes and deposited dusts in Coventry, UK. *Physics and Chemistry of the Earth,* 22, 203-206.

CHARLESWORTH, S.M. & LEES, J.A. (1999(a)) The distribution of heavy metals in deposited urban dusts and sediments, Coventry, England. *Environmental Geochemistry and Health,* 21, 97-115.

CHARLESWORTH, S.M. & LEES, J.A. (1999(b)) The transport of particulate-associated heavy metals form source to deposit in the urban environment, Coventry, UK. *The Science of the Total Environment,* 235, 351-353.

CHARLESWORTH, S.M. & FOSTER, I.D.L. (1999) Sediment budgets and metal fluxes in two contrasting urban lake catchments in Coventry, UK. *Applied Geography,* 19, 199-210.

CHESHIRE COUNTY COUNCIL & ENGLISH HERITAGE (2003) Cheshire Historic Towns Survey: Runcorn and Halton Archaeological Assessment. *Chester, Cheshire County Council.*

CIVIL AVIATION AUTHORITY *UK airport statistics: historical annual report tables.* http://www.caa.co.uk/statistics [accessed 17/08/2009].

CLAES, M., GYSELS, K., VAN GRIEKEN, R. & HARRISON, R.M. (1998) Inorganic composition of atmospheric aerosols. IN HARRISON, R.M. & VAN GRIEKEN, R. (Eds.) Atmospheric particles. *Chichester, Wiley.*

CLARK, R.B. (1989) Marine Pollution. *Oxford, Oxford University Press.*

CLARKE, G., KERNAN, M., MARCHETTO, A., SORVARI, S. & CATALAN, J. (2005) Using diatoms to assess geographic patterns of change in high-altitude European lakes from pre-industrial times to the present day. *Aquatic Sciences,* 67, 224-236.

CLIFTON, J., McDONALD, P., PLATER, A. J. & OLDFIELD, F. (1999) Derivation of a grain-size proxy to aid the modelling and prediction of radionuclide activity in salt marshes and mud flats of the eastern Irish Sea. *Estuarine, Coastal and Shelf Science,* 48, 511-518.

COHEN, A.S., PALACIOS-FEST, M.R., MCGRILL, J., SWAERZENSKI, P.W., VERSCHUREN, D., SINYINZA, R., SONGORI, T., KAKAGOZO, B., SYAMPILA, M., O'REILY, C.M., & ALIN, S.R. (2005) Paleolimnological investigations of anthropogenic environmental change in Lake Tanganyika. I: an Introduction to the project. *Journal of Paleolimnology,* 34, 1-18.

COKER, W.B. (1995) Processes effecting mercury and associated metals in lake sediment columns. *Proceedings of 1995 Canadian mercury workshop.* Ecological Monitoring and Assessment Network (EMAN), Toronto, Ontario.

COLLS, J. (1997) Air Pollution: An Introduction. *London, E & FN Spon.*

COLMAN, S.M., KING, J.W., JONES, G.A., REYNOLDS, R.L. & BOTHNER, M.H. (2000) Holocene and recent sediment accumulation rates in Southern Lake Michigan. *Quaternary Science Reviews,* 19, 1563-1580.

COLVILE, R.N., STEVENS, E.C., NIEUWENHUIJSEN, M.J. & KEEGAN, T.J. (2001) Atmospheric dispersion modelling for assessment of exposure to arsenic for epidemiological studies in the Nitra Valley, Slovakia. *Journal of Geophysical Research,* 106, 17421-17432.

CONNOR, S. E. & THOMAS, I. (2003) Sediments as archives of industrialisation: Evidence of atmospheric pollution in coastal wetlands of southern Sydney, Australia. *Water, Air, & Soil Pollution,* 149, 189-210.

COUILLARD, Y., CATTANEO, A., GALLON, C. & COURCELLES, M. (2008) Sources and chronology of fifteen elements in the sediments of lakes affected by metal deposition in a mining area. *Journal of Paleolimnology,* 40, 97-114.

COUILLARD, Y., COURCELLES, M., CATTANEO, A. & WUNSAM, S. (2004) A test of the integrity of metal records in sediment cores based on the documented history of metal contamination in Lac Dufault (Québec, Canada). *Journal of Paleolimnology,* 32, 149-162.

COX, P.A. (1995) The elements on earth: inorganic chemistry in the environment. *Oxford, Oxford University Press.*

CROUDACE, I.W. & CUNDY, A.B. (1995) Heavy metal and hydrocarbon pollution in recent sediments from Southampton Water, southern England: a geochemical and isotopic study. *Environmental Science and Technology,* 29, 1288-1296.

CROWTHER, J. & BARKER, P. (1995) Magnetic susceptibility: distinguishing anthropogenic effects from natural. *Archaeological Prospection,* 2, 207-215.

DAMMAN, A.W.H. (1978) Distribution and movement of elements in ombrotrophic peat bogs. *Oikos,* 30, 480-495.

DAUVAL'TER, V.A. (2004) Effects of atmospheric emissions of the Vorkuta Industrial Region on the chemical composition of lake sediments. *Water Resources.* 31, 668-672.

DAVID, C., DEARING, J. & ROBERTS, N. (1998) Land-use history and sediment influx in lowland lake catchment: Groby Pool. Leicestershire, UK. *The Holocene,* 8, 383-394.

DE MIGUEL, E., LLAMAS, J.F., CHACÓN, E., BERG, T., LARSSEN, S., RØYSET, O. & VADSET, M. (1997) Origin and patterns of distribution of trace elements in street dusts: unleaded petrol and urban lead. *Atmospheric Environment,* 31, 2733-2740.

DEAN, W.E. & SCHWALB, A. (2000) Holocene environmental and climatic change in the Northern Great Plains as recorded in the geochemistry of sediments in Pickerel Lake, South Dakota. *Quaternary International,* 67, 5-20.

DEAN, W.E. (1974) Determination of carbonate and organic matter in calcareous sediments and sedimentary rocks by loss on ignition: comparison with other methods. *Journal of Sedimentary Petrology,* 21, 375-393.

DEARING, J. A. (1999(a)) Magnetic Susceptibility. IN WALDEN, J., OLDFIELD, F. & SMITH, J. (Eds.) Environmental Magnetism: a practical guide. *Quaternary Research Association Technical Guide No.6.* pp.35-62.

DEARING, J. A., DANN, R. J. L., HAY, K., LEES, J. A., LOVELAND, P. J., MAHER, B. A. & O'GRADY, K. (1996) Frequency-dependent susceptibility measurements of environmental materials. *Geophysical Journal International*, 124, 228-240.

DEARING, J.A. & JONES, R.T. (2003) Coupling temporal and spatial dimensions of global sediment flux through lake and marine sediment records. *Global and Planetary Change*, 39, 147-168.

DEARING, J.A., BOYLE, J.F., APPLEBY, P.G., MACKAY, A.W. & FLOWER, R.J. (1998) Magnetic properties of recent sediments in Lake Baikal, Siberia. *Journal of Paleolimnology*, 20, 163-173.

DEARING. J.A. (1999(b)) Environmental magnetic susceptibility: using the Bartington MS2 system. *Kenilworth, Chi Publishing.*

(DEFRA) (2007) *The air quality strategy for England, Scotland, Wales and Northern Ireland.* http://www.defra.gov.uk/environment/quality/air/airquality/strategy/documents/airqualitystrategy-vol1.pdf [accessed 17/08/2008].

DEKKERS, M. J. (1997) Environmental magnetism: an introduction. *Geologie en Mijnbouw*, 76, 163-182.

DEKKERS, M.J. & PIETERSEN, H.S. (1992) Magnetic properties of low-Ca fly ash: a rapid tool for Fe- assessment and a survey for potentially hazardous elements. *Materials Research Society*, 245, 37-47.

DEMORY, F., OBERHÄNSLI, H., NOWACZYK, N.R., GOTTSCHALK, M., WIRTH, R., & NAUMANN, R. (2005) Detrital input and early diagenesis in sediments from Lake Baikal revealed by rock magnetism. *Global and Planetary Change*, 46, 145-166.

(DEPARTMENT OF TRANSPORT) (2008) *Transport statistics of Great Britain.* http://dft.gov.uk/transtat.tsgb [accessed 28/03/2008].

DIAZ, J., GARCIA, R., RIBERA, P., ALBERDI, J.C., HERNANDEZ, E., PAJARES, M.S. & OTERO, A. (1999) Modelling of air pollution and its relationship with mortality and morbidity in Madrid Spain. *International Archives of Occupational and Environmental Health, 72, 366-376.*

DIGEFELDT, G., OLSSON, S. & SANDGREN, P. (2000) Reconstruction of lake-level changes in lake Xinias, central Greece, during the last 40 000 years. *Palaeogeography, Palaeoclimatology , Palaeoecology,* 158, 65-82.

DIGGLE, REV.G.E. (1961) A history of Widnes. *Corporation of Widnes.*

DINARÉS-TURELL, J., HOOGSKKER, A.A., ROBERTS, A.P., ROHLING, E.J. & SAGNOTTI, L. (2003) Quaternary climatic control of biogenic magnetite production and eolian dust input in cores from the Mediterranean Sea. *Palaeogeography, Palaeoclimatology, Palaeoecology*, 190, 195-209.

DINESCU, I.C., STYEINNES, E., DULIU, O.G., CIOETEA, C., SJØBAKK, T.E., DUMITRIU, D.E., GUGIU, M.M. & HARALAMBIE, M. (2004) Distribution of some major and trace elements in Danube Delta lacustrine sediment and soil. *Journal of Radioanalytical and Nuclear Chemistry*, 262, 345-354.

DINGLE, A.E. (1982) 'The monster nuisance of all': Landowners, alkali manufacturers and air pollution 1828-64. *Economic History Review*, 35, 529-548.

DISSANAYAKE, C.B. (1983) Metal-organic interactions in environmental pollution. *International Journal of Environmental Studies*, 22, 25-42.

DOCKERY, D.W. & POPE III, C.A. (1994) Acute respiratory effects of particulate air pollution. *Annual Reviews of Public Health*, 15, 107-113.

DOCKERY, D.W., POPE III, C.A., XU, X., SPENGLER, J.D., WARE, J,.H., FAY, M.E., FERRIS, B.G., & SPEOZER, F.E. (1993) An association between air pollution and mortality in six US cities. *New England Journal of Medicine*, 329, 1753-1759.

DONALDSON, K., LI, X.Y. & MACNEE, W. (1998) Ultrafine (nanometer) particle mediated lung injury. *Jounral of Aerosol Science*, 29, 553-560.

DONER, L. (2003) Late-Holocene paleoenvironments of northwest Iceland from lake sediments. *Palaeogeography, Palaeoclimatology, Palaeoecology*, 193, 535-560.

DOUGLAS, I. (1985) Urban Sedimentology. *Processes in physical geography*, 9, 255-280.

DOUGLAS, I., HODGSON, R., & LAWSON, N. (2002) Industry, environment and health through 200 years in Manchester. *Ecological Economics*, 41, 235-255.

DUBNOV, J., BARCHANA, M., RISHPON, S., LEVEBTHAL, A., SEGAL, I., CAREL, R., PORTNOV, B.A. (2007) Estimating the effect of air pollution form a coal-fired power station on the development of children's pulmonary function. *Environmental Research*, 103, 87-98.

DUNLOP, D. J. (1973) Superparamagnetic and single-domain threshold sizes in magnetite. *Journal of Geophysical Research*, 78, 1780-1793.

ĎURZA, O. (1999) Heavy metals contamination and magnetic susceptibility in soils around metallurgical plant. *Physics and Chemistry of the Earth*, 24, 541-543.

DWIVEDI, D., AGARWAL, A.K. & SHARMA, M. (2006) Particulate emission characterization of a biodiesel vs diesel-fuelled compression ignition transport engine: a comparative study. *Atmospheric Environment*, 40, 5586-5595.

EBBINGHAUS, A & WIESEN, P (2001) Aircraft fuels and effect upon engine emissions. *Air and Space Europe*, 3, 101-103.

EDWARDS, K.J. & WHITTINGTON, G. (2001) Lake sediments, erosion and landscape change during the Holocene in Britain and Ireland. *Catena*, 42,143-173.

EIMERS, M.C., PATERSON, A.M., DILLON, P.J., SCHIFF, S.L. CUMMING, B.F. & HALL, R.I. (2006) Lake sediment core records of sulphur accumulation and sulphur isotopic composition in Central Ontario, Canada lakes. *Journal of Paleolimnology*, 35, 99-109.

EL BILALI, L., RASMUSSEN, P.E., HALL, G.E.M. & FORTIN, D. (2002) Role of sediment composition in trace metal distribution in lake sediments. *Applied Geochemistry*, 17, 1171-1181.

ENGLERT, N. (2004) Fine particulates and human health – a review of epidemiological studies. *Toxicology Letters*, 149, 235-242.

(ENVIRONMENT AGENCY) (2005) Pollution Inventory data (air pollution) for Halton. http://www.environment-agency.gov.uk [accessed 17/05/2005].

(ENVIRONMENT AGENCY) (2007) *Pollution Inventory Reporting: guidance notes.* Environment Agency. http://www.environment-agency.co.uk/pi_guidance.pdf [accessed 21/01/2008].

ERIKSSON, M.G. & SANDGREN, P. (1999) Mineral magnetic analyses of sediment cores recording recent soil erosion history in central Tanzania. *Palaeogeography, Palaeoclimatology, Palaeoecology,* 152, 365-383.

EVANS, M.E. & HELLER, F. (2003) Environmental Magnetism. Principles and Applications of Enviromagnetics. *London, Academic Press.*

EVANS, M.F. & SMITH, V.K. (2005) Do new health conditions support mortality air pollution effects? *Journal of Environmental Economics and Management*, 50, 496-518.

FAEGRI, K. (1990) Palaeolimnology and lake acidification: A summary. IN THE ROYAL SOCIETY. Palaeolimnology and lake acidification. *Cambridge, University Press.* pp. 215-219.

FARR, K.M., JONES, D.M., O'SULLIVAN, P.E., EGLINGTON, G., TARLING, D.H & HEDGES, R.E.M. (1990) Palaeolimnological studies of laminated sediments from the Shropshire-Cheshire Meres. *Hydrobiologica*, 214, 279-292.

FERNANDÉZ, P., ROSE, N.L., VILANOVA, R.M. & GRIMALT, J.O. (2002) Spatial and temporal comparisons of polycyclic aromatic hydrocarbons and spheroidal carbonaceous particles in remote European lakes. *Water, Air and Soil Pollution: Focus,* 2, 261-274.

FISHER, G.L., PRENTICE, B.A., SILBERMAN, D., ONDOV, J.M., BIERMANN, A., RAGAINI, R.C. & MCFARLAND, A.R. (1978) Physical and morphological studies of size-classified coal fly ash. *American Chemical Society,* 12, 447-451.

FLANDERS, P.J. (1994) Collection, measurement, and analysis of airborne magnetic particulates from pollution in the environment. *American Institute of Physics,* 75, 5931-5936.

FOSTER, I.D.L. & CHARLESWORTH, S.M. (1996) Heavy metals in the hydrological cycle: trends and explanation. *Hydrological Processes,* 10, 277-261.

FOSTER, I.D.L., CHARLESWORTH, S.M., DEARAING, J.A., KEEN, D.H. & DALGLEISH, H. (1991) Lake sediments: a surrogate measure of sediment associated heavy metal transport in fluvial systems? *Sediment and stream water quality in a changing environment: trends and explanation.* Proceedings of the Viena Symposium, (August) pp. 321-328.

FOSTER, I.D.L., GREW, R. & DEARING, J.A. (1990) Magnitude and frequency of sediment transport in agricultural catchments; a paired lake-catchment study in Midland England. IN BORDMAN, J., FOSTER, I.D.L. & DEARING, J.A. (Eds.) Soil erosion on agricultural land. *Chichester, Wiley.* pp. 153-171.

FOTT, J., VUKIC, J. & ROSE, N.L. (1998). The spatial distribution of characterised fly-ash particles and trace metals in lake sediments and catchment mosses: Czech Republic. *Water Air and Soil Pollution,* 106, 241-261.

FOWLER, REV.G. (1834) Visitor's Guide to Runcorn and its vicinity. *Runcorn, Walker.*

FOX, W.M., CONNOR, L., COPPLESTONE, D., JOHNSON, M.S. & LEAH, R.T. (2001) The organochlorine contamination history of the Mersey estuary, UK, revealed by analysis of sediment cores from salt marshes. *Marine Environmental Research,* 51, 213-227.

FOX, W.M., JOHNSON, M.S., JONES, S.R., LEAH, R.T. & COPPLESTONE, D. (1999) The use of sediment cores from stable and developing salt marshes to reconstruct historical contamination profiles in the Mersey Estuary, UK. *Marine Environmental Research,* 47, 311-329.

FRENCH, P. W. (1996) Implications of a salt marsh chronology for the Severn estuary based on independent lines of dating evidence. *Marine Geology,* 135, 115-125.

FRENCH.P.W. (1998) The impact of coal production on the sediment record of the Severn Estuary. *Environmental Pollution,* 103, 97-43.

FRIGNANI, M., BELLUCCI, L.G., CARRARO, C. & FAVOTTO, M. (2004) Accumulation of polychlorinated biphenyls in sediments of the Venice Lagoon and the industrial area of Porto Marghera. *Chemosphere,* 54, 1563-1572.

GALLOWAY, J.N., THORNTON, J.D., NORTON, S.A., VOLCHOR, H.L. & MCLEAN, R.A.N. (1982) Trace metals in atmospheric deposition: a review and assessment. *Atmospheric Environment,* 16, 1677-1700.

GAO, N., HOPKE, P.K. & REID, N.W. (1996) Possible sources for some trace elements found in airborne particles and precipitation in Dorset, Ontario. *Air and Waste Management Association.,* 46, 1035-1047.

GAUTAM, P., BLAHA, U. & APPEL, E. (2005) Intergration of magnetism and heavy metal chemistry of soils to quantify the environmental pollution in Kathmandu, Nepal. *The Island Arc,* 14, 424-435.

GAUTAM, P., BLAHA, U., & APPEL, E. (2005) Magnetic susceptibility of dust-loaded leaves as a proxy of traffic related heavy metal pollution in Kathmandu City, Nepal. *Atmospheric Environment,* 39, 2201-2211.

GAUTAM, P., BLAHA, U., APPEL, E. & NEUPANE, G. (2004) Environmental magnetic approach towards the quantification of pollution in Kathmandu urban area, Nepal. *Physics and Chemistry of the Earth,* 29, 973-984.

GEORGEAUD, V.M., ROCHETTE, P., AMBROSI, J.P., VANDAMME, D. & WILLIAMSON, D. (1997) Relationship between heavy metals and magnetic properties in a large polluted catchment: the Etang de Berre. *Physics and Chemistry of the Earth,* 22, 211-214.

GHIO, A.J. & COHEN, M.D. (2005) Disruption of iron homeostasis as a mechanism of biological effect by ambient air pollution particles. *Inhalation Toxicology,* 17, 709-716.

GIBBS-EGGAR, Z., JUDE, B., DOMINIK, J., LOIZEAU, J. & OLDFIELD, F. (1999) Possible evidence for dissimilatory bacterial magnetite dominating the magnetic properties of recent lake sediments. *Earth and Planetary science Letters,* 168, 1-6.

GILBERTSON, D.D., GRATTAN, J.P., CRESSEY, M. & PYATT, F.B. (1997) An air pollution history of metallurgical innovation in iron and steel making: a geochemical archive of Sheffield. *Water, Air and Soil Pollution,* 100, 327-34.

GODBEER, W.C. & SWAINE, D.J. (1995) The deposition of trace elements in the environs of a power station. IN SWAINE, D.J. & GOODARZI, F. (Eds.) Energy and Environment: environmental aspects of trace elements in coal. *London, Kluwer Academic Publishers.* pp. 178-203.

GOLDBERG, E.D., HODGE, V.F., GRIFFIN, J.J. & MINORU, K. (1981) Impact of fossil fuel combustion on the sediments of Lake Michigan. *Environmental Science and Technology,* 15, 466-471.

GOLDBERG, E.D., HODGE, V.H.M., KOIDE.M., GRIFFIN, J., GAMBLE, E., BRICKER, O.P., MATISOFF, G., HOLDREN, G.R. & BRAUN, R. (1978) A pollution history of Chesapeake Bay. *Geochimica et Cosmochimica Acta,* 42, 1413-1425.

GOODWIN, J.W.L., SALWAY, A.G., EGGLESTON, H.S., MURRELLS, T.P. & BERRY, J.E. (1999) *UK emissions of air pollutants 1970 to 1996.* National Atmospheric Emissions Inventory. http://www.aeat.co.uk/netcen/airqual/naei/annreport/annrep96/sect4_1.html [accessed 29/01/2008].

GÖTSCHI, T., HAZANKAMP-VON ARX, M.E., HEINRICH, J., BONO, R., BURNEY, P., FORSBERG, B., JARVIS, D., MALDONADO, J., NORBÄCK, D., STERN, W.B., SUNYER, J., TORÉN, K., VERLATO, G., VILLANI, S. & KÜNZLI, N. (2005) Elemental composition and reflectance of ambient fine particles at 21 European locations. *Atmospheric Environment,* 39, 5947-5958.

GOYER, R.A. (1997) Toxic and essential metal interactions. *Annual Review of Nutrition,* 17, 37-50.

GOUDIE, A., ANDERSON, M., BURT, T., LEWIN, J., RICHARDS, K., WHALLEY, B. & WORSLEY, P. Geomorphological Techniques (2nd edition). *Cambridge, Unwin Hyman Ltd.*

GRANEY, J.R. & ERIKSEN, T.M. (2004) Metals in pond sediments as archives of anthropogenic activities: a study in response to health concerns. *Applied Geochemistry,* 19, 1177-1188.

GRAYSON, R.P. & PLATER, A.J. (2009) A lake sediment record of Pb mining from Ullswater, English Lake District, UK. *Journal of Paleolimnology,* 42, 183-197.

GREENWOOD, E.F. (Ed.) (1999) Ecology and landscape development: a history of the Mersey Basin. *Liverpool, Liverpool University Press.*

GRIFFIN, J. & GOLDBERG, E.D. (1979) Morphologies and origin of elemental carbon in the environment. *Science,* 206, 563-565.

GRIFFIN, J.J. & GOLDBERG, E.D. (1983) Impact of fossil fuel combustion on the lake sediments of Lake Michigan: a reprise. *Environmental Science and Technology,*17, 244-245.

GRIFFIN, J.J. & GOLDBERGE, E.D. (1981) Sphericity as a characteristic of solids from fossil fuel burning in a Lake Michigan sediment. *Geochimica et Cosmochimica Acta,* 45, 763-769.

HABERLE, S.G. & LUMLEY, S.H. (1998) Age and origin of tephras recorded in postglacial lake sediments to the west of the southern Andes, 44°S to 47°S. *Journal of Volcanology and Geothermal Research,* 84, 239-256.

HALLETT, D.J., MATTHEWS, R.W. & FOIT, Jr. F.F. (2001) Mid-Holocene Glacier Peak and Mount St. Helens we tephra layers detected in lake sediments from Southern British Columbia using high-resolution techniques. *Quaternary Research,* 55, 584-292.

HALTON PRIMARY CARE TRUST. (2004) *An Equity Profile for Halton.* www2.Halton.gov.uk/pdfs/councilanddemocracy/equityprofile2004 [accessed 15/08/2007].

(HALTON BOROUGH COUNCIL) (1991) *The Halton Legacy.* www2.Halton.gov.uk/pdfs/environment/planning/thehaltonlegacy [accessed 15/08/2007].

(HALTON BOROUGH COUNCIL) (2003) *Contaminated Land Strategy for Inspection.* www2.Halton.gov.uk/pdfs/environment/conlandinspectionstrategy [accessed 02/10/2007].

(HALTON BOROUGH COUNCIL) (2005(a)) *'Halton: Gateway to prosperity' a new economic and tourism development strategy for Halton 2005-2008.* Halton Borough Council. www2halton.gov.uk/pdfs/business/gatewaytoprosperity2005-2008 [accessed 15/08/2007].

(HALTON BOROUGH COUNCIL) (2005(b)) *Halton Science Report.* www.wheresciencesucceds.co.uk/downloads/Halton%20Chem%20report.pdf [accessed 15/08/2007].

HAN, J. & JIANG, W. (1999) Particle size contributions to bulk magnetic susceptibility in Chinese loess and paleosol. *Quaternary International,* 62, 103-110.

HANESCH, M. & SCHOLGER, R. (2002) Mapping of heavy metal loadings in soils by means of magnetic susceptibility measurements. *Environmental Geology,* 42, 857-870.

HANESCH, M., SCHOLGER, R. & REY, D. (2003) Mapping dust distribution around an industrial site by measuring magnetic parameters of tree leaves. *Atmospheric Environment,* 37, 5125-5133.

HARDIE, D.W.F. (1950) A history of the chemical industry in Widnes. *Imperial Chemicals Industries Limited, General Chemicals Division.*

HARLAND, B.J., TAYLOR, D. & WITHER, A. (2000) The distribution of mercury and other trace metals in the sediments of the Mersey Estuary over 25 years 1974-1998. *The Science of the Total Environment,* 253, 45-62.

HARRISON, R., & VAN GRIEKEN, R. (Eds.) (1999) IUPAC series on analytical and physical chemistry of environmental systems: atmospheric particulates. *Chichester, John Wiley & Sons.*

HARRISON, R.M. (2004) Key pollutants – airborne particles. *Science of the Total Environment,* 334, 3-8.

HAY, K.L., DEARING, J.A., BABAN, S.M.J. & LOVELAND, P. (1997) A preliminary attempt to identify atmospherically-derived pollution particles in English topsoils from magnetic susceptibility measurements. *Physics and Chemistry of the Earth,* 22, 207-210.

HEIRI, O., LOTTER, A.F., LERNCKE, G. (2001) Loss on Ignition as a method for estimating organic and carbonate content in sediments: reproducibility and comparability of results. *Journal of Palaeolimnology,* 25, 101-110.

HEIT, M., TAN, Y., KLUSEK, C. & BURKE, J.C. (1981) Anthropogenic trace elements and polycyclic aromatic hydrocarbon levels in sediment cores from two lakes in Adirondack acid lake region. *Water, Air and Soil Pollution,* 15, 441-464.

HELLER, F. (1998) Magnetic record of industrial pollution in forest soils of Upper Silesia, Poland. *Journal of Geophysical Research,* 103, 17,767-17,774.

HITCHINS. J., MORAWSKA, L., WOLFF, R. & GILBERT, D. (2000) Concentrations of submicron particles from vehicle emissions near a major roadway. *Atmospheric Environment,* 34, 51-59.

HODGDON, S., NIEUWENHUIJSEN, M.J., ELLIOTT, P. & JARUP, L. (2006) Kidney disease mortality and environmental exposure to mercury. *American Journal of Epidemiology,* 165, 72-77.

HODGSON, S. (2005) Renal effects in a population exposed to chlor alkali plant emissions. *Unpublished PhD Thesis. London Imperial College of Science Technology and Medicine.*

HODGSON, S., NIEUWENHUIJSEN, M.J., HANSELL, A., SHEPPERD, S., FLUTE, T., STAPLES, B., ELLIOTT, P,. & JARUP, L. (2004) Excess risk of kidney disease in a population living near industrial plants. *Occupational and Environmental Medicine,* 61, 717-719.

HOFFMAN, V., KNAB, M. & APPEL, E. (1999) Magnetic susceptibility mapping of roadside pollution. *Journal of Geochemical exploration,* 66, 313-326.

HOLDEN, VJ.C. (2009) Sedimentary accretion of the North Sefton coast. *Unpublished PhD Thesis, University of Lancaster/ Edge Hill University.*

HOPKE, P.K., LAMB, R.E. & NATUSCH, D.F.S. (1980) Multielemental Characterization of urban roadway dust. *Environmental Science and Technology,* 14, 164-172.

HOSSEINPOOR, A.R., FOROUZANFAR, M.H., YUNESIAN, M., ASGHARI, F., NAIENI, K.H. & FARHOOD, D. (2005) Air pollution and hospitalisation due to angina pectoris in Tehran, Iran: A time-series study. *Environmental Research,* 99, 126-131.

HU, S., APPEL, E., WANG, S., WU, J., XUE, B., WANG, Y., QIAN, J. & XIANG, L. (1999) A preliminary magnetic study on lacustrine sediments from Zoigê Basin, eastern Tibetain Plateau, China: Magnetostratigraphy and environmental implications. *Physics and Chemistry of the Earth,* 24, 811-816.

HU, S., WANG, Y., APPEL, E., ZHU, Y., HOFFMANN, V., SHI, C. & YU, Y. (2003) Magnetic responses to acidification Lake Yangzonghai, SW China. *Physics and Chemistry of the Earth,* 28, 711-717.

HUANG, C.C AND O'CONNELL, M. (2000) Recent land-use and soil erosion history within a small catchment in Connemara, western Ireland: evidence from lake sediments and documentaery sources. *Catena,* 41, 293-335.

HUANG, C.C. (2002) Holocene landscape development and human impact in the Connemara Uplands, Western Ireland. *Journal of Biogeography,* 29, 153-165.

HUANG, K.M. & LIN, S. (2003) Consequences and implications of heavy metal spatial variation in sediments of the Keelong River drainage basin Taiwan. *Chemosphere,* 53, 1113-1121.

HUEGLIN, CH., GAEGAUF, CH., KÜNZEL, S. & BURTSCHER, H. (1997) Characterisation of wood combustion particles: Morphology, mobility and photoelectric activity. *Environmental Science and Technology*, 31, 3239-3447.

HUNT, A. (1986) The application of mineral magnetic methods to atmospheric aerosol discrimination. *Physics of the Earth and Planetary Interiors*, 42, 10-21.

HUNT, A., JONES, J. & OLDFIELD, F. (1984) Magnetic measurements and heavy metals in atmospheric particulates of anthropogenic origin. *The Science of the Total environment*, 33, 129-139.

IP, C.C.M., LI, X.D., ZHANG, G., FARMER, J.G., WAI, O.W.H. & LI, Y.S. (2004) Over one hundred years of trace metal fluxes in sediments of the Pearl River Estuary, south China. *Environmental Pollution*, 132, 157-172.

JANSSEN, N.A.H., LANKI, T., HOEK, G., VALLIUS, M., DE HARTOG, J.J., VAN GRIAKEN, R., PEKKANEN, J. & BRUNEKREEF, B. (2005) Associations between ambient, personal and indoor exposure to fine particulate matter constituents in Dutch and Finnish panels of cardiovascular patients. *Occupational and Environmental Medicine*, 62, 868-877.

JENKINS, A. WHITEHEAD, P.G., COSBY, B.J. & BIRKS, H.J.B. (1990) Modelling long-tem acidification: A comparison with diatom reconstructions and the implications for reversibility. IN THE ROYAL SOCIETY. (1990) Palaeolimnology and lake acidification. *Cambridge, University Press*. pp. 209-214.

JENNER, M. (1995) The politics of London air John Evelyn's fumifugium and restoration. *The Historical Journal*, 38, 535-551.

JENNETT, J.C., EFFLER, S.W. & WIXSON, B.G. (1980) Mobilisation and toxicological aspects of sedimentary contaminants. IN BAKER, R.A. (Ed.) Contaminants and sediments volume 1: fate and transport case studies, modelling toxicity. *Michigan,, Ann Arbor Science*. pp. 429-444.

JERRET, M., BUZZELI, M., BURNETT, T. & DELUCA, P.F. (2005) Particulate air pollution, social confounders, and mortality in small areas of an industrial city. *Social Science and Medicine*, 60, 2845-2863.

JOHNSON, K.S., ZUBERI, B., MOLINA, L.T., MOLINA, M.J., IEDEMA, M.J., COWIN, J.P., GASPAR, D.J., WANG, C. & LASKIN, A. (2005) Processing of soot in an urban environment: case study from the Mexico City Metropolitan Area. *Atmospheric Chemistry and Physics*, 5, 3033-3043.

JONES. A.D. (1969) *Industry & Runcorn 1750 to 1960.* Publicity & Information services Department. Halton Borough Council (January 1969).

JORDAN, P., RIPPEY, B. & ANDERSON, N.J. (2002) The 20th century whole-basin trophic history of an inter-drumlin lake in an agricultural catchment. *The Science of the Total Environment*, 279, 161-173.

KAMAT, S.R. & DOSHI, V.B. (1987) Sequential health effect study in relation to air pollution in Bombay, India. *European Journal of Epidemiology*, 3, 265-277.

KAPIČKA, A., PETROVSKÝ, E., JORDANOVA, N. & PODRÁZSKÝ, V. (2001) Magnetic parameters of forest top soils in Krkonoše Mountains, Czech Republic. *Physics and Chemistry of the Earth (A)*, 26, 917-922.

KAPIČKA, A., PETROVSKÝ, E., USTJAK, S. & MACHÁČKOVÁ, K. (1999) Proxy mapping of fly-ash pollution of soils around a coal-burning power plant: a case study in the Czech republic. *Journal of Geochemical Exploration*, 66, 291-297.

KAPLAN, M.R., WOLFE, A.P. & MILLER, G.H. (2002) Holocene environmental variability in Southern Greenland inferred from lake sediments. *Quaternary Research*, 58, 149-159.

KATSOUYANNI, K., SCHWARTZ, J., SPIX, C., TOULOUMI, G., ZMIROU, D., ZANOBETTI, A., WOJTYNIAK, B., VONK, J.M., TOBIAS, A., PONKA, A., MEDINA, S., BACHAROVA, L. & ANDERSON, H.R. (1996) Short term effects of air pollution on health: a European approach using epidemiologic time series data: the APHEA protocol. *Journal of Epidemiology Community Health*, 50, 12-18.

KEEGAN, T., HOG, B., THORNTON, I., FARAGO, M., JAKUBIS, P., JAKUBIS, M., PESCH, B., RANFT, U., NIEUWENHUIJSEN, M.J. & THE EXPASCAN STUDY GRIUO. (2002) Assessment of environmental arsenic levels in Prievidza district. *Journal of Exposure Analysis and Environmental Epidemiology*, 12, 179-185.

KEMP, A.L. & THOMAS, R.L. (1976) The impacts of man's activities on the composition of sediments in Lake Ontario, Erie and Huron. *Water, Air and Soil Pollution*, 5, 2018-2022.

KEYWOOD, M.D., AYERS, G.P., GRAS, J.L., GILLETT, R.W., COHEN, D.D. (1999) Relationships between size segregated mass concentration data and ultrafine particle number concentrations in urban areas. *Atmospheric Environment*, 33, 2907-2913.

KIENEL, U., SCHWAB, M.J. & SCHETTLER, G. (2005) Distinguishing climatic form direct anthropogenic influences during the past 400 years in varved sediments from Lake Holzmaar (Eifel, Germany). *Journal of Paleolimnology*, 33, 327-347.

KIM, J.G. (2005) Assessment of recent industrialization in wetlands near Ulsan, Korea. *Journal of Paleolimnology*, 33, 433-444.

KING, J.W. & CHANNEL, J.E.T. (1991) Sedimentary magnetism, environmental magnetism and magnetostratigraphy. *Reviews of Geophysics*, April, 358-370.

KIRWIN, T. (*Pers. Comm.*) Conversation with Tim Kirwin, Woodland Trust, Cheshire, regarding pond sites within Woodland Trust Management sites (15/11/04) timkirwin@woodland-trust.org.uk.

KLOSE, S., TÖLLE, R., BÄUCKER, E. & MAKESCHIN, F. (2003) Stratigraphic distribution of lignite-derived atmospheric deposits in forest soils of the Upper Lusatian Region, East Germany. *Water, Air and Soil Pollution*, 142, 3-25.

KNIGHT, C. (1979) Urbanization and natural stream channel morphology: the case of two English new towns. IN HOLLIS, G.E. (Ed.) Man's impact on the hydrological cycle in the United Kingdom. *Norwich, Geo Abstracts Ltd.* pp. 181-199.

(KNOWSLEY METROPOLITAN BOROUGH COUNCIL) (1998) *Primary Care Trust Board Meeting: IPPC application- Jaguar Cars Limited (Halewood combustion plant).* Thursday 2nd November 2006.

(KNOWSLEY PCT) (2008) *Knowsley local history its people and heritage.* http://history.knowsley.gov.uk [accessed 148/08/2009].

KOZLOV, M. (2004) Retrospective analysis of the age at death of two heavily polluted and two unpolluted Russian towns. *Chemosphere*, 56, 405-410.

KUKIER, U., ISHAK, C.F., SUMMER, M.E. & MILLER, W.P. (2003) Composition and element solubility of magnetic and non-magnetic fly ash fractions. *Environmental Pollution*, 123, 255-266.

KUNZENDORF, H., EMEIS, K-C. & CHRISTISIANSEN, C. (1998) Sedimentation in the Central Baltic Sea as viewd by non-destructive Pb-210-dating. *Danish Journal of Geography*, 98, 1-9.

KUTCHKO, B.G. & KIM, A.G. (2006) Fly ash characterisation by SEM-EDS. *Fuel*, 85, 2537-2544.

LALL, R., KENDALL, M., ITO, K. & THURSTON, G.D. (2004) Estimations of historical annual PM2.5 exposures for health effects assessment. *Atmospheric Environment*, 38, 5217-5226.

LAST, W.M. & SMOL, J.P. (Eds.) (2001) Tracking Environmental Change using Lake Sediments: Volume 2 Physical and Geochemical Methods. *Dordrecht, The Netherlands, Kluwer Academic Publishers*.

LAST, W.M. (2001) Textural analysis of lake sediments. IN LAST, W.M. & SMOL, J.P. (Eds) Tracking environmental change using lake sediments. *London, Kluwer Academic Publishers.* pp. 239-269.

LAZARO, T.R. (1979) Urban Hydrology: a multidisciplinary perspective. *Michigan, Ann Arbor Science.*

LE TERTRE, A., MEDINA, S., SAMOLI, E., FORSBERG, B., MICHELOZZI, P., BOUMGHAR, A., VONK, J.M., BELLINI, A., ATKINSON, R., AYRES, J.G., SUNYER, J., SCHWARTZ, J,& KATSOUYANNI, K. (2002) Short-term effects of particulate air pollution on cardiovascular diseases in eight European cities. *Journal of Epidemiology and Community Health*, 56, 773-779.

LECOANET, H., LEVEQUE, F. & AMBROSI, J. P. (2001) Magnetic properties of salt-marsh soils contaminated by iron industry emissions (southeast France). *Journal of Applied Geophysics*, 48, 67-81.

LEE, S.V. & CUNDY, A.B. (2001) Heavy metal contamination and mixing processes in sediments from the Humber Estuary, eastern England. *Estuarine, Coastal and Shelf Science*, 53, 519-636.

LEES, J. A. (1999) Evaluating magnetic parameters for use in source identification, classification and modelling of natural and environmental materials. IN WALDEN, J., OLDFIELD, F. & SMITH, J. (Eds.) Environmental Magnetism: a practical guide. *London, QRA Technical Guide No.6.* pp.113-138.

LEHNER, D., KELLNER, G., SCHNABLEGGER, H. & GLATTER, O. (1998) Static light scattering on dense colloidal systems: new instrumentation and experimental results. *Journal of Colloid and Interface Science*, 201, 34-47.

LEONG, L.S. & TANNER, P.A. (1999) Comparison of methods for determination of organic carbon in Marine sediments. *Marine Pollution Bulletin*, 38, 875-879.

LEROY, S., KAZANCI, N., ILERI, Ö., KIBAR, M., EMRE, O., MCGEE, E. & GRIFFITHS, H.I. (2002) Abrupt environmental changes within a late Holocene lacustrine sequence south of the Marmara Sean (Lake Manyas N-W Turkey): possible links with seismic events. *Marine Geology*, 190, 531-552.

LEWIS, T.E. & MCINTOSH, A.W. (1989) Covariation of selected trace elements with binding substrate in cores collected from two contaminated sediments. *Bulletin of Environmental Contamination and Toxicology*, 43, 518-528.

LIN, J-L., TAN, D-.T., HSU, K-H., & YU, C-C. (2001) Environmental lead exposure and progressive renal insufficiency. *Archives of International Medicine*, 161, 264-271.

LING, A. (1967) Runcorn Development Corporation: Runcorn New Town. *Nottingham, Hawthorns of Nottingham Ltd.*

LOCKE, G. & BERTINE, K.K. (1986) Magnetite in sediments as an indicator of coal combustion. *Applied Geochemistry*, 1, 345-356.

LOPEZ, M.T., ZUK, M., GARIBAY, V., TZINTZUN, G., INIESTRA, R. & FERNÁNDEZ, A. (2005) Health impacts from power plant emissions in Mexico. *Atmospheric Environment*, 39, 119-129.

LOTTER, A.F., EICHER, U., SIEGENTHALER, U. & BIRKS, H.J.B. (1992) Late-glacial climatic oscillations as recorded in Swiss lake sediments. *Journal of Quaternary Science*, 7, 187-204.

LOWE, J.J. & WALKER, M.J.C. (1997) Reconstructing Quaternary Environments: Second Edition. *Essex, Longman.*

LUMBY, J.H. (1939) Norris Papers. *Record Society of Lancashire and Cheshire*, 93, 1-289.

MACDONALD, K. & YOUNG, M. (2007) *The UK oil industry over the past 100 years. Special Feature- UK Oil Industry.* http://www.berr.gov.uk/files/file43856pdf [accessed 19th August 2010].

MACKERETH, F.J.H. (1966) Some chemical observations on post-glacial lake sediments. *Philosophical Transactions of the Royal Society: biological sciences*, 250, 165-213.

MADDEN, E.F. & FOWLER, B.A. (2000) Issues in risk assessment of chemicals of concern to department of defence and other agencies session. Mechanisms of nephrotoxicity from metal combinations: a review. *Drug and Chemical Toxicology*; 23, 1-12.

MAHER, B. A. (1986) Characterisation of soils by mineral magnetic measurements. *Physics of Earth and Planetary Interiors*, 42, 76-92.

MAHER, B.A. & THOMPSON, R. (1999) Climates, Environments and Magnetism. *Cambridge, Cambridge University Press.*

MAHER, B.A., THOMPSON, R. & HUNSLOW, M.W. (1999) Introduction to Quaternary climates, environments and magnetism. IN MAHER, B.A. & THOMPSON, R. (Eds.) Quaternary climates, environments and magnetism. *Cambridge, Cambridge University Press.* pp. 1-48.

(MALVERN INSTRUMENTS) *Transfer of methods from the Mastersizer W and Mastersizer X to the Mastersizer 2000.* http://malver.co.uk/Malvern/kbase.nsf/albino/KB000485/pfile/MRK525-01%20_Method%20Transfer_pdf [accessed 21/06/2006].

MAMANE, Y., MILLER, J.L. & DZUBAY. T.G. (1986) Characterisation of individual fly ash particles emitted from coal and oil fired power plants. *Atmospheric Environment,* 20, 2125-2135.

MANTA, D.S., ANGELONE, M., BELLANCA, A., BERI, R. & SPROVIERI, M. (2002) Heavy metals in urban soils: a case study from the city of Palermo (Sicily), Italy. *The Science of the Total Environment,* 300, 229-243.

MATTHIAS, A.D. & BOHN, H.L. (1996) Physical processes affecting atmospheric pollution. IN PEPPER, I.L., GERBA, C.P. & BRUSSEAU, M.L. (Eds.) Pollution Science. *London, Academic Press.* pp. 19-30.

MATZKA, J. & MAHER, B.A. (1999) Magnetic biomonitoring of roadside tree leaves: identification of spatial and temporal variations in vehicle-derived particulates. *Atmospheric Environment,* 33, 4565-4569.

MAYNARD, R. (2004) Key airborne pollutants- the impacts on health. *Science of the Total Environment,* 334-335, 9-13.

MCCALLY, M. (2002) Life support: the Environment and Human Health. *Cambridge, MIT Press.*

McCAVE, I.N. & SYVITSKI, J.P.M. (1991) Principles and Methods of Geological Particle Size Analysis. IN SYVITSKI, J.P.M. (Ed.) Principles, Methods, and Application of Particle Size Analysis. *Cambridge, Cambridge University Press.*

MCELROY, M.W.M., CARR, R.C., ENSOR, D. & MARKOWSKI, G.R. (1982) Size distribution of fine particles from coal combustion. *Science,* 215, 13-19.

MCLEAN, D. (1991) Magnetic spherules in recent lake sediments. *Hydrobiology,* 214, 91-97.

MEADE, M., FLORIN, J. & GESLER, W. (1988) Medical Geography. *London, The Guilford Press.*

MEHARG, A.A. & KILLHAM, K. (2003) A pre-industrial source of dioxins and furans. *Nature,* 421, 909-910.

MEIJ, R. (1995) The distribution of trace elements during combustion of coal. IN SWAINE, D.J. & GOODARZI, F. (Eds.) Energy and environment: environmental aspects of trace elements in coal. *London, Kluwer Academic Publishers.* pp. 111-127.

MERILÄINEN, J.J., HNYNEN, J., PALOMÄKI, A., MÄNTYKOSKI, K. & WITICK, A. (2003) Environmental history of an urban lake: a palaeolimnological study of Lake Jyväsjärvi, Finland. *Journal of Paleolimnology,* 30, 387-406.

MEYERS, P.A. & TERANES, J.L. (2001) Sediment organic matter. IN LAST, W.M. & SMOL, J.P. (Eds) Tracking environmental change using lake sediments. *London, Kluwer Academic Publishers.* pp. 239-269.

MIGHALL, T.M., ABRAHAMS, P.W., GRATTAN, J.P., HAYES, D., TIMBERLAKE, S. & FORSYTH, S. (2002) Geochemical evidence for atmospheric pollution derived from prehistoric copper mining at Copa Hill, Cwmystwyth, mid-Wales, UK, *Science of the Total Environment,* 292 69-80.

MILKO, S., MESIĆ, S., PROHIĆ, E. & PEH, Z. (2003) Trace element distribution in surface sediemnts of Lake Vrana and topsoil of Cres Island, Croatia. *Natura Croatica*, 12, 93-111.

MINGRAM, J. ALLEN, J.R.M., BRÜCHMANN, C., LIU, J., LUO, X., NEGENDANK, J.F.W., NOWACZYK, N. & SCHETTLER, G. (2004) Maar- and crater lakes of the Long Gang Volcanic Field (N.E. China) – overview, laminated sediments and vegetation history of the last 900 years. *Quaternary International*, 123-125, 135-147.

MOHOROVIC, L. (2004) First two months of pregnancy – critical time for pre-term delivery and low birth weight caused by adverse effects of coal combustion toxics. *Early Human Development.*, 80, 115-123.

MORAWSKA, L. & ZHANG, J. (2002) Combustion sources of particles.1: health relevance and source signatures. *Chemosphere*, 49, 1045-1058.

MORAWSKA, L., BOFINGER, N.D., KOCIS, L. & NWANKWOALA, A. (1998) Submicron and supermicron particles from diesel vehicle emissions. *Environmental Science and Technology*, 32, 2033-2042.

MORENO, E., SAGNOTTI, L., DINARÈS-TURELL, J., WINKLER, A. & CASCELLA, A. (2003) Biomonitoring of traffic air pollution in Rome using magnetic properties of tree leaves. *Atmospheric Environment*, 37, 2967-2977.

MORRIS, W.A., VERSTEEG, J.K., BRYANT, D.W., LEGZDINS, A.E., MCCARRY, B.E. & MARVIN, C.H. (1995) Preliminary comparisons between mutagenicity and magnetic susceptibility of respirable airborne particulate. *Atmospheric Environment*, 29, 3441-3450.

MUKHOPADHYAY, K. & FORSSELL, O. (2005) An empirical investigation of air pollution from fossil fuel combustion and its impact on health in India during 1973-1974 to 1996-1997. *Ecological Economics*, 55, 235-250.

MUXWORTHY, A. R. (2001) Effect of grain interactions on the frequency dependence of magnetic susceptibility. *Geophysical Journal International*, 144, 441-447.

MUXWORTHY, A.R., MATZKA, J. & PETERSEN, N. (2001) Comparison of magnetic parameters of urban atmospheric particulate matter with pollution and meteorological data. *Atmospheric Environment*, 35, 4379-4386.

MUXWORTHY, A.R., MATZKA, J., DAVILA, A.F. & PETERSEN, N. (2003) Magnetic signature of daily sampled atmospheric particulates. *Atmospheric Environment*, 37, 4163-4169.

MUXWORTHY, A.R., SCHMIDBAUER, E. & PERETSON, N. (2002) Magnetic properties and Mössbauer of urban atmospheric particulate matter: a case study from Munich, Germany. *Geophysical Journal. International*, 150, 558-570.

NAGEOTTE, S.M. & DAY, J.P. (1998) Lead concentrations and isotope ratios in street dusts determined by electrothermal atomic absorption spectrometry and inductively coupled plasma mass spectrometry. *The Analyst*, 123, 59-62.

NATIONAL RIVERS AUTHORITY. (1995). *The Mersey Estuary: a Report on Environmental Quality*. Water Quality Series No. 23. National Rivers Authority, Bristol.

(NATIONAL STATISTICS) (2002) *Road Traffic, 1951-1998: social trends 30*. Office for National Statistics. http://www.statistics.gov.uk/statbase/xsdataset.asp [accessed 14/09/2009].

(NATIONAL STATISTICS) (2008) *Transport Trends*. London, Department for Transport. http://www.dft.gov.uk/pgr/statistics/databasepublications/trends [accessed 14/09/2009].

NG, S.L. & KING, R.H. (2004) Geochemistry of lake sediments as a record of environmental change in a high Artic watershed. *Chemie der Erde*, 64, 257-275.

NICHOLSON, S.M. (1983) Farming at Speke Hall 1066-1795. *Merseyside Archaeological Society Journals*, 3.

NICKSON, C. (1887) History of Runcorn. *London, Mackie & Co.*

NORTON, S.A. (1986) A review of the chemical record in lake sediment of energy related air pollution and its effects on lakes. *Water, Air and Soil Pollution*, 30, 331-345.

NORTON, S.A., BIENERT, R.W., BINFORD, M.W.JR. & KAHL, J.S. (1992) Stratigraphy of total metals in PIRLA sediment cores. *Journal of Palaeolimnology*, 7, 191-214.

NOWIERSKI, M., DIXON, D.G. & BORGMANN, U. (2006) Lac Dufault sediment core trace metal distribution bioavailability and toxicity to *Hyalella azteca*. *Environmental Pollution*, 139, 532-540.

NRIAGU, J.O. & COKER, R.D. (1980) Trace metals in humic and fulvic acids from Lake Ontario sediments. *Environmental Science and Technology*, 14, 443-446.

O'NEIL, M.S., JERRETT, M., KAWACHI, I., LEVY, J.I., COHEN, A.J., GOUVEIA, N., WILKINSON, P., FLETCHER, T., CIFUENTES, L., SCHWARTZ, J. (2003) Health, wealth and air pollution: advancing theory and methods. *Environmental Health Perspectives*, 111, 1861-1870.

OBERDÖRSTER, G. (2000) Toxicology of ultrafine particles: *in vivo* studies. *Philosophical Transactions of the Royal Society. London A*, 358, 2719-2740.

OLDFIELD, F. & APPLEBY, P.G. (1984) Empirical testing of ^{210}Pb-dating models for lake sediments. IN HAWORTH, E.Y. & LUND, J.W.G. Lake Sediments and Environmental History. *Leicester, Leicester University Press*. pp. 93-124.

OLDFIELD, F. & APPLEBY, P.G. (1985) The role of 210Pb dating in sediment based erosion studies. IN LOUGHRAN, R.L., SOIL CONSERVATION SERVICE OF NEW SOUTH WALES & UNIVERSITY OF NEWCASTLE (N.S.W). Drainage basin erosion and sedimentation. *New South Wales, University of Newcastle*. pp. 175-182.

OLDFIELD, F. & RICHARDSON, N. (1990(a)) Lake sediment magnetism and atmospheric deposition. *Phil. Trans. Royal Society London*, 327, 325-330.

OLDFIELD, F. & RICHARDSON, N. (1990(b)) Peats and lake sediments: formation, stratigraphy, description and nomenclature IN GOUDIE, A., ANDERSON, M., BURT, T., LEWIN, J., RICHARDS, K., WHALLEY, B. & WORSLEY, P. Geomorphological Techniques (2nd edition). *Cambridge, Unwin Hyman Ltd*. pp 496-528.

OLDFIELD, F. & WU, R. (2000) The magnetic properties of the recent sediments of Brothers Water, N W England. *Journal of Paleolimnology*, 23, 165-174.

OLDFIELD, F. & YU, L. (1994) The influence of particle size variations on the magnetic properties of sediments from the north-eastern Irish Sea. *Sedimentology*, 41, 1093-1108.

OLDFIELD, F. (1981) History of particulate atmospheric pollution from magnetic measurements in dated Finnish peat profiles. *Ambio*, 10, 185-188.

OLDFIELD, F. (1990) Magnetic measurements of recent sediments from Big Moose Lake, Adirondack Mountains, N.Y., USA. *Journal of Paleolimnology*, 4, 93-101.

OLDFIELD, F. (1991) Environmental magnetism - personal perspective. *Quaternary Science Reviews*, 10, 73-83.

OLDFIELD, F. (1994) Toward the discrimination of fine-grained ferrimagnets by magnetic measurements in lake and near-shore marine sediments. *Journal of Geophysical Research*, 99, 9045-9050.

OLDFIELD, F. (1999) Environmental Magnetism; the range of applications. IN WALDEN, J., OLDFIELD, F., & SMITH, J.P. (Eds.). Environmental Magnetism: a practical guide. Technical Guide No. 6. *London, Quaternary Research Association.*

OLDFIELD, F. (2007) Sources of fine-grained magnetic minerals in sediments: a problem revisited. *The Holocene*, 17, 8, 1265-1271.

OLDFIELD, F., APPLEBY, P. G. & VAN DER POST, K. D. (1999) Problems of core correlation, sediment source ascription and yield estimation in Ponsonby Tarn, West Cumbria, UK. *Earth Surface Processes and Landforms*, 24, 975-992.

OLDFIELD, F., ASIOLI, A., ACCORSI, C.A., MERCURI, A.M., JUGGINS, S., LANGONE, L., ROLPH, T., TRINCARD, F., WOLFF, G., GOBBS, Z., VIGLIOTTI, L., FRIGNANI, M., VAN DER POST, K. & BRANCH, N. (2003) A high resolution late Holocene palaeoenvironmental record from the central Adriatic Sea. *Quaternary Science Reviews*, 22, 319-342.

OLDFIELD, F., BARNOSKY, C., LEOPOLD, E.B. & SMITH, J.P. (1983) Mineral magnetic studies of lake sediments. *Hydrobologia*, 103, 37-44.

OLDFIELD, F., DARNLEY, I., YATES, G., FRANCE, D. E. & HILTON, J. (1992) Storage diagenesis versus sulphide authigenesis: possible implications in environmental magnetism. *Journal of Palaeolimnology*, 7, 179-189.

OLDFIELD, F., HUNT, A., JONES, M.D.H., CHESTER, R., DEARING, J.A., OLSSON, L. & PROSPERO, J.M. (1985) Magnetic differentiation of atmospheric dusts. *Nature*, 317, 516-518.

OLDFIELD, P. (*Pers. Comm.*) Email from Paul Oldfield, Ecologist at Halton Borough Council, regarding management of pond sites in Halton (06/01/2005) paul.oldfield@halton-borough.gov.uk.

OLIVER, B.B., CHARLTON, M.W. & DURHAM, R.W. (1989) Distribution, redistribution and geochronology of polychlorinated biphenyl congers and other chlorinated hydrocarbons in Lake Onatrio sediments. *Environmental Science and Technology*, 23, 200-208.

OLIVEIRA, S.M.B., PESSENDA, L.C.R., GUOVEIA, A.E.M., BABINSKI, M. & FAVARO, D.I.T. (2009) A geochemical and lead isotope record from a small pond in a remote equatorial island, Fernando de Noronha, Brazil. *The Holocene*, 19, 469-448.

OLSSON, I.U. (1986) Radiometric Dating. IN BERGLUND, B.E. Handbook of Holocene Palaeoecology. *Chichester, John Wiley & Sons Ltd.* pp. 273-312.

PACYNA, E.G., PACYNA, J.M., FUDALA, J., STRZELECKA-JASTRZAB, E., HLAWICZKA, S., PANASIUK, D., NITTER, S., PREGGER, T., PFEIFFER, H. & FRIEDRICH, R. (2007) Current and future emissions of selected heavy metals to the atmosphere from anthropogenic sources in Europe. *Atmospheric Environment,* 41, 8557-8566.

PACYNA, J.M. & PACYNA, E.G. (2001) An assessment of global and regional emissions of trace metals to the atmosphere from anthropogenic sources worldwide *Environmental Reviews*, 30, 269-298.

PALMGREN, F., HANSEN, A.B., BERKOWICZ, R. & SKOV, H. (2001) Benzene emission from the actual car fleet in relation to petrol composition in Denmark. *Atmospheric Environment*, 35, S35-S42.

PARODI, S., S.E., CASELLA, C., PUPPO, A., DAMINELLI, E., FONTANA, V., VALERIO, F. & VERCELLI, M. (2005) Lung cancer in an urban area in Northern Italy near a coke oven plant. *Lung Cancer,* 47, 155-164.

PEGLAR, S.M. (1998) The Mid-Holocene *Ulmus* decline at Diss Mere, Norfolk, UK: a year-by-year pollen stratigraphy from annual laminations. *The Holocene 3*1, 1-13.

PELED, R., FRIGER, M., BOLOTIN, A., BIBI, H., EPSTEIN, L., PILPEL, D. & SCHARF, S. (2005) Fine particles and meteorological conditions are associated with lung function in children with asthma living near two power plants. *Public Health,* 199, 418-425.

PENG, C., WU, X., LIU, G., JOHNSON, S. AND GUTTIKUNDA, S. (2002) Urban air quality and health in China. *Urban Studies,* 39, 2283-2300.

PENTTINEN, P., ALM, S., RUUSKANEN, J. AND PEKKANEN, J. (2000) Measuring reflectance of TSP-filters for retrospective health studies. *Atmospheric Environment*, 34, 2581-2586.

PETERS, A., SKORKOVSKY, J., KOTESOVEC.F., BRYNDA, J., SPIX, C., WICHMANN, H.E., & HEINRICH, J. (2000) Associations between mortality and air pollution in central Europe. *Environmental Health Perspectives,* 108, 283-287.

PETERS, C. & DEKKERS, M. J. (2003) Selected room temperature magnetic parameters as a function of mineralogy, concentration and grain size. *Physics and Chemistry of the Earth*, 28, 659-667.

PETROVSKỲ, E. & ELWOOD, B.B. (1999) Magnetic monitoring of air- land- and water-pollution. IN MAHER, B.A. & THOMPSON, R. Quaternary Climates, Environments and Magnetism. *Cambridge, Cambridge University Press*. pp. 279-231.

PETROVSKÝ, E., KAPIČKA, A., JORDANOVA, N. & BORŮVKA, L. (2001) Magnetic properties of alluvial soils contaminated with lead, zinc and cadmium. *Journal of Applied Geophysics,* 48, 127-136.

PETROVSKỲ, E., KAPIČKA, A., JORDANOVA, N., KNAB, M. & HOFFMAN, V. (2000) Low-field magnetic susceptibility: a proxy method of estimating increased pollution of different environmental systems. *Environmental Geology*, 39, 312-318.

PHALEN, R.F. (2002) The particulate air pollution controversy: a case study and lessons learned. *London, Kluwer Academic Publishers.*

PHILLIPOTS, G. & COHEN, D (2004) *National Statistics region in figures: northwest.* http://www.statistics.gov.uk/download/theme_compendia/region_in_figures_winter04/North_West.pdf [accessed 29/01/2005].

PIGOT & CO. (1828-1829) Directory of Cheshire, Cumberland, Derbyshire, Durham, Lancashire, Lincolnshire and Northumberland. *London and Manchester, Pigot.* pp. 49-51.

PIGOT & CO. (1834) Commercial Directory for the country of Cheshire *London and Manchester, Pigot.* pp. 52-55.

PIRRONE, N., ALLEGRINI, I., KELLER, G.J., NRIAGU, J.O., ROSSMANN, R. & ROBBINS, J.A. (1998) Historical atmospheric mercury emissions and deposits in North America compared to mercury accumulations in sedimentary records. *Atmospheric Environment,* 5, 929-940.

PLATER, A. J. & APPLEBY, P. G. (2004) Tidal sedimentation in the Tees Estuary during the 20th century: radionuclide and magnetic evidence of pollution and sedimentary response. *Estuarine, Coastal and Shelf Science*, 60, 179-192.

PLATER, A.J., RIDGWAY, J., APPLEBY, P.G., BERRY, A. & WRIGHT, M.R. (1998) Historical contaminant fluxes in the Tess Estuary, UK: geochemical, magnetic and radionuclide evidence. *Marine Pollution Bulletin,* 37, 343-360.

PLESS-MULLOLI, T., PHILLIMORE, P., MOFFATT, S., BHOPAL, R., FOY, C., DUNN, C. & TATE, J. (1998) Lung cancer, proximity to industry and poverty in Northeast England. *Environmental Health Perspectives*, 106, 1–8.

POOLE, C. (1906) Old Widnes and its neighbourhood. *Widnes, Swale.*

POPE III, C.A. (1989) Respiratory disease associated with community air pollution and a steel mill, Utah Valley. *American Journal of Public Health*, 79,623-628.

POPE III, C.A., BURNETT, R.T., THUN, M.J., CALLE, E.E., KREWSKI, D., ITO, K. & THURSTON, G.D. (2002). Lung cancer, cardiopulmonary mortality, and long-term exposure to fine particulate air pollution. *Journal of the American Medical Association*, 287, 1132-1141.

POPE III, C.A., BATES, D.V., RAIZENNE, M.E. (1995) Health effects of particulate air pollution: time for reassessment? *Environmental Health Perspectives*, 103, 472-480.

POWER, A. L., WORSLEY, A.T. & BOOTH, C.A. (2009) Magneto-biomonitoring of intra-urban spatial variations of particulate matter using tree leaves. *Environmental Geochemistry and Health*, 31, 315-325.

POWER, A.L., WORSLEY, A.T., BOOTH, C.A. & FARR, K.M. (2006) Preliminary insights of magneto-biomonitoring (Tilia europaea and Acer pseudoplatanus) as an alternative roadside particulate air pollution technology. IN LONGHURST, J.W.S & BREBBIA, C.A. (Eds.) Air Pollution XIV. *Southampton, WIT Press.* pp. 525-534.

POZZA, M.R., BOYCE, J.I. & MORRIS, W.A. (2004) Lake-based magnetic mapping of contaminated sediment distribution, Hamilton Harbour, Lake Ontario, Canada. *Journal of Applied Geophysics*, 57, 323-41.

PUFFER, J.H., RUSSEL, E.W.B. & RAMPINO, M.R. (1980) Distribution and origin of magnetite spherules in air, waters and sediments of the Greater New York city area and the North Atlantic Ocean. *Journal of Sedimentary Petrology,* 50, 247-256.

PUNNING, J-M., LIBLIK, V. & ALLIKSAAR, T. (1997) History of fly-ash emissions and palaeorecords of atmospheric deposition in the oil shale combustion area. *Oil Shale*, 14, 347-362.

PUNNING, M-J., BOYLE, J.F., TERASMAA, J., VAASMA, T. & MIKOMÄGI, A. (2007) Changes in lake-sediment structure and composition caused by human impact: repeated studies of Lake Martiska, Estonia. *The Holocene*, 17, 145-151.

QUALITY OF URBAN AIR GROUP, (1993) *Urban air quality in the United Kingdom.* (First report of the Urban Air Review Group). London, Department of the Environment.

RAINHAM, D.G.C., SMOYER-TOMIC, K.E., SHEVIDAN, S.C. & BURNETT, R.T. (2005) Synoptic weather patterns and modification of the association between air pollution and human mortality. *International Journal of Environmental Health Research*, 15, 347-360.

RALOFF, J. (2003) Air sickness: how microscopic dust particles cause subtle but serious harm. *Science News,* 164, 72-75.

RENBERG, I. & WIK, M. (1984) Dating recent lake sediments by soot particulate counting. *Verh.Internat. Verin. Limnol,* 22, 712-718.

RENBERG, I. &WIK, M. (1995) Soot particle counting in recent lake sediments: an indirect dating method. *Ecological Bulletins*, 37, 53-57.

RENBERG, I. (1986) Concentration and annual accumulation values of heavy metals in lake sediments: their significance in studies of the history of heavy metal pollution. *Hydrobiologia*, 143, 379-385.

RENBERG, I., BINDLER, R. & BRÄNNVALL, M-L. (2001) Using the historical atmospheric lead-deposition record as a chronological marker in sediment deposits in Europe. *The Holocene*, 11, 511-516.

REVICH, B., ASKEL, E., USHAKOVA, T., IVANOVA, I., ZHUCHENKO, N., KLYUEV, N., BRODSKY, B. & SOTSKOV, Y. (2001) Dioxin exposure and public health in Chapaevsk, Russia. *Chemosphere*, 43, 951-966.

RICHARDSON, N. (1986) The mineral magnetic record in recent ombriotrophic peat synchronised by fine resolution pollen analysis. *Physics of the Earth and Planetary Interiors*, 42, 48-56.

RICHARDSON, N. (Pers. Comm.) Conversation with Nigel Richardson (Edge Hill University) regarding calculation of magnetic flux (04/02/2009).

RINTOUL, G. (1984) *Chemical Manufacture in Runcorn and Weston 1800-1930.* http://www.catalyst.org.uk [accessed 02/08/07]

ROBERTS, N. (1989) The Holocene: an environmental history. *New York, Blackwell.*

ROBERTSON, D.J., TAYLOR, K.G. & HOON, S.R. (2003) Geochemical and mineral magnetic characterisation of urban sediment particulates, Manchester, UK. *Applied Geochemistry*, 18, 269-282.

ROBERTSON, D.J. & TAYLOR, K.G. (2007) Temporal variability of metal contamination in urban-deposited Manchester UK: Implications for urban pollution monitoring. *Water, Air and Soil Pollution,* 186, 209-220.

ROBINSON, S.G. (1986) The late Pleistocene palaeoclimatic record of North Atlantic deep-sea sediments revealed by mineral-magnetic measurements. *Physics of the Earth and Planetary Interiors*, 42, 22-47.

ROLPH, T.C., OLDFIELD, F. & VAN DER POST, K.D. (1996) Palaeomagnetism and rock-magnetism results from Lake Albano and the central Adriatix Sea (Italy). IN GUILIZZONI, P. & OLDFIELD, F. (Eds.) Palaeoenvironmental analysis of Intalioan crater lake and Adriatic sediments. *Memorie dell'Istituto Italiano di Idrobiologia*, 55, 265-283.

ROLPH, T.C., VIGLIOTTI, L., & OLDFIELD, F. (2004) Mineral magnetism and geomagnetic secular variation of marine and lacustrine sediments from central Italy: timing and nature of local and regional Holocene environmental change. *Quaternary Science Reviews*, 23, 1699-1722.

ROMIEU, I., MENSES, F., RUIZ, S., SIENRA, J.J., HUERTA, J., WHITE, M.C. & ETZEL, R.A. (1996) Effects of air pollution on the respiratory health of asthmatic children living in Mexico City. *American Journal of Respiratory and Critical care Medicine*, 154, 300-307.

ROSE, N.L. & MONTEITH, D.T. (2004) Temporal trends in spheroidal carbonaceous particle deposition derived from annual sediment traps and lake sediment cores and their relationship with non-marine sulphate. *Environmental Pollution*, 137, 151-163.

ROSE, N.L., BOYLE, J.F., DU, Y., YI, C., DAI, X., APPLEBY, P.G BENNION, H., CAI, S. & YU, L. (2004(b)) Sedimentary evidence for changes in the pollution status of Taihu in the Jiangsu region of eastern China. *Journal of Paleolimnology*, 32, 41-51.

ROSE, N.L., HARLOCK, S. & APPLEBY, P.G. (1999) Within-basin profile variability and cross correlation of lake sediment cores using the spheroidal carbonaceous particle record. *Journal of Paleolimnology,* 21, 85-96.

ROSE, N.L. & HARLOCK, S. (1998) The spatial distribution of characterized fly-ash particles and trace metals in lake sediments and catchment mosses in the United Kingdom. *Water, Air and Soil Pollution,* 106, 287-308.

ROSE, N.L. (1990) A method for the extraction of carbonaceous particles from lake sediments. *Journal of Paleolimnology,* 3, 45-53.

ROSE, N.L. (1994(a)) A note on further refinements to a procedure for the extraction of carbonaceous fly-ash particles from sediments. *Journal of Paleolimnology*, 11, 201-204.

ROSE, N.L. (1994(b)) Characterisation of carbonaceous particles from lake sediments. (Proceedings of the international symposium "Limnology of mountain lakes" Stara Lesna, Czechoslovakia. July 1-7, 1991) *Hydrobiologia,* 274, 127-132.

ROSE, N.L. (1995) The carbonaceous particle record in lake sediments from the Arctic and other remote areas of the northern hemisphere. *The Science of the Total Environment,* 160/161, 487-496.

ROSE, N.L. (1996) Inorganic fly-ash spheres as pollution tracers. *Environmental Pollution,* 91, 245-252.

ROSE, N.L. (2001) Fly-ash particles. IN LAST, W.M.& SMOL, J.P. (Eds.) Tracking environmental change using lake sediments. Volume 2: Physical and Geochemical methods. *Dordrecht, The Netherlands, Kluwer Academic Publishers.*

ROSE, N.L. JUGGINS, S. & WATT, J. (1999(a)) The characterisation of carbonaceous fly-ah particles from major European fossil-fuel types and applications to environmental samples. *Atmospheric Environment,* 33, 2699-2713.

ROSE, N.L., ALLIKSAAR, T., BOWMAN, J.J., FOTT, J., HARLOCK, S., PUNNING, J.M., ST.CLAIR-GRIBBLE, K., VUKIC, J. & WATT, J. (1998(a)) The FLAME project: general discussion and conclusions. *Water, Air and Soil Pollution,* 106, 329-351.

ROSE, N.L., ALLIKSAAR, T., BOWMAN, J.J., FOTT, J., HARLOCK, S., PUNNING, J.M., ST. CLAIR-GRIBBLE, K., VUKIC, J. & WATT, J. (1998(b)) The FLAME research project: introduction and methods. *Water, Air and Soil Pollution,* 106, 205-218.

ROSE, N.L., APPLEBY, P.G., BOYLE, J.F., MACKAY, A.W. & FLOWER, R.J. (1998(c)) The spatial and temporal distribution of fossil-fuel derived pollutants in the sediment record of Lake Baikal, eastern Siberia. *Journal of Palaeolimnology*, 20, 151-162.

ROSE, N.L., HARLOCK, S. & APPLEBY, P.G. (1999(b)) The spatial and temporal distributions of spheroidal carbonaceous fly-ash particles (SCP) in the sediment record of European mountain lakes. *Water, Air and Soil Pollution,* 113, 1-32.

ROSE, N.L., HARLOCK, S., APPLEBY, P.G. & BATTARBEE, R.W. (1995) Dating of recent lake sediments in the United Kingdom and Ireland using spheroidal carbonaceous particle (SCP) concentration profiles. *The Holocene,* 5, 328-335.

ROSE, N.L., JUGGINS, S. & WATT, J. (1996) Fuel-type characterisation of carbonaceous fly-ash particles using EDS-derived surface chemistries and its application to particles extracted from lake sediments. *Proceedings of the Royal Society of London (Series A),* 452, 881-907.

ROSE, N.L., JUGGINS, S., WATT, J. & BATTARBEE, R.W. (1994 (c)) Fuel-type characterisation of spheroidal carbonaceous particles using surface chemistry. *Ambio,* 23, 296-299.

ROSE, N.L., ROSE, C.L., BOYLE, J.F. & APPLEBY, P.G. (2004(a)) Lake sediment evidence for local and remote sourced of atmospherically derived pollutants in Svalbard. *Journal of Paleolimnology*, 31, 499-513.

ROSE, N.L., SHILLAND, E., YANG, H., BERG, T., CAMERERO, L., HARRIMAN, R., KOINIG, K., LIEN, L., NICKUC, U., STUCHLIK, E., THEIS, H. & VENTURA, M. (2002) Deposition and storage of spheroidal carbonaceous fly-ash particulates in European mountain lake sediments and catchment soils. *Water, Air and Soil Pollution: Focus*, 2, 251-260.

ROUND, F.E. (1990) Diatom communities- their response to changes in acidity. IN THE ROYAL SOCIETY. Palaeolimnology and lake acidification. *Cambridge, University Press.* pp. 17-23.

RUIZ-FERNÁNDEZ, A.C., PÁEZ-OSUNA, F., URRUTIA-FUCUGAUCHI, J. & PREDA, M. (2005) ^{210}Pb geochronology of sediment accumulation rates in Mexico City Metropolitan Zone as recorded at Espejo de los Livios lake sediments. *Catena*, 61, 31-48.

(RUNCORN & DISTRICT HISTORIC SOCIETY) *Runcorn: a historical sketch. Runcorn & District Historical Society.* http://www.runcornhistsoc.org.uk/runcorn_historical_sketch.html [accessed 30/03/2006].

SACK, D. (2001) Shoreline and basin configuration techniques in paleolimnology. IN LAST, W.M. & SMOL, J.P. (Eds.) Tracking environmental change using lake sediments. *Dordrech, The Netherlands, Kulwer.* pp. 49-71.

SAGER, M. (1993) Determination of arsenic, cadmium, mercury, stibium, thallium and zinc in coal and coal fly-ash. *Fuel,* 72, 1327-1330.

SAINSBURY, P., HUSSEY, R., ASHTON, J. & ANDREWS, B. (1996) Industrial atmospheric pollution, historical land use patterns and mortality. *Journal of Public Health Medicine,* 18, 87-93.

SANDERS, G., JONES, K.C. & HAMILTON-TAYLOR, J. (1995) PCB and PAH fluxes to a dated UK peat core. *Environmental Pollution,* 89, 17-25.

SANDERS, G., JONES, K.C., HAMILTON-TAYLOR, J. & DOERR, H. (1992) Historical inputs of polychlorinated biphenyls and other organochlorines to a dated lacustrine sediment core in rural England. *Environmental Science and Technology,* 26, 1815-1821.

SANDGREN, P. & SNOWBALL, I. (2001) Application of mineral magnetic techniques to paleolimnology. IN LAST, W.M. & SMOL, J.P. (Eds) Tracking environmental change using lake sediments. *London, Kluwer Academic Publishers.* pp. 217-237.

SANTSCHI, P.H., NIXON, S., PILSON, M. & HUNT, C. (1984) Accumulation of sediments, trace metals, (Pb, Cu) and total hydrocarbons in Narragansett Bay, Rhode Island. *Estuarine, Coastal and Shelf Science,* 19, 427-449.

SCHÄDLICH, G., WEIßFLOG, L. & SCHÜÜRMANN, G. (1995) Magnetic susceptibility in conifer needles as indicators of fly ash deposition. *Fresenius Environmental Bulletin,* 4, 7-12.

SCHMELING, M. (2004) Characterization of urban air pollution by total reflection x-ray florescence. *Spectrochimica Acta Part B,* 59, 1165-1171.

SCHOLGER, R. (1997) Magnetic susceptibility as a tool for mapping of heavy metal contamination of sediments and soils: case study from Styria, Austria. *Annals of Geophysics.* abstract 2, supplement 1, part 1, pp. C105.

SCHOLGER, R. (1998) Heavy metal pollution monitoring by magnetic susceptibility measurements applied to sediments of the river Mur (Styria, Austria). *European Journal of Environmental Geophysics and Engineering,* 3, 25-37.

SCHWARTZ, J. (1993) Particulate air pollution and chronic respiratory disease. *Environmental Research,* 62, 7-13.

SCHWARTZ, J. (1996) Air pollution and hospital admissions for respiratory disease. *Epidemiology,* 7, 20-28.

SCOULLOS, M. & OLDFIELD, F. (1979) Magnetic monitoring of marine particulate pollution in the Elefsis Gulf, Greece. *Marine Pollution Bulletin,* 10, 287-291.

SHI, J-B., IP, C.C.M., TANG, C.W.Y., ZHANG, G., WU, R.S.S. & LI, X-D. (2007) Spatial and temporal variations of mercury ion sediments from Victoria Harbour, Hong Kong. *Marine Pollution Bulletin,* 54, 464-488.

SHILTON, V. F., BOOTH, C. A., SMITH, J. P., GIESS, P., MITCHELL, D. J. & WILLIAMS, C. D. (2005) Magnetic properties of urban street dust and their relationship with organic matter content in the West Midlands, UK. *Atmospheric Environment,* 39, 3651-3659.

SHU, J., DEARING, J.A., MORSE, A.P., YU, L. & YUAN, N. (2001) Determining the sources of atmospheric particles in Shanghai, China, from magnetic and geochemical properties. *Atmospheric Environment,* 35, 2615-2625.

SHU. J., DEARING, J.A., MORSE, A.P., YU, L.Z. & LI, C.Y. (2000) Magnetic properties of daily sampled total suspended particulates in Shanghai. *Environmental Science and Technology,* 34, 2393-2400.

SIOUTAS, C., DELFINO, R.J. & SINGH, M. (2005) Exposure assessment for atmospheric ultrafine particulates (UFPs) and implications in epidemiology research. *Environmental Health Perspectives,* 113, 947-955.

SMITH, J. P. (1999) An introduction to the magnetic properties of natural materials. IN WALDEN, J., OLDFIELD, F. & SMITH, J. P. (Eds.) Environmental Magnetism: a practical guide. *London, QRA Technical Publication.* pp. 5-25.

SMITH, K.R. (1993) Fuel combustion, air pollution exposure and health: the situation in developing countries. *Annual Review of Energy and the Environment,* 18, 529-566.

SMOL, J.P. (2002) Pollution of lakes and rivers: a palaeoenvironmental perspective. *London, Arnold Publishers.*

SNOWBALL,I. (1999) Electromagnetic units and their use in environmental magnetic studies. IN WALDEN, J., OLDFIELD, F. & SMITH, J. P. (Eds.) Environmental Magnetism: a practical guide. Technical Guide No. 6. *London, Quaternary Research Association.* pp. 89-112.

SNOWBALL, I. & TORII, M. (1999) Incidence and significance of magnetic iron sulphides in Quaternary sediments and soils. IN MAHER, B.A. & THOMPSON, R. Quaternary Climates, Environments and Magnetism. *Cambridge, Cambridge University Press.* pp. 279-321.

SNOWBALL, I.F. (1994) Bacterial magnetite and magnetic properties of sediments in a Swedish lake. *Earth and Planetary Science Letters,* 126, 129-142.

SOLOVIEVA, N., JONES, V.J., NAZAROVA, L., BROOKS, S.J., BIRKS, H.J.B., GRYTNES, J-A., APPLEBY, P.G., KAUPPILA, T., KONDRATENOK, B., RENBERG, I. & PONOMAREV, V. (2005) Palaeolimnological evidence for recent climate change in lakes from the northern Urals, arctic Russia. *Journal of Paleolimnology,* 33, 463-482.

SPASSOV, S., EGLI, R., NOURGALIEV, D.K. & HANNAM, J. (2004) Magnetic quantification of urban pollution sources in atmospheric particulate matter. *Geophysical Journal International,* 159, 555-564.

SPURNY, K.R. (1996) Chemical mixtures in atmospheric aerosols and their correlation to lung disease and lung cancer occurrence in the general population. *Toxicology Letters,* 88, 271-277.

STAPLES, B., HOWSE, M.L.P., MASON, H. & BELL, G.M. (2003) Land contamination and urinary abnormalities: cause for concern? *Occupational and Environmental Medicine*, 60, 463-467.

STARKEY, H.F. (1981) Schooner Port: Two centuries of Upper Mersey Sail. *Ormskirk, G.W. and A Hesketh.*

STARKEY, H.F., (1990) Old Runcorn. *Halton, Halton Borough Council.*

STEWART, A. (*Pers. Comm.*) Northwest Health Protection Agency. Led field visit around contaminated land in Halton, as part of the Environment and Human Health Conference and Workshop (Society of Environmental Geochemistry and Health) on 06/06/2007, alex.stewart@hpa.org.uk.

STOBART, J. (1996) The spatial organization of a regional economy: central places in northwest England in the early-eighteenth century. *Journal of Historical Geography*, 22, 147-159.

STOCKHAUSEN, H. & ZOLITSCHKA, B. (1999) Environmental changes in 13,000 cal. BP reflected in magnetic and sedimentological properties of sediments from Lake Holzmaar (Germany). *Quaternary Science Reviews*, 18, 913-925.

STONE, R. (2002) Counting the costs of London's killer smog. *Science*, 298, 2106-2107.

STRZYSZCZ, Z. (1993) Magnetic susceptibility of soils in the areas influenced by industrial emissions. IN SHULLIN, R., DESAULES, A., WEBSTER, R. & VON STEIGER, B. Soil monitoring: early detection and surveying of soil contamination and degradation. *Basel, Switzerland, Birkhäuser Verlag.* pp. 255-269.

STRZYSZCZ, .Z. & MAGIERA, T. (1996) The influence of industrial emissions on the magnetic susceptibility of soils in Upper Silesia. *Studia Geophysica et Geodaetica*, 40, 276-286.

STRZYSZCZ, Z., MAGIERA, T. & HELLER, F. (1996) The influence of industrial emissions on the magnetic susceptibility of soils of southern Poland. *Physics and Chemistry of the Earth*, 23, 1127-1131.

SWAINE, D.J. (1995) The formation, composition and utilisation of flyash. IN SWAINE, D.J. & GOODARZI, F. (Eds.) Energy and Environment: environmental aspects of trace elements in coal. *London, Kluwer Academic Publishers*. pp. 204-220.

SZNETER, S. & MOONEY, G. (1998) Urbanization, mortality and the standard f living debate; new estimates of the expectation of life at birth in nineteenth-century British cities. *Economic History Review*, 1, 84-112.

TAYLOR, P.I., NUSBAUM, R.L., FRONABARGER, A.K., KATUNA, M.P., & SUMMER, N. (1996) Magnetic spherules in coastal plain sediments, Sullivan's Island, South Carolina, USA. *Meteoritics and Planetary Science*, 31, 77-80.

THOMPSON, R. & OLDFIELD, F. (1986) Environmental Magnetism. *London, George Allen & Unwin.*

THOMPSON, R. BATTARBEE, R.W., O'SULLIVAN, P.E. & OLDFIELD, F. (1975) Magnetic susceptibility of lake sediments. *Limnology and Oceanography*, 20, 687-698.

THOMPSON, R., BLOEMENDAL, J., DEARING, J. A., OLDFIELD, F., RUMMERY, T. A., STOBER, J. C. & TURNER, G. M. (1980) Environmental applications of magnetic measurements. *Science*, 207, 481-486.

THOMSON, J., DYER, F.M. & CROUDACE, I.W. (2002) Records of radionuclide deposition in two salt marshes in the United Kingdom with contrasting redox and accumulation conditions. *Geochimica et Cosmochimica Acta*, 66, 1011-1023.

TIKKANEN, M., KORHOLA, A., SEPPÄ, H. & VIRKANEN, J. (1997) A long-term record of human impacts on an urban ecosystem in the sediments of Töölönlahti Bay in Helsinki, Finland. *Environmental Conservation*, 24,326-337.

TOLONEN, K.R., HAAPALAHTI, R. & SUKSI, J. (1990) Comparison of varve dated soot ball chronology and lead-210 dating in Finland. IN SAARNISTO, M. & KAHRA, A. (Eds.) Laminated sediments. *Geological Survey of Finland, Special Paper*, 14, 65-75.

TOLONEN, K. & OLDFIELD, F. (1986) The record of magnetic-mineral and heavy metal deposition at Regent Street Bog, Fredriction, New Brunswick,Canada. *Physics of the Earth and Planetary Interiors*, 42, 57-66.

TORO, M., FLOWER, R.J., ROSE, N.L. & STEVENSON, A.C. (1993) The sedimentary record of the recent history in a high mountain lake in central Spain. *Verhandlugen ddes Internationalen Verein Limnologie*, 25, 1108-1112.

TURNER, A. (1999) Diagnosis of chemical reactivity and pollution sources from particulate trace metal distributions in estuaries. *Estuarine, Coastal and Shelf Science*. 48, 177-191.

TYLMANN, W. (2004) Sedimentation rates using 210Pb on the example of morphologically complex lake, Copper Lake Radunskie, north Poland. *Geochronometria*, 23, 21-26.

TYLMANN, W. (2005) Lithological and geochemical record of anthropogenic changes in recent sediments of a small and shallow lake (lake Pusty Staw, northern Poland). *Journal of Paleolimnology*, 33, 313-325.

UK EMISSIONS INVENTORY TEAM (2007) *UK emissions of air pollutants 1970-2005.* http://www/airquality.co.uk/reports/cat07/0801140937_2005_Report_FINAL.pdf [accessed 13/07/2008].

ULLRICH, S.M., ILYUSHCHENKO, M.A., KAMBEROV, I.M. & TANTON, T.W. (2007) Mercury contamination in the vicinity of a derelict chlor-alkali plant. Part I: sediment and water contamination of Lake Balkyldak and the River Irtysh. *Science of the Total Environment*, 381, 1-16.

UN: ECONOMIC AND SOICIAL COUNCIL (2005) *Summary of health risks of particulate matter from long-range transboundary air pollution.* United Nations. http://www/unece.org/env/documents/2005/eb/wg1/EB.AIR.WG1.20051.e.pgf [accessed on 05/08/2008]

(US ENVIRONMENT PROTECTION AGENCY) (2003) *National air quality and emissions trends report.* http://epa.gov/airtredns [accessed 28/03/2004].

(US ENVIRONMENT PROTECTION AGENCY) (2008) *Lead emissions from the use of leaded aviation gasoline in the United States.* http://www.epa.gov/nonroad/aviation/420r08020.pdf [accessed 18th April 2009].

URBAT, M., LEHNDROFF, E. & SCHWARK, L. (2004) Biomonitoring of air quality in the Cologne conurbation using pine needles as a passive sampler – Part 1: magnetic properties. *Atmospheric Environment,* 38, 3781-3792.

VALI, H., FÖRSTER, O., AMARANTIDIS, G. & PETERSEN, N. (1987) Magnetotactic bacteria and their magnetofossils in sediments. *Earth and Planetary Science Letters,* 86, 389-400.

330.

VAN LOON, G.W.T. & DUFFY, S.J. (2005) Environmental chemistry: a global perspective. *Oxford, Oxford University Press.*

VAN METRE, P.C. & CALLENDER, E. (1997) Water-quality trends in White Rock Creek Basin from 1912-1994 identified using sediment cores from White Rock Lake reservoir, Dallas, Texas. *Journal of Paleolimnology,* 17, 239-249.

VARDY, P.I. (2005) *Cleanliness and Godliness.* Runcorn and District Historic Society. www.runcornhistsoc.org.uk [accessed 14/8/07].

VARGAS, V.M.F. (2003) Mutagenic activity as a parameter to assess ambient air quality for protection of the environment and human health. *Mutation Research,* 544, 313-319.

VEDAL, S. (1997) Ambient particles and health: lines that divide. *Air and Waste Management Association,* 47, 551-581.

VERMETTE, S.J., IRVINE, K.N. & DRAKE, J.J. (1991) Temporal variability of the elemental composition in urban street dust. *Environmental Monitoring and Assessment,* 18, 69-77.

VEROSUB, K.L. & ROBERTS, A.P. (1995) Environmental magnetism: past, present and future. *Journal of Geophysical Research,* 100, 2175-2192.

VERSTEEG, J.K., MORRIS, W.A., & RUKAVINA, N.A. (1995) The utility of magnetic properties as a proxy for mapping contamination in Hamilton Harbour sediment. *Journal of Great Lakes and Reservoirs,* 21, 71-83.

VESELÝ, J., ALMQUIST-JACOBSON, H., MILLER, L.M., NORTON, S.A., APPELBY, P., DIXIT, A.S. & SMOL, J.P. (1993) The history and impact of air pollution on Čertovo lake, southwestern Czech Republic. *Journal of Palaeolimnology,* 8, 211-231.

VIDAL, J. (2000) Toxic Shock. *The Guardian.* 11th February.

VINEIS, P., FORASTIERE, F., HOEK, G. & LIPSETT, M. (2004) Outdoor air pollution and lung caner: recent epidemiologic evidence. *International Journal of Cancer,* 111, 647-652.

VINZENTS, P.S., MOLLER, P., SORENSEN, M., KNUDSEN, L.E., HERTEL, O., JENSEN, F.P., SCHIBYE, B. & LOFT, S. (2005) Personal exposure to ultrafine particulates and oxidative DNA damage. *Environmental Health Perspectives,* 113, 1485-1490.

VON GUNTEN, H.R., STRUM, M. & MOSER, R.N. (1997) 200-year record of metals in lake sediments and natural background concentrations. *Environmental Science and Technology*, 31, 2193-2197.

VON KLOT, S., PETERS, A., AALTO, P., BELLADER, T., BERGLIND, N., D'IPPOLITI, D., ELOSUA, R. HORMANN, A., KULMALA, M., LAUKI, T., LOWEL, H., PEKKANEN, J., PICCIOTTO, S., SUNYER, J. & FORASTIERE, F. (2005) Ambient air pollution is associated with increased risk of hospital cardiac readmissions of myocardial infarction survivors in five European cities. *Circulation*, 112, 3073-3079.

WALDEN, J. (1999(b)) Sample collection and preparation. IN WALDEN, J., OLDFIELD, F. & SMITH, J. P. (Eds.) Environmental Magnetism: a practical guide. Technical Guide, No. 6. *London, Quaternary Research Association*. pp. 26-34.

WALDEN, J. (1999(a)) Remanence Measurements. IN WALDEN, J., OLDFIELD, F. & SMITH, J. P. (Eds.) Environmental Magnetism: a practical guide. Technical Guide No. 6. *London, Quaternary Research Association*. pp. 63-84.

WANG, X. & MAUZERALL, D.L. (2006). Evaluating impacts of air pollution in China on public health: implications for future air pollution and energy policies. *Atmospheric Environment*, 40, 1706-1721.

WARREN, K. (1980). Chemical Foundations: The Alkali Industry in Britain to 1926. *Oxford, Clarendon Press*.

WATANABE, T., NARAOKA, H., NISHIMURA, M. & KAWAI, T. (2004) Biological and environmental changes in Lake Baikal during the late Quaternary inferred from carbon, nitrogen and sulfur isotopes. *Earth and Planetary Science Letters*, 222, 285-299.

WEBER, S., HOFFMANN, P., ENSLING, J., DEDIK, A.N., WEINBRUCH, S., MIEHE, G., GÜTLICH, P. & ORTNER, H.M. (2000) Characterization of iron compounds from urban and rural aerosol sources. *Journal of Aerosol Science*, 31, 987-997.

WEST, R.G. (1977) Pleistocene Geology and Biology: Second Edition. *London, Longman Group Limited.*

WHITELEGG, J. & WILLIAMS, N. (2000) The plane truth; aviation and the environment. *London, The Ashden Trust & Transport 2000 Trust.*

WILLIAMS, M. (1991) Ferrimagnetic sulfide formation in recent sediments of Loch Ba, Scotland and implications for magnetostratigraphic interpretation. *Quaternary Research*, 35, 208-221 .

WILLIAMS, M.L. (2000) Atmospheric pollution: contribution of automobiles. *Revue Française d'Allergologie et d'Immunologie Clinique*, 40, 216-21.

WILSON, J.G., KINGHAM, S., PEARCE, J., STYRMAN, A.P. (2005) A review of intraurban variations in particulate air pollution: implications for epidemiological research. *Atmospheric Environment*, 39, 6444-6462.

WOLMAN, M.G. (1967) A cycle of sedimentation and erosion un urban river channels. *Geografiska Annaler*, 49, 385-395.

WORSLEY, A.T., BOOTH, C.A., POWER, A.L., RICHARDSON, N., APPLEBY, P.G. & WRIGHT, E.J. (2005) Atmospheric pollution and human health: the significance of a datable sedimentary archive from a small urban lake in Merseyside, UK. IN BREBBIA, C.A., POPOV, V. & FAYZIEVA, D. (Eds.) Environmental Health Risk II. *Southampton, Wessex Institute Technology Press*. pp. 199-208.

WORSLEY, A.T., POWER, A.L., BOOTH, C.A., RICHARDSON, N., APPLEBY, P.G. & ORTON, C. (2006) Air pollution records from urban lake sediments: the implications of datable, lacustrine sedimentary archives for epidemiology. IN LONGHURST, J.W.S & BREBBIA, C.A. (Eds.) Air Pollution XIV. *Southampton, Wessex Institute Technology Press*. pp 735-744.

WORSLEY, A.T. & POWER, A.L. (2007) Atmospheric pollution and human health: the significance of a datable sedimentary archives from a small urban lake in Merseyside UK. *Environment and human health conference and workshop.* Society of Environmental Geochemistry and Health, Liverpool. (4th June).

WRIGHT, Jr H.E. (1980) Cores of soft lake sediments. *Boreas*, 9, 107-114.

WRIGHT, Jr H.E. (1991) Coring Tips. *Journal of Paleolimnology*, 6, 37-49.

WU, Y-S., FANG, G-C., CHEN, J-C., LIN, C-P. HUANG, S-H., RAU, J-Y. & LIN, J-G. (2006) Ambient air particulate dry deposition, concentrations and metallic elements at Taichung Harbor near Taiwan Strait. *Atmospheric Research*, 79, 52-66.

XIE, R.K., SEIP, H.M., LEINUM, J.R., WINJE, T. & XIAO, J.S. (2005) Chemical characterization of individual particles (PM10) from ambient air in Guiyang City, China. *Science of the Total Environment*, 343, 261-272.

XIE, S., DEARING, J.A. & BLOEMENDAL, J. (1999) A partial susceptibility approach to analysing the magnetic properties of environmental materials: a case study. *Geophysical Journal International*, 138, 851-856.

XIE, S., DEARING, J.A. & BLOEMENDAL, J. (2000) The organic matter content of street dust in Liverpool, UK, and its association with dust magnetic properties. *Atmospheric Environment*, 34, 26-275.

XIE, S., DEARING, J.A., BLOEMENDAL, J. & BOYLE, J.F. (1999) Association between the organic matter content and magnetic properties in street dusts, Liverpool, UK. *Science of the Total Environment*, 241, 205-214.

XIE, S., DEARING, J.A., BOYLE, J.F., BLOEMENDAL, J. & MORSE, A.P. (2001) Association between magnetic properties and element concentrations of Liverpool street dust and its implication. *Journal of Applied Geophysics*, 48, 83-92.

YANG, C., CHANG, C., CHUANG, H., TSAI, S., WU, T. & HO, C. (2004) Relationships between air pollution and daily mortality in a subtropical city: Taipei, Taiwan. *Environment International*, 30, 519-523.

YANG, H. & ROSE, N. (2005) Trace element pollution records in some UK lake sediments, their history, influence factors and regional differences. *Environment International*, 31, 63-75.

YANG, H. & ROSE, N.(2004) Trace element pollution records in some UK lake sediments, their history, influence factors and regional differences. *Environment International*, 31, 63-75.

YANG, H., BATTEARBEE, RW., TURNER, S.D., ROSE, N.L., DERWENT, R.G., WU, G. & YANG, R. (2010) Historical reconstruction of mercury pollution across the Tibetan Plateau using lake sediments. *Environmental Science and Technology*, 44, 2918-2924.

YANG, H., HE, B., CAI, S., OLDFIELD, F. & YU, L. (1997) Environmental implications of magnetic measurements on recent sediments from Lake Donghu, Wuhan. *Water, Air and Soil Pollution*, 98, 187-195.

YANG, H., ROSE, N.L. & BATTERBEE, R.W. (2001(a)) Dating of recent catchment peats using Spheroidal carbonaceous particle (SCP) concentration profiles with particular reference to Lochnagar, Scotland. *The Holocene*, 11, 593-597.

YANG, H., ROSE, N.L., BATTERBEE, R.W. & BOYLE, J. (2001(b)) Storage and distribution of trace metals and spheroidal carbonaceous particles (SCPs) from atmospheric deposition in the catchment peats of Lochnagar, Scotland. *Environmental Pollution*, 115, 231-238.

YANG, H-H., CHIANG, C-F., LEE, W-J., HWANG, K.P. & WU, E.M-Y. (1999) Size distribution and dry deposition of road dust PAHs. *Environment International*, 25, 585-597.

YANG, T., LIU, Q., LI, H., ZENG, Q. & CHAN, L. (2010) Anthropogenic magnetic particles and heavy metals in the road dust: magnetic identification and its implications. *Atmospheric Environment*, 44, 1175-1185.

YANG, H., ROSE, N.L.& BATTARBEE, R.W. (2002) Distribution of some trace metals in Lochnagar, a Scottish mountain lake ecosystem and its catchment. *Science of the Total Environment*, 285, 197-208.

YELOFF, D.E., LABADZ, J.C. & HUNT, C.O. (2005) The suitability of a south Pennine (UK) reservoir as an archive of recent environmental change. *Journal of Paleolimnology*, 34, 339-348.

YU, L. & OLDFIELD, F. (1989) A multivariate mixing model for identifying sediment sources from magnetic measurements. *Quaternary Research*, 32, 168-181.

YU, L. & OLDFIELD, F. (1993) Quantitative sediment source ascription using magnetic measurements in a reservoir-catchment system near Nijar, SE Spain. *Earth Surface Processes and Landforms*, 18, 441-454.

ZHANG, Q.W., KUSAKA, Y., SATO, K., NUKAKUKI, K., KOHYAMA, N. & DONALDSON, K. (1998) Differences in the extent of inflammation caused by intratracheal exposure to three ultrafine metals: role of free radicals. *Journal of Toxicology and Environmental Health*, 53, 423-438.

ZHU, Y., HINDS, W.C., KIM, S., SHEN, S. & SIOUUTAS, C. (2002) Study of ultrafine particles near a major highway with heavy duty diesel traffic. *Atmospheric Environment*, 36, 4323-4335.